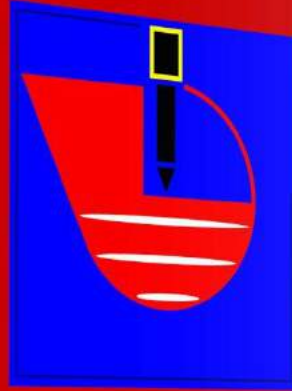


**Pile Buck**  
INTERNATIONAL, INC.

**Basics of Foundation Design**



# Basics of Foundation Design

Electronic Edition, January 2017

**Bengt H. Fellenius**  
Dr. Tech., P. Eng.

email: [Bengt@Fellenius.net](mailto:Bengt@Fellenius.net)  
website: [www.Fellenius.net](http://www.Fellenius.net)

**Pile Buck**  
INTERNATIONAL, INC.

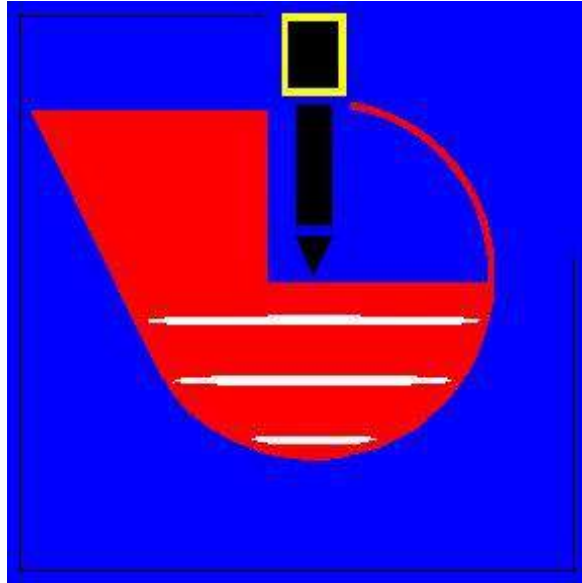
Pile Buck International, Inc. | P.O. Box 64-3609 | Vero Beach, FL 32964-3299



**Reference:**

Fellenius, B.H., 2018. Basics of foundation design.  
Pile Buck International, Inc., Vero Beach, FL,  
Electronic Edition, [www.Fellenius.net](http://www.Fellenius.net), 466 p.

Order a hard copy at this link. <http://www.pilebuck.com/product/basics-foundation-design-book/>



# Basics of Foundation Design

*Electronic Edition, January 2018*

**Bengt H. Fellenius**

**Dr. Tech., P. Eng.**

2375 Rothesay Avenue  
Sidney, British Columbia  
Canada, V8L 2B9

E-address: <[Bengt@Fellenius.net](mailto:Bengt@Fellenius.net)>  
Web site: [www.Fellenius.net](http://www.Fellenius.net)

---



# BASICS OF FOUNDATION DESIGN

## TABLE OF CONTENTS

### Contents

### Preface

#### 1. Classification, Effective Stress, and Stress Distribution (18 pages)

- 1.1 Introduction
- 1.2 Phase Parameters
- 1.3 Soil Classification by Grain Size
- 1.4 Effective Stress
- 1.5 Stress Distribution
- 1.6 Boussinesq Distribution
- 1.7 Newmark Influence Chart
- 1.8 Westergaard Distribution
- 1.9 Characteristic Point

#### 2. Cone Penetration Testing (54 pages)

- 2.1 Introduction
- 2.2. Brief Survey of Soil Profiling Methods
  - 2.21 Begeman (1965)
  - 2.22 Sanglerat et al., (1974)
  - 2.23 Schmertmann (1978)
  - 2.24 Douglas and Olsen (1981)
  - 2.25 Vos (1982)
  - 2.26 Robertson et al., (1986) and Campanella and Robertson (1988)
  - 2.27 Robertson (1990)
- 2.3 The Eslami-Fellenius CPTU Profiling and Classification
- 2.4 The Eslami-Fellenius and Robertson (1990) Methods
- 2.5 Comparisons
- 2.6 Profiling Case Example
- 2.7 Dissipation Time Measurement
- 2.8 Inclination Measurement
- 2.9 Shear-wave Measurement
- 2.10 CPT Depth and Stress Adjustment
- 2.11 Determining the Janbu Modulus Number,  $m$ , from CPT
- 2.12 Determining Soil Parameters from CPTU Measurements
  - 2.12.1 Undrained Shear Strength
  - 2.12.2 Overconsolidation Ratio, OCR
  - 2.12.3 Earth Stress Coefficient,  $K_0$
  - 2.12.4 Friction Angle
  - 2.12.5 Density Index,  $I_D$
  - 2.12.6 Conversion to SPT N-index
  - 2.12.7 Determining the E-Modulus from CPT Cone-stress

- 2.12.8 Assessing Liquefaction Susceptibility
  - 2.12.8.1 Cyclic Stress Ratio, CSR, and Cyclic Resistance Ratio, CRR
  - 2.12.8.2 Factor of Safety,  $F_s$ , against Liquefaction
  - 2.12.8.3 Comparison to Liquefaction Susceptibility Determined from SPT N-indices
  - 2.12.8.4 Determining Liquefaction Risk and Achieving Compaction/Densification; Example
  - 2.12.8.5 Compaction/Densification from Pile Driving

### **3. Settlement Calculation (26 pages)**

- 3.1 Introduction
- 3.2 Movement, Settlement, and Creep
- 3.3 Linear Elastic Deformation
- 3.4 Non-Linear Elastic Deformation
- 3.5 The Janbu Tangent Modulus Approach
  - 3.5.1 General
  - 3.5.2 Cohesionless Soil,  $j > 0$
  - 3.5.3 Dense Coarse-Grained Soil,  $j = 1$
  - 3.5.4 Sandy or Silty Soil,  $j = 0.5$
  - 3.5.5 Cohesive Soil,  $j = 0$
  - 3.5.6 Typical values of Modulus Number,  $m$
- 3.6 Evaluating oedometer tests by the  $e$ - $\lg p$  and the strain-stress methods
- 3.7 The Janbu Method vs. Conventional Methods
- 3.8 Time Dependent Settlement
- 3.9 Secondary Compression
- 3.10 Magnitude of Acceptable Settlement
- 3.11 Calculation of Settlement
- 3.12 Special Approach — Block Analysis
- 3.13 Determining the Modulus Number from In-Situ Plate Tests
- 3.14 Comments
  - 3.14.1 Immediate Compression
  - 3.14.2 Consolidation Settlement
  - 3.14.3 Secondary Compression

### **4. Vertical drains to accelerate settlement (18 pages)**

- 4.1 Introduction
- 4.2 Conventional Approach to Dissipation and Consolidation
- 4.3 Combined Vertical and Horizontal Flow
- 4.4 Practical Aspects Influencing the Design of a Vertical Drain Project
  - 4.4.1 Drainage Blanket on the Ground Surface
  - 4.4.2 Effect of Winter Conditions
  - 4.4.3 Depth of Installation
  - 4.4.4 Width of Installation
  - 4.4.5 Effect of Pervious Horizontal Zones, Lenses, and Layers
  - 4.4.6 Surcharging
  - 4.4.7 Stage Construction
  - 4.4.8 Loading by Means of Vacuum
  - 4.4.9 Pore Pressure Gradient and Artesian Flow
  - 4.4.10 Secondary Compression
  - 4.4.11 Monitoring and Instrumentation

- 4.5. Sand Drains
- 4.6. Wick Drains
  - 4.6.1 Definition
  - 4.6.2 Permeability of the Filter Jacket
  - 4.6.3 Discharge Capacity
  - 4.6.4 Microfolding and Crimping
  - 4.4.6 Handling on Site
  - 4.6.6 Axial Tensile Strength of the Drain Core
  - 4.6.7 Smear Zone
  - 4.6.8 Site Investigation
  - 4.6.9 Spacing of Wick Drains
- 4.7 Closing remarks
  
- 5. Earth Stress (14 pages)**
  - 5.1 Introduction
  - 5.2 The earth Stress Coefficient
  - 5.3 Active and Passive Earth Stress
  - 5.4 Surcharge, Line, and Strip Loads
  - 5.5 Factor of Safety and Resistance Factors
  - 5.6 Aspects of Structural Design
  - 5.7 Anchored Sheet-Pile Wall Example
  - 5.8 Retaining Wall on Footing Example
  - 5.9 Retaining with multiple horizontal supports
  - 5.10 Collapse of shored trench
  
- 6. Bearing Capacity of Shallow Foundations (14 pages)**
  - 6.1 Introduction
  - 6.2 The Bearing Capacity Formula
  - 6.3 Inclined and Eccentric Loads
  - 6.4 Inclination and Shape factors
  - 6.5 Overturning
  - 6.6 Sliding
  - 6.7 Combined Calculation of a Wall and Footing
  - 6.8 Numerical Example
  - 6.9 Presumptive Stress
  - 6.10 Words of Caution
  
- 7. Static Analysis of Pile Load Transfer (84 pages)**
  - 7.1 Introduction
  - 7.2 Static Analysis
    - 7.2.1 Shaft Resistance
    - 7.2.2 Toe Resistance
    - 7.2.3 Ultimate Resistance
    - 7.2.4 Service Conditions
  - 7.3 Load-movement and load transfer
  - 7.4 Critical Depth
  - 7.5 Effect of Installation
  - 7.6 Residual Force
  - 7.7 Analysis of Capacity for Tapered Piles
  - 7.8 Standard Penetration Test, SPT
  - 7.9 Cone Penetrometer Test, CPTU
    - 7.9.1 Schmertmann and Nottingham

- 7.9.2 deRuiter and Beringen (Dutch)
- 7.9.3 LCPC (French)
- 7.9.4 Meyerhof
- 7.9.5 Tumay and Fakhroo
- 7.9.6 The ICP
- 7.9.7 Eslami and Fellenius
- 7.9.8 Comments on the Methods
- 7.10 The Lambda Method
- 7.11 Field Testing for Determining Axial Pile Capacity
- 7.12 Installation Phase
- 7.13 Structural Strength
- 7.14 The Location of the Neutral Plane and Magnitude of the Drag Force
- 7.15 The Unified Design Method for Capacity, Drag Force, Settlement, and Downdrag
  - 7.15.1 Drag Force
  - 7.15.2 A case History of Applying the Unified Design Method
- 7.16 Piles in Swelling Soil
- 7.17 Settlement of a Wide Piled Foundation
  - 7.17.1 Load-Transfer Movement of single piles
  - 7.17.2 Settlement below the Pile Toe Level due to Consolidation and Secondary Compression
  - 7.17.3 Downdrag
- 7.18 Wide Piled Foundations
  - 7.18.1 Settlement due to compression of pile and soil body
  - 7.18.2 Settlement due to load transfer
  - 7.18.3 Settlement due to compression of the soil below the pile toe level
  - 7.18.4 Contact stress
  - 7.18.5 Load distribution across the raft and between piles
- 7.19 Piled Raft and Piled Pad Foundations
- 7.20 A Few Related Comments on Pile Groups
  - 7.20.1 Pile Spacing
- 7.21 A few related comments
  - 7.21.1 Pile Spacing
  - 7.21.2 Pile Size
  - 7.21.3 Design of Piles for Horizontal Loading
  - 7.21.4 Seismic Design of Lateral Pile Behavior
  - 7.21.5 Pile Testing
  - 7.21.6 Pile Jetting
  - 7.21.7 Bitumen Coating
  - 7.21.8 Pile Buckling
  - 7.21.9 Plugging of Open-Toe Pipe Piles and in-between Flanges of H-piles
  - 7.21.10 Contact Stress
  - 7.21.11 Sweeping and Bending of Piles
  - 7.21.12 Influence on Adjacent Foundations
- 7.22 Capacity as a function of time
- 7.23 Scour
- 7.24 A Piled Foundation Example
- 7.25 Conclusions

## **8. Analysis of Results from the Static Loading Test (60 pages)**

- 8.1 Introduction
- 8.2 Davisson Offset Limit
- 8.3 Hansen 80-% and 90-% Criteria
  - 8.3.1 Hansen 80-% Criterion



- 8.3.2 Hansen 90-% Criterion
- 8.4 Chin-Kondner Extrapolation
- 8.5 Decourt Extrapolation
- 8.6 De Beer Yield Load
- 8.7 The Creep Method
- 8.8 Load at Maximum Curvature
- 8.9 Factor of Safety
- 8.10 Choice of Criterion
- 8.11 Loading Test Simulation
  - 8.11.1 The Ratio Function
  - 8.11.2 The Hyperbolic Function
  - 8.11.3 The Exponential Function
  - 8.11.4 The 80-% Function
  - 8.11.5 The Zhang Function
  - 8.11.6 The Vijayvergiya Function
  - 8.11.7 The Five Function-Curves Compiled
  - 8.11.8 Procedure for Fitting a Simulated Test Curve to a Measured Curve Using t-z and q-z Functions
- 8.12 Effect and Mechanism of Residual Force
- 8.13 Instrumented Tests
  - 8.13.1 Telltale Instrumentation
  - 8.13.2 Determining Load Distribution from Telltale Measurements
  - 8.13.3 Brief Notes on Strain-Gage Instrumentation
- 8.14 The Bidirectional Test
- 8.15 Residual Load in an Instrumented Pile
  - 8.15.1 Case History of Residual Force and Other Influences
  - 8.15.2 Case History on Calculation True Load Distribution
- 8.16 Modulus of 'Elasticity' of the Instrumented Pile
  - 8.16.1 Aspects to Consider
  - 8.16.2 Converting Strain to Load Using the Pile Modulus
  - 8.16.3 Mathematics of the Tangent Modulus Method
  - 8.16.4 Comparison between Secant and Tangent Modulus Methods
  - 8.16.4 Unloading/Reloading cycles
- 8.17 Concluding Remarks

## **9. Pile Dynamics (50 pages)**

- 9.1 Introduction
- 9.2. Principles of Hammer Function and Performance
- 9.3. Hammer Types
  - 9.3.1 Drop Hammers
  - 9.3.2 Air/Steam Hammers
  - 9.3.3 Diesel Hammers
  - 9.3.4 Direct-Drive Hammers
  - 9.3.5 Vibratory Hammers
- 9.4 Basic Concepts
- 9.5 Wave Equation Analysis of Pile Driving
- 9.6 Hammer Selection by Means of Wave Equation Analysis
- 9.7 Aspects to Consider In Reviewing Results of Wave Equation Analysis
- 9.8 High-Strain Dynamic Testing with the Pile Driving Analyzer
  - 9.8.1 Wave Traces
  - 9.8.2 Transferred Energy
  - 9.8.3 Movement
- 9.9 Pile Integrity

- 9.9.1 Integrity Determined from High-strain Testing
  - 9.9.2 Integrity Determined from Low-strain Testing
- 9.10 Case Method Estimate of Capacity
- 9.11 CAPWAP determined pile capacity
- 9.12 Results of a PDA Test
- 9.13 Long Duration Impulse Testing Method—The Statnamic and Fundex Methods
- 9.14 Vibratory Pile Driving
  - 9.14.1 Pile Shaft Resistance
  - 9.14.2 Pile Toe Resistance
  - 9.14.3 Vibrator Performance Parameters
  - 9.14.4 Vibratory Driving Planned from Penetration Tests
- 9.15 Vibration Caused by Pile Driving
- 9.16 Settlement, Compaction, and Densification Caused by Pile Driving Vibrations
- 9.17 Vibratory Compaction
- 10. Working Stress and Load and Resistance Factor Design (16 pages)**
  - 10.1 Introduction
  - 10.2 The Factor of Safety
  - 10.3 Limit States and Load and Resistance Factor Design
  - 10.4 Factor of Safety and Resistance Factors for Piled Foundations
    - 10.4.1 The Eurocode
    - 10.4.2 The AASHTO Specs
  - 10.5 Serviceability Limit States
  - 10.6 Concluding Remarks
- 11. Slope Stability (10 pages)**
  - 11.1 Introduction
  - 11.2 Example of Slip Circle Analysis
  - 11.3 Friction Circle
  - 11.4 Logarithmic Spiral
  - 11.5 Analysis for  $c'$ - $\phi'$  Conditions
  - 11.6 Software
- 12. Specifications and Dispute Avoidance (8 pages)**
  - 12.1 Introduction and examples
  - 12.2 A few special pointers
- 13. Terminology and Style (16 pages)**
  - 13.1 Introduction and Basic Definitions
  - 13.2 Brief compilation of some definitions and terms
  - 13.3 Units
  - 13.4 Spelling rules and special aspects on style
  - 13.5 References and bibliography
  - 13.6 Re-use of figures and data
  - 13.7 Some useful unit conversions
- 14. Examples (28 pages)**
  - 14.1 Introduction
  - 14.2 Stress Calculations
  - 14.3 Settlement Calculations
  - 14.4 Earth Pressure and Bearing Capacity of Retaining Walls
  - 14.5 Pile Capacity and Load-Transfer
  - 14.6 Analysis of Pile Loading Tests

- 15. Problems (10 pages)**
  - 15.1 Introduction
  - 15.2 Stress Distribution
  - 15.3 Settlement Analysis
  - 15.4 Earth Stress and Bearing Capacity of Shallow Foundations
  - 15.5 Deep Foundations
- 16. References (18 pages)**
- 17. Index (4 pages)**



## P R E F A C E

The “Red Book” presents a background to conventional foundation analysis and design. The origin of the text is two-fold. It started as a compendium of the contents of courses in foundation design given during my years as Professor at the University of Ottawa, Department of Civil Engineering. Later on, it became a background document to the software developed by former students of mine and marketed by UniSoft Ltd.

The text is not intended to replace the much more comprehensive ‘standard’ textbooks, but rather to support and augment these in a few important areas, supplying methods applicable to practical cases handled daily by practicing engineers and providing the basic soil mechanics background to those methods.

It concentrates on the static design of foundations. Although the topic is far from exhaustively treated, it does intend to present most of the basic material needed for a practicing engineer involved in routine geotechnical design, as well as provide the tools for an engineering student to approach and solve common geotechnical design problems. Indeed, I make the somewhat brazen claim that the text actually goes a good deal beyond what the average geotechnical engineers usually deals with in the course of an ordinary design practice, but not beyond what they should deal with.

The text emphasizes two main aspects of geotechnical analysis, the use of effective stress analysis and the understanding that the distribution of pore pressures in the field is fundamental to the relevance of any foundation design. Indeed, foundation design requires a solid understanding of the, in principle simple, but, in reality, very complex, interaction of solid particles with the water and gas present in the pores, as well as an in-depth recognition of the most basic principle in soil mechanics, the *principle* of effective stress.

To avoid the easily introduced errors of using buoyant unit weight, I strongly advise you to use the straight-forward method of calculating the effective stress from determining separately the total stress and pore pressure distributions, finding the effective stress distribution quite simply as a subtraction between the two. The method is useful for the student and the practicing engineer alike.

The text starts with a brief summary of phase system calculations and how to determine the vertical distribution of stress underneath a loaded area applying the methods of 2:1, Boussinesq, and Westergaard.

I have long held that the piezocone (CPTU) is invaluable for the engineer charged with determining a soil profile and estimating key routine soil parameters at a site. Accordingly, the second chapter gives a background to the soil profiling from CPTU data. This chapter is followed by a summary of methods of routine settlement analysis based on change of effective stress. More in-depth aspects, such as creep and lateral flow are very cursorily introduced or not at all, allowing the text to expand on the influence of adjacent loads, excavations, and groundwater table changes being present or acting simultaneously with the foundation analyzed.

Consolidation analysis is treated sparingly in the book, but for the use and design of acceleration of consolidation by means of vertical drains, which is a very constructive tool for the geotechnical engineers that could be put to much more use in the current state-of-the-practice.

Earth stress—‘earth pressure’—is presented with emphasis on the Coulomb formulas and the effect of sloping retaining walls and sloping ground surface with surcharge and/or limited area surface or line loads per the requirements in current design manuals and codes. Conventional methods of analyzing bearing capacity of shallow foundations is introduced and the importance of combining the bearing capacity design analysis with earth stress and horizontal and inclined loading is emphasized. The Limit States Design, or Load and Resistance Factor Design, for retaining walls and footings is also addressed in this context.

The design of piles and pile groups is only very parsimoniously treated in most textbooks, and the treatment is often misleading a practicing engineer. In this book, therefore, I have spent a good deal of effort on presenting the static design of piles considering capacity, negative skin friction, and settlement, emphasizing the interaction of load-transfer and settlement (downdrag), which I have termed “the Unified Piled Foundation Design”. The settlement analysis of piles and pile groups combines load-transfer movement and settlement due to increase of effective stress in the soil due to the load applied to the piles and to the other effects in the immediate area of the pile group. The use of basic principles for design analysis of wide piled foundations is detailed.

The pile analysis chapter is followed by a separate chapter on the analysis of static loading tests, and modeling the static loading test, including the bidirectional test. In my opinion, no analysis of piles is completed until the results of the test are presented in terms of load distributions correlated to an effective stress analysis referencing the observed and/or expected foundation movement. The load-movement response expressed in t-z and q-z curves is emphasized.

Basics of pile driving dynamic testing are presented. The treatment is not directed toward serving the expert, but is intended to serve as background to the general practicing engineer. The dynamics chapter includes aspects of vibratory driving and how vibrations from pile driving can affect neighboring areas and building and concludes with aspects of vibratory compaction.

I have some critique on the use of working stress and limits states (factor of safety and load and resistance factors) , indeed, on the use of "capacity" and present a chapter on background and principles of this use.

A brief chapter on slope stability analysis is also included.

Frequently, many of the difficulties experienced by the student in learning to use the analytical tools and methods of geotechnical engineering, and by the practicing engineer in applying the 'standard' knowledge and procedures, lie with a less than perfect feel for the terminology and concepts involved. To assist in this area, a brief chapter on preferred terminology and an explanation to common foundation terms is also included.

Everyone surely recognizes that the success of a design to a large extent rests on an equally successful construction of the designed project. However, many engineers appear oblivious to the key prerequisite for success of the construction: a dispute-free interaction between the engineers and the contractors during the construction, as judged from the many acutely inept specs texts common in the field. I have added a strongly felt commentary on the subject at the end of the book.

A set of solved examples and problems for individual practice. The problems are of different degree of complexity, but even when very simple, they intend to be realistic and have some relevance to the practice of engineering design.

Finally, most facts, principles, and recommendations put forward in this book are those of others. Although several pertinent references are included, these are more to indicate to the reader where additional information can be obtained on a particular topic, rather than to give professional credit. However, I am well aware of my considerable indebtedness to others in the profession from mentors, colleagues, friends, and collaborators throughout my career, too many to mention. The opinions and sometimes strong statements are my own, however, and I am equally aware that time might suggest a change of these, often, but not always, toward the mellow side.

The "Red Book" is available for free downloading from my web site, [[www.Fellenius.net](http://www.Fellenius.net)] and dissemination of copies is encouraged. I have appreciated receiving comments and questions triggered by the earlier versions of the book and hope that this revised and expanded text will bring additional e-messages with questions and suggestions (<Bengt@Fellenius.net>). Not least welcome are those pointing out typos and mistakes in the text to correct in future updated versions. Note that the downloading link on my web site includes copies of several technical articles that provide a wider treatment of the subject matters. A non-color, hard-copy of the book can be ordered from PileBuck International Inc. E: [info@pilebuck.com](mailto:info@pilebuck.com).

The 2018 edition is updated from previous edition by correction of a few typos, some reformatting and rephrasing, expansion of a few issues, and adding of views on design of wide piled rafts, Chapter 7.

I am indebted to Dr. Mauricio Ochoa, PE, for his careful editing review of my text as well as making many most pertinent and much appreciated suggestions for clarifications and add-ons.

Sidney January 2018

Bengt H. Fellenius

# CHAPTER 1

## CLASSIFICATION, EFFECTIVE STRESS, and STRESS DISTRIBUTION

### 1.1 Introduction

Before a foundation design can be embarked on, the associated soil profile must be well established. The soil profile is compiled from three cornerstones of information:

- assessment of the overall site geology
- in-situ testing results, particularly continuous tests, such as the CPTU
- laboratory classification and testing of recovered soil samples
- pore pressure (piezometer) observations

Projects where construction difficulties, disputes, and litigations arise often have one thing in common: borehole logs and soundings were thought sufficient when determining the soil profile, disregarding information on the geology.

The essential part of the foundation design is to devise a foundation type and size that will result in acceptable values of deformation (settlement) and an adequate margin of safety to failure (the degree of utilization of the soil strength). Deformation is *due to change* of effective stress and soil shear resistance is *proportional* to effective stress. Therefore, all foundation designs must start with determining the effective stress distribution of the soil around and below the foundation unit. That initial distribution then serves as basis for the design analysis. The "initial" condition may well be many years back in time and the long-term—final—condition years ahead in time.

Effective stress is the total stress minus the pore pressure (the water pressure in the voids). Determining the effective stress requires that the basic parameters of the soil are known. The basic parameters are the pore pressure distribution and the Phase Parameters, such as water content<sup>1)</sup> and total density. Unfortunately, far too many soil reports on site conditions lack adequate information on both the pore pressure distribution and the phase parameters.

### 1.2 Phase Parameters

Soil is an "interparticulate medium". A soil mass consists of a heterogeneous collection of solid particles with voids in between. The solids are made up of grains of minerals or organic material. The voids contain water and gas. The water can be clean or include dissolved salts and gas. The gas is similar to ordinary air, sometimes mixed with gas generated from decaying organic matter. The *solids*, the *water*, and the *gas* are termed the three **phases** of the soil.

---

<sup>1)</sup> The term "moisture content" is sometimes used in the same sense as "water content". Most people, even geotechnical engineers, will consider that calling a soil "moist", "damp", or "wet" signifies three different conditions of the soils (though undefined). It follows that laymen, read lawyers and judges, will believe and expect that "moisture content" is something different to "water content", perhaps thinking that the former indicates a less than saturated soil. However, there is no difference. It is only that saying "moisture" instead of "water" implies, or intends to imply, that the speaker possesses a greater degree of sophistication than conveyed by simply saying "water content" and, because the term is not immediately understood by the layman, it intends to send the message that the Speaker is in the "know", a specialist of some stature. Don't fall into that trap. Use "water content". Remember, we should strive to use simple terms that laymen can understand. (Abbreviated quote from Chapter 11).

To aid a rational analysis of a soil mass, the three phases are “disconnected”. Soil analysis makes use of basic definitions and relations of volume, mass, density, water content, saturation, void ratio, etc., as indicated in Fig. 1.1. The definitions are related and knowledge of a few will let the geotechnical engineer derive all the others.

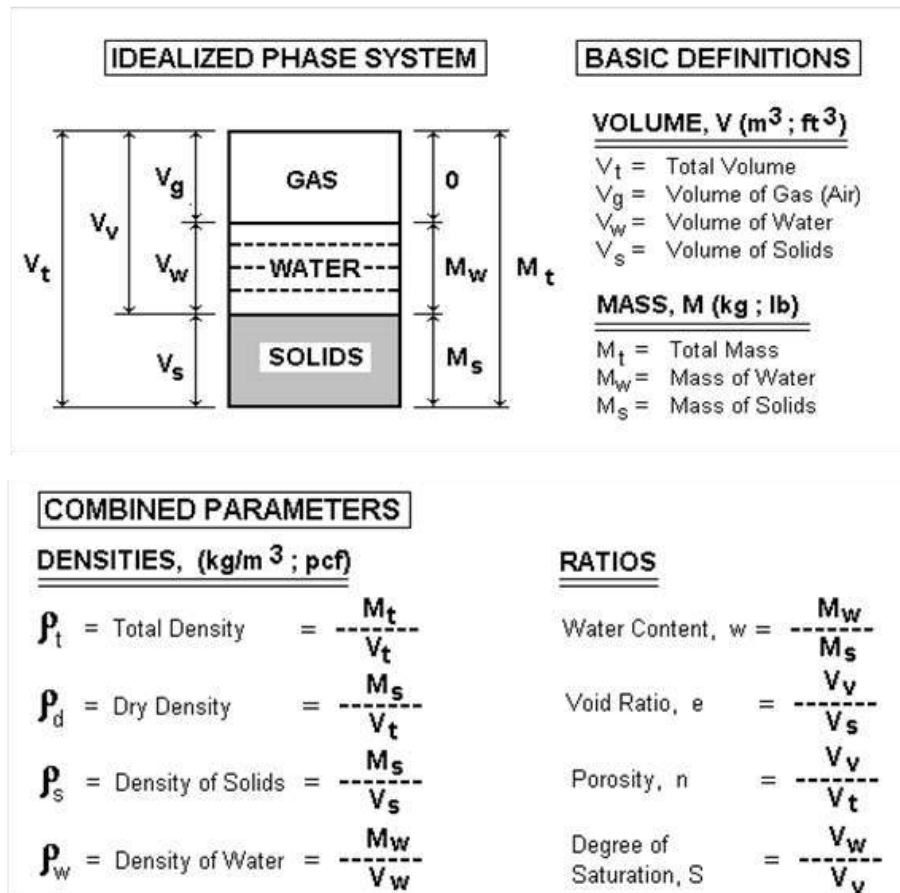


Fig. 1.1 The Phase System definitions

The need for phase systems calculation arises, for example, when the engineer wants to establish the effective stress profile at a site and does not know the total density of the soil, only the water content. Or, when determining the dry density and degree of saturation from the initial water content and total density in a Proctor test. Or, when calculating the final void ratio from the measured final water content in an oedometer test. While the water content is usually a measured quantity and, as such, a reliable number, many of the other parameters reported by a laboratory are based on an assumed value of solid density, usually taken as  $2,670 \text{ kg/m}^3$  plus the assumption that the tested sample is saturated. The latter assumption is often very wrong and the error can result in significantly incorrect soil parameters.

Starting from the definitions shown in Fig. 1.1, a series of useful formulae can be derived, as follows:

$$(1.1) \quad S = \frac{w}{\rho_w} \times \frac{\rho_s \rho_d}{\rho_s - \rho_d} = \frac{w}{e} \times \frac{\rho_s}{\rho_w}$$

$$(1.2) \quad w = S \rho_w \times \frac{\rho_s - \rho_d}{\rho_s \rho_d} = \frac{\rho_t}{\rho_d} - 1$$



$$(1.3) \quad \rho_{SAT} = \frac{M_w + \rho_w V_g + M_s}{V_t} = \rho_d + \rho_w \left(1 - \frac{\rho_d}{\rho_s}\right) = \frac{\rho_d}{\rho_s} (\rho_s + e\rho_w) = \rho_s \frac{1+w}{1+e}$$

$$(1.4) \quad \rho_d = \frac{\rho_s}{1+e} = \frac{\rho_t}{1+w} = \frac{\rho_w S}{w + \frac{\rho_w}{\rho_s} S}$$

$$(1.5) \quad \rho_t = \frac{\rho_s(1+w)}{1+e} = \rho_d(1+w)$$

$$(1.6) \quad e = \frac{n}{1-n} = \frac{\rho_s}{\rho_d} - 1 = \frac{w}{S} \times \frac{\rho_s}{\rho_w}$$

$$(1.7) \quad n = \frac{e}{1+e} = 1 - \frac{\rho_d}{\rho_s}$$

When performing phase calculations, the engineer normally knows or assumes the value of the density of the soil solids,  $\rho_s$ . Sometimes, the soil can be assumed to be fully saturated (however, presence of gas in fine-grained soils may often result in their not being fully saturated even well below the groundwater table; organic soils are rarely saturated and fills are almost never saturated). Knowing the density of the solids and one more parameter, such as the water content, all other relations can be calculated using the above formulae (they can also be found in many elementary textbooks, or easily be derived from the basic definitions and relations). I have included a few of the equations in an Excel "365 Cribsheet", which can be downloaded from my web site: [www.Fellenius.net](http://www.Fellenius.net).

The density of water is usually  $1,000 \text{ kg/m}^3$ . However, temperature and, especially, salt content can change this value by more than a few percentage points. For example, places in Syracuse, NY, have groundwater that has a salt content of up to 16 % by weight. Such large salt content cannot be disregarded when determining distribution of pore pressure and effective stress.

While most silica-based clays can be assumed to be made up of particles with a solid density of  $2,670 \text{ kg/m}^3$  (165 pcf), the solid density of other clay types may be quite different. For example, calcareous clays can have a solid density of  $2,800 \text{ kg/m}^3$  (175 pcf). However, at the same time, calcareous soils, in particular coral sands, can have such a large portion of voids that the bulk density is quite low compared to that of silica soils. Indeed, mineral composed of different materials can have a very different mechanical response to load. For example, just a few percent of mica in a sand will make the sand weaker and more compressible, all other aspects equal (Gilboy 1928).

Organic materials usually have a dry density that is much smaller than inorganic material. Therefore, when soils contain organics, their in-place average solid density is usually smaller than for inorganic materials. Moreover, if the organic content is 3 % (of dry weight) or larger, the soil should be called "slightly organic" and at 5 % organic content, the soil should be called "organic" (as adjective). Organic soils will have smaller shear strength and larger compressibility as opposed to inorganic soils. For example, an organic clay will exhibit much increased secondary compression (Section 3.9).

Soil grains are composed of minerals and the solid density varies between different minerals. Table 1.1 below lists some values of solid density for minerals that are common in rocks and, therefore, common in soils. The need for listing the density parameters with units could have been avoided by giving the densities in relation to the density of water, which is called "relative density". The term relative density, as used in modern international terminology, was termed "specific gravity" in old terminology, now abandoned. However, presenting the density parameter with units, as opposed to relative to the density of water, avoids the conflict of which of the two mentioned terms to use; either the correct term, which many, but not all, would misunderstand, or the incorrect term, which all understand, but the use of which would suggest ignorance of current terminology convention. (Shifting to a home-made term, such as "specific density", which sometimes pops up in the literature, does not make the ignorance smaller).

**Table 1.1 Solid Density for Minerals**

Mineral Type	Solid Density	
	kg/m <sup>3</sup>	pcf
Amphibole	≅3,000+	190
Calcite	2,800	180
Quartz	2,670	165
Mica	2,800	175
Pyrite	5,000	310
Illite	2,700	170

The term "relative density" is also used when describing a state of "compactness" or "compactness condition" termed "relative density", " $D_r$ ", which can range from very loose, loose, compact, dense, through very dense state. The relative density is not expressed in mass/volume, but is correlated to the N-index of the Standard Penetration test, SPT.

Depending on the soil void ratio and degree of saturation, the total density of soils can vary within wide boundaries. Tables 1.2 and 1.3 list some representative values.

**Table 1.2 Total saturated density for some typical soils**

Soil Type	<u>Saturated Total Density</u>	
	Metric (SI) units kg/m <sup>3</sup>	English units pcf
Sands; gravels	1,900 - 2,300	118 - 144
Sandy Silts	1,700 - 2,200	105 - 138
Clayey Silts and Silts	1,500 - 1,900	95 - 120
Soft clays	1,300 - 1,800	80 - 112
Firm clays	1,600 - 2,100	100 - 130
Glacial till	2,100 - 2,400	130 - 150
Peat	1,000 - 1,200	62 - 75
Organic silt	1,200 - 1,900	75 - 118
Granular fill	1,900 - 2,200	118 - 140

**Table 1.3 Total saturated density for uniform silica sand**

“Relative” Density	Total Saturated Density (kg/m <sup>3</sup> )	Water Content (%)	Void Ratio (approximate) (- - -)
Very dense	2,200	15	0.4
Dense	2,100	19	0.5
Compact	2,050	22	0.6
Loose	2,000	26	0.7
Very loose	1,900	30	0.8

A frequently applied expression is the "density index",  $I_D$ . The definition of the density index,  $I_D$ , is based on the assumption that the void ratio of the soil can be reliably determined for standardized procedures to create "maximum" and "minimum" density of a natural soil [ $I_D = (e_{\max} - e)/(e_{\max} - e_{\min})$ ]. Over the years, the density index has been used as a parameter to describe geotechnical parameters of sand deposits and correlations have been developed to estimate the angle of internal friction, liquefaction potential, and soil modulus. However, as has been shown by many, e.g., Tavenas and LaRochelle (1972), the density index is a highly imprecise and non-reproducible parameter as explained below.

A void ratio value determined on a soil sample, usually coarse-grained, is usually provided with two-decimal precision. However, the void ratio value is rarely more precise than by about  $0.05 \pm$ . For loose to compact sand, the in-situ void ratio typically ranges from about 0.40 through 0.60, depending on grain size gradation. Therefore, for a given sample, say, with an in-situ void ratio of 0.40, where typically, the maximum and minimum void ratios lie between 0.30 and 0.70, the  $I_D$  is 75 %. However, considering that the error, very likely, would be 0.05 up or down for each of the three values, the error in a particular  $I_D$  could be almost 20 %. (A 0.05 change in void ratio corresponds to a less than 2 % change in water content for a sand with  $e = 0.40$ , assuming that the degree of saturation,  $S$ , is 100 %, which is difficult to ensure for a sand sample). Tavenas and LaRochelle (1972) presented an extensive and detailed study of the Density Index and indicated that the average error is 18 % and concluded that the index “*cannot be used as a base parameter of any calculation*”. Indeed, any formula or numerical expression applying the  $I_D$  should be considered suspect and only applied with great caution, if at all.

### 1.3 Soil Classification by Grain Size

All languages describe "clay", "sand", "gravel", etc., which are terms primarily based on grain size. In the very beginning of the 20th century, Atterberg, a Swedish scientist and agriculturalist, proposed a classification system based on specific grain sizes. With minor modifications, the Atterberg system is still used and are the basis of the International Geotechnical Standard, as listed in Table 1.4.

Soil is made up of grains with a wide range of sizes and is named according to the portion of the specific grain sizes. Several classification systems are in use, e.g., ASTM, AASHTO, and International Geotechnical Society. Table 1.5 indicates the latter, which is also the Canadian standard (CFEM 1992).

The International (and Canadian) naming convention differs in some aspects from the AASHTO and ASTM systems which are dominant in US practice. For example, the boundary between silt and sand in the international standard is at 0.060 mm, whereas the AASHTO and ASTM standards place that boundary at Sieve #200 which has an opening of 0.075 mm. Table 1.5 follows the International standard. For details and examples of classification systems, see Holtz and Kovacs (1981) and Holtz et al. (2011).

**Table 1.4 Classification of Grain Size Boundaries (mm)**

<b>Clay</b>	<0.002		
<b>Silt</b>			
Fine silt	0.002	—	0.006
Medium silt	0.006	—	0.02
Coarse silt	0.02	—	0.06
<b>Sand</b>			
Fine sand	0.06	—	0.2
Medium sand	0.2	—	0.6
Coarse sand	0.6	—	2.0
<b>Gravel</b>			
Fine gravel	2	—	6
Medium gravel	6	—	20
Coarse gravel	20	—	60
<b>Cobbles</b>	60	—	200
<b>Boulders</b>	>200		

**Table 1.5 Classification of Grain Size Combinations (mm)**

"Noun" (Clay, Silt, Sand, Gravel)	35	< 100 %
"and" plus "noun"	20 %	< 35 %
"adjective" (clayey, silty, sandy)	10%	< 20%
"trace" (clay, silt, sand, gravel)	1 %	< 10 %

The grain size distribution for a soil is determined using a standard set of sieves. Conventionally, the results of the sieve analysis are plotted in diagram drawn with the abscissa in logarithmic scale as shown in Fig. 1.2. The three grain size curves, A, B, and C, shown are classified according to Table 1.5 as A: "*Sand trace gravel trace silt*". B: *Sandy clay some silt*, and C: would be named *clayey sandy silt some gravel*. Samples A and B are alluvial soils and are suitably named. However, Sample C, having 21 %, 44 %, 23 %, and 12 % of clay, silt, sand, and gravel size grains, is from a glacial till, for which soil, all grain size portions are conventionally named as adjective to the noun "till", i.e., Sample C is a "*clayey sandy silty glacial till*".

The grain-size fractions are fundamental parameters for a foundation design. The above classification follows the Canadian standard (and the international). Several other systems are in use. In the US, the Unified Soil Classification System (USCS) is the dominant (e.g., Holtz and Kovacs 1981 and Holtz et al. 2011). Therefore, in addition to the soil description, every borehole log in a geotechnical engineering report should include the numerical results of grain size analyses to allow the users to apply their preferred system.

Note that soils are also classified by grain angularity, constituent minerals, organic content, etc.

Sometimes, grain-size analysis results are plotted in a three-axes diagram called "ternary diagram" as illustrated in Fig. 1.3, which allows for a description according to grain size portions Clay+Silt+Sand to be obtained at a glance.

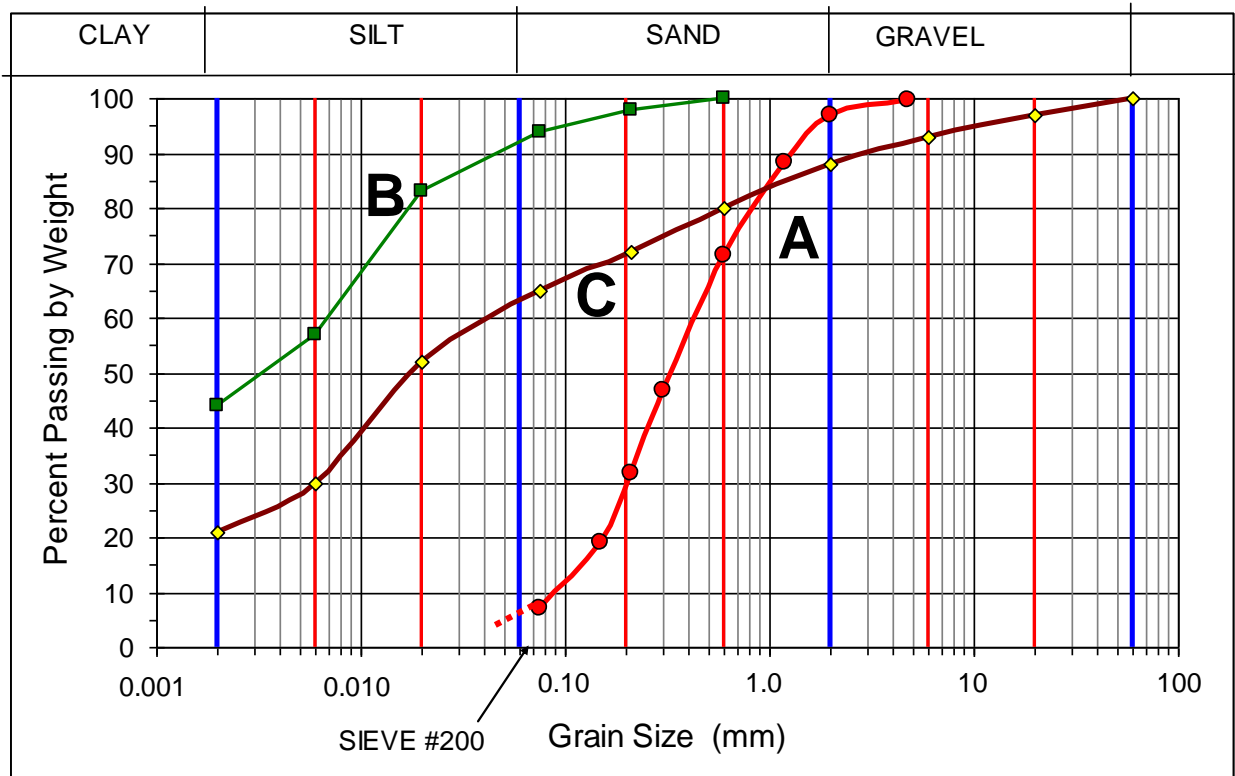


Fig. 1.2 Grain size diagram

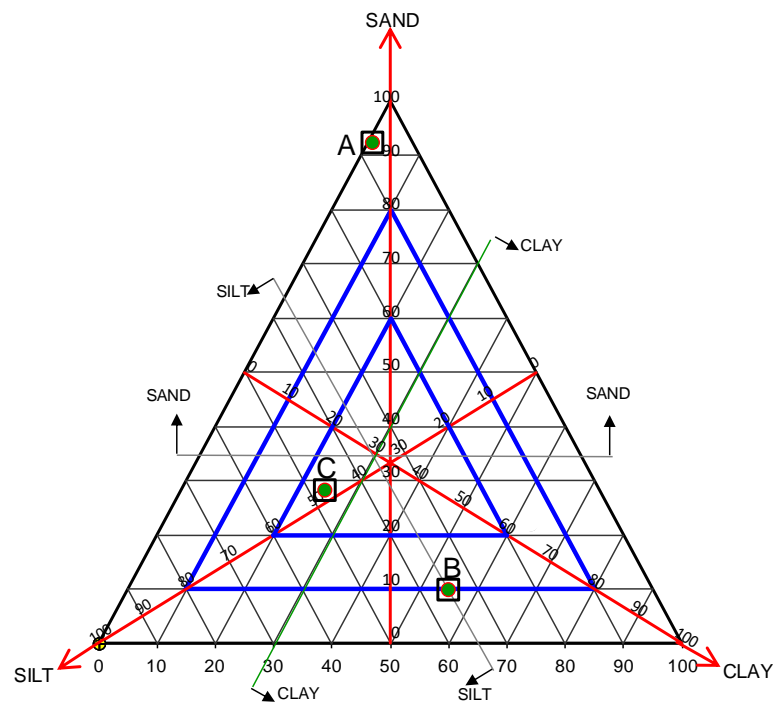


Fig. 1.3 Example of a ternary diagram

### 1.4. Effective Stress

As mentioned, effective stress is the total stress minus the pore pressure (the water pressure in the voids). Total stress at a certain depth below a level ground surface is the easiest of all values to determine as it is the summation of the total unit weight (total density times gravity constant) and depth. Where the pore pressure is hydrostatically distributed below the groundwater table, which is defined as the uppermost level of zero pore pressure (equal to atmospheric pressure), the pore pressure at a certain depth is equal to the density of water times the distance from that depth up to the groundwater table. (Notice, the soil can be partially saturated also above the groundwater table. Then, because of capillary action, pore pressures in the partially saturated zone above the groundwater table may be negative. In routine calculations, pore pressures are usually assumed to be zero in the zone above the groundwater table).

Notice, however, the pore pressure distribution is not always hydrostatic, far from always, actually. Hydrostatic pore water pressure has a vertical pressure gradient that is equal to unity (no vertical flow). However, the pore pressure at a site may have a downward gradient from a perched groundwater table, or an upward gradient from an **aquifer** down below (an aquifer is a soil layer containing free-flowing water, or a layer sandwiched between soil layers that are less "free-flowing", i.e., less pervious). Moreover, in areas below or close to the seashore and in areas close to bedrock containing salt (NaCl), the pore water may include dissolved salt and its density may be correspondingly larger than 1,000 kg/m<sup>3</sup>.

Frequently, the common method of determining the effective stress,  $\Delta\sigma'$ , contributed by a specific soil layer is to multiply the buoyant unit weight,  $\gamma'$ , of the soil with the layer thickness,  $\Delta h$ , as indicated in Eq. 1.8a.

$$(1.8a) \quad \Delta\sigma' = \gamma' \Delta h$$

The effective stress at a depth,  $\sigma'_z$  is the sum of the contributions from the soil layers, as follows.

$$(1.8b) \quad \sigma'_z = \sum(\gamma' \Delta h)$$

The buoyant unit weight,  $\gamma'$ , is often thought to be equal to the total unit weight ( $\gamma_t$ ) of the soil minus the unit weight of water ( $\gamma_w$ ) which presupposes that there is no vertical gradient of water flow in the soil,  $i = 0$ , defined below. However, this is only a special case. Because most sites display either an upward flow (maybe even artesian; the head is greater than the depth) or a downward flow, calculations of effective stress must consider the effect of the gradient—the buoyant unit weight is a function of the gradient in the soil as follows (Eq. 1.8c).

$$(1.8c) \quad \gamma' = \gamma_t - \gamma_w(1-i)$$

where  $\sigma'$  = effective overburden stress

$\Delta h$  = layer thickness

$\gamma'$  = buoyant unit weight

$\gamma_t$  = total (bulk) unit weight

$\gamma_w$  = unit weight of water

$i$  = gradient; the head at two points (difference in water elevation) divided by the distance the water has to flow between these two points (equal head means no flow,  $i = 0$  and upward flow is defined as the negative direction, i.e.,  $i < 0$ ).

A vertical flow is a non-hydrostatic condition. If the flow is upward, the gradient is negative; if downward it is termed positive. The flow can be minimal, that is, no obvious velocity. For artesian conditions, which is a non-hydrostatic condition, the gradient is larger than unity and the buoyant weight is smaller than for

the hydrostatic condition. Then, the effective stress is smaller too and, therefore, the soil strength is reduced. For example, a "quick sand" condition occurs when the upward gradient is so large that the effective stress (and buoyant unit weight,  $\gamma'$ ), approaches zero. Note that "quick sand" is not a particularly "quick" type of sand, but a soil, usually a silty fine sand, subjected to an upward pore pressure gradient.

The gradient in a non-hydrostatic condition is often awkward to determine. However, the difficulty can be avoided, because the effective stress is most easily found by calculating the total stress and the pore water pressure separately. The effective stress is then obtained by simple subtraction of the latter from the former.

Note, the difference in terminology—effective *stress* and pore *pressure*—which reflects the fundamental difference between forces in soil as opposed to in water. Stress is directional, that is, stress changes depend on the orientation of the plane of action in the soil. In contrast, pressure is omni-directional, that is, independent of the orientation; equal in all directions. Don't use the term "*soil pressure*", it is a misnomer.

The soil stresses, total and effective, and the water pressures are determined, as follows: The **total vertical stress** (symbol  $\sigma_z$ ) at a point in the soil profile (also called "total overburden stress") is calculated as the stress exerted by a soil column determined by multiplying the soil total (or bulk) unit weight with the height of the column (or the sum of separate weights when the soil profile is made up of a series of separate soil layers having different unit weights). The symbol for the total unit weight is  $\gamma_t$  (the subscript "t" stands for "total").

$$(1.9) \quad \sigma_z = \gamma_t z \quad \text{or:} \quad \sigma_z = \sum \Delta \sigma_z = \sum (\gamma_t \Delta h)$$

Similarly, the **pore pressure** (symbol  $u$ ), as measured in a stand-pipe, is equal to the unit weight of water,  $\gamma_w$ , times the height of the water column,  $h$ , in the stand-pipe. (If the pore pressure is measured directly, the head of water (height of the water column) is equal to the pressure divided by the unit weight of the water,  $\gamma_w$ ).

$$(1.10) \quad u = \gamma_w h$$

The height of the column of water (the head) representing the water pressure is usually not the distance to the ground surface nor, even, to the groundwater table. For this reason, the height is usually referred to as the "phreatic height" or the "piezometric height" to separate it from the depth below the groundwater table or depth below the ground surface.

The pore pressure distribution is determined by applying the fact that (in stationary situations) the pore pressure distribution can be assumed linear in each individual, or separate, soil layer, and, in pervious soil layers "sandwiched" between less pervious layers, the pore pressure is hydrostatic (that is, the vertical gradient within the sandwiched layer is unity. Note, if the pore pressure distribution within a specific soil layer is not linear, then, the soil layer is undergoing consolidation, which is not a stationary condition).

The **effective overburden stress** (symbol  $\sigma'_z$ ), also called "effective vertical stress", is then obtained as the difference between total stress and pore pressure.

$$(1.11) \quad \sigma'_z = \sigma_z - u_z = \gamma_t z - \gamma_w h$$

Usually, the geotechnical engineer provides a unit density,  $\rho$ , instead of the unit weight,  $\gamma$ . The unit density is mass per volume and unit weight is force per volume. Because in the customary English system

of units, both types of units are given as lb/volume, the difference is not clear (that one is pound-mass and the other is pound-force is not normally indicated, though pound-force is the most common variant). In the SI-system, unit density is given in  $\text{kg/m}^3$  and unit weight is given in  $\text{N/m}^3$ . Unit weight is unit density times the gravitational constant,  $g$ . (For most foundation engineering purposes, the gravitational constant can be taken to be  $10 \text{ m/s}^2$  rather than the overly exact value of  $9.81 \text{ m/s}^2$ ; besides, the second decimal varies across the Earth). Beware of asinine terms such as “weight density”.

$$(1.12) \quad \gamma = \rho g$$

Many soil reports do not indicate the bulk or total soil density,  $\rho_t$ , and provide only the water content,  $w$ , and the dry density,  $\rho_d$ . Knowing the dry density, the total density of a saturated soil can be calculated as:

$$(1.13) \quad \rho_t = \rho_d (1 + w)$$

## 1.5 Stress Distribution

Load applied to the surface of a body distributes into the body over a successively wider area. The simplest way to calculate the stress distribution is by means of the 2(V):1(H) method. This method assumes that the load is distributed over an area that increases in width in proportion to the depth below the loaded area, as is illustrated in Fig. 1.4. Since the vertical load,  $Q$ , acts over the increasingly larger area, the stress (load per surface area) diminishes with depth. The mathematical relation is as follows.

$$(1.14) \quad q_z = q_0 \times \frac{B \times L}{(B + z) \times (L + z)}$$

where  $q_z$  = stress at Depth  $z$   
 $z$  = depth where  $q_z$  is considered  
 $B$  = width (breadth) of loaded area  
 $L$  = length of loaded area  
 $q_0$  = applied stress =  $Q/B \times L$

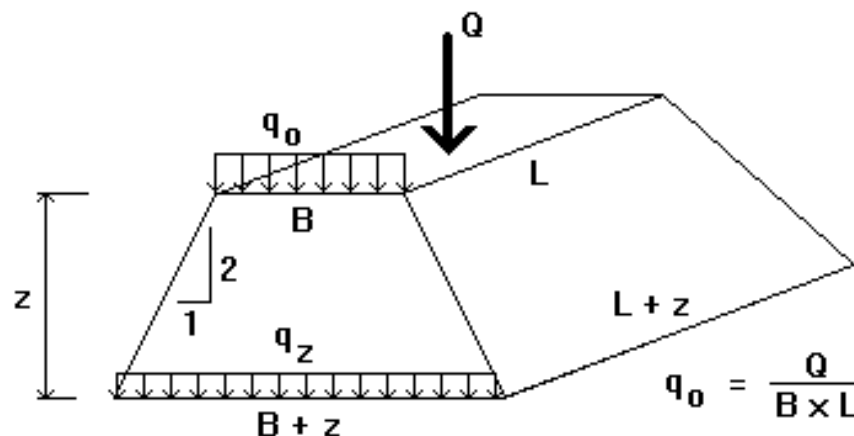


Fig. 1.4 The 2:1 method

Note, the 2:1 distribution is only valid inside (below) the footprint of the loaded area and must never be used to calculate the stress outside the footprint.



**Example 1.1** The principles of calculating effective stress and stress distribution are illustrated by the calculations involved in the following soil profile: An upper 4 m thick layer of normally consolidated sandy silt is deposited on 17 m of soft, compressible, slightly overconsolidated clay, followed by 6 m of medium dense silty sand and, hereunder, a thick deposit of medium dense to very dense sandy ablation glacial till. The densities of the four soil layers and the earth fill are: 2,000 kg/m<sup>3</sup>, 1,700 kg/m<sup>3</sup>, 2,100 kg/m<sup>3</sup>, 2,200 kg/m<sup>3</sup>, and 2,000 kg/m<sup>3</sup>, respectively. The groundwater table lies at a depth of 1.0 m. For “original conditions” (or initial condition), the pore pressure is hydrostatically distributed from the groundwater table throughout the soil profile. For “final conditions”, the pore pressure in the sand has increased to a phreatic height above ground of 5 m; the fact that the phreatic height reaches above ground makes the pressure condition “artesian”. It is still hydrostatically distributed in the sand (as is the case when a more pervious soil layer is sandwiched between less pervious soils—a key fact to consider when calculating the distribution of pore pressure and effective stress). Moreover, the pore pressure in the clay has become non-hydrostatic. Note, however, that it is linear, assuming that the “final” condition is long-term, i.e., the pore pressure has stabilized. The pore pressure in the glacial till is assumed to remain hydrostatically distributed. Finally, for those “final conditions”, a 1.5 m thick earth fill has been placed over a square area with a 36 m side.

Calculate the distribution of total and effective stresses, and pore pressure underneath the center of the earth fill before and after placing the earth fill. Distribute the earth fill, by means of the 2:1-method, that is, distribute the load from the fill area evenly over an area that increases in width and length by an amount equal to the depth below the base of fill area (Eq. 1.14).

Table 1.6 presents the results of the stress calculation for the Example 1.1 conditions. The calculation results are presented in the format of a spread sheet, a “hand calculation” format, to ease verifying the computer calculations. Notice that performing the calculations at every metre depth is normally not necessary. The table includes a comparison between the non-hydrostatic pore pressure values and the hydrostatic, as well as the effect of the earth fill, which can be seen from the difference in the values of total stress for “original” and “final” conditions.

The stress distribution below the center of the loaded area shown in Table 1.1 was calculated by means of the 2:1-method. However, the 2:1-method is rather approximate and limited in use. Compare, for example, the vertical stress below a loaded footing that is either a square or a circle with a side or diameter of  $B$ . For the same contact stress,  $q_0$ , the 2:1-method, strictly applied to the side and diameter values, indicates that the vertical distributions of stress,  $[q_z = q_0/(B + z)^2]$  are equal for the square and the circular footings. Yet, the total applied load on the square footing is  $4/\pi = 1.27$  times larger than the total load on the circular footing. Therefore, if applying the 2:1-method to circles and other non-rectangular areas, they should be modeled as a rectangle of an equal size (‘equivalent’) area. Thus, a circle is modeled as an equivalent square with a side equal to the circle radius times  $\sqrt{\pi}$ .

Notice, the 2:1-method is inappropriate to use for determining the stress distribution below a point at any other location than well within the loaded area. For this reason, it cannot be used to combine stress from two or more loaded areas unless the footprints are similar and have the same center. To calculate the stresses induced from more than one loaded area and/or below an off-center location, more elaborate methods, such as the Boussinesq distribution, are required.

**TABLE 1.6**  
**STRESS DISTRIBUTION (2:1 METHOD) BELOW CENTER OF EARTH FILL**  
 [Calculations by means of UniSettle]

ORIGINAL CONDITION (no earth fill)				FINAL CONDITION (with earth fill)		
Depth (m)	$\sigma_0$ (kPa)	$u_0$ (kPa)	$\sigma_0'$ (kPa)	$\sigma_1$ (kPa)	$u_1$ (kPa)	$\sigma_1'$ (kPa)
<b>Layer 1 Sandy silt <math>\rho = 2,000 \text{ kg/m}^3</math></b>						
0.00	0.0	0.0	0.0	30.0	0.0	30.0
1.00 (GWT)	20.0	0.0	20.0	48.4	0.0	48.4
2.00	40.0	10.0	30.0	66.9	10.0	56.9
3.00	60.0	20.0	40.0	85.6	20.0	65.6
4.00	80.0	30.0	50.0	104.3	30.0	74.3
<b>Layer 2 Soft Clay <math>\rho = 1,700 \text{ kg/m}^3</math></b>						
4.00	80.0	30.0	50.0	104.3	30.0	74.3
5.00	97.0	40.0	57.0	120.1	43.5	76.6
6.00	114.0	50.0	64.0	136.0	57.1	79.0
7.00	131.0	60.0	71.0	152.0	70.6	81.4
8.00	148.0	70.0	78.0	168.1	84.1	84.0
9.00	165.0	80.0	85.0	184.2	97.6	86.6
10.00	182.0	90.0	92.0	200.4	111.2	89.2
11.00	199.0	100.0	99.0	216.6	124.7	91.9
12.00	216.0	110.0	106.0	232.9	138.2	94.6
13.00	233.0	120.0	113.0	249.2	151.8	97.4
14.00	250.0	130.0	120.0	265.6	165.3	100.3
15.00	267.0	140.0	127.0	281.9	178.8	103.1
16.00	284.0	150.0	134.0	298.4	192.4	106.0
17.00	301.0	160.0	141.0	314.8	205.9	109.0
18.00	318.0	170.0	148.0	331.3	219.4	111.9
19.00	335.0	180.0	155.0	347.9	232.9	114.9
20.00	352.0	190.0	162.0	364.4	246.5	117.9
21.00	369.0	200.0	169.0	381.0	260.0	121.0
<b>Layer 3 Silty Sand <math>\rho = 2,100 \text{ kg/m}^3</math></b>						
21.00	369.0	200.0	169.0	381.0	260.0	121.0
22.00	390.0	210.0	180.0	401.6	270.0	131.6
23.00	411.0	220.0	191.0	422.2	280.0	142.2
24.00	432.0	230.0	202.0	442.8	290.0	152.8
25.00	453.0	240.0	213.0	463.4	300.0	163.4
26.00	474.0	250.0	224.0	484.1	310.0	174.1
27.00	495.0	260.0	235.0	504.8	320.0	184.8
<b>Layer 4 Ablation Till <math>\rho = 2,200 \text{ kg/m}^3</math></b>						
27.00	495.0	260.0	235.0	504.8	320.0	184.8
28.00	517.0	270.0	247.0	526.5	330.0	196.5
29.00	539.0	280.0	259.0	548.2	340.0	208.2
30.00	561.0	290.0	271.0	569.9	350.0	219.9
31.00	583.0	300.0	283.0	591.7	360.0	231.7
32.00	605.0	310.0	295.0	613.4	370.0	243.4
33.00	627.0	320.0	307.0	635.2	380.0	255.2

## 1.6 Boussinesq Distribution

The Boussinesq distribution (Boussinesq 1885, Holtz and Kovacs 1981, Holtz et al. 2011) assumes that the soil is a homogeneous, isotropic, linearly elastic half sphere (Poisson's ratio equal to 0.5). The following relation gives the vertical distribution of the stress resulting from the point load. The location of the distribution line is given by the radial distance to the point of application (Fig. 1.5) and calculated by Eq. 1.15.

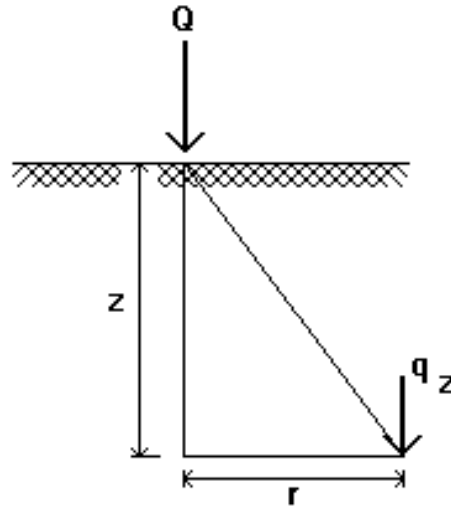


Fig. 1.5. Definition of terms used in Eq. 1.15.

$$(1.15) \quad q_z = Q \frac{3z^3}{2\pi (r^2 + z^2)^{5/2}}$$

where  $Q$  = the point load (the total load applied)  
 $q_z$  = stress at Depth  $z$   
 $z$  = depth where  $q_z$  is considered  
 $r$  = radial distance to the point of application

A footing is usually placed in an excavation and often a fill is placed next to the footing. When calculating the stress increase from a footing load, the changes in effective stress from the excavations and fills must be included, which, therefore, precludes the use of the 2:1-method (unless all such excavations and fills are concentric with the footing).

By means of integrating the point load relation (Eq. 1.15) along a line, a relation for the stress imposed by a line load,  $P$ , can be determined as given in Eq. 1.16.

$$(1.16) \quad q_z = P \frac{2z^3}{\pi (r^2 + z^2)^2}$$

where  $P$  = line load (force/ unit length)  
 $q_z$  = stress at Depth  $z$   
 $z$  = depth where  $q_z$  is considered  
 $r$  = radial distance to the point of application

### 1.7 Newmark Influence Chart

Newmark (1935) integrated Eq. 1.15 over a finite area and obtained a relation, Eq. 1.17, for the stress,  $q_z$ , under the **corner of a uniformly loaded rectangular** area, for example, a footing, as a function of an Influence Factor,  $I$ .

$$(1.17) \quad q_z = q_0 \times I \quad I = \frac{A \times B + C}{4\pi}$$

$$\text{where} \quad A = \frac{2mn\sqrt{m^2 + n^2 + 1}}{m^2 + n^2 + 1 + m^2n^2}$$

$$B = \frac{m^2 + n^2 + 2}{m^2 + n^2 + 1}$$

$$C = \arctan \left[ \frac{2mn\sqrt{m^2 + n^2 + 1}}{m^2 + n^2 + 1 - m^2n^2} \right]$$

and

- $m = x/z$
- $n = y/z$
- $x =$  length of the loaded area
- $y =$  width of the loaded area
- $z =$  depth to the point under the corner  
where the stress is calculated

Notice that Eq. 1.17 provides the stress in only one point; for stresses at other points, for example when determining the vertical distribution at several depths below the corner point, the calculations have to be performed for each depth. To determine the stress below a point other than the corner point, the area has to be split in several parts, all with a corner at the point in question and the results of multiple calculations summed up to give the answer. Indeed, the relations are rather cumbersome to use. Also restricting the usefulness in engineering practice of the footing relation is that an irregularly shaped area has to be broken up in several smaller rectangular areas. Recognizing this, Newmark (1942) published diagrams called influence charts by which the time and effort necessary for the calculation of the stress below a point was considerably shortened even for an area with an irregularly shaped footprint.

Until the advent of the computer and spread-sheet programs, the influence chart was faster to use than Eq. 1.17, and the Newmark charts became an indispensable tool for all geotechnical engineers. Others developed charts using the Boussinesq basic equation to apply to non-rectangular areas and non-uniformly loaded areas, for example, a uniformly loaded circle or a the trapezoidal load from a sloping embankment. Holtz and Kovacs (1981 and Holtz et al. 2011) include several references to developments based on the Boussinesq basic relation.

A detailed study of the integration reveals that, near the base of the loaded area, the formula produces a sudden change of values. Fig. 1.6 shows the stress distribution underneath the center of a 3-m square footing exerting a contact stress of 100 kPa. Below a depth of about one third of the footing width, the stress diminishes in a steady manner. However, at about one third of the width, there is a kink and the stress above the kink decreases whereas a continued increase would have been expected. The kink is due to the transfer of the point load to stress, which no integration can disguise.

For the same case and set of calculations, Fig. 1.7 shows the influence factor,  $I$  for the corner of an 1.5 m wide square footing. The expected influence factor immediately below the footing is 0.25, but, for the same reason of incompatibility of point load and stress, it decreases from  $m = n$  = about 1.5 (side of “corner” footing =  $0.67z$ ; side of “square” footing =  $0.33z$ ). Newmark (1935) resolved this conflict by extending the curve, as indicated by the extension lines in Figs. 1.6 and 1.7 by means of adjusting Eq. 1.17 to Eq. 1.17a. The relation shown below the equations, indicates when each equation controls. Although Newmark (1935) included the adjustment, it is not normally found in textbooks.

$$(1.17a) \quad q_z = q_0 \times I = \frac{A \times B + \pi - C}{4\pi}$$

which is valid where:  $m^2 + n^2 + 1 \leq m^2 n^2$ . "A", "B", and "C" are as in Eq. 1.17.

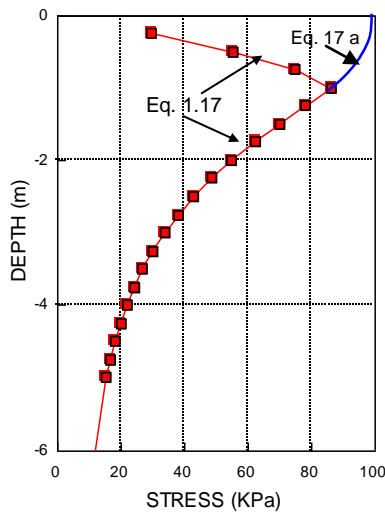


Fig. 1.6. Calculated stress distribution

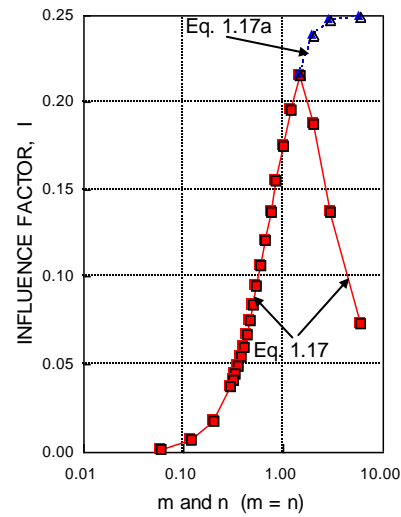


Fig. 1.7. Influence factor

## 1.8 Westergaard Distribution

Westergaard (1938) suggested that in soil with horizontal layers that restrict horizontal expansion, it would appropriate to assume that the soil layers are rigid horizontally (Poisson's ratio equal to zero) allowing only vertical compression for an imposed stress. Westergaard's solution for the stress caused by a point load is given in Eq. 1.18.

$$(1.18) \quad q_z = \frac{Q}{\pi z^2} = \frac{1}{[1 + 2(r/z)^2]^{3/2}}$$

where  $Q$  = total load applied  
 $q_z$  = stress at Depth  $z$   
 $z$  = depth where  $q_z$  is considered  
 $r$  = radial distance to the point of application

An integration of the Westergaard relation similar to the integration of the Boussinesq relation (Eq. 1.16) results in Eq. 1.19 (Taylor 1948). For the same reason of incompatibility of dimensions between Load and Stress, a “kink” appears also for the Westergaard solution.

$$(1.19) \quad q_z = q_0 \times I = q_0 \frac{1}{2\pi} \arctan \left[ \frac{1}{\sqrt{D + E + F}} \right]$$

$$\text{where} \quad D = \frac{1}{2m^2} \quad E = \frac{1}{2n^2} \quad F = \frac{1}{4m^2 n^2}$$

where  $m = x/z$   
 $n = y/z$   
 $x =$  length of the loaded area  
 $y =$  width of the loaded area  
 $z =$  depth to the point under the corner  
for where the stress is calculated

Influence charts similar to the Newmark charts for the Boussinesq relation have been developed also for the Westergaard relation. The difference between stresses calculated by one or the other method is small and considered less significant than the differences between reality and the idealistic assumptions behind either theory. The Westergaard method is often preferred over the Boussinesq method when calculating stress distribution in layered soils and below the center portion of wide areas of flexible load.

### 1.9 Characteristic Point

A small diameter footing, of about 1 metre width, can normally be assumed to distribute the contact stress evenly over the footing contact area. However, this cannot be assumed to be the case for wider footings. Both the Boussinesq and the Westergaard distributions assume ideally flexible footings (and ideally elastic soil), which is not the case for real footings, which are neither fully flexible nor absolutely rigid and soils are only approximately elastic in loading. Kany (1959) and Steinbrenner (1934; 1936) showed that below a so-called **characteristic point**, the vertical stress distribution is equal for flexible and rigid footings. In an ideally elastic soil, the characteristic point is located at a distance of 0.13B and 0.13L in from the side (edge) of a rectangular footing of width, B, and length, L, and at a distance of 0.08R in from the perimeter of a circular footing of radius R. The distances from the center are 0.37 times B or L and 0.42 times the circle radius, respectively, i.e., about 0.4 times width, length, or diameter of either a footing or circle. Thus, when applying Boussinesq method of stress distribution to a regularly shaped, more or less rigid footing, the stress below the characteristic point is normally used rather than the stress below the center of the footing to arrive at a representative stress distribution for the settlement calculation. Indeed, with regard to vertical stress distribution, we can live with the fact that footings are not ideally flexible or rigid and natural soils are far from perfectly elastic.

The calculations by either of Boussinesq or Westergaard methods are time-consuming. The 2:1 method is faster to use and it is therefore the most commonly used method in engineering practice. Moreover, the 2:1 distribution lies close to the Boussinesq distribution for the characteristic point. However, for calculation of stress imposed by a loaded area outside its own footprint, the 2:1 method cannot be used. Unfortunately, the work involved in a "hand calculation" of stress distribution according the Boussinesq or Westergaard equations for anything but the simplest case involves a substantial effort. To reduce the effort, before-computer calculations were normally restricted to involve only a single or very few loaded areas. Stress history, e.g., the local preconsolidation effect of previously loaded areas at a site, was rarely included. Computer programs are now available which greatly simplify and speed up the calculation effort. In particular, the advent of the UniSettle program (Goudreault and Fellenius 2011) has drastically reduced the routine calculation effort even for the most complex conditions and vastly increased the usefulness of the Boussinesq and Westergaard methods.

**Example.** Fig. 1.8 illustrates the difference between the three stress calculation methods for a square flexible footing with a side ("diameter") equal to "B" and loaded at its center, and, forestalling the presentation in Chapter 3, Fig. 1.9 shows the distribution of settlement for the three stress distributions shown in Fig. 1.8. The settlement values have been normalized to the settlement calculated for the Boussinesq method.

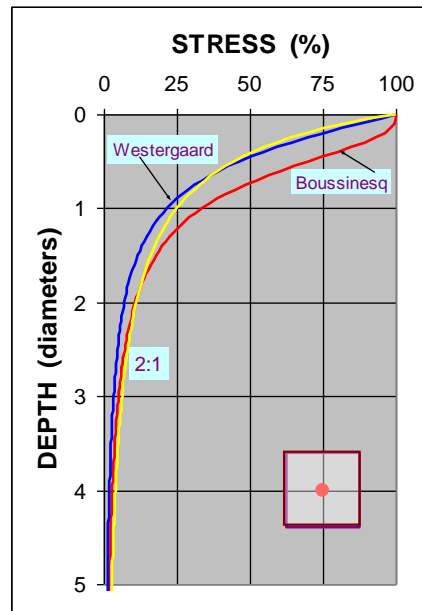


Fig. 1.8 Comparison between the methods

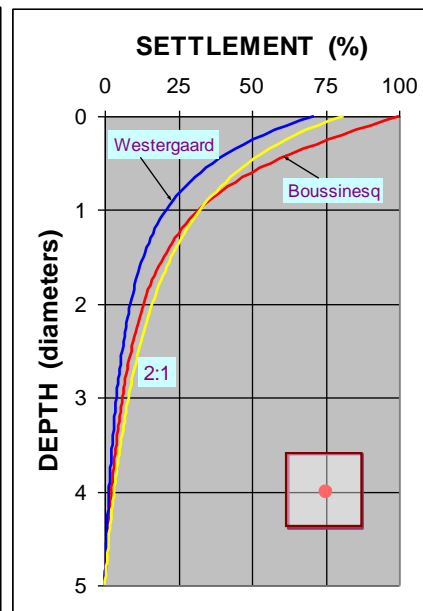


Fig. 1.9 Settlement distributions

Figs. 1.10 and 1.11 shows the stress and settlement distributions for when the load is applied at the so-called characteristic point ( $x = y = 0.37B$  from the center of the footing), below which the stress distributions are the same for a flexible as for a rigid footing.

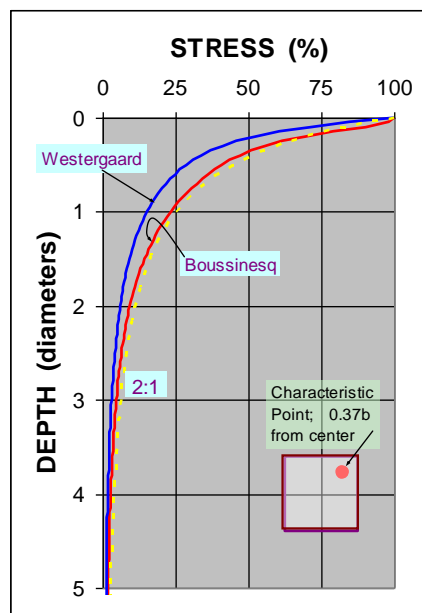


Fig. 1.10 Comparison between the methods

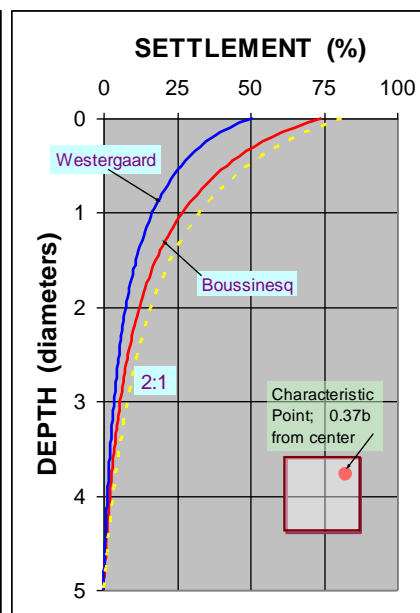


Fig. 1.11 Settlement distributions

As illustrated in Fig. 1.12, calculations using Boussinesq distribution can be used to determine how stress applied to the soil from one building may affect an adjacent existing building.

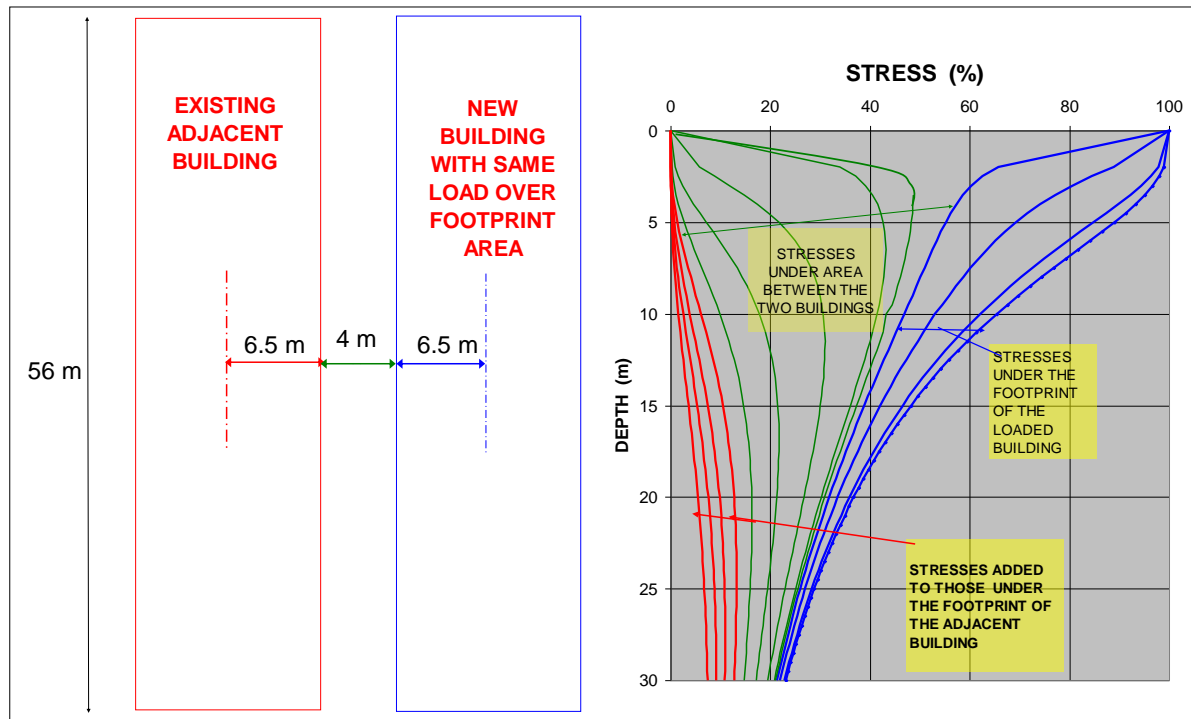


Fig. 1.12 Influence on stress from one building over to an adjacent building.

The stress exerted by the "existing building" is quite close to the preconsolidation margin of the soil, which means that the settlement is small. The "new building" exerts the same stress on the soil, and its stress adds to the stress from the existing building to the soils below this building, resulting in additional settlement for the "existing building". At the same time, the settlement due to the stress from the "existing building" acting under the footprint of the "new building" has already occurred when the "new building" is constructed. Therefore, the settlement of the new building will be smaller than that for the first building. The analysis of the second building settlement needs to consider that the first building reduced or eliminated the preconsolidation margin underneath the footprint of the new building. Simple stress calculations will make the problem and potential undesirable effect very clear. (For aspects on settlement analysis, see Chapter 3).



## CHAPTER 2

### SOIL PROFILING WITH THE CONE PENETROMETER

#### 2.1 Introduction

Design of foundations presupposes that the soil conditions (profile and parameters) at the site have been established by a geotechnical site investigation. Site investigations employ soil sampling and in-situ sounding methods. Most methods consist of intermittent sampling, e.g., the standard penetration test with split-spoon sampling and probing for density—the N-index. Other intermittent methods are the vane, dilatometer, and pressuremeter tests. The only continuous in-situ test is the cone penetrometer test.

In-situ sounding by standardized penetrometers came along early in the development of geotechnical engineering. For example, the Swedish weight-sounding device (Swedish State Railways Geotechnical Commission 1922), which still is in use in Sweden and Finland. The cone stress obtained by this device and other early penetrometers included the influence of soil friction along the rod surface. In the 1930s, a “mechanical cone penetrometer” was developed in the Netherlands where the rods to the cone point were placed inside an outer pipe (a sleeve), separating the cone rods from the soil (Begemann 1963). The mechanical penetrometer was advanced by first pushing the entire system to obtain the combined resistance. Intermittently, every even metre or so, the cone point was advanced a small distance while the outer tubing was held immobile, thus obtaining the cone stress separately. The difference was the total shaft resistance.

Begemann (1953) introduced a short section sleeve, immediately above the cone point. The sleeve arrangement enabled measuring the shaft resistance over a short distance (“sleeve friction”) near the cone. Sensors were placed in the cone and the sleeve to measure the cone stress and sleeve friction directly and separately (Begemann 1963). This penetrometer became known as the “electrical cone penetrometer”.

In the early 1980s, piezometer elements were incorporated with the electrical cone penetrometer, leading to the modern cone version, “the piezocone”, which provides values of cone stress, sleeve friction, and pore pressure at close distances, usually every 25 mm, but frequently every 10 mm—indeed, there is no reason for not recording at every 10 mm. (The shear resistance along the sleeve, the “sleeve friction” is regarded as a measure of the undrained shear strength—of a sort—the value is recognized as not being accurate; e.g., Lunne et al. 1986, Robertson 1990). Fig. 2.1 shows an example of a piezocone to a depth of 30 m at the site where the soil profile consists of three layers: an upper layer of soft to firm clay, a middle layer of compact silt, and a lower layer of dense sand. The groundwater table lies at a depth of 2.5 m. The CPT values shown in the diagram have been determined at every 50 mm. (Note, nothing is gained by widening distance between measuring points. Instead, valuable information may be lost.).

While a CPT sounding is always aimed vertical, it might bend and drift in the soil, which will cause the cone point to deviate from the vertical below the starting point. This also means that the sounding depth will be shorter; the cone point “lifts”. For most cone soundings, deviation from the depth and exact location vertically below the “cone location” is inconsequential. However, for deep soundings, both deviations can be substantial. Modern CPT equipment will always measure the deviation from the vertical in two directions, which allows the operator and user to calculate the deviation from the ideal. Curiously, the inclination measurements are often not included with a final report. They should be.

The cone penetrometer does not provide a measurement of static resistance, but records the resistance at a certain penetration rate (now standardized to 20 mm/s). Therefore, pore water pressures develop in the soil at the location of the cone point and sleeve that add to the “neutral” pore water pressure. In dense fine sands, which are prone to dilation, the induced pore pressures can significantly reduce the neutral pressure. In pervious soils, such as sands, the pore pressure changes are small, while in less pervious soils, such as silts and clays, they can be quite large. Measurements with the piezocone showed that the cone stress must be corrected for the pore pressure acting on the cone shoulder (Baligh et al. 1981; Campanella et al. 1982, Campanella and Robertson 1988). See Section 2.2.6 and Eq. 2.1 below.

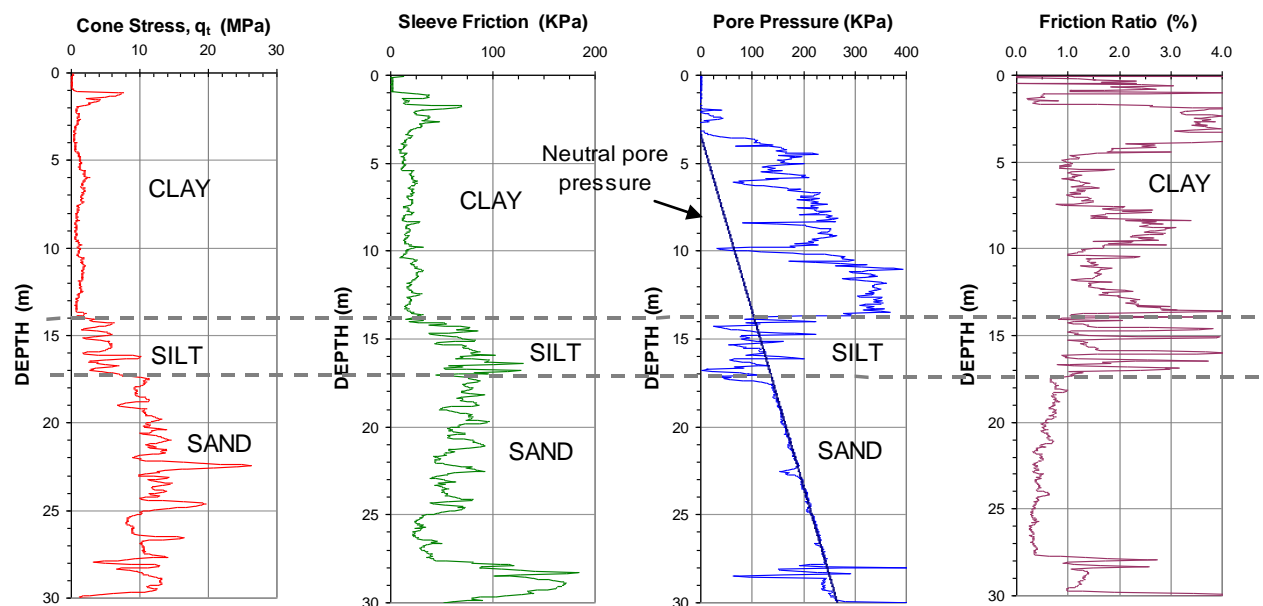


Fig. 2.1 Results from a piezocone to a depth of 30 m

The cone penetrometer test, is simple, fast to perform, economical, supplies continuous records with depth, and allows a variety of sensors to be incorporated with the penetrometer. The direct numerical values produced by the test have been used as input to geotechnical formulae, usually of empirical nature, to determine capacity and settlement, and for soil profiling.

Early cone penetrometers gave limited information that could be used for determining soil type and were limited to determining the location of soil type boundaries. The soil type had to be confirmed from the results of conventional borings. Empirical interpretations were possible but they were limited to the geological area where they had been developed. Begemann (1965) is credited with having presented the first rational soil profiling method based on CPT soundings. With the advent of the piezocone, the CPTU, the cone penetrometer was established as an accurate site investigation tool.

This chapter is a summary to indicate some of the uses of the cone penetrometer test. For a more thorough account, the reader is directed to the many reports and papers by Tom Lunne, Paul Mayne, and Peter Robertson, specifically, Kulhawy and Mayne (1990), Lunne et al. (1986), Lunne et al. (1997), Mayne et al. (1990), Mayne et al. (2001), Mayne et al. (2002), Mayne (2007), Robertson and Campanella (1983), and Robertson 2007.

An account of the use of results from CPTU soundings to analyze the response of a pile to applied load belongs here, but it is instead treated in Chapter 7, Static Analysis of Pile Load Transfer to present it in the context of how it is applied.

## 2.2 Brief Survey of Soil Profiling Methods

### 2.2.1 Begemann (1965)

Begemann (1965) pioneered soil profiling from the CPT, showing that, while coarse-grained soils generally demonstrate larger values of cone stress,  $q_c$ , and sleeve friction,  $f_s$ , as opposed to fine-grained soils, the soil type is not a strict function of either cone stress or sleeve friction, but of the combination of the these values.

Figure 2.2 presents the Begemann soil profiling chart, showing (linear scales)  $q_c$  as a function of  $f_s$ . Begemann showed that the soil type is a function of the ratio, the “friction ratio”,  $f_R$ , between the sleeve friction and the cone stress, as indicated by the slope of the fanned-out lines. Table 2.1 shows the soil types for the Begemann data base correlated to friction ratio. The Begemann chart and table were derived from tests in Dutch soils with the mechanical cone. That is, the chart is site-specific, i.e., directly applicable only to the specific geologic locality where it was developed. For example, the cone tests in sand show a friction ratio smaller than 1 %. A distinction too frequently overlooked is that Begemann did not suggest that the friction ratio alone governs the soil type. Aspects, such as overconsolidation, whether a recent or old sedimentary soil, or a residual soil, mineralogical content, etc. will influence the friction ratio, and, therefore, the interpretation, as will a recent fill or excavation. It is a mistake to believe that the CPTU can duplicate the sieve analysis, or replace it in a soils investigation.

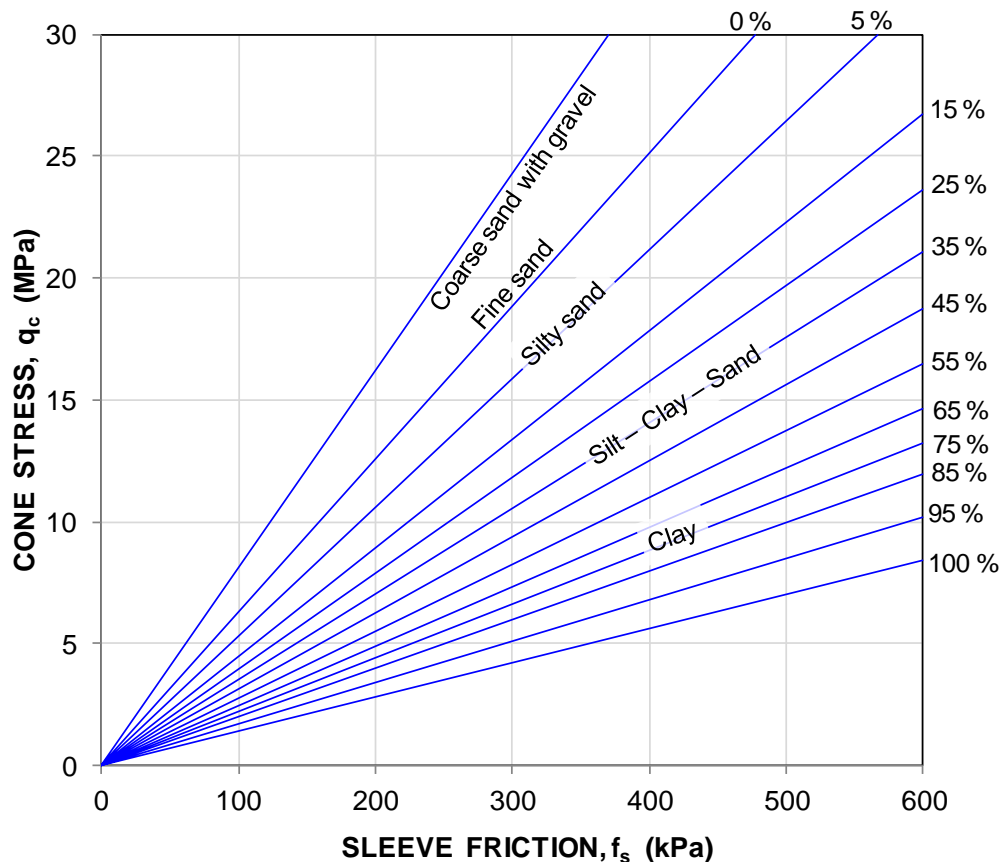


Fig. 2.2 The Begemann original profiling chart. The %-values refer to percent fines (Begemann, 1965)

**Table 2.1 Soil Type as a Function of Friction Ratio (Begemann, 1965)**

Coarse sand with gravel through fine sand	1.2 %	-	1.6 %
Silty sand	1.6 %	-	2.2 %
Silty sandy clayey soils	2.2 %	-	3.2 %
Clay and loam, and loam soils	3.2 %	-	4.1 %
Clay	4.1 %	-	7.0 %
Peat			>7 %

## 2.2.2 Sanglerat et al. (1974)

Sanglerat et al. (1974) proposed the chart shown in Fig. 2.3A presenting cone stress,  $q_c$ , (logarithmic scale) versus sleeve friction from soundings using a 80 mm diameter research penetrometer. Figure 2.3B shows the same graph but with the cone stress in linear scale. The green curves indicate the range of values ordinarily encountered. The change from Begemann's type of plotting to plotting against the friction ratio is unfortunate. This manner of plotting has the apparent advantage of combining the two important parameters, the cone stress and the friction ratio. However, plotting the cone stress versus the friction ratio implies, falsely, that the values are independent of each other; the friction ratio would be the independent variable and the cone stress the dependent variable. In reality, the friction ratio is the inverse of the ordinate and the values are patently not independent—the cone stress is plotted against its own inverse self, multiplied by a variable that ranges, normally, from a low of about 0.01 through a high of about 0.07.

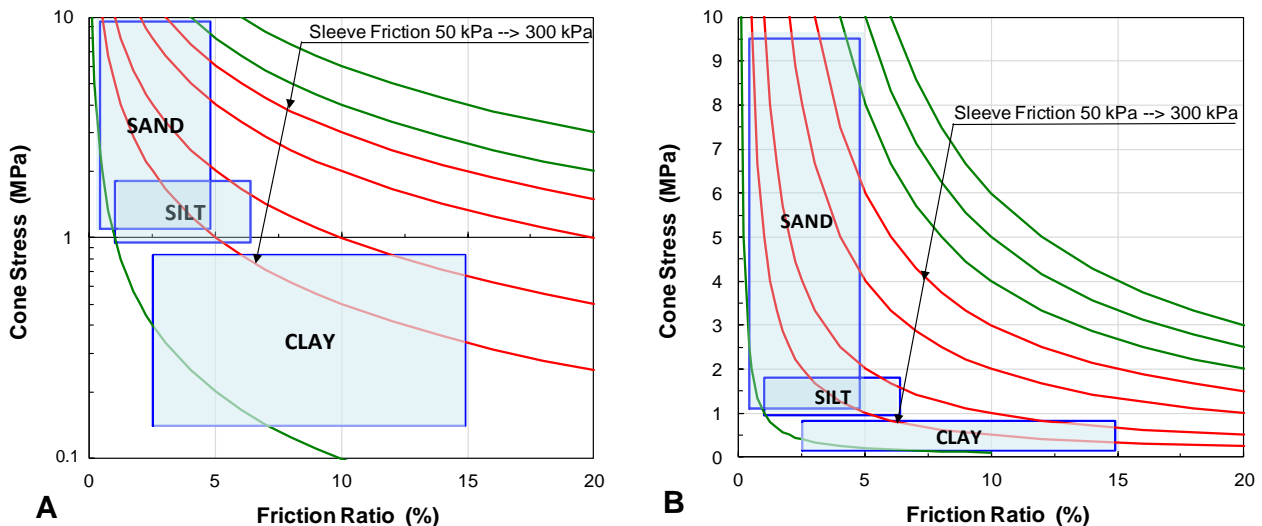


Fig. 2.3 Plot of data from research penetrometer with the cone stress in log scale and linear scale (after Sanglerat et al. 1974)

As is very evident in Fig. 2.3, regardless of the actual values, the plotting of data against own inverse values will predispose the plot to a hyperbolically shaped zone ranging from large ordinate values at small abscissa values through small ordinate values at large abscissa values. The resolution of data representing fine-grained soils is very much exaggerated as opposed to the resolution of the data representing coarse-grained soils. This is made obvious in the right graph, which has the cone stress shown in linear scale. Simply, while both cone stress and sleeve friction are important soil profiling parameters, plotting one as a function of the other distorts the information. Obviously, plotting against the Friction Ratio restricts the usable area of the graph, and, therefore, the potential resolution of the test data.

Notice, however, that Fig. 2.3 defines the soil type also by its upper and lower limit of cone stress and not just by the friction ratio. The boundary between compact and dense sand is usually placed at a cone stress of 10 MPa, however..

From this time on, the Begemann manner of plotting the cone stress against the sleeve friction was discarded in favor of Sanglerat's plotting cone stress against the friction ratio. However, this development—plotting the cone stress against itself (its inverted self) modified by the sleeve friction value—is unfortunate.

### 2.2.3 Schmertmann (1978)

Schmertmann (1978) proposed the soil profiling chart shown in Fig. 2.4A. The chart is based on results from mechanical cone data in “North Central Florida” and also incorporates Begemann's CPT data. The chart indicates envelopes of zones of common soil type. It also presents boundaries for density of sands and consistency (undrained shear strength) of clays and silts, which are imposed by definition and not related to the soil profile interpreted from the CPT results.

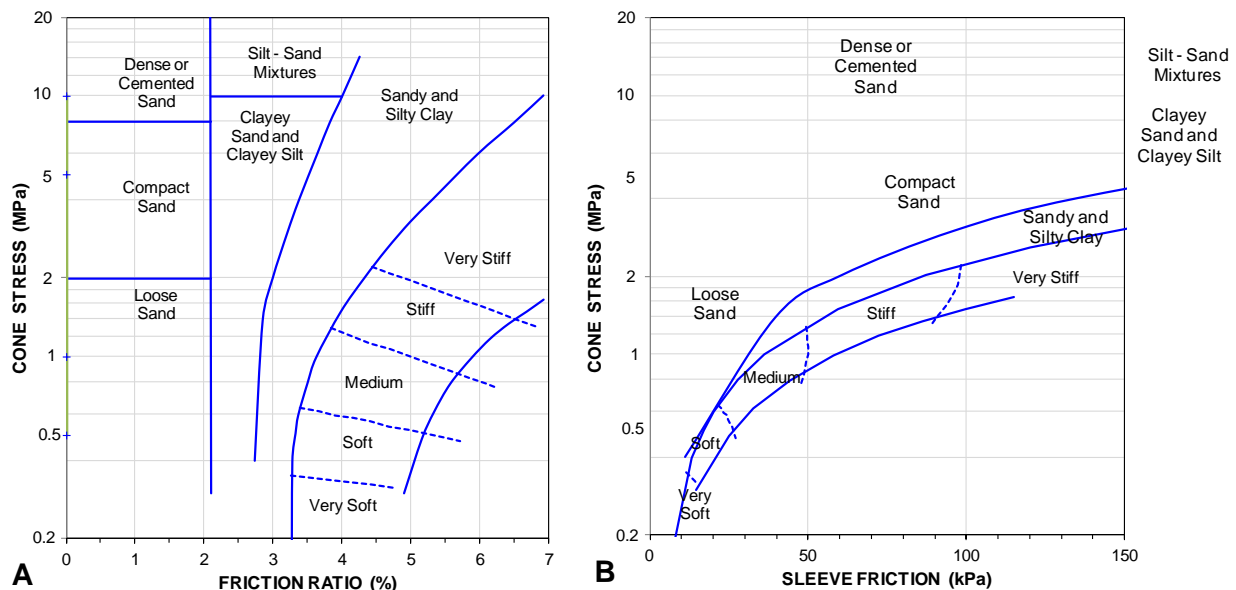


Fig. 2.4 The Schmertmann profiling chart (Schmertmann, 1978). (A) the original axes, (B) The Schmertmann profiling chart converted to a Begemann type profiling chart.

Also the Schmertmann chart plots the cone stress against the friction ratio, that is, the data are plotted against their inverse self. Fig. 2.4B shows the Schmertmann chart converted to a Begemann type graph. When the plotting of the data against own inverse values is removed, a qualitative, visual effect comes forth that is quite different from that of Fig. 2.4A. Note also that the consistency boundaries do not any longer appear to be very logical.

Schmertmann (1978) stated that the correlations shown in Fig. 2.4A may be significantly different in areas of dissimilar geology. The chart is intended for typical reference and includes two warnings: “*Local correlations are preferred*” and “*Friction ratio values decrease in accuracy with low values of  $q_c$* ”. Schmertmann also mentions that soil sensitivity, friction sleeve surface roughness, soil ductility, and pore pressure effects can influence the chart correlation. Notwithstanding the caveat, the Schmertmann chart is very commonly applied “as is” in North American practice.

### 2.2.4 Douglas and Olsen (1981)

Douglas and Olsen (1981) proposed a soil profiling chart based on tests with the electrical cone penetrometer. The chart, which is shown in Fig. 2.5A, appends classification per the unified soil classification system to the soil type zones. The chart also indicates trends for liquidity index and earth stress coefficient, as well as sensitive soils and “metastable sands”. The Douglas and Olsen chart envelopes several zones using three upward curving lines representing increasing content of coarse-grained soil. The chart distinguishes where soils are sensitive or “metastable”.

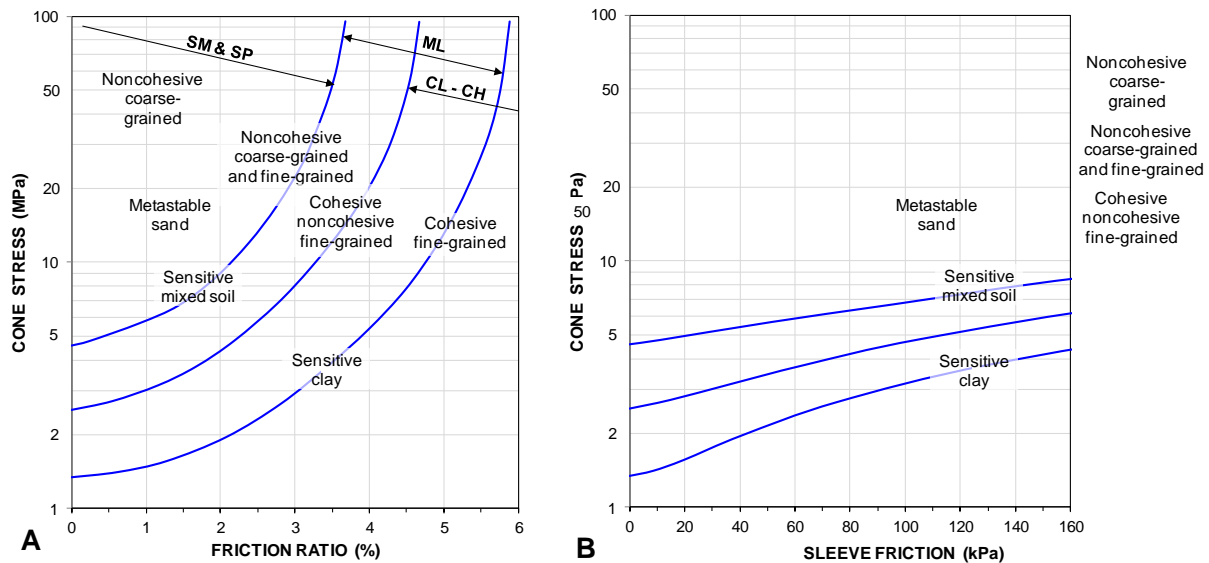


Fig. 2.5 The Douglas and Olsen profiling chart (Douglas and Olsen 1981). (A) the original axes, (B) The Douglas and Olsen profiling chart converted to a Begemann type profiling chart.

Comparing the Douglas and Olsen chart (Fig. 2.5A) with the Schmertmann chart (Fig. 2.4A), a difference emerges in implied soil type response: while in the Schmertmann chart the soil type envelopes curve downward, in the Douglas and Olsen chart they curve upward. Zones for sand and for clay are approximately the same in the two charts, however.

A comparison between the Douglas and Olsen and Schmertmann charts is more relevant if the charts are prepared per the Begemann type of presentation. Thus, Fig. 2.5B shows the Douglas and Olsen chart converted to a Begemann type graph. The figure includes the three curved envelopes. The sleeve friction is limited to 160 kPa, which is a practical limit for actual conditions. Three of the labels in the original chart fall outside this limit (two were combined here to fit). Moreover, it is hard to accept that the areas indicated as metastable or sensitive are correctly identified in the original chart

Obviously, plotting the cone stress versus the friction ratio, i.e., against its inverse self will easily lead to distorted conclusions from the graph.

### 2.2.5 Vos (1982)

Vos (1982) suggested using the electrical cone penetrometer for Dutch soils to identify soil types from the friction ratio, as shown in Table 2.2 (Vos, 1982). The percentage values are similar but not identical to those recommended by Begemann (1965).

**TABLE 2.2 Soil Behavior Categories as a Function of Friction Ratio**

Coarse sand and gravel		<1.0%
Fine sand	1.0 %-	1.5 %
Silt	1.5 %-	3.0 %
Clay	3.0%-	7.0%
Peat	>7 %	

### 2.2.6 Robertson et al. (1986)

Robertson et al. (1986) and Campanella and Robertson (1988) presented a chart, which was the first chart to be based on the piezocone, i.e., the first to include the correction of cone stress for pore pressure at the shoulder according to Eq. 2.1. It is indeed bizarre that many still disregard the effect of pore pressure on the cone shoulder and continue to employ and apply the uncorrected stress,  $q_c$ , to their analyses, thus, knowingly applying erroneous data.

$$(2.1) \quad q_t = q_c + U2(1-a)$$

where  $q_t$  = cone stress corrected for pore water pressure on shoulder  
 $q_c$  = measured cone stress  
 $U2$  = pore pressure measured at cone shoulder  
 $a$  = ratio between shoulder area (cone base) unaffected by the pore water pressure to total shoulder area

The Robertson et al. (1986) profiling chart is presented in Fig. 2.6. The chart identifies numbered areas that separate the soil behavior categories in twelve zones, as follows.

- |                                |  |
|--------------------------------|--|
| 1. Sensitive fine-grained soil | 7. Silty sand to sandy silt                          |
| 2. Organic soil                | 8. Sand to silty sand                                |
| 3. Clay                        | 9. Sand  |
| 4. Silty clay to clay          | 10. Sand to gravelly sand                            |
| 5. Clayey silt to silty clay   | 11. Very stiff fine-grained soil                     |
| 6. Sandy silt to clayey silt   | 12. Overconsolidated or cemented sand to clayey sand |

A novel information in the profiling chart is the delineation of Zones 1, 11, and 12, representing somewhat extreme soil responses, enabling the CPTU to uncover more than just soil grain size. The rather detailed separation of the in-between zones, Zones 3 through 10 indicate a gradual transition from fine-grained to coarse-grained soil.

As mentioned above, plotting of cone stress value against the friction ratio is plotting the cone stress against itself (its inverted self) modified by the sleeve friction value, distorting the results. Yet, as indicated in Fig. 2.7, the measured values of cone stress and sleeve friction can just as easily be plotted separately. The friction ratio is a valuable parameter and it is included as an array of lines ranging from a ratio of 0.1 % through 25 %.

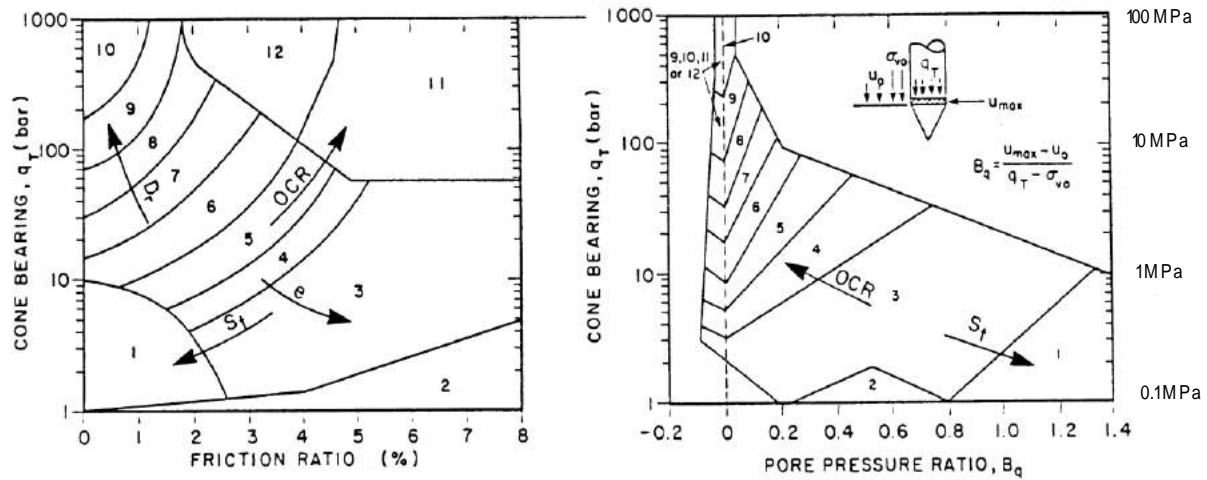


Fig. 2.6 Profiling chart per Robertson et al. (1986; used with permission)

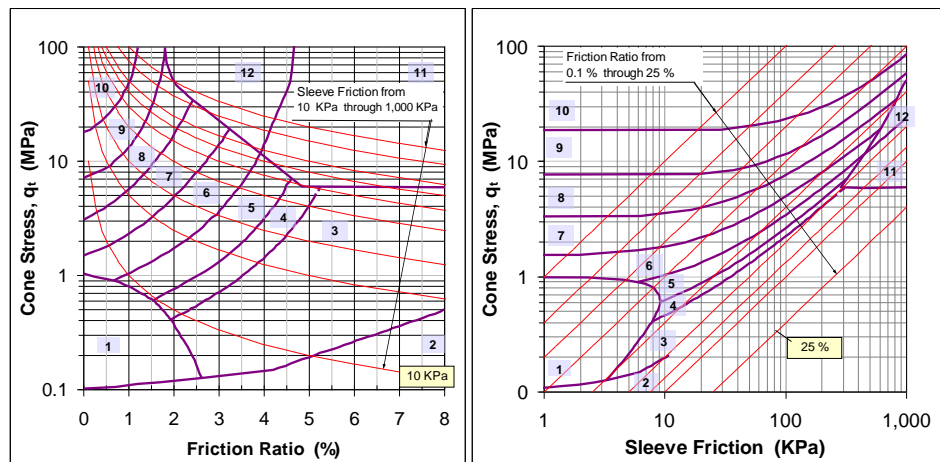


Fig. 2.7A The profiling chart shown in Fig. 2.6

Fig. 2.7B The profiling chart plotted as Cone Stress vs. Sleeve Friction

The Robertson et al. (1986) profiling chart (Fig. 2.6) introduced a pore pressure ratio,  $B_q$ , defined by Eq. 2.2, as follows.

$$(2.2) \quad B_q = \frac{u_2 - u_0}{q_t - \sigma_v}$$

where

- $B_q$  = pore pressure ratio
- $u_2$  = pore pressure measured at cone shoulder
- $u_0$  = in-situ pore pressure
- $q_t$  = cone stress corrected for pore water pressure on shoulder
- $\sigma_v$  = total overburden stress



Essentially, the  $B_q$ -value shows the change of pore pressure divided by the cone stress,  $q_t$  (the cone stress is very much larger than the total stress). Directly, the  $B_q$ -chart (Fig. 2.8) shows zones where the U2 pore pressures become smaller than the neutral pore pressures ( $u_0$ ) in the soil during the advancement of the penetrometer, resulting in negative  $B_q$ -values. Otherwise, the  $B_q$ -chart appears to be an alternative rather than an auxiliary chart; one can use one or the other depending on preference. However, near the upper envelopes, a CPTU datum plotting in a particular soil-type zone in the friction ratio chart will not always appear in the same soil-type zone in the  $B_q$ -chart. Robertson et al. (1986) points out that “occasionally soils will fall within different zones on each chart” and recommends that the users study the pore pressure rate of dissipation (if measured) to decide which zone applies to questioned data.

The pore pressure ratio,  $B_q$ , is an inverse function of the cone stress,  $q_t$ . Therefore, also the  $B_q$ -plot represents the data as a function of their own self values.

**Eslami and Fellenius (1996)** proposed a pore pressure ratio,  $B_E$ , defined, as follows.

$$(2.3) \quad B_E = \frac{u_2 - u_0}{u_0}$$

where  $B_E$  = pore pressure ratio  
 $u_0$  = neutral pore pressure  
 $u_2$  = pore pressure measured at the cone shoulder

The  $B_E$ -value shows the relative change of pore pressure introduced by pushing the cone.

There is little information obtained from the pore pressure ratios that is not available directly from the measured pore pressure (U2) and friction ratio,  $f_R$ .

### 2.2.7 Robertson (1990)

Robertson (1990) proposed a development of the Robertson et al. (1986) profiling chart, shown in Fig. 2.8, plotting a “normalized cone stress”,  $q_{cnrm}$ , against a “normalized friction ratio”,  $R_{fnrm}$ , in a cone stress chart. The accompanying pore pressure ratio chart plots the “normalized cone stress” against the pore pressure ratio,  $B_q$ , defined by Eq. 2.2 applying the same  $B_q$ -limits as the previous chart (Zone 2 is not included in Fig. 2.8).

The normalized cone stress is defined by Eq. 2.4.

$$(2.4) \quad q_{cnrm}' = \frac{q_t - \sigma'_v}{\sigma_v}$$

where  $q_{cnrm}'$  = cone stress normalized according to Robertson (1990)  
 $q_t$  = cone stress corrected for pore water pressure on shoulder  
 $\sigma_v$  = total overburden stress  
 $\sigma'_v$  = effective overburden stress  
 $(q_t - \sigma_v)$  = net cone stress

The normalized friction ratio is defined as the sleeve friction over the net cone stress, as follows.

$$(2.5) \quad R_{fmm} = \frac{f_s}{q_t - \sigma_v}$$

where  $f_s$  = sleeve friction  
 $q_t$  = cone stress corrected for pore water pressure on shoulder  
 $\sigma_v$  = total overburden stress

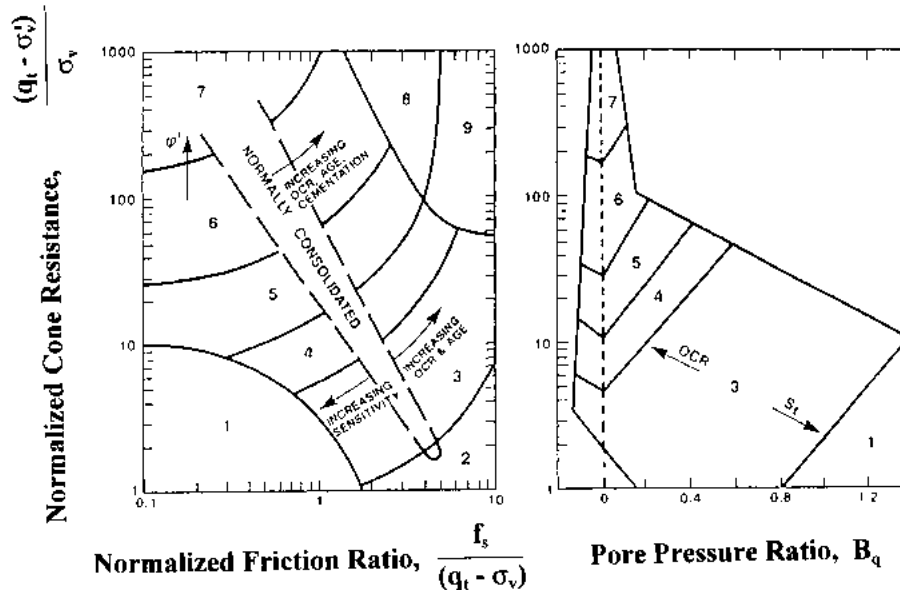


Fig. 2.8 Profiling chart per Robertson (1990; used with permission)

The numbered areas in the profiling chart separate the soil behavior categories in nine zones, as follows.

- |  |  |
|--|--|
| 1. Sensitive, fine-grained soils             | 6. Sand [silty sand to clean sand]                             |
| 2. Organic soils and peat                    | 7. Sand to gravelly sand                                       |
| 3. Clays [clay to silty clay]                | 8. Sand – clayey sand to “very stiff” sand                     |
| 4. Silt mixtures [silty clay to clayey silt] | 9. Very stiff, fine-grained, overconsolidated or cemented soil |
| 5. Sand mixtures [sandy silt to silty sand]  |  |

The two first and two last soil types are the same as those used by Robertson et al. (1986) and Types 3 through 7 correspond to former Types 3 through 10. The Robertson (1990) normalized profiling chart has seen extensive use in engineering practice (as has the Robertson et al. 1986 chart).

The normalization is professedly to compensate for that the cone stress is influenced by the overburden stress. Therefore, when analyzing deep CPTU soundings (i.e., deeper than about 30 m), a profiling chart developed for more shallow soundings does not apply well to the deeper sites. At very shallow depths, however, the proposed normalization will tend to lift the data in the chart and imply a coarser soil than necessarily the case. Moreover, where soil types alternate between light-weight and soils (which soil densities can range from 1,400 kg/m<sup>3</sup> through 2,100 kg/m<sup>3</sup>) and/or where upward or downward pore pressure gradients exist, the normalization is unwieldy. For these reasons, it would appear that the normalization merely exchanges one difficulty for another.

More important, the chart still includes the plotting of data against the inverse of own self. This is not necessary. A chart with the same soil zones could just as well have been produced with normalized cone stress against a normalized sleeve friction.

Accepting the Robertson (1990) normalization, Figs. 2.9A and 2.9B show the envelopes of the Robertson (1990) chart (Fig. 2.8) converted to a Begemann type chart. The ordinate is the same and the abscissa is the multiplier of the normalized cone stress and the normalized friction factor of the original chart (the normalized sleeve friction is the sleeve friction divided by the effective overburden stress). Where needed, the envelopes have been extended with a thin line to the frame of the diagram.

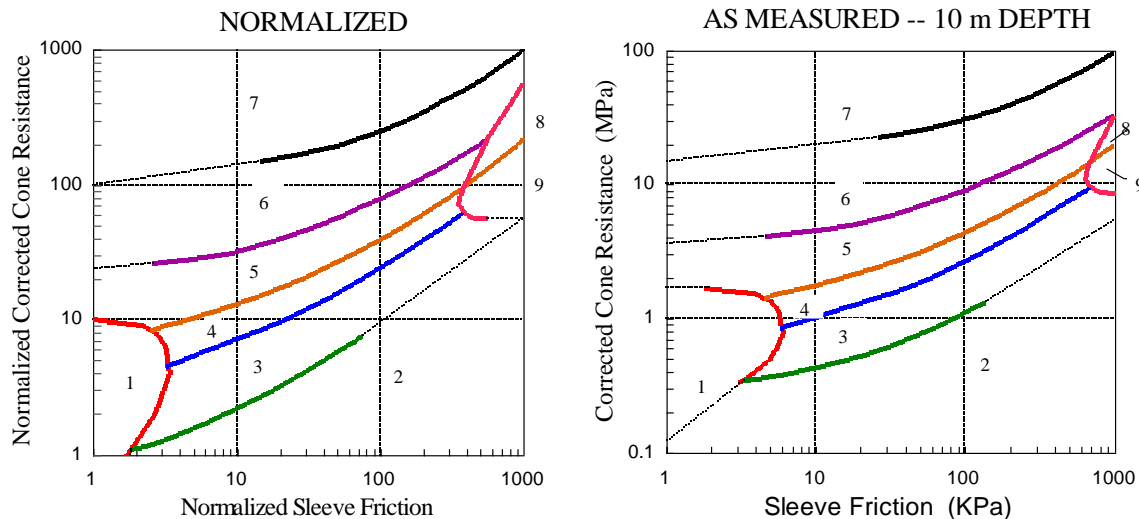


Fig. 2.9A Normalized corrected cone stress vs. normalized sleeve friction

Fig. 2.9B Pore-pressure corrected cone stress vs. sleeve friction

As reference to Figs. 2.4B and 2.5B, Fig. 2.9b presents the usual Begemann type profiling chart converted from Fig. 2.8 under the assumption that the data apply to a depth of about 10 m at a site where the groundwater table lies about 2 m below the ground surface. This chart is approximately representative for a depth range of about 5 m to 30 m. Comparing the “normalized” chart with the “as measured” chart does not indicate that normalization would be advantageous.

Other early profiling charts were proposed by Searle (1979), Jones and Rust (1982), Olsen and Farr (1986), Olsen and Malone (1988), Erwig (1988). CPTU charts similar to that of Robertson (1990) were proposed by Larsson and Mulabdic (1991), Jefferies and Davies (1991, 1993), and Olsen and Mitchell (1995). Robertson (2016) has further developed his CPTU classification approach to separate classification per grain size from the per soil response.

### 2.3 The Eslami-Fellenius CPTU Profiling and Soil Behavior Type Classification Method

To investigate the use of cone penetrometer data in pile design, Eslami and Fellenius (1997) compiled a database consisting of CPT and CPTU data linked with results of boring, sampling, laboratory testing, and routine soil characteristics. The cases are from 18 sources reporting data from 20 sites in 5 countries. About half of the cases are from piezocone tests, CPTU, and include pore pressure measurements (U2). Non-CPTU tests are from sand soils and were used with the assumption that the U2-values are approximately equal to the neutral pore pressure ( $u_0$ ). The database values are separated on five main soil behavior categories as follows.

- |  |                             |
|--|-----------------------------|
| 1. Very soft Clay or<br>Sensitive and Collapsible Clay and/or Silt | 4a. Sandy Silt              |
| 2. Clay and/or Silt  | 4b. Silty Sand              |
| 3. Silty Clay and/or Clayey Silt                                   | 5. Sand and/or Sandy Gravel |

The data points were plotted in a Begemann type profiling chart and envelopes were drawn enclosing each of the five soil types. The envelopes are shown in Fig. 2.10. The database does not include cases with cemented soils or very stiff clays, and, for this reason, no envelopes for such soil types are included in the chart.

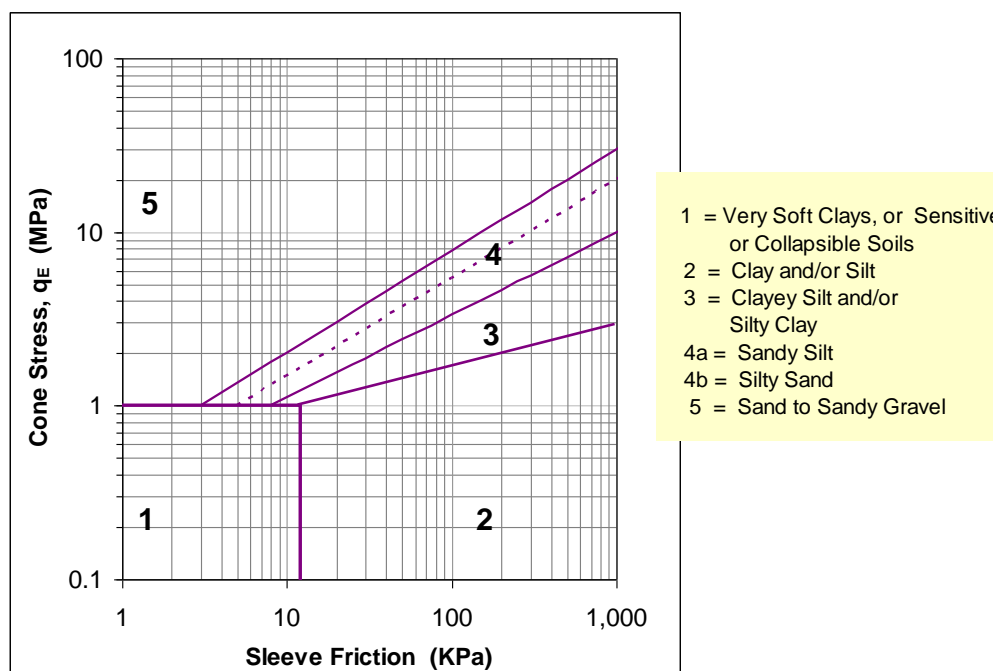


Fig. 2.10 The Eslami-Fellenius profiling chart (Eslami 1996; Eslami and Fellenius, 1997)

Plotting the “effective” cone stress,  $q_E$ , defined by Eq. 2.6 is a filtering action that was found to provide a more consistent delineation of envelopes than a plot of only the pore pressure corrected stress,  $q_t$ . Moreover, “ $q_t$ ” is corrected, i.e., true, cone stress, and “ $q_E$ ” is  $q_t$  with the  $U_2$  pore pressure subtracted). (Note, subtracting the pore pressure does not suggest that the value is an effective stress. The subscript “E” is simply a short for “Eslami”. In developing the method, it was found that the subtraction of  $U_2$  made the data come together in more easily delineated zones).

$$(2.6) \quad q_E = (q_t - U_2)$$

where  $q_E$  = Eslami cone stress  
 $q_t$  = cone stress corrected for pore water pressure on shoulder (Eq. 2.1)  
 $U_2$  = pore pressure measured at cone shoulder

The  $q_E$ -value was shown to be a consistent value for use in relation to soil responses, such as pile shaft and pile toe resistances (Eslami 1996, Eslami and Fellenius 1995; 1996; 1997). Notice again that, as mentioned by Robertson (1990), the measured pore water pressure is a function of where the pore pressure gage is located. Therefore, the  $q_E$ -value is by no means a measurement of effective stress in conventional sense. Because the sleeve friction is a rather approximate measurement, no similar benefit

was found in producing an “effective” sleeve friction. In dense, coarse-grained soils, the  $q_E$ -value differs only marginally from the  $q_t$ -value. In contrast, cone tests in fine-grained soils could generate substantial values of excess pore water pressure causing the  $q_E$ -value to be much smaller than the  $q_t$ -value, indeed, even negative, in which case the value should be taken as equal to zero.

The Eslami-Fellenius chart is simple to use and requires no adjustment to estimated value of the overburden stresses. The chart is primarily intended for soil type (profiling) analysis of CPTU data. With regard to the grain-size boundaries between the main soil fractions (clay, silt, sand, and gravel), international and North American practices agree. In contrast, differences exist with regard to how soil-type names are modified according to the contents of other than the main soil fraction. The chart assumes the name convention summarized in Section 1.3 as indicated in the Canadian Foundation Engineering Manual (1992, 2006).

The data from the CPT diagrams presented in Fig. 2.1 are presented in the chart shown in Fig. 2.11. The three layers are presented with different symbols.

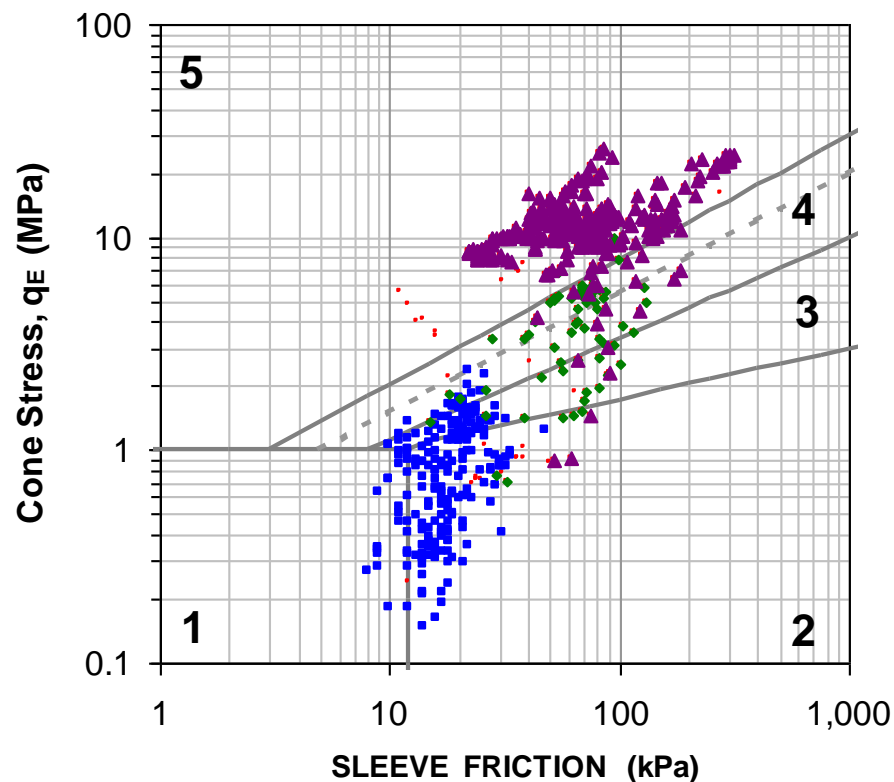


Fig. 2.11 The CPT sounding shown in Fig. 2.1 plotted in a Eslami-Fellenius profiling chart.

## 2.4 Comparison between the Eslami-Fellenius and Robertson (1990) Methods

To provide a direct comparison between the Robertson (1990) profiling chart and the Eslami-Fellenius chart, three short series of CPTU data were compiled from sites with very different geologic origin where the soil profiles had been established independently of the CPTU. The borehole information provides soil description and water content of recovered samples. For one of the cases, the grain size distribution is also available. The CPTU-diagrams from the site are shown in Fig. 2.12. The soil and CPTU information for the specific points are compiled in Table 2.3. The three sites are:

1. North Western University, **Evanston**, Illinois (Finno 1989). CPTU data were obtained in a soil profile consisting of 7 m of sand deposited on normally consolidated silty clay. The piezometer was attached to the cone face ( $u_1$ ) and not behind the shoulder ( $u_2$ ). The method of converting the pore pressure measurement to the  $u_2$ -value presented by Finno (1989) has been accepted here, although the conversion is disputed. For comments, see Mayne et al. (1990).
2. Along the shore of Fraser River, **Vancouver**, British Columbia (personal communication, V. Sowa, 1998). A 20 m thick mixed soil profile of deltaic deposits of clay, silt, and sand. The first four data points are essentially variations of silty clay or clayey silt. The fifth is a silty sand.
3. University of Massachusetts, **Amherst**, Massachusetts (personal communication, P. Mayne, 1998). A soil profile (Lutenegger and Miller 1995) consisting of 5 m of a thick homogeneous overconsolidated clayey silt. This case includes also information on grain size distribution. The borehole records show the soil samples for data points Nos. 3 through 7 to be essentially identical. Notice that the  $u_2$ -measurements indicate substantial negative values, that is, the overconsolidated clay dilates as the cone is advanced.

For each case, the soil information in Table 1 is from depths where the CPTU data were consistent over a 0.5 m length. Then, the CPTU data from 150 mm above and below the middle of this depth range were averaged using geometric averaging, preferred over the arithmetic average as it is less subject to influence of unrepresentative spikes and troughs in the data (a redundant effort, however, as the records contain no such spikes and troughs). The CPTU data were analyzed by the Eslami-Fellenius (1996) and the Robertson (1990) profiling methods and the results are shown in Fig. 2.13.

**Evanston data:** The first three samples are from a sand soil and both methods identify the CPTU data accordingly. The remaining data points (Nos. 4 through 7) given as Silty Clay in the borehole records are identified as Clay/Silt by the Eslami-Fellenius and as Clay to Silty Clay by the Robertson method, that is, both methods agree with the independent soil classification.

**Vancouver data:** Both methods properly identify the first four data points to range from Clayey Silt to Silty Clay in agreement with the independent soil classification. The fifth sample (Silty Sand) is identified correctly by the Eslami-Fellenius method as a Sand close to the boundary to Silty Sand and Sandy Silt. The Robertson method identifies the soil as a Sandy Silt to Clayey Silt, which is essentially correct, also.

**Amherst data:** Both methods identify the soils to be silt or clay or silt and clay mixtures. Moreover, both methods place Points 3 through 7 on the same soil type boundary line, that is, confirming the similarity between the soil samples. However, the spread of plotted points appear to be larger for the Robertson method; possibly due that its profiling does not consider the pore pressures developed by the advancing penetrometer (but for the pore pressure on the shoulder, of course), while the Eslami-Fellenius method does account for the substantial negative pore pressures that developed.

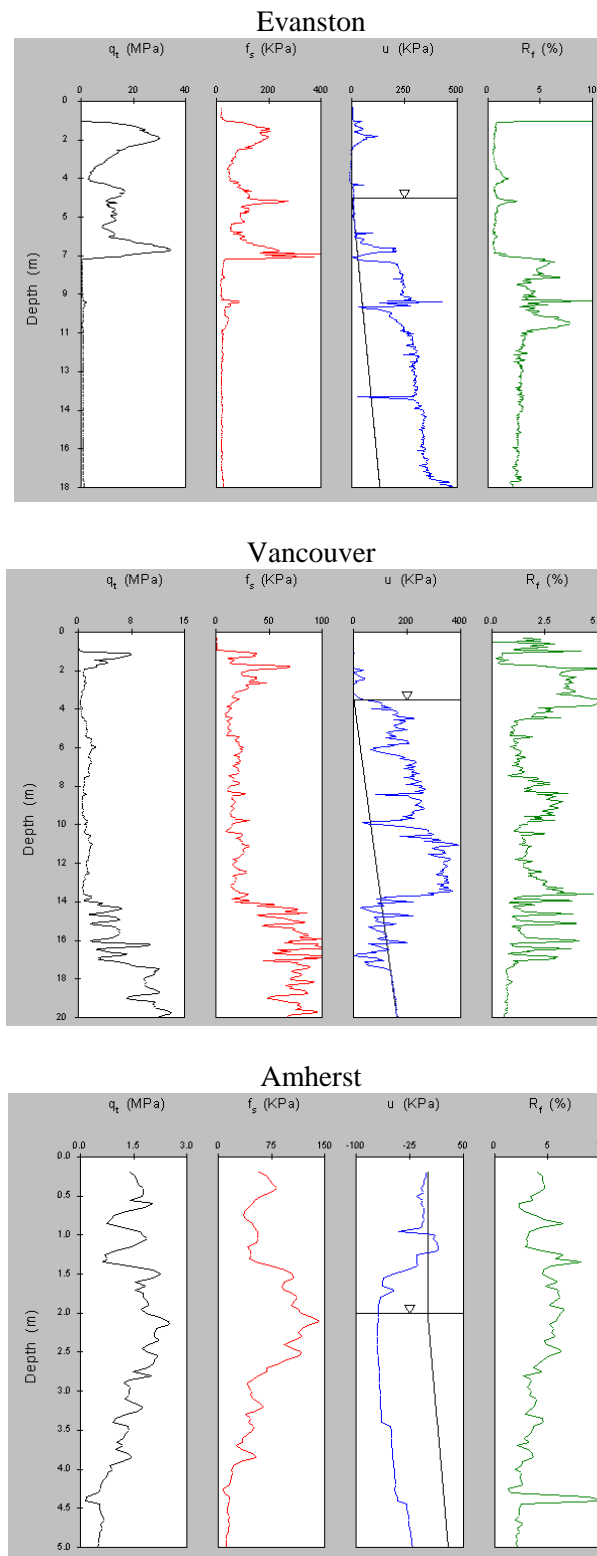


Fig. 2.12 CPTU diagram from the three sites

**TABLE 2.3 Soil and CPTU information**

No.	Depth (m)	Description	Water		Soil Fractions		CPTU Data		
			Content (%)	(%)	$q_t$ (MPa)	$f_s$ (kPa)	U2 (kPa)		
<b>Evanston, IL (Groundwater table at 4.5 m)</b>									
1	1.5	SAND, Fine to medium, trace gravel	29		25.08	191.5	49.8		
2	3.4	SAND, Medium, trace gravel	16		3.48	47.9	-16.0		
3	6.7	SAND, Fine, trace silt, organics	26		32.03	162.8	111.7		
4	8.5	Silty CLAY, trace sand	28		0.51	21.1	306.4		
5	9.5	Silty CLAY, little gravel	22		0.99	57.5	39.6		
6	12.8	Silty CLAY, little gravel	23		0.69	19.2	383.0		
7	16.5	Silty CLAY, little gravel	24		0.77	17.2	427.1		
<b>Vancouver, BC (Groundwater table at 3.5 m)</b>									
1	3.7	CLAY to Clayey SILT	52		0.27	16.1	82.5		
2	5.8	Clayey SILT to SILT	34		1.74	20.0	177.1		
3	10.2	Silty CLAY	47		1.03	13.4	183.5		
4	14.3	Silty CLAY	40		4.53	60.2	54.3		
5	17.5	Silty SAND	25		10.22	77.8	118.5		
<b>Amherst, MA (Groundwater table at 2.0 m)</b>									
				Clay Silt Sand					
1	0.6	SAND and SILT, trace clay	20	10	30	60	2.04	47.5	- 9.4
2	1.5	Clayey SILT, trace sand	28	23	67	10	2.29	103.3	-47.3
3	2.0	Clayey SILT, trace sand	36	21	75	4	1.87	117.0	-69.5
4	2.5	Clayey SILT, trace sand	29	33	65	2	1.86	117.0	-70.3
5	3.0	Clayey SILT, trace sand	40	36	62	2	1.37	46.8	-66.3
6	3.5	Clayey SILT, trace sand	53	40	58	2	1.38	48.9	-50.7
7	4.0	Clayey SILT, trace sand	60	40	58		0.91	17.9	-46.9
8	4.5	Clayey SILT	30	42	57	1	0.55	12.9	-29.3



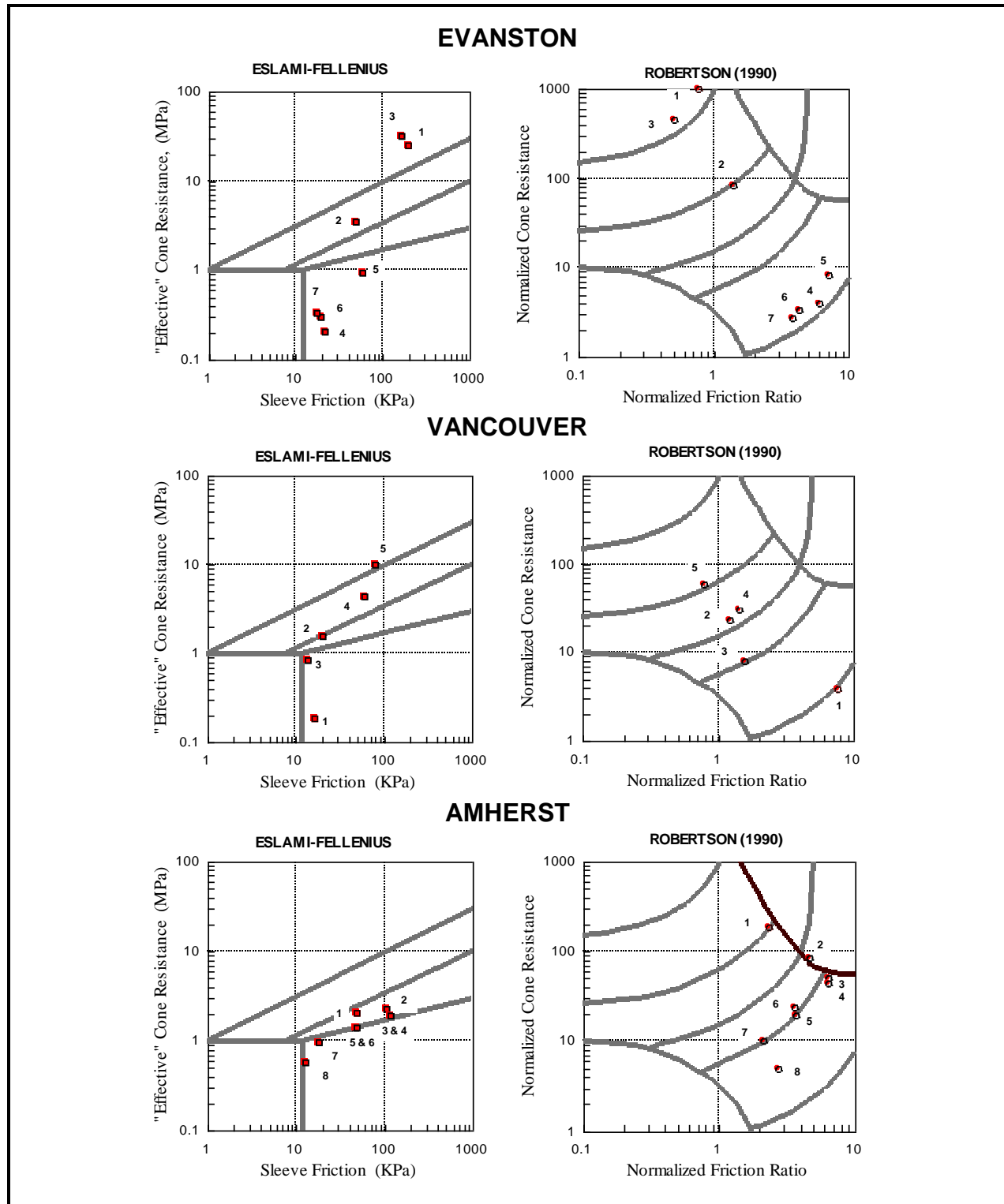


Fig. 2.13 Comparison between the Table 1 data plotted in Eslami-Fellenius and Robertson profiling charts. [Note that the boundary line between silty sand ("Area 4") and Sand (Area "5") in the former chart is drawn rising from sleeve friction of 1 kPa, per an early definition from when the method was first developed].

## 2.5 Comparisons

- I. The CPT methods (mechanical cones) do not correct for the pore pressure on the cone shoulder and the profiling developed based on CPT data may not be relevant outside the local area where they were developed. The error due to omitting the pore water pressure correction is large in fine-grained soils and small in coarse-grained soils.
- II. Except for the profiling chart by Begemann (1965) and Eslami-Fellenius (1997), all of the referenced soil profiling methods plot the cone stress versus its own inverse value in one form or another. This generates data distortion and violates the rule that dependent and independent variables must be rigorously separated.
- III. Some profiling methods, e.g., Robertson (1990), include normalization which require unwieldy manipulation of the CPT data. For example, in a layered soil, should a guesstimated “typical” density value be used in determining the overburden stress or a value that accurately reflects the density? Moreover, regardless of soil layering, determining the effective overburden stress (needed for normalization) requires knowledge of the pore pressure distribution, which is not always hydrostatic but can have an upward or downward gradient and this information is rarely available.
- IV. The normalization by division with the effective overburden stress does not seem relevant. For example, the normalized values of fine-grained soils obtained at shallow depth (where the overburden stress is small) will often plot in zones for coarse-grained soil.
- V. The Robertson (1990) and the Eslami-Fellenius (1997) CPTU methods of soil profiling were applied to data from three geographically apart sites having known soils of different types and geologic origins. Both methods identified the soil types accurately.
- VI. Eslami-Fellenius (1996) method has the advantage over the Robertson (1990) that it avoids the solecism of plotting data against their own inverted values and associated distortion of the data.
- VII. Eslami-Fellenius (1997) method has the additional advantage over other referenced piezocone methods in that it allows the user to directly assess a value without first having to determine distribution of total and effective stress to use in a subtraction and multiplication effort in calculating a “normalized” set of values.
- VIII. A soil profiling chart based on a Begemann type plot, such as the Eslami-Fellenius (1996) method can easily be expanded by adding delineation of strength and consistency of fine-grained soils and relative density and friction angle of coarse-grained soils per the user preferred definitions or per applicable standards.
- IX. No doubt, CPTU sounding information from a specific area or site can be used to further detail a soil profiling chart and result in delineation of additional zones of interest. However, there is a danger in producing a very detailed chart inasmuch the resulting site dependency easily gets lost leading an inexperienced user to apply the detailed distinctions beyond their geologic validity.
- X. The CPTU is an excellent tool for the geotechnical engineer in developing a site profile. Naturally, it cannot serve as the exclusive site investigation tool and soil sampling is still required. However, when the CPTU is used govern the depths from where to recover soil samples for detailed laboratory study, fewer sample levels are needed, reducing the costs of a site investigation while simultaneously increasing the quality of the information because important layer information and layer boundaries are not overlooked.

## 2.6 Profiling case example

Figure 2.14 shows  $q_t$ ,  $f_s$ ,  $U_2$ ,  $u_0$ , and  $f_R$  diagrams from a CPTU sounding in a sand deposit (in the Fraser River delta outside Vancouver, BC). Borehole samples indicate the soil profile to consist of loose to medium to fine silty sand containing layers or zones of silt, silty clay, and clay. As indicated in the figure, the borehole records agree well with the layering established using the profiling methods of Eslami-Fellenius (1997). The reading spacing is 10 mm. The depth measurements are corrected for the CPT rod inclination (deviation was in the form of a gentle sweep), resulting in an indicated maximum depth of 94 m, whereas the actual maximum depth is 90.5 m (see Section 2.8).

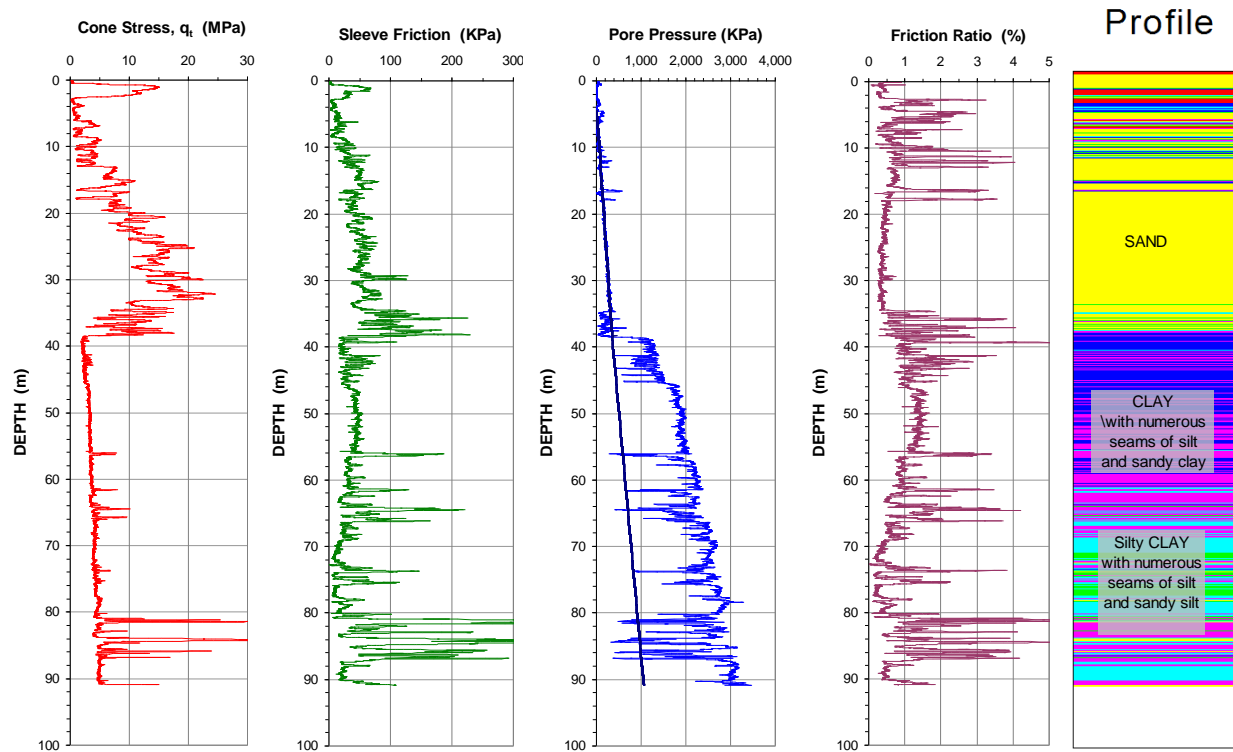


Fig. 2.14 CPTU sounding diagrams with profiling according to the Eslami-Fellenius(1997) method. Data from Amini et al. (2008).

The overall soil profile can be separated on four main zones, as indicated below. The soil descriptions was confirmed from bore hole samples. The colored block diagrams to the right are obtained from soil profiling using the CPTU data directly.

0 m	-	2.6 m	Coarse SAND
2.6 m	-	6.0 m	CLAY, Silty CLAY
6.0 m	-	13.0 m	Medium to fine SAND and Silty SAND (Fine sand portion = 30 % to 80 %)
12.5 m	-	16.0 m	Fine SAND trace silt
16.0 m	-	34.0 m	Fine to medium SAND
34.0 m	-	38.0 m	Silty SAND
38.0 m	-	70.0 m	CLAY with numerous silt seams and sandy clay
70 m	====>		Silty CLAY with seams of silt and sandy silt

Established by the pore pressure dissipation measurements (see Section 2.7), the pore pressure distribution in the clay layer below 38 m depth is artesian; the pore pressure head above ground is about 7 m.

The soil profile determined from CPTU data is usually in agreement with the soil profile determined from the conventional grain size distribution. In normally consolidated sedimentary soils, the CPTU-determined soil profile usually agrees well with grain-size description determined from soil samples. However, in overconsolidated or residual soils, the CPTU soil profile can often deviate from the soil sample description. Every site investigation employing CPTU sounding should include soil sampling. It is not necessary to obtain the soil samples in regular boreholes. Modern CPTU equipment includes the means to push down a plastic sampling tube inside a steel pipe of the same size as the cone rod. A continuous core of soil is recovered from where "disturbed" samples can be selected for detailed study. Figure 2.15 shows sections of four such cores recovered next to a CPTU sounding.



Fig. 2.15 Sections of soil cores , ranging from fill, sandy clay, clay, through sand with pieces of gravel. Sampling by means of CPTU device equipped with separate sampler.

Figure 2.16 shows all cone data for the upper 20 m plotted in a Eslami-Fellenius profiling chart with Figure 2.16A showing the data plotted using axes in the usual logarithmic scales. However, the logarithmic plot only serves the purpose of compressing data so that all can be shown together. The log scale makes small relative changes of small values show up and yet includes similarly relative changes for larger values. However, when, as in the example case, the span between the small and the larger values is limited, the plot can preferably be made using linear scales, as shown in Fig. 2.16B.

Figure 2.17 (on Page 2-22) shows the data in profiling charts according to the Robertson 1986 method in logarithmic and linear scales. The linear plot indicates that the organic soil distinction (Layer 2) is probably not practical and that the separation between Layers 4 and 5 could well be considered as one layer. Figure 2.18 (on Page 2-23) shows the same for Robertson 1990 method. It is clearly evident from Fig. 2.18B that the method is not suitable for linear plotting even for a relatively small range of values of the example.

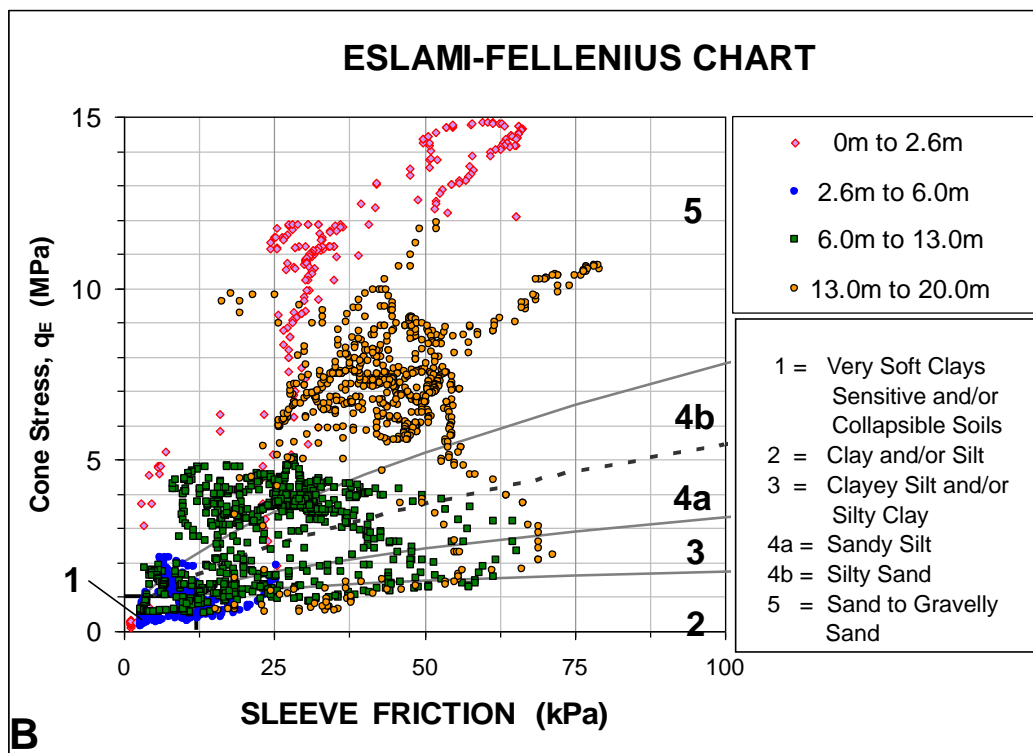
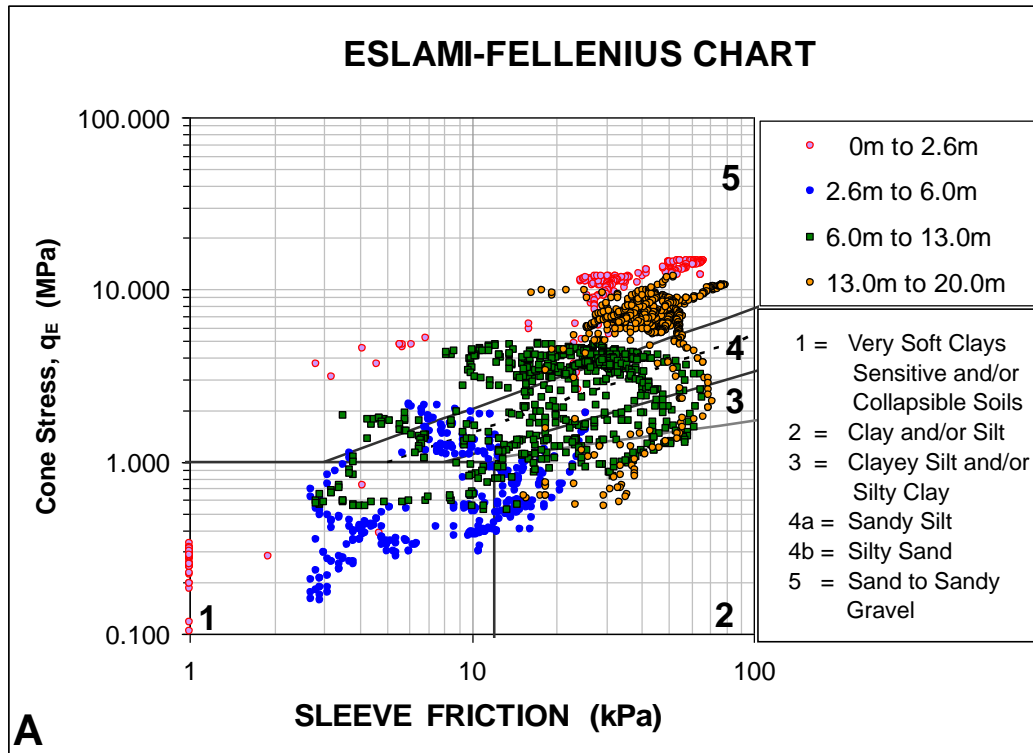


Fig. 2.16 A. Eslami-Fellenius profiling chart with axes in logarithmic scale  
 B. Eslami-Fellenius profiling chart with axes in linear scale

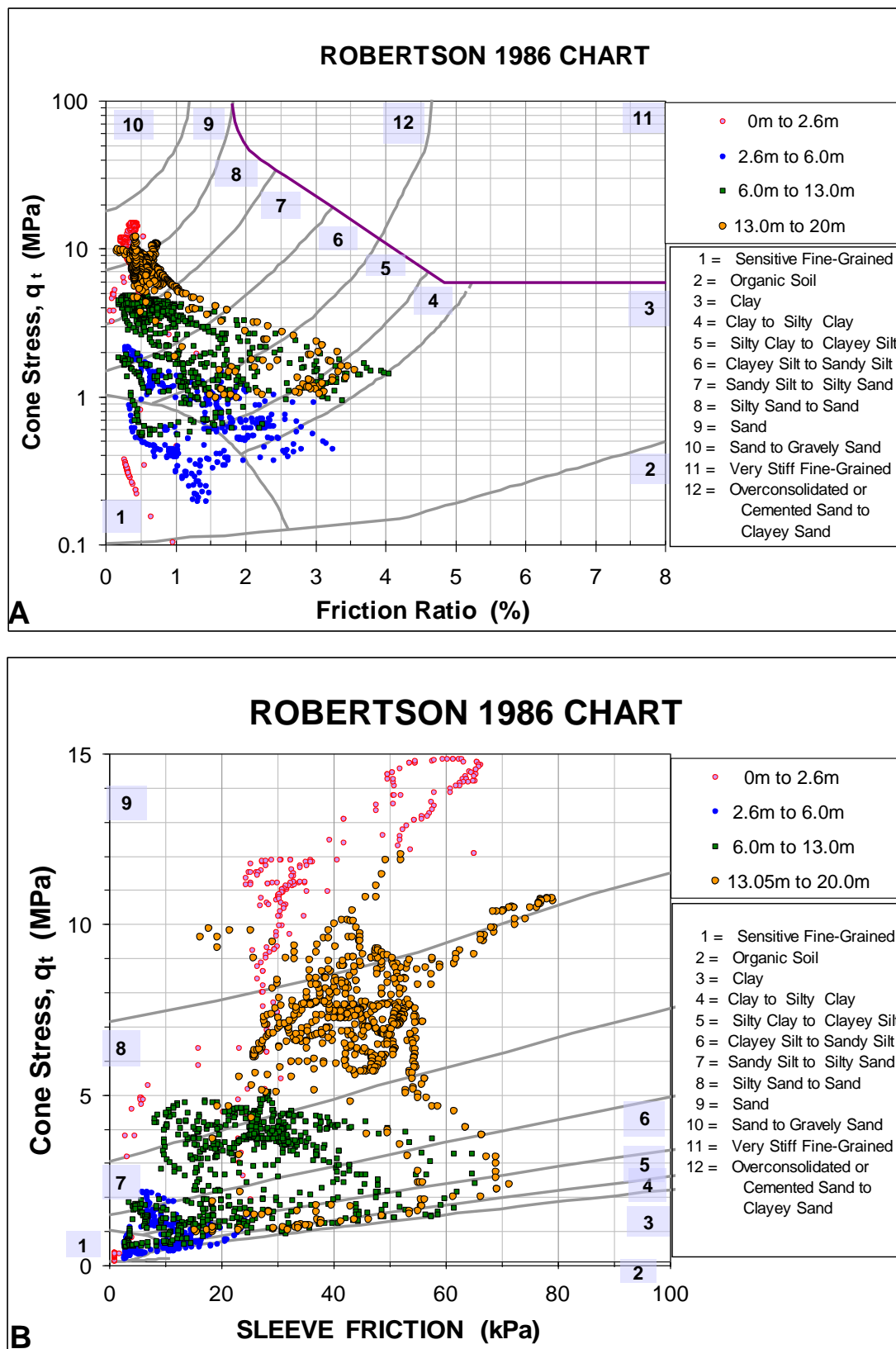


Fig. 2.17 A. Robertson 1986 profiling chart with axes in logarithmic scale  
B. Robertson 1986 profiling chart with axes in linear scale

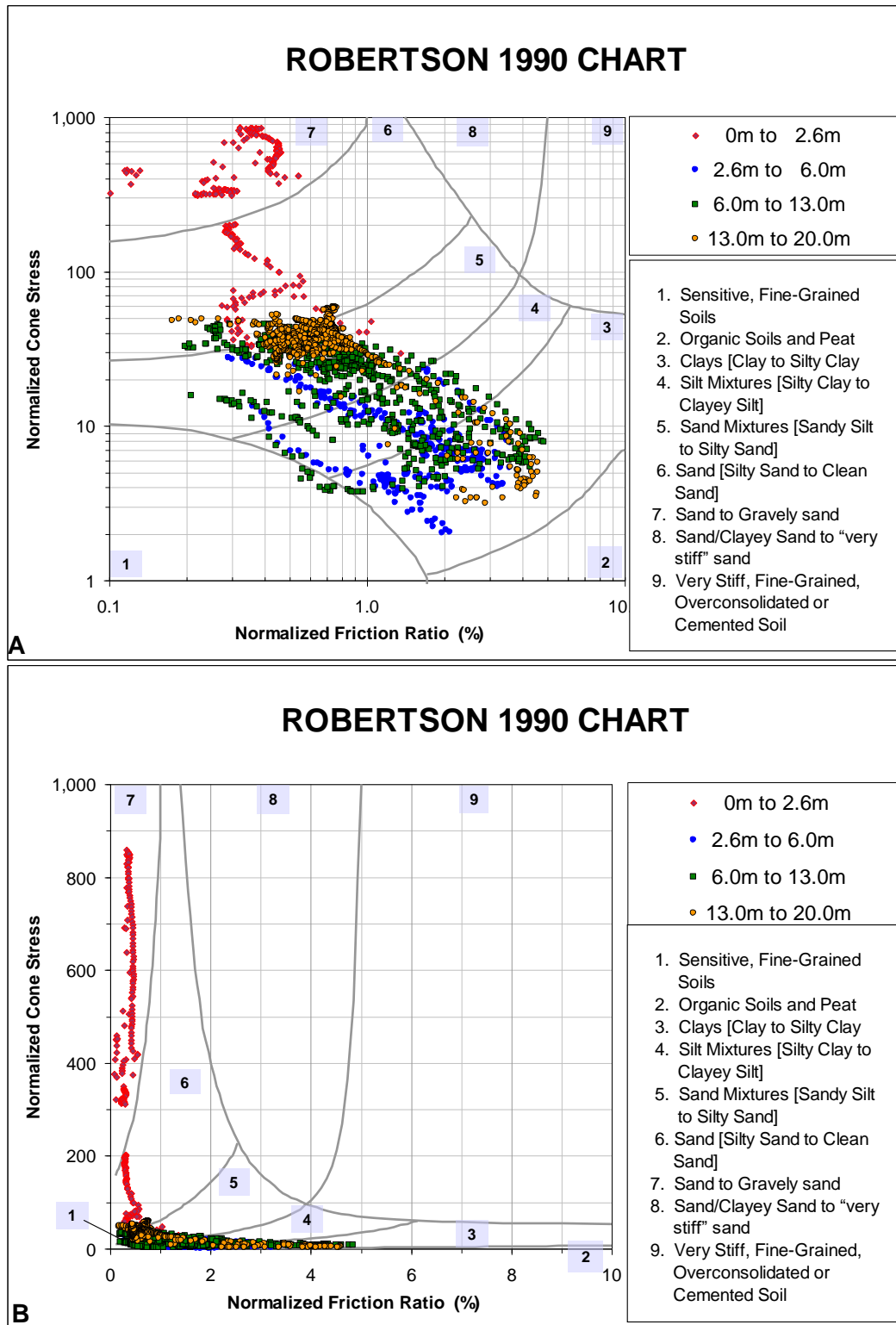


Fig. 2.18 A. Robertson 1990 profiling chart with axes in logarithmic scale  
 B. Robertson 1990 profiling chart with axes in linear scale



## 2.7 Dissipation Time Measurement

In fine-grained soils, the time for the dissipation of the generated pore pressure is of interest. Usually in conjunction with adding a rod to the rod assembly, the cone is kept unmoving and the pore pressures ( $U_2$ ) are recorded. The dissipation time to neutral pore pressure is considered a measure of the coefficient of consolidation,  $c_H$ . (Mayne et al. 1990; 2001). The pore pressure after full dissipation is a measure of the phreatic height at that depth and can be used as indication of pore pressure gradient in the soil (as was done in the case of the CPTU sounding shown in Fig. 2.14).

## 2.8 Inclination Measurement

When a cone is pushed into the ground it is started vertically, but, understandably, the cone rod assembly will start to bend in the soil and the cone will deviate from the vertical line through the starting point on the ground. All CPT systems incorporate inclination measurements and the inclination is recorded for each measurements of cone stress, sleeve friction, and pore pressure. Sometimes, only a value of the maximum inclination is recorded. This will allow a calculation of the radial and vertical deviation of the cone, but not the direction. Other cones show the inclination in two perpendicular directions, which measurements then allow for a calculation of the maximum inclination and the location of the cone at each depth. Down to depths of about 30 m, the deviation is usually not significant. Fig. 2.19 shows deviation records that are unmistakably large; the cone moved 12 m laterally away from the starting point and the bending caused the depth measurement of 30 m to in reality have been slightly less than 28 m — "the cone is lifting its foot". Inclination measurements are not often reported. Obviously, they should be checked and the cone data corrected for depth deviation, when appropriate.

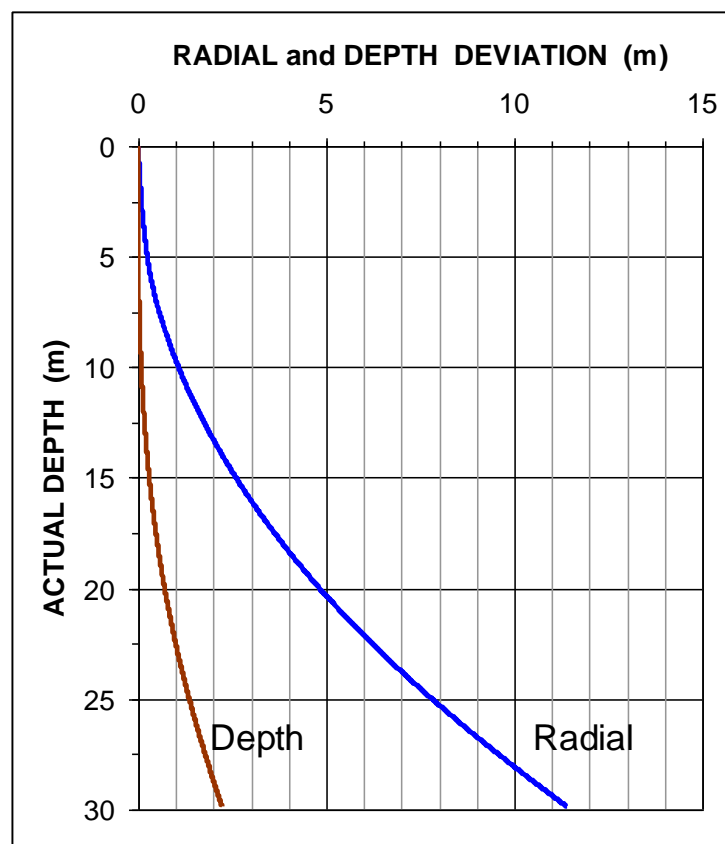


Fig. 2.19 Radial and depth deviation for a 30 m deep cone sounding in Squamish, BC



## 2.9 Shear -wave Measurement

The seismic CPTU, the SCPTU, incorporates a geophone for measuring the arrival time of a shear wave generated on the ground surface close to the cone rod. The shear-wave is generated by giving a horizontal impact to a steel plate placed on the ground surface and the time for generating the impact and arrival at the geophone are recorded. The test is normally performed when adding a cone rod to the rod length (that is, the cone is not moving). Impacts are given at intermittent depths and the results are evaluated as the difference in travel time between geophone from the previous test depth and the current depth, resulting in the shear wave velocity for the soil between the two depths. The shear wave velocity is then used directly in analysis or converted to low-strain dynamic shear modulus ( $G_{\max}$ ). Or combined with vibration velocity when assessing the risk for vibration settlement due to pile driving (see Chapter 9, Section 9.14).

## 2.10 Depth and Stress Adjustment\*)

The results of cone and sleeve friction measurements as used for compressibility reference are believed affected by the effective overburden stress (Jamiolkowski et al., 1988). Therefore, it is necessary to consider this effect when interpreting CPT results used for settlement analysis. For the depth adjustment of the cone stress, Massarsch (1994) proposed to apply a dimensionless adjustment factor,  $C_M$ , to the cone stress according to Eq. 2.7, based on the mean effective stress,  $\sigma'_m$ .

$$(2.7) \quad C_M = \left[ \frac{\sigma_r}{\sigma'_m} \right]^{0.5}$$

where  $C_M$  = stress adjustment factor  $\leq 2.5$   
 $\sigma_r$  = reference stress = 100 kPa  
 $\sigma'_m$  = mean effective stress

The mean effective stress is determined according to Eq. 2.8.

$$(2.8) \quad \sigma'_m = \frac{\sigma'_v (1 + 2K_0)}{3}$$

where  $\sigma'_m$  = mean effective stress  
 $\sigma'_v$  = vertical effective stress  
 $K_0$  = coefficient of horizontal earth stress at rest (effective stress condition)

The stress-adjusted (or depth-adjusted) cone penetration stress,  $q_{tM}$ , is

$$(2.9) \quad q_{tM} = q_t C_M = q_t \left( \frac{\sigma_r}{\sigma'_m} \right)^{0.5}$$

---

\*) The information in Section 2.10 is quoted from Massarsch and Fellenius (2002)

where  $q_{tM}$  = stress-adjusted (depth-adjusted) cone stress  
 $q_t$  = unadjusted—as measured—cone stress (but corrected for pore pressure on the shoulder)  
 $C_M$  = stress adjustment factor  $\leq 2.5$   
 $\sigma_r$  = reference stress = 100 kPa  
 $\sigma'_m$  = mean effective stress

Near the ground surface, values per Eq. 2.9 increase disproportionally and it is necessary to limit the adjustment factor to a value of 2.5.

Determining the mean stress (Eq. 2.10) requires knowledge of the coefficient of earth stress at rest,  $K_0$ . In normally consolidated soils, the magnitude of the horizontal earth stress is usually assumed to follow Eq. 3.29 (Jaky 1948).

$$(2.10) \quad K_0 = 1 - \sin \phi'$$

where  $K_0$  = coefficient of horizontal earth stress (effective stress condition)  
 $\phi'$  = effective friction angle

The effective friction angle for normally consolidated sand and silt ranges between 30° and 36°, which range corresponds to the relatively narrow range of a  $K_0$  of about 0.4 through 0.6.

Compaction results in an increase of the earth stress coefficient at rest,  $K_0$ . However, in overconsolidated soils, that is, compacted soils, it is more difficult to estimate  $K_0$ . Several investigators have proposed empirical relationships between the earth stress coefficient of normally and overconsolidated sands and the overconsolidation ratio, OCR, as given in Eq. 2.11.

$$(2.11) \quad \frac{K_1}{K_0} = OCR^\beta \quad \text{which converts to: (2.11a)} \quad OCR = \left[ \frac{K_1}{K_0} \right]^{\frac{1}{\beta}}$$

where  $K_0$  = coefficient of earth stress at rest for normally consolidated sand  
 $K_1$  = coefficient of earth stress at rest for overconsolidated sand  
 $\beta$  = empirically determined exponent, usually assumed equal to about 0.4

## 2.11 Determining the Janbu Modulus Number, m, from CPT

The most important aspect of a soils investigation and a geotechnical design of a foundation is to assess the settlement of the foundation. For cohesive soils the necessary soil parameters are determined from laboratory tests on 'undisturbed' samples. For coarse-grained soil layers, acceptably undisturbed samples are difficult to obtain and test. The CPTU tool allows a determination of the soil compressibility in terms of the Janbu modulus number, m, which is a parameter that for cohesive soil is equal to the conventional  $C_c e_0$  relation. It also is used for expressing compressibility of soils that can be assumed to respond linearly to a load change, conventionally expressed by an E-modulus. It is particularly useful when assessing potential settlement in intermediate soils, such as silty sand and sandy silt. The background and application of the Janbu modulus number is shown in detail in Section 3.5.

Massarsch (1994) proposed a semi-empirical relationship shown in Eq. 2.12 between the modulus number and the cone stress adjusted for depth according to Section 2.10.

$$(2.12) \quad m = a \left( \frac{q_{tM}}{\sigma_r} \right)^{0.5}$$

where  $m$  = modulus number  
 $a$  = empirical modulus modifier, which depends on soil type  
 $q_{tM}$  = stress-adjusted cone stress  
 $\sigma_r$  = reference stress = 100 kPa

The modulus modifier,  $a$ , has been determined from the evaluation of extensive field and laboratory data (Massarsch, 1994) and shown to vary within a relatively narrow range for each soil type. Massarsch et al. (1997) proposed the values for silt, sand, and gravel listed in Table 2.4.

**TABLE 2.4** Modulus Modifier Factor,  $a$ , for different soil types, Massarsch et al. (1997)

Soil Type	Modulus Modifier, $a$
Soft clay	3 <sup>*)</sup>
Firm clay	5 <sup>*)</sup>
Silt, organic soft	7
Silt, loose	12
Silt, compact	15
Silt, dense	20
Sand, silty loose	20
Sand, loose	22
Sand, compact	28
Sand, dense	35
Gravel, loose	35
Gravel, dense	45

<sup>\*)</sup> These values are based on my limited calibration to consolidometer tests in normally consolidated lacustrine and marine clays. Clays at other sites may differ considerably from the shown values.

Eqs. 2.7 through 2.12 can be combined in a single equation, Eq. 2.13.

$$(2.13) \quad m = a \left[ \left( \frac{q_t}{(\sigma'_r \sigma'_v)^{0.5}} \right) \left( \frac{3}{1 + 2K_0} \right)^{0.5} \right]^{0.5}$$

where  $m$  = modulus number  
 $a$  = empirical modulus modifier, which depends on soil type  
 $q_t$  = unadjusted—as measured—cone stress (but corrected for pore pressure on the shoulder)  
 $\sigma_r$  = reference stress = 100 kPa

For a soil with  $K_0$  ranging from 0.5 through 5.0, the term  $[3/(1 + K_0)^{0.5}]$  ranges from 1.2 to 0.8, that is, the term can be approximated to unity and Eq. 2.13 becomes Eq. 2.14. Notice, compaction can increase the earth stress coefficient beyond a value of 5 and Eq. 2.14 should then be used for the evaluation of the results of the compaction effort.

$$(2.14) \quad m = a \left[ \frac{q_t}{(\sigma'_r \sigma'_v)^{0.5}} \right]^{0.5}$$

CPT readings are taken intermittently at closely spaced distances, normally every 20 mm, preferably every 10 mm. It is often beneficial to filter the cone stress values,  $q_t$ , so that the peaks and troughs in the data are removed. The most useful filtering is obtained by a geometric average over a short length, say, about 0.5 m.

The values of the Modulus Modifier,  $a$ , given in Table 3.4 have been verified in compacted hydraulic fills. They have yet to be verified in naturally deposited soils. Therefore, use of the values should be done with cautionary judgment. At sites where oedometer testing of recovered ‘undisturbed’ samples can be performed, the CPT data from the corresponding layer can, and should be, calibrated to verify the Modulus Modifier for the site.

The effect of filtering and depth-adjusting the  $q_t$  values and calculation of the modulus number profile is illustrated in Fig. 2.20 using the CPT soundings of Fig. 2.1.

The CPTU sounding used as example in Chapter 2 to show profiles of various soil parameters has also been used to calculate the compressibility (modulus number) profile for a site in Alberta (Fellenius 2004).

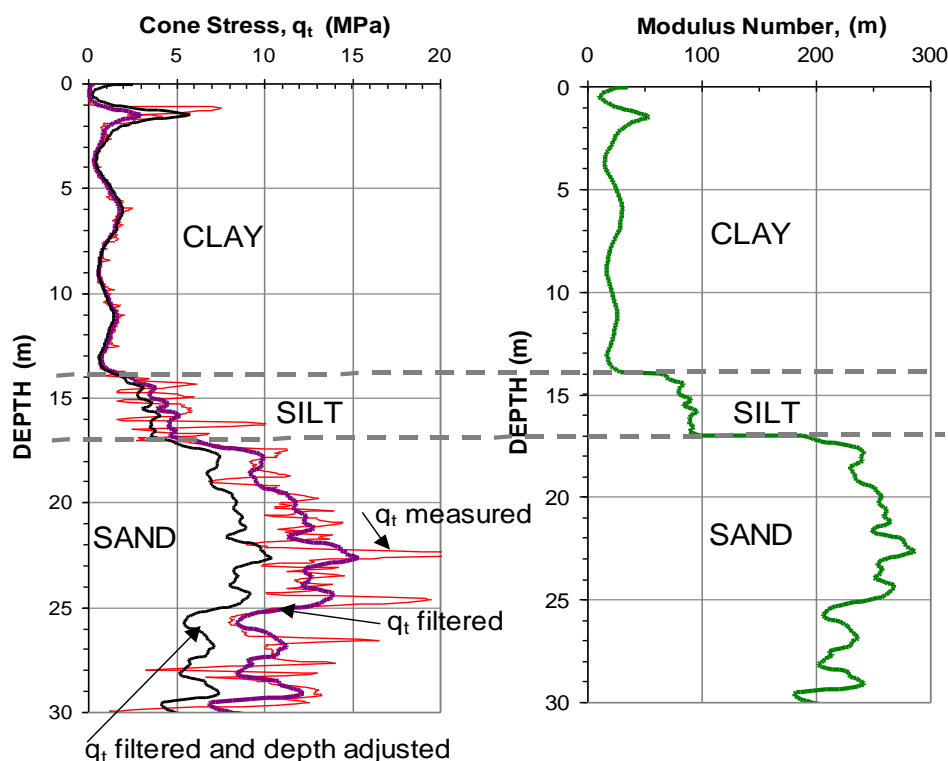


Fig. 2.20 Example of filtered and depth-adjusted  $q_t$  and profile of the resulting modulus number,  $m$

Fig. 2.21 shows the unfiltered  $q_t$ -profile, the filtered  $q_t$ -profile, and the depth-adjusted values. The second of the three diagrams shows the calculated modulus number profile and the modulus numbers from oedometer tests to which the CPTU curve is fitted. The third shows a profile of the modulus modifiers and the "a-exponents" resulting from the fitting of the data.

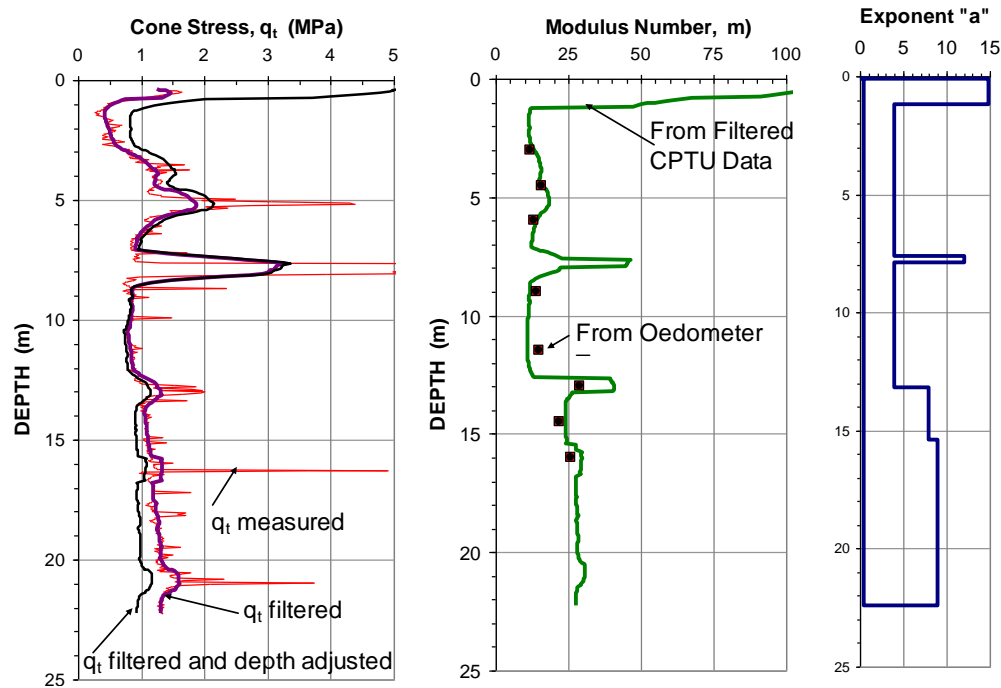


Fig. 2.21 Example of filtered and depth-adjusted  $q_t$  values and profile of the resulting modulus number,  $m$ , fitted by means of the "a-exponent" to values determined in oedometer tests.

## 2.12 Determining Soil Parameters from CPTU Measurements

Many geotechnical parameters are diffuse by themselves. Their reliability depends to a large extent on how they are applied, in what geology, for what design problem, and foremost, on what experience the user of the relation has in the application of the parameter. When a parameter is obtained through correlation to the cone penetrometer results, the user's direct experience becomes even more important. **No formula promoting a relation between a geotechnical parameter and the CPT results should be accepted without thorough correlation to independent test results at the site considered.** However, when such correlation, which by necessity is intermittent, has proven a consistent relation at a site, then, it can be used to establish a more detailed distribution of the parameters at a site from the CPTU profile.

### 2.12.1 Undrained Shear Strength

A popular application for CPT results is to estimate values of undrained shear strength and several correlations exist. The popularity exists despite that undrained shear strength can be determined by so many methods, such as in-situ vane, unconfined compression test, triaxial testing, direct shear, simple shear, etc. The method of determining the undrained shear strength often varies with the design problem to be addressed. Eq. 2.7 is typical of the relations which have been proposed for determining the undrained shear strength from CPTU data. (Kulhawy and Mayne 1990).

$$(2.15) \quad \tau_u = \frac{q_t - \sigma_v}{N_{kt}}$$

where  $\tau_u$  = undrained shear strength  
 $q_t$  = cone stress corrected for pore water pressure on shoulder (Eq. 2.1)  
 $\sigma_v$  = total overburden stress  
 $N_{kt}$  = a coefficient;  $10 < N_{kt} < 20$

An example of undrained shear strength values calculated from Eq. 2.15 is presented in Fig. 2.22A along with the main cone-stress profile. The sounding is from a site in Alberta 185 km north of Edmonton described by Fellenius (2008). The groundwater table lies at a depth of 1.5 m and the pore water pressure is hydrostatically distributed. The soil profile consists of 7.5 m of soft silty clay with a water content of about 35 % through 70 %, a Liquid Limit of about 60 % through 70 %, a Plastic Limit of about 15 through 40 , and a Plasticity Index of about 25. The Janbu modulus number ranges from about 12 through 20. The upper about 7 m of the clay is overconsolidated with an OCR of about 2 through 5. Triaxial consolidated and undrained tests and direct shear testing on the clay indicated a strain-softening soil having a friction angle ranging from 21° through 25° with a residual (post peak) value of about 21°. A small cohesion intercept was found in the range of 10 kPa through 25 kPa. The clay is a re worked, transported, and re deposited glacial till clay. The clay is interrupted at 5 m depth by an about 0.5 m thick layer of silty sand. At a depth of 7.5 m lies a second 0.5 m thick layer of silty sand. The sand is followed by soft silty sandy gravelly ablation clay till that continues to the end of the borehole at a depth of about 25 m. The ranges of water content and indices of the clay till are about the same as those of the upper clay layer. Consolidation tests on samples from the clay till show the Janbu modulus number of the clay to range from 20 through 30. No recompression modulus is available, but the sandy clay till is clearly overconsolidated.

A second example of undrained shear strength values calculated from Eq. 2.7 is presented in Fig. 2.22B. The sounding is from the Langley, BC. Below 5 m depth, the soils consist of lightly to over-consolidated stiff clay to large depth. Some thin sand layers exist between 33 m and 37 m depth.

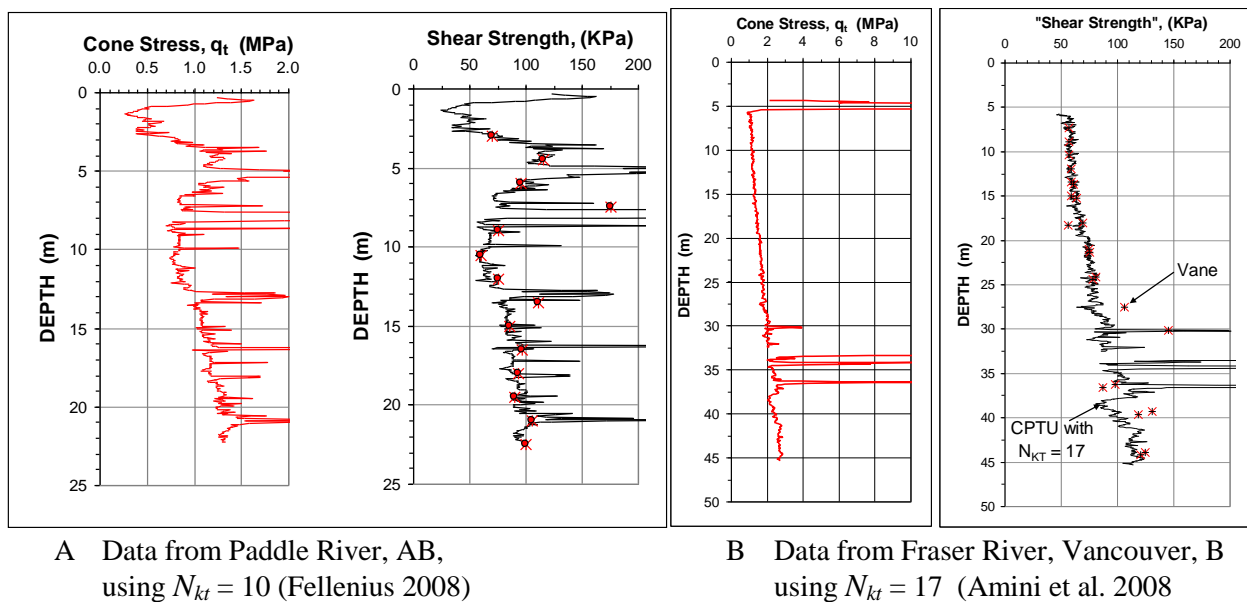


Fig. 2.22 Cone stress ( $q_t$ ) and undrained shear strength profiles fitted to a vane shear profile from tests next to CPTU sounding.

### 2.12.2 Overconsolidation Ratio, OCR

Correlations between the CPTU test data and the overconsolidation ratio, OCR, have also been proposed. Eq. 2.16 presents one method (Kulhawy and Mayne 1990).

$$(2.16) \quad OCR = C_{OCR} \frac{q_t - \sigma_v}{\sigma'_v}$$

where  $OCR$  = overconsolidation ratio

$C_{OCR}$  = a coefficient;  $\cong 0.2 < C_{OCR} < \cong 0.3$

$q_t$  = cone stress corrected for pore water pressure on shoulder (Eq. 2.1)

$\sigma_v$  = total overburden stress

$\sigma'_v$  = effective overburden stress

An OCR profile from the Alberta CPTU sounding is shown in Fig. 2.23 fitted to OCR values determined in eight oedometer tests on Shelby sample recovered in a bore hole next to the CPTU sounding. The fit was obtained with an OCR-coefficient,  $C_{OCR}$ , of 0.2.

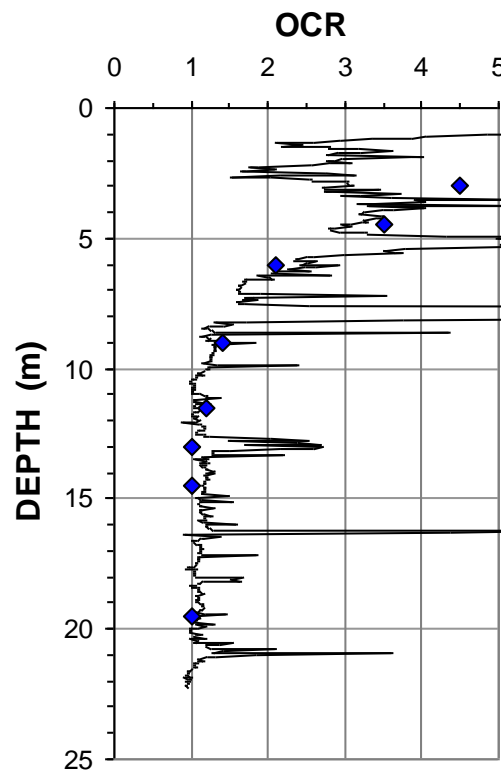


Fig. 2.23 OCR profile fitted to OCR values determined from oedometer tests on Shelby samples. Data from Paddle River site, Alberta (Fellenius 2008).

### 2.12.3 Earth Stress Coefficient, $K_0$

Also the earth stress coefficient,  $K_0$ , can be correlated to CPTU test results. Eq. 2.17 presents one method (Kulhawy and Mayne 1990).

$$(2.17) \quad K_0 = C_K \frac{q_t - \sigma_v}{\sigma'_v}$$

where  $K_0$  = earth stress coefficient  
 $C_K$  = a coefficient;  $C_K \cong 0.1$   
 $q_t$  = cone stress corrected for pore water pressure on shoulder (Eq. 2.1)  
 $\sigma_v$  = total overburden stress  
 $\sigma'_v$  = effective overburden stress

A  $K_0$ -profile from the Alberta CPTU sounding is shown in Fig. 2.24.

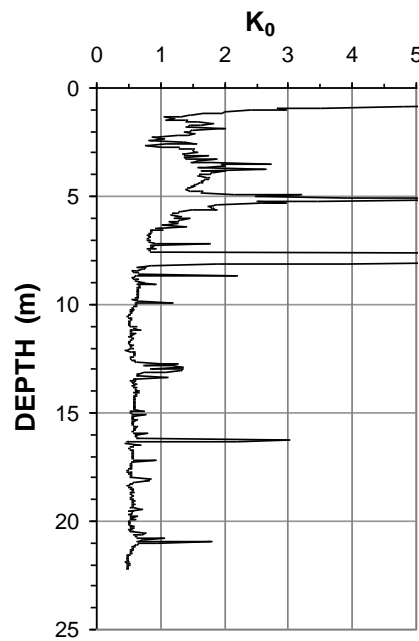


Fig. 2.24  $K_0$  profile determined from the CPTU sounding.  
 Data from Paddle River site, Alberta (Fellenius 2006).

#### 2.12.4 Friction Angle

The CPTU results are frequently used to estimate a value for the effective friction angle of sand, typically, using the relation shown in Eq. 2.18 (Robertson and Campanella 1983).

$$(2.18) \quad tg\phi' = C_\phi \lg \frac{q_t}{\sigma'_v} + K_\phi$$



where  $\phi'$  = effective friction angle  
 $C_\phi$  = a coefficient;  $C_\phi \cong 0.37$  ( $= 1/2.68$ )  
 $K_\phi$  = a coefficient;  $K_\phi \cong 0.1$   
 $q_t$  = cone stress corrected for pore water pressure on shoulder (Eq. 2.1)  
 $\sigma'_v$  = effective overburden stress

A  $\phi'$ -profile from the Alberta CPTU sounding is shown in Fig. 2.23. The profile also includes three friction angle values determined in triaxial tests. The basic 0.37  $C_\phi$ - and 0.1  $K_\phi$  coefficients are used..

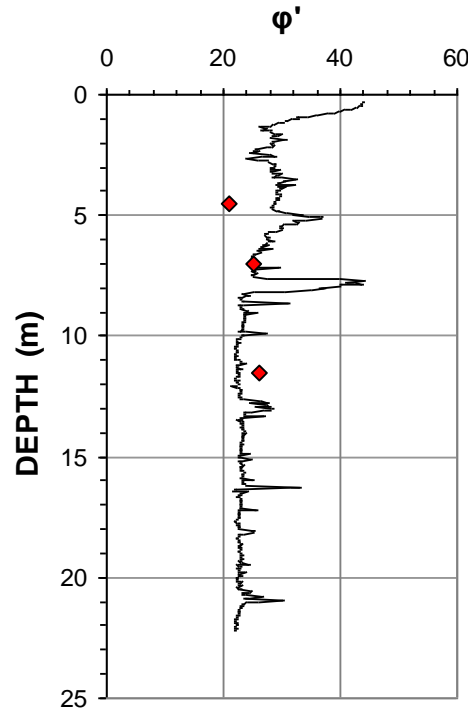


Fig. 2.25 Friction angle,  $\phi'$ , profile determined from the CPTU sounding with three values from triaxial tests. The basic 0.37  $C_\phi$  and  $K_\phi$  coefficients are used. Data from Paddle River site, Alberta (Fellenius 2006).

### 2.12.5 Density Index, $I_D$

Equation 2.19 shows an empirical relation for the Density Index (Kulhawy and Mayne 1990) determined from the cone stress. Note, however, that any formula or numerical expression applying the  $I_D$  should be considered suspect and only applied with great caution. For details, see Chapter 1, Section 1.2.

$$(2.19) \quad I_D = \sqrt{\frac{q_d}{305 F_{OCR} F_{AGE}}} = \sqrt{\frac{q_d}{300}}$$

where  $I_D$  = density index  
 $q_{cl}$  = normalized cone stress ( $1/\sqrt{(\sigma'_v \sigma_r)}$ , where  $\sigma_r = 100$  kPa)  
 $F_{OCR}$  = adjustment factor for overconsolidation ratio (OCR)  $\sim 1$   
 $F_{AGE}$  = adjustment factor for age  $\sim 1$

Baldi et al. (1986) presented an empirical relation for the Density Index shown in Eq. 2.20.

$$(2.20) \quad I_D = \left( \frac{1}{2.61} \right) \ln \left( \frac{q_c}{181 \sigma_m'^{0.55}} \right)$$

where

- $I_D$  = density index
- $q_c$  = cone stress
- $\sigma_m'$  = mean effective overburden stress =  $\sigma_v'(1 + K_0)/3$
- $\sigma_v'$  = effective overburden stress
- $K_0$  = earth stress coefficient

The density index is primarily intended to be applied to sands. Fig. 2.26 shows the results from a CPT sounding in a loose sand at Vilano Beach Florida (McVay et al. 1999).

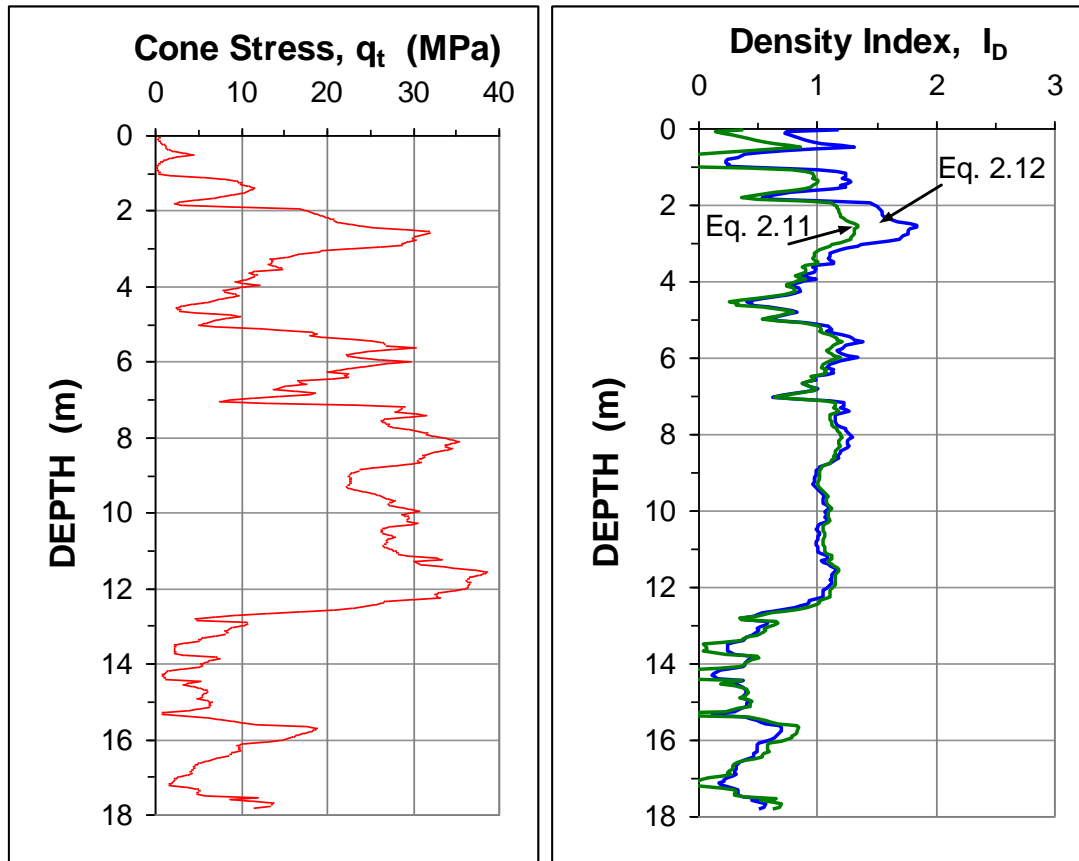


Fig. 2.26 Profiles of cone stress and Density Index,  $I_D$ , determined from the CPTU sounding according to Eq. 2.11 and 2.12. No reference values are available from the site. (CPT data from McVay et al. 1999).

### 2.12.6 Conversion to SPT N-index

Robertson et al. (1983) presented correlations between CPT cone stress values and N-indices from SPTs at 18 sites, as shown in Fig. 2.27A. The conversion ratios are plotted to the mean grain size determined for the SPT samples. The log-scale on the abscissa overemphasizes the data in the fine-grained soils. The data are therefore shown also with the abscissa in linear scale, Fig. 2.27B, which demonstrates that the scatter in the ratio values is rather large.

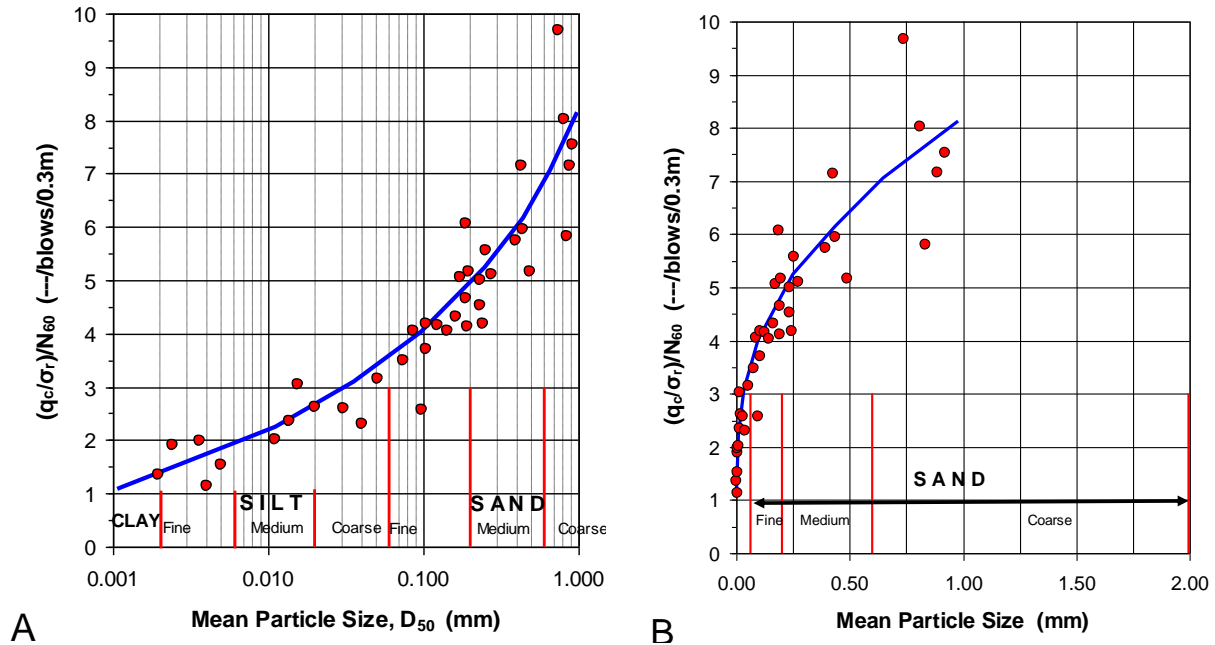


Fig. 2.27 Correlations between CPT cone stress values,  $q_c$  (kPa) divided by  $\sigma_r$  ( $= 100$  kPa) and SPT  $N_{60}$ -indices from 18 sites. Fig. 2.27A abscissa is in Log-scale and Fig. 2.27B abscissa is in linear scale. Data from Robertson et al. 1983.

The conversion curve shown by Robertson et al. (1983) has seen much use for determining N-indices from CPT soundings in order to apply the so-determined "N"-values to various calculations. Actually, these days, the cone stress is the pore pressure corrected stress,  $q_t$ . The conversion results are rather questionable, however. The conversions do not just show a scatter, conversions at other sites are often very different to those shown in Fig. 2.27. For example, Fig. 2.28 shows a plot of the same data supplemented with conversions obtained from N-indices presented by McVay et al. (1999) for the Vilano Beach site, Florida. The mean grain diameter for the Florida site is not known and all data points are plotted at  $d = 0.65$  mm, which is a reasonably representative value for the sand at the site. However, even if the actual mid-range grain size had been known, the plot would still neither have shown any relation to the 1983 curve, nor to any other correlation.

In-situ classification of "relative density" of coarse-grained soils is usually referenced to the SPT-index value. However, the cone stress of the CPTU provides a more consistent and reliable such reference. Thus, in very loose soils  $q_t$  is  $< 2$  MPa, in loose soils,  $q_t$  ranges from 2 through 4, in compact from 4 through 12, in dense from 12 - 20, and in very dense soil,  $q_t$  is  $> 20$  MPa.

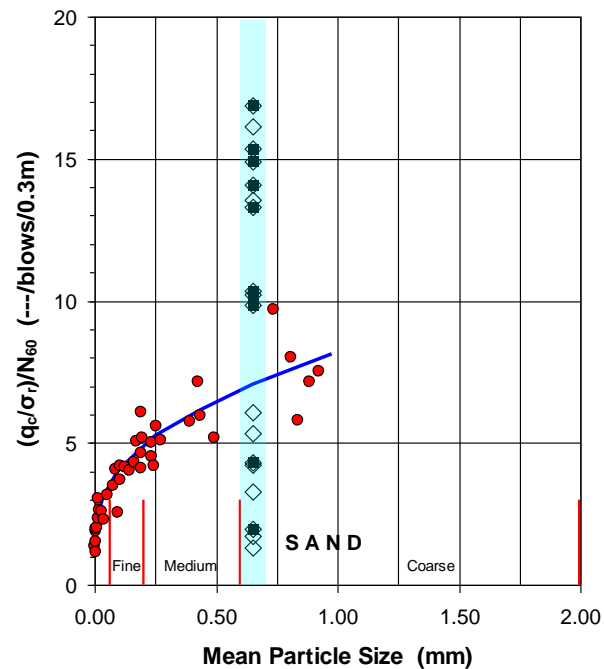


Fig. 2.28 The SPT-CPT correlations of Fig. 2.25 supplemented with correlations from Vilano Beach site, Florida. Data from McVay et al. 1999.

### 2.12.7 Determining the E-Modulus from CPT cone-stress

When calculating settlement, the E-modulus of interest is the modulus for an average applied stress limited to a value equal to about 25 % of the estimated ultimate bearing resistance. The modulus is called  $E_{25}$ , and it can be related to the average cone stress according to the relationship given in Eq. 2.21.

$$(2.21) \quad E_{25} = \alpha q_t$$

where  $E_{25}$  = secant modulus for a stress equal to about 25 % of the ultimate stress  
 $\alpha$  = an empirical coefficient  
 $q_t$  = cone stress

Test data indicate that the empirical coefficient,  $\alpha$ , varies considerably and depends on the soil type and stress conditions as well as on the applied load level. According to the Canadian Foundation Engineering Manual (1985, 1992), when correlated to plate load tests on sand,  $\alpha$  varies between 1.5 and 4. Based on a review of results of cone tests in normally consolidated, uncemented sand in calibration chambers, Robertson and Campanella (1986) proposed a range for  $\alpha$  between 1.3 and 3.0. This range agrees well with recommendation by Schmertmann (1970) for use of CPT data to analyze settlement of isolated footings on coarse-grained soils. Dahlberg (1975) performed tests in overconsolidated sand and found that  $\alpha$  ranged from 2.4 through 4, increasing with increasing value of  $q_t$ . The Canadian Foundation Engineering Manual (1992) states that  $\alpha$  is a function of soil type and compactness, as listed in Table 2.5. The values of  $\alpha$  shown in the table apply to a settlement analysis in soils that can be assumed to have a linear ("elastic") response to a load increase.

**TABLE 2.5**  $\alpha$  from Static Cone Penetration Tests (CFEM 1992)

Soil type	$\alpha$
Silt and sand	1.5
Compact sand	2.0
Dense sand	3.0
Sand and gravel	4.0

### 2.12.8 Assessing Liquefaction Susceptibility

When an earthquake hits, as the name implies, the soil will "quake in shear"; movements back and forth occur (or, more rarely, up and down). If the shear movements, as is most commonly the case, make smaller grains move into the voids between larger grains, the soil volume reduces—the soil contracts—and pore pressure increases and effective stress decreases. In a series of repeated shaking—cyclic shear—the pore pressure increases can accumulate, affect a large volume of soil, and cause a complete loss of effective stress, i.e., the soil liquefies. If so, the volume loss in the liquefied zone will cause the foundations placed on the ground above to settle by the amount of the volume decrease. Shear movements of magnitude associated with an earthquake in fine-grained and cohesive soils are considered less susceptible to liquefaction, as the soil grains in such soil cannot as easily be rearranged by the shaking. Moreover, dense coarse-grained soil will not liquefy, because when the grains in such soils are rearranged and move relative each other, they "climb over each other"<sup>1</sup> and the soil elements affected will actually increase in volume—dilate, and the pore pressures will decrease rather than increase—the soil does not liquefy. However, loose coarse-grained soil are contractant and the looser the soil, the more prone to liquefaction it is. Figure 2.29 illustrates the sometime drastic consequence of liquefaction.

In the following, principles of the assessment of liquefaction susceptibility are presented. The material is not exhaustive and the reader is strongly recommended to review the references for additional information.

#### 2.12.8.1 Cyclic Stress Ratio, CSR, and Cyclic Resistance Ratio, CRR

Data from CPTU soundings are often employed to assess susceptibility due to earthquake induced liquefaction. The following summarizes the procedures of Robertson and Wride (1998) and Youd et al. (2001). The analysis starts by determining the driving effect, called **Cyclic Stress Ratio, CSR**, calculated from Eqs. 2.22 through 2.24 (Seed and Idriss 1971).

$$(2.22) \quad CSR = 0.65 (MWF) \frac{a_{\max}}{g} \frac{\sigma_v}{\sigma_v'} r_d$$

$$(2.23) \quad MWF = \left( \frac{M}{7.5} \right)^{2.56}$$

$$(2.24) \quad r_d = 1 - 0.015z$$

<sup>1</sup> When subjected to a shear movement, initially, also a dense sand will contract, but when the movement gets larger, as in the case of an earthquake shaking, dense sand will dilate.



Fig. 2.29 Effect of liquefaction from the 7.4 Magnitude Kocaeli Earthquake of August 17, 1999 in Turkey. Courtesy of Dr. N.J. Gardner, University of Ottawa.

where

$CSR$	=	Cyclic Stress Ratio
$MWF$	=	Earthquake Magnitude Weighting Factor, dimensionless; increases with increasing earthquake magnitude, $M$
$M$	=	earthquake magnitude per Richter scale, dimensionless
$a_{max}$	=	maximum horizontal acceleration at ground surface ( $m/s^2$ )
$g$	=	gravity constant ( $m/s^2$ ), dimensionless
$r_d$	=	stress reduction coefficient for depth, dimensionless
$z$	=	depth below ground surface (m)

Usually the term  $a_{max}/g$  is given as a ratio to the gravity constant, "g", e.g., 0.12g. When  $M$  is equal to a magnitude of 7.5,  $MWF$  becomes equal to unity. (For, say, magnitudes ranging from 6.0 through 8.0,  $MWF$  ranges from 0.57 through 1.19).  $MWF$  is the inverse of the Magnitude Scaling Factor,  $MSF$ , also commonly used for weighting or scaling earthquake magnitudes. For recommendations regarding choice of  $MWF$  or  $MSF$ , see Youd et al. (2001). Note that while the energy per the Richter scale,  $M$ , is the energy at source, the maximum horizontal acceleration pertains to the site considered. The two are somewhat proportional, in that a large earthquake (large "M") will normally cause a large "a", although the  $CSR$  depends exponentially on the "M" input, whereas the influence of "a" is linear.

The depth factor or stress reduction coefficient,  $r_d$ , serves to respond to the observation that the incidence of liquefaction reduces with depth. Different authors have proposed slightly larger values for the constant applied to the depth,  $z$ , in Eq. 2.15, as summarized by Youd et al. (2001) and Moss et al. (2006).

The ability of the soil to resist liquefaction is calculated using a **Cyclic Resistance Ratio, CRR**, applied to CPTU results as determined according to an approach proposed by Robertson and Campanella (1985) further developed by Robertson and Wride (1998), who correlated information for a large number of earthquakes. Figure 2.30 shows the CSR-values as calculated from Eqs. 2.22 through 2.24 and plotted against values of Normalized Cone Stress,  $q_{c1}$ , as defined by Eq. 2.25. The plotted data points are from where liquefaction occurred and where it did not occur, and the boundary between the two scenarios is termed the CRR-curve. It is considered applicable to clean sand defined as sand with a fines content smaller than 5 %, which is also the upper boundary for free-draining sand.

$$(2.25) \quad q_{c1} = q_t \sqrt{\frac{\sigma_r}{\sigma_v}}$$

where  $q_{c1}$  = cone stress normalized for liquefaction calculation ( $q_{c1} \leq 1.7q_t$ )  
 $q_t$  = cone stress. In sand, whether the cone stress is uncorrected  $q_c$ , or corrected,  $q_t$ , for the pore pressure,  $U_2$ , on the cone shoulder makes very little difference to the normalized cone stress value  
 $\sigma_r$  = reference stress = 100 kPa (= atmospheric pressure)

The boundary line is the Cyclic Resistance Ratio Curve, CRR, which is also shown as a linear regression curve (Eq. 2.18) for the boundary values ( $M=7.5$ ). The two dashed curves show the boundary curves for sand with fines contents of 15 % and 35 %, respectively (copied from Stark and Olsen 1995, Eqs. 2.19a and 2.19b). The original diagram divided the cone stress,  $q_c$ , by atmospheric pressure to make the number non-dimensional.

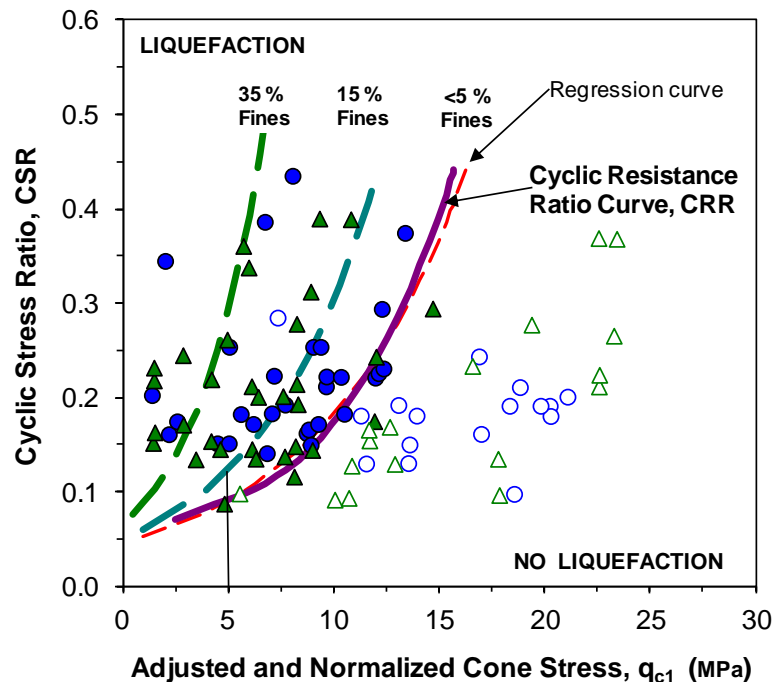


Fig. 2.30 Correlations between CRR-values calculated from actual earthquakes versus  $q_{c1}$ -values for cases of liquefaction (solid symbols) and no liquefaction (open symbols), and boundary curve (solid line) according to Robertson and Wride (1998) and Youd et al. (2001).

According to the sources of Fig. 2.28, sand containing fines will be less liquefiable, that is, the boundary line moves to the left for increasing fines contents. Stark and Olsen (1995) presented a graph similar to that shown, which included boundary lines for fines contents of 15 % and 35 %. These curves have been



added to the graph. However, recent findings have questioned that fines content would reduce seismic susceptibility (Bray and Sancio 2006; 2007, Boulanger and Idriss 2006; 2007, Boardman 2007).

The boundary curve for the Cyclic Resistance Ratio Curve, CRR, applicable to clean sand is determined according to Eqs. 2.26a and 2.26b. The curve can be approximated by means of regression analysis, which gives Eq. 2.19.

$$(2.26a) \quad CRR = 0.833 \left( \frac{q_{c1}}{100} \right) + 0.05 \quad \text{for } q_{c1} < 50 \text{ MPa}$$

$$(2.26b) \quad CRR = 93 \left( \frac{q_{c1}}{100} \right)^3 + 0.08 \quad \text{for } 50 < q_{c1} < 160 \text{ MPa}$$

$$(2.26) \quad CRR = 0.045(e^{0.14q_{c1}})$$

where      CRR      =    Cyclic Resistance Ratio  
 $q_{c1}$       =    cone stress normalized for liquefaction calculation; (MPa) (Eq. 2.24)  
 $e$           =    base of the natural logarithm = 2.718

N.B., the constants "0.833" are as quoted; there's no typo; notice the exponent:  $(q_{c1}/100)^3$  in Eq. 2.26.

The two curves for fines contents of 15 % and 35 % correspond to Eqs. 2.27a and 2.27b, respectively.

$$(2.27a) \quad CRR = 0.045(e^{0.20q_{c1}})$$

$$(2.27b) \quad CRR = 0.065(e^{0.30q_{c1}})$$

Juang and Jiang (2000) presented the graph shown in Fig. 2.31, similar to that in Fig. 2.30, showing boundary curves for probability of liquefaction,  $P_L$ , ranging from 0.1 through 0.9. Mathematical expressions for the curves are given by Eqs. 2.28a through 2.28f. The curve (Eq. 2.28d) for a probability of 0.5 is almost identical to the boundary curve (Eq. 2.26) of Fig. 2.29.

$$(2.28a) \quad CRR_{P_L=0.1} = 0.025(e^{0.14q_{c1}})$$

$$(2.28b) \quad CRR_{P_L=0.2} = 0.033(e^{0.14q_{c1}})$$

$$(2.28c) \quad CRR_{P_L=0.3} = 0.038(e^{0.014q_{c1}})$$

$$(2.28d) \quad CRR_{P_L=0.5} = 0.046(e^{0.14q_{c1}})$$

$$(2.28e) \quad CRR_{P_L=0.7} = 0.057(e^{0.14q_{c1}})$$

$$(2.28f) \quad CRR_{P_L=0.9} = 0.085(e^{0.14q_{c1}})$$



where  $CRR$  = Cyclic Resistance Ratio from the CPTU data  
 $P_L$  = probability of liquefaction  
 $e$  = base of the natural logarithm = 2.718  
 $q_c$  = cone stress (kPa)

Moss et al. (2006) presented methodologies for deterministic and probabilistic assessment of seismic soil liquefaction triggering potential based on the cone penetration test. The data base includes observations at 18 earthquake events and studies of the response of sand layers at 182 localities affected by the earthquake. Of these, liquefaction was observed at 138 cases and the sand did not liquefy in 44 cases. Two of the case histories (Kocaeli, Turkey, and Chi-Chi, Taiwan, involving 32 observations) were from quakes occurring after 1998. The Moss et al. (2006) assessment makes use of probabilistic and statistics as well as information in addition to the cone sounding information. For deterministic assessment, the approach is similar to the approach by Robertson and Wride (1998) as illustrated in Fig. 2.32.

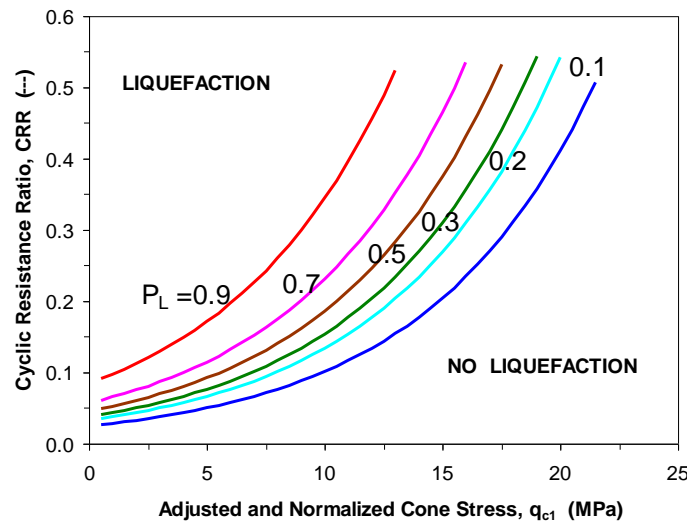


Fig. 2.31 Correlations between CRR-values and  $q_{c1}$ -values for different probabilities of liquefaction,  $P_L$ . Data from Juang and Jiang (2000).

For cases of liquefaction (solid symbols) and no liquefaction (open symbols), according to Moss et al. (2006) and boundary curve (solid line) according to Robertson and Wride (1998) and Youd et al. (2001). The boundary line is the Cyclic Resistance Ratio Curve, CRR. The two dashed curves show the boundary curves for sand with fines contents of 15 % and 35 %, respectively (copied from Stark and Olsen 1995, Eqs. 2.19a and 2.19b).

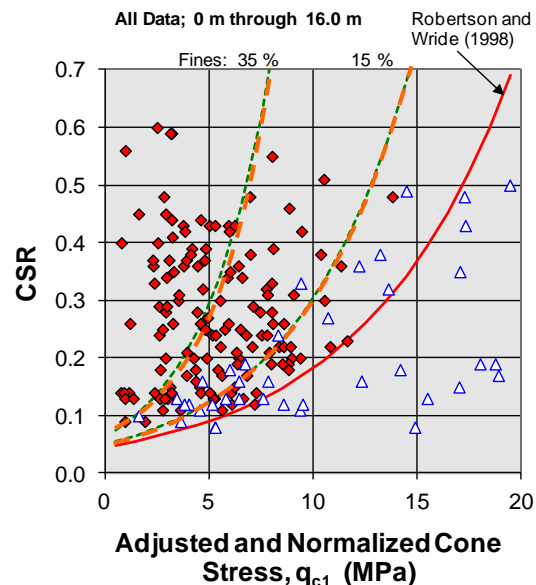


Fig. 2.32 Correlations between CRR-values calculated from actual earthquakes versus  $q_{c1}$ -values

Figs. 2.33A and 2.33B present the Moss et al. (2006) data plotted as earthquake acceleration ( $q_{\max}/g$ ) versus not-normalized cone stress (the as-measured cone stress). In an actual case, this is the format of the first information available and the figures are useful as aid toward whether or not a detailed liquefaction study is necessary. Fig. 2.33A shows only the data from ground surface to depth of 6.0 m. Fig. 2.33B shows all data in the data base. The dashed curve is the Robertson and Wride CRR curve plotted against the  $q_c$ -values as if they were  $q_{c1}$ -values. The curve is only included in the figures to serve as reference to Fig. 2.32. Fig. 2.33A demonstrates that for shallow depth (<6 m), and a moderate magnitude earthquake (<0.25g), liquefaction was not observed for as-measured cone stress larger than 5 MPa.

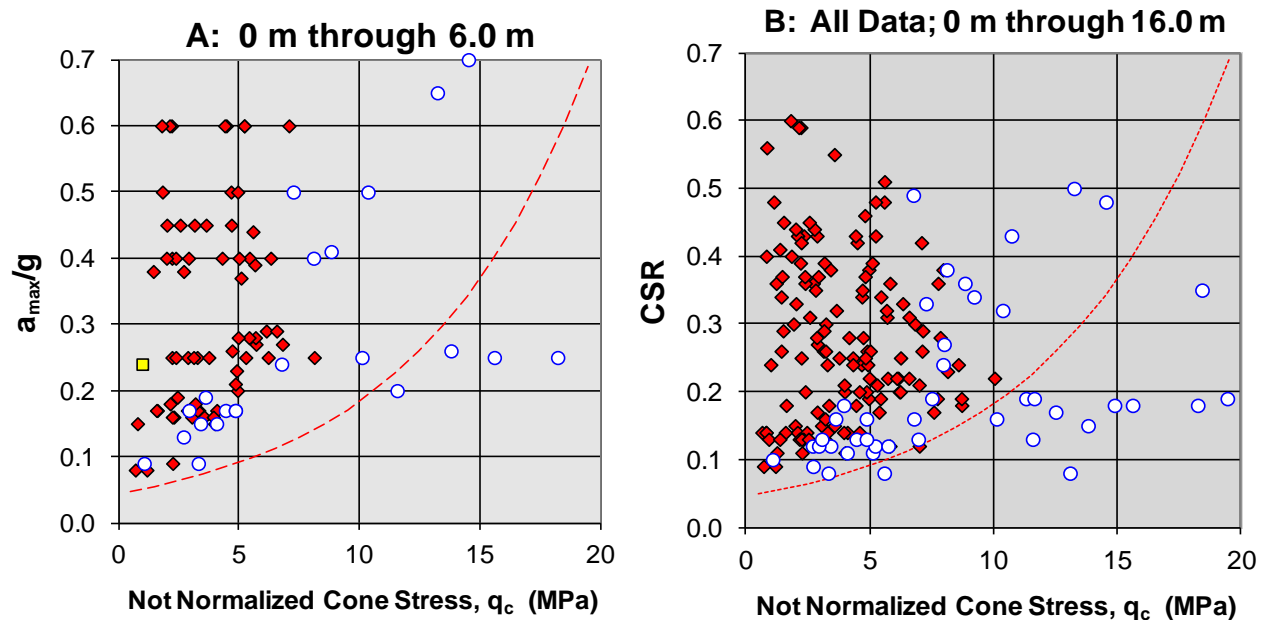


Fig. 2.33 The data points presented as earthquake acceleration ( $q_{\max}/g$ ) versus not-normalized cone stress (the as-measured cone stress).

#### 2.12.8.2 Factor of Safety, $F_s$ , against Liquefaction

The factor of safety ( $F_s$ ) against liquefaction is the ratio between the resisting condition represented by the CRR-value and the earthquake condition represented by the CSR-value, according to Eq. 2.29.

$$(2.29) \quad F_s = \frac{CRR}{CSR} MWF$$

where

- $F_s$  = factor of safety against liquefaction
- $CRR$  = Cyclic Resistance Ratio from the CPTU data
- $CSR$  = Cyclic Stress Ratio from the seismic conditions
- $MWF$  = Magnitude Weighting Factor

A  $F_s$  smaller than unity does not necessarily mean that liquefaction will occur for the considered earthquake magnitude. However, it does indicate the need for a closer look at the risk and susceptibility and a detailed study of the current main references, e.g., Youd et al. (2001) and Moss et al. (2006).

### 2.12.8.3 Comparison to Liquefaction Susceptibility Determined from SPT N-indices

Evaluation of liquefaction resistance was formerly—and still is in many places—based on the SPT Index. It is generally considered necessary to adjust the N-index to depth, i.e., overburden stress, by means of a coefficient called "normalization factor",  $C_N$ , proposed by Seed 1976 for earthquake applications specifically. The N-index is also adjusted to a value for standard condition of energy. The latter is obtained by using transducers for measuring impact stress and acceleration (see Chapter 9) to determine the energy transferred to the SPT rods. As "standard" transferred energy is 60 % of the nominal energy, the measured N-index is proportioned to the actually transferred energy. (Note deviation of the actual transferred energy from 60 % of nominal by more than 25% up or down is not acceptable). The so-adjusted index is expressed in Eqs. 2.30 and 2.31.

$$(2.30) \quad (N_1)_{60} = C_N N_{60}$$

where  $N_I$  = stress-adjusted (depth-adjusted) N-index  
 $C_N$  = normalization factor expressed  
 $N_{60}$  = SPT N-index energy corrected

$$(2.31) \quad C_N = 1 - 1.25 \log \left( \frac{\sigma'_v}{\sigma_r} \right)$$

where  $\sigma'_v$  = effective overburden stress  
 $\sigma_r$  = reference stress = 100 kPa

The normalization factors, Eqs. 2.16 and 2.23, are very similar as indicated in Fig. 2.34, where they are plotted together. The assumptions are a soil with a density of 2,000 kg/m<sup>3</sup> and a groundwater table at the ground surface. Below a depth of about 3 m, the factors are almost identical. At a depth of about 10 m, both normalization factors are about equal to unity (effective overburden stress is about equal to the reference stress).

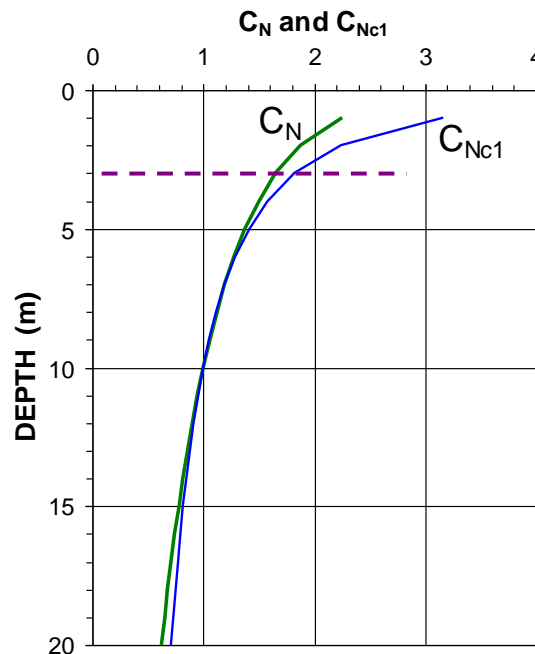


Fig. 2.34 Comparison between the normalization factors for SPT-index and CPT cone stress,  $q_c$ .

Figure 2.35 shows calculated  $CSR$ -values versus corresponding  $(N_1)_{60}$ -values from sites where liquefaction effects did or did not occur for earthquakes with magnitudes of approximately 7.5. The  $CRR$  curve on this graph was conservatively positioned to separate data points from sites where liquefaction occurred from data points from sites with no liquefaction. Curves were developed for granular soils with fines contents of 5% or less, 15%, and 35% as shown on the plot. The  $CRR$  curve for fines contents smaller than 5% is the basic penetration criterion for the simplified procedure and is called the "SPT clean sand base curve". The curves are valid only for magnitude 7.5 earthquake, but the values can be adjusted by means of the  $MWF$  according to Eq. 2.13 (for other suggested relations see Moss et al. 2006).

The boundary  $CRR$  curve in the original graph is plotted per Eq. 2.32 (Figure 2.35). The dashed curve next to the boundary curve is a regression curve fitting the boundary curve per Eq. 2.33a. Similarly, the two dotted curves showing the boundary curves for fines contents are approximately fitted to Eqs. 2.33b and 2.33c.

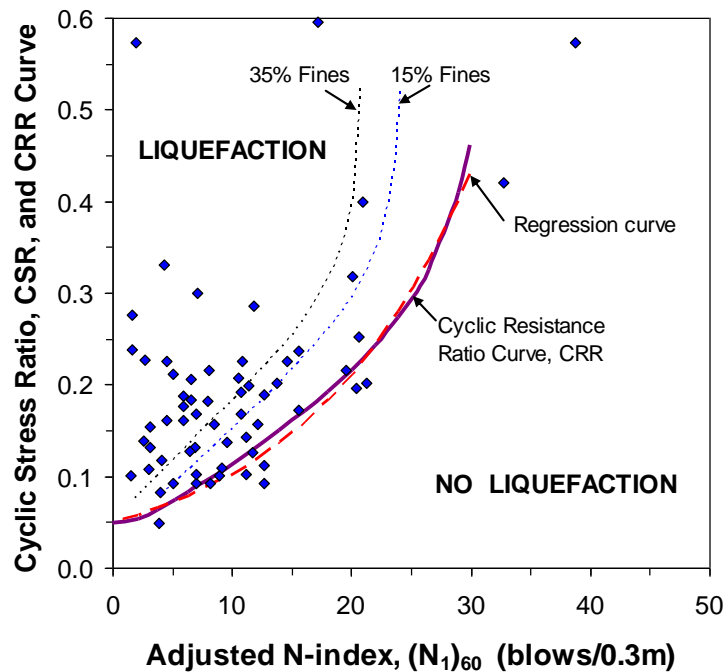


Fig. 2.35 Correlations between  $CRR$ -values and Adjusted  $N$ -indices. Data from Youd et al. (2001).

$$(2.32) \quad CRR = \frac{1}{34 - N} + \frac{N}{135} + \frac{50}{(10N + 45)^2} - \frac{1}{200}$$

$$(2.33a) \quad CRR_{FC < 5\%} = 0.050(e^{0.072N_{60}})$$

$$(2.33b) \quad CRR_{FC = 0.13\%} = 0.060(e^{0.084N_{60}})$$

$$(2.33c) \quad CRR_{FC = 0.33\%} = 0.070(e^{0.092N_{60}})$$

The adjusted SPT-N indices,  $(N_1)_{60}$ , can be correlated to the adjusted and normalized cone stress,  $q_{cl}$ , over the respective values of cyclic stress resistance,  $CSR$ . For equal  $CSR$ -values, the relation between the two is approximately linear—the ratio is 0.18, that is,  $(N_1)_{60} = 1.8q_{cl}$  (the linear regression coefficient is 0.99). As mentioned, at a depth of 10 m, the normalization factor  $C_N$  is approximately equal to unity, i.e., the  $(N_1)_{60}$ -values is equal to  $N_{60}$ , (Eqs. 2.22 and 2.23). Similarly, the factor  $\sqrt{(\sigma_r/\sigma'_v)}$  in Eq. 2.15 is equal to unity at this depth. Therefore, the normalized cone stress,  $q_{cl}$ , is equal to  $q_c$ . So, the ratio at 10 m depth between  $q_c$  and  $(N)_{60}$  becomes about 2. This means, for example, that at about 10 m depth, a loose sand, as indicated by a cone stress of, say, 3 MPa, correlates to an  $N$ -index of 6 blows/0.3 m, which does correspond to a loose relative density when judged from the  $N$ -index.

As the normalization factors are very similar, the mentioned about-2 ratio is independent of depth (once below 3 m depth). Referring to Section 2.12.6, the  $q_c/\sigma_r$ -ratio between a  $q_c$  equal to 3 MPa and an  $N_{60}$  equal to 6 bl./0.3m is 5. To lie on the curve of Fig. 2.27, this value would apply to a "fine sand". The agreement is hardly coincidental, however. Much of the experience behind Fig. 2.30 and its curves was transferred from the data behind Fig. 2.35. It is obvious from the discussion in Section 2.12.8.1 that correlation between the SPT index and the cone stress is highly variable. It is questionable how relevant and useful a conversion from an SPT Index value to a cone stress would be for an actual site. One would be better served pushing a cone in the first place.

#### 2.12.8.4 Determining Liquefaction Risk and Achieving Compaction/Densification; Example

As an example of calculations of factor of safety against liquefaction, results are presented of cone penetration soundings performed small trial area (12 m by 12 m) at Hong Kong Chek Lap Kok Airport in a sand fill before and after seven days after vibratory densification. The sand fill consisted partly of calcareous material (fragments of shells and clams), and contained about 15 % of fines and occasional layers of silt and silty sand. It was placed by bottom dumping, where the water depth exceeded 4 m, and by spraying, where the water depth was shallower. The final thickness of the sand fill prior to compaction was about 10 m. The groundwater level was located about 1 m below the fill surface. The sand fill was specified to contain less than 10 % of fines. The compaction study of the case is reported by Massarsch and Fellenius (2002).

Figure 2.36 present the results of four CPTU soundings through the as-placed fill before compaction, illustrating that the fill consists mainly of loose sand to a depth of about 4 m below which the sand contain frequent layers of silty sand and an occasional lens of silty clay and even clay. The homogeneity of the fill is demonstrated in the profiling chart shown in Fig. 2.37. The figures include all CPT records (readings were taken every 20 mm) from one CPT sounding. The data points in Zones 4a and 4b indicating silt, sandy silt, and silty sand are all from below 4 m depth. The silty clay and clay lens indicated in the figure at about 6 m depth is 60 mm thick and the profiling chart shows it to be made up of three closely located values, one value indicating clay and two values indicating silty clay.

The site was densified using the Müller Resonance Compaction (MRC) method (Massarsch and Westerberg 1995). By changing the vibration frequency, the system makes use of the vibration amplification, which occurs when the soil deposit is excited at the resonance frequency. Different vibration frequencies are used during the particular phases of the compaction process in order to achieve optimal probe penetration and soil densification, as well as facilitate of probe extraction and to avoid undoing the compaction ("uncompacting" the soil) when extracting the Müller tool.

The results of three cone soundings performed seven days after the vibratory compaction are shown in Fig. 2.38. The diagrams show that the compaction has resulted in increased values of cone stress and sleeve friction, more directly demonstrated in Fig. 2.39 (only the average curves are shown). The friction ratio is approximately the same, however. The average curves are produced by means of a geometric

average running over a distance of 500 mm, that is 25 values. The purpose of the averaging is to reduce the influence of thin layers of soft material that could cause a smaller than actual cone stress and, therefore, indicate a larger than actual susceptibility to liquefaction.

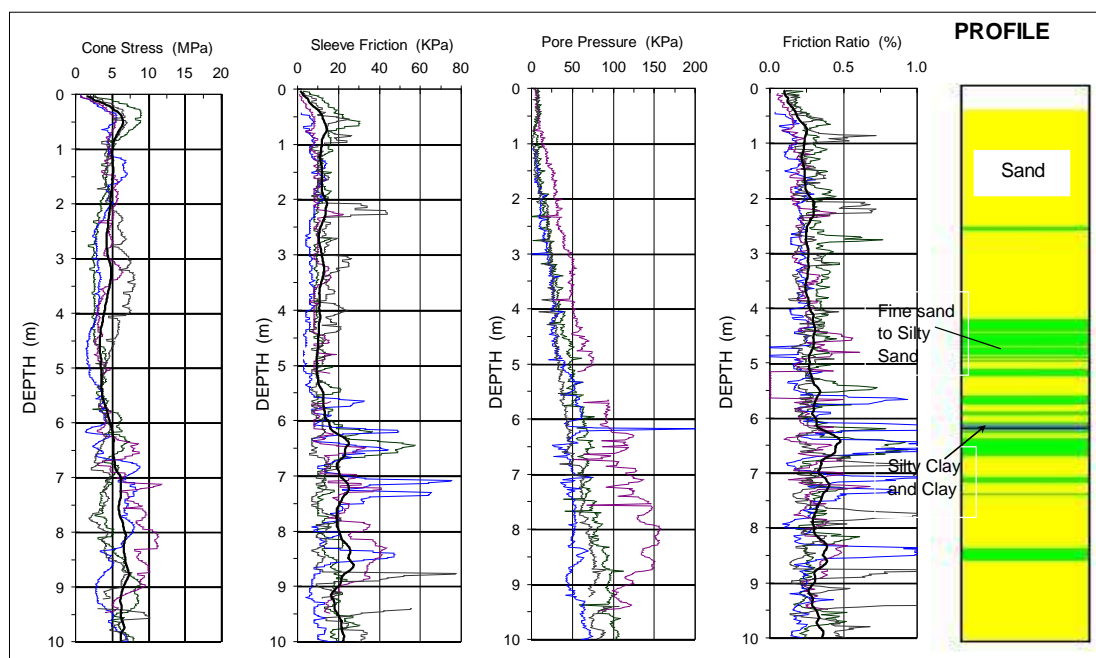


Fig. 2.36 Results of four CPTU initial (before compaction) soundings at Chek Lap Kok Airport. The heavy lines in the cone stress, sleeve friction, and friction ratio diagrams are the geometric averages for each depth of the four soundings.

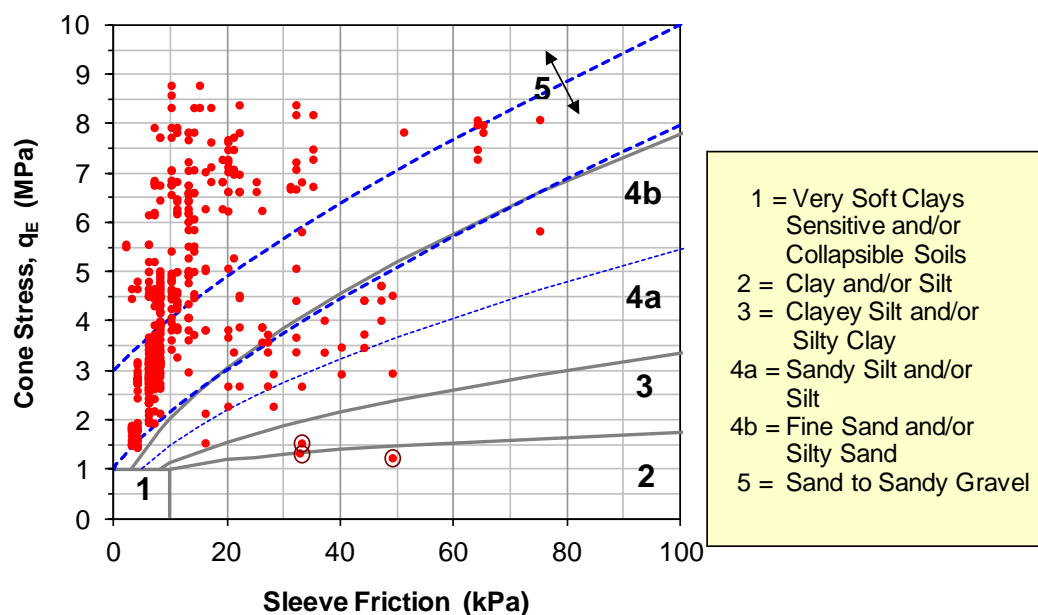


Fig. 2.37 The CPT data from one of the initial cone soundings plotted in an Eslami-Fellenius CPT profiling chart (Eslami and Fellenius 2000). The three separate dots near the boundary between Zones 2 and 3 are from the clay layer at Depth 6.1 m. (Data from Massarsch and Fellenius 2002).

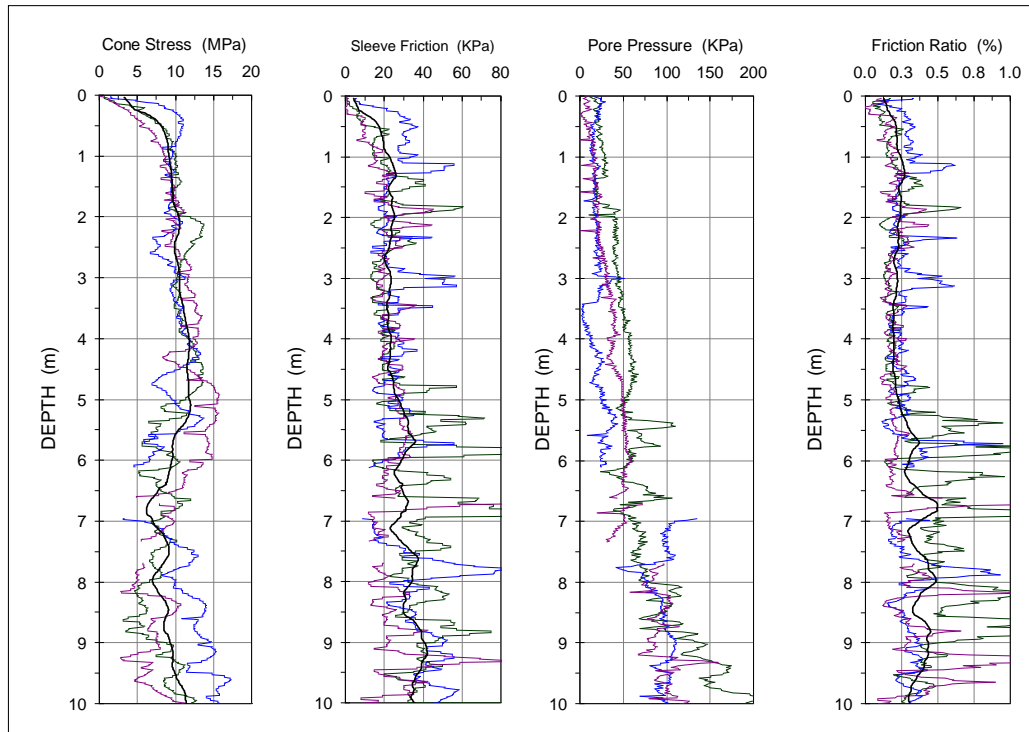


Fig. 2.38 Results of three CPTU soundings at Chek Lap Kok Airport seven days after the vibratory compaction. The heavy lines in the cone stress, sleeve friction, and friction ratio diagrams are the geometric averages for each depth of the four soundings

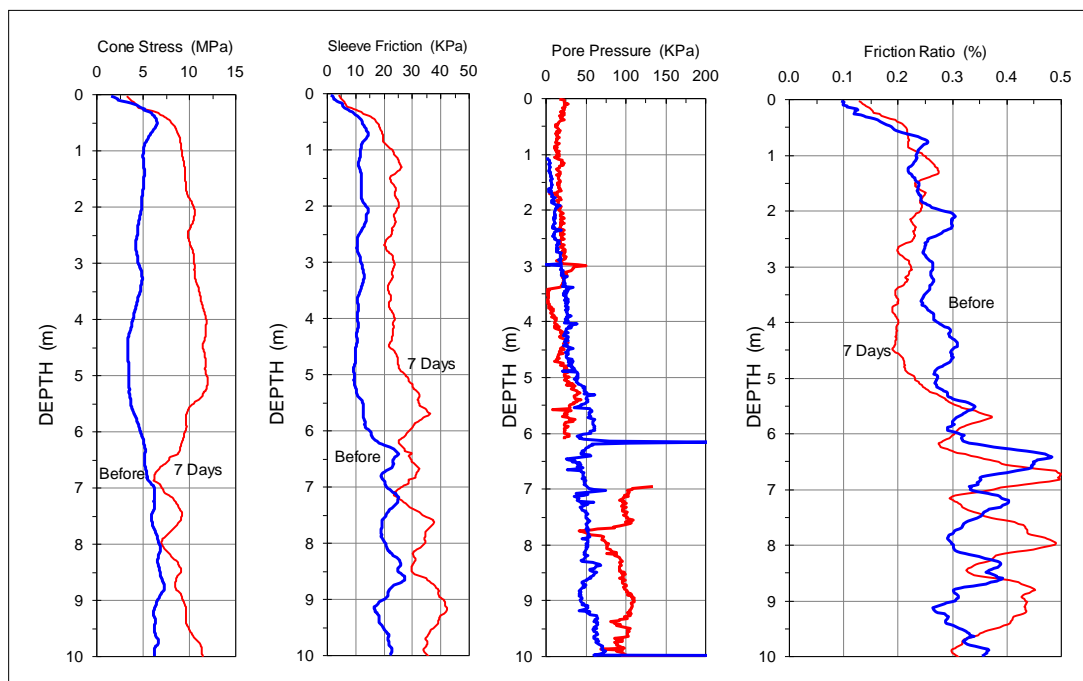


Fig. 2.39 Geometric average values of cone stress, sleeve friction, and friction ratios and measured pore pressures from CPTU soundings at Chek Lap Kok Airport before and seven days after the vibratory compaction

Figure 2.40 shows the data points in an Eslami-Fellenius profiling chart, implying a coarser soil than that shown by the sounding before the compaction (Figure 2.38). Of course, the soil composition is the same (but for minor variation below about 9 m depth, where the seven-day sounding encountered clay lenses not found in the "before" sounding). The densification has changed the sand from a normally consolidated sand to an overconsolidated sand. As a result, the points plot higher up in the chart implying a coarser soil than found in the "before" sounding.

For purpose of demonstrating the seismic analysis described above, the susceptibility for liquefaction at the site is assumed to be affected by an earthquake of magnitude of 7.5 and a seismic acceleration of 30 % of gravity. This assumption determines the site-specific Cyclic Resistance Ratio,  $CRR$ , according to Eqs. 2.13 through 2.15. The cone stress measurements determine the Cyclic Stress Ratio,  $CSR$ , from the "before" and "after" soundings, and the factor of safety against liquefaction is the  $CSR$  divided by the  $CRR$  as defined in Eq. 2.20. Figure 2.41 shows the calculated factors of safety for the before-and-after compaction and Figure 2.42 the before-and-after compaction Janbu modulus numbers. The results demonstrate that the compaction was highly efficient above about 6 m depth and plain efficient in the finer soils below (fine sand and silt are not as suitable for compaction as sand; Massarsch 1991).

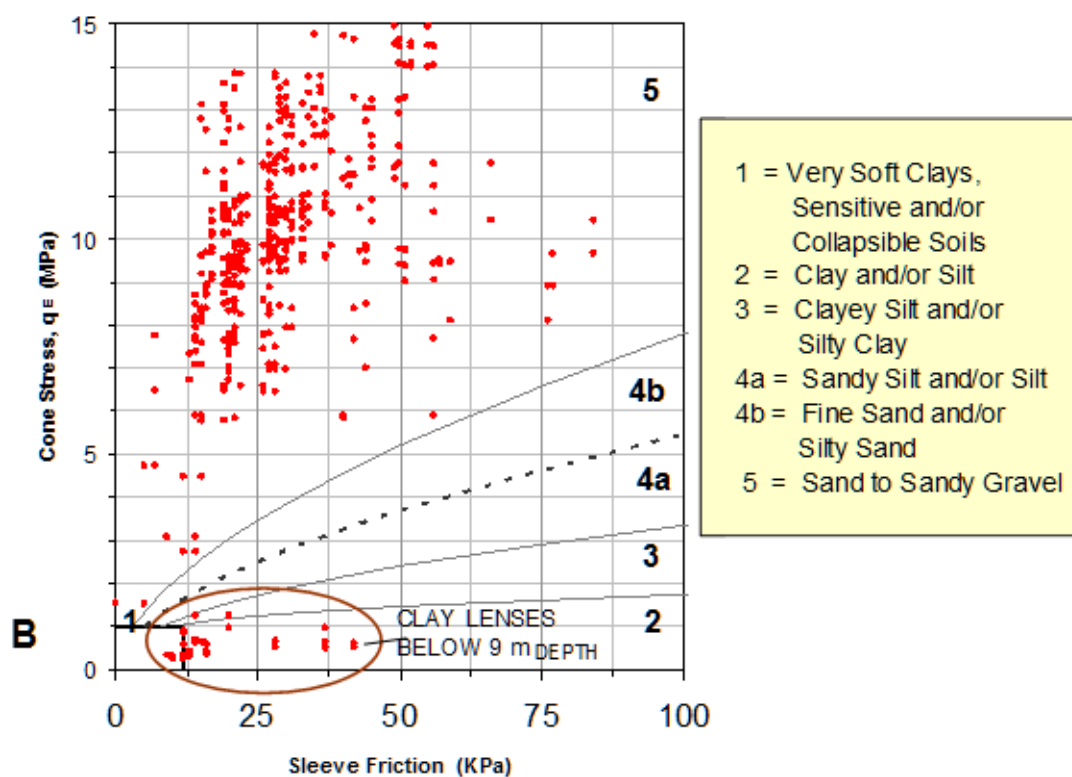


Fig. 2.40 The CPT data from one of the 7-day after compaction cone soundings plotted in an Eslami-Fellenius profiling chart (Eslami and Fellenius 2000)



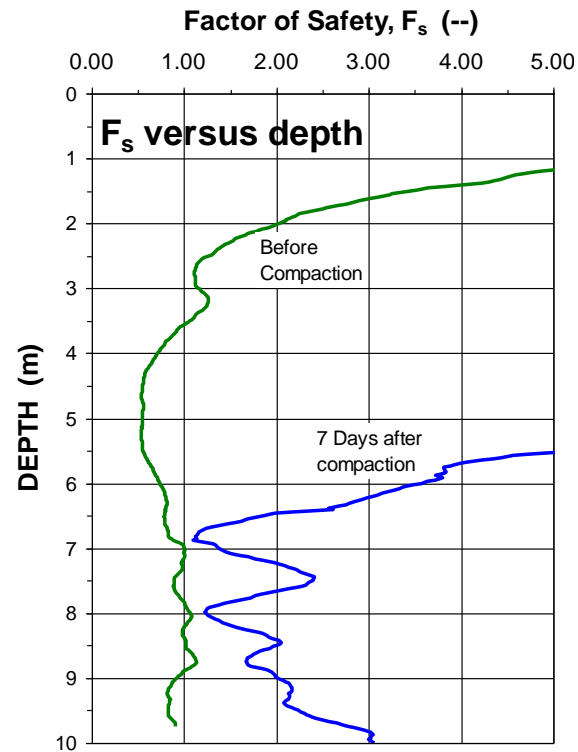


Fig. 2.41 Factor of safety against liquefaction before and after vibratory compaction

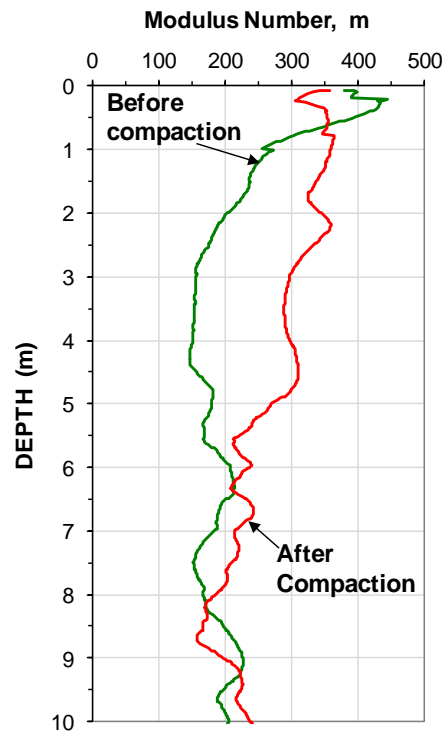


Fig. 2.42 Modulus number,  $m$ , before and after vibratory compaction

### 2.12.8.5      **Compaction/Densification from Pile Driving**

Driving pile in loose sand frequently raises concern for the pile driving vibration causing settlement for adjacent foundations, as is discussed in section 9.14 and 9.15. Section 2.12.8.5 presented seismic remediation (densification) of a site exhibiting loose sand by means of vibratory treatment. An alternative treatment is densification achieved by driving piles, usually wood piles. A small densification effect results from the fact that the piles force the soil to occupy a smaller volume, sharing the original volume with the piles, as it were. However, this effect is marginal, about 50 % of the pile volume is displacement and heave and, unless the pile spacing is very small, the remainder volume does not make for any significant reduction (i.e., densification of the soil). The desired densification effect is mainly achieved by the dynamic forces transmitted from the pile to the soil from the pile driving. The larger the dynamic force, the more pronounced the densification effect. A quandary is that some hammers do not produce much dynamic force when driving a pile in loose soil. A good soil resistance is needed, in particular toe resistance, before a sufficient dynamic force that densifies the soil can be imparted. The pile driving hammer impact produces a dynamic force along a pile that is transmitted to the soil. The impact force is a function of the impact velocity of the drop weight or ram. However, for diesel hammers, the dynamic force is also a function of the soil response. This is because, when the pile toe is in loose soil, the reflected force wave is weaker and cannot send the ram back up as high as opposed to when the soil resistance is larger. When ram travel of the diesel hammer is thus shortened, the impact force is smaller and cannot compress the fuel mix in the combustion chamber as much and, therefore, a smaller combustion force will develop as opposed to when the pile toe encounters stronger soil resistance (see Chapter 9). This was demonstrated at the Mission Bridge in B.C., Canada, where wood piles were driven in order to provide liquefaction remediation (D.W. Mitchell, Vancouver Pile Driving Ltd.; personal communication).

Figure 2.43 contains the records of two CPTU soundings, "Area A" and "Area B", pushed before any piles were driven at the site (courtesy of W. Schwartz, Sky to Sea Drilling Ltd., Vancouver). The soundings show that the soil profile consists of about 9 m of mostly compact (Area A) and mostly very loose to loose (Area B) sand with silt, both followed by mostly compact sand with occasional loose layers. The sand became dense below about 20 m depth. The curve labeled "(B)F<sub>s</sub>" is the safety against liquefaction according to Eq. 2.22 for the CPTU in Area B determined from input of an earthquake magnitude, *M*, of 7.5 (i.e., *MWF* = 1.0) and a peak horizontal acceleration, *a*<sub>max</sub>, of 0.3 g (Vancouver, BC, lies in a high-risk earthquake zone). The *F<sub>s</sub>* is larger than unity above 9 m depth for this CPTU sounding, but considering the small *q<sub>t</sub>*-values, the upper 9 m of sand would probably liquefy if a large earthquake would strike the area (or rather, when it does). Figure 2.44 shows the CPTU soil classification chart (linear abscissa scale). Open and closed symbols are from Areas A and B, respectively.

The two figures show that upper 9 m thick zones are different in the two areas. In Area A, it is coarser than in Area B and not loose, but compact. In contrast, below 9 m depth, there is little difference.

The densification wood piles were about 10 to 13-inch top diameter (top of tree; pile toe) and 13 to 15-inch butt diameter driven in 12 m lengths that were spliced at the site. Splicing was with joining the two lengths by a plate with a short dowel attached to each side. The pile spacing was 1.25 m (about 3.5 pile diameters). The project specifications called for driving the piles with a diesel hammer or hydraulic hammer (at pile locations where the headroom was low). However, nobody wants to do a splice with a heavy diesel hammer 15 m up in the air nor attempt to carry out the light tapping needed for completing the splice with a diesel hammer. It was therefore proposed to shift to using a gravity hammer (drop hammer). To meet the somewhat surprising argument that a drop hammer could not achieve the desired level of densification, a limited test was carried out comprised of one CPTU sounding pushed in each area before and one pushed after piles had been driven. In Area A, the piles were driven with a Birmingham B300 diesel hammer (1,700 kg ram). In Area B, the piles were driven with an APE7.5, a hydraulic hammer with a 5,500 kg ram and a stroke limited to 0.6 m and with a 2,500-kg drop hammer.

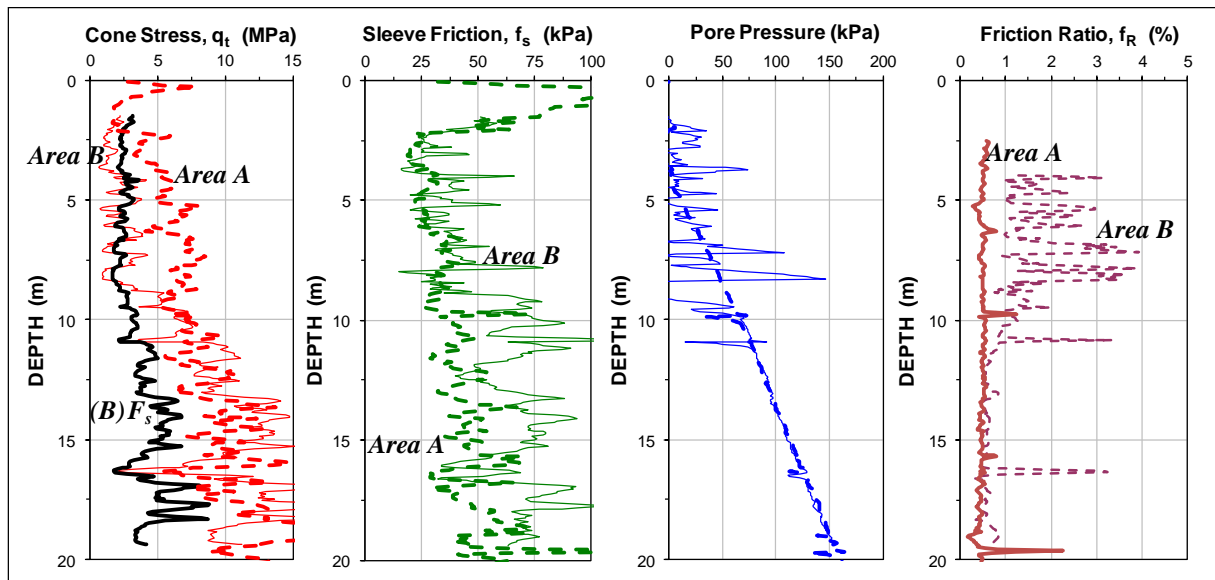


Fig. 2.43 Typical CPTU sounding from before the pile driving

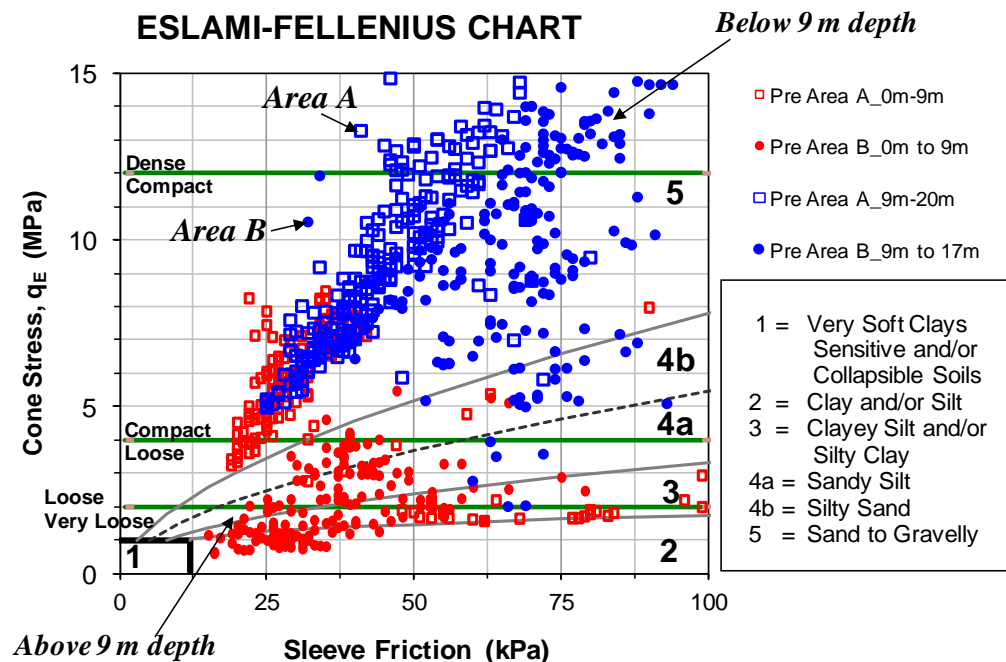


Fig. 2.44 Classification chart from the CPTU sounding shown in Figure 2.41

Similar to the study of the effect of the vibratory compaction project summarized in Section 2.12.8.4, assessing before and after results of densification—compaction—can be by direct qualitative comparison between pre- and post- cone-stress distributions. The best quantitative comparison is by means of the modulus number calculated from the CPTU results, as shown in Figures 2.45 through 2.47. The figures show the cone stress and modulus number records from before and after the driving in Area A (Berminghammer B300) and Area B (hydraulic and drop hammers). No information is available on

hammer setting and no dynamic or geophysical monitoring was undertaken in the test (see Chapter 9), which is regrettable, as such monitoring provides the best means for assessing the densification effect of the vibrations introduced by the compaction work.

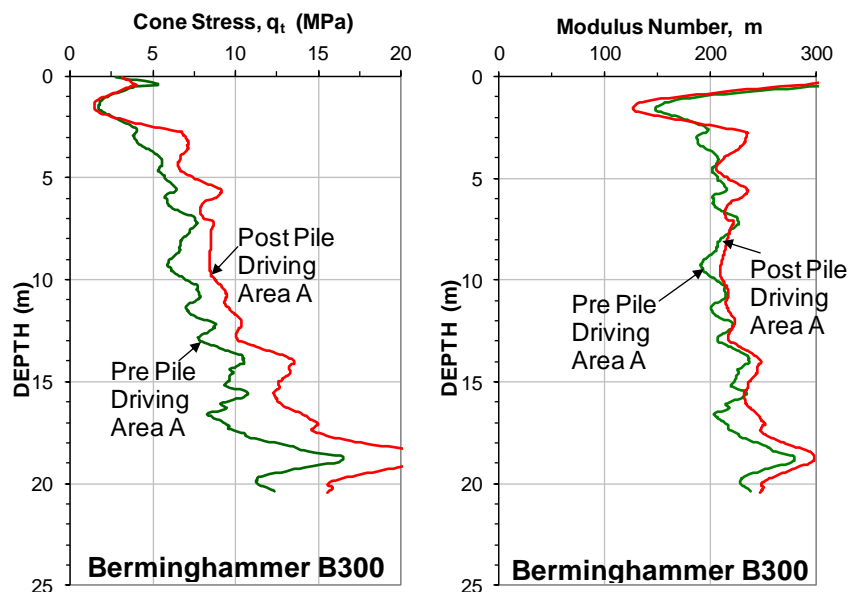


Fig. 2.45 Distribution of cone stress,  $q_t$ , and modulus number,  $m$ .  
Area A, zone of piles driven with Berminghammer 300 diesel hammer

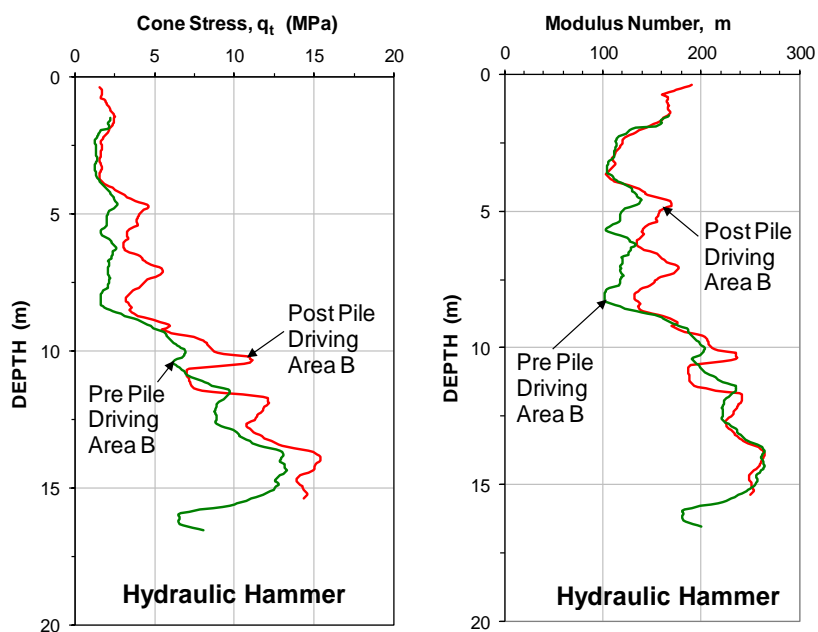


Fig. 2.46 Distribution of cone stress,  $q_t$ , and modulus number,  $m$ .  
Area B, zone of piles driven with APE 7.5a Hydraulic hammer

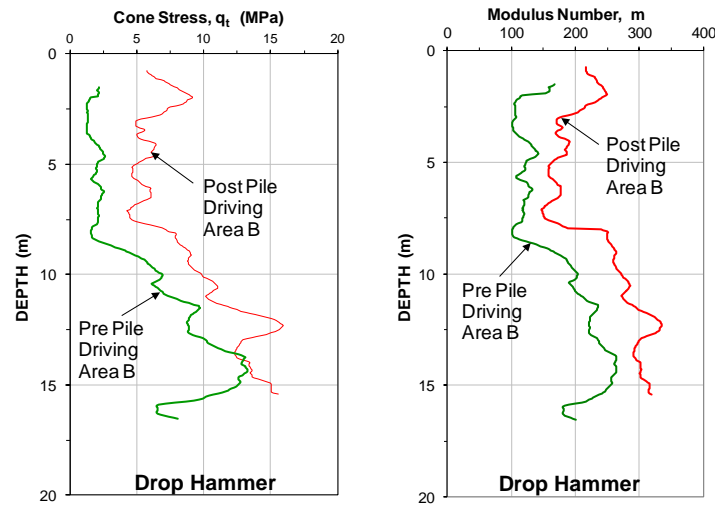


Fig. 2.47 Distribution of cone stress,  $q_t$ , and modulus number,  $m$ , Area B, zone of piles driven with a drop hammer

The Berminghammer B300 and the hydraulic hammers appear to have achieved a moderate densification. In contrast, where the piles were driven with the drop hammer, the results show that the drop hammer not only densified the sand, the densification was also more pronounced than for the mechanical hammers, illustrating, as mentioned, that the dynamic force transmitted to the soil can, when desired, be maintained when using the drop hammer.

Figure 2.48 shows a comparison between the pre- and post pile driving CPTU records indicating a pronounced increase of cone stress and sleeve friction to about 9 m depth. Also below 9 m, an increase of cone stress due to the compaction effect is evident, but not so for the sleeve friction as would have been expected. This is also indicated in the classification chart shown in Figure 2.49. The pile driving was with the drop hammer for the first pile segment and with the ASPE 7.5a after the splicing. It should be noted that the locations of the pre and post CPT-soundings are some 15 m apart.

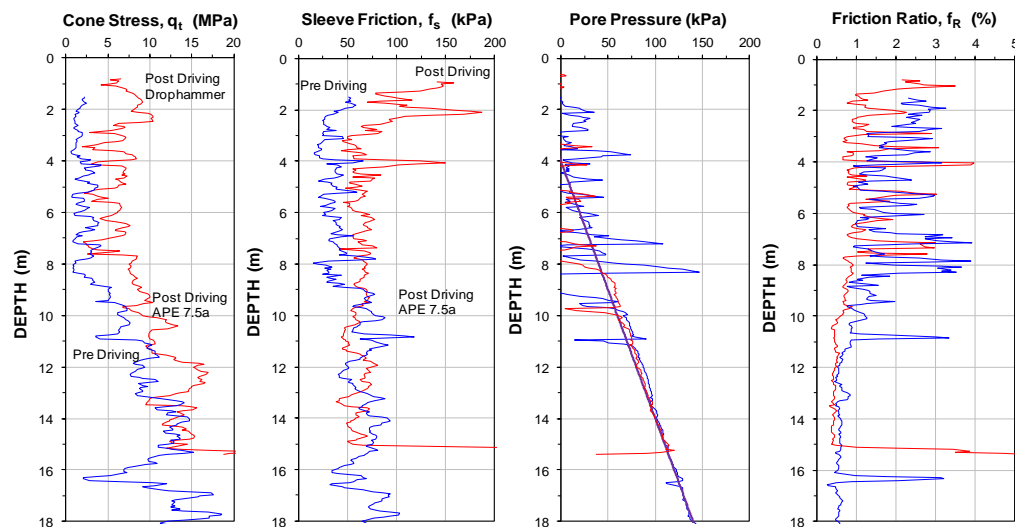


Fig. 2.48 Distribution of cone stress,  $q_t$ , sleeve friction,  $f_s$ , and pore pressure,  $U_2$ , before and after the pile driving

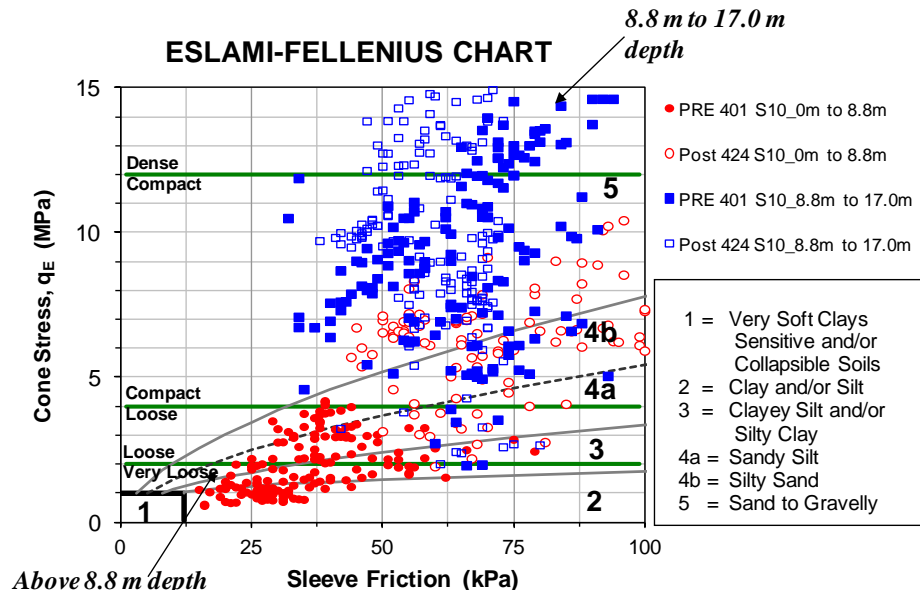


Fig. 2.49 Area B, pre and post CPTU classification Chart (Eslami-Fellenius)

The post-driving sleeve friction versus the pre-driving sleeve friction is shown in Figure 2.48. Above 8.8 m depth, the post-driving sleeve friction increased. However, below 8.8 m there was no significant increase and the ratio between post-driving and pre-driving records stayed at about unity.

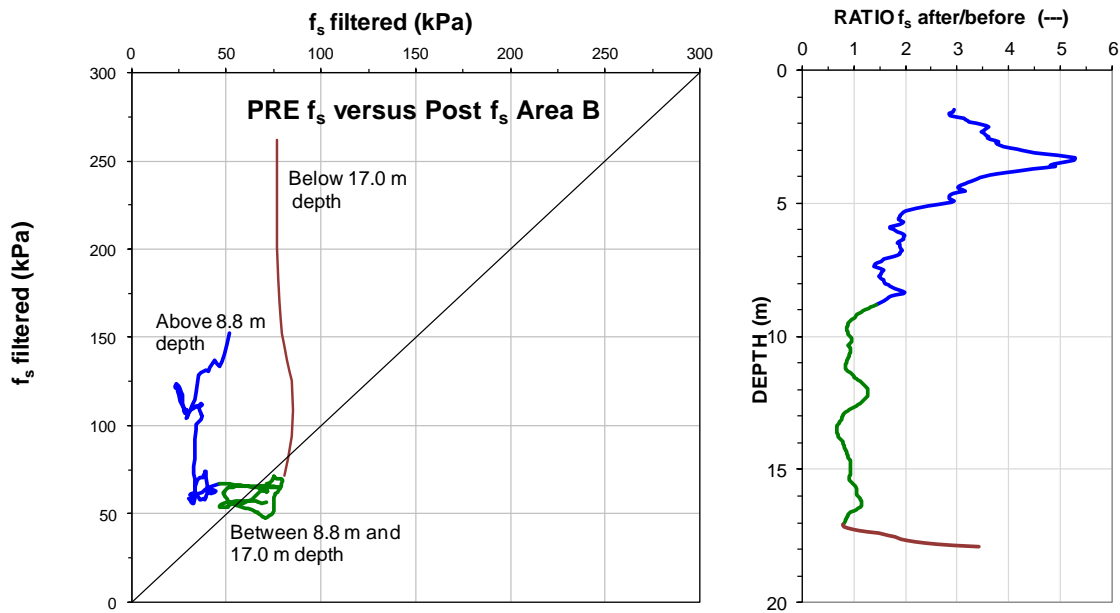


Fig. 2.50 Post-driving versus pre-driving sleeve friction,  $f_s$ , and distribution of the ratio between post-driving and pre-driving sleeve friction,  $f_s$ ,

## CHAPTER 3

### SETTLEMENT CALCULATION

#### 3.1 Introduction

A foundation is a constructed unit that transfers the load from a superstructure to the ground. With regard to vertical loads, most foundations receive a more or less concentrated load from the superstructure and transfer this load to the soil underneath the foundation, distributing the load as a stress over the “footprint” of the foundation. The foremost requirement for a proper foundation is that the change of stress due to the soil-structure interaction must not give rise to a deformation of the soil that results in a settlement of the superstructure in excess of what the superstructure can tolerate.

Deformation is expressed by the terms movement, displacement, and settlement. The terms are not synonyms—they are related, but not equal. It is important not to confuse them.

Settlement analysis must combine the classical, well-established consolidation theory with immediate and secondary compression. Calculating settlement as a part of a design, which is in fact a prediction, is relatively easy. The problem is knowing what input parameters to apply. The knowledge is gained by back-calculating records of actual measurements. There are quite a few available.

#### 3.2 Movement, Settlement, Consolidation, and Secondary Compression

**Movement** occurs as a response when a stress is applied to a soil, but the term should be reserved to deformation due to *increase of total stress*. Movement is the result of a transfer of stress to the soil (the movement occurs as necessary to build up the resistance to the load), when the involved, or influenced, soil volume successively increases as the stress increases. For example, movement results when load increments are added to a pile or to a plate in a static loading test (where, erroneously, the term “settlement” is often used instead of “movement”). As a term, movement is used when the involved, or affected, soil volume increases as the load gets larger.

**Settlement** is volume reduction of soil volume as a consequence of an *increase in effective stress* (and it should not be used when referring to deformation due to incremental increase of total stress, such as in a loading test). Settlement consists of either one or the sum of immediate compression, consolidation settlement, and secondary compression (secondary compression is included here because it is initiated by a change of effective stress although it occurs without change of effective stress, see below). As a term, “settlement” is used when the total stress is constant and the involved, or influenced, soil zone stays the same during the increase of the effective stress.

**Immediate compression** (also often called immediate settlement) is the result of compression of the soil grains (soil skeleton) and of volume reduction of any free gas present in the voids. It is usually assumed to be linearly proportional to the change of stress (i.e., assumed ‘elastic’). The immediate compression is therefore often called ‘elastic’ compression. It occurs quickly and is normally small (it is not associated with expulsion of water, i.e., consolidation).

**Consolidation** (also called primary consolidation) is volume reduction due to increase in effective stress with dissipation of pore pressures (expelling water from the soil body). In the process, the imposed stress, initially carried by the pore water, is transferred to the soil structure. Consolidation occurs quickly in coarse-grained soils, but slowly in fine-grained soils.

**Secondary Compression** is a term for compression (of the soil skeleton) occurring *without an increase of effective stress*, but it is triggered by the change of effective stress. Of course, there is an expulsion of water in the process, but the slow long-term compression occurs without appreciable increase or change of stress or pore pressure. Sometimes, the term "creep" is used to mean secondary compression, but avoid this because "creep" should be restricted to conditions of shear. Secondary compression is usually small, approximately similar in magnitude to the immediate compression, but it may over time add significantly to the total deformation of the soil. Secondary compression can be very large in organic soils and then actually result in an increase of pore pressure or a continuously maintained small excess pore pressure—a "self-induced consolidation" (Chang 1981).

The magnitude of the consolidation settlement is a function of the *relative increase of effective stress*: The larger the existing effective stress before a specific additional stress is applied, the smaller the induced settlement. For this reason, most soil materials do not show a linear relation between stress and strain. Cohesive soils, in particular, have a distinct stress-strain non-linearity. The exception being, for example, very dense soils, such as glacial clay tills, where the stress-strain behavior can be approximated to a linear relation. A special case of non-linearity occurs for a stress-increase beyond the preconsolidation stress in an over-consolidated soil ("pre-consolidation" is stress that is larger than the current effective overburden stress in the soil), resulting in a stress-strain behavior that is much more compressible beyond the preconsolidation stress than below. An increase of effective stress within the preconsolidation range does not trigger consolidation unless the stress increase has caused an increase of pore pressure, then, usually only to a small degree.

The amount of deformation for a given contact stress depends on the distribution of that stress change (relative existing stress) in the affected soil mass and the compressibility of the soil layer. The change of effective stress is the difference between the initial (original) effective stress and the final effective stress. (See Chapter 1 and Table 1.6 for an example of how to calculate the distribution of the effective stresses at a site).

### 3.3 Linear Deformation ("Elastic")

Linear stress-strain behavior follows Hooke's law ("elastic modulus method") according to Eq. 3.1.

$$(3.1) \quad \varepsilon = \frac{\Delta\sigma'}{E}$$

where

$\varepsilon$	=	induced strain in a soil layer
$\Delta\sigma'$	=	imposed change of effective stress in the soil layer
$E$	=	elastic modulus of the soil layer

The "elastic modulus" is often called Young's modulus. Strictly speaking, however, Young's modulus is the modulus when lateral expansion is allowed. When no, or next to no, lateral expansion is "allowed", the modulus is called "constrained modulus",  $D$  (or  $M$ ), and it is larger than the Young modulus,  $E$ . The constrained modulus is also called the "oedometer modulus". For ideally elastic soils, the ratio between  $D$  and  $E$  is shown in Eq. 3.2.

$$(3.2) \quad \frac{D}{E} = \frac{(1 - \nu)}{(1 + \nu)(1 - 2\nu)}$$



where       $D$     =    constrained modulus  
                $E$     =    Young's modulus  
                $\nu$    =    Poisson's ratio

Poisson's ratio expresses how a compression in the direction of loading is counteracted by lateral expansion in the perpendicular direction. Incompressible materials have a Poisson's ratio of 0.5. Such materials may compress in the direction of loading, but the volume is unchanged. For a soil material with a Poisson's ratio of 0.3, a common value, the constrained modulus is 35 % larger than the Young's modulus. (As an illustration, unrelated to settlement of soils, but not to foundation engineering: the concrete inside a concrete-filled thick-wall pipe pile behaves as a constrained material as opposed to the concrete in a concrete pile. Therefore, when analyzing the deformation under load, the constrained modulus needs to be used for the former and the Young's modulus for the latter).

The deformation of a soil layer,  $s$ , is the strain,  $\varepsilon$ , times the thickness,  $h$ , of the layer. The settlement,  $S$ , of the foundation is the sum of the deformations of the soil layers below the foundation (Eq. 3.3).

$$(3.3) \quad S = \sum s = \sum (\varepsilon h)$$

### 3.4 Non-Linear Deformation

Stress-strain behavior is non-linear for most soils. The non-linearity cannot be disregarded when analyzing compressible soils, such as silts and clays, that is, the linear elastic modulus approach is not appropriate for these soils. Non-linear stress-strain behavior of compressible soils is conventionally modeled by Eq. 3.4.

$$(3.4) \quad \varepsilon = \frac{C_c}{1 + e_0} \lg \frac{\sigma'_1}{\sigma'_0} = CR \lg \frac{\sigma'_1}{\sigma'_0}$$

where     $\varepsilon$     =    strain induced by increase of effective stress from  $\sigma'_0$  to  $\sigma'_1$   
            $C_c$    =    compression index  
            $e_0$    =    initial void ratio  
            $\sigma'_0$    =    original (or initial) effective stress  
            $\sigma'_1$    =    final effective stress  
            $CR$    =    compression ratio =  $C_c/(1 + e_0)$ ; see explanation in the paragraph immediately before Eq. 3.6.

The compression index and the void ratio parameters,  $C_c$  and  $e_0$ , are determined by means of oedometer (consolidometer; compressometer) tests in the laboratory.

If the soil is overconsolidated, that is, consolidated to a stress (called preconsolidation stress),  $\sigma'_p$ , larger than the existing effective stress, Eq. 3.4 changes to Eq. 3.5.

$$(3.5) \quad \varepsilon = \frac{1}{1 + e_0} \left( C_\sigma \lg \frac{\sigma'_p}{\sigma'_0} + C_c \lg \frac{\sigma'_1}{\sigma'_p} \right) \quad \text{and} \quad \varepsilon = \frac{1}{1 + e_0} C_\sigma \lg \frac{\sigma'_1}{\sigma'_0} \quad \text{when } \sigma'_1 < \sigma'_p$$

where  $\sigma'_p$  = preconsolidation stress ( $=\sigma'_0 + \Delta\sigma'_c$ )  
 $\Delta\sigma'_c$  = preconsolidation margin  
 $C_c$  = re-compression index

Thus, in conventional engineering practice of settlement design, two compression parameters need to be established; the  $C_c$  and the  $e_0$ . Actually, on surprisingly many occasions, geotechnical engineers only report the  $C_c$ , neglecting to include the  $e_0$ . Worse, when they do report both parameters, they often report the  $C_c$  from the oedometer test and the  $e_0$  from a different soil specimen than that used for determining the compression index! This is not acceptable, of course. The undesirable challenge of ascertaining what  $C_c$ -value goes with what  $e_0$ -value is removed by using the Janbu tangent modulus approach instead of the  $C_c$  and  $e_0$  approach, applying the Janbu modulus number,  $m$ , instead, as determined directly from the oedometer test as presented in Section 3.5.

The inconvenience of having to employ two parameters is also avoided by the MIT approach, where the compressibility of the soil is characterized by the ratios  $C_c/(1 + e_0)$  and  $C_{cr}/(1 + e_0)$  as single parameters (usually called Compression Ratio, CR, and Recompression Ratio, RR, respectively). See Section 3.7.

As an aside, Swedish and Finnish practices apply a strain value, called  $\varepsilon_2$ , equal to the strain for a doubling of the applied stress. For the latter, Eq. 3.5 becomes:

$$(3.6) \quad \varepsilon = \frac{\varepsilon_{2r}}{\lg 2} \lg \frac{\sigma'_p}{\sigma'_0} + \frac{\varepsilon_2}{\lg 2} \lg \frac{\sigma'_1}{\sigma'_p}$$

where  $\varepsilon_{2r}$  = " $\varepsilon_2$ -compressibility" for reloading  
 $\varepsilon_2$  = " $\varepsilon_2$ -compressibility" for virgin loading

### 3.5 The Janbu Approach

#### 3.5.1 General

The Janbu approach, proposed by Nilmar Janbu in the early 1960s (Janbu 1963; 1965; 1967), and referenced by the Canadian Foundation Engineering Manual, CFEM (1985, 1992), combines the basic principles of linear and non-linear stress-strain behavior. The method applies to all soils, clays as well as sand. By the Janbu method, the relation between stress and strain is simply a function of two non-dimensional parameters that are unique for any soil: a stress exponent,  $j$ , and a modulus number,  $m$ . (Strictly, the modulus is for constrained ("oedometer") condition). Professor Janbu has presented a comprehensive summary of his method (Janbu 1998).

The Janbu approach is based on the definition of the conventional tangent modulus,  $M_t = \partial\sigma/\partial\varepsilon$ , by the following expression (Eq. 3.7).

$$(3.7) \quad M_t = \frac{\partial\sigma}{\partial\varepsilon} = m\sigma_r \left(\frac{\sigma'}{\sigma_r}\right)^{1-j}$$

where  $\varepsilon$  = strain induced by increase of effective stress  
 $\sigma'$  = effective stress  
 $j$  = a stress exponent  
 $m$  = a modulus number (with a subscript,  $m_r$ , for recompression modulus number)  
 $\sigma'_r$  = a reference stress, a constant, which for all practical purposes is equal to 100 kPa ( $\approx 1$  tsf  $\approx 2$  ksf  $\approx 1$  kg/cm<sup>2</sup>  $\approx 1$  at)

The Janbu expressions for strain are derived as follows.

### 3.5.2 Cohesionless Soil — $j > 0$

For cohesionless soil, the stress exponent is larger than zero,  $j > 0$ . Integrating Eq. 3.7 results in Eq. 3.8.

$$(3.8) \quad \varepsilon = \frac{1}{mj} \left[ \left( \frac{\sigma'_1}{\sigma'_r} \right)^j - \left( \frac{\sigma'_0}{\sigma'_r} \right)^j \right]$$

where  $\varepsilon$  = strain induced by increase of effective stress  
 $\sigma'_0$  = original effective stress  
 $\sigma'_1$  = final effective stress  
 $j$  = stress exponent  
 $m$  = modulus number, which is determined from laboratory and/or field testing  
 $\sigma'_r$  = reference stress, a constant, which is equal to 100 kPa ( $\approx 1 \text{ tsf} \approx 2 \text{ ksf} \approx 1 \text{ kg/cm}^2 \approx 1 \text{ at}$ )

Mathematically, any stress exponent value larger than zero can be used. An exponent equal to unity indicates a linear stress-deformation response to load. A value smaller than unity agrees with the observation that for each increment stress the deformation of a soil volume becomes progressively smaller. A value larger than unity implies a soil where the incremental deformation increases with increasing stress. The latter has no practical application other than the fact that it, on occasion, can be useful in curve-fitting to observed records of stress or load versus movement, e.g., in dilative soil subjected to shear forces.

### 3.5.3 Dense Coarse-Grained Soil — $j = 1$

The stress-strain behavior (settlement) in dense coarse-grained soils, such as glacial till, can be assumed to be 'elastic', which means that the stress exponent is equal to unity ( $j = 1$ ) and the compression is 'linearly elastic'. It is normally assumed that **immediate compression** is linearly elastic, i.e.,  $E_i$  and  $m_i$  are constant and the stress exponent,  $j$ , is equal to unity. By inserting  $j = 1$  and considering that the reference stress,  $\sigma_r$ , is equal to 100 kPa, Eq. 3.7 becomes Eq. 3.9.

$$(3.9) \quad \varepsilon = \frac{1}{100 m} (\sigma'_1 - \sigma'_0) = \frac{1}{100 m} \Delta \sigma'$$

Notice, because the reference stress is inserted with a value in the SI-system of units, Eq. 3.9 presupposes that  $E$  is given in the same system of units, i.e., in Pa. If the units for  $E$  are in tsf or ksf, Eq. 3.9 changes to Eqs. 3.9a or 3.9b, respectively.

$$(3.9a) \quad \varepsilon = \frac{1}{m} (\sigma'_1 - \sigma'_0) = \frac{1}{m} \Delta \sigma' \quad (3.9b) \quad \varepsilon = \frac{1}{2 m} (\sigma'_1 - \sigma'_0) = \frac{1}{2 m} \Delta \sigma'$$

Comparing Eqs. 3.1 and 3.9 for soils with a stress exponent of unity and considering that the reference stress,  $\sigma_r$ , is equal to 100 kPa, for  $E$  in units of kPa, tsf, and ksf, the respective relations between the modulus number and the  $E$ -modulus are (again, the "E" is, strictly speaking, the constrained modulus, and I should really be using the symbol "M" and not "E"):

$$(3.10) \quad m = E/100 \quad (3.10a) \quad m = E \quad (3.10b) \quad m = E/2$$

### 3.5.4 Sandy or Silty Soil — $j = 0.5$

Janbu's original concept considered a gradual increase of the stress exponent,  $j$ , from zero to unity when going from clay to dense gravel, though applying a gradual change is considered unnecessary in practice. Values of " $j$ " other than  $j = 0$  or  $j = 1$ , are only used for **sandy or silty** soils, where the stress exponent is often taken as equal to 0.5. (It actually reduces with decreasing grain size, but  $j = 0.5$  is usually an acceptable average). By inserting this value and considering that the reference stress is 100 kPa, Eq. 3.7 simplifies to Eq. 3.11. For a soil, which is expected to have a non-linear response ( $j = 0.5$ ), where an average E-modulus is known for a range of stress, combining Eqs. 3.9 and 3.11 can enable a modulus number to be calibrated from (i.e., fitted to) a known E-modulus and stress range.

The Janbu modulus number can also be estimated from results of a CPTU sounding, as described in Section 2.11. This is an advantage of the Janbu approach because determining compressibility of coarse-grained soils in the laboratory is difficult.

$$(3.11) \quad \varepsilon = \frac{1}{5m} (\sqrt{\sigma'_1} - \sqrt{\sigma'_0}) \quad \text{units in kPa}$$

Notice, Eq. 3.11 is not independent of the choice of units and the stress values must be inserted in kPa. That is, a value of 5 MPa is to be inserted as "5,000" and a value of 300 Pa as "0.3".

In English units and with stress in units of tsf or, alternatively, in ksf, Eq. 3.11 becomes

$$(3.11a) \quad \varepsilon = \frac{2}{m} (\sqrt{\sigma'_1} - \sqrt{\sigma'_0}) \quad \text{units in tsf} \quad (3.11b) \quad \varepsilon = \frac{\sqrt{2}}{m} (\sqrt{\sigma'_1} - \sqrt{\sigma'_0}) \quad \text{units in ksf}$$

Take care, the equations are not independent of units—to repeat, in Eqs. 3.10a and 3.10b, the stress units must be inserted in units of tsf and ksf, respectively.

If the soil is **overconsolidated** and the final stress exceeds the preconsolidation stress, Eqs. 3.11, 3.11a and 3.11b change to:

$$(3.12) \quad \varepsilon = \frac{1}{5m_r} (\sqrt{\sigma'_p} - \sqrt{\sigma'_0}) + \frac{1}{5m} (\sqrt{\sigma'_1} - \sqrt{\sigma'_p}) \quad \text{units in kPa}$$

$$(3.12a) \quad \varepsilon = \frac{2}{m_r} (\sqrt{\sigma'_p} - \sqrt{\sigma'_0}) + \frac{2}{m} (\sqrt{\sigma'_1} - \sqrt{\sigma'_p}) \quad \text{units in tsf}$$

$$(3.12b) \quad \varepsilon = \frac{\sqrt{2}}{m_r} (\sqrt{\sigma'_p} - \sqrt{\sigma'_0}) + \frac{\sqrt{2}}{m} (\sqrt{\sigma'_1} - \sqrt{\sigma'_p}) \quad \text{units in ksf}$$

where  $\sigma'_0$  = original effective stress (kPa, tsf, and ksf, respectively)  
 $\sigma'_p$  = preconsolidation stress (kPa, tsf, and ksf, respectively)  
 $\sigma'_1$  = final effective stress (kPa, tsf, and ksf, respectively)  
 $m$  = modulus number (dimensionless)  
 $m_r$  = recompression modulus number (dimensionless)

If the soil is overconsolidated and the imposed stress does not result in a new (final) stress that exceeds the preconsolidation stress, Eqs. 3.12, 3.12a, and 3.12b become:

$$(3.13) \quad \varepsilon = \frac{1}{5m_r} (\sqrt{\sigma'_1} - \sqrt{\sigma'_0}) \quad \text{units in kPa}$$

$$(3.13a) \quad \varepsilon = \frac{2}{m_r} (\sqrt{\sigma'_1} - \sqrt{\sigma'_0}) \quad \text{units in tsf}$$

$$(3.13b) \quad \varepsilon = \frac{\sqrt{2}}{m_r} (\sqrt{\sigma'_1} - \sqrt{\sigma'_0}) \quad \text{units in ksf}$$

In a cohesionless soil, where the stress exponent is 0.5 and where previous experience exists from settlement analysis using the elastic modulus approach (Eqs. 3.1 and 3.3), a direct conversion can be made between E and m, which results in Eq. 3.14.

Notice, stress and E-modulus (or D-modulus) must be input in the same units, normally kPa for analyses using SI-units. When using English units (stress and modulus in tsf or ksf), Eqs. 3.14a and 3.14b apply).

$$(3.14) \quad m = \frac{E}{5(\sqrt{\sigma'_1} + \sqrt{\sigma'_0})} = \frac{E}{10\sqrt{\sigma'}} \quad \text{units in kPa}$$

$$(3.14a) \quad m = \frac{2E}{(\sqrt{\sigma'_1} + \sqrt{\sigma'_0})} = \frac{E}{\sqrt{\sigma'}} \quad \text{units in tsf}$$

$$(3.14b) \quad m = \frac{\sqrt{2} E}{(\sqrt{\sigma'_1} + \sqrt{\sigma'_0})} = \frac{E}{\sqrt{2}\sigma'} \quad \text{units in tsf}$$

### 3.5.5 Cohesive Soil — $j = 0$

In cohesive soil, the stress exponent is zero,  $j = 0$ . For **normally consolidated** cohesive soils, the integration of Eq. 3.6 then results in Eq. 3.15 (the formula is independent of the stress units).

$$(3.15) \quad \varepsilon = \frac{1}{m} \ln \frac{\sigma'_1}{\sigma'_0}$$

Most natural soils other than very young or organic clays are **overconsolidated**. Thus, in an overconsolidated, cohesive soil, Eq. 3.16 applies:

$$(3.16) \quad \varepsilon = \frac{1}{m_r} \ln \frac{\sigma'_p}{\sigma'_0} + \frac{1}{m} \ln \frac{\sigma'_1}{\sigma'_p}$$

Notice, the ratio  $(\sigma'_p/\sigma'_0)$  is equal to the **Overconsolidation Ratio**, OCR. However, the measure of overconsolidation is better expressed as a stress difference, or "**Preconsolidation Margin**":  $\sigma'_p - \sigma'_0$ . An oedometer test determines the preconsolidation margin for the sample, not the OCR for the profile. An OCR should therefore never be stated without being coupled to the depth to which it applies. Better then to use the preconsolidation margin as the main parameter. For example, an area that has had 2 m of soil removed now would exhibit a preconsolidation margin of about 40 kPa throughout the soil body. However, at a depth of 1 m below the new ground surface (also the groundwater table), the OCR would be about 5, reducing to only about 1.2 at 10 m depth.

By the way, soils can be normally consolidated or overconsolidated, but never "underconsolidated". The latter is just a misnomer for soils that are "undergoing consolidation". In soils undergoing consolidation, the actual effective overburden stress is equal to the actual preconsolidation stress. If piezometer measurements at a site would indicate that the effective overburden stress (remember, effective stress is equal to total stress minus pore pressure) is larger than the preconsolidation stress determined in consolidation testing, then, either, or both, of the results of the consolidation test or of the determination of effective overburden stress are wrong. "Undergoing consolidation" means that pore pressure dissipation is occurring at the site and that the pore-pressure distribution is non-linear. N.B., so is the distribution of effective stress.

If the applied foundation stress does not result in a new stress that exceeds the preconsolidation stress, Eq. 3.16 becomes Eq. 3.17.

$$(3.17) \quad \varepsilon = \frac{1}{m_r} \ln \frac{\sigma'_1}{\sigma'_0}$$

### 3.5.6 Typical Values of Modulus Number, $m$

With knowledge of the original effective stress, the increase of stress, and the type of soil involved (without which knowledge, no reliable settlement analysis can ever be made), the only soil parameter required is the modulus number. The modulus numbers to use in a particular case can be determined from conventional laboratory testing, as well as in-situ tests. As a reference, Table 3.1 shows a range of normally conservative modulus numbers,  $m$ , which are typical of various soil types (quoted from the Canadian Foundation Engineering Manual 1992). Re-compression modulus numbers,  $m_r$ , can often, but always, be expected to range from 8 to 12 times the numbers for normally consolidated conditions. A smaller ratio is often an indication of sample disturbance.

The modulus numbers in the table are approximate and mixed soils will be different. For example, a silty sand will be more compressible than a clean sand (Huang et al. 1999). Similarly, a sand containing even a small amount of mica, a few percent is enough, will be substantially more compressible than a sand with no mica (Gilboy 1928).

Designing for settlement of a foundation is a prediction exercise. The quality of the prediction, that is, the agreement between the calculated and the actual settlement value, depends on how accurately the soil

profile and stress distributions applied to the analysis represent the site conditions, and how closely the loads, fills, and excavations at the site resemble those actually occurring. The quality depends also on the quality of the soil parameters used as input to the analysis. Soil parameters for cohesive soils depend on the quality of the sampling and laboratory testing. Clay samples tested in the laboratory should be from carefully obtained ‘undisturbed’ samples. When testing overconsolidated clays, paradoxically, the more disturbed the sample is, the less compressible the clay appears to be. The error which this could cause is to a degree ‘compensated for’ by the simultaneous apparent reduction in the preconsolidation value. Furthermore, high quality sampling and oedometer tests are costly, which limits the amounts of information procured for a routine project. The designer usually runs the tests on the ‘worst’ samples and arrives at a ‘conservative’ prediction. This may be acceptable, but never so when the word ‘conservative’ is nothing but a disguise for the more appropriate terms of ‘erroneous’ and ‘unrepresentative’. Then, the end results may perhaps not even be on the ‘safe side’.

Non-cohesive soils cannot easily be sampled and tested (however, as indicated in Section 3.13, CPT sounding can be used to estimate a compressibility profile for a site). Therefore, settlement analysis of foundations in such soils must rely on empirical relations derived from in-situ tests and experience values. Usually, non-cohesive soils are less compressible than cohesive soils and have a more pronounced overconsolidation. Therefore, testing of compressibility and analysis of settlement is often considered less important for non-cohesive soils. However, considering the current trend toward larger loads and foundation stresses, cautious foundation design must address also the settlement expected in non-cohesive soils.

**TABLE 3.1 Typical and Normally Conservative Modulus Numbers**

SOIL TYPE		MODULUS NUMBER	STRESS EXP.
Till, very dense to dense		1,000 — 300	(j=1)
Gravel		400 — 40	— " —
Sand	dense	400 — 250	(j=0.5)
	compact	250 — 150	— " —
	loose	150 — 100	— " —
Silt	dense	200 — 80	(j=0.5)
	compact	80 — 60	— " —
	loose	60 — 40	— " —
<b>Clays</b>			
Silty clay	hard, stiff	60 — 20	(j=0)
	stiff, firm	20 — 10	— " —
Clayey silt	soft	10 — 5	— " —
Soft marine clays and organic clays		20 — 5	(j=0)
Peat		5 — 1	(j=0)

Regardless of which methods that are used for calculating—predicting—the settlement, it is necessary to refer the analysis results back to basics. That is, if the settlement values used for the assessment of the foundation design are not determined from a so backed-up analysis, the foundation should be evaluated

to indicate what range of compressibility parameters (Janbu modulus numbers) the settlement values represent for the actual soil profile and conditions of effective stress and load. For example, if the design of the superstructure indicates that a settlement of 35 mm is the acceptable limit, the foundation design engineer should calculate—back-calculate—the modulus numbers that correspond to the limit under the given conditions of soil profile and effective stress and compare the results to the parameters obtained from the soils investigation. This back-calculation is a small effort that will provide a worthwhile check on the reasonableness of the results as well as assist in building up a reference data base for future analyses and design cases.

### **3.5.7 Application to Compacted Soils and Proctor Tests**

Compacted fills usually consist of coarse-grained soil, e.g., sand and gravel, which are brought to a certain at-least density by various means of compaction. Often, a standard laboratory compaction test, such as the Proctor test (Holtz and Kovacs 1981, Holtz et al. 2011), is used to provide a reference density, i.e., “optimum dry density”. Then, satisfactory field compaction requires that the dry density of the fill is shown to be at least a certain percentage of the Proctor optimum value. Note, the reference is dry density. Because of the ease of determining water content as opposed to determining density (density requires a known volume of the soil sample before the sampling), frequently, the acceptance criterion in the field is the water content relative to the “water content at optimum density”. However, because the degree of saturation varies in the fill, using a water-content criterion is a poor substitute for reference to the actual dry density.

Proctor density tests are performed on unsaturated soil specimens, which means that compression is fast as it does not require squeezing out any water and therefore, strictly, means that consolidation is not involved. The common conception is that consolidation is settlement—well it is part of it—leads many to think “no-consolidation, so no-settlement”. This could be an explanation for why nobody ever indicates the compressibility of the densified soil as a reference in addition to the Proctor density value. Apart from the fact that a soil compacted on the dry side of the optimum dry density might compress if later on becoming saturated, compacted soils have compressibility and will compress when loaded.

It is usually assumed that a fill compacted to 95 % of Proctor optimum dry density will neither settle under its own weight nor when loaded by a footing, and this with some justification, too. However, fills are sometimes subjected to very large loads and sometimes the compaction is to a lower Proctor value, say 90%. Then, settlement will occur. Therefore, information on the compressibility, that is the E-modulus, or better still, the modulus number (with the stress exponent,  $j$ , equal to unity) are important for the design decisions, as are the preconsolidation stress and the preconsolidation margin. Note, compacted soils are invariably preconsolidated (“precompressed”).

Requiring a specific compaction result, i.e., density, means that a certain at-least compressibility (E-modulus or modulus number) is *de-facto* required. It is desirable (indeed, so desirable that it should be mandatory) that every compaction specification in addition to listing the percentage of the Proctor dry density value (be it Standard Proctor or Modified Proctor) also declares what compressibility that this represents and provides the maximum settlement this represents for the load applied in the project. As mentioned, if the maximum settlement and the maximum stress are known, if only from a judgment call, then, a back-calculation will produce the equivalent compressibility for the case.

Because of sample disturbance and other influences, the fact that most soils are preconsolidated is often overlooked. Some even believe that preconsolidation only applies to clays. Actually, coarse-grained soils, indeed, sand, are almost always overconsolidated, and significantly so. However, the values of OCR or preconsolidation margin are difficult to determine by conventional soil investigation methods. Note, the compressibility values (modulus numbers or E-values) employed in an analysis are often empirical values



obtained from relatively low stress levels applicable to the preconsolidation condition. When a foundation exerting larger stress is considered, the stress level might exceed the preconsolidation stress level. The settlement is then governed by the virgin compressibility of the soil. If so, the settlements will be larger, much larger, than those based on low-stress level experience values.

### 3.6 Evaluating oedometer tests by the e-log p and the strain-stress methods

To repeat, with regard to the options of linearly elastic response to an applied load, the Janbu method with the stress exponent set equal to unity is mathematically the same as using an E-modulus. Similarly, the Janbu method with the stress exponent equal to zero, is mathematically the same as using the  $C_c/e_0$  method. The Janbu method adds a third option, that of  $j = 0.5$ , which is applicable to silty sand and sandy silt, which method is not covered by the conventional methods.

The Janbu modulus numbers are easy to use. For clays, it provides a single unified parameter, the modulus number. With only one parameter, it is easy for the geotechnical engineer to establish a reference data base of values.

Figure 3.1 presents the results of an oedometer test (consolidation test; data from Bowles, 1988) plotted both in the conventional (North American) manner (Fig. 3.1A) of  $e$  versus  $\lg p'$  and as strain ( $\varepsilon$ ) versus  $\lg p'$  (Fig. 3.1B). The same test data are used for both diagrams. The compression index,  $C_c$ , is determined to 0.38 in the first diagram as the void ratio distance for one log cycle. The modulus number,  $m$ , is determined to 12 from the second diagram as the inverse of the strain obtained for a stress change from  $\sigma'_0 = p$  to  $\sigma'_1 = 2.718p$  (Eq. 3.15).

The recompression index and recompression modulus number are determined in similar manner. Most geotechnical textbooks include details on how to analyze the results of an oedometer test, for example Holtz and Kovacs (1981), Holtz et al. (2011), and Bowles (1988), including advice about correction for sample disturbance.

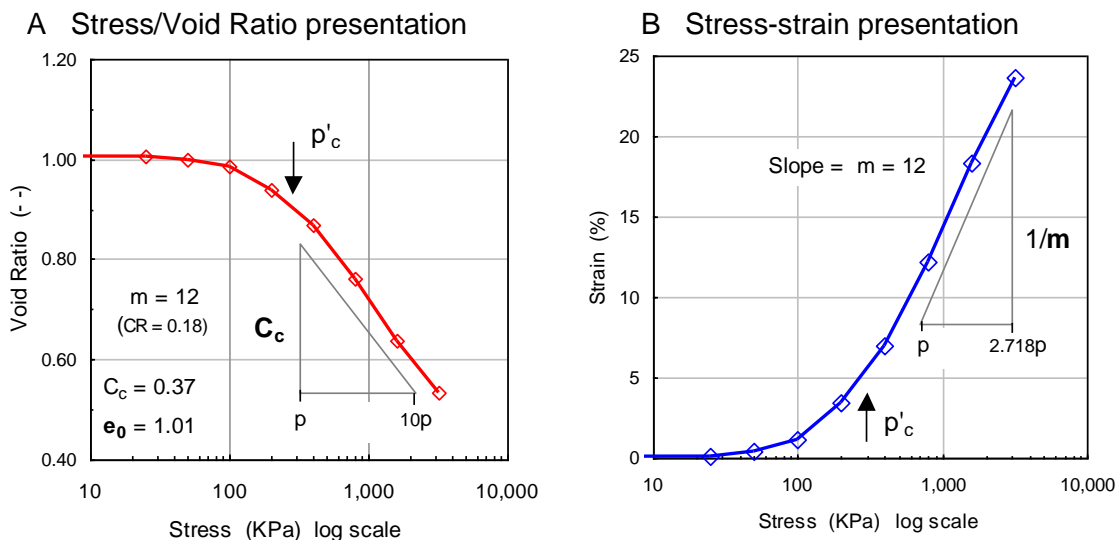


Fig. 3.1 Results from a consolidometer test (data from Bowles, 1988). (The preconsolidation stress is taken directly from the source where it was indicated to have been determined "by eye-balling" to 280 kPa).

Preconsolidation stress is often difficult to determine even from oedometer tests on high quality (undisturbed) samples. Janbu (1998) recommends to obtain it from a plot of the slope of the tangent modulus line, as shown in Fig. 3.2. For the subject example, the preconsolidation stress is clearly noticeable at the applied stress of 200 kPa. Most text books include several conventional methods of determining the preconsolidation stress. Grozic et al. (2003) describe the methods in details and offer an interesting discussion on the processes. See also Tanaka et al. (2002) and references therein.

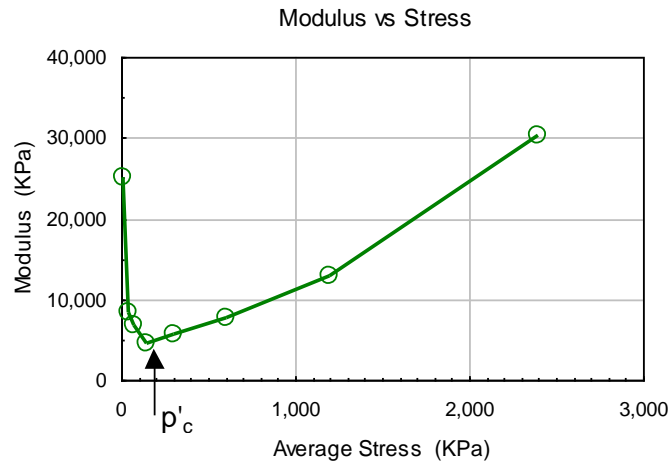


Fig. 3.2 The tangent modulus plot to determine preconsolidation stress according to Janbu (1998)

### 3.7 The Janbu Method versus Conventional Methods

The Janbu tangent modulus method is not different to—does not contrast or conflict with—the 'conventional' methods. The Janbu method for calculation of settlements and the conventional elastic modulus approach give identical results, as do the Janbu method and the conventional  $C_c e_0$ -method (Eqs. 3.4 and 3.5, and Eqs. 3.13, 3.14, and 3.15). There are simple direct conversions between the modulus numbers and the E-modulus (or D-modulus) and the  $C_c e_0$  values. The relation for a linearly elastic soil ("E-modulus soils") is given in Eq. 3.10 (the equation is repeated below).

$$(3.10) \quad m = E/100 \quad \text{E in units of kPa} \quad \text{or} \quad (3.10a) \quad m = E \cdot 10^{-5} \quad \text{E in units of Pa}$$

$$(3.10b) \quad m = E \quad \text{E in units of tsf} \quad (3.10c) \quad m = E/2 \quad \text{E in units of ksf}$$

The conversion relation between the conventional  $C_c$  and  $e_0$  method and the Janbu modulus method is given in Eq. 3.18 (also repeated below).

$$(3.18) \quad m = \ln 10 \frac{1+e_0}{C_c} = 2.3 \frac{1+e_0}{C_c} = 2.3/CC$$

Although mathematically equal, the MIT approach (Section 3.4) has a disadvantage over the Janbu method in that its compressibility values (CR) are smaller than unity, requiring expressing values with decimals, while the Janbu modulus numbers are larger than unity and whole numbers. For example, for modulus numbers of 5, 10, 50, to 100, which span most of the compressibility range of cohesive soil, become CR-values of 0.46, 0.23, 0.046, and 0.023. Moreover, apart from the unwieldy three-decimal format required for the later numbers in the series, the MIT CR-values have no apparent correlation to the E-modulus that might be applied to compressibility of non-cohesive soils, which correlation the Janbu method provides.

Similarly, a strict mathematical relation can be determined for the Swedish-Finnish  $\varepsilon_2$ -approach (Eq. 3.6), as described in Eq. 3.19.

$$(3.19) \quad m = \ln 10 \frac{\lg 2}{\varepsilon_2} = 2.3 \frac{\lg 2}{\varepsilon_2} = \frac{0.69}{\varepsilon_2}$$

The Janbu method of treating the intermediate soils (sandy silt, silty sand, and sand) is “extra” to the  $C_c$ - $e_0$  method and the elastic method (Eqs. 3.12 and 3.13).

It is not possible to express the relative degree of compressibility using the  $C_c$ - $e_0$  approach. That is, a specific  $C_c$ -value cannot be referred to as representing a high compressibility or medium compressibility, etc., without also coupling it with the  $e_0$ -value and few can correlate to two numbers simultaneously. The following couple of examples will demonstrate the advantage of the Janbu modulus number approach as opposed to the conventional  $C_c/e_0$  approach.

Figure 3.3 shows results from oedometer tests on an overconsolidated Texas Gulf Clay (Beaumont clay), with void ratios ranging from about 0.4 through 1.2 (Endley et al. 1996). Figure 3.3A presents a range of  $C_c$ -values, which imply that the compressibility expressed as increased  $C_c$ -value, would be increasing with depth (the associated values of voids ratio,  $e$ , are not shown). However, Fig. 3.3B, which shows the  $C_c$ - $e_0$ -values converted to Janbu modulus numbers, demonstrates that there is no such trend with depth. The modulus numbers range—from about 10 through almost 40—is quite wide, going from high through low compressibility.

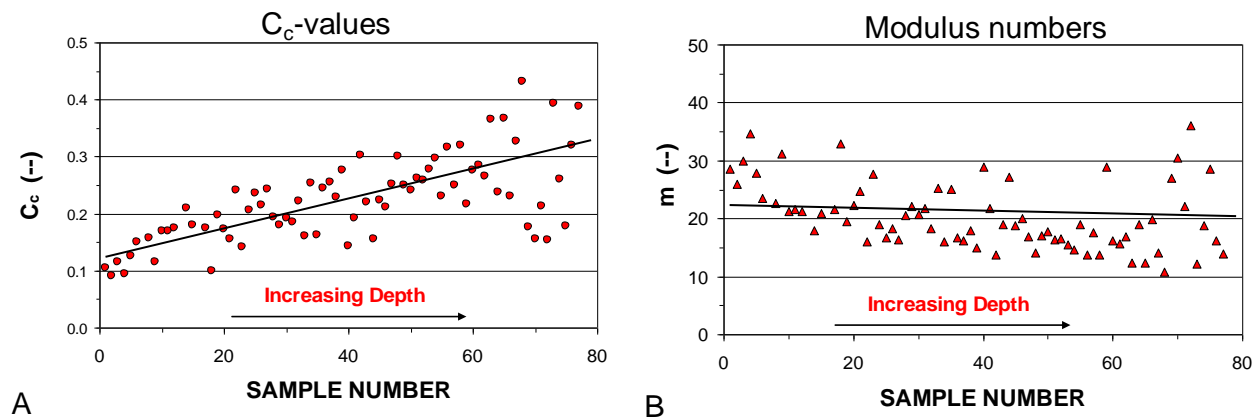


Fig. 3.3  $C_c$ -values and modulus numbers from Beaumont clay. Data from Endley et al. 1996.

Figure 3.4 presents results from oedometer tests on a normally consolidated to slightly overconsolidated silty clay outside Vancouver, BC with void ratios ranging from about 0.8 through 1.4. The relative range between the smallest and largest  $C_c$ -value (a factor of 2) suggests a somewhat wider range of compressibility than the actual, represented by the modulus number where the relative range between the smallest and largest value is a factor of 1.3. The average modulus number is approximately 10, which is the upper boundary of a very compressible soil.

The Janbu method is widely used internationally and by several North American engineering companies and engineers. However, many others are yet reluctant to use the Janbu approach, despite its obvious advantages over the conventional  $C_c/e_0$  method. The approach has been available for more than twenty years in the second and third editions of the broadly used Canadian Foundation Engineering Manual, CFEM (1985; 1992). (Regrettably, by accident or other, the committee revising the CFEM for the fourth

Edition published in 2006 omitted to keep the Janbu approach in the Manual). Moreover, the Janbu modulus number has important application for assessing liquefaction risk and soil densification as described in Section 2, Clauses 12.8,4 and 2.12.8.5.

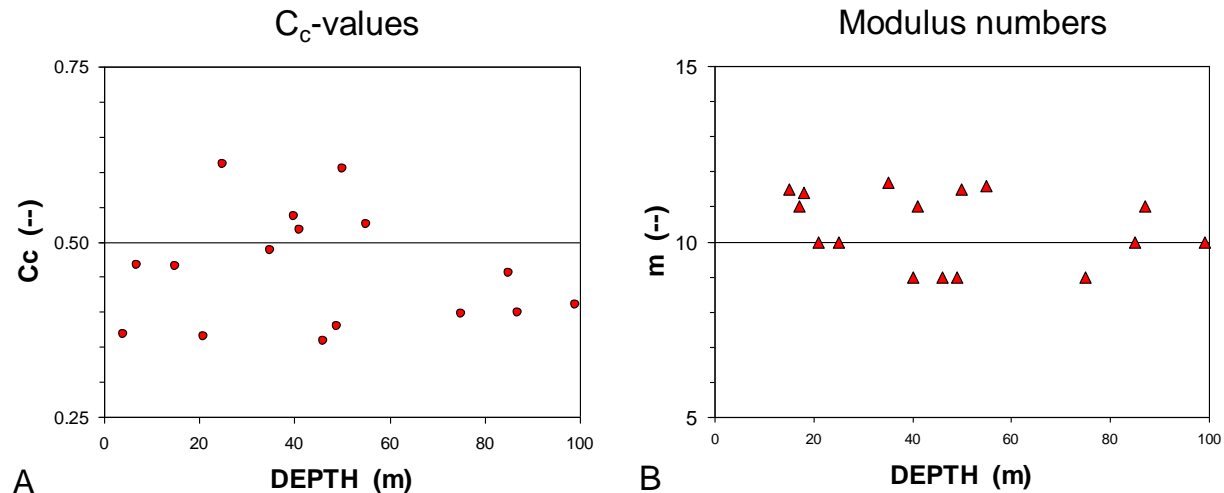


Fig. 3.4  $C_c$ -values and modulus numbers from Fraser River clay, BC.

Those not fully convinced by the previous examples, should reflect on the results shown in Fig. 3.5 and 3.6. Figure 3.5A shows a fairly typical array of  $C_c$ -values ranging from about 0.3 through 0.9, implying a rather randomly varying compressibility. However, when coupled with the associated  $e_0$ -values, admittedly judiciously selected, as shown in Fig. 3.5B, the different picture evolves: the compressibility is constant for the  $C_c$ -values. Figure 3.6A shows a set of constant  $C_c$ -values, that is, they imply a constant compressibility. Similarly, however, when coupled with their associated  $e_0$ -values, again admittedly judiciously selected, as shown in Fig. 3.6B, the different picture evolves: the compressibility is highly variable despite the constant  $C_c$ -values.

Engineers working in a well-known area where the soils have a familiar range of water contents and void ratios well-known to those engineers, can work well only classifying compressibility from  $C_c$ -values. However, when encountering foundation problems in different geologies, a good advice is to start using the modulus number as the measure of and reference to soil compressibility.

### 3.8 Time Dependent Settlement

Because soil solids compress very little, settlement is mostly the result of a change of pore volume. However, compression of the solids ("immediate compression") does still occur and it occurs quickly. It is usually considered elastic, that is, the stress-strain response is linear.

Moreover, when addressing settlement due to a fill placed on the ground, we do not usually pay attention to settlement due to immediate compression. But the as-placed fill thickness is the difference between the elevation of the original ground surface and the elevation of the final fill surface. That is, the thickness includes the settlement due to the immediate compression. As often is the case, if the added stress is calculated based on the elevation of the original ground surface, it is therefore underestimated.

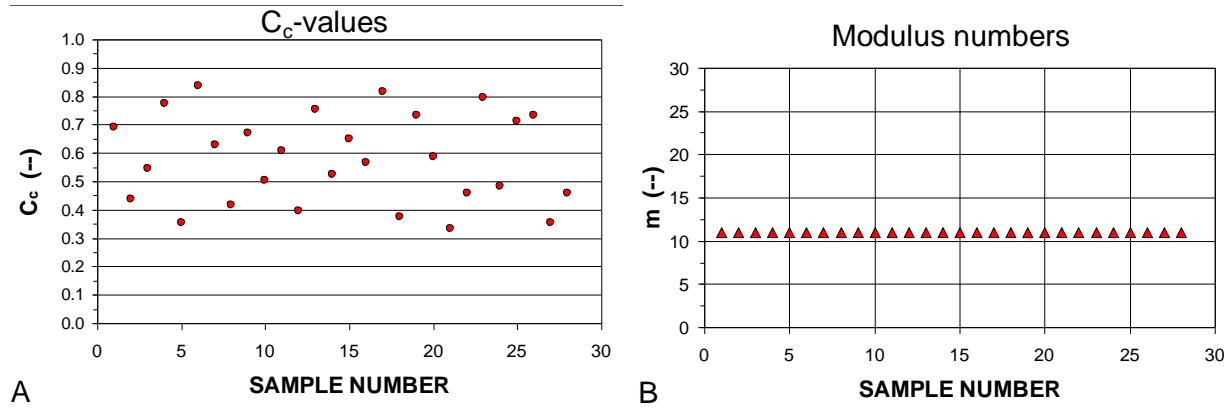


Fig. 3.5 Typical, but "selected"  $C_c$ -values, and converted via associated "selected"  $e_0$ -values to "m"-values.

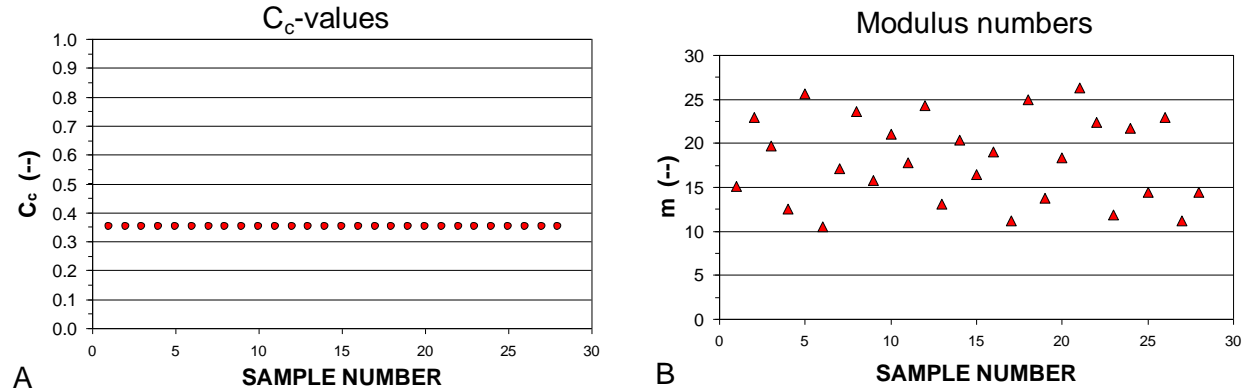


Fig. 3.6 "Selected" constant  $C_c$ -values, and converted via associated "selected"  $e_0$ -values to "m"-values.

No change of pore volume will occur before the water occupying the pores is expelled ("squeezed out") by the stress increase, which process is rapid in coarse-grained soils and slow in fine-grained soils. The process is called consolidation, and it usually occurs with an increase of both undrained and drained soil shear strength. In very fine clays, the consolidation can even take a longer time than the life expectancy of the building, or of the designing engineer, at least. By analogy with heat dissipation in solid materials, the Terzaghi consolidation theory indicates simple relations for the time required for the consolidation. The most commonly applied theory builds on the assumption that water is leaving the soil at one surface boundary (upper or lower) and not at all at the opposite boundary (nor horizontally). The consolidation is rapid in the beginning, when the driving (forcing) pore pressures are greater and slows down with time as the pressures reduce. The analysis makes use of the relative amount of consolidation obtained at a certain time, called average degree of consolidation, which is defined in Eq. 3.20.

$$(3.20) \quad U_{v,AVG} = \frac{S_t}{S_f} = 1 - \frac{u_t}{u_0}$$

where  $U_{v, AVG} =$  **average** degree of consolidation for vertical drainage  
 $S_t =$  settlement at Time  $t$   
 $S_f =$  final settlement at full consolidation  
 $u_t =$  *average* pore pressure at Time  $t$   
 $u_0 =$  initial *average* pore pressure (on application of the load at Time  $t = 0$ )

Notice that the pore pressure varies throughout the soil layer and that Eq. 3.20 assumes an average value through the soil profile. In contrast, the settlement values are not the average, but the accumulated values.

Eq. 3.20 shows that the degree of consolidation is the same whether determined by settlement or pore pressure dissipation. If you believe in the classical theory, and why not, the 100-% consolidation is the same as the difference between final and initial effective stress and the dissipated pore pressure is the degree of consolidation times that effective stress change. Of course, a measured settlement is an average for an appreciable body of soil, whereas a pore pressure is a pressure in a point. There is always the question whether or not that pore pressure is representative for the soil body. Moreover, the degree determined from measured settlement cannot be determined until all the settlement has occurred, whereas the degree determined from pore pressure is known from the start and any time, so questionable or not, that degree is the one we can determine when the settlement is ongoing. Further confusing the matter is that the two definitions of the degree of consolidation are not quite equal at any one time. And, what is 100 % consolidation? It only occurs at infinite time. In practice, the settlement calculated for a degree of consolidation of 90 or 95 % is what most consider the "100-% value".

The time for a achieving certain degree consolidation is then, as follows (Eq. 3.21).

$$(3.21) \quad t = T_v \frac{H^2}{c_v}$$

where  $t =$  time to obtain a certain degree of consolidation  
 $T_v =$  a dimensionless time coefficient  
 $c_v =$  coefficient of consolidation expressed as area/time  
 $H =$  length of the longest drainage path

The time coefficient,  $T_v$ , is a function of the type of pore pressure distribution. Of course, the shape of the distribution affects the average pore pressure values and a parabolic shape is usually assumed.

The interrelations for  $T_v$  and  $U_{v, AVG}$  are given in Eqs. 3.22a through 3.22c (Holtz and Kovacs 1981, Holtz et al. (2011), and in Chapter 9 and Appendix B). Eqs. 3.22a and 3.22b are valid for  $U_{v, AVG} > 60$  %. For  $U_{v, AVG} < 60$  %, Eqs. 3.22c and 3.22d apply.

$$(3.22a) \quad U_{v, AVG} = 1 - \frac{8}{\pi^2} \exp\left(-\frac{\pi^2}{4} T_v\right) \quad \text{if } U_{v, AVG} > 0.60$$

$$(3.22b) \quad T_v = 1.781 - 0.933 \lg(1 - U_{v, AVG}) \quad \text{if } U_{v, AVG} > 0.60$$

$$(3.22c) \quad U_{v, AVG} = \sqrt{\frac{4T_v}{\pi}} \quad \text{if } U_{v, AVG} < 0.60$$

$$(3.22d) \quad T_v = \frac{\pi}{4} U_{v,AVG} \quad \text{if } U_{v,AVG} < 0.60$$

Approximate values of  $T_v$  for different average values of the average degree of consolidation,  $U_{AVG}$ , are given in Table 3.2. For more exact values and values to use when the pore pressure distribution is different, see, for example, Holtz and Kovacs (1981), Holtz et al. (2011).

**TABLE 3.2** Approximate values of  $T_v$  for different average values of the degree of consolidation,  $U_{AVG}$

$U_{AVG}$	0.25	0.50	0.70	0.80	0.90	“1”
$T_v$	0.05	0.20	0.40	0.57	0.85	$\approx 1.00$

Note  $U_{AVG}$  is usually given in percent. However, here it is used as a ratio, a number between 0 and 1.

The SI base units for the parameters of Eq. 3.21 are s (time in seconds),  $\text{m}^2/\text{s}$  (coefficient of consolidation,  $c_v$ ), and m (metre; length). Often, practitioners desire to obtain the time directly in everyday units, such as days, months, or years with different persons preferring different units, which means that a Babylonian confusion can easily develop with numbers produced in an assortment of units, such as  $\text{m}^2/\text{year}$ ,  $\text{cm}^2/\text{year}$ , and  $\text{cm}^2/\text{month}$ , even  $\text{ft}^2/\text{month}$  and  $\text{ft}^2/\text{year}$ , instead of the more appropriate base SI-unit,  $\text{m}^2/\text{s}$ . (Take care to avoid confusion and risk of mistakes by ensuring that equations are always designed for input of values in base SI-units). To convert to units of  $10^{-8} \text{ m}^2/\text{s}$  from the following non-SI units, multiply with the respective conversion and report the resulting number with a multiple of  $10^{-8}$ : To convert to  $10^{-8} \text{ m}^2/\text{s}$  from  $\text{m}^2/\text{year}$ , multiply by 3.2; from  $\text{m}^2/\text{month}$ , multiply by 38; from  $\text{m}^2/\text{day}$ , multiply by 1,160; from  $\text{ft}^2/\text{year}$ , multiply by 0.29; from  $\text{ft}^2/\text{month}$ , multiply by 3.5; from  $\text{ft}^2/\text{day}$ , multiply by 108; and from  $\text{ft}^2/\text{s}$ , multiply by  $9.29 \times 10^6$ .

This said, it can be argued that an exception from the requirement of using base SI-units is justified in order to avoid the  $10^{-8}$  number or decimals and apply the units  $\text{m}^2/\text{year}$  in the SI-system and  $\text{ft}^2/\text{year}$  in the English system of units. To convert from  $\text{m}^2/\text{year}$  to  $\text{ft}^2/\text{year}$ , multiply by 10.76. To convert from  $\text{ft}^2/\text{s}$  to  $\text{m}^2/\text{year}$ , multiply by 0.093. [Roy E. Olson (Olson 1998) suggested that in order to honor Terzaghi, the base units for the  $c_v$ -coefficient should be given the symbol “T”. Thus, a value of  $1 \text{ m}^2/\text{s} \times 10^{-8}$  ( $= 0.32 \text{ m}^2/\text{year}$ ) would become 10 nT, where “n” stands for “nano” and is equal to  $10^{-9}$ . It is a pity that the suggestion did not catch on].

Holtz and Kovacs (1981), Holtz et al. (2011) reported common  $c_v$ -values ranging from a low of  $0.5 \times 10^{-8} \text{ m}^2/\text{s}$  in Swedish sensitive clays, about  $3 \times 10^{-8} \text{ m}^2/\text{s}$  in San Francisco Bay Mud, through about  $40 \times 10^{-8} \text{ m}^2/\text{s}$  in Boston Blue Clay (0.16, 0.95, and  $12.6 \text{ m}^2/\text{year}$ , respectively).

The coefficient of consolidation is determined in the laboratory oedometer test (some in-situ tests can also provide  $c_v$ -values) and it can rarely be obtained more accurately than within a ratio ranging from 2 to 3.

The longest drainage path,  $H$ , for a soil layer that drains at both surface boundaries is half the layer thickness. If drainage only occurs at one boundary,  $H$  is equal to the full layer thickness. Naturally, in layered soils, the value of  $H$  is difficult to ascertain, as each layer drains into its adjacent layers.

In saturated soils, water has to be expelled from the soil before the pore volume can reduce. In soils containing gas and in partially saturated soils, however, initially the process appears to be rapid, because

gas (air) will readily compress when subjected to an increase of pressure, allowing the pore volume to decrease rapidly. Settlement due to the latter change is often mistaken for the immediate compression of the soil. Well, it is immediate, but it is not due to compression of the soil skeleton. The compression of the soil skeleton is permanent, whereas the compression of the gas bubbles is temporary.

Inorganic soils below the groundwater table are usually saturated and contain no gas. In contrast, organic soils will invariably contain gas in the form of small bubbles (as well as gas dissolved in the water, which gas becomes free gas on release of confining pressure when sampling the soil) and these soils will appear to have a large immediate compression when load is applied. During the consolidation process, as the pore pressure gradually reduces, the bubbles expand to their original size and the consolidation process will appear to be slower than the actual rate, indeed, measurements of the development will appear to suggest that the consolidation is completed. The remaining settlement, which inevitably will occur, will be believed to be caused by secondary compression, (Section 3.9). As such, the secondary compression will appear to be unusually large.

Generally, the determination—prediction—of the time for a settlement to develop is filled with uncertainty and it is difficult to reliably estimate the amount of settlement occurring within a specific time after the load application. The prediction is not any easier when one has to consider the development during the build-up of the load. For details on the subject, see Ladd (1991).

Loading a soil by placing a certain thickness of fill over a certain area takes time. Most case analyses assume that all the fill is placed simultaneously so all monitoring has a common starting date (time). However, if the placing of the fill invariably occurs over time, therefore, a back-analysis needs to input of the fill as a number of loaded areas placed at the actual times—if now that information is available in the back-analyzed case record.

Of old, the consolidation theory recognizes two cases: either a double-drained or a single-drained layer. The problem with reality, though, is that soils are made up of more than one layer and, therefore, they drain into each other—Here, Nature has thrown a most inconsiderate monkey wrench into our wheels. I do know of a few very complex computer models that can tackle a case having a profile made up of couple of such layers by assuming special numerical relations for each soil layer that slow down the classical relations as based on numerous more or less sophisticated conditions. The trouble is that the input to the software built into the models has no acceptable field data to verify the veracity of the assumed functions involved. There are only a few full-scale case histories where the consolidation process was monitored individually in "sandwiched" soil layers in a multi-layered clay profile. However, the results of most of these cases are muddled up by varying loading times, disturbance effects, and ratio between horizontal and vertical dissipation directions. The main difficulty, though, is that full-scale case studies have to be carried over many years, more likely longer than the usual life span of an engineer; definitely longer than the attention span of professors and their graduate students. Cases involving wickdrains will require much shorter time—the shorter time is the very reason for using the wickdrains—but the drainage is horizontally to the drains and the monitoring does not allow for separating the response in one soil layer from that in another.

I have found that practicing engineers with long experience are quite good at estimating the time for consolidation of a compressible layer by applying judgment. There is usually a main soil layer, an "alpha", that dominates the settlement response to load. So, for design (or back-calculation), the time for full consolidation in that  $\alpha$ -layer is first estimated. The consolidation times for all other layers are then considered in relation to the  $\alpha$ -layer allowing for a longer or shorter time as deemed appropriate (the process also includes re-assessing the time for the  $\alpha$ -layer). The process includes assessing the input of layer thickness, densities, compressibilities, preconsolidation margin, etc., as guided by the site investigation information. (First, input the time for full consolidation of the " $\alpha$ -layer". Second, go to the



other layers and input the consolidation time for these—now, a shorter or longer time value, as you judge applicable in reference to your " $\alpha$ -layer". Note that once the time for full consolidation is chosen, the coefficient of consolidation,  $c_v$ , is decided by the geometry, and you need to convince yourself that the values are reasonable for each layer. Anyway, chances are that you will obtain an acceptable distribution of the time-dependent settlement of each layer and, therefore, of the ground surface or the foundation.

An additional, and sometimes not so marginal, factor is that the settlement means lowering a portion of the soil from a position immediately above the groundwater table to immediately below, which creates a gradual buoyancy effect (reduction of the effective stress throughout the soil profile). When it needs to be considered, simply input of a corresponding time-spaced series of appropriate negative loads.

The rather long consolidation time in clay soils can be shortened considerably by means of vertical drains (see Chapter 4). Vertical drains installed at a spacing ranging from about 1.0 m through 3.0 m have been very successful in accelerating consolidation to develop in weeks or months as opposed to requiring years. In the past, vertical drains consisted of sand drains and installation disturbance in some soils often made the drains cause more problems than they solved (Casagrande and Poulos 1969). However, the sand drain is now replaced by premanufactured band-shaped drains ("wick drains"), most which do not share the difficulties and adverse behavior of sand drains (some do, however, and quality and performance of wick drains vary from type to type, usually in inverse to the cost of material).

Theoretically, when vertical drains have been installed, the drainage is in the horizontal direction. Therefore, the design formulae are developed based on radial drainage. However, vertical drains connect horizontal layers of greater permeability, which frequently are interspersed in natural soils (See Section 5.3.5). This must be addressed in the design. The way to determine the existence and frequency of such horizontal permeable layers, is by careful scrutiny of continuous Shelby-tube sampling or by CPT in-situ sounding. If the extruded Shelby-tube samples are left to dry in room temperature, then, after a few days or so, pervious layers or bands of silt and sand will show up as light-colored partitions in the sample. After full drying, the layers will no longer be visible. The CPT in-situ sounding needs to be performed with readings taken every 10 mm (which does not infer any extra costs and, anyway, should be the norm for all CPTU soundings).

Where settlement at a certain time after start of loading needs to be calculated and the degree of consolidation in the various soil layers is known (or has been calculated) for that time, a short-cut value of consolidation settlement can be obtained by dividing the modulus number with the value of the degree of consolidation and using the so-adjusted modulus number for the calculation.

Consolidation, or time-dependent settlement, is not an exclusive domain of cohesive soils. Settlement of coarse-grained soils, indeed sand, can sometimes display a time-dependent response, which can be modeled by consolidation theory as expressed in Eq. 3.21.

### 3.9 Secondary Compression

Theoretically and approximately so also in practice, settlement values plotted in a linear vs. log-time plot will be a straight line until close to the end of the consolidation process. The settlements will continue after the end of the consolidation due to slow continued compression of the soil skeleton, albeit at a flatter slope, which process is called "secondary compression" (note, secondary compression must not be called "secondary consolidation", as there is no consolidation, i.e., dissipation of pore pressures, involved). The process is a function of a "coefficient of secondary compression,  $C_\alpha$ " (See Holtz and Kovacs 1981, Holtz et al. 2011). Eq. 3.23 shows a relation for the amount of compression developing over time after the

consolidation is completed. Notice that secondary compression is not a function of the applied load itself, but of the actual time considered relative to the time for the consolidation.

$$(3.23a) \quad \varepsilon_{2nd} = \frac{C_\alpha}{1 + e_0} \lg \frac{t_\alpha}{t_{CONS}}$$

where

- $\varepsilon_{2nd}$  = secondary compression strain
- $C_\alpha$  = coefficient of secondary compression
- $t_\alpha$  = length of time considered from time of start of consolidation ( $t_\alpha > t_{CONS}$ )
- $t_{CONS}$  = time for achieving the primary consolidation (Eq. 3.21), which is time between placing the load and the completion of the consolidation

The value of  $C_\alpha$  is usually expressed as a ratio to the consolidation coefficient,  $C_c$ , ranging from 0.01 through 0.10 with an average of about 0.05. For example, the ratio of a soft clay having  $C_c$  of about 0.3 and void ratio of about unity (i.e., a modulus number of 15), the ratio  $C_\alpha/C_c$  would be about 0.01 (Holtz and Kovacs 1981, Holtz et al. 2011).

When the ratio  $C_\alpha/C_c$  and the Janbu modulus number are known, applying Eq. 3.18, Eq. 3.23a changes to Eq. 3.23b.

$$(3.23b) \quad \varepsilon_{2nd} = \frac{C_\alpha}{C_c} \frac{1}{m \ln 10} \lg \frac{t_\alpha}{t_{CONS}} \quad [\ln 10 = \lg e = 2.3]$$

Time  $t_{CONS}$  is theoretically the time for 100 % consolidation. However, that time is theoretically infinitely long. Usually,  $t_{CONS}$  is taken as the time determined for achieving 90 % of primary consolidation.

The current consensus appear to be that secondary compression starts when the consolidation process starts. Therefore, the secondary compression is added to the consolidation settlement at the beginning of the consolidation process, instead of adding it at the end, recognizing that secondary compression is triggered when an increase of effective stress is imposed. However, the secondary compression is small compared to the consolidation and, therefore, secondary compression can be thought as only starting at the end of consolidation. Indeed, even after about the first twenty years after the end of consolidation, it has rarely become larger than the immediate compression. (Although it could be substantial in organic soils, e.g., Chang 1981). Note, when the soil contains gas, the slow-down of settlement with time may erroneously be interpreted as indication of large secondary compression (See Sections 3.2 and 3.8).

Secondary compression is often defined as the settlement that develops when the consolidation is over. If so, this would mean that, close to the drainage (layer) boundaries, it would start earlier than at the center of a layer. Indeed, secondary compression is a rather equivocal concept and the formula is correspondingly dubious. For example, should the total consolidation time be estimated at 85%, 90 %, or 95 % consolidation? There is little scientific weight in the concept. Unfortunately, there is also very little of long-term observations to use for correlations between the formula and reality.

Most projects involve several load areas influencing the stresses and the time for start and duration of consolidation below each other. Therefore, it is difficult to decide when the consolidation starts and when it is completed, which values govern the start and the development with time of the secondary compression (Eq. 3.23). Invariably, in a actual case, a judgment call is required in deciding what input to use for the calculation. Moreover, for the secondary compression to start requires a start of consolidation, and, because applying a load smaller than the preconsolidation stress results in a minimal pore pressure

increase and a short "consolidation" time, practice is to assume much smaller coefficient of secondary compression for layers where the applied load has not exceeded the preconsolidation margin. Some mean that secondary compression does not occur unless consolidation has been triggered.

Eqs. 3.23a and 3.23b mean that secondary compression would increase if the consolidation time would decrease, e.g., by shortening the drainage path. This does not make sense, of course. It is a consequence of the fact that secondary compression is an empirical concept without proper theoretical basis that tries to rationalize the factual observation that settlement continues (at a diminishing rate) for a long time after the induced pore pressures have dissipated.

### 3.10 Magnitude of Acceptable Settlement

Settlement analysis is often limited to ascertaining that the expected settlement would not exceed one inch. (Realizing that 25 mm is too precise a value when transferring this limit to the SI-system, some have argued whether "the metric inch" should be 20 mm or 30 mm!). However, in evaluating settlement in a design, the calculations need to provide more than just an upper boundary. The actual settlement value and both total and differential settlements must be evaluated. The Canadian Foundation Engineering Manual (1992) lists acceptable displacement criteria in terms of maximum deflection between point supports, maximum slope of continuous structures, and rotation limits for structures. The multitude of limits demonstrate clearly that the acceptable settlement varies with the type and size of structure considered. Moreover, modern structures often have small tolerance for settlement and, therefore, require that the design engages a more thorough settlement analysis than was required in the past. The advent of the computer and development of sophisticated yet simple to use design software has enabled the structural engineers to be very precise in the analysis of deformation of a structure and the effect of deformations on the stress and strain in various parts of a structure. As a not-so-surprising consequence, requests for "settlement-free" foundations have increased. This means that the geotechnical analysis must determine also the magnitude of small values of settlement.

When the geotechnical engineer is vague on the predicted settlement, the structural designer "plays it safe" and increases the size of footings or changes the foundation type, which may increase the costs of the structure. These days, in fact, the geotechnical engineer can no longer just offer an estimated "less than one inch" value, but must provide a more accurate value by performing a thorough analysis considering soil compressibility, soil layering, and load variations. Moreover, the analysis must be put into the full context of the structure, which necessitates a continuous communication between the geotechnical and structural engineers during the design effort. Building codes have started to recognize the complexity of the problem and mandate that the designers collaborate continuously during the design phases as well as during the construction. See, for example, the Canadian Highway Bridge Design Code, CAN/CSA-S6 2006 (Canadian Standards Council 2006).

### 3.11 Calculation of Settlement

Calculation of settlement should be performed in the following steps.

1. Determine the soil profile (i.e., the soil layering and pore pressure distribution; Chapter 2) at the initial state for the site and foundation unit(s) so that the initial effective stress ( $\sigma'_0$ ) distribution is adequately established (Chapter 1).
2. Determine and compile the soil compressibility parameters, i.e., the modulus number and stress exponents (or the "conventional" parameters), and for consider both virgin and reloading conditions, as well as preconsolidation margin.

3. Determine the stress distribution (e.g., Boussinesq) imposed by the foundation unit(s) and any changes to the initial site conditions (excavations, fills, groundwater table lowering, etc.) and calculate the new (the final) distribution of effective stress,  $\sigma'_1$ .
4. Divide each soil layer in a suitable number of sub layers and calculate the initial and final effective stress representative for each sub layer using the suitable equations given in this chapter. (Perform the calculations in either the middle of each sub layer, or at top and bottom of each and take an average of these two; if the sub layers are reasonably thin, the two approaches will give equal result).
5. Calculate for each sub layer the strain caused by the change of effective stress from  $\sigma'_0$  to  $\sigma'_1$  (Section 3.5 contains the formulae to use).
6. Multiply each calculated strain value with its appropriate layer thickness to determine the settlement for each sub layer and add up to find the accumulated settlement value (Eq. 3.3).
7. When desired, calculate also the immediate settlement and secondary compression.

Software, such as UniSettle (Goudreault and Fellenius 2006; 2011) greatly simplify the calculation process. In particular, where Step 3 includes several components and when loads are applied at different times so that consolidation starts and finishes at different times.

A settlement analysis must incorporate all relevant facts. Because the person performing the analysis does not know all details of a project, important facts may get overlooked, such as that the site information does not include that the ground has either been or will be excavated or backfilled prior to construction, or that stress from an adjacent structure or embankment will have affect the existing stresses underneath the foundation that is being analyzed. Often, even though all the relevant facts from the local site are applied, regional conditions must also be included in the analysis. For example, in the Texas Gulf Coast Region, notably in Greater Houston area, past lowering of the groundwater table due water mining in deep wells (starting in the 1920s) have resulted in a regional subsidence—in places as much or larger than 2 m—and a large downward water gradient. Downward gradients ('negative head') larger than 0.25 (100 m) have been measured at depths of 400 m. The groundwater table is now rising (since ceasing to pump in the mid-1970s). Figure 3.7 presents observations in three deep wells from 1930 onward.

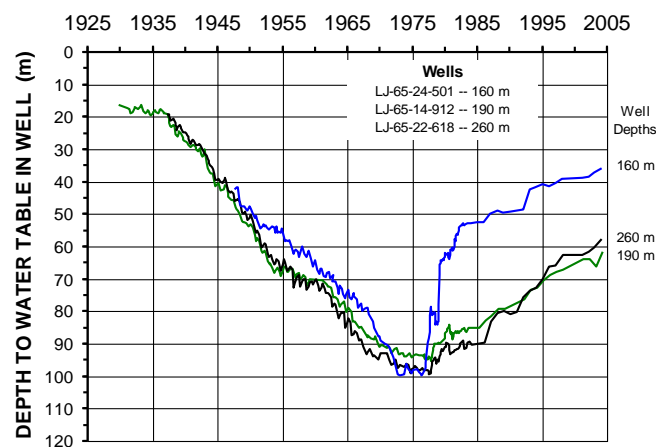


Fig. 3.7 Example of measured depth to water level in 160 m through 350 m deep wells near the San Jacinto Monument. (Data from Barbie et al. 2005 and Fellenius and Ochoa 2009).

The clay soils in the Greater Houston area are desiccated and overconsolidated from ancient desiccation and from the recent lowering of the pore pressures. The overconsolidation degree is getting larger as the water pressures now are returning to pre-1920 levels. Old and new foundations need to take the changing pore pressure gradient into account. Figure 3.8 shows settlement observations for the San Jacinto Monument (Briaud et al. 2007) and how, after completed construction in 1936, the initial moderate groundwater mining did not affect the consolidation settlement of the monument, but how the accelerated lowering of the groundwater from 1940 onward appreciably affect the settlement development. The heavy blue line with solid dots shows the measured settlement of the Monument. The dashed line marked "Monument only" is the assumed settlement of the monument had there been no groundwater lowering.

For either back analysis (for future reference) or for design calculations of expected settlement, the local regional pore pressure conditions must be carefully established and, therefore, all site investigations must include installing piezometers geared to establish the pore pressure distribution.

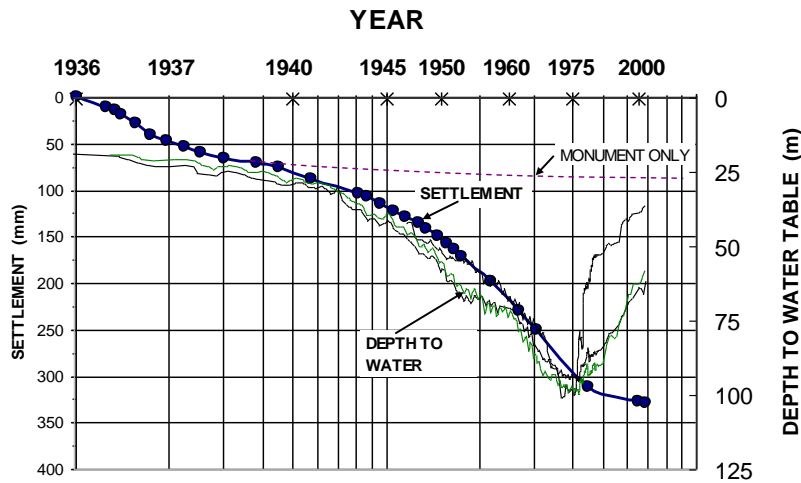


Fig. 3.8 Observed settlement of the San Jacinto Monument plotted together with the observed depths to water in wells near the Monument. (Data from Fellenius and Ochoa 2009).

### 3.12 Special Approach -- Block Analysis

When a foundation design analysis indicates a likelihood that ordinary foundations (footings, rafts, or mats) would experience excessive settlement, site improvement techniques are frequently employed. For example, deep vibratory compaction, dynamic consolidation, stone-columns, or lime-cement columns. Common for these techniques is that the compressibility of an upper soil zone (the depth of the treatment) at the site is improved. The result of the treatment is rarely uniform. It usually consists of treating vertical zones (columns) leaving untreated soil in between, e.g., installing piles, which is in a sense a soil improvement method. Provided the overall treated area is equal or larger than the footprint of the foundation, the settlement analysis consists of determining the average (proportional) modulus number of the treated zone as indicated in Eq. 3.24. This average is then applied to calculations for the treated zone replacing the original soil modulus.

$$(3.24) \quad m_{AVG} = \frac{m_{UNTR} \times A_{UNTR} + m_{TR} \times A_{TR}}{A_{UNTR} + A_{TR}}$$

where  $m_{AVG}$  = average modulus number for the treated zone  
 $m_{UNTR}$  = modulus number for untreated soil

$m_{TR}$	=	modulus number for treated soil
$A_{UNTR}$	=	area of untreated soil
$A_{TR}$	=	area of treated soil

When the size of the footprint is at least about equal to the treated area, the imposed stress is assumed to be transferred undiminished through the treated zone (taken as a block of soil), i.e., *no stress distribution within the treated zone (or out from its side)*. The block will compress for the load and the compression (settlement contribution) is determined using the average modulus and applying elastic stress-strain (stress exponent = unity). At the bottom of the block, the imposed stress is now distributed down into the soil and the resulting strains and settlements are calculated as before.

### 3.13 Determining the Modulus Number from In-Situ Plate Tests

To supplement results from laboratory tests, the compressibility parameters (modulus number, as well as E-moduli) can be determined by back-calculation using settlement data from structures with a well-defined footprint placed on a well-investigated soil. However, the results are approximate, as no information is obtained on preconsolidation or on settlement for applied stresses different from that stress causing the observed settlement. Moreover, if the soil is layered, the compressibility parameter is a blend (average) of the values in whole soil body affected. Values for a specific soil layer can be determined in in-situ plate tests. Plate tests have the advantage of enabling settlements to be determined from a range of applied load. The plate test is usually performed at the ground surface or at shallow depth. For the latter case, the plate is placed at the bottom of an excavated hole. Use of a screw-plate can extend the depth, but the depth is still limited as screw-plates can rarely be “screwed-in” more than a few metre. Janbu applied 0.3 m diameter screw-plates and evaluated the modulus number assuming that the strain induced by the applied load increments was the measured settlement divided by half the plate diameter. The Canadian Foundation Engineering Manual (1992) indicates how the modulus number can be established from the so-determined stress-strain values. It is of course better to actually measure the strain induced by the loading of the plate. This can be done by equipping the test plate with a small centrally placed screw-plate that can be moved down, say, a distance below the main plate. The central plate is not loaded, but its movement due to the load applied to the main test plate is measured. The difference in movement between the main plate and the small central plate divided by the distance is the induced strain. The distance of the central plate below the main plate can be determined from Boussinesq stress distribution calculation, fitting the distance to a depth corresponding to the calculated average strain.

Figure 3.9 presents the results of loading tests in sand on three square footings of 1.0 m, 1.5 m, and 2.5 m, and two footings of 3.0 m diameter. Figure 3.9A shows the load-movement for the individual footings and Fig. 3.9B shows the results as stress versus movement divided with the footing width. Figure 3.9B is important because it shows that the load-movement in sand is independent of scale.

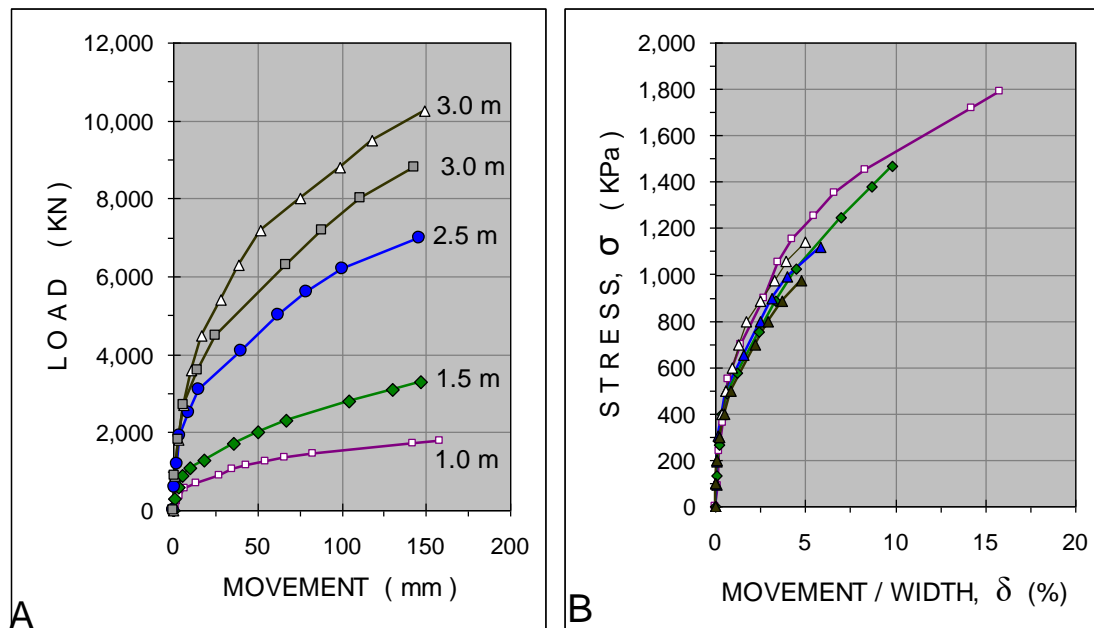


Fig. 3.9 Observed load-movement (A) and stress-normalized movement (B) of five footings tested at Texas A&M University (data from Briaud and Gibbens 1994, 1999).

By dividing each stress values with its relative movement value, a "secant modulus"<sup>1</sup> is established for each such data pair. Similarly, by for each pair dividing the change of stress with the change of relative movement, a tangent modulus is determined. The results are shown in Figs. 3.10A and 3.10B, respectively, and indicate as many modulus values as there are applied values of stress. This is no surprise, the movements of the example tests are affected by immediate deformation, creep during load-holding, increased volume of soil affected from one applied load to the next, and, primarily, by a significant cementation or preconsolidation condition for the example case—most sands are preconsolidated and this sand is no exception.

In Fig. 3.10B, the large initial tangent modulus value is influenced by the reloading modulus, while toward the end of the loading tests, the tangent modulus is mostly influenced by the virgin modulus of the sand. The curves can be used to estimate the starting point for a fitting of the test data to a theoretical calculation, employing a common "preconsolidation stress" and fixed values of reloading and virgin modulus numbers. The process involves a rather laborious trial and error series of calculations, assuming either a linear elastic response,  $j = 1$ , or Janbu's mid-type response,  $j = 0.5$ , Boussinesq distribution, and calculating the settlement at the characteristic point (Chapter 1, Section 1.9). For the linear elastic assumption ( $j=1$ ), the calculated values match the observed values when applying a preconsolidation stress of about 500 kPa and modulus numbers,  $m$  and  $m_r$ , about 60 and 900, respectively. The corresponding  $E$ -values are about 6 MPa and 90 MPa, respectively. (For additional reference to this important case history, see Section 6.10).

<sup>1</sup> In contrast, the tangent modulus curve reflects the correct material response.

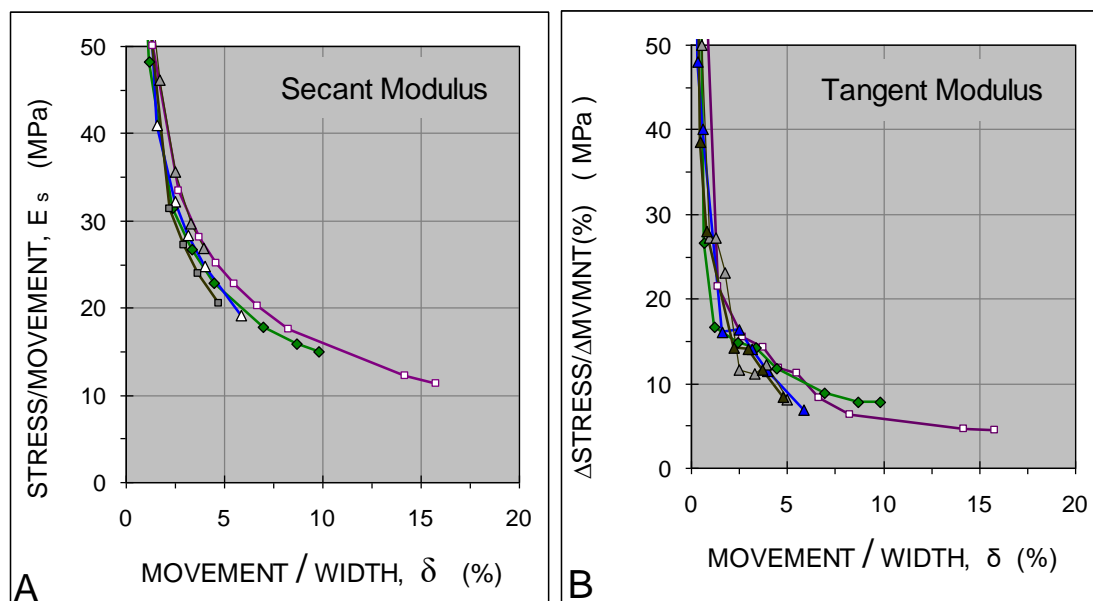


Fig. 3.10 Calculated Secant and tangent modulus curves for the five footing tests shown in Fig. 3.9.



## CHAPTER 4

### VERTICAL DRAINS TO ACCELERATE SETTLEMENT

#### 4.1 Introduction

All materials will undergo volume change when subjected to stress change and soils are no exception. Unlike steel or concrete and other solids, soils are made up of granular materials: grains. Moreover, the pores between the grains are usually filled with water, often a water and air (gas) mix. This fact makes the response of soil to an increase of stress more complex as opposed to other building materials. The shear strength of soil is more important for foundation design than the compressive strength, for example. The central aspect, however, is that in order for a volume change (other than the ‘elastic’ compression of the grains themselves) to take place, the space between the grains, the pores, must be able to reduce in volume. In a saturated soil, this requires that the water and/or gas first leaves the pore volume—can be squeezed out of the soil pores. The process is as follows. An increase of stress results in a small immediate, ‘initial’ or ‘elastic’, compression of the soil skeleton. If the pores contain free gas (‘bubbles’), the bubbles will compress, some of it may go into solution. This effect, too, is immediate, and the corresponding volume change (settlement) cannot be distinguished from the immediate compression. In inorganic soils, the immediate compression is small compared to the compression due to the reduction of the pore volume. However, reduction of pore volume cannot take place without the water in the pores simultaneously leaving the pores. The driving force in the latter process is the increase of pore pressure, which at first is about equal to the average of the imposed stress increase. As the water leaves the soil, the pressure reduces, “dissipates”, until, finally, all the imposed stress is carried as contact stress between the grains. The process is called “consolidation” and it is presented in Section 3.8.

The consolidation time is governed by how easy or difficult is for the water to flow through the soil along with the drainage path, the latter is the length the water has to flow to leave the zone of increased stress. The measure of the “difficulty” of the water to flow is the soil hydraulic conductivity (“permeability”) and the time is more or less a linear function of the “permeability” (related to the “coefficient of consolidation”), but it is an exponential function (square) of the drainage path. Therefore, if the drainage path can be shortened, the time for the consolidation settlement, which is the largest part of the three components of the settlement, can be shortened, “accelerated”, substantially. This is achieved by inserting drains into the soil, providing the water with the easy means of travel—“escape”—from the zone of stress increase. The spacing between the drains controls the length of the drainage path. For example, drains installed at a spacing that is a tenth of the thickness of a soil layer that is drained on both sides could, theoretically, shorten the consolidation time to a percentage point or two of the case without drains. An additional benefit is that because the water flows horizontally toward the drains (radially, rather), the flow makes use of the horizontal hydraulic conductivity of the soil, which normally is much larger than that in the vertical direction.

The potential benefit of using vertical drains became obvious very soon after Terzaghi in 1926 published his theory of consolidation. Thus, vertical drains have been used in engineering practice for almost 100 years. At first, vertical drains were made of columns of free-draining sand (sand drains) installed by various means (Barron 1947). In about 1945, premanufactured bandshaped drains, termed “wick drains”, were invented (Kjellman 1947) and, since about 1970, the technical and economical advantages of the wick drain have all but excluded the use of sand drains. Holtz et al. (1991) have presented a comprehensive account of the history of vertical drains. Lately, the preferred name is “Premanufactured Vertical Drains”, PVD. However, I have retained the “wick drain” term in this chapter.

#### 4.2 Conventional Approach to Pore Pressure Dissipation and Consolidation of a Drain Project

The basic principles of the behavior of consolidation in the presence of vertical drains is illustrated in Fig. 4.1. The dissipation of the excess pore pressures in the soil body is governed by the water flowing horizontally toward the drain and then up to the groundwater table. (Vertical flow toward draining layers above and below the soil body is usually disregarded). The pore water pressure distribution inside the drain is assumed to be hydrostatic at all times.

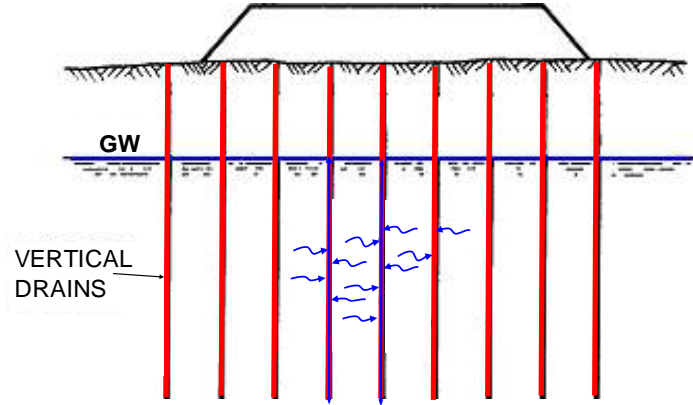


Fig. 4.1 Basic principles of consolidation process in the presence of vertical drains

For the analysis of acceleration of pore pressure dissipation in fine-grained soils (consolidation) for a vertical drain project and subsequent settlement, Barron (1948) and Kjellman (1948) developed a theory based on radial flow toward a circular drain in the center of a cylinder of homogeneous soil with an impervious outer boundary surface (Hansbo 1960; 1979; 1981; 1994). Vertical flow (drainage) was assumed not to occur in the soil. The theory is summarized in the Kjellman-Barron formula, Eq. 4.1. The Kjellman-Barron formula is based on the assumption of presence of horizontal (radial) flow only and a homogeneous soil.

$$(4.1) \quad t = \frac{D^2}{8c_h} \left[ \ln \frac{D}{d} - 0.75 \right] \ln \frac{1}{1-U_h}$$

where

- $t$  = time from start of consolidation (s)
- $D$  = zone of influence of a drain (m)
- $d$  = equivalent diameter of a drain (m)
- $U_h$  = average degree of consolidation for radial (horizontal) flow (--)
- $c_h$  = coefficient of horizontal consolidation ( $\text{m}^2/\text{s}$ )  
[ $1 \text{ m}^2/\text{s} = 3.2 \times 10^8 \text{ m}^2/\text{year}$ ; Section 3.8]

Eq. 4.1 can be rearranged to give the relation for the average degree of consolidation,  $U_h$ .

$$(4.1a) \quad U_h = 1 - \exp \left[ \frac{-8 c_h t}{D^2 \left( \ln \frac{D}{d} - 0.75 \right)} \right]$$

Fig. 4.2 shows a simplified sketch of the principle for consolidation of a soil layer. Fig. 4.2A shows a soil layer sandwiched between free-draining boundaries: the ground surface and a free-draining soil layer below the consolidating layer. The parabolic shape curve indicates the pore pressure distribution at a particular time. The time required for a certain degree of consolidation (in addition to the soil parameters of the case) is primarily a function of the longest drainage path, that is, half the thickness of the clay layer and assuming vertical flow. Fig. 4.2B shows the corresponding picture where vertical drains have been installed. Here, the consolidation time is primarily a function of the spacing of the drains and horizontal flow.

Note that the pore pressure in the drain is essentially hydrostatic. That is, the flow through the drain to the boundaries (ground surface and drain bottom) is a low-gradient flow. Indeed, the theoretical analysis assumes no gradient inside the drain. Therefore, testing the flow characteristics (conductivity; "ease of flow") of wick drains should be at very low gradients. Test under a gradient of unity is common, but it could show unrealistic drain response (see Section 4.5.3).

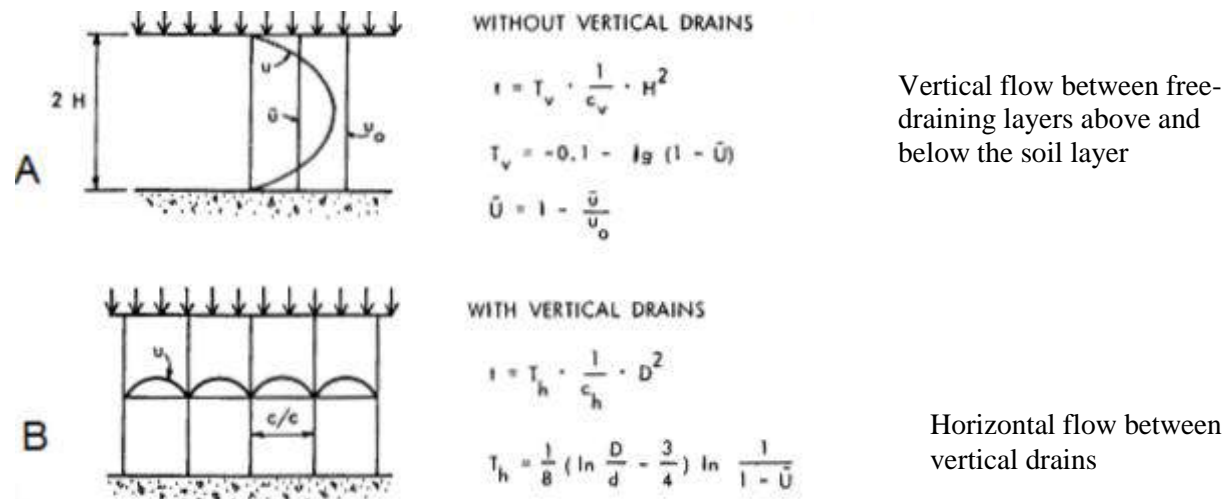


Fig. 4.2 Principles and formulae for consolidation of a soil layer

Relations for average degree of consolidation combining horizontal and vertical flows have been developed for vertical drains. However, the contribution of vertical drainage to the rate of consolidation is very small as opposed to the contribution by the horizontal drainage—the drainage toward the drains. In a typical case, vertical drainage alone could require 20 years, while installing drains to facilitate horizontal drainage could shorten the time to 3 months. Obviously, the contribution of the vertical drainage is usually minimal.

The zone of influence of a drain is defined as the diameter of a cylinder having the same cross section area as the area influenced by the drain. That is, if in a given large area of Size  $A$  there are  $n$  drains placed at some equal spacing and in some grid pattern, each drain influences the area  $A/n$ . Thus, for drains with a center-to-center spacing,  $c/c$ , in a square or triangular pattern, the zone of influence,  $D$ , is  $1.13 c/c$  or  $1.05 c/c$ , respectively, as illustrated in Fig. 4.3.

In the case of sand drains, the equivalent diameter,  $d$ , is often taken as equal to the nominal diameter of the sand drain. In the case of wick drains (Section 4.5), no agreement exists on what to use as the equivalent diameter of the drain. One approach used is simply to equalize the outside surface area of the

wick drain with a circular sand drain of the same surface. However, this approach does not recognize the difference between the usually open surface of the premanufactured drain and the rather closed surface of the sand drain, nor the differences between various makes of wick drains. Strictly speaking, the equivalent diameter of a wick drain should be termed “the equivalent cylinder diameter” to separate it from ‘the equivalent sand drain diameter’. Fellenius (1977) suggested that the equivalent cylinder diameter of a sand drain is the nominal diameter of the sand drain multiplied by the porosity of the sand in the drain. The porosity of loose, free-draining sand is normally about 0.4 to 0.5. Thus, the equivalent cylinder diameter of a sand drain is about half of the nominal diameter.

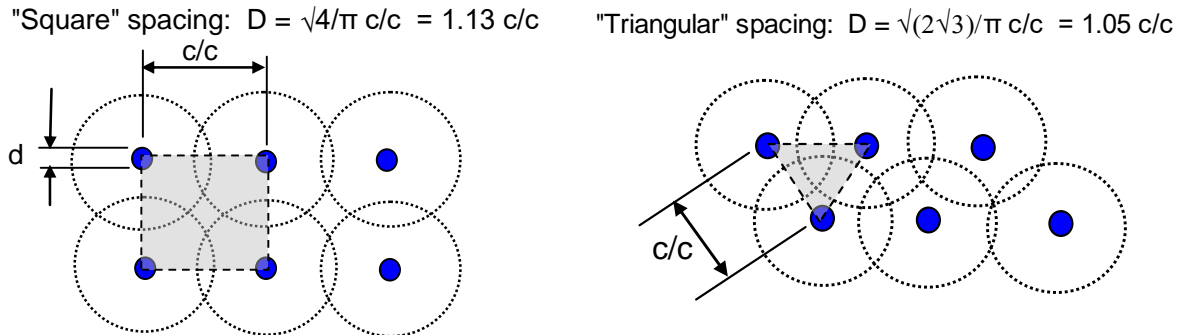


Fig. 4.3 Width of the Zone of influence for square and triangular spacings,  $c/c$ , between drains.

However, the question of what value of equivalent diameter to use is not of importance in practice because the consolidation time is not very sensitive to the variations of the value of the equivalent cylinder diameter. (In contrast, the consolidation time is very sensitive to the spacing of the drains). For wick drains of, commonly, 100-mm width, values proposed as the equivalent cylinder diameter have ranged between 30 mm and 80 mm, and full-scale studies have indicated that the performance of such drains have equaled the performance of sand drains of 200 mm to 300 mm in nominal diameter (Hansbo 1960; 1979; 1981; 1994).

The average degree of consolidation at a certain time,  $\bar{U}$ , is defined as the ratio between the average increase of effective stress,  $\Delta\sigma'$ , in the soil over the applied stress causing the consolidation process, i.e.,  $\Delta\sigma'/q$ . In practice, average degree of consolidation is determined from measurements of either pore pressure increase or settlement and defined as 1 minus the ratio between the average pore pressure increase in the soil over the total pore-pressure increase resulting from the applied stress,  $\bar{U} = 1 - u/u_0$ , or,  $\bar{U} = \Delta S/S_f$ , the amount of settlement obtained over the final amount of settlement at completed consolidation. Because pore pressures can be determined at the start of a project, whereas the value of the final settlement is not obtained until after the project is completed, the degree of consolidation is usually based on pore pressure measurements. However, pore pressures and pore-pressure dissipation vary with the distance to the draining layer and, in particular, with the distance to the drains. Seasonal variation is also a factor. Therefore, and in particular because pore-pressure measurements are usually made in only a few points, pore pressure values are very imprecise references to the average degree of consolidation.

The rate of consolidation may differ at different depths and locations due not least to variations of layer thickness. Therefore, also the average degree of consolidation based on settlement observations is also a rather ambiguous value, unless related to measurements of the compression of each specific layer (difference between settlement at top and bottom of the layer) and as the average of several such layers.

In a homogeneous soil layer, the horizontal coefficient of consolidation,  $c_h$ , is usually several times larger than the vertical coefficient,  $c_v$ . Moreover, dissipation time calculated according to the Kjellman-Barron formula (Eq. 4.1), is inversely proportional to the  $c_h$ -value. Note, however, that the drain installation will disturb the soil and break down the horizontal pathways nearest the drain (create a "smear zone") and, therefore, the benefit of the undisturbed horizontal coefficient may not be available. For sand drains, in particular displacement-type sand drains, a  $c_h$ -value greater than the  $c_v$ -value can rarely be mobilized.

For a detailed theoretical calculation, to consider the effect of a smear zone would seem necessary. However, in practice, other practical aspects (See Section 4.3) are far more influential for the process of accelerating settlement and theoretical refinements are rarely justified (see also Section 4.6.7) and Considering smear zone effect could distract the attention from the far more important aspects of choosing representative parameters and assessing the site conditions correctly.

The coefficient of consolidation,  $c_v$ , varies widely in natural soils (see Section 3.8). In **normally consolidated** clays, it usually ranges from  $1 \times 10^{-8} \text{ m}^2/\text{s}$  to  $30 \times 10^{-8} \text{ m}^2/\text{s}$  (3 to 100  $\text{m}^2/\text{year}$ ). In silty clays and clayey silts, it can range from  $5 \times 10^{-8} \text{ m}^2/\text{s}$  to  $50 \times 10^{-8} \text{ m}^2/\text{s}$  (16 to 160  $\text{m}^2/\text{year}$ ).

The coefficient of consolidation,  $c_v$ , is normally determined from laboratory testing of undisturbed soil samples or, preferably, in-situ by determining the pore-pressure dissipation time in a piezocone (CPTU; see Chapter 2). The actual  $c_h$ -coefficient to use requires considerable judgment in its selection, and it can, at best, not be determined more closely than within a relative range of three to five times. This means that engineering design of a project requires supporting data for selection of the  $c_h$ -coefficient in order to avoid the necessity of employing an excessively conservative approach.

The duration of the primary consolidation without the presence of vertical drains can take many years. When drains have been installed, the duration is typically shortened to a few months. Also a vertical drain project will include estimating the magnitude and rate of the secondary compression (Chapter 3, Section 3.9), which involves calculations with input of coefficient of secondary compression,  $C_\alpha$ , and duration of the primary consolidation  $t_{\text{CONS}}$ . First, the  $C_\alpha$  is considered to be a soil parameter that is independent of whether the consolidation is achieved by vertical or horizontal drainage. Then, using the, typically, 50 to 100 times shorter time for  $t_{\text{CONS}}$  for horizontal drainage (wick drains case) as opposed to that for vertical drainage will result in that the calculated settlement due to secondary compression will come out as an order of magnitude larger for a project where the consolidation process is having accelerated by means of vertical drains, as opposed to the number for where no vertical drains are used. Secondary compression is not governed by the direction of water flow nor can it reasonably be a function of the length of the drainage path. Therefore, the discrepancy is not true. It is the result of the fact mentioned in Section 3.9 that the secondary compression concept is an empirical approach to fit observations to some reasonable way of calculating and predicting the process. To resolve the discrepancy, when estimating the magnitude of secondary compression developing after the end of consolidation for a vertical drain project, the duration required for the consolidation had there been no drains should be estimated and used in calculating the settlement due to secondary compression.

### 4.3 Combined vertical and horizontal flow

Carillo (1942 and Asaoka (1978) developed Eq. 4.2 to express the average degree of consolidation for the case of combined horizontal and vertical consolidation. Note, however, that (1) the small distance between the drains (the drain spacing), (2) that the horizontal coefficient of consolidation,  $c_h$ , is larger than the vertical coefficient,  $c_v$ , and (4) the fact that the thickness of the clay layer is normally much larger than the drain spacing. The combined effect of this is that the effect of vertical drainage is normally insignificant.

$$(4.2) \quad \bar{U}_{omb.} = 1 - \frac{1 - \bar{U}_h}{1 - \bar{U}_v}$$

where

$\bar{U}_{omb.}$	=	Combined average degree of consolidation
$\bar{U}_h$	=	Average degree of horizontal consolidation
$\bar{U}_v$	=	Average degree of vertical consolidation

For example, if the horizontal degree of consolidation in the absence of vertical flow is 80 % and the vertical degree is 20 % in the absence of horizontal flow, the combined degree is 75 %, which is not that much smaller than the horizontal degree alone.

#### 4.4 Practical Aspects Influencing the Design of a Vertical Drain Project

In addition to the theoretical aspects, a design of a vertical drain project is affected by several practical matters, as outlined in this section. (The simplifications of the Kjellman-Barron formula is addressed in Section 4.7.1 as they affect the outcome of a design calculation).

##### 4.4.1 Drainage Blanket on the Ground Surface and Back Pressure

Unless the drains are taken into a free-draining soil layer below the fine-grained layer to be drained, the ground surface must be equipped with a drainage blanket and/or trenches to receive and lead away the water discharged from the drains. Drainage of the “below” layer is rarely assured and, therefore, most projects will include a drainage blanket on the ground surface. Sometimes, the natural ground may provide sufficient drainage to serve as the drainage blanket. Absence of a suitable drainage blanket may result in water ponding in the bowl-shaped depression that develops as the soil settles, creating a back pressure in the drains that impairs the consolidation process. This is illustrated in Fig. 4.4. Ponding due to insufficient horizontal drainage on the ground surface is not acceptable, of course. In a design of a vertical drain project, the expected amount of settlement must be calculated and a surface drainage scheme designed that ensures a horizontal gradient away from the treated area at all times.

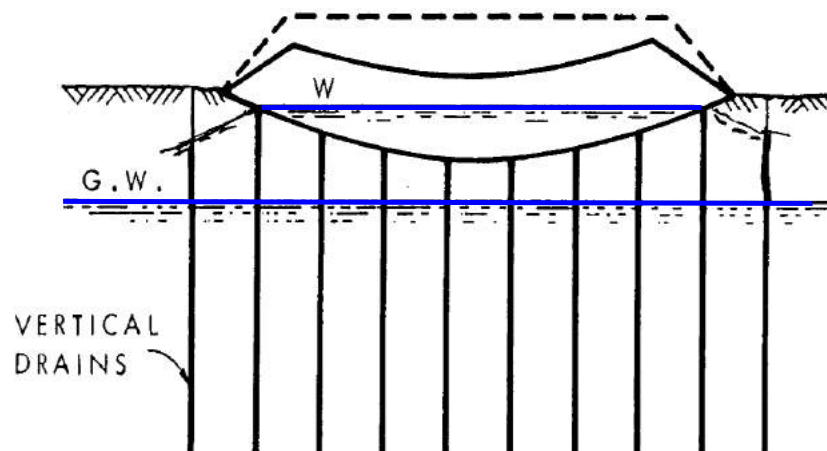


Fig. 4.4 Effect of water ponding below the embankment in the absence of a surface drainage blanket

The build-up of back pressure will halt or slow down the time development of the consolidation settlement, which, if the process is monitored, is discernible as a flattening out of the time-settlement curve or a curve with a humpback appearance. This may lead to the false conclusion that all of the primary settlement has been obtained. However, eventually, the back pressure will disappear, and the settlement, delayed due to the back pressure, will recur. If the back-pressure is temporary, the settlement versus time curve will show a hump back, a slow-down followed by an increased of the settlement rate.

It is also important to realize that as the embankment settles, the total vertical stress imposed to the original ground surface over and above the existing vertical stress reduces accordingly, which the modeling needs to take into consideration (because the height of the original ground surface above the groundwater table reduces). This is particularly important where the groundwater level lies close to the original ground surface.

#### **4.4.2 Effect of Winter Conditions**

In areas where Winter conditions prevail, consideration must be given to the risk of the ground frost reducing or preventing the drain discharge at the groundwater table or into the drainage blanket at the ground surface building up a back pressure. The result is similar to that of ponding: a slow-down of the settlement, which can be mistaken for the project having reached the end of the primary consolidation. After the Spring thaw, the settlement will recur.

#### **4.4.3 Depth of Installation**

The installation depth is governed by several considerations. One is that drains will not accelerate consolidation unless the imposed stress triggering the consolidation brings the effective stress in the soil to a value that is larger than the preconsolidation stress. i.e., the imposed stress is larger than the preconsolidation margin. The imposed stress decreases with depth (as, for example, determined by Boussinesq formulae; Chapter 3). From this consideration, the optimum depth of the drains is where the imposed stress is equal to the preconsolidation margin. However, other considerations may show that a deeper installation is desirable, e.g., to assure water discharge into a deeper located pervious soil layer.

#### **4.4.4 Width of Installation**

Drains installed underneath an embankment to accelerate consolidation must be distributed across the entire footprint of the embankment and a small horizontal distance beyond. A rule-of-thumb is to place the outermost row of the drains at a distance out from the foot of the embankment of about a third to half the height of the embankment. If the drains are installed over a smaller width, not only will differential settlement (bowing or dishing) increase during the consolidation period, the consolidation time will become longer.

#### **4.4.5 Effect of Pervious Horizontal Zones, Lenses, Bands, and Layers**

The assumption of only homogeneous soil, whether with only radial flow or radial flow combined with vertical flow, used in the derivation of the formulae is not realistic. In fact, most fine-grained clay soils contain horizontal zones of pervious soil consisting of thin lenses, bands, or even layers of coarse-grained soil, such as silty sand or sand. These layers have no influence on the consolidation process where and when no drains are used. However, where vertical drains have been installed, the drainage is to a large extent controlled by the vertical communication between these zones as facilitated by the drains. As illustrated in Fig. 4.5, the consolidation is then by way of slow vertical flow in the fine-grained soil to the lenses, followed by rapid horizontal flow in the lens to the vertical drain, and, then, in the drain to the

surface blanket. In effect, the lenses take on the important function of drainage boundaries of the less pervious layers of the soil body sandwiched between the lenses. That is, the mechanism is still very much that of a vertical flow.

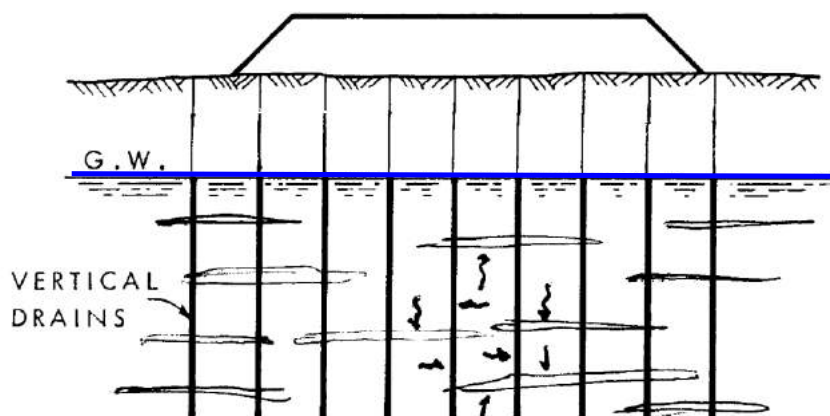


Fig. 4.5 Actual flow in a soil containing pervious lenses, bands, or layers

It is vital for a design of vertical drain project to establish the presence of such lenses, bands, or layers of coarse-grained soil and their vertical spacing. Conventional boreholes and laboratory analysis of recovered samples are rarely fully suitable for this purpose and, usually, once it becomes clear that vertical drains are considered for a project, additional field investigation involving both undisturbed sampling, CPTU tests, and special laboratory testing may become necessary.

#### 4.4.6 Surcharging

The rate of consolidation always slows down significantly toward the end of the consolidation period. The time between about 80 % and 95 % of primary consolidation can require as long time as that from start to 80 %, and the time from 95 % to, say, 98 % can take a very long time. It is not practical to design for a target completion level greater than an average degree of consolidation of 80 %. To reach even that level within a reasonable time requires a surcharge ("overload") to be placed along with embankment. The surcharge is an extra embankment load (extra height) that is removed when the average degree of consolidation has reached the target level, usually about 80 % of the average degree of consolidation for the embankment plus surcharge. The magnitude of the surcharge load should be designed so that after removal, the consolidation of the remaining embankment is completed, resulting in more than a "100 % consolidation" for the embankment without the surcharge. The timing of the removal of the surcharge normally coincides with preparing the embankment for paving of the road bed.

The results of a vertical drain project must always be monitored. This means that the programme must include a carefully designed schedule of ground surface measurements of settlement as well as a good number of depth-anchors or similar gages to monitor the distribution of settlement. Piezometers to measure pore pressures are also required (the analysis of pore pressure records must be made with due respect to fact that the distance between a piezometer tip and a drain cannot be known with good accuracy). The time to remove the surcharge must depend on the measurement data. It is helpful to plot the settlement values a settlement versus log-time as the project proceeds. Such lin-log plots will show the settlement plot to appear in an approximately straight line on reaching 80+ % consolidation. Such plots should represent the development in individual soil layers, not just be from ground surface values.



A monitoring programme should include several stations measuring pore pressure distribution and settlement distribution with depth (not just settlement of the ground surface) and monitoring should commence very early in the project; immediately on preparing the ground and before placing the first lift of the fill.

It is absolutely necessary to realize that the purpose of the monitoring programme is not just to confirm that the project performed satisfactorily, that is, performed as intended and expected. The monitoring programme must be designed to respond to the key purpose of providing records for early discovery and analysis in case the project would not perform satisfactorily and, also, to provide data that will be sufficient for a comprehensive study of the conditions so that a remedial programme can be designed if needed (see also Section 4.4.10). To the same end, it is very worthwhile to include in the monitoring arrangement a station away from the drain area to monitor the performance for conditions of no drains but otherwise identical to those of the project. For a case history reporting an unsatisfactory performance of a wick drain project, see Fellenius and Nguyen 2013.

Figure 4.6 shows settlements measured in one point below a test embankment, where wick-drains were installed. The dotted lines indicate the reducing fill height due to the ongoing settlement. On removal of the surcharge (to half height), settlement essentially ceased (a small heave is expected to occur, provided full consolidation has had time to develop for the remaining embankment height).

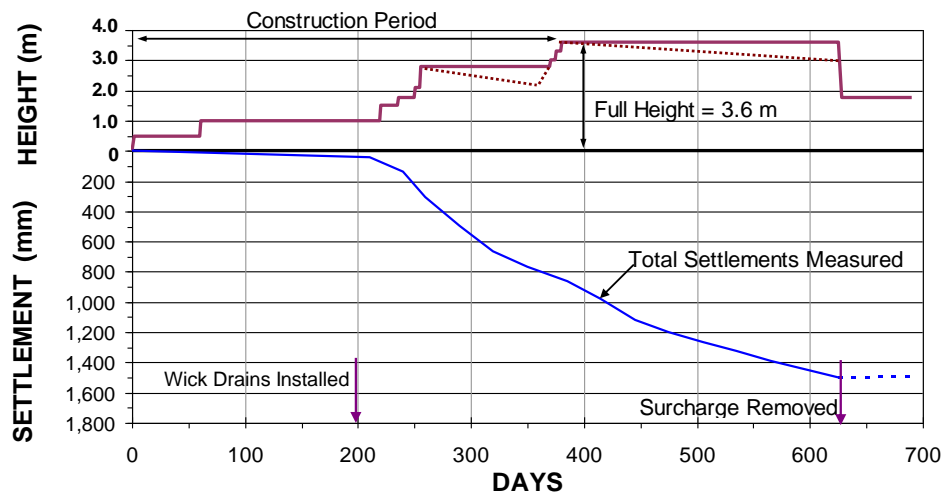


Fig. 4.6 Settlement measured for a stage-constructed test embankment.  
Data from Moh and Lin (2006).

On completion of the consolidation, the soil supporting the embankment is normally consolidated. This means that future settlement may occur due to small additional loading of the soil from, for example, a moderate raising of the elevation of the road bed or widening the embankment during future maintenance work, or, indeed, even from a load increase due to seasonal variation of the groundwater table (a lowering of the groundwater table will increase the effective stress and initiate—renew—the consolidation). For this reason, it is advisable that the project be designed so as to leave the soil underneath the final structure at a suitable level of preconsolidation stress. This means that the design of a vertical drain project should always incorporate a surcharge (i.e., an "overload"; an extra embankment load to be removed on completion of the consolidation).

#### 4.4.7 Stage Construction

Constructing an embankment to full height in one stage may give rise to concern for the stability of the embankment. Lateral soil spreading will be of concern and not just slope failure. Usually, the instability occurs in the beginning of construction and the risk subsides as the pore pressures reduce due to the consolidation. The stability of the embankment can be ensured during the construction by building in stages—stage construction—and with careful monitoring and evaluation (engineering review) of the consolidation progress. The construction time can be very long, however, unless accelerated by means of vertical drains.

Vertical drains are very effective means to minimize lateral spreading and improve embankment stability. The drains accelerate the consolidation process so that the construction rate is not at all, or only moderately, affected by the stability concern, whereas constructing the embankment without drains would have necessitated stage construction and generally prolonged the construction time and/or necessitated incorporating relief embankments or other resource-demanding methods to offset the concern for stability and lateral movements.

Figure 4.7 shows observed settlements and movements for a stage-constructed 3.6 m high test embankment during the construction of the new Bangkok International Airport, Thailand. Settlement was monitored in center and at embankment edges and horizontal movement was monitored near the sides of embankment. Time from start to end of surcharge placement was nine months. Observation time after end of surcharge placement was eleven months. Compare the maximum lateral movements at the embankment edges, about 180 mm, to the settlements, 1,400 mm. The lateral movements are large. However, without the drains they could easily have twice as large. Note also that the lateral movement is the reason for that the edges of the embankment settle more than the center.

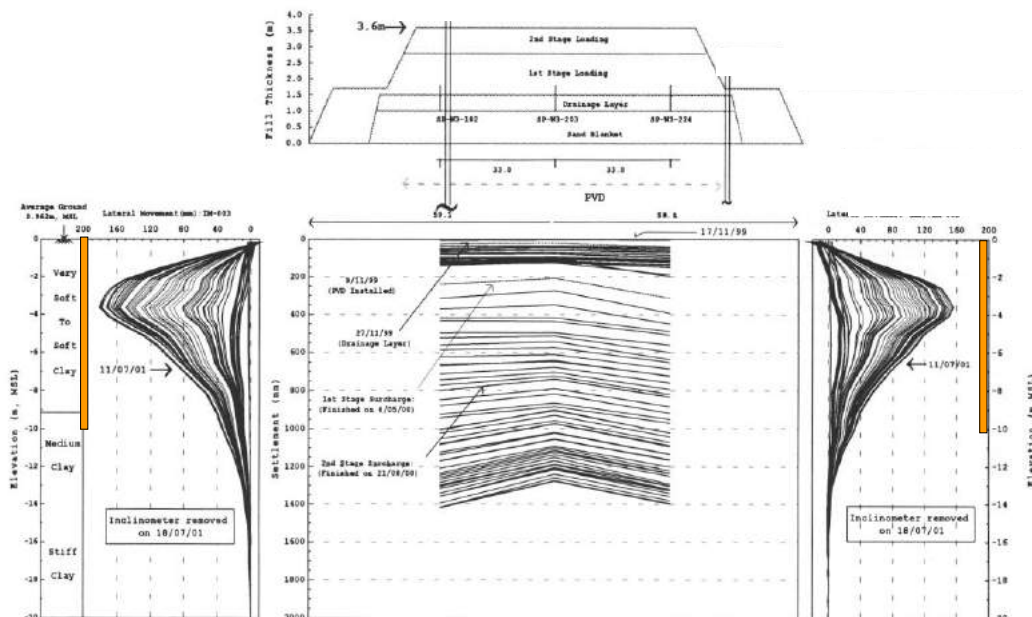


Fig. 4.7 Settlement and lateral movement for a stage-constructed 3.6 m high test embankment. From Moh and Lin (2006; used with permission).

#### 4.4.8 Loading by Means of Pumping to Achieve Vacuum Effect

Instead of, or in conjunction with, an embankment load, the stress increase driving the consolidation process can be by means of suction, that is, applying a vacuum on the ground surface with vertical drains installed in the ground (Holtz and Wager 1975). Usually, the vacuum method involves placing an impervious membrane (a tarp) on the ground and pumping out the air underneath it. (Chai et al. 2005; 2006). The vacuum method involves many practical issues not mentioned here. One alternative application of the method includes connecting each drain to a suction pipe (Cortlever et al. 2006).

The theoretical maximum vacuum is equal to the atmospheric pressure (100 kPa), which corresponds to an about 5 m high embankment. However, the actual vacuum possible is no more than about half the theoretical maximum. A difference between applying a stress using the vacuum method is that the stress does not cause outward lateral movement, but inward, albeit small. Also, even in very soft soils, no slope stability concerns exists. Combining the vacuum method with an embankment loading may eliminate the need for stage-construction.

Pumping in wells drilled to pervious sand lenses or layers in or below the layer to consolidate will also accelerate the consolidation. The primary effect of the pumping is to reduce the pore pressure in the drains at the location of the pervious layers and, thus, lower the pore pressures in the full length of the vertical drains, which will increase the horizontal gradient toward the drains. Some effect will be achieved from the lowering of the pore pressures in the drainage zone below the consolidating layer, which improves also the vertical drainage of the layer; shortens the consolidation time.

#### 4.4.9 Pore Pressure Gradient and Artesian Flow

Bridges and associated embankments are usually placed near rivers, in valleys, or other low-lying areas. Most of these areas are characterized by a clay layer underlain by pervious soils that function as an aquifer separated from the surficial water table. Commonly, the pore pressure distribution in the lower layers at the site has an upward gradient, it may even be artesian. Drains installed at these sites will not change the pore pressure in the lower soils. However, the drains may change the pore pressure gradient to hydrostatic. This change will offset some of the increase of effective stress due to the embankment and have the beneficial effect of reducing the magnitude of the embankment-induced settlement. However, the change of the pore pressure distribution from upward gradient to hydrostatic distribution will act as a back pressure and slow down the consolidation rate. To adjust for this, an extra surcharge may be required. Moreover, arranging for a proper surface drainage of the site will be important as water may be transported up to the ground surface from the lower soil layers for a very long time.

#### 4.4.10 Monitoring and Instrumentation

It is imperative to verify that the consolidation proceeds as postulated in the design. Therefore, a vertical drain project must always be combined with an instrumentation programme to monitor the progress of the consolidation in terms of **settlement and pore pressure** development during the entire consolidation period, and often include also lateral movement during the construction. Pore pressures must be monitored also outside the area affected by either the embankment or the drains to serve as independent reference to the measurements.

Instrumentation installed at a construction site has a poor survival rate. It is very difficult to protect the instrumentation from inadvertent damage. Sometimes, to avoid disturbing the construction work, the monitoring may have to be postponed. Often, a scheduled reading may have to be omitted as it may be too risky for a technician to approach the gage readout unit. Therefore, the monitoring programme should include buried gages and readings by remote sensing. As it is normally not possible for the monitoring

programme to control the construction and to ensure that records are taken at important construction milestones, the programme should include automatic data logging set to take readings at frequent intervals. Still, the possibility of damage to the gages cannot be discounted. Therefore, a certain level of redundancy in the layout of instrumentation is necessary.

The monitoring programme must include frequent correlations between the monitoring results and the design to catch any anomalies that can adversely affect the project. To this end, the design should include calculations of expected response at the locations of planned instrumentation. However, a design can never anticipate every event that will arise at a construction project. Therefore, the design should preauthorize provisions for performing analysis of the effect of unexpected events, such as extreme rainfall or drought during the monitoring period, unanticipated construction events involving fill, excavation, or pumping of groundwater, delays of completion of the construction, etc., so that necessary calculations are not delayed because time otherwise required for authorizing the subsequent analyses and adding supplemental instrumentation. Instrumentation design (type, placement depths and locations etc.) is a task for a specialist—the inexperienced must solicit assistance.

#### **4.5 Sand Drains**

The sand drain was the first type of vertical drain to be used for accelerating the pore pressure dissipation (during the mid-1930s). The following aspects are specific to the use of sand drains.

Sand drains are usually made by driving or vibrating a pipe into the ground, filling it with sand and withdrawing it. As indicated by Casagrande and Poulos (1969), the installation of full-displacement sand drains (driven drains) in soils that are sensitive to disturbance and displacement may decrease hydraulic conductivity and increase compressibility. As a consequence, the settlement could actually increase due to the construction of the drains.

The sand used in a sand drain must be free draining (not just "clean"), which means that the portion of fine-grained soil in the sand—in the completed sand drain—must not exceed 5 % by weight and preferably be less than 3 %. Constructing sand drains by pouring sand down a jetted water-filled hole will have the effect that silt and clay under suspension in the water will mix with the sand and cause the fines contents to increase to the point that the sand is no longer free-draining. In theory, this can be avoided by washing the hole with water until the water is clear. However, in the process, the hole will widen and the site will become very muddy and, potentially, the mud will render useless the drainage blanket on the ground. Simply put, a free-standing hole that can be washed clear of fines is made in a soil that does not need drains. If the hole is created by washing out the soil, then, before the sand is placed, a pipe must be inserted into which the sand is poured. The pipe is withdrawn after the pipe has been filled with sand. It is advisable to withdraw using vibratory equipment to make sure that the sand does not arch inside the pipe.

Sand drains are apt to neck and become disrupted during the installation work, or as a consequence of horizontal movements in the soil. The function of a necked or disrupted drain is severely reduced.

Sand drains have been constructed in the form of sand-filled long bags, hoses, called "sand wicks", which are inserted into a drilled hole

The stated disadvantages notwithstanding, sand drains can be useful where large flows of water are expected, in soils less sensitive to disturbance by the installation, and where the ratio of length to the nominal diameter of the drain is not greater than 50, and the ratio of spacing to nominal diameter is larger than 10.

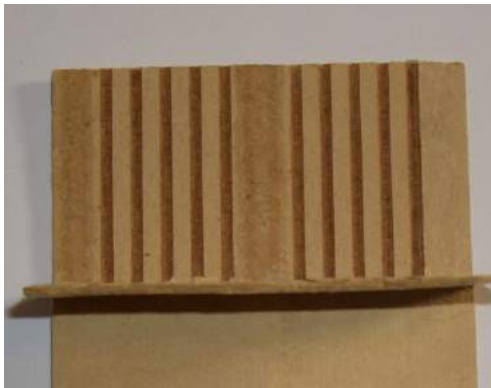
Since the advent of the prefabricated bandshaped drain, the wick drain, sand drains are rarely used as vertical drains to accelerate consolidation in fine-grained soils.

## 4.6 Wick Drains

### 4.6.1 Definition

A wick drain is a prefabricated band-shaped about 100 mm wide and 5 mm to 10 mm thick unit consisting in principle of a channeled (grooved or studded) core wrapped with a filter jacket (Figs. 4.8 -4.10). Installation is usually by means of a mandrel pushed into the ground (Fig. 4.11). The filter jacket serves the purpose of letting water into the drain core while preventing fine soil particles from entering. The channels lead the water up to a drainage layer on the ground surface, or to the groundwater table, or down to a draining layer below the consolidating soil layer. For details see Holtz et al. (2011).

The Kjellman Cardboard Wick; 1942



The Geodrain; 1976



The Alidrain or Burcan Drain; 1978



The Mebra Drain; 1984 (Castle board Drain; 1979)



Fig. 4.8 Photos of four types of wick drains





Fig. 4.9 View over a site after completed wick drain installation



Fig. 4.10 Water discharging from a drain immediately outside the embankment

#### 4.6.2 Permeability of the Filter Jacket

There are statements in the literature (e.g., Hansbo 1979) that the drain filter would not need to be any more pervious to water than the soil is, that is, have a hydraulic conductivity of about  $1 \times 10^{-8}$  m/s. This value is representative to that of a practically impervious membrane and the statement is fundamentally wrong. The filter must be able to accept an inflow of water not only from clay soil, but also from coarser soils, such as silty, fine sand typically found in lenses, or layers in most fine-grained soils—plentiful in most clays. In such soils, the portion reaching the drain through the clay is practically negligible. Moreover, the **outflow**, i.e., the discharge, of water must also be considered: **what enters the drain must exit the drain** (c.f., Fig. 4.10). While the drain receives water over its full length, typically, 5 m through over 20 m, it must be capable of discharging this water through a very short distance of its length (discharge through the end of the drain is a rather special case). Therefore, the hydraulic conductivity of the filter must not be so small as to impede the outflow of water. Generally, the filter must have a hydraulic conductivity (permeability coefficient) no smaller than that of coarse silt or fine sand, approximately  $1 \times 10^{-6}$  m/s.



Fig. 4.11 Installation of wick drains type Alidrain (courtesy of J.C. Brodeur, Burcan Industries Ltd.)

If the permeability of the drain filter is such that a head above the groundwater table appears inside the drain, the so developed back pressure (Fig. 4.12) will slow down the consolidation process and impair the function of the drain. Examples exist where, due to a too low hydraulic conductivity of the filter jacket, the water has risen more than two metre inside the drain above the groundwater table before a balance was achieved between inflow in the soil below and outflow in the soil above the groundwater table (Fellenius 1981). The effect was that about one metre of surcharge was wasted to compensate for the two metre rise of the water above the groundwater table. It is the rare occasion that the cut-off end of the drain is placed at the groundwater table (removing the need for the water to leave the drain through the filter jacket).

#### 4.6.3 Discharge Capacity

An aspect of importance to a wick drain is the discharge capacity (well resistance) of the drain. Holtz et al. (1991) define the discharge capacity of a drain as the longitudinal flow under a gradient of unity (1.00). However, when this definition is coupled with the, by others, oft-repeated statement that the discharge capacity of most drain wicks is greater than  $100 \text{ m}^3/\text{year}$ , i.e.,  $20 \text{ cm}^3/\text{minute}$  (the volume in a small-size glass of water), the inevitable conclusion is that the discharge capacity is not important. The face value of this conclusion is correct, discharge capacity at a gradient of unity is not important. However, discharge capacity at low gradient is very important! The flow in a drain occurs under a very small gradient, about 0.01, not 1.00. Note that the basic premise of the Kjellman-Barron relation that the pore pressure distribution inside the drain is hydrostatic is not quite true—a gradient of zero means no flow! As to the actual discharge, in the extreme, consolidation settlement accelerated by means of drains can amount to about 0.1 m to 0.5 m, for the first month. A drain typically discharges water from a plan area, "footprint", of about  $2 \text{ m}^2$ . Therefore, the corresponding discharge per drain is approximately  $0.2 \text{ m}^3$  to  $1 \text{ m}^3$  per month, or  $0.005$  to  $0.02 \text{ cm}^3/\text{minute}$ . To achieve this flow of water under the more realistic small gradient, adequate discharge capacity and well resistance to outflow are important factors to consider.

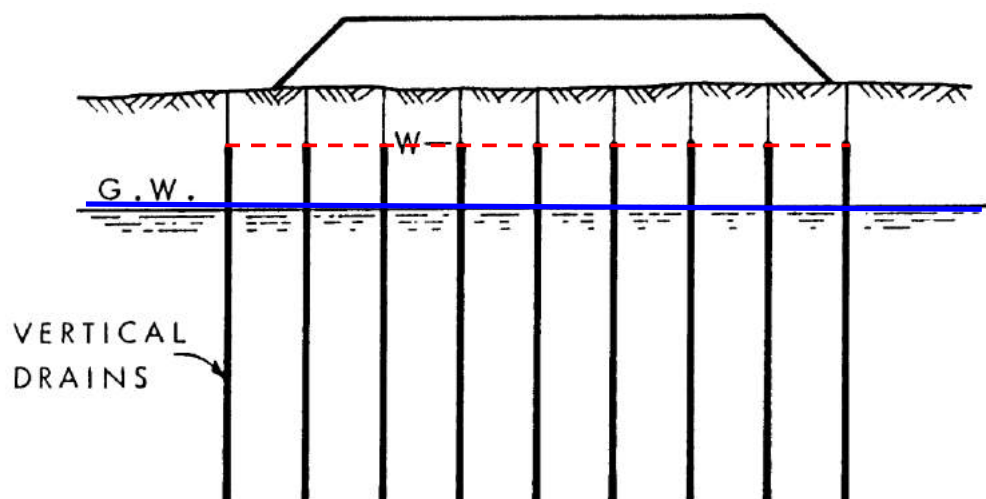


Fig. 4.12 Back pressure in wick drains with filter jacket inadequate for discharge of water

Nevertheless, laboratory tests suggest that most modern prefabricated drains have adequate discharge capacity and acceptably small well resistance. That is, water having entered through the filter is not appreciably impeded from flowing up toward the groundwater table through the drain (or down into pervious non-consolidating layers, if the drains have been installed to reach into such layers). *Nota Bene*, this is conditional on that one can assume that the drains stay straight and have no kinks or folds (microfolds) crimping the drain core. However, this one cannot assume, because, as the soil consolidates, the drains shorten and develop a multitude of kinks and folds, as explained in the following.

Not all drain are alike. Some drains are less suitable for use to large depth. A drain that has a soft compressible core will compress due to the large soil stress at depth and the water flow through the drain will be impeded. The drain core must be strong enough to resist large, lateral (confining) soil stresses without collapsing as this could close off the longitudinal drainage path. For example, at a depth of 20 m in a clay soil underneath a 10-m high embankment, the effective soil stress can exceed 400 kPa, and it is important that the drain can resist this stress without the function of the drain becoming impaired. Fellenius and Nguyen (2013) report a case where the wick drains did not function below about 20 m depth due to the drain core having become compressed.

#### 4.6.4 Microfolding and Crimping

Settlement is the accumulation of relative compression of the soil which for most cases ranges from about 5 % through 20 % and beyond. A drain cannot buckle out into the soil, nor can it compress elastically, but must accommodate the soil compression in shortening through developing series of folds—microfolds, also called crimping. Microfolds will reduce the discharge capacity if the grooves or channels block off the flow of the water when folded over. Some drain types are more susceptible to the crimping effect of microfolding than others. Most of the time, though, the filter jacket will channel the water so as to circumvent a blocked location. Drains where the filter jacket is kept away from the central core by a series of studs, which maintain the open flow area inside the drain, as opposed to longitudinal grooves or channels, can accommodate microfolding without impeding the flow of water. It is important to verify that a wick drain considered for use at a site, will be able to resist the significant soil forces at depth without becoming compressed the point of ceasing to function. Several disastrous examples exist of flimsy wick drains that ceased to function below certain shallow depth.



#### **4.6.5 Handling on Site**

The wick drain is often manhandled on the construction site: it is dragged on a truck floor and on the ground, it is left in the sun and in the rain, it gets soaked and is then allowed to freeze, it is stepped on, etc. This puts great demands on strength, in particular wet strength, on the filter and the glue, or weld, used to hold the longitudinal filter seam together. Clay or mud can easily enter and block off the flow in the drain core through a rip or tear in the filter. One such spot in a drain may be enough to considerably impair its function. The filter must have an adequate strength, dry or wet.

#### **4.6.6 Axial Tensile Strength of the Drain Core**

A factor also affecting the proper function of a drain and its discharge ability is the tensile strength of the drain core. Wick drains are installed from a roll placed near the ground from where they are pulled up to the top of the installation rig, where they pass over a pulley and go down into an installation mandrel that is forced into the ground. Ever so often, the mandrel tip meets resistance in an interbedded dense layer. This resistance is often overcome very suddenly resulting in an abrupt increase of mandrel installation velocity with the consequence that the drain is yanked down. The filter jacket is usually loose and able to accommodate the sudden pull, but many types of wick drains have thin and weak cores that can easily be torn apart. A drain with a partial or full-width tear of the core will not function well and, as the damage cannot be seen by the field inspection, adequate tensile strength of the drain core is an important condition to consider in the selection of a drain.

#### **4.6.7 Smear Zone**

When moving the installation mandrel down and up in a clay, a zone nearest the mandrel is remolded. This zone is called the smear zone. The Kjellman-Barron solution can be refined by incorporating a smear zone into the formula apparatus. It is questionable how important a role smear plays, however. A wick drain has typically a cross sectional area of  $5 \text{ cm}^2$ . It is sometimes installed using a flattened mandrel having a cross section of about  $100 \text{ cm}^2$ , or, more commonly, using a circular mandrel having a cross section of  $200 \text{ cm}^2$ . The installation, therefore, leaves a considerable void in the ground, which, on withdrawing the mandrel, is partially and more or less immediately closed up. In the process, fissures open out from the drain and into the soil. The fissuring and “closing of the void” may be affected by the installation of the next drain, placing of fill on the ground, and/or by the passing of time. The net effect will vary from locality to locality. However, the creation of a void and its closing up, and creation of fissures is far more important than what thickness and parameters to assign to a smear zone. Smear requires careful modeling of the soil hydraulic conductivity and coefficient of consolidation in both horizontal and vertical directions, as well as of all other pertinent soil parameters. To incorporate smear in the Kjellman-Barron radial flow formula mostly serves as a fudge concept to fit the formula to data in a back-calculation. Incorporating smear zone effects in a design of a wick-drain project is not meaningful.

#### **4.6.8 Site Investigation**

A properly designed and executed subsurface investigation is vital to any geotechnical design. Unfortunately, it is the rare project where the designer has the luxury of knowing the soil in sufficient detail. On many occasions, the paucity of information forces the designer to base the design on “playing it safe”. The design of a wick drain project will be very much assisted by having CPTU soundings and continuous tube sampling, as both will aid in determining the presence and extent of lenses, bands, and seams in the soil.

#### **4.6.9 Spacing of Wick Drains**

The design of the spacing to use for a wick drain project can be calculated by means of the Kjellman-Barron formula (Eq. 4.1) with input of the coefficient of consolidation and the desired time for the desired degree of consolidation to be achieved with due consideration of the amount of surcharge to use, etc. More sophisticated analysis methods are available. However, the accuracy of the input is frequently such that the spacing can only be determined within a fairly wide range, be the calculation based on the simple or the sophisticated methods. It is often more reliable to consider that a suitable spacing of drains in a homogeneous clay is usually between 1.0 m and 1.6 m, in a silty clay between 1.2 m to 1.8 m, and in a coarser soil between 1.5 m to 2.0 m. The low-range values apply when presence of appreciable seams or lenses have not been found and the upper-range values apply to sites and soils where distinct seams or lenses of silt or sand have been established to exist. It is often meaningful to include an initial test area with a narrow spacing (which will provide a rapid response) and monitor the pore pressures and settlement for a month or so until most of the consolidation has developed. The observations can then be used to calibrate the site and the design of the rest of the site can then be completed with a wider and more economical spacing.

#### **4.7 Closing remarks**

Acceleration of settlement by means of vertical wick drains an approach with many spin-off benefits. The drains will accelerate the settlement, maybe to the point that, for example in case of a highway, when the road is about to be paved, most of the consolidation settlement has occurred, which minimizes future maintenance costs. If a structure, be it a bridge or a building is to be placed on piles and downdrag (i.e., settlement) is a concern for the piles, a quite common situation, accelerating the settlement with drains so that the settlement occurs before the structure is completed, may alleviate the downdrag problem. If lateral spreading (horizontal movements in the soil) due to fills or embankments imposes lateral movements in the soil that cause the piles to bend, wick drains will reduce the maximum pore pressures and reduce the lateral spreading (Harris et al. 2003).

The analysis of the site conditions aided by the more careful site investigation will have the beneficial effect that the designers will become more aware of what the site entails and be able to improve on the overall geotechnical design for the site and the structures involved. In this regard, note my comments in Section 4.4.10 on monitoring a wick drain project.

## CHAPTER 5

### EARTH STRESS —EARTH PRESSURE

#### 5.1 Introduction

“Earth stress” is the term for soil stress exerted against the side of a foundation structure—a “wall”. Many use the term “earth pressure” instead, which is incorrect in principle because “pressure” denotes an omni-directional situation, such as pressure in water, whereas the stress in soil is directional, a vector. The misnomer is solidly anchored in the profession and to try to correct it is probably futile. Nevertheless, this chapter applies the term “earth stress”.

Earth stress is stress against a wall from a retained soil body. Loads supported on or in the soil body near the wall will add to the earth stress. The magnitude of the stress against a wall is determined by the physical parameters of the soil, the physical interaction between the soil and the wall, the flexibility of the wall, and the direction and magnitude as well as manner of movement (tilting and/or translation) of the wall. The latter aspect is particularly important. When the wall moves outward, that is, away from the soil—by the soil pushing onto the wall, moving out it or tilting it away, an ‘active’ condition is at hand and the earth stress is said to be “active”. If instead the wall moves toward the soil—by outside forces pushing the wall into the soil— the earth stress is said to be “passive”. In terms of magnitude, the active stress against the wall is much smaller than the passive stress; the relative magnitude can be a factor of ten, and, in terms of amount of movement required for full development of stress, the active stress requires a smaller movement than that required for developing the passive stress. The displacement necessary for full active condition is about 1 % of the wall height; less in dense sand, more in soft clay, and that necessary for full passive condition is about 5 % of the wall height; less in dense sand, more in soft clay. Many text books and manuals include diagrams illustrating the relative displacement necessary to fully develop the active stress (reduce the intensity) and ditto for the passive stress (increase the intensity) for a range of conditions.

In non-cohesive soils, conventionally, the unit stress at a point on the wall is proportional to the overburden stress in the soil immediately outside the wall. The proportionality factor is called “earth stress coefficient” and given the symbol “ $K$ ” (the word “coefficient” is spelled “Koefficient” in German, Terzaghi’s first language). The earth stress acting against the wall at a point is a product of the  $K$ -coefficient and the overburden stress. In a soil deposited by regular geologic process in horizontal planes, the horizontal stress is about half of the stress in vertical direction, that is, the earth stress coefficient is about 0.5 (notice, the value can vary significantly; see also Section 3.13.3). It is called the “coefficient of earth stress at rest” (“coefficient of earth pressure at rest”) and denoted  $K_0$  (pronounced “K-nought”). Once a movement or an unbalanced force is imposed, the ratio changes. If the wall is let to move and the soil follows suit, the earth stress coefficient reduces to a minimum value called “coefficient of active earth stress” and denoted  $K_a$ . Conversely, if the wall forced toward the soil, the earth stress coefficient increases to a maximum value called “coefficient of passive earth stress” and denoted  $K_p$ .

The earth stress coefficient is a function of many physical parameters, such as the soil strength expressed by the friction angle, the roughness of the wall surface in contact with the soil, the inclination of the wall, and the effective overburden stress. The effective overburden stress is governed by the weight of the soil, the depth of the point below the ground surface, and the pore pressure acting at the point. Despite this complexity, the earth stress coefficient is determined from simple formulae.

## 5.2 The Earth Stress Coefficient

Fig. 5.1 shows an inclined, rough-surface gravity retaining wall subjected to earth stress from a non-cohesive soil body with an inclined ground surface. The unit active earth stress against the wall acts at an angle of  $\delta$  formed by a counter-clockwise rotation to a line normal to the wall surface. The unit active earth stress is calculated as  $K_a$  times the effective overburden stress and the coefficient,  $K_a$ , is given in Eq. 5.1a.

$$(5.1a) \quad K_a = \frac{\sin(\beta - \phi')}{\sin \beta [\sqrt{\sin(\beta + \delta)} + \sqrt{\sin(\delta + \phi') \sin(\phi' - \alpha) / \sin(\beta - \alpha)}]}$$

where

- $\alpha$  = slope of the ground surface measured counter clock-wise from the horizontal
- $\beta$  = inclination of the wall surface measured counter clock-wise from the base
- $\phi'$  = effective internal friction angle of the soil
- $\delta$  = effective wall friction angle and the rotation of the earth stress measured counter clock-wise from the normal to the wall surface

Fig. 5.1 shows that for active earth stress, the earth stress has a counter clock-wise rotation,  $\delta$ , relative the normal to the wall surface and the passive earth stress coefficient,  $K_a$ , is given in Eq. 5.1a.

The horizontal component of the active earth stress,  $K_{ah}$ , is given in Eq. 5.1b

$$(5.1b) \quad K_{ah} = K_a \sin(\beta + \delta)$$

If the wall is vertical and smooth, that is,  $\beta = 90^\circ$  and  $\delta = 0^\circ$ , then, Eqs. 5.1a and 5.1b both reduce to Eq. 5.1c.

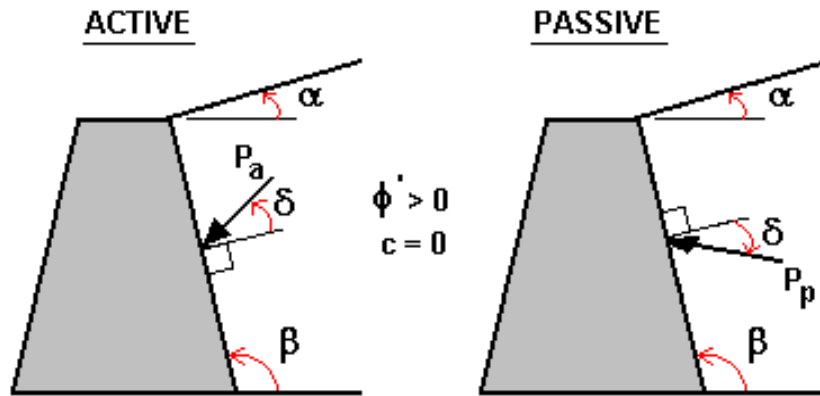


Fig. 5.1 Earth stress against the face of a rough surface gravity wall from a soil body with an inclined ground surface.

$$(5.1c) \quad K_{ah} = K_a = \frac{1 - \sin \phi'}{1 + \sin \phi'} = \tan^2(45^\circ - \phi'/2)$$

Fig. 5.1 shows that for passive earth stress, the earth stress has a clock-wise rotation,  $\delta$ , relative the normal to the wall surface and the passive earth stress coefficient,  $K_p$ , is given in Eq. 5.2a.

$$(5.2a) \quad K_p = \frac{\sin(\beta + \phi')}{\sin \beta [\sqrt{\sin(\beta - \delta)} + \sqrt{\sin(\delta + \phi') \sin(\phi' + \alpha) / \sin(\beta - \alpha)}]}$$

The horizontal component of the passive earth stress,  $K_{ph}$ , is given in Eq. 5.2b

$$(5.2b) \quad K_{ph} = K_p \sin(\beta - \delta)$$

If the wall is vertical and smooth, that is,  $\beta = 90^\circ$  and  $\delta = 0^\circ$ , Eqs. 5.2a and 5.2b both reduce to Eq. 5.2c

$$(5.2c) \quad K_{ph} = K_p = \frac{1 + \sin \phi'}{1 - \sin \phi'} = \tan^2(45^\circ + \phi'/2)$$

Notice that in Fig. 5.1 the wall friction angle (the rotation of the normal force against the wall surface) occurs in different directions for the active and passive cases. The directions indicate the situation for the soil wedge movement relative to the wall—downward in the active case and upward in the passive case. That is, in the active case, the wall moves outward and down; in the passive case, the wall is forced inward and up. For special cases, an outside force may move (slide) the wall in a direction that is opposite to the usual direction (for example, a wall simultaneously retaining soil and supporting a vertical load). The corresponding effect on the earth stress coefficient can be determined by inserting the wall friction angle,  $\delta$ , with a negative sign in Eqs. 5.1a and 5.2a.

### 5.3 Active and Passive Earth Stress

The unit active earth stress,  $p_a$ , in a soil exhibiting both cohesion and friction is given by Eq. 5.3

$$(5.3) \quad p_a = K_a \sigma'_z - 2c' \sqrt{K_a}$$

where  $\sigma'_z$  = effective overburden stress  
 $c'$  = effective cohesion intercept

The unit passive earth stress,  $p_p$ , in a soil exhibiting both cohesion and friction is given by Eq. 5.4

$$(5.4) \quad p_p = K_p \sigma'_z + 2c' \sqrt{K_p}$$

Usually, if pore water pressure exists in the soil next to a retaining wall, it can be assumed to be hydrostatic and the effective overburden stress be calculated using a buoyant unit weight. However, when this is not the case, the pore pressure gradient must be considered in the determination of the effective stress distribution, as indicated in Eq. 1.8c.

The pressure of the water must be added to the earth stress. Below the water table, therefore, the active and passive earth stress are given by Eqs. 5.5 and 5.6, respectively.

$$(5.5) \quad p_a = K_a \sigma'_z - 2c' \sqrt{K_a} + u$$

$$(5.6) \quad p_p = K_p \sigma'_z + 2c' \sqrt{K_p} + u$$

where  $u$  = the pore water pressure

In total stress analysis, which may be applicable to cohesive soils with  $\phi = 0$ , Eqs. 5.1a and 5.2a reduce to Eq. 5.7a and Eqs. 5.1b and 5.2b reduce to Eq. 5.7b.

$$(5.7a) \quad K_a = K_p = \frac{1}{\sin \beta} \quad \text{and} \quad (5.7b) \quad K_{ah} = K_{ap} = 1$$

where  $\beta$  = inclination of the wall from Eq. 5.1a

Where  $\phi = 0$ , and where the undrained shear strength,  $\tau_u$ , of the soil is used in lieu of effective cohesion, Eqs. 5.5 and 5.6 reduce to Eqs. 5.8a and 5.8b.

$$(5.8a) \quad p_a = \sigma_z - 2\tau_u$$

$$(5.8b) \quad p_p = \sigma_z + 2\tau_u$$

where  $\sigma_z$  = the total overburden stress

Notice, however, that if a crack develops near the wall that can be filled with water, the force against the wall will increase. Therefore, the earth stress calculated by Eqs. 5.8a and 5.8b should always be assumed to be at least equal to the water pressure,  $u$ , acting against the wall from the water-filled crack (even if the soil away from the wall could be assumed to stay “dry”).

Fig. 5.2 illustrates an inclined, rough-surface wall having on the side to the right (“active side” or “inboard side”) a soil (a backfill, say) with a sloping ground surface. A smaller height soil exists on the other side (the “passive side” or the “outboard side”). The inboard soil is saturated and a water table exists at about mid-height of the wall. The inboard soil is retained by the wall and the soil is therefore in an active state. The soil layer on the outboard side aids the wall in retaining the active side soil and water. It is therefore in a passive state.

The figure includes the angles  $\alpha$ ,  $\beta$ , and  $\delta$ , which are parameters used in Eqs. 5.1a and 5.2a. They denote the slope of the ground surface, the slope of the wall surface, and the wall friction angle and rotation of the earth stress acting on the wall surface. (The equations also include the angle  $\phi'$ , but this angle cannot be shown, because the soil internal friction angle is not a geometric feature).

Fig. 5.2 includes two stress diagrams illustrating the horizontal passive and active earth stress ( $p_{ph}$  and  $p_{ah}$ ) acting against the wall (proportional to the vertical effective stress within the soil layers). The distribution of water pressure,  $u$ , against the passive and active side of the wall is also shown in the stress diagram.

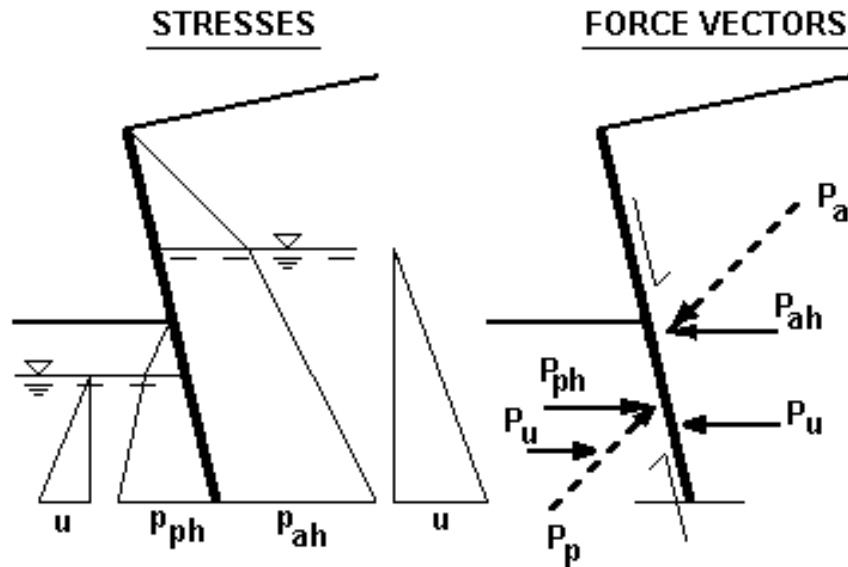


Fig. 5.2 Stresses and force vectors against an inclined wall

The force vectors ( $P_{ph}$  and  $P_{ah}$ ) are the sum of all the horizontal earth stresses and act in the centroids of the stress diagrams. Notice, because of the wall friction, the total earth stress force vectors ( $P_p$  and  $P_a$ , the dashed vectors) are not normal to the wall surface. Notice also that the wall friction vectors acting along the wall surface on the active and passive side point in opposing directions. (The weight of the wall and the forces at the base of the wall are not shown, and neither is the net bending moment).

In developing the forces, movements will have occurred that mobilize the active and passive states (and, also, the contact stresses and sliding resistance at the base of the wall). However, the wall as shown is in equilibrium, that is, the movements have ceased. The movements may well have been sufficiently large to develop active stress (and, probably, also the full sliding resistance, depending on the type of soil present under the base of the wall). However, no more passive resistance has developed than that necessary to halt the movement of the wall. (Remember, the movement necessary for full passive resistance is larger than for full active resistance).

When cohesion dominates in the retained soil, Eq. 5.3 may result in a negative active earth stress near the ground surface. Negative earth stress implies a tension stress onto the wall, which cannot occur. Therefore, when calculating earth stress, the negative values should be disregarded.

#### 5.4 Surcharge, Line, and Strip Loads

A surcharge over the ground surface increases the earth stress on the wall. A uniform surcharge load can be considered quite simply by including its effect when calculating the effective overburden stress. However, other forces on the ground surface, such as strip loads, line loads, and point loads also cause earth stress. Strip loads, which are loads on areas of limited extent (limited size footprint), and line and point loads produce non-uniform contribution to the effective overburden stress and, therefore, their

contribution to the earth stress is difficult to determine. Terzaghi (1954) applied Boussinesq stress distribution to calculate the earth stress from line loads and strip loads. This approach has been widely accepted in current codes and manuals (e. g., Canadian Foundation Engineering Manual 1992; 2006, NAVFAC DM7 1982). According to Terzaghi (1954), the earth stress against the wall is twice the Boussinesq stress.

Fig. 5.3 illustrates the principles of the stress acting on a wall due to surface loads calculated according to Boussinesq distribution. The so calculated stress is independent of the earth stress coefficient, the soil strength parameters, and, indeed, whether an active or a passive state exists in the soil. The figure shows the Boussinesq distributions for the horizontal stress at a point,  $z$ , below the ground surface from a line load, a uniformly loaded strip load, and a strip load with a linearly varying load on the ground surface, are given by Eqs. 5.9a through 5.9.c. For symbols, see Fig. 5.4. Notice, the angles  $\alpha$  and  $\beta$  are not the same as those used in Eq. 5.1,  $\alpha$  is the angle between the vector to the edge of the strip load, and  $\beta$  is the angle between the wall and the left vector to the strip.

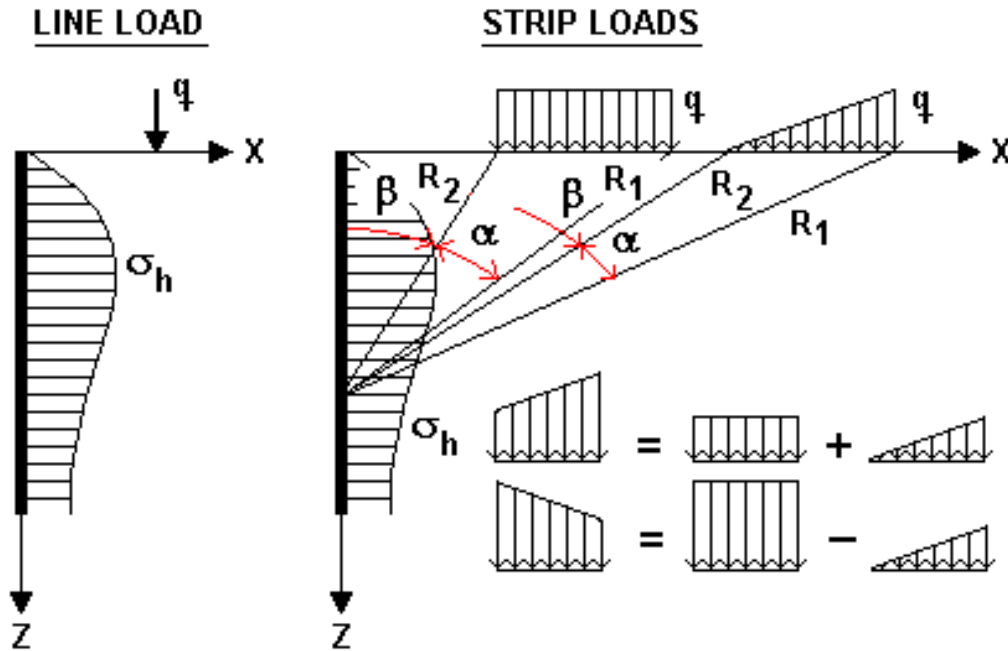


Fig. 5.3 Earth stress on a wall from line and strip loads on the ground surface as determined by Boussinesq distribution

Stress from a line load,  $q$ :

$$(5.9a) \quad \sigma_h = \frac{2q}{\pi} \frac{x^2 z}{(x^2 + z^2)^2}$$

Stress from uniform strip load,  $q$ :

$$(5.9b) \quad \sigma_h = \frac{q}{\pi} [\alpha - \sin \alpha \cos(\alpha + 2\beta)]$$



Stress from a uniform strip load that varies linearly from zero at one side to  $q$  at the other side:

$$(5.9c) \quad \sigma_h = \frac{q}{\pi} \left[ \frac{x\alpha}{\beta} - \frac{z}{\beta} \ln\left(\frac{R_1^2}{R_2^2}\right) + \frac{\sin 2\beta}{2} \right]$$

Integration of the equations gives the expression for the horizontal earth stress acting against a wall resulting from the line and strip loads. As mentioned above, the integrated value is doubled to provide the earth stress acting on the wall. A linearly varying (increasing or decreasing) strip load can be determined by combining Eqs. 5.9b and 5.9c.

Terzaghi (1953) presented nomograms for finding the point of application of the resultant of the unit earth stress acting against a vertical wall. By means of applying numerical computer methods, the location of the earth stress resultant and its magnitude can be directly located and, moreover, also the solution for inclined walls be determined.

According to Terzaghi (1954), the earth stress calculated according to Eq. 5.9a is not valid for a line load acting closer to the wall than a distance of 40 % of the wall height. For such line loads, the earth stress should be assumed equal to the earth stress from a line load at a distance of 40 % of the height. The resulting force on the wall is 55 % of the line load and its point of application lies about 60 % of the wall height above the wall base.

For a cantilever wall having a base or a footing, a surface load will, of course, also act against the horizontal surface of the base, as indicated in Fig 5.4. The vertical stress on the base can be determined from Eqs. 5.10a through 5.10c applying the symbols used in Fig. 5.3 and Eqs. 5.9a through 5.9c.

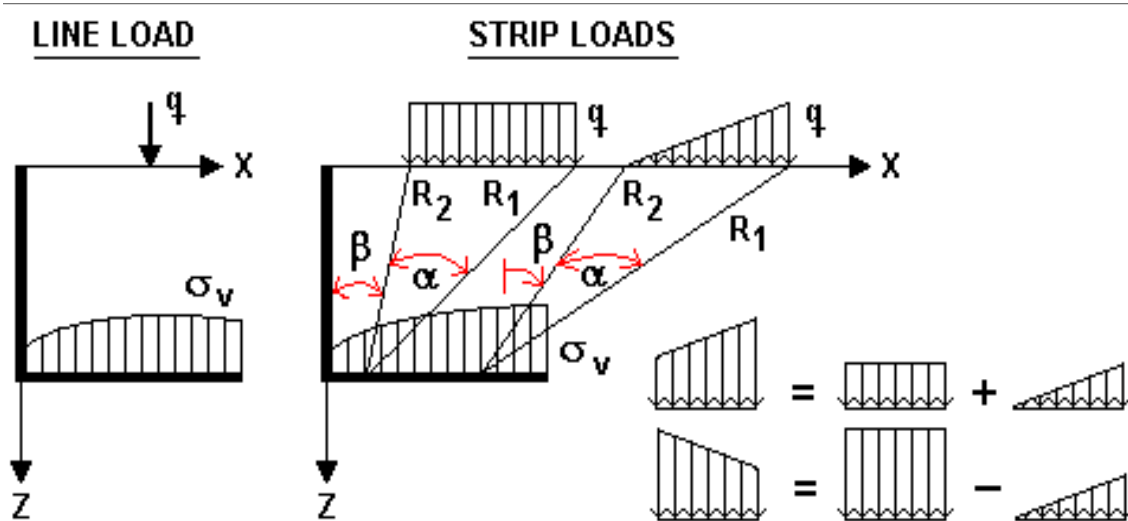


Fig. 5.4 Vertical earth stress on the base of a cantilever wall from line and strip loads on the ground surface as determined by Boussinesq distribution

Vertical stress from a line load,  $q$ :

$$(5.10a) \quad \sigma_v = \frac{2q}{\pi} \frac{z^3}{(x^2 + z^2)^2}$$

Vertical stress from a uniform strip load,  $q$ :

$$(5.10b) \quad \sigma_v = \frac{q}{\pi} [\alpha + \sin \alpha \cos(\alpha + 2\beta)]$$

Vertical stress from uniform strip load that varies linearly from zero at one side to  $q$  at the other side:

$$(5.10c) \quad \sigma_v = \frac{q}{\pi} \left[ \frac{x\alpha}{\beta} - \frac{\sin 2\beta}{2} \right]$$

Integration of the equations gives the resulting vertical earth stress acting against the base and, also, its location. A linearly varying (increasing or decreasing) strip load can be determined by combining Eqs. 5.10b and 5.10c. Notice, the stress according to Eqs. 5.10a through 5.10c acting on the base can have a stabilizing influence on a footing foundation.

## 5.5 Factors of Safety and Resistance Factors

In a design for earth stress forces, the factors of safety (resistance factors in LRFD) appropriate to the structures and types of loads involved should be applied. Note, however, that "safety" against overturning and location of the resultant, should be applied without any factor of safety or resistance factor on the loads and earth forces, but the stability be ensured per the location of the resultant. See also Section 6.6.

## 5.6 Aspects of Structural Design

Once the geometry of the structure and the geotechnical aspects of the design (such as the bearing resistance, settlement, and sliding resistance) are acceptable, the structural engineer has to ensure that the retaining structure itself is able to sustain the forces acting on each of its parts, such as the stem, the toe, and the heel. The stem is the vertical portion of the structure supporting the horizontal components of all loads. The toe is the portion of the footing located on the "outboard side" of the retaining structure and the heel is the portion of the footing located on the "inboard side" of the retaining structure.

While the overall geometry of the footing supporting a wall structure is often dictated by the external stability of the retaining wall (active stress), the structural design (member thickness, reinforcing steel, etc.) is based entirely on the internal stability (backfill stress).

### 5.6.1 Stem Design

The stem must be designed for shear, compression, and, most important, bending stresses. The shear forces acting on the stem are the summation of all horizontal forces acting above the top of the footing toe. In addition to shear forces, the stem must be capable of resisting compression forces. These forces

can include the weight of the stem, the vertical components of the soil forces acting along the face of the stem (inclined stem and/or wall friction exist), and other vertical forces acting directly on the stem.

Bending forces acting on the stem are obtained by multiplying all shear and compression forces by their respective distances to the base of the stem. The design of the stem must consider both the loads applied during the construction stage as well as loads during service conditions. Often in the design of the stem, the effect of the passive forces will be excluded while loads are added that are induced by the compaction of the backfill on the active side of the stem.

For concrete walls, the thickness of the stem and the amount and spacing of reinforcing steel should be sized based on the interaction of the shear, compression, and bending forces.

### **5.6.2 Toe Design**

The footing toe area is designed to resist the upward stresses created by the bearing layer at equilibrium condition. The design assumes that there is no deformation of the footing or the stem following installation of the backfill. It is also assumed that sliding or bearing failure will not occur. According to the Ontario Highway Bridge Design Code (OHBDC 1991), the design of the toe should consider both a uniform and a linear contact stress distribution. The design must include shear and bending forces. For concrete structures, these forces will usually dictate the amount and spacing of the bottom reinforcing steel in the footing.

### **5.6.3 Heel Design**

The footing heel area is designed to resist the downward stresses caused by the fill and forces on the inboard side. The design assumes that the structure will rotate around a point located at the toe of the footing. All loads from the active side, included in the external stability design, must be included also in the bending and shear design of the heel. For concrete structures, the heel design will usually dictate the amount and spacing of upper surface reinforcing steel in the footing.

### **5.6.4 Drainage**

Apart from design cases involving footings and walls designed in water, such as a sea wall, both footing and wall should be provided with drainage (pinholes, french drains, etc.) to ensure that no water can collect under the footing or behind the wall. This is particularly important in areas where freezing conditions can occur or where swelling soils exist under the footing or behind the wall. The commonly occurring tilting and cracking condition of walls along driveways etc. is not due to earth stress from the weight of the retained soil, but to a neglect of frost and/or swelling conditions.

## **5.7 Anchored Sheet-Pile Wall Example**

An anchored sheet-pile wall will be constructed in a 5 m deep lake to retain a reclaimed area, as indicated in Figure 5.5. The original soil consists of medium sand. The backfill will be medium to coarse sand and the fill height is 7 m. A tie-back anchor will be installed at a 1.5-m depth. Calculate the sheet-pile installation depth and the force in the anchor assuming the sheet pile is a free-end case. Cohesion,  $c'$ , can be assumed to be 0 and all shear forces along the sheet-pile wall can be disregarded. For now, do not include any safety margin for the input or any factors of safety. The example is taken from Taylor (1948) with some adjustment of numbers. It also appears, with similar number changes, in many, if not most, modern textbooks.

Proceed by first determining the sheet-pile length on the condition of equal rotating moment around the anchor level (i.e., net moment = 0) and then the anchor tension on the condition that the sum of all horizontal forces must be zero. The procedure is easily performed in an Excel spreadsheet.

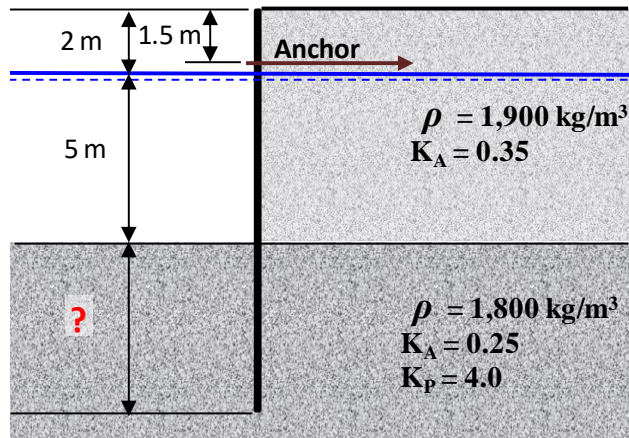


Fig. 5.5 Vertical view of sheet-pile wall

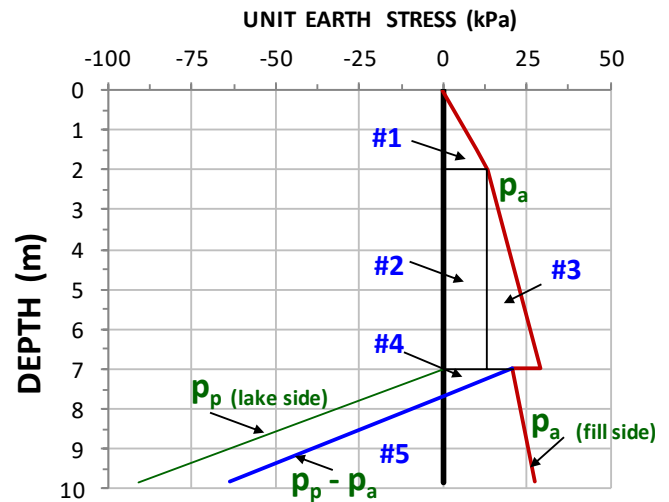


Fig. 5.6 Distribution of active and passive earth stress

Active side					Passive side				
DEPTH	$\sigma$	$u$	$\sigma'$	$p_a$	$\sigma$	$u$	$\sigma'$	$p_p$	$ p_p - p_a $
0.0	0.0	0.0	0.0	0.0					
1.5	28.5	0.0	28.5	10.0					
2.0	38.0	0.0	38.0	13.3					
7.0	133.0	50.0	83.0	29.1					
7.0	133.0	50.0	83.0	20.8	50.0	50.0	0.0	0.0	20.8
7.7	145.6	57.0	88.6	22.2	62.6	57.0	5.6	-22.4	$\approx 0$ (7.7 m by interpolation)
9.579	182.6	75.8	103.3	25.9	96.4	75.8	20.6	-82.5	56.6 (9.579 m is by trial and error' for $M = 0$ )
		$\Sigma 121.6$			$\Sigma 102.3$				

	Area	Arm	M	$\Sigma M$
#1	13.3	0.2	2.3	2.3
#2	66.5	3.0	199.5	201.8
#3	39.4	3.8	150.8	352.6
#4	7.3	6.0	43.3	395.9
#5	53.1	-7.5	-395.9	$\approx 0$

Anchor 73.3 kN (the balance between lake-side and fill-side forces)

The shown solution procedure disregards axial stiffness and bending of the sheet piles, which come into play when assuming that the sheet-pile end condition is fixed. The axial stiffness and bending of the sheet-pile wall will have a large influence on the embedment depth and the anchor force. The 'ultimate sheet-pile' with a fixed end is a cantilever pile, i.e., a sheet-pile wall with no tie back anchor. The penetration (embedment depth) necessary is then a function also of the pile bending stiffness.

### 5.8 Retaining Wall on Footing Example

A retaining wall with dimensions as shown in the figure has been constructed on an existing ground. The area behind and in front of the wall was then backfilled with a coarse-grained soil having a total density,  $\rho_t$ , of 1,750 kg/m<sup>3</sup> and an internal friction angle,  $\phi'$ , of 32°. Cohesion,  $c'$ , can be assumed to be 0. There is no water table and the backfill is free-draining. Calculate the active and passive earth stresses acting on the wall and where the resultant to all forces cuts the base of the footing. (Assume that the thickness of the wall and its footing is small).

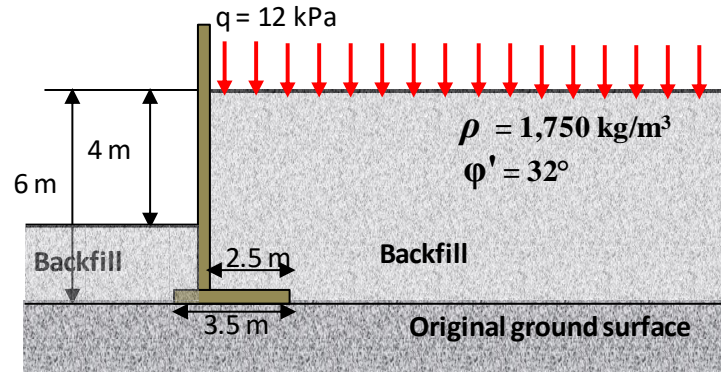


Fig. 5.7 Vertical view of retaining wall

Eqs. 5.1c and 5.2c give  $K_a = 0.31$  and  $K_p = 3.25$ .

Seven gravity forces, loads, and earth stresses affect the wall as indicated in Figure 5.8. They can be combined to show a single force, the resultant.

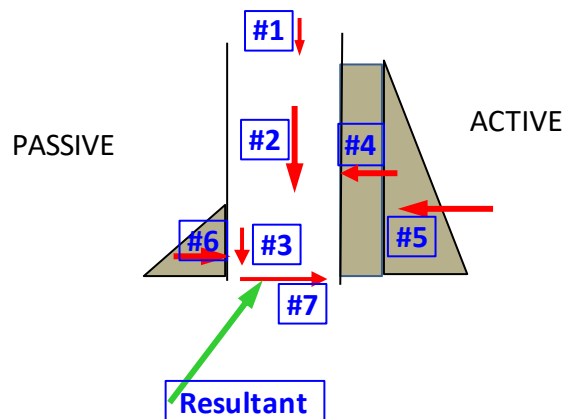


Fig. 5.8 Forces and stresses affecting the wall

The governing condition is the location of the resultant. To determine this, calculate the rotational moment around the footing toe (left edge of the footing in Figure 5.7).

#### Forces and rotational moment

	Force (kN)	Arm to toe (m)	M (kNm)
#1 = $12 \times 2.5$	= 30	2.25	67.5
#2 = $17.5 \times 2.5 \times 6$	= 262.5	2.25	590.6
#3 = $17.5 \times 1 \times 2$	= 35	0.5	18.0
#4 = $0.31(12 \times 6)$	= 22.3	3.0	66.9
#5 = $0.31(17.5 \times 6 \times 6/2)$	= 97.7	2.0	195.4
#6 = $3.25(17.5 \times 2 \times 2/2)$	= 114	0.7	-76.4
#7 = $(30+262+35) \times \tan 32$	= 204	0	0

### Moments around the footing toe

Vertical:  $Q=(30+262+35) = 327$ ;  $M=(67.5+590.6+18) = 676 \implies v_{\text{off toe}} = 676/327 = 2.1 \text{ m}$

Horizontal:  $Q=(22+98-114) = 6$ ;  $M=(67+195-76) = 186 \implies h_{\text{above}} = 186/6 = 31.0 \text{ m}$

Figure 5.9 indicates how to determine the location of the resultant.

$X/31 = 6/327 \implies X = 0.6 \text{ m}$   
well within the middle third.

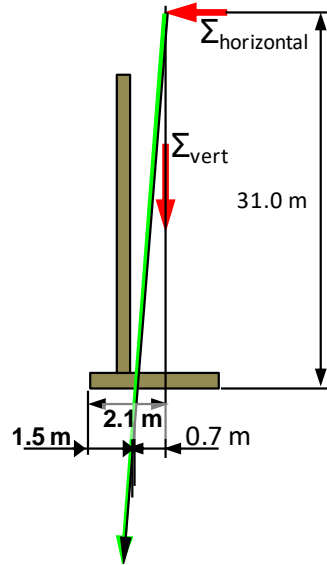


Fig. 5.8 Forces and stresses affecting the wall

### 5.9 Retaining with multiple horizontal supports

In case of a wall retaining a backfill, it is common to assume that the anchor forces increase proportionally to the increase of earth stress (triangularly distributed) acting on the wall, as the height of the retained soil increases. However, the conventional method to construct a shoring, a retaining wall, involves step-by-step excavation and installation horizontal supports (struts, anchors, tie-backs, raker supports, etc.) designed to hold back the earth stress acting on the wall. The wall can consist of a series of soldier piles with the distance between them covered by "wood lagging", a slurry trench with the slurry replaced by concrete, pile-in-pile walls (secant walls), and others. The earth stress against a wall retaining soil during a gradually deepening excavation, will be larger than that imposed by a backfill. Moreover, the force in the uppermost anchor row will be larger than that in the uppermost row of the backfill-supporting wall. Terzaghi and Peck (1948) recommended that the total earth stress be increased by a factor of 1.3 and the anchor forces be set equal as shown in Figure 5.9, thus redistributing the earth stress.

A similar redistribution is recommended for walls retaining cohesive soil, soft to firm and stiff to hard, respectively.

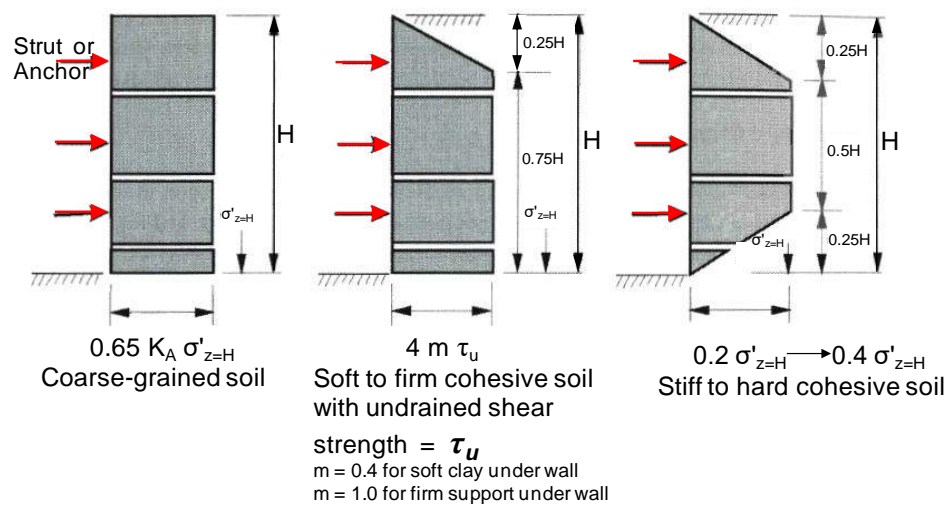


Fig. 5.9 Redistribution of earth stress for effect of progressive excavation and strut placement

Figure 5.10 shows an anchored sheet-pile wall constructed to shore up a 6 m deep excavation in a medium to coarse sand with three tie-back anchors at depths of 1.5, 3.0, and 5.0 m. A fill is placed on the ground surface.

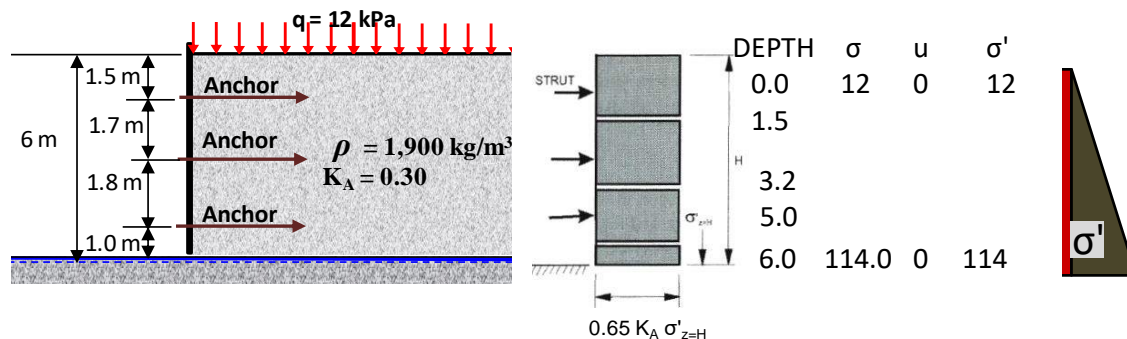


Fig. 5.10 Example

The total earth stress per metre of wall is:

$$\text{Total Earth Stress} = K_A h (\sigma'_{\text{ground}} + \sigma'_{\text{bottom}}) = 0.3 \times 6.0 \times (12 + 114)/2 = 113 \text{ kN}$$

$$\text{The force in each anchor} = 0.65 \times 113/3 = 25 \text{ kN}$$

As each row of anchors is installed as the excavation proceeds, it makes sense to prestress them to at least 1.5 times the expected force, i.e., to about 40 kN and, also, to have anchors that can take an overstress to about twice the expected force without breaking.

### 5.10 Collapse of shored trench

It is not always recognized that the shear force along the inside of the wall assists in reducing the strut force. Figure 5.11 shows an about 1.8 m deep trench excavated between two sheet pile walls shored up by one strut. The force vector diagram indicates the strut force. N.B., the force at the bottom of the trench is disregarded and the diagram is not to scale.

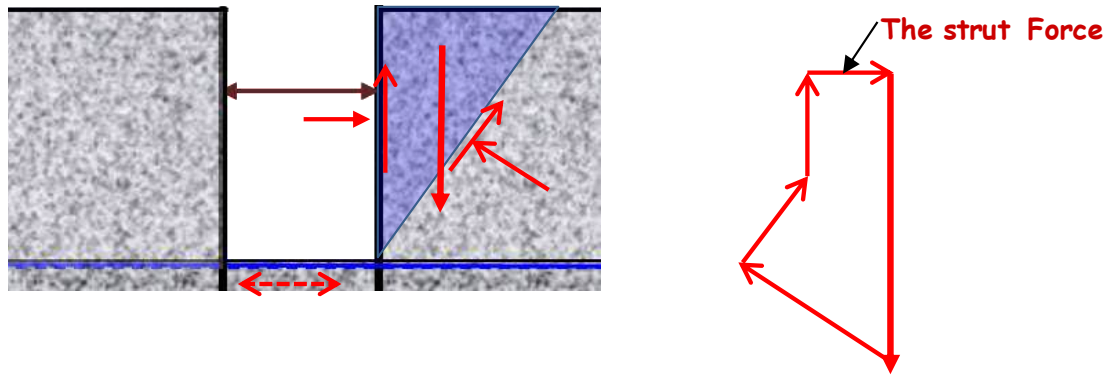


Fig. 5.11 A trench shored up with one strut and showing a force vector diagram of the forces

As indeed happened in a real case, assume that the excavator starts traveling with one track on the top of the sheet pile wall. In the real case, it was observed that this caused a small movement downward of the wall. Coincidentally, a couple of struts broke and the trench collapsed. Was the collapse really coincidental? Figure 5.12 shows a similar force vector diagram for the condition of the sheet piles moving downward.

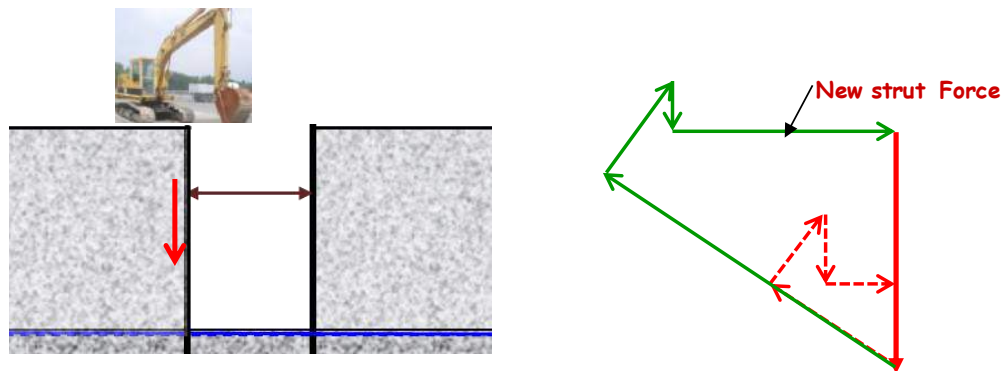


Fig. 5.12 The force vector diagram for when travels on top of the sheet pile wall

As suggested by the force vector diagram, when the shear force along the inside of the sheet pile wall reverted direction, the strut force increased significantly. In the illustrated case, the increase was sufficient to buckle the strut. The single coincidence of the case is the unfortunate fact that the collapse took the life of one person who was in the trench at the location of the collapse.



## CHAPTER 6

### BEARING CAPACITY OF SHALLOW FOUNDATIONS

#### 6.1 Introduction

When Society started building structures imposing large concentrated loads onto the soil, occasionally, catastrophic failures occurred. Initially, the understanding of foundation behavior merely progressed from the lessons of one failure to the next. Later, much later, laboratory tests were run of model footings on different soils and the test results were extrapolated to the behavior of full-scale foundations by means of theoretical analysis. For example, loading tests on model size footings gave load-movement curves with a distinct peak value—a "bearing capacity failure"—agreeing with a theoretical analysis that the capacity (not the settlement) controlled the response of a footing to load. Such tests further suggested that the "bearing capacity" in terms of stress of a model footing in clay is independent of the footing size, while, in contrast, tests on model footings in sand resulted in "capacities" in terms of stress that increased with the footing size (see Section 6.10).

However, tests on full-size footings have shown that bearing capacity in terms of an ultimate resistance at which failure occurs, does not exist. It has been shown conclusively that the theoretical treatment of bearing capacity provides an incorrect picture of actual response of footings to load. The correct modeling of footing response is a settlement analysis (Chapter 3). That the subject treatment in Section 6.2 through 6.5 is at all presented here is primarily in order to serve as a piece of historical geotechnics. The practicing design engineer is strongly advised against actually applying the formulas and relations presented. The details behind this recommendation are presented in Section 6.10. Sections 6.2 through 6.9 are only provided to present the historical or conventional approach. I do not suggest that the approach would in any way be correct.

#### 6.2 The Bearing Capacity Formula

Buisman (1935; 1940) and Terzaghi (1943) developed the "bearing capacity formula" given in Eq. 6.1 with details in Eqs. 6.2a through 6.2d. The premise of the formula is that the footing foundation has infinite length (is continuous) and the load is vertical and concentric with the footing center line, the soil is homogeneous, and the ground surface is horizontal.

$$(6.1) \quad r_u = c' N_c + q' N_q + 0.5 B \gamma' N_\gamma$$

where	$r_u$	=	ultimate unit resistance of the footing
	$c'$	=	effective cohesion intercept
	$B$	=	footing width
	$q'$	=	overburden effective stress at the foundation level
	$\gamma'$	=	average effective unit weight of the soil below the foundation
	$N_c, N_q, N_\gamma$	=	non-dimensional bearing capacity factors

When the groundwater table lies above or at the base of a footing, the effective unit weight,  $\gamma'$ , is the buoyant unit weight of the soil. When it lies below the base and at a distance equal to the width,  $B$ ,  $\gamma'$  is equal to the total unit weight. When the groundwater table lies within a distance of  $B$ , the value of  $\gamma'$  in Eq. 6.1a is equal to the average buoyant value. The formula as based on the model shown in Figure 6.1.

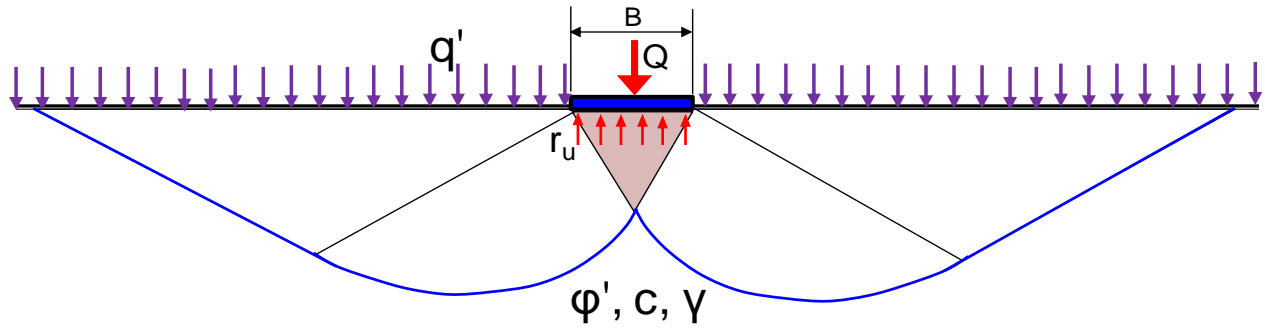


Fig. 6.1 The model for the Triple-N Formula

The bearing capacity factors are a function of the effective friction angle of the soil. Notice, for friction angles larger than about  $37^\circ$ , the bearing capacity factors increase rapidly. The factors were originated by Buisman (1935; 1940) and Terzaghi (1943), later modified by Meyerhof (1951; 1963), Hansen (1961), and others. According to the Canadian Foundation Engineering Manual (1992), the bearing capacity factors, which are somewhat interdependent, are as follows.

$$(6.2a) \quad N_q = e^{\pi \tan \phi'} \left( \frac{1 + \sin \phi'}{1 - \sin \phi'} \right) \quad \phi' \rightarrow 0 \quad N_q \rightarrow 1$$

$$(6.2b) \quad N_c = (N_q - 1)(\cot \phi') \quad \phi' \rightarrow 0 \quad N_c \rightarrow \pi + 2 = 5.14$$

$$(6.2c) \quad N_\gamma = 1.5(N_q - 1)(\tan \phi') \quad \phi' \rightarrow 0 \quad N_\gamma \rightarrow 0$$

where  $\phi'$  = the effective internal friction angle of the soil

Terzaghi and many others refined the original coefficients of the "triple N formula", relying mainly on results of test on model footings. The range of published values for the  $N_q$  coefficient is about 50 through about 600. (This wide range of the key parameter should have alerted the profession to that perhaps the pertinence of the formula could be questionable).

Equation 6.2c is not the only one used for determining the  $N_\gamma$  bearing capacity coefficient. Eq. 6.2d, for example, is a commonly applied relation that was developed by Vesic (1973; 1975) by means of fitting a curve to a set of values from values in a table produced by Caquot and Kerisel (1953):

$$(6.2d) \quad N_\gamma = 2(N_q + 1)(\tan \phi') \quad \phi' \rightarrow 0 \quad N_\gamma \rightarrow 0$$

Vesic (1975) presented a table listing the factors according to Eq. 6.1e ranging from  $0^\circ$  through  $50^\circ$ , which table is reproduced in the AASHTO Specifications (1992).

There are many other expressions in use for the  $N_\gamma$  bearing capacity factor. For example, the German code DIN 4017 uses  $N_\gamma = 2(N_q - 1)(\tan \phi')$  in its expression, that is, a “-” sign instead of a “+” sign (Hansbo 1994). For details, see Tomlinson (1980), Bowles (1988), and (Hansbo 1994).

### 6.3 Inclined and Eccentric Loads

Fig. 6.2 shows a cross sections of two strip footings of width,  $B$ , subjected to vertical load,  $Q$  and  $Q_v$ , respectively. The load on the left footing is vertical and concentric. The applied contact stress,  $q$ , is stress per unit length ( $q = Q/B$ ) and it mobilizes an equally large soil resistance,  $r$ .

However, loads on footings are normally eccentric and inclined, as shown for the footing to the right. Loading a footing eccentrically will reduce the bearing capacity of the footing. An off-center load will increase the stress (edge stress) on one side and decrease it on the opposing side. A large edge stress can be the starting point of a bearing failure. The edge stress is taken into account by replacing the full footing width ( $B$ ) with an effective footing width ( $B'$ ) in the bearing capacity formula (Eq. 6.1a; which assumes a uniform load).

The effective footing width is the width of a smaller footing having the resultant load in its center. That is, the calculated ultimate resistance is decreased because of the reduced width ( $\gamma$ -component in Eq. 6.1) and the applied stress is increased because it is calculated over the effective area as  $q = Q/(B'L)$ . The approach is approximate and its use is limited to the requirement that the contact stress must not be reduced beyond a zero value at the opposite edge ("no tension at the heel"). This means that the resultant must fall within the middle third of the footing, that is, the eccentricity must not be greater than  $B/6$  (= 16.7 % of the footing width). Fig. 6.3 illustrates the difference in contact stress between a footing loaded within its middle third area as opposed to outside that area.

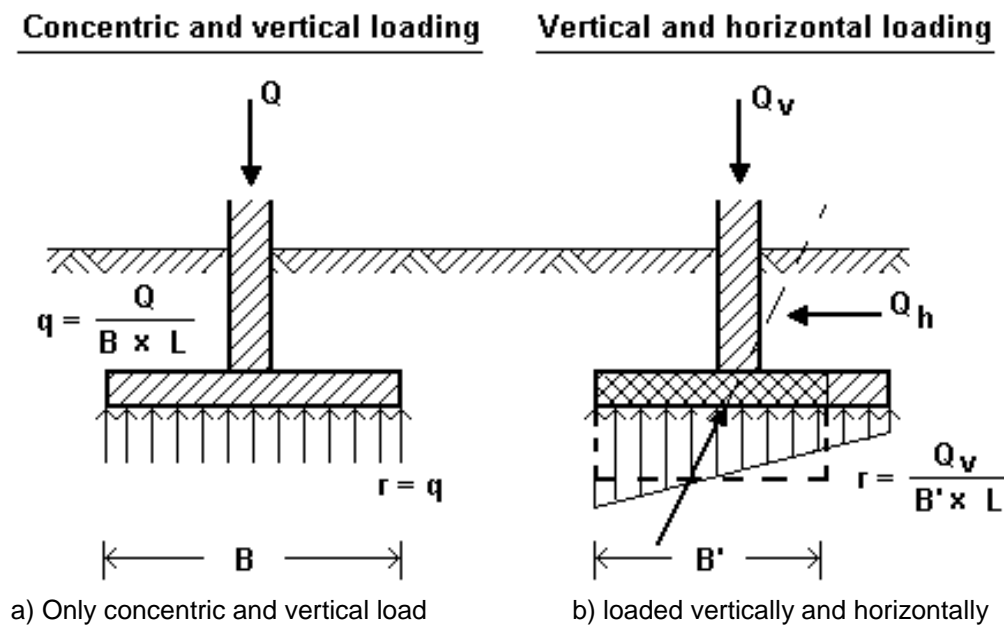


Fig. 6.2 A strip footing

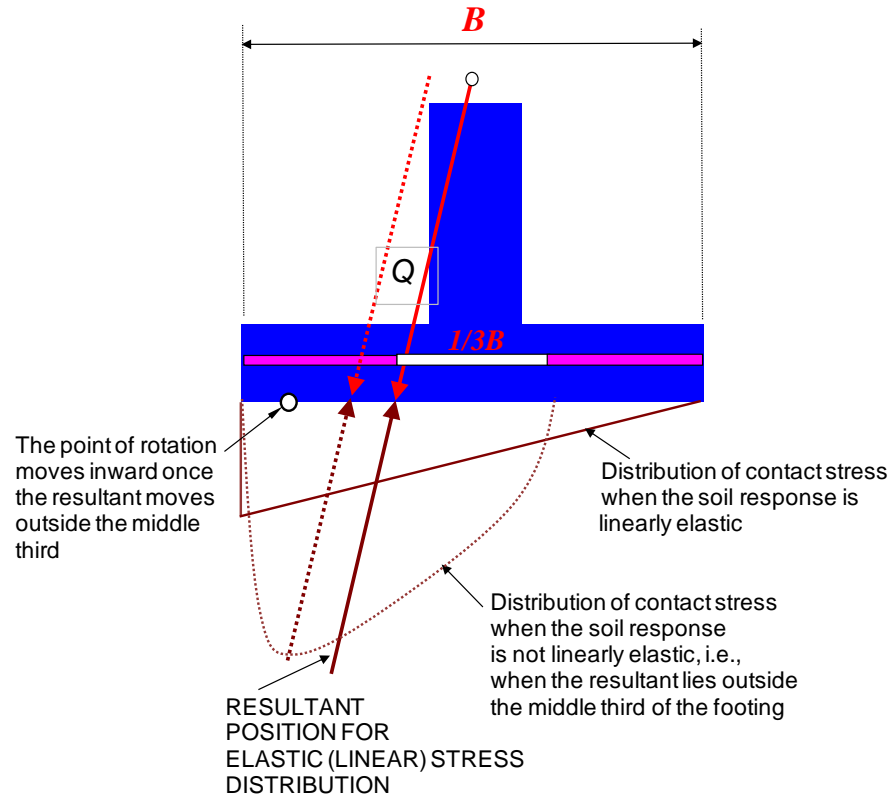


Fig. 6.3 Contact stress distributions when the resultant lies within the middle third and outside.

#### 6.4 Inclination and Shape Factors

Combining a vertical load with a horizontal load, that is, inclining the resultant load, will also reduce the bearing capacity of a footing. The effect of the inclination is expressed by means of reduction factors called Inclination Factors,  $i$ . An inclination may have an indirect additional effect due to that the resultant to the load on most occasions acts off center, reducing the effective area of the footing.

Also the shape of the footing influences the capacity, which is expressed by means of reduction factors called Shape Factors,  $s$ . The bearing capacity formula is derived under the assumption of an infinitely long strip footing. A footing with finite length,  $L$ , will have a contribution of soil resistance from the footing ends. This contribution is what the shape factors adjust for, making the formula with its bearing capacity factors applicable also to rectangular shaped footings. Notice, Eq. 6.3 does not include Depth Factors. However, many will consider the depth of the footing by including the overburden stress,  $q'$ .

Thus, to represent the general case of a footing subjected to both inclined and eccentric load, Eq. 6.1a changes to Eq. 6.2.

$$(6.3) \quad r_u = s_c i_c c' N_c + s_q i_q q' N_q + s_\gamma i_\gamma 0.5B' \gamma' N_\gamma$$

where factors not defined earlier are

$$\begin{aligned} s_c, s_q, s_\gamma &= \text{non-dimensional shape factors} \\ i_c, i_q, i_\gamma &= \text{non-dimensional inclination factors} \\ B' &= \text{equivalent or effective footing width} \end{aligned}$$

When the load is offset from the center of the footing toward the long side, the L-side, rather than toward the short side, the B-side, the bearing stress is assumed to act over a footing area of  $B$  times  $L'$ . When the resultant is eccentric in the directions of both the short and long sides of the footing, the effective area according to the Ontario Highway Bridge Design Code (1991) takes the shape of a triangle with the resultant in its centroid. In contrast, the AASHTO Specifications (1992) defines the effective area as a rectangle with sides  $B'$  and  $L'$ .

As long as the resultant falls within the middle third of the footing width, it can acceptably be assumed that the stress distribution below the footing is approximately linear. However, when the resultant moves beyond the third point, that is, closer to the edge of the footing, not only does the edge stress increase rapidly, the assumption of linearity is no longer valid. The requirement of having the resultant in the middle third is, therefore, very important in the design. In fact, if the resultant lies outside the middle third, the adequacy of the design becomes highly questionable. See also Section 6.6.

The shape factors are given in Eqs. 6.4a through 6.3k.

$$(6.4a) \quad s_c = s_q = 1 + \frac{B'}{L'} \frac{N_q}{N_c}$$

$$(6.4b) \quad s_\gamma = 1 - 0.4 \frac{B'}{L'}$$

where  $B'$  = equivalent or effective footing width

$L'$  = equivalent or effective footing length

According to the Canadian Foundation Engineering Manual (1992) and the OHBDC (1991), the inclination factors are:

$$(6.4c) \quad i_c = i_q = \left(1 - \frac{\alpha}{90^\circ}\right)^2$$

$$(6.4d) \quad i_\gamma = \left(1 - \frac{\alpha}{\phi'}\right)^2$$

where  $\alpha$  = the inclination of the resultant (angle to the vertical)

$\phi'$  = the effective internal friction angle of the soil

As for the case of the bearing capacity factor  $N_\gamma$ , different expressions for the inclination factor  $i_\gamma$  are in use. Hansen (1961) proposed to use

$$(6.4e) \quad i_\gamma = \left(1 - \frac{P}{Q + B' L' c' \cot \phi'}\right)^2$$

where  $P$  = the horizontal resultant to the forces  
 $Q$  = the vertical resultant to the forces  
 $c'$  = effective cohesion intercept  
 $\phi'$  = effective friction angle  
 $B'$  = equivalent or effective footing width  
 $L'$  = equivalent or effective footing length

Vesic (1975) proposed to use an expression similar to Eq. 6.4e, but with an exponent “m” instead of the exponent of “2”, where m is determined as follows:

$$(6.4f) \quad m = \frac{2 + \frac{L}{B}}{1 + \frac{L}{B}}$$

The AASHTO Specifications (AASHTO 1992) includes a somewhat different definition of the inclination factors, as follows:

$$(6.4g) \quad i_c = i_q - \frac{1 - i_q}{N_c \tan \phi'} \quad \text{for } \phi' > 0$$

$$(6.4h) \quad i_c = 1 - \frac{n P}{B' L' c' N'_c} \quad \text{for } \phi' = 0$$

$$(6.4i) \quad i_q = 1 - \frac{n P}{\theta + B' L' c' \cot \phi'}$$

$$(6.4j) \quad i_\gamma = 1 - \frac{(n+1) P}{\theta + B' L' c' \cot \phi'}$$

The factor “n” is determined as follows:

$$(6.4k) \quad n = \frac{2 + \frac{L'}{B'}}{1 + \frac{L'}{B'}} \cos^2 \theta + \frac{2 + \frac{B'}{L'}}{2 + \frac{B'}{L'}} \sin^2 \theta$$

where  $\theta$  = angle of load eccentricity (angle of the force resultant with the long side of the footing)  
 $B'$  = equivalent or effective footing width  
 $L'$  = equivalent or effective footing length

Notice, all the above inclination factors as quoted from the various sources can result in values that are larger than unity. Such a calculation result is an indication of that the particular expression used is not valid.

Many textbooks present a basic formulae multiplied with influence factors for shape and inclination of the resultant. These influence factors are calculated from formulae similar to the ones listed above and are often to be determined from nomograms as opposed to from formulae. They may also include considerations of stress distribution for different shapes (or with separate influence factors added). Such influence factors are from before the advent of the computer, when calculations were time-consuming.

## 6.5 Overturning

Frequently, one finds in text books and codes that the stability of a footing is expressed as an overturning ratio: “Factor-of-Safety against overturning”. This is the ratio between rotating moment around the toe of the footing taken as the quotient between the forces that try to topple (overturn) the footing and the forces that counteract the overturning. Commonly, the recommended “factor-of-safety against overturning” is 1.5. However, while the ratio between the calculated moments may be 1.5, the Factor of Safety,  $F_s$ , is not 1.5. For the factor of safety concept to be valid, a value of  $F_s$  close to unity must be possible, which is not the case when the resultant moves beyond the third point. For such a situation, the combination of increasing edge stress and progressively developing non-linearity causes the point of rotation to move inward (see Fig. 6.3). At an overturning ratio of about 1.2, failure becomes imminent. Ballerinas dance on toe, real footings do not, and the overturning ratio must not be thought of as being the same as a factor of safety. **Safety against overturning cannot be by a factor of safety. It is best guarded against by keeping the resultant inside the middle third of the footing.**

## 6.6 Sliding

The calculation of a footing stability must include a check that the safety against horizontal sliding is sufficient. The calculation is simple and consists of determining the ratio between the sum of the horizontal resistance and the sum of all horizontal loads,  $\Sigma R_h / \Sigma Q_h$  at the interface between the footing underside and the soil. This ratio is taken as the factor of safety against sliding. Usually, the safety against sliding is considered satisfactory if the factor of safety lies in the range of 1.5 through 1.8. The horizontal resistance is made up of friction ( $\Sigma Q_v \tan \phi'$ ) and cohesion components ( $c'BL$ ).

## 6.7 Combined Calculation of a Retaining Wall and Footing

Fig. 6.4 illustrates the general case of earth stress acting on a ‘stubby’ cantilever wall. The bearing capacity of the footing has to consider loads from sources not shown in the figure, such as the weight of the wall itself and the outside forces acting on the wall and the soil. The earth stress governing the structural design of the wall (P1) is determined from the product of the active earth stress coefficient ( $K_a$ ) and the effective overburden stress. The calculations must consider the soil internal friction angle ( $\phi$ ), inclination of the wall ( $\beta$ ), wall friction ( $\tan \delta$ ), as well as sloping of the ground surface ( $\alpha$ ). When the heel of the footing and/or the ground surface are sloping, the average height ( $H_1$ ) is used in the calculation of the effective overburden stress used for P1, as shown in the figure. Notice, many codes postulates that the backfill soil nearest the wall stem may not relax into full active condition. These codes therefore require a larger earth stress coefficient (closer to  $K_0$ ) in the calculation of the earth stress acting directly on the stem. The vertical component of the earth stress is often disregarded because including it would necessitate the corresponding reduction of the weight of the soil resting on the base.

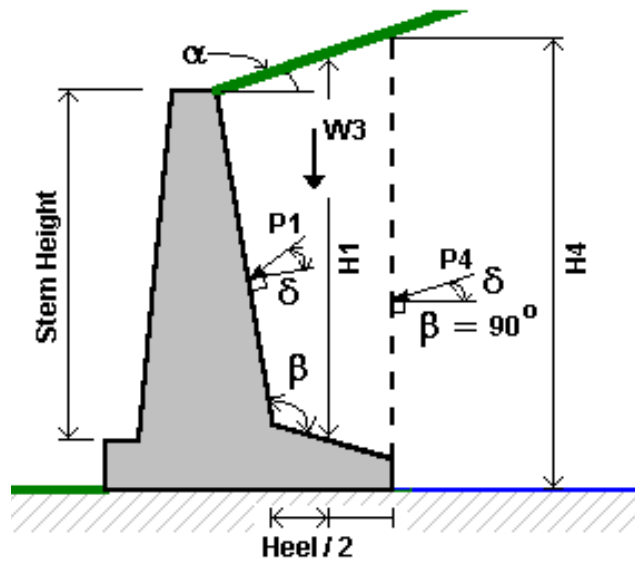


Fig. 6.4 Example of forces acting on a cantilever wall

The geotechnical design for bearing capacity and overturning requires the calculation of the resultant of all loads acting on a free body comprised by the wall and footing and the soil resting on the heel. The earth stress ( $P_4$ ) to include in the calculation of the force resultant the acts against the boundary of the free body, which is a normal rising from the heel, that is, its earth stress coefficient is determined from a  $\beta$  equal to  $90^\circ$ . Notice also that the height of the normal ( $H_4$ ) is used in determining the overburden stress applied in calculating  $P_4$ .

In contrast to the case for the earth stress against the stem, the earth stress acting on the normal from the heel should be calculated disregarding wall friction in the soil (Tschebotarioff 1978).

In summary, the design for capacity of a footing consists of ensuring that the factors of safety on bearing capacity of a uniformly loaded equivalent footing and on sliding are adequate, and verifying that the edge stress is not excessive.

## 6.8 Numerical Examples

### 6.8.1 Example 1

Calculate the factor of safety against bearing capacity failure for a 5-ft square spread footing placed at a depth of 2 ft below ground well above the groundwater table and loaded by 76 kips. The soil consists of sand with a 121 pcf total density,  $\rho_t$ . Cohesion,  $c'$ , is zero.

The working stress is 4.75 ksf, the effective stress,  $q'$ , at the foundation depth is 242 psf, and the bearing capacity factors,  $N_q$ , and  $N_\gamma$  are 21 and 19, respectively. Because the footing is square, shape factors apply:  $s_{q, \text{square}} = 1.6$  and  $s_{\gamma, \text{square}} = 0.6$ . The calculated  $r_u$  is 15.45 ksf and the factor of safety,  $F_s$ , is  $(15.45 - q')/4.75 = 3.2$ . The more logical approach would be to add the  $q'$  to the applied stress. However, this would only make a decimal change to  $F_s$  for the example, as for most cases.



A factor of safety of 3 or larger would for most imply a design with a solid safety against an undesirable outcome. However, the question of safe or not safe does not rest with the issue of capacity, but with the deformation—settlement—of the footing. If the sand in the example has a Janbu modulus number of, say, 100 and is essentially elastic in response ( $E = 200$  ksf), then the settlement of the footing for the load will be about 0.9 inch, which probably would be an acceptable value. However, if the sand deposit is not 5 ft thick below the footing but 30 ft, then the calculated settlement (Boussinesq distribution) would increase by about 30 % and perhaps approach the limit of acceptance. The calculated bearing capacity would not change however.

### 6.8.2 Example 2

The bearing capacity calculations are illustrated in a numerical example summarized in Fig. 6.5. The example involves a 10.0 m long and 8.0 m high, vertically and horizontally loaded retaining wall (bridge abutment). The wall is assumed to be infinitely thin so that its weight can be neglected in the calculations. It is placed on the surface of a ‘natural’ coarse-grained soil and a coarse material (backfill) is placed behind the wall. A 1.0 m thick fill is placed in front of the wall and over the toe area. The groundwater table lies close the ground surface at the base of the wall and the ground surface is horizontal.

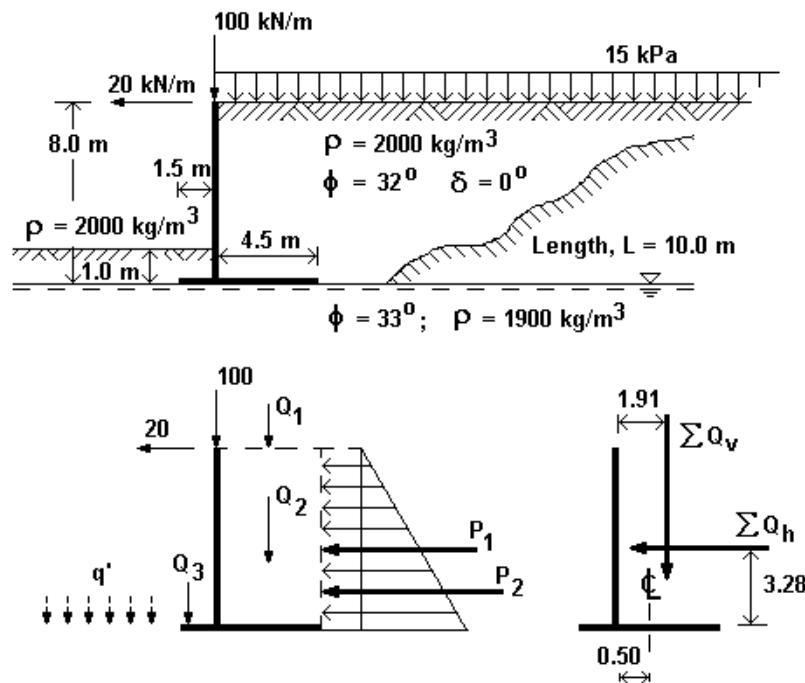


Fig. 6.5 Cantilever wall example (Fellenius 1995)

In any analysis of a foundation case, a free-body diagram is necessary to ensure that all forces are accounted for in the analysis, such as shown in Fig. 6.5. Although the length of the wall is finite, it is normally advantageous to calculate the forces per unit length of the wall (the length,  $L$ , then only enters into the calculations when determining the shape factors).

The vertical forces denoted  $Q_1$  and  $Q_2$  are loads on the base (heel portion).  $Q_1$  is from the surcharge on the ground surface calculated over a width equal to the length of the heel.  $Q_2$  is the weight of the soil on the heel. The two horizontal forces denoted  $P_1$  and  $P_2$  are the active earth stress forces acting on a fictitious wall rising from the heel, which wall is the boundary of the free body. Because this fictitious wall is soil, it is commonly assumed that wall friction does not occur (Tschebotarioff, 1978).

Because of compaction of the backfill and the inherent stiffness of the stem, the earth stress coefficient to use for earth stress against the stem is larger than that for active stress. This earth stress is of importance for the structural design of the stem and it is quite different from the earth stress to consider in the stability analysis of the wall.

Fig. 6.5 does not include any passive earth stress in front of the wall, because this front wall earth stress is normally neglected in practice. The design assumes that movements are large enough to develop active earth stress behind the wall, but not large enough to develop fully the passive earth stress against the front of the wall. Not just because the passive earth stress is small, but also because in many projects a more or less narrow trench for burying pipes and other conduits is often dug in front of the wall. This, of course, eliminates the passive earth stress, albeit temporarily.

Calculations by applying the above quoted equations from the Canadian Foundation Engineering Manual (CFEM 1985) result in the following.

$$\begin{aligned}\phi' &= 32^\circ \implies K_a = 0.307 & K_p \text{ is assumed to be zero} \\ \phi' &= 33^\circ \implies N_q = 26.09 & N_c = 38.64 \quad N_\gamma = 25.44 \\ i_q &= i_c = 0.69 & i_\gamma = 0.28 & s_q = s_c = 1.34 & s_\gamma = 0.80 \\ e &= 0.50 \text{ m} & B' &= 5.0 \text{ m} & r_u &= 603 \text{ kPa} & q &= 183 \text{ kPa} \\ F_{s\text{-bearing}} &= 3.29 & F_{s\text{-sliding}} &= 2.35 & \text{Overturning ratio} &= 3.76\end{aligned}$$

The design calculations show that the factors of safety (see Chapter 10) against bearing failure and against sliding are 3.29 and 2.35, respectively. The resultant acts at a point on the base of the footing at a distance of 0.50 m from the center, which is smaller than the limit of 1.00 m. Thus, it appears as if the footing is safe and stable and the edge stress acceptable. However, a calculation result must always be reviewed in a “*what if*” situation. That is, what if for some reason the backfill in front of the wall were to be removed? Well, this seemingly minor change results in a reduction of the calculated factor of safety to 0.90. The possibility that this fill is removed at some time during the life of the structure is real. Therefore, despite that under the given conditions for the design problem, the factor of safety for the footing is adequate, the wall structure may not be safe.

### 6.8.3 Example 3

A very long footing will be constructed in a normally consolidated sand (dimensions and soil parameters are shown in Figure 6.6). The resultants to all vertical and horizontal forces are denoted  $V$  and  $H$ , respectively and act along lines as shown. The counteracting resultant to all activating forces is denoted  $R$ . The sand deposit is 9 m thick and followed by bedrock.

- A. Is the resultant within the middle third?
- B. Calculate the factor of safety,  $F_{s, \text{bearing}}$ , according to the Bearing Capacity Formula
- C. Calculate the factor of safety,  $F_{s, \text{sliding}}$
- D. Calculate the settlement of the footing. Assume that the modulus number indicated in the figure covers both immediate and long-term settlement. Use stress distribution per the 2V:1H-method.

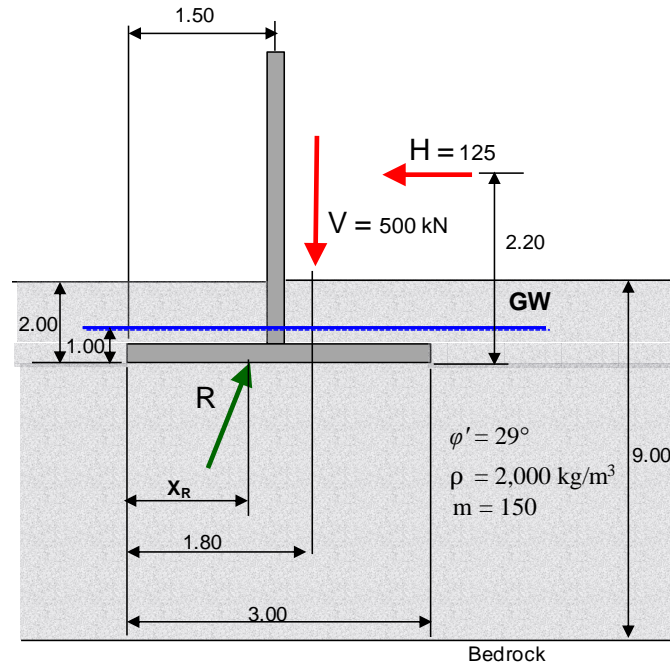


Fig. 6.6 Continuous footing in sand

Determine first the location of the resultant, i.e., its distance,  $x_R$ , from the left side of the footing, by taking static moment over the footing side.

$$1.80V - 2.20H = x_R V \implies 1.80 \cdot 500 - 2.20 \cdot 125 = x_R \cdot 500 \implies x_R = 1.25 \text{ m from the toe (side)}$$

**A.** The middle third limit is 1.00 m from the footing side, so the resultant lies within the middle third.

**B.** The Bearing Capacity Formula:  $r_u = q' N_q + 0.5 B' \gamma' N_\gamma$

$$q' = \sigma'_{z=2.00} = 1.0 \cdot 20 + 1.0 \cdot 10 = 30 \text{ kPa}$$

$$N_q = 16 \quad N_\gamma = 13 \quad \gamma' = 20 - 10 \quad B' = 2 \times x_R = 2.50 \text{ m}$$

$$r_u = 30 \cdot 6 + 0.5 \cdot 2.50 \cdot 10 \cdot 13 = 643 \text{ kPa}$$

$$q_{\text{applied}} = V/B' = 500/2.5 = 200 \text{ kPa}$$

$$F_{s, \text{bearing}} = 643/200 = 3.21$$

**C.** The sliding force is  $H = 125 \text{ kN}$

$$\text{The shear resistance is } V \tan \phi' = 500 \cdot 0.50 = 250$$

$$F_{s, \text{sliding}} = 250/125 = 2.0$$

**D.** Determine the effective stress at initial condition,  $\sigma'_0$ , and add the 2(V):1(H) distribution from the 500-kN stress over the  $B'$  area ( $= 200 \text{ kPa}$ ) to obtain  $\sigma'_1$ . Use the basic relations in Chapter 3 for strain and settlement ( $s = \sum \epsilon \Delta H$ ) to find the total settlement for the footing. Calculations are best carried out in a spread sheet table, as follows.

### Calculation table

Depth	$\sigma$	u	$\sigma'_0$	Footing	$\sigma'_1$	Settlement
0.0	0	0	0	0	0	43.0
1.0 GW	10	0	10	0	20	43.0
2.0	40	10	30	0	35	43.0
2.0	40	10	30	200.0	230.0	43.0
3.0	60	20	40	140.1	180.1	31.2
4.0	80	30	50	106.9	156.9	22.4
5.0	100	40	60	85.8	145.8	15.7
6.0	120	50	70	71.3	141.3	10.4
7.0	140	60	80	60.6	140.6	6.2
8.0	160	70	90	52.6	142.6	2.8
9.0	180	80	100	46.2	138.5	0

Had the full width, B, been used instead of B', the calculated settlement would have been 40 mm. Though the analysis should then consider the fact that the stress along one side is larger than along the other because of the horizontal load and the stress distribution should be with the Boussinesq method, which results in a calculated settlement of 29 mm along one side and 36 along the other. B.t.w., using Boussinesq distribution for the B' case results in 30 mm calculated settlement.

### 6.9 Presumptive Stress

Frequently, footing designs based on a so-called presumptive-stress approach that applies certain, intentionally conservative working stress values governed by assessment of the soil profile and the local geology at the site according to the local practice of the geology. Table 6.1 present a typical such an array of values.

**TABLE 6.1** Presumed Stress

Soil Type	Condition	Presumed Stress	
Clay	Stiff to hard	300 to 600	kPa
	Stiff	150 to 300	kPa
	Firm	75 to 150	kPa
	Soft	<75	kPa
Sand	Dense	>300	kPa
	Compact	100 to 300	kPa
	Loose	<100	kPa
Sand + Gravel	Dense	>600	kPa
	Compact	200 to 600	kPa
	Loose	<200	kPa
Shale, sound sedimentary rock	Medium strength	3	MPa
	Weak to medium	1 to 3	MPa
	Very weak	0.5	MPa

### 6.10 Words of Caution

Some words of caution: Footing design must emphasize settlement analysis. The bearing capacity formula approach is, mildly put, very approximate and should never be taken as anything beyond a simple estimate for purpose of comparing a footing design to previous designs. Most current codes and standards put an unrealistic reliance on the formula, which is made worse by the modern trend toward LFRD or ULS applying partial factors of safety (or resistance factors) to the various parameters.

The bearing capacity formula applies best to the behavior of small model footings in dense sand. When applying load to actual, real-life footings, the formula's relevance is very much in question. Full-scale tests show that no clear ultimate value can be obtained even at very large deformations. When critical state soil mechanics came about (Roscoe et al. 1958, advancing the concept proposed by Casagrande 1935), the reason for the model tests reaching an ultimate value became clear: Model tests affect only the soil to shallow depth, where even the loosest soil behaves as an overconsolidated soil. That is, in loading, after some initial volume change, the soil first dilates and then contracts resulting in a stress-deformation curve that implies an ultimate resistance (e.g., Been and Jefferies 1991, Altaee and Fellenius 1994).

Fig. 6.7 presents results from loading tests performed by Ismael (1985) on square footings with sides of 0.25 m, 0.50 m, 0.75 m, and 1.00 m at a site where the soils consisted of fine sand 2.8 m above the groundwater table. The sand was compact, as indicated by a N-index equal to 20 blows/0.3 m. The footings were placed at a depth of 1.0 m. The measured stress-movement behavior of the footing is shown in the left diagram. The diagram to the right shows the same data plotted as stress versus relative movement, i.e., the measured movement divided by the footing side. Notice that the curves are gently curving having no break or other indication of failure despite relative movements as large as 10 % to 15 % of the footing side.

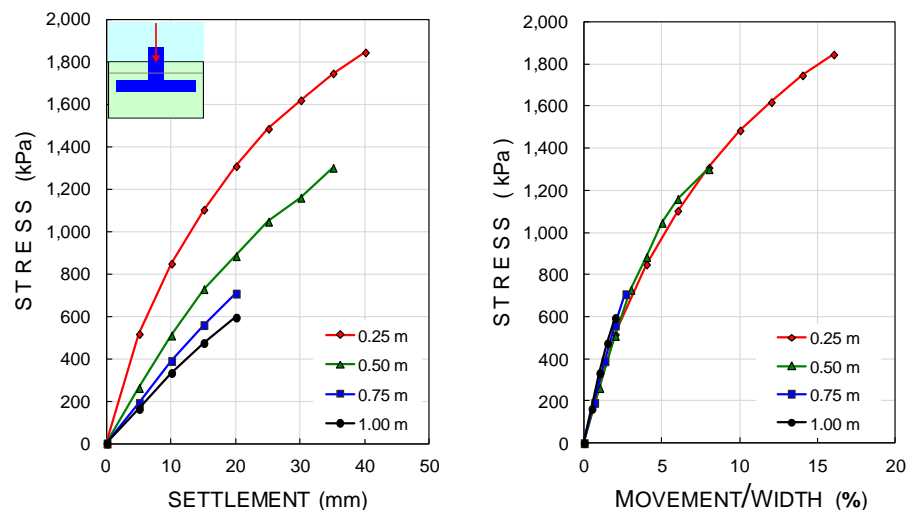


Fig. 6.7 Results of static loading tests on square footings in well graded sand (Data from Ismael, 1985)

Loading a footing in cohesive soil will generate pore pressures and a subsequent consolidation process during the dissipation. The soil layers below a footing conditions are rarely absolutely uniform in compressibility and layer thickness, which means that the consolidation settlement will vary across the footings and the structure will tilt toward the side where the settlement is the largest. The tilting will move the resultant toward that site, which in turn will increase the settlement and tilt and might increase to pore pressures until the footing fails, ostensibly as a bearing capacity failure, but in reality a result of excessive and settlement and gradually increasing stress applied to the foundation side.

Similar static loading tests on square footings placed at a depth of 0.8 m in sand were performed by Briaud and Gibbens (1994) and Briaud et al. (1999) in a slightly preconsolidated, silty fine sand well above the groundwater table (also presented in Section 3.14.1). The natural void ratio of the sand was 0.8. The footing sides were 1.0 m, 1.5 m, 2.0 m, and 3.0 m. Two footings were of the size 3.0 m. The results of the test are presented in Fig. 6.8, which, again, shows no indication of failure despite the large relative movements.

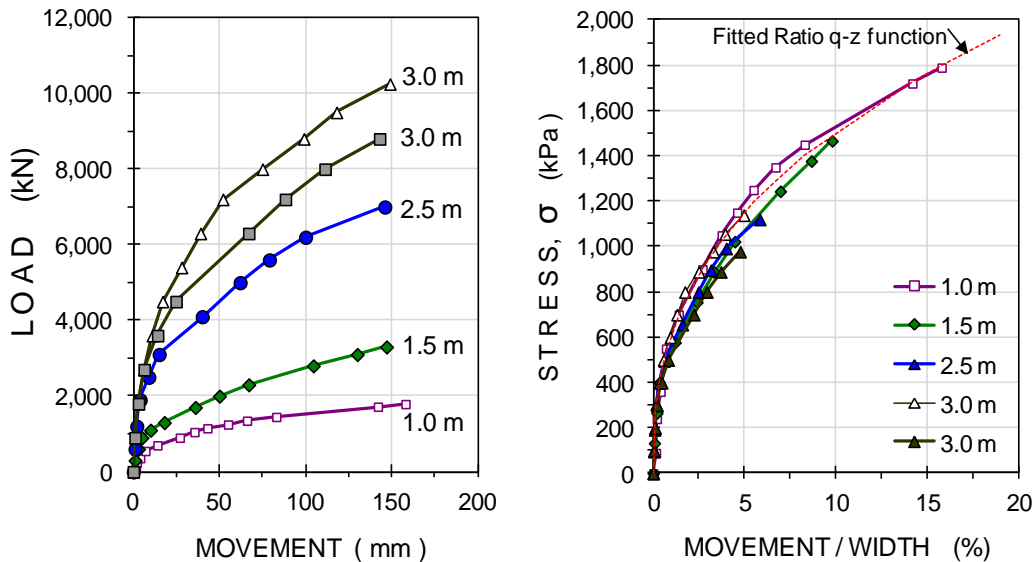


Fig. 6.8 Results of static loading tests on square footings in well graded sand  
(Data from Briaud and Gibbens 1994)

The indisputable fact is that bearing capacity of a real-size footing does not really exist. The concept of capacity is a condition associated with shear failure. However, in contrast to a body sliding against a soil (the case of a footing sliding along its base or of shaft resistance when a pile slides against the soil), the movement of soil body affected by the applied load is governed by deformation characteristics of the soil and the fact that the affected soil body increases for each load applied. That is, the volume of soil involved changes all through the loading. When the basic concept for a response is wrong, simply, any interpretation of the results based on that concept is also wrong!

The foregoing two tests and several others available in the literature, e.g., Fellenius (2009; 2011) show conclusively that bearing failure, i.e., capacity or ultimate resistance, does not exist for a normal loading case. (Fellenius 2016). As mentioned, the exception is in clays when the imposed loading is rapid enough to generate pore pressures and uneven settlement, and when the soil is preconsolidated so the loading generates negative pore pressures and failure occurs when the pore pressures return to normal values.

The fallacies of the bearing capacity formula notwithstanding, the formula is frequently applied to current foundation designs and most building codes, handbooks, and guidelines recommend its use. Therefore, applying the bearing capacity formula to routine designs is still considered within the accepted standard of care. Moreover, there is a fundamental difference between the movements recorded in a loading test and the settlement of a footing for a long-term unchanging load. This should be recognized and a footing design, therefore, should be based on deformation analysis, not on capacity.

Finally, the design must consider the construction of the footing. The footing base must be prepared so it is "undisturbed": free of remolded and loosened soils and not affected by running water or freezing. If the foundation level is raised, the backfill must be engineered, that is, be compacted to a satisfactory density.

## CHAPTER 7

### STATIC ANALYSIS OF PILE LOAD-TRANSFER

#### 7.1 Introduction

Where designing on shallow foundations would mean unacceptable settlement, or where scour and other environmental hazards exist that could impair the structure in the future, deep foundations are used. Deep foundations are usually piled foundations, that is, foundations supported on piles installed by driving, pushing ("jacked-in"), or constructed in-situ, to competent soils through soft compressible soil layers. Piles can be made of wood, concrete, or steel, or of composite materials, such as concrete-filled steel pipes or an upper concrete section connected to a lower wood, steel, or helical section, or open or closed cross sections such as pipe pile, H-piles, or helical piles. They can be round, square, hexagonal, octagonal, rectangular (e.g., "barrettes"), even triangular, and straight-shafted, step-tapered, or conical. They can be short or long, or slender or stubby. In order to arrive at a reliable design, all the particulars of the pile, including the method of construction, must be considered together with the soil data and desired function of the pile.

Design of a piled foundation for axial load starts with an analysis of how the load is transferred to the soil, often thought limited to determining only the pile "capacity", sometimes separating the "capacity" on components of shaft and toe resistances. (The term "capacity" is a very imprecise concept, which is why I here write it inside quotation marks). The load-transfer analysis is often called static analysis or "capacity" analysis. The load-transfer analysis is also a necessary part of a settlement analysis, because in contrast to the design of shallow foundations, settlement analysis of piles cannot be separated from load-transfer.

Total-stress analysis using undrained shear strength (so-called  $\alpha$ -method) has very limited application, because the load transfer between a pile and the soil is governed by effective stress behavior (i.e., the pile resistance is proportional to the effective overburden stress). Therefore, an effective stress analysis (also called  $\beta$ -method) is the preferred method. Sometimes, the  $\beta$ -method includes an adhesion (effective cohesion intercept) component. The adhesion component is normally not applicable to driven piles, but may sometimes be useful for bored piles ("cast-in-situ piles", "drilled-shafts", "caissons", "augercasts", etc. — "it's a sweet child that has many names"). The total stress and effective stress approaches apply to both shaft and toe resistances, although " $\alpha$ - and  $\beta$ -methods", usually refer to shaft resistance, specifically.

All foundation design methods are primarily based on empirical correlations, of course, whether by total stress or effective stress analyses. Any case analyzed by total stress can also be analyzed by effective stress. However, I have seen cases where an effective stress method analysis ( $\beta$ -coefficients) that was matched to results of a static loading test also matched the reduced resistance of a same-depth pile tested after the site had been excavated. In contrast, a total stress analysis ( $\alpha$ -values) matched to the results of the first static loading test would not match the softer response of the second test.

In bedrock, which is a cohesive material, total stress is usually applied, as the shaft shear is mostly a function of the bond between the pile shaft and the bedrock surface, which in sound bedrock is not proportional to overburden stress. However, in weathered bedrock consisting of a conglomerate of rock pieces in a matrix of soil, the shaft resistance is indeed proportional to the surrounding effective stress, usually proportional to the overburden stress.

This chapter will address theoretical analysis. However, it is imperative that every analysis is correlated to results of actual field tests so that the parameters applied to the analysis are from reality. Analysis of load transfer for piles cannot be removed from reference to good experience, direct or indirect.

## 7.2 Static Analysis

### 7.2.1 Shaft Resistance

Static analysis of axial pile response involves considering the load—sustained (dead) and transient (live)—applied to the head of a pile and transferred to the soil by means of shaft and toe resistance as indicated in Fig. 7.1.

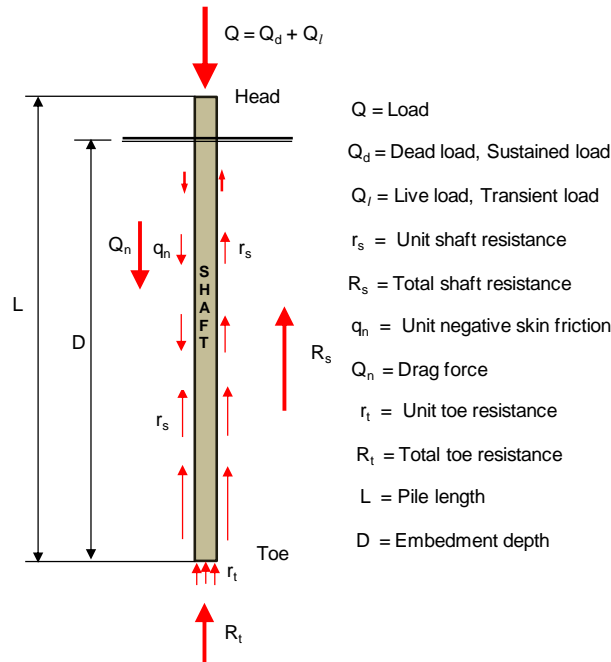


Fig. 7.1 Transfer of load to a pile and from a pile to the soil

Not shown in the figure, but intimately associated with the resistance indicated by the arrows, is the movement associated with the load-transfer. This will be addressed in Chapter 8.

The general numerical relation for the ultimate unit shaft resistance,  $r_s$ , of a short pile element is

$$(7.1a) \quad r_s = c' + \beta \sigma'_z$$

where  $c'$  = effective cohesion intercept (or, simply: shear strength—undrained or otherwise), usually,  $c'$  is not included in the analysis  
 $\beta$  = Bjerrum-Burland coefficient (or "effective-stress proportionality-coefficient")  
 $\sigma'_z$  = effective overburden stress

When, as is usual, the adhesion component,  $c'$ , is set to zero, Eq. 7.1a expresses that unit shaft resistance is directly proportional to the effective overburden stress. This proportionality is a very simplified approach and disregards rotation of principle stresses, relative movement and shear angle, and many other aspects. Eq. 7.1a presumes a specific relative movement between the pile, and the soil and the resistance, unit or total, must, therefore, always refer to its related movement.



N.B., the interaction between the pile surface and the soil occurs in a zone or band around the pile, not as a sudden slip. Thus, nearest the pile, shear forces develop along with compression and the "movement" is the relative movement between the boundaries of the affected zone, one close to the pile surface, but not necessarily right at the surface, but the other away from the pile. Measurements on piles near a loaded piles (as in a static loading test) have shown that loading the test pile imposed "passive" movements on piles located several pile diameters away (Caputo and Viggiani 1984, Lee and Xiao 2001)

The direction of the movement has no effect on the load-movement for the shaft resistance. That is, push or pull, positive or negative, the shear stress is the same. Moreover, the movement necessary for the mobilization of shaft resistance is independent of the diameter of the pile.

The accumulated shaft resistance from Depth 0 through Depth  $z$  is

$$(7.1b) \quad R_s = \int A_s r_s dz = \int A_s (c' + \beta \sigma'_z) dz$$

where  $R_s$  = accumulated shaft resistance  
 $A_s$  = circumferential area of the pile at Depth  $z$   
 (i.e., surface area over a unit length of the pile)

The beta-coefficient varies with soil gradation, mineralogical composition, density, depositional history (genesis), grain angularity, etc. Table 7.1 shows what approximate range of  $\beta$ -coefficients to expect from basic soil types compiled by Fellenius (2008) from different case histories. The values are derived from pile tests in mechanically weathered, inorganic, alluvially transported and deposited soils. Other soils, in particular, highly overconsolidated soils (see O'Neill and Reese 1999), or soils with organics (e.g., "muck"), residual soils, calcareous soils, micaceous soils, and many others may—nay, will—exhibit different ranges of  $\beta$ -coefficients.

**TABLE 7.1**  
**Approximate Ranges of Beta-coefficients**

SOIL TYPE	Phi	Beta
Clay	25 - 30	0.15 - 0.35
Silt	28 - 34	0.25 - 0.50
Sand	32 - 40	0.30 - 0.90
Gravel	35 - 45	0.35 - 0.80

The beta-coefficients can deviate significantly from the values shown in Table 7.1. For example, Rollins et al. (2005) compiled back-calculated average beta-coefficients from a large number of case histories on results of uplift tests for different types (material) of piles in sand as shown in Fig. 7.2a (my trend line) and Fig. 7.2.b. Also included are average beta-coefficients back-calculated from a large number of case histories reporting results of uplift tests for different types (material) of piles in sand (Clausen et al. (2005).

Clausen et al. (2005) also compiled cases from piles in clay: beta-coefficients versus plasticity index, as shown in Fig. 7.3.

Available analysis results from measurements of distribution of shaft resistance indicate unquestionably that the unit shaft resistance increases more or less linearly with depth. That is, effective stress governs the unit shaft resistance. As mentioned, the actual proportionality coefficient, the  $\beta$ -coefficient, can obviously vary within rather large ranges and depends on not just grain size distribution, but also on mineral composition, overconsolidation ratio, whether sedimentary or weathered residual soil, etc.

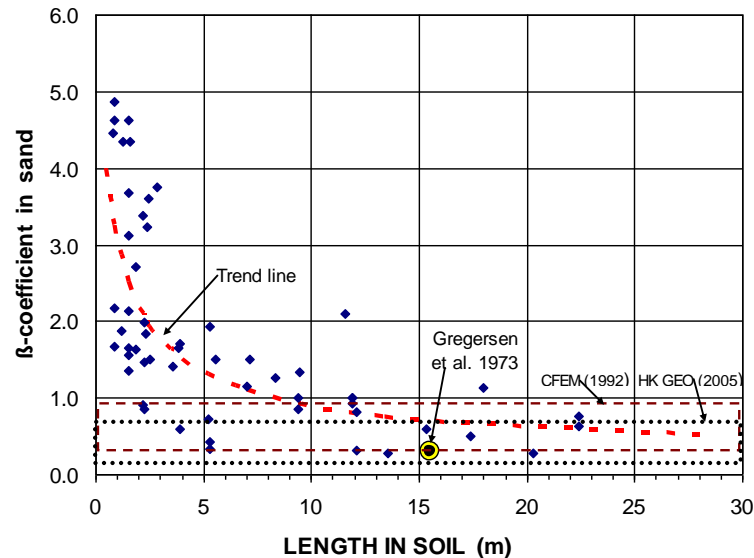


Fig. 7.2a Beta-coefficient for piles in sand versus embedment length. (Data from Rollins et al. 2005 with ranges suggested by CFEM 1992, Gregersen et al. 1973, and Hong Kong Geo 2006).

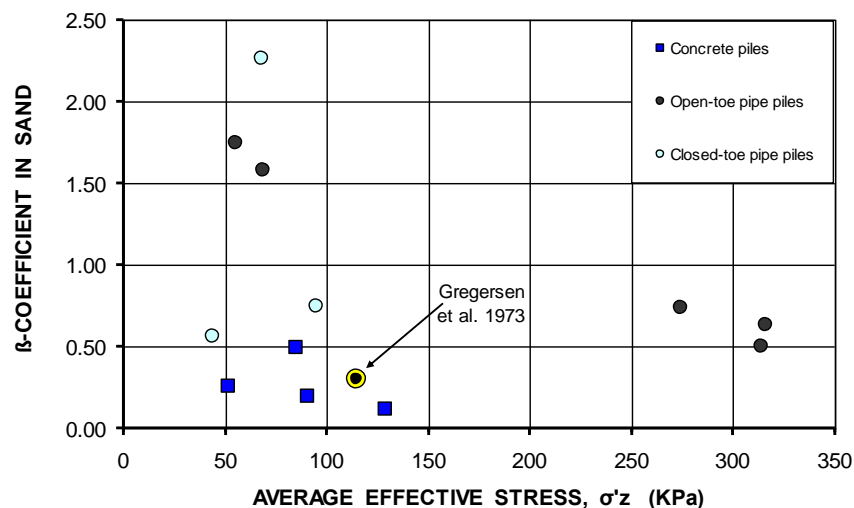


Fig. 7.2b Beta-coefficient in sand versus average effective stress. (Data from Clausen et al. 2005)

In soils that exhibit plastic shear response (i.e., ultimate shear resistance) to an imposed movement, ultimate resistance is usually mobilized for very small relative movement between the pile and the soil, often only a few millimetre. Such soils are soft clays and non-dilating sand. Fig. 7.4 presents unit shaft resistance measured along a bored 1.8 m diameter test pile constructed in HoChiMinh City in the Mekong delta, Vietnam, for the Sunrise City Towers at depths of 73, 75, 77, and 83 m. At the peak resistance, sudden large movements developed; no records were obtained between about 5 mm and 35 mm (Fellenius and Nguyen 2013; 2014).

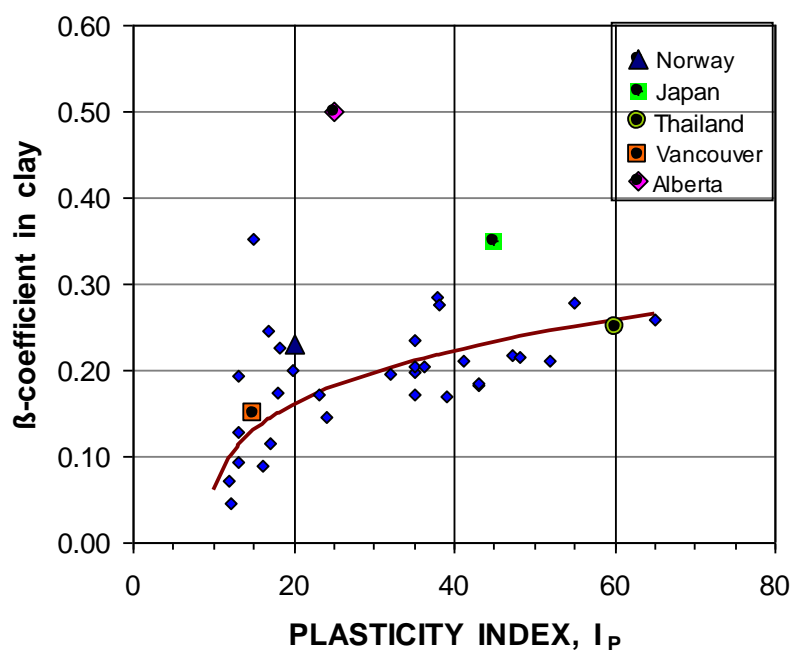


Fig. 7.3 Beta-coefficient for piles in clay versus plasticity index,  $I_p$ . (Data from Clausen et al. 2005 with results from five cases added; Fellenius 2006).

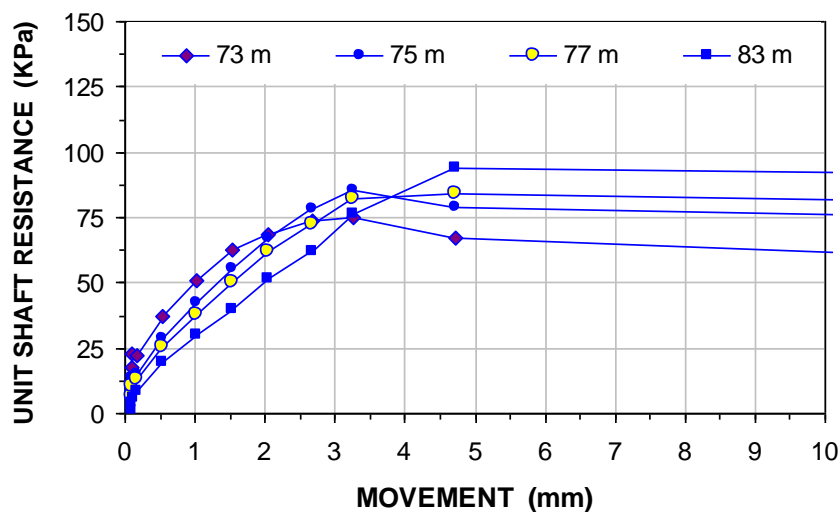


Fig. 7.4 Unit shaft resistance measured in a 1.8 m diameter bored pile constructed in silty sandy clay and clayey sand. (Fellenius and Nguyen 2013; 2014).

Most accounts of shaft resistance response in the literature report similar almost elastic-plastic shape. However, other than in soft clays, the shaft resistance response is usually more in the shape of a gently rising curve showing no sudden peak or change that could be taken as an indication of ultimate resistance. The beta-coefficient (as well as an  $\alpha$ -method shear resistance) should always be coupled to the movement between the pile shaft and the soil at which the particular shear resistance has or will be developed.

### 7.2.2 Toe Resistance

Also the ultimate unit toe resistance is considered proportional to the effective stress, i.e., the effective stress at the pile toe. Based on this premise (actually, false premise, actually), the unit toe resistance is:

$$(7.2a) \quad r_t = N_t \sigma'_{z=D}$$

where  $r_t$  = unit toe resistance  
 $N_t$  = toe bearing "capacity" coefficient  
 $D$  = embedment depth  
 $\sigma'_{z=D}$  = effective overburden stress at the pile toe

The total toe resistance is

$$(7.2b) \quad R_t = A_t r_t = A_t N_t \sigma'_{z=D}$$

where  $R_t$  = total toe resistance  
 $A_t$  = toe area (normally, the cross sectional area of the pile)

Also the toe-coefficient,  $N_t$ , varies widely. Table 7.2 (CFEM 1992) shows an approximate range of values for the four basic soil types. These values are typical of those determined in a static loading test to "failure" (see Chapter 8, Sections 8.2 - 8.8), which usually occurs at a pile head movement of 30 mm and beyond. Notice that the pile toe movement is normally only about  $10 \pm$  mm; a larger test-imposed toe movement is rare.

**TABLE 7.2 Approximate Range of  $N_t$**

SOIL TYPE	Phi	$N_t$
Clay	25 - 30	3 - 30
Silt	28 - 34	20 - 40
Sand	32 - 40	30 - 150
Gravel	35 - 45	60 - 300

The value of the toe proportionality coefficient,  $N_t$ , is sometimes stated to be of some relation to the conventional bearing "capacity" coefficient,  $N_q$ , but the validity of any such relation is not real. The truth is that neither the  $N_q$ -coefficient for a footing (See Chapter 6) nor the  $N_t$ -coefficient correctly represent the pile toe behavior for an imposed load. As discussed by Fellenius (1999; 2011), the concept of bearing "capacity" does not apply to a pile toe. Instead, the pile toe load-movement is a function of the stiffness (compressibility) of the soil below the pile toe in combination with the effective overburden stress in a relation called  $q$ - $z$  curve (See Section 8.12) and toe resistance does not exhibit an ultimate value, but continues to increase with increasing toe movement. Even for piles tested to an ultimate resistance, as judged from the pile head load-movement response, the actual toe movement is usually, no more than about 5 mm to 12 mm from the start of the test. Therefore, the value represented by the  $N_t$ -coefficient determined from most tests corresponds to the resistance at that toe movement. Fig. 7.5 shows unit toe resistances measured in two bored test piles of 1.5 m and 1.8 m diameter constructed with the pile toe in silty sandy clay and clayey sand at the same site as the example shown in Fig. 7.4. The absence of indication of approaching "failure" despite the large movements is typical for a pile toe response (and footing response; compare Section 6.10).

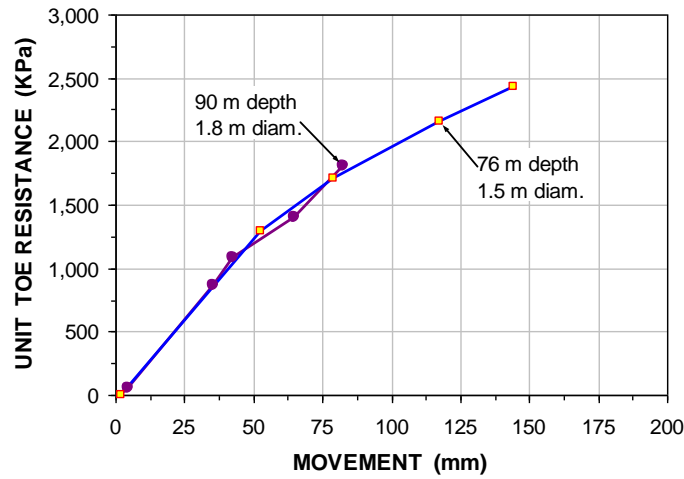


Fig. 7.5 Unit toe resistance measured in the same two bored piles as addressed in Fig. 7.4

### 7.2.3 Ultimate Resistance ("capacity")<sup>1,2</sup>

As indicated in Eq. 7.3, the "capacity" of the pile,  $Q_{ult}$ , (alternatively written  $R_{ult}$ ) is the sum of the shaft and toe resistances.

$$(7.3) \quad Q_{ult} = R_s + R_t$$

Eq. 7.4 shows the relation for the load in pile,  $Q_z$ , at depth,  $z$ , for a certain load at the pile head,  $Q_{ult}$ , when the shaft and toe resistances are fully mobilized

$$(7.4) \quad Q_z = Q_{ult} - \int A_s \beta \sigma'_z dz = Q_{ult} - (R_s)_z$$

Both shaft and toe resistances develop due to movement. The movement can either be in response to a load applied to the pile or be due to downdrag. In the ideal elastic-plastic load-movement case, the magnitude of the movement beyond the small values necessary before the plastic state is reached is not important. However, in most cases of shaft resistance and in every case of toe resistance, a single ultimate resistance value does not exist; the resistance is always a function of the movement. It follows that **pile capacity is a fudge concept**. The current overreliance in the design of piled foundations (as well as footings) on factors of safety (or resistance factors) applied to "capacity" is neither logical nor safe. As will be outlined below, design should be based on deformation and settlement analysis.

<sup>1</sup> Notice, the commonly used term "ultimate capacity" is a misnomer, a tautology. The term is a mix of the synonym terms "ultimate resistance" and "capacity". Although one cannot be mistaken of the meaning of "ultimate capacity", the adjective should not be used, because it makes the use of other adjectives seem proper, such as "load capacity", "allowable capacity", "design capacity", "working capacity", "carrying capacity", which are at best awkward and at worst misleading. Sometimes, even the person modifying "capacity" with these adjectives is unsure of the meaning. The only modifiers to use with the term "capacity" for piles are "long-term capacity" as opposed to "short-term capacity", "axial capacity" as opposed to "lateral capacity", and "bearing capacity", or "geotechnical capacity" (often used to contrast "structural strength"; the term "structural capacity" is awkward and it should be avoided. Better to use the term "structural strength").

#### 7.2.4 Service Conditions

During service conditions, loads from the structure ("working loads") will be applied to the pile head via a pile cap. The working loads are normally separated on permanent (or 'dead' or "sustained") loads,  $Q_{\text{dead}}$ , and transient (or 'live') loads,  $Q_{\text{live}}$ . (See definitions of "dead" and "live" in Chapter 13). Not generally recognized is that, even if soil settlements are small, even when too small to be readily noticeable, the soil will in the majority of cases, move down in relation to the pile and in the process transfer load to the pile by negative skin friction. (An exception is a pile in swelling soils and the exception is limited to the length of pile in the swelling zone, where then 'positive skin friction' develops; for analysis swelling response, see Section 7.17). Already the small relative movements always occurring over time between a pile shaft and the soil are sufficient to develop significant negative skin friction (as well as positive skin friction, and positive and negative shaft resistances—the separation of the terms on "friction" and "resistance" signifies whether the shear is introduced by the soil or by outside forces). Therefore, every pile develops an equilibrium of forces between, on the one side, the sum of the dead load applied to the pile head,  $Q_{\text{dead}}$ , and a drag force,  $Q_n$ , induced by negative skin friction in the upper part of the pile, and, on the other side, the sum of positive shaft resistance and toe resistance in the lower part of the pile. The point of "**force equilibrium**" is called the **neutral plane**, is the depth where the shear stress along the pile changes over from negative skin friction into positive shaft resistance. This is also where there is no relative displacement between the pile and the soil, that is, the neutral plane is also the "**settlement equilibrium**". Note, where the soil settlements are small, the height of the transition zone will be large.

The key aspect of the foregoing is that the development of a neutral plane and drag force due to negative skin friction is an always occurring phenomenon in piles and not limited to where large soil settlement occurs around the piles. Numerous well-documented case histories testify to the veracity of the underlined statement (Fellenius 2004).

For piles designed with a normal margin against failure (e.g., designed with a factor-of-safety on the "capacity"), the neutral plane lies below the mid-point of a pile. The extreme case is for a pile bearing on bedrock, where the location of the neutral plane is at the pile toe, at the bedrock elevation. For a lightly loaded, dominantly shaft-bearing pile 'floating' in a homogeneous soil with linearly increasing shear resistance, the neutral plane typically lies at a depth which is about equal to the lower third point of the pile embedment length<sup>3)</sup>. See also comments on "Piled Raft and Pile Pad Foundations" in Section 7.5.

The larger the toe resistance, the deeper lies the neutral plane. And, the larger the dead load, the shallower the neutral plane.

The analysis is illustrated in the following example: A pile group of 355-mm diameter pipe piles is to be installed at a site where the soil profile consists of an upper layer of silt deposited on soft clay followed by dense silty sand on glacial till. A 1.5 m thick earth fill will be placed over a large area surrounding the pile group resulting in a stress of 30 kPa. Each pile will be subjected to dead and live loads of 800 kN and 200 kN, respectively.

The calculation begins with a load-transfer analysis, which is best performed using a range (boundary values) of  $\beta$  and  $N_t$ -parameters which provide upper and lower limits of reasonable values. We can assume that the particular ranges of soil parameter values necessary for the calculations have been established in a soils investigation. The soil parameters are density, and the parameters  $\beta$  and  $N_t$ <sup>4)</sup>

---

<sup>3)</sup> This is the basis for the "Terzaghi-Peck" rule of calculating the settlement of a pile group consisting of shaft bearing piles in uniform soil as the settlement for an equivalent raft placed at the lower third point of the pile.

<sup>4)</sup> The unit toe resistance is better input as the unit resistance generated by estimating an imposed toe movement.

**TABLE 7.3** CALCULATION OF PILE "CAPACITY" [by means of UniPile Version 5]

Size, $\Phi = 355$ mm	Live Load, $Q_l = 200$ kN	Shaft Resistance, $R_s = 1,671$ kN		
Area, $A_s = 1.115$ m <sup>2</sup> /	Dead Load, $Q_d = 800$ kN	Toe Resistance, $R_t = 1,147$ kN		
Area, $A_t = 0.099$ m <sup>2</sup>	Total Load = 1,000 kN	Total Resistance, $R_u = 2,817$ kN		
$F_s = 3.01$	Depth to N. P. = 25.46 m	Load at N. P., $Q_{max} = 1,809$ kN		
-DEPTH TOTAL STRESS (m) (kPa)	PORE PRES. (kPa)	EFFECTIVE STRESS (kPa)	$Q_d+Q_n$ (kN)	$Q_u-R_s$ (kN)
<b>LAYER 1 Sandy Silt</b> $\rho = 2,000$ kg/m <sup>3</sup> $\beta = 0.40$				
0.00 30.00	0.00	30.00	800	2,817
1.00(GWT)48.40	0.00	48.40	818	2,800
4.00 104.30	30.00	74.30	900	2,718
<b>LAYER 2 Soft Clay</b> $\rho = 1,700$ kg/m <sup>3</sup> $\beta = 0.30$				
4.00 104.30	30.00	74.30	900	2,718
5.00 120.10	43.50	76.60	925	2,693
6.00 136.00	57.10	79.00	951	2,667
7.00 152.00	70.60	81.40	978	2,640
8.00 168.10	84.10	84.00	1,005	2,612
9.00 184.20	97.60	86.60	1,034	2,584
10.00 200.40	111.20	89.20	1,063	2,554
11.00 216.60	124.70	91.90	1,094	2,524
12.00 232.90	138.20	94.60	1,125	2,493
13.00 249.20	151.80	97.40	1,157	2,461
14.00 265.60	165.30	100.30	1,190	2,428
15.00 281.90	178.80	103.10	1,224	2,394
16.00 298.40	192.40	106.00	1,259	2,359
17.00 314.80	205.90	109.00	1,295	2,323
18.00 331.30	219.40	111.90	1,332	2,286
19.00 347.90	232.90	114.90	1,370	2,248
20.00 364.40	246.50	117.90	1,409	2,209
21.00 381.00	260.00	121.00	1,449	2,169
<b>LAYER 3 Silty sand</b> $\rho = 2,100$ kg/m <sup>3</sup> $\beta = 0.50$				
21.00 381.00	260.00	121.00	1,449	2,169
22.00 401.60	270.00	131.60	1,519	2,098
23.00 422.20	280.00	142.20	1,595	2,022
24.00 442.80	290.00	152.80	1,678	1,940
25.00 463.40	300.00	163.40	1,766	1,852
26.00 484.10	310.00	174.10	1,758	1,758
27.00 504.80	320.00	184.80	1,657	1,657
<b>LAYER 4 Ablation Till</b> $\rho = 2,200$ kg/m <sup>3</sup> $\beta = 0.55$				
27.00 504.80	320.00	184.80	1,657	1,657
31.00 591.70	360.00	231.70	1,147	1,147
				<b><math>N_t = 50</math></b>

The unit shaft resistance is calculated using the average effective stress between Depths  $z_{(n-1)}$  and  $z_n$  assumed to represent a plastic state of resistance) used in the effective stress calculations of load transfer. The example does not include a settlement analysis. Had that been considered as a part of the analysis, additional input would have been needed, such as compressibilities (such as for immediate compression, consolidation, and secondary compression conditions), consolidation coefficient (See Chapter 3) of the soil within and beyond the pile embedment depth. The analysis includes several steps. The pile has reached well into the competent sand layer, which will not compress much for the increase of effective stress due to the pile loads and the earth fill. Therefore, the settlement of the pile group will be minimal and not govern the design. Settlement analysis will be discussed in Section 7.16.

Determine first the range of installation length (using the range of effective stress parameters) as based on the required at-least "capacity". The at-least "capacity" is the "capacity" that when divided with the factor of safety represents the "allowable load", which must not be smaller than the "working load" actually applied to the pile. A factor-of-safety of 3.0 is usually applied to an analysis not referenced to direct test records of pile response:  $3,000/3.0 = 1,000 = 800 + 200$  kN. The calculations show that to achieve a 3,000-kN "capacity" ("capacity" that, of course, must agree with some definition based on pile head movement), when applying the lower boundary values of  $\beta$  and  $r_t$  or  $N_t$ , the piles have to be installed to a penetration into the sandy till layer of 4 m, i.e., depth of 31 m.

The calculated load and resistance distributions for the example pile are given in the two rightmost columns in Table 7.3, which presents the results of the load-transfer calculations for this embedment depth. The calculations have been made with the UniPile program (Goudreault and Fellenius 2014) and the results are presented in the format of a spread-sheet "hand calculation" to simplify verifying the computer calculations. The two-decimal precision serves to assist in the verification.

The calculations results are plotted in Fig. 7.6a in the form of two curves: a resistance curve and a load-transfer curve. The resistance curve (Eq. 7.4) starts at the mentioned "capacity" of 3,000 kN and decreases with depth due to the shaft resistance (ultimate conditions are assumed). The value plotted at the pile toe is the calculated toe resistance. The curve is assumed to represent the long-term conditions at a site.

The load distribution in the pile during long-term conditions down to the neutral plane is given by Eq. 7.5. The curve starts at the dead load of 800 kN and increases due to negative skin friction to a maximum at the neutral plane, where it intersect with the resistance curve and then is the same as the resistance curve. Note, the load-transfer curve represents the **extreme case of a relative movement** between the pile(s) and the soil at a movement that is large enough to fully mobilize the shaft shear, resulting in a transition zone of a minimal length, including a significant toe resistance. That is, the load-transfer curve assumes that the movement of the pile toe into the soil is about equal to that found in a static loading test to "failure".

$$(7.5) \quad Q_z = Q_d + \int A_s q_n dz = Q_d + Q_n$$

where  $Q_d$  = dead load on the pile  
 $Q_n$  = drag force at the neutral plane  
 $A_s$  = circumferential pile area  
 $q_n$  = unit negative skin friction;  $q_n = r_s = \beta \sigma'_z$

As is obvious from the equations, at the depth to the pile toe ( $z = D$ ),  $Q_z$  is equal to  $R_t$ . The curves are based on the assumption that the change—transition—from negative to positive direction unit shear occurs over a **transition zone** with a certain length (height) along the pile.



The transition between the resistance curve (Eq. 7.4) and the load-transfer curve (Eq. 7.5) is in reality not the sudden kink the equations suggest, but, as suggested by in Fig. 6A, a gradual curve from increasing to decreasing trend. The corresponding change from negative skin friction to positive shaft resistance shown as the line marked "T\*" in Fig. 7.6B is not really linear, but somewhat S-shaped, starting almost horizontal at the left and then bending down aiming for the neutral plane, continuing from there gradually bending back to finish at almost a horizontal portion over to the right. This is because a smooth transition from fully developed negative skin friction to fully developed positive shaft resistance occurs over some length of pile above and below the neutral plane, a 'transition zone'. The length of the transition zone varies with the type of soil and the rate or gradient of the relative movement between the pile and the soil at the neutral plane. Its length can be estimated to be the length over which the relative movement between the pile and the soil is smaller than about 2 mm to 5 mm. Thus, if disregarding the transition zone, the theoretically calculated value of the load in the pile at the neutral plane, the maximum load, is higher than the real value and it is easy to overestimate the magnitude of the drag force and, therefore, the maximum load in the pile. Notice, also, that the calculations are interactive inasmuch that a change of the value of the dead load applied to a pile will change the location of the neutral plane and the magnitude of the maximum axial load in the pile (which occurs at the neutral plane).

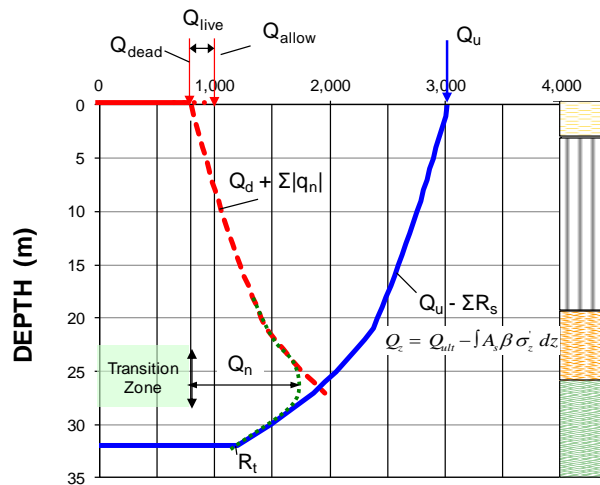


Fig. 7.6A Load-transfer and resistance curves

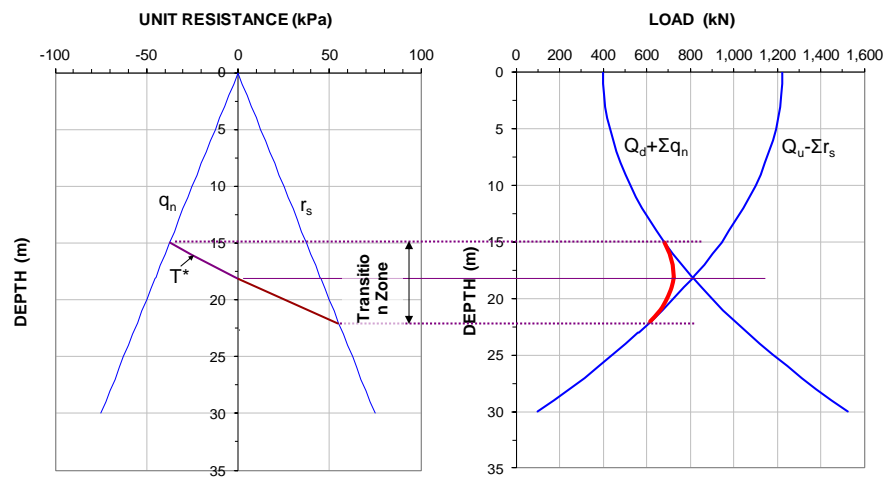


Fig. 7.6B Transition from unit negative skin friction to unit positive shaft resistance and from increasing load to decreasing load distribution (*not the same example as in 7.6a*)

### 7.3 Load-movement and Load Transfer

The foregoing presents the conventional bearing-"capacity" ultimate-resistance approach, based on a pile having a specific resistance value called "capacity" (subject to definition; See Chapter 8) amounting to the sum of the ultimate resistances—usually presumed plastic—of all the elements making up the pile. The reality is very different, even for the case of a definite ultimate resistance, as illustrated by the t-z curve in Fig. 7.7. The pile element is in a strain-softening soil and the resistance build up to a peak at a small initial shear movement, whereafter it reduces—softens. For reasons of simplicity, we assume here that all pile elements making up the pile have the same t-z strain-softening shaft-resistance relation. The pile toe response follows a q-z relation (for information on t-z and q-z functions, see Chapter 8), and a pile toe response never reaches an ultimate condition, but continuous as a gently rising load-movement curve. When the pile (assumed to be a 300-mm diameter, 30 m long concrete pile), is subjected to a head-down static loading test that combines all the responses of the various pile elements and their stiffness (EA), and the effect of the pile toe element is added, the results are as shown in Fig. 7.7. Everyone would probably take the red dot at the peak of the pile-head load-movement curve to represent the pile "capacity". The figure shows that, at that stage in the test, however, only one or a few of the pile elements would be at a stage representing their peak resistance. The elements in the upper part of the pile will be at a post-peak state and the elements closer to the pile toe will be at pre-peak state. The pile toe has hardly begun to move and the mobilized toe resistance is small. Chapter 8 shows pile-head load-movement curves and strain-hardening t-z responses, where no "capacity" is obvious and special definitions are needed in order to obtain one from the test results. Those cases share with the case shown in Fig. 7.7 the condition that whatever the definition of pile "capacity" applied to the pile-head curve, it will not harmonize with or correlate to the ultimate resistance defined or chosen for the individual pile elements.

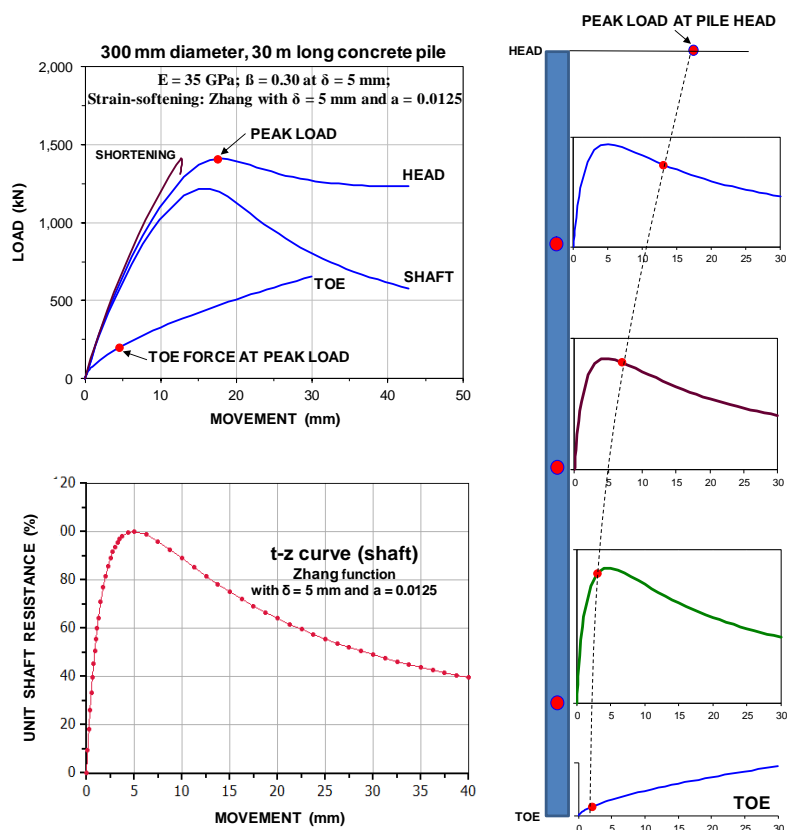


Fig. 7.7 Comparison between load-movement curves and t-z curves

## 7.4 Critical Depth

Many texts suggest the existence of a so-called ‘critical depth’ below which the shaft and toe resistances would be constant and independent of the increasing effective stress. This concept is a fallacy and based on incorrect interpretation of test data and should not be applied. Fellenius and Altae (1994; 1996) discussed the “Critical Depth” and the reasons for how such an erroneous concept could come about. (Some authors have applied the term “critical depth” to the phenomenon of reduction of the unit shaft resistance along very long offshore piles, where the resistance at depth in a homogeneous soil can start to decrease, but that is not the generally understood meaning of the term as applied "on shore").

## 7.5 Effect of Installation

Whether a pile is installed by driving or by other means, the installation affects—disturbs—the soil. Before the disturbance from the pile installation has subsided, it is difficult to determine the magnitude of what shaft and toe resistances to expect. For instance, presence of dissipating excess pore pressures causes uncertainty in the magnitude of the effective stress in the soil and the strength gain (set-up) due to reconsolidation is hard to estimate. Such installation effects can take long time to disappear, especially in clays. They can be estimated in an effective stress analysis using suitable assumptions as to the distribution of pore pressure along the pile at any particular time. Usually, to calculate the installation effect, a good estimate can be obtained by imposing excess pore pressures in the fine-grained soil layers—the finer the soil, the larger the induced pore pressures—taking care that the pore pressure must not exceed the total overburden stress. The reconsolidation process returns the pore pressures to the original conditions and when all the induced excess pore pressures have dissipated, the long-term "capacity" is established. For a case-history example, see Fellenius (2008). Notice, in some soils, even sands, the increase of "capacity", the set-up, can continue also well after the pore pressures induced during the driving have dissipated (Bullock et al. 2005). See also Section 7.20.

## 7.6 Residual Force

The dissipation of induced excess pore pressures (called “reconsolidation”) imposes force (axial) in the pile by negative skin friction in the upper part of the pile, which is resisted by positive shaft resistance in the lower part of the pile and some toe resistance. In driven piles, residual force also results from strain built in or locked-in during the driving. Residual force, as well as "capacity", may continue to increase also after the excess pore pressures have dissipated.

The quantitative effect of not recognizing the residual force in the evaluation of results from a static loading test, is that erroneous conclusions will be drawn from the test: the shaft resistance appears larger than the true value, while the toe resistance appears correspondingly smaller. Typically, when the residual force is not recognized, the distribution of axial load in the pile evaluated from the test records will be with a decreasing curvature with depth, indicating a unit shaft resistance that gets smaller with depth, as opposed to the more realistic shape (in a homogeneous soil) of increasing curvature, indicating a progressively increasing shaft resistance.

The existence of residual force in piles has been known for a long time. Nordlund (1963) was probably the first to point out its importance for evaluating load distribution from the results of an instrumented static pile loading test. However, it is not easy to demonstrate that test data are influenced by residual force. To quantify the effect is even more difficult. Practice is, regrettably, to consider the residual force to be small and not significant to the analysis and to proceed with an evaluation based on “zeroing” all gages immediately before the start of the test. That is, the problem is 'solved' by declaring it not to exist. This is

why the soil mechanics literature includes theories applying “critical depth” and statements that unit shaft resistance would reduce as a function of depth in a homogeneous soil. For more details on this effect and how to analyze the test data to account for residual force, see Hunter and Davisson 1969, Bozozuk et al. 1978, O'Neill et al. (1982), Altae et al. (1992; 1993), Fellenius and Altae (1994; 1996), and Fellenius (2002).

Notice, “capacity” as a term means ultimate resistance, and, in contrast to ultimate shaft resistance, ultimate toe resistance does not exist. As used in the practice, the “capacity” of a pile determined from a static loading test is the load for which the load movement of the pile head appears to show continued movement for a small increase of applied load, failure occurs, the pile “plunges”. This ‘failure’ value is a combination of shaft resistance and toe resistance as indicated in Fig. 7.9, which illustrates how a strain-softening (post-peak) behavior for the shaft resistance combined with an increasing toe resistance, implies an ultimate failure that easily can be assumed to occur also at the pile toe. The toe load-movement curve includes a suggested effect of a residual (locked-in) toe force in addition to that introduced in the test. Additional discussion on this topic is offered in Chapter 8.

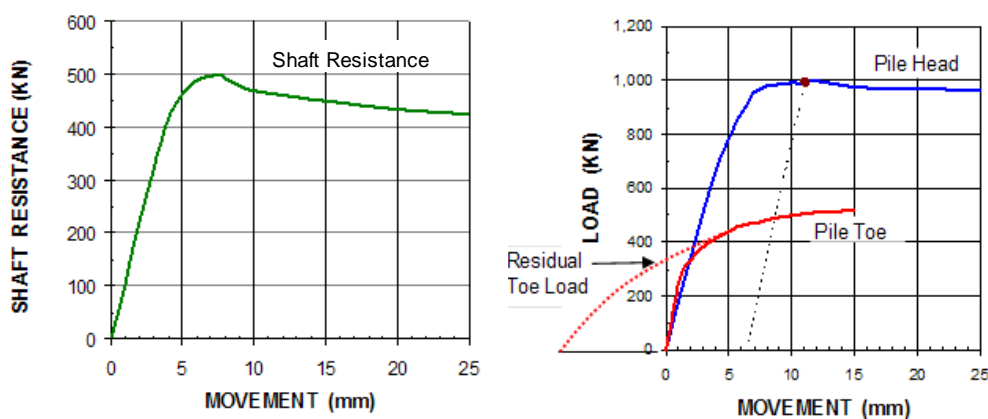


Fig. 7.9 Load-Movement curves for shaft resistance and for total ("Pile Head") and toe resistances.

## 7.7 Analysis of Tapered Piles

Many piles are not cylindrical or otherwise uniform in shape throughout the length. The most common example is the wood pile, which has a conical shape. Step-tapered piles are also common, consisting of two or more concrete-filled steel tubes (pipes) of different diameters connected to each other, normally, the larger above the smaller. Sometimes, a pile can consist of a steel pipe with a lower conical section, for example, the Monotube pile, and the Steel-Taper-Tube pile which typically have a 25 feet (7.6 m) long conical toe section, tapering the diameter down from 14 inches (355 mm) to 8 inches (203 mm). Composite piles can have an upper concrete section joined to a smaller diameter H-pile extension.

For the step-tapered piles, each ‘step’ provides an extra resistance point, which needs to be considered in an analysis. (The GRLWEAP wave equation program, for example, can model a pile with a diameter change as having a second pile toe at the location of the ‘step’). In a static analysis, each such step can be considered as an extra pile toe with a donut-shaped area,  $A_t$ , and assigned a corresponding toe resistance per Eq. 7.2b, or toe unit resistance value,  $r_t$ , times the donut area. Each such extra toe resistance value is then added to the shaft resistance calculated using the actual pile diameter.

The analysis of how a helical pile—single helix or multiple helices—is best analyzed as each helix serving as an extra pile toe with its representative “toe” resistance. Naturally, no such analysis can be meaningful without correlation to the movement generating the resistance. Closely spaced helices can result in the pile responding as a straight-shaft pile with a diameter equal to the helix diameter.

Piles with a continuous taper (conical piles) are less easy to analyze. Nordlund (1963) suggested a taper adjustment factor to use to increase the unit shaft resistance in sand for conical piles. The adjustment factor is a function of the taper angle and the soil friction angle. A taper angle of 1° (0.25-inch/foot) in a sand with a 35° friction angle would give an adjustment factor of about 4. At 0.5° taper angle, the factor would be about 2. I prefer a more direct calculation method consisting of dividing the soil layers into sub-layers of some thickness and, at the bottom of each such sub-layer, project the diameter change. This donut-shaped area is then treated as an extra toe similar to the analysis of the step-taper pile. The shaft resistance is calculated using the mean diameter of the pile over the same "stepped" length. The shaft resistance over each such particular length consists of the sum of the shear resistance over the shaft area and the toe resistance of the "donut" area. This method requires that a toe coefficient,  $N_t$ , or a unit toe resistance value,  $r_t$ , be assigned to each "stepped" length. The "donut" method applies also to piles in clay.

The taper does not come into play for negative skin friction. This means that, when determining the response of a pile to tension loading, the effect of the taper (the "donut") should be excluded. In addition, the analysis must consider that the shear response along the tapered length is considerably smaller in "pull" as opposed to in "push" (in contrast to straight-shaft pile for which the shaft resistance in pull" and "push" are the same). Similarly, when assessing negative skin friction, the "donut effect" of the taper must be disregarded. Below the neutral plane, however, the effect should be included. Note, including it will influence the location of the neutral plane (because the "donut effect" of the taper increases the positive shaft resistance below the neutral plane, thus lowering the force equilibrium).

## 7.8 Standard Penetration Test, SPT, Method for Determining Axial Pile "Capacity"

For many years, the N-index of standard penetration test has been used to calculate "capacity" of piles. However, the standard penetration test (SPT) is a subjective and highly variable test. The Canadian Foundation Engineering Manual (1992) lists the numerous irrational factors influencing the N-index. The person doing the analysis using of the N-index must consider the split-spoon sample of the soil obtained in the test and relate the analysis to the site and to area-specific experience of the SPT-test. These days, N-indices are usually adjusted to the  $N_{60}$ -value, which is the value after correction to an impact energy equal to 60 % of the nominal positional energy of the 63.5 kg-weight falling from 760-mm height. Several additional adjustments have also been proposed. It is wise not to rely too much on N-indices. Indeed, using the "N-values" numerically in a formula is in my opinion using make-believe engineering.

The test and the N-index have substantial qualitative value, but should be used only very cautiously for quantitative analysis. So, although I quote the equations for calculations using SPT N-indices, I believe that using the N-index numerically in formulae, such as Eqs. 7.6 through 7.11, is unsafe and imprudent.

Meyerhof (1976) compiled and rationalized some of the experience then available and recommended that the "capacity" be a function of the N-index, as follows: N.B., Meyerhof "calibrated" the coefficients to primarily Franki-piles in Eastern Canada glacial till and coarse-grained soils.

$$(7.6) \quad R = R_t + R_s = mN_t A_t + n\bar{N}_s A_s D$$

where

- $m$  = a toe coefficient
- $n$  = a shaft coefficient
- $N_t$  = N-index at the pile toe (taken as a pure number)
- $\overline{N_s}$  = N-index average along the pile shaft (taken as a pure number)
- $A_t$  = pile toe area
- $A_s$  = unit shaft area; circumferential area
- $D$  = embedment depth

For values inserted into Eq. 7.6 using base SI-units, that is, **R** in newton, **D** in metre, and **A** in m<sup>2</sup>/m, the toe and shaft coefficients, **m** and **n**, become:

$$\begin{aligned} m &= 400 \cdot 10^3 \text{ for driven piles and } 120 \cdot 10^3 \text{ for bored piles (N/m}^2\text{)} \\ n &= 2 \cdot 10^3 \text{ for driven piles and } 1 \cdot 10^3 \text{ for bored piles (N/m}^2\text{)} \end{aligned}$$

For values inserted into Eq. 7.6 using English units with **R** in kips, **D** in feet, and **A** in ft<sup>2</sup>/ft, the toe and shaft coefficients, **m** and **n**, become:

$$\begin{aligned} m &= 8 \text{ for driven piles and } 2.4 \text{ for bored piles (ksf)} \\ n &= 0.04 \text{ for driven piles and } 0.02 \text{ for bored piles (ksf)} \end{aligned}$$

Decourt (1989; 1995) suggested that the pile "capacity" should be calculated according to Eq. 7.7. The equation presumes that values are input in base SI-units, that is, **R** in newton, **D** in metre, and **A** in m<sup>2</sup>/m

$$(7.7) \quad R = R_t + R_s = K N_t A_t + \alpha (2.8 \overline{N_s} + 10) A_s D$$

where

- $R_t$  = total toe resistance
- $R_s$  = total shaft resistance
- $K$  = a toe coefficient per soil type and construction method as listed in Table 7.4
- $\alpha$  = a shaft coefficient per soil type and construction method as listed in Table 7.5
- $N_t$  = N-index at the pile toe (taken as a pure number)
- $\overline{N_s}$  = N-index average along the pile shaft (taken as a pure number)
- $A_t$  = pile toe area
- $A_s$  = unit shaft area; circumferential area
- $D$  = embedment depth

**TABLE 7.4 Toe Coefficient K (Decourt 1989; 1995)**

Soil Type	Displacement Piles	Non-Displacement Piles
Sand	$325 \cdot 10^3$	$165 \cdot 10^3$
Sandy Silt	$205 \cdot 10^3$	$115 \cdot 10^3$
Clayey Silt	$165 \cdot 10^3$	$100 \cdot 10^3$
Clay	$100 \cdot 10^3$	$80 \cdot 10^3$

**TABLE 7.5 Shaft Coefficient  $\alpha$**  (Decourt 1989; 1995)

Soil Type	Displacement Piles	Non-Displacement Piles
Sand	$1 \cdot 10^3$	$0.6 \cdot 10^3$
Sandy Silt	$1 \cdot 10^3$	$0.5 \cdot 10^3$
Clayey Silt	$1 \cdot 10^3$	$1 \cdot 10^3$
Clay	$1 \cdot 10^3$	$1 \cdot 10^3$

O'Neill and Reese (1999) suggested calculating the toe resistance of a drilled shaft in cohesionless soil as given in Eq. 7.8. For piles with a toe diameter larger than 1,270 mm (50 inches), the toe resistance calculated according to Eq. 7.8 should be reduced by multiplication with a factor,  $f_t$ , according to Eq. 7.9 with units per the system used—SI or US customary).

$$(7.8) \quad r_t = 0.59 \left( N_{60} \frac{\sigma'_{ref}}{\sigma'_z} \right)^{0.8} \sigma'_z$$

$$(7.9) \quad f_t = \frac{1,270}{b} \quad \text{with } b \text{ in millimetre and} \quad f_t = \frac{50}{b} \quad \text{with } b \text{ in inches}$$

where  $N_{60}$  = N-index (blows/0.3 m) energy-corrected taken as a pure number  
 $\sigma'_{ref}$  = a reference stress, a constant, which for all practical purposes is equal to 100 kPa (= 1 tsf = 2 ksf = 1 kg/cm<sup>2</sup> = 1 at)  
 $\sigma'_z$  = overburden stress at the depth of the pile toe  
 $b$  = diameter of the pile toe (mm or inch)

With regard to the shaft resistance, O'Neill and Reese (1999) suggested calculating the beta-coefficient (Section 7.2) for drilled shafts in cohesionless soil directly, as given in Eqs. 7.10 and 7.11. The calculated unit shaft resistance,  $r_s = \beta \sigma'_z$ , must not exceed 200 kPa (originally 4 ksf). Note that for  $N_{60} \geq 15$ , the O'Neill-Reese beta-coefficient only depends on the depth,  $z$ .

$$(7.10) \quad \beta = \frac{N_{60}}{15} (1.5 - 0.245\sqrt{z}) \quad \text{for } N_{60} \leq 15$$

$$(7.11) \quad \beta = 1.5 - 0.245\sqrt{z} \quad \text{for } N_{60} \geq 15$$

where  $\beta$  = the beta-coefficient (the effective stress proportionality coefficient)  
 $z$  = the SPT sampling depth  
 $N_{60}$  = N-index (blows/0.3 m) energy-corrected

Eqs. 7.8 through 7.11 are also included in AASHTO (2010).

## 7.9 Cone Penetration Test, CPTU, Method for Determining Axial Pile "Capacity"

The static cone penetrometer resembles a pile. There is shaft resistance in the form of the sleeve friction measured immediately above the cone, and there is toe resistance in the form of the directly applied and measured cone stress. Despite the resemblance, there is little scientific reason for why cone stress and sleeve friction measured for a small diameter cone pushed at a constant rate into the soil would have any correlation to the long-term static resistance of a pile. That is, other than that site-specific correlations can

be and have been found. Without such specific site correlations—"calibrations"—, relying on the analysis of "capacity" using results from the static cone makes for a very uncertain design.

Two main approaches for application of cone data to pile design has evolved: indirect and direct methods.

**Indirect CPT methods** employ soil parameters, such as friction angle and undrained shear strength estimated from the cone data as based on bearing "capacity" and/or cavity expansion theories, which introduces significant uncertainties. The indirect methods disregard horizontal stress, apply strip-footing bearing "capacity" theory, and neglect soil compressibility and strain softening. These methods are not particularly suitable for use in engineering practice and are here not further referenced.

**Direct CPT methods** more or less equal the cone resistance with the pile unit resistances. Some methods may use the cone sleeve friction in determining unit shaft resistance. Several methods modify the resistance values to consider the difference in diameter between the pile and the cone, a "scaling" effect. The influence of mean effective stress, soil compressibility, and rigidity affect the pile and the cone in equal measure, which eliminates the need to supplement the field data with laboratory testing and to calculate intermediate values, such as  $K_s$  and  $N_q$ .

Since its first development in the Netherlands, the cone penetrometer test, CPT, has been applied as tool for determining pile "capacity". Seven methods are presented in the following. The first six are based on the mechanical or the electric cones and do not correct for the pore pressures acting on the cone shoulder. The seventh method is the Eslami-Fellenius method, which is based on the piezocone, CPTU. Of course, the Eslami-Fellenius method can also be applied to CPT results, subject to suitable assumptions made on the distribution of the pore pressure, usually applying the neutral pore pressure,  $u_0$ .

1. Schmertmann and Nottingham
2. deRuiter and Beringen (commonly called the "Dutch Method" or the "European Method")
3. Bustamante and Gianselli (commonly called the "LCPC Method" or the "French Method")
4. Meyerhof (method for sand)
5. Tumay and Fakhroo (method limited to piles in soft clay)
6. The ICP method
7. Eslami and Fellenius

Often, CPT and CPTU data include a small amount of randomly distributed extreme values, "peaks and troughs", that may be representative for the response of the cone to the soil characteristics, but not for a pile having a much larger diameter. Keeping the extreme values will have a minor influence on the pile shaft resistance, but it will have a major influence on the pile toe resistance not representative for the pile resistance at the site. Therefore, when calculating pile toe "capacity", it is common practice to manually filter and smoothen the data by either applying a "minimum path" rule or, more subjectively, by reducing the influence of the peaks and troughs from the records. To establish a representative value of the cone resistance to the pile unit toe resistance, the first five methods determine an arithmetic average of the CPT data averaged over an "influence zone", whereas the sixth method (Eslami-Fellenius method) applies geometric mean to achieve the filtering for the toe resistance determination.

### 7.9.1 Schmertmann and Nottingham

#### Toe resistance

The **Schmertmann and Nottingham** method is based on a summary of the work on model and full-scale piles presented by Nottingham (1975) and Schmertmann (1978). The unit toe resistance,  $r_t$ , is a "minimum



path" average obtained from the cone stress values in an influence zone extending from  $8b$  above the pile toe ( $b$  is the pile diameter) and  $0.7b$  or  $4b$ , as indicated in Fig. 7.9.

The procedure consists of five steps of filtering the  $q_c$  data to "minimum path" values. Step 1 is determining two averages of cone stress within the zone below the pile toe, one for a zone depth of  $0.7b$  and one for  $4b$  along the path "a" through "b". The smaller of the two is retained. (The zone height  $0.7b$  applies to where the cone stress increases with depth below the pile toe). Step 2 is determining the smallest cone stress within the zone used for the Step 1. Step 3 consists of determining the average of the two values per Steps 1 and 2. Step 4 is determining the average cone stress in the zone above the pile toe according to the minimum path shown in Fig. 7.10. (Usually, just the average of the cone stress within the zone is good enough). Step 5, finally, is determining the average of the Step 3 and Step 4 values. This value is denoted  $q_{ca}$ .

The pile toe resistance is then determined according to Eq. 7.12.

$$(7.12) \quad r_t = C q_{ca}$$

where

- $r_t$  = pile unit toe resistance; an upper limit of 15 MPa is imposed
- $C$  = correlation coefficient governed by the overconsolidation ratio, OCR
- $q_{ca}$  = the cone stress filtered in the influence zone per the above procedure

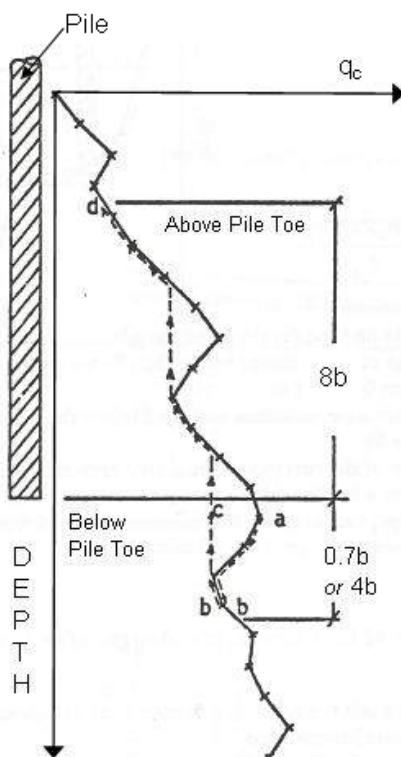


Fig. 7.10 Determining the influence zone for toe resistance (Schmertmann, 1978)

The correlation coefficient,  $C$ , ranges from 0.5 through 1.0 depending on overconsolidation ratio, OCR, according to one of the "1" through "3" slopes between the toe resistance,  $r_t$ , and the minimum-path average of the cone stress ("filtered in the influence zone"), as indicated in Fig. 7.11. For simplicity, the relations are usually also applied to a pile toe located in clay.

### Unit shaft resistance

The unit shaft resistance,  $r_s$ , may be determined from the sleeve friction as expressed by Eq. 7.13.

$$(7.13) \quad r_s = K_f f_s$$

where

- $r_s$  = pile unit shaft resistance; an upper limit of 120 kPa is imposed
- $K_f$  = a dimensionless coefficient
- $f_s$  = sleeve friction

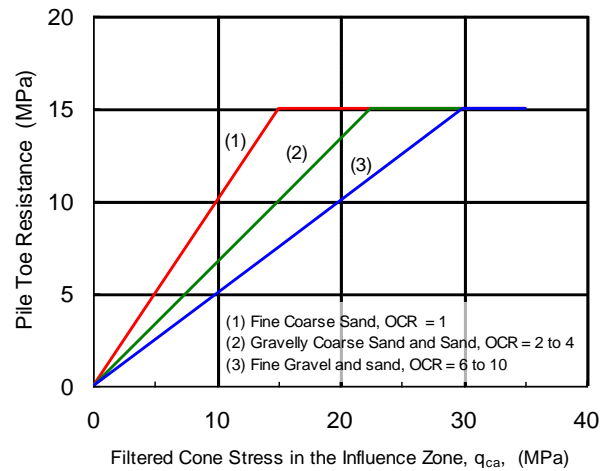


Fig. 7.11 Adjustment of unit toe resistance to OCR

Fig. 7. 12 shows that, in clay,  $K_f$  is a function of the sleeve friction and ranges from 0.2 through 1.25.

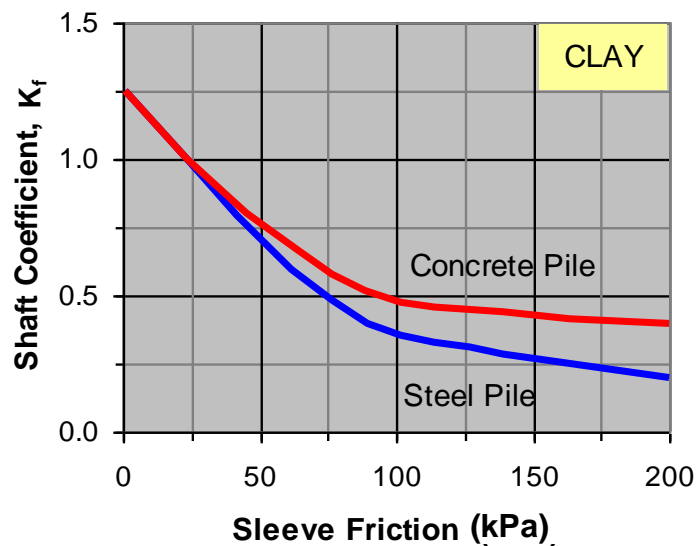


Fig. 7.12 Shaft coefficients for use in Eq. 7.11

In sand,  $K_f$  is assumed to be a function of the pile embedment ratio,  $D/b$ . Within a depth of the first eight pile diameters below the ground surface ( $D/b = 8$ ), the  $K_f$ -coefficient is linearly interpolated from zero at the ground surface to 2.5. Hereunder, the value reduces from 2.5 to 0.891 at an embedment of 20  $D/b$ . Simply applying  $K_f = 0.9$  straight out is usually satisfactory. Alternatively, in sand, but not in clay, the shaft resistance may be determined from the cone stress,  $q_c$ , according to Eq. 7.14.

$$(7.14) \quad r_s = K_c q_c$$

where  $r_s$  = unit shaft resistance; an upper limit of 120 kPa is imposed  
 $K_c$  = a dimensionless coefficient; a function of the pile type.  
                     for open toe, steel piles       $K_c = 0.008$   
                     for closed-toe pipe piles       $K_c = 0.018$   
                     for concrete piles       $K_c = 0.012$   
 $q_c$  = cone stress

### 7.9.2 deRuiter and Beringen

#### Toe resistance

The “Dutch” method was presented by deRuiter and Beringen (1979). For unit toe resistance of a pile in sand, the method is the same as the Schmertmann and Nottingham method. In clay, the unit toe resistance is determined from total stress analysis applied according to conventional bearing “capacity” theory as indicated in Eqs. 7.15 and 7.16.

$$(7.15) \quad r_t = 5 S_u$$

$$(7.16) \quad S_u = \frac{q_c}{N_k}$$

where  $r_t$  = pile unit toe resistance; an upper limit of 15 MPa is imposed  
 $S_u$  = undrained shear strength  
 $N_k$  = a dimensionless coefficient, ranging from 15 through 20, usually = 20

#### Shaft resistance

In **sand**, the unit shaft resistance is the smallest of the sleeve friction,  $f_s$ , and  $q_c/300$ .

In **clay**, the unit shaft resistance may also be determined from the undrained shear strength,  $S_u$ , as given in Eq. 7.17.

$$(7.17) \quad r_s = \alpha S_u = \alpha \frac{q_c}{N_k}$$

where  $r_s$  = pile unit shaft resistance  
 $\alpha$  = adhesion factor equal to 1.0 for normally consolidated clay  
                     and 0.5 for overconsolidated clay  
 $S_u$  = undrained shear strength according to Eq. 7.14

An upper limit of 120 kPa is imposed on the unit shaft resistance.

### 7.9.3 LCPC

The **LCPC** method, also called the “**French**” or “**Bustamente**” method (LCPC = Laboratoire Central des Ponts et Chaussées) method is based on experimental work of Bustamante and Gianselli (1982) for the French Highway Department. For details, see CFEM 1992. The method does not include either of sleeve friction,  $f_s$ , and correction of the cone stress for the pore pressure,  $U_2$ , acting on the cone shoulder.

#### Toe resistance

The unit toe resistance,  $r_t$ , is determined from the cone resistance within an influence zone of  $1.5b$  above and  $1.5b$  below the pile toe, as illustrated in Fig. 7.13 (“ $b$ ” is the pile diameter). First, the cone resistance within the influence zone is averaged to  $q_{ca}$ . Next, an average,  $q_{caa}$ , is calculated of the average of the  $q_{ca}$ -values that are within a range of  $0.7$  through  $1.3$  of  $q_{ca}$ . Finally, the toe resistance is obtained from multiplying the equivalent value with a correlation coefficient,  $C_{LCPC}$ , according to Eq. 7.18.

$$(7.18) \quad r_t = C_{LCPC} q_{caa}$$

where

$r_t$	=	pile unit toe resistance; an upper limit of 15 MPa is imposed
$C_{LCPC}$	=	correlation coefficient (Table 7.5A)
$q_{caa}$	=	average of the average cone resistance in the influence zone

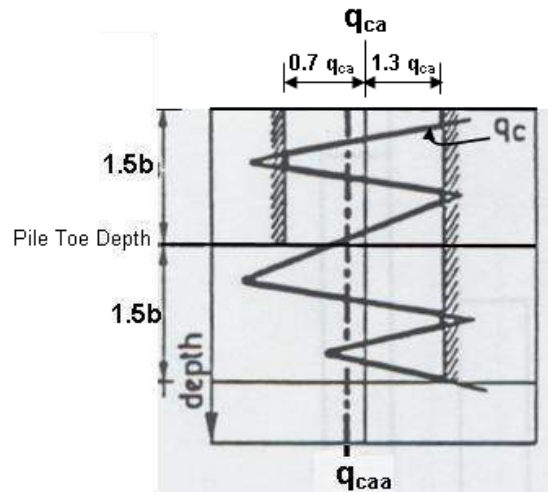


Fig. 7.13 Averaging the cone resistance according to the LCPC method. The “ $b$ ” stands for pile toe diameter. (Bustamante and Gianselli, 1982).

As indicated in Table 7.5A, for driven steel piles and driven precast piles, the correlation coefficient,  $C_{LCPC}$ , ranges from 0.45 through 0.55 in clay and from 0.40 through 0.50 in sand. For bored piles, the values are about 20 % smaller.

#### Shaft resistance

The unit shaft resistance,  $r_s$ , is determined from Eq. 7.19 with the  $K_{LCPC}$ -coefficient ranging from 0.5 % through 3.0 %, as governed by magnitude of the cone resistance, type of soil, and type of pile. Table 7.5B shows upper limits of the unit shaft resistance, ranging from 15 kPa through 120 kPa depending on soil type, pile type, and pile installation method.

$$(7.19) \quad r_s = K_{LCPC} q_c \leq J \quad (\text{see Table 7.5B})$$

where  $r_s$  = unit shaft resistance; for imposed limits  
 $K_{LCPC}$  = a dimensionless coefficient; a function of the pile type and cone resistance  
 $J$  = upper limit value of unit shaft resistance  
 $q_c$  = cone resistance (note, uncorrected for pore pressure on cone shoulder)

**TABLE 7.5A Coefficients of Unit Toe Resistance in the LCPC Method**  
 (Bustamante and Gianselli 1982)

Soil Type	Cone Stress (MPa)	Bored Piles $C_{LCPC}$ (- - -)	Driven Piles $C_{LCPC}$ (- - -)
CLAY	-- $q_c < 1$	0.40	0.50
	1 < $q_c < 5$	0.35	0.45
	5 < $q_c$ - - -	0.45	0.55
SAND	- - - $q_c < 12$	0.40	0.50
	12 < $q_c$ - - -	0.30	0.40

**TABLE 7.5B Coefficients and Limits of Unit Shaft Resistance in the LCPC Method**  
 Quoted from the CFEM (1992)

Soil Type	Cone Stress (MPa)	Concrete Piles & Bored Piles $K_{LCPC}$ (- - -)	Steel Piles $K_{LCPC}$ (- - -)	Maximum $r_s$ $J$ (kPa)
CLAY	-- $q_c < 1$	0.011 (1/90)	0.033 (=1/30)	15
	1 < $q_c < 5$	0.025 (1/40)	0.011 (=1/80)	35
	5 < $q_c$ - - -	0.017 (1/60)	0.008 (=1/120)	35
	(for $q_c > 5$ , the unit shaft resistance, $r_s$ , is always larger than 35 kPa)			
SAND	- - - $q_c < 5$	0.017 (1/60)	0.008 (=1/120)	35
	5 < $q_c < 12$	0.010 (1/100)	0.005 (=1/200)	80
	12 < $q_c$ - - -	0.007 (1/150)	0.005 (=1/200)	120

The values in the parentheses are the inverse of the  $K_{LCPC}$ -coefficient

The limits shown in Table 7.5B are developed in its own practice and geologic setting, and it is questionable if they have any general validity. It is common for users to either remove the limits or to adjust them to new values. Many also apply other values, personally preferred, of the  $K$  and  $J$  coefficients, as well as the  $C$ -coefficient for toe resistance. Therefore, where the LCPC method or a "modified LCPC method" is claimed to be used, the method is often not the actual method by Bustamante and Gianselli (1982), but simply a method whereby the CPT cone resistance by some correlation is used to calculate pile shaft and toe resistances. Such adjustments do not remove the rather capricious nature of the limits.

The correlation between unit shaft resistance and cone stress,  $q_c$ , is represented graphically in Figs. 7.14A and 7.14B with Fig. 7.14A showing the values in "CLAY" and Fig. 7.14B in "SAND". Note, the LCPC method does not correct the cone stress for the pore pressure on the cone shoulder.

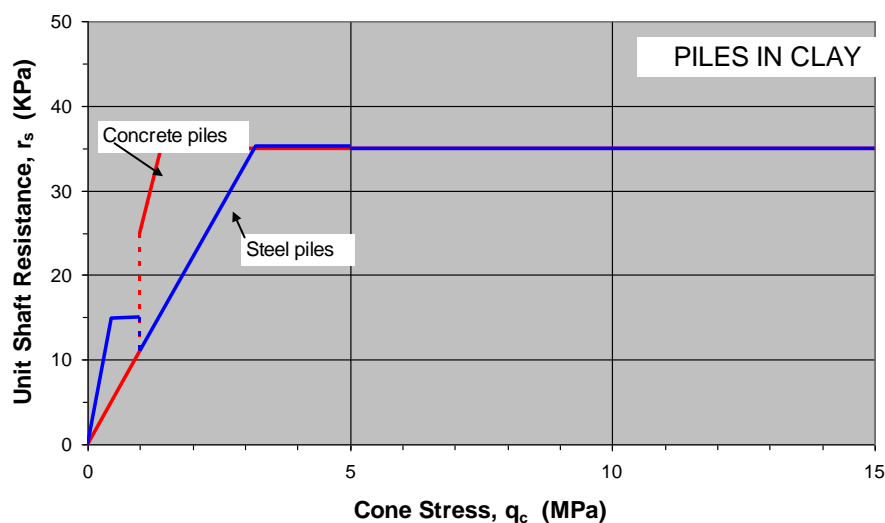


Fig. 7.14A Unit shaft resistance versus cone stress,  $q_c$ , for piles in clay according to the LCPC method.

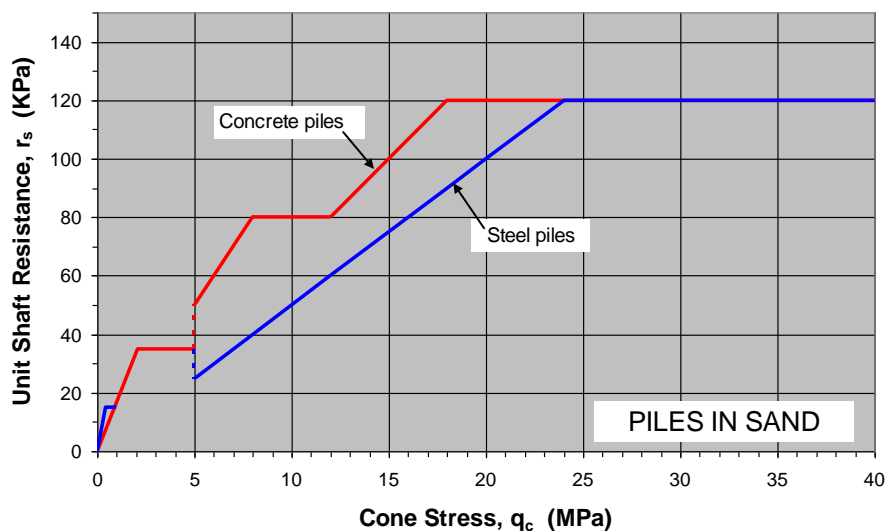


Fig. 7.14B Unit shaft resistance versus cone stress,  $q_c$ , for piles in sand according to the LCPC method.

## 7.9.4 Meyerhof

### Toe resistance

The **Meyerhof** method (Meyerhof 1951; 1963; 1976) is intended for calculating the "capacity" of piles in sand. For unit toe resistance, the influence of scale effect of piles and shallow penetration in dense sand strata is considered by applying two modification factors,  $C_1$  and  $C_2$ , to the  $q_c$  average. The unit toe resistance for driven piles is given by Eq. 7.20.

$$(7.20) \quad r_t = q_{ca} C_1 C_2$$

where

- $r_t$  = unit toe resistance; for bored piles, reduce to 70 % of  $r_t$  per Eq. 7.13
- $q_{ca}$  = arithmetic average of  $q_c$  in a zone ranging from "1b" below through "4b" above pile toe
- $C_1$  =  $[(b + 0.5)/2b]^n$ ; modification factor for scale effect  
when  $b > 0.5$  m, otherwise  $C_1 = 1$
- $C_2$  =  $D/10b$ ; modification for penetration into dense strata  
when  $D < 10b$ , otherwise  $C_2 = 1$
- $n$  = an exponent equal to  
1 for loose sand ( $q_c < 5$  MPa)  
2 for medium dense sand ( $5 < q_c < 12$  MPa)  
3 for dense sand ( $q_c > 12$  MPa)
- $b$  = pile diameter
- $D$  = embedment of pile in a dense sand layer

### Shaft resistance

For driven piles, the unit shaft resistance is either taken as equal to the sleeve friction,  $f_s$ , or 50 % of the cone stress,  $q_c$ , as indicated in Eqs. 7.21 and 7.22. For bored piles, reduction factors of 70 % and 50 %, respectively, are applied to these calculated values of shaft resistance.

$$(7.21) \quad r_s = K_f f_s \quad K_f = 1.0$$

$$(7.22) \quad r_s = K_c q_c \quad K_c = 0.5$$

where

- $r_s$  = unit shaft resistance
- $K_f$  = sleeve resistance modification coefficient
- $K_c$  = cone resistance modification coefficient
- $f_s$  = unit sleeve friction, **kPa**
- $q_c$  = unit cone stress, **kPa**

### 7.9.5 Tumay and Fakhroo

#### Toe resistance

The **Tumay and Fakhroo** method is based on an experimental study in clay soils in Louisiana (Tumay and Fakhroo 1981). The **unit toe resistance** is determined in the same way as in the Schmertmann and Nottingham method, Eq. 7.12.

#### Shaft resistance

The unit shaft resistance is determined according to Eq. 7.23 with the  $K_f$ -coefficient determined according to Eq. 7.24. Note, the  $K$ -coefficient is not dimensionless in Eq. 7.24.

$$(7.23) \quad r_s = K_f f_s$$

where

- $r_s$  = pile unit shaft resistance, kPa
- $K_f$  = a coefficient

$f_s$  = unit sleeve friction, **kPa**

$$(7.24) \quad K_f = 0.5 + 9.5e^{-90f_s}$$

where  $e$  = base of natural logarithm = 2.718

$f_s$  = unit sleeve friction, **MPa**

### 7.9.6 ICP Method

Jardine et al. (2005) present the Imperial College method of using CPT results to determine pile "capacity" in sand and clay. As in the other CPT methods, the sleeve friction is not considered and the cone stress is not corrected for the effect of the pore pressure acting on the cone shoulder. The following description is limited to the method for sand, as it is a bit simpler than the method for clay.

#### Toe resistance in sand

The ICP method applies the cone stress with adjustment to the relative difference between the cone diameter and the pile toe diameter as indicated in Eq. 7.25.

$$(7.25) \quad r_t = q_{ca} \left[ 1 - 0.5 \lg\left(\frac{b_{pile}}{b_{cone}}\right) \right]$$

where  $r_t$  = pile unit toe resistance

$q_{ca}$  = unit cone resistance filtered according to the LCPC method

$b_{pile}$  = pile toe diameter

$b_{cone}$  = cone diameter; 36 mm for a cone with 10 cm<sup>2</sup> base area

For pile diameters larger than 900 mm, a lower limit of  $r_t = 0.3q_c$  applies. Moreover, for piles driven open-toe, a different set of equations apply, which depends on whether or not the pile is plugged.

#### Shaft resistance in sand

According to the ICP method, the unit shaft resistance of closed-toe piles driven in sand is determined according to Eqs. 7.26 and 7.27, which I offer without comments, leaving the reader to judge the engineering relevance of the equations.

$$(7.26) \quad r_s = K_J q_c$$

where  $K_J$  is determined according to Eq. 7.27.

$$(7.27) \quad K_J = \left\{ 0.0145q_c \left( \frac{\sigma'_z}{\sigma_r} \right)^{0.13} \left( \frac{b}{h_f} \right)^{0.38} + [2q_c(0.0203 + 0.00125q_c(\sigma'_z/\sigma_r)^{-0.5} - 1.216 \times 10^{-6} (\frac{q_c^2}{\sigma'_z \sigma_r})]^{-1} \frac{0.01}{b} \right\} \tan \delta$$

where  $\sigma'_z$  = effective overburden stress

$\sigma'_r$  = effective radial stress

$b$  = pile diameter

$h_f$  = depth below considered point to pile toe; limited to 8b

$\delta$  = interface angle of friction



Eq. 7.25 employs principles of "Coulomb failure criterion", "free-field vertical effective stress ( $\sigma'_z$ ) normalized by absolute atmospheric pressure", "local radial effective stress ( $\sigma'_r$ ) with dilatant increase", "interface angle of friction at constant volume test" (or estimate from graph), is "uncorrected for overconsolidation", and applies to compression loading. The method has been developed by fitting to results from six field tests listed by Jardine et al. (2005).

### 7.9.7 Eslami and Fellenius

The Eslami-Fellenius method makes use of the piezocone, CPTU, which is a cone penetrometer equipped with a gage measuring the pore pressure at the cone (usually immediately behind the cone; at the cone shoulder, the so-called U2-position), which is a considerable advancement on the static cone. By means of the piezocone, the cone information can be related more dependably to soil parameters and a more detailed analysis be performed.

#### Toe resistance

In the Eslami and Fellenius CPTU method (Eslami 1996; Eslami and Fellenius 1995, 1996, 1997, Fellenius and Eslami 2000), the cone stress is transferred to an apparent "effective" cone stress,  $q_E$ , by subtracting the measured pore pressure,  $U_2$ , from the measured total cone stress (corrected for pore pressure acting against the shoulder). The pile **unit toe resistance** is the geometric average of the "effective" cone stress over an influence zone that depends on the soil layering, which reduces — removes — potentially disproportionate influences of odd "peaks and troughs", which the simple arithmetic average used by the CPT methods does not do. When a pile is installed through a weak soil into a dense soil, the average is determined over an **influence zone** extending from  $4b$  below the pile toe through a height of  $8b$  above the pile toe. When a pile is installed through a dense soil into a weak soil, the average above the pile toe is determined over an influence zone height of  $2b$  above the pile toe as opposed to  $8b$ . The relation is given in Eq. 7.28.

$$(7.28) \quad r_t = C_t q_{Eg}$$

where

$r_t$	=	pile unit toe resistance
$C_t$	=	toe correlation coefficient (toe adjustment factor)—equal to unity in most cases
$q_{Eg}$	=	geometric average of the cone stress over the influence zone after correction for pore pressure on shoulder and adjustment to "effective" stress

The toe correlation coefficient,  $C_t$ , also called toe adjustment factor, is a function of the pile size (toe diameter). The larger the pile diameter, the larger the movement required to mobilize the toe resistance. Therefore, the "usable" pile toe resistance diminishes with increasing pile toe diameter. For pile diameters larger than about 0.4 m, the adjustment factor should be determined by the relation given in Eq. 7.29.

$$(7.29) \quad \begin{array}{lll} C_t = \frac{1}{3b} & C_t = \frac{12}{b} & C_t = \frac{1}{b} \\ \text{[ 'b' in metre ]} & \text{[ 'b' in inches ]} & \text{[ 'b' in feet ]} \end{array}$$

where  $b$  = pile diameter in units of either metre (or inches or feet)

#### Shaft resistance

Also the pile unit shaft resistance is correlated to the average "effective" cone stress with a modification according to soil type per the approach detailed below. The  $C_s$  correlation coefficient is determined from the soil profiling chart (Chapter 2, Fig. 2.10), which uses both cone stress and sleeve friction. However,

because the sleeve friction is a more variable measurement than the cone stress, the sleeve friction value is not applied directly, but follows Eq. 7.30.

$$(7.30) \quad r_s = C_s q_E$$

where

- $r_s$  = pile unit shaft resistance
- $C_s$  = shaft correlation coefficient, which is a function of soil type determined from the Eslami-Fellenius soil profiling and Table 7.6
- $q_E$  = cone stress after correction for pore pressure on the cone shoulder and adjustment to apparent “effective” stress;  $q_E = q_t - U_2$

Fig. 7.15 compares the unit shaft resistances for piles in sand according to the LCPC method, which does not differentiate between different types of sand and the Eslami-Fellenius method, which separates the sand (Types 4a, 4b, and 5 in Table 7.6) as determined from the actual cone sounding. The difference between  $q_c$  and  $q_t$  is disregarded in the figure. The comparison shows the difference in principle between the methods in that the resistance determined by the LCPC method is definite for the two types of pile material for any specific value of  $q_c$  making no difference between types of sand, while the E-F method indicates a range of values as a function of the sand gradation (as determined from the CPTU soil indication).

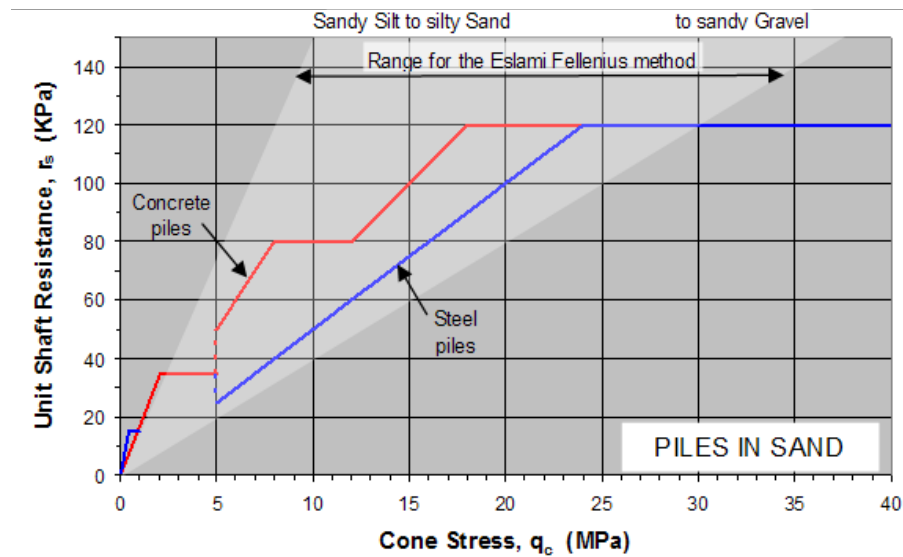


Fig. 7.15 Unit Shaft resistance versus cone stress,  $q_c$ , for piles in sand according to the LCPC method (the red and blue lines) and the Eslami-Fellenius method

**TABLE 7.6 Shaft Correlation Coefficient,  $C_s$**

Soil Type	$C_s$
1. Soft sensitive soils	0.08
2. Clay	0.05
3. Silty clay, stiff clay and silt	0.025
4a. Sandy silt and silt	0.015
4b. Fine sand or silty sand	0.010
5. Sand to sandy gravel	0.004

Notice, all analysis of pile "capacity", whether from laboratory data, SPT-data, CPT-data, or other methods should be correlated back to an effective stress calculation and the corresponding beta-coefficients and  $N_t$ -coefficients be determined from the calculation for future reference.

Soil is variable, and digestive judgment of the various analysis results can and must be exercised to filter the data for computation of pile "capacity", and site-specific experience is almost always absolutely necessary. The more representative the information is, the less likely the designer is to jump to false conclusions, but one must always reckon with an uncertainty in the prediction.

While the soil types indicate a much larger differentiation than the "clay/sand" division of the CPT-methods, the shaft correlation coefficients values shown in Table 7.6 still present sudden changes when the  $q_t$  and  $f_s$  values change from plotting above and below a line in the soil classification chart. It is advisable to always plot the data in the soil classification chart and apply the same shaft correlation coefficient to soil layers that show data points that are grouped together even if they straddle a boundary line. If results from measured shaft distribution is available, the correlation coefficient should be determined by fitting to the measured shaft resistance.

### **7.9.8 Comments on the CPT and CPTU Methods**

When using either of the CPT methods (the six first methods) or the CPTU-method, difficulties arise in applying some of the recommendations of the methods. For example:

1. Although the recommendations are specified to soil type (clay and sand; very cursorily characterized), the CPT methods do not include a means for identifying the actual soil type from the data. Instead, the soil profile governing the coefficients relies on information from conventional boring and sampling, and laboratory testing, which may not be fully relevant to the CPT data.
2. All the CPT methods include random smoothing and filtering of the CPT data to eliminate extreme values. This results in considerable operator-subjective influence of the results.
3. The CPT methods were developed before the advent of the piezocone and, therefore, omit correcting for the pore pressure acting on the cone shoulder (Campanella and Robertson, 1988). The error in the cone stress value is smaller in sand, larger in clay.
4. All of the CPT methods are developed in a specific geographic area with more or less unique geological conditions, that is, each method is based on limited types of piles and soils and may not be relevant outside its related local area.
5. The upper limit of 15 MPa, which is imposed on the unit toe resistance in the Schmertmann and Nottingham, and European methods, is not reasonable in very dense sands where values of pile unit toe resistance higher than 15 MPa frequently occur. Excepting Meyerhof method, all CPT methods impose an upper limit also to the unit shaft resistance. For example, the upper limits (15 kPa, 35 kPa, 80 kPa, and 120 kPa) imposed in the French (LCPC) method quoted in Table 7.5B. Values of pile unit shaft resistance higher than the recommended limits occur frequently. Therefore, the limits are arbitrary and their general relevance is questionable.
6. All CPT methods involve a judgment in selecting the coefficient to apply to the average cone resistance used in determining the unit toe resistance.

7. In the Schmertmann and Nottingham and the European methods, the overconsolidation ratio, OCR is used to relate  $q_c$  to  $r_t$ . However, while the OCR is normally known in clay, it is rarely known for sand.
8. In the European (Dutch) method, considerable uncertainty results when converting cone data to undrained shear strength,  $S_u$ , and, then, in using  $S_u$  to estimate the pile toe "capacity".  $S_u$  is not a unique parameter and depends significantly on the type of test used, strain rate, and the orientation of the failure plane. Furthermore, drained soil characteristics govern long-term pile "capacity" also in cohesive soils. The use of undrained strength characteristics for long-term "capacity" is therefore not justified. (Nor is it really a direct CPT method).
9. In the French method, the length of the influence zone is very limited, and perhaps too limited. (The influence zone is the zone above and below the pile toe in which the cone resistance is averaged). Particularly if the soil strength decreases below the pile toe, the soil average must include the conditions over a depth larger than  $1.5b$  distance below the pile toe.
10. The French (LCPC) and the ICP methods make no use of sleeve friction, which disregards an important aspect of the CPT results and soil characterization.
11. The maximum unit shaft shear values imposed in a few of the methods are arbitrary and do not have general validity.
12. The correlations between CPT or CPTU values to pile shaft and toe resistances are totally empirical and each depends on the data-base used for its development. In fact, there is no scientifically defensible reason that the stress recorded by a cone pushed slowly into the soil would correlate to the long-term resistance of a pile of often 50 to 100 times wider size—other than the fact that, on many occasions, it has shown to work.
13. While some CPT/CPTU methods may have more appeal to a designer than others, the fact is that which method works at a site varies with site geology, pile type and may other conditions specific to a site. No one method is at all times better than the others. It is necessary to always establish for the site involved which method to use by direct tests or careful correlation to other non-CPT/CPTU methods.
14. Ever so often a "new" CPT or CPTU method for determining pile "capacity" is published. Mostly, these methods are modifications of the old methods. Surprisingly many of these apply the cone stress,  $q_c$ , uncorrected for pore pressure acting on the cone shoulder. This is understandable for the "old" methods developed before the pore pressure effect was known. However, those methods were indeed developed against a data base that included such errors—small for piles in sand, variable and potentially larger for piles in clay.
15. All estimates of "capacity" based on cone sounding results by any method are uncertain and should not be accepted without reference to observations—calibrations—proving their suitability for the particular geology and site.
16. All CPT/CPTU methods are statistical correlations to a data base of test records and pile capacities estimated from the test by a variety of methods that can results in capacity values differing more than by a factor of 2 from each other, include errors due to residual load, and involve incorrect separation of shaft resistance from toe resistance components. No pile response derived from an in-situ method should be accepted unless the method has shown to agree with actual pile response established at the particular site or at a site acceptably representative for the actual site conditions, construction, and geology.

### 7.10 The Lambda Method

Vijayvergia and Focht (1972) compiled a large number of results from static loading tests on essentially shaft bearing piles in reasonably uniform soil and found that, for these test results, the mean unit shaft resistance is a function of depth and could be correlated to the sum of the mean overburden effective stress plus twice the mean undrained shear strength within the embedment depth, as shown in Eq. 7.31.

$$(7.31) \quad r_m = \lambda(\sigma'_m + 2c_m)$$

where

- $r_m$  = mean shaft resistance along the pile
- $\lambda$  = the 'lambda' correlation coefficient
- $\sigma'_m$  = mean overburden effective stress
- $c_m$  = mean undrained shear strength

The correlation factor is called "lambda" and it is a function of pile embedment depth, reducing with increasing depth, as shown in Table 7.7.

**TABLE 7.7**  
**Approximate Values of  $\lambda$**

Embedment		$\lambda$
(Feet)	(m)	(-)
0	0	0.50
10	3	0.36
25	7	0.27
50	15	0.22
75	23	0.17
100	30	0.15
200	60	0.12

The lambda method is almost exclusively applied to the Gulf of Mexico soils to determine the shaft resistance for heavily loaded pipe piles for offshore structures in relatively uniform soils. Again, the method should be correlated back to an effective stress calculation and the corresponding beta-ratios and  $N_t$ -coefficients be determined from the calculation for future reference.

### 7.11 Field Testing for Determining Axial Pile "Capacity"

The static capacity of a pile is most reliable when determined in a full-scale static-loading test on an instrumented pile or in bidirectional tests (see Chapter 8). However, the test determines the "capacity" of the specific tested pile(s), only. The load response of other piles at the site must still be determined by analysis, albeit one that now can be calibrated by the field testing. As several times emphasized in the foregoing, all resistances and parameters should be referenced to a static analysis using effective stress parameters and also combined with the relative movement between the pile and the soil at which they were determined. Moreover, despite the numerous static loading tests that have been carried out and the many papers that have reported on such tests and their analyses, the understanding of static pile testing in current engineering practice leaves much to be desired. The reason is that engineers have concerned themselves with mainly one question, only "does the pile have a certain least capacity?", finding little of practical value in analyzing the pile-soil interaction and the load-transfer, i.e., determining the distribution of resistance along the pile and the load-movement behavior of the pile, which aspects are of major importance for the safe and economical design of a piled foundation.

The field test can also be in the form of a dynamic test (Chapter 9), that is, during the driving or restriking of the pile, measurements are taken and later analyzed to determine the static resistance of the pile mobilized during a blow from the pile driving hammer. The uncertainty involved in transferring the dynamic data to static behavior is offset by the ease of having results from more than one test pile. Of course, also the "capacity" and load distribution found in the dynamic test should be referenced to a static analysis.

## 7.12 Installation Phase

Most design analyses pertain to the service condition of the pile and are not quite representative for the installation (construction) phase. However, as implied above (Section 7.6), it is equally important that the design includes an analysis of the conditions during the installation (the construction, the drilling, the driving, etc.) of the piles. For example, when driving a pile, the stress conditions in the soil are different from those during the service condition, and during the pile driving, large excess pore pressures are induced in a soft clay layer and, probably, also in a silty sand, which further reduces the effective stress.

The design must include the selection of the pile driving hammer, which requires the use of software for wave equation analysis, called WEAP analysis (Goble et al. 1980; GRL 2002; Hannigan 1990). This analysis requires input of soil resistance in the form as result of static load-transfer analysis. For the installation (initial driving) conditions, the input is calculated considering the induced pore pressures. For restriking conditions, the analysis should consider the effect of soil set-up.

By means of wave equation analysis, pile penetration resistance (blow-count) at end-of-initial-driving (EOID) and restriking (RSTR) can be estimated. However, the analysis also provides information on what driving stresses to expect, indeed, even the length of time and the number of blows necessary to drive the pile. The most commonly used result is the bearing graph, that is, a curve showing the ultimate resistance ("capacity") versus the penetration resistance (blow count). As in the case of the static analysis, the parameters to input to a wave equation analysis can vary within upper and lower limits, which results in not one curve but a band of curves within envelopes as shown in Fig. 7.16.

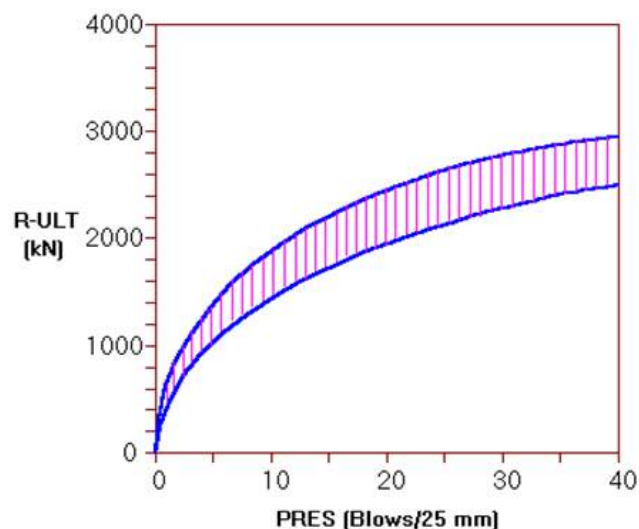


Fig. 7.16 Bearing graph from WEAP analysis

The input parameters consist of the distribution of static resistance, which requires a prior static analysis. Additional input consists of the particular hammer to use with its expected efficiency, etc., the dynamic parameters for the soil, such as damping and quake values, and many other parameters. It should be obvious that no one should expect a single answer to the analysis. The figure shows that at an EOID "capacity" of about 2,200 kN, the penetration resistance (PRES) will range from about 10 blows/25 mm through about 20 blows/25 mm.

Notice that the wave equation analysis postulates observation of the actual penetration resistance when driving the piles, as well as a preceding static analysis. Then, common practice is to combine the analysis with a factor of safety ranging from 2.5 (never smaller) through 3.0.

Fig. 7.16 demonstrates that the hammer selected for the driving cannot drive the pile against a "capacity" of about 3,000 kN "capacity" expected after full set-up. That is, restriking cannot prove out the "capacity". This is a common occurrence. Bringing in a larger hammer, may be a costly proposition. It may also be quite unnecessary. If the soil profile is well known, the static analysis correlated to the soil profile and to careful observation during the entire installation driving for a few piles, sufficient information is usually obtained to support a satisfactory analysis of the pile "capacity" and load-transfer. That is, the "capacity" after set-up is inferred and sufficient for the required factor of safety.

When conditions are less consistent, when savings may result, and when safety otherwise suggests it to be good practice, the pile "capacity" is tested directly. Conventionally, this is made by means of a static loading test. Since about 1975, also dynamic tests are often performed (Chapter 9). Static tests are costly and time-consuming, and are, therefore, usually limited to one or a few piles. In contrast, dynamic tests can be obtained quickly and economically, and be performed on several piles, thus providing assurance in numbers. For larger projects, static and dynamic tests are often combined.

### **7.13 Structural Strength**

Design for structural strength includes consideration of the conditions at the pile head and at the neutral plane. At the pile head, the axial loads consist of dead and live load (combined with bending at the pile head), but no drag force. At the neutral plane, the loads consist of dead load and drag force, but no live load. (Live load and drag force cannot occur at the same time and must, therefore, not be combined in the analysis).

Most limitations of allowable axial load or factored resistance for piles originate in considerations of the conditions at the pile head, or pile cap, rather, and driving conditions. At the pile cap, the axial load is combined with bending and shear forces. In the driving of a pile, the achievable "capacity" is not determined by the axial strength of the pile but by the combination of the hammer ability and the pile impedance,  $EA/c$ . It does not make sense to apply the same limits to the portion of structural strength to the condition at the neutral plane as at the pile cap. Moreover, it should be recognized that, for axial structural strength of the pile, the design considers a material that is significantly better known and which strength varies less than the soil strength. Therefore, the restrictions on the axial force (the safety factor) should be smaller than those applied to soil strength.

Very long piles installed in soils where the settlement is large over most of the length of the piles can be subjected to drag forces that raise concerns for the structural strength of the piles. This is rarely the case before the depth to the neutral plane is about 80 to 100 pile diameters.

For straight and undamaged piles, I recommend that the allowable maximum load at the neutral plane be limited to 70 % of the pile axial strength. However, for composite piles, such as concrete-filled pipe piles and axially reinforced concrete piles, one cannot calculate the allowable stress by adding the "safe" values for the various materials, but must design according to strain compatibility in recognition of that all parts of the pile cross section deforms at the same strain. Good steel in poor concrete cannot be used to its full advantage because the concrete will fail before the steel is substantially engaged. I then recommend that the unfactored axial load at the neutral plane be limited to a value that induces a maximum unfactored compression strain of 1 millistrain into the pile with no material becoming stressed beyond 70 % of its structural strength. See Section 7.15 for a discussion on the location of the neutral plane and the magnitude of the drag force.

### 7.14 The Location of the Neutral Plane and the Magnitude of the Drag Force

The rules for the static analysis presented in this chapter include merely the most basics of the topic. They are derived from many well-documented case histories from around the world. Some of which are summarized by Fellenius (1998, 2006). One major reference is a case history presented by Endo et al. (1969) from which work Fig. 7.17 is quoted. The figure shows two diagrams which clearly demonstrates the interdependence of the load-transfer and the movement and settlement behavior.

The left diagram in Fig. 7.17 shows the load distribution measured during almost three years after the installation of a telltale-instrumented steel pile. The loads in the pile increase due to negative skin friction to a maximum drag force value at the neutral plane (N.P.) and reduce from there due to positive shaft resistance.

The diagram to the right in Fig. 7.17 shows the measured settlement of the soil and the pile over the same time period. Note that the distributions of settlement for the pile and the soil intersect at the neutral plane.

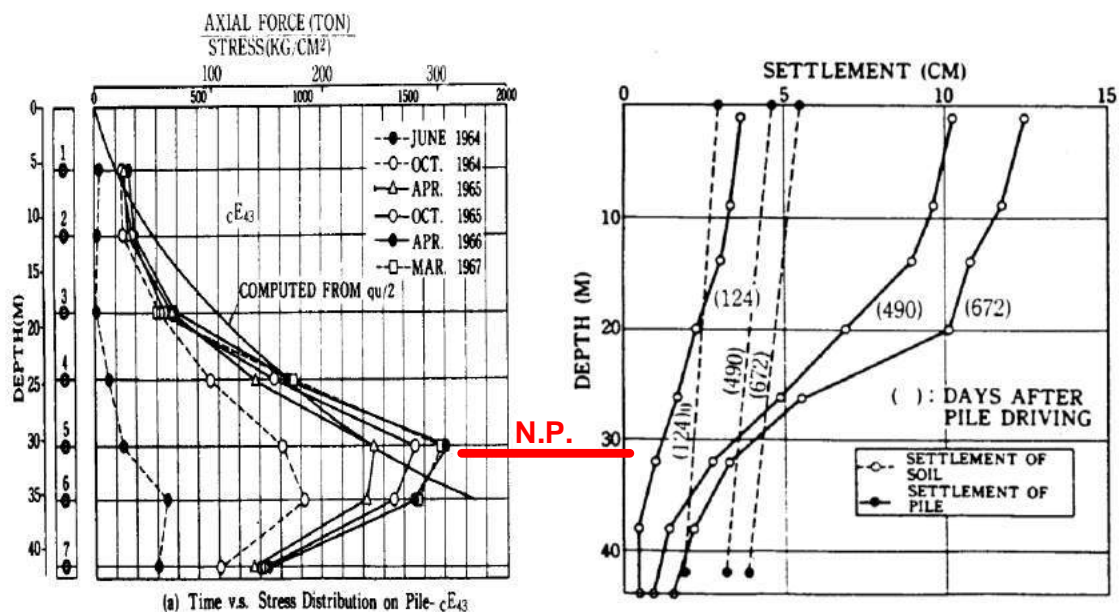


Fig. 7.17 Combination of two diagrams taken from Endo et al. (1969)



Note that the shear forces increased with depth and that, during the last three years of monitoring, the negative skin friction in the upper portion of the pile did not appreciably increase despite the ongoing soil settlement. The paper also presents measurements of pore pressure development showing that, in the upper portion of the soil, the pore pressures did not change much during the last few years of observation. This means that the effective stress did not change appreciably during that time in that zone. At depth, however, the pore pressures dissipated with time, and, consequently, the effective stress increased, and, the negative skin friction and positive shaft resistance increased accordingly. Clearly, the shear forces are proportional to the effective overburden stress and they and their development with time are independent of the magnitude of the settlement.

The main principle of determining the interaction between load-transfer and settlement, as well as the associated magnitude of the drag force is shown in Fig. 7.18. The left diagram in the figure shows load-and-resistance curves with distribution of ultimate resistance and two long-term load distributions (marked “1” and “2”), which both start from the dead load applied to the pile. (The dashed extension of the bar at the level of the ground surface indicates the live load also applied to the pile at times, but live load has no influence on a long-term load distributions). The right diagram shows the distribution with depth of soil and pile settlement.

Case 1 and Case 2 are identical with regard to the distributions of ultimate resistance. That is, the two cases would have shown the same load-movement diagram in a static loading test. However, Case 1 is associated with small long-term settlement of the soil. The settlement diagram to the right side diagram shows that the relative movement between the soil and the pile is sufficient to fully mobilize negative skin friction along the upper portion of the pile and positive shaft resistance in the lower portion, but for an in-between transition zone. The length of the transition zone is governed by the distance for which the relative movement between the pile and the soil is very small, smaller than the few millimetre necessary to fully mobilize the shear forces (Section 7.2). At a site where the total settlement is small, this minimal relative movement does not materialize nearest the neutral plane and the length of the transition zone can be significant.

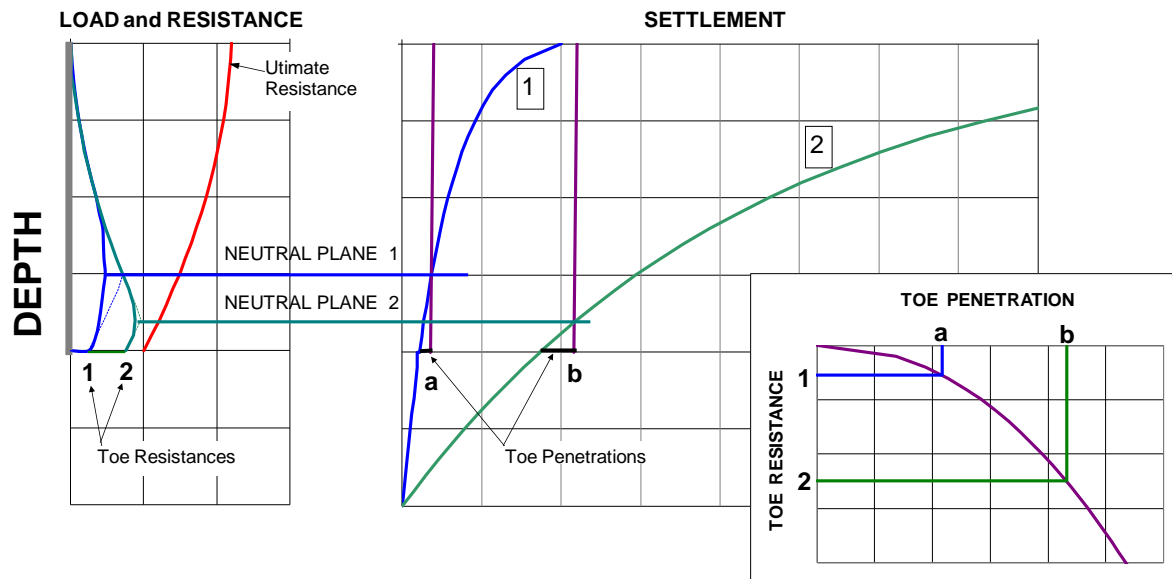


Fig. 7.18 Combination of load-and-resistance diagram and settlement diagram

The figure demonstrates a second important principle. The toe resistance shown in the load diagram is small compared to the ultimate value indicated by the resistance diagram. This is because the toe

resistance is a function of the imposed pile toe movement. The toe movement is illustrated as the “toe penetration” in the settlement diagram. The penetration shown for Case 1 is the one that results in the toe resistance shown in the resistance diagram.

Case 2 presents a case where the soil settlement is no longer small. The effect of the larger settlement is that the toe movement is larger. As a result, the mobilized toe resistance is larger and the point of equilibrium, the neutral plane, has moved down. Moreover, the transition zone is shorter. The maximum load, that is, the sum of the dead load and the drag force, is therefore larger. If the settlement were to become even larger, the toe penetration would increase, the neutral plane would move further down, transition zone would become even shorter, and the drag force would become larger.

For a given resistance distribution, the figure illustrates that the magnitude of the relative movement between the pile and the soil is one of the factors governing the magnitude of the drag force and the location of the neutral plane. If a pile is installed well into a non-settling layer with a neutral plane located in that layer or at its upper boundary, then, the toe resistance will be small, and the transition zone will be long. The drag force will be correspondingly small (as opposed to a drag force calculated using maximum values of shaft shear and toe resistance and minimal length of the transition zone).

Many use the terms “drag force” and “downdrag” as interchangeable terms. Even in combination: “downdrag force”! However, although related, the terms are not synonyms. “Drag force” is the integration of the negative skin friction. Its maximum value occurs at the neutral plane. Its action on a pile is similar to that of the prestressing force in a prestressed concrete pile. N.B., the latter is never called “prestressing load”. “Downdrag” refers to pile settlement caused by the soil hanging on the pile and dragging it down. The two terms can be said to be the inverse of each other. Where drag force is at its maximum, e.g., for a pile supported on bedrock, the downdrag is minimal. On the other hand, when the downdrag is large, the drag force is small. Provided the pile axial strength is not exceeded by the sum of the dead load and the drag force, presence of drag force is beneficial as it merely prestresses the pile, minimizes the ‘elastic’ compression of the pile due to live loads, etc. In contrast, downdrag is usually undesirable. At a site where the soils are expected to settle due to general subsidence or effect of fills, groundwater lowering, adjacent structures, etc., the problem to watch for is the downdrag, not the drag force.

Fig. 7.19 shows two alternatives of the typical distribution of load in the pile, representing the distribution in a soil that settles appreciably and in one that does not settle much at all. Therefore, the former results in an insignificant length of the transition zone from fully mobilized negative skin friction to ditto positive shaft resistance, whereas the latter shows a very long length. It is assumed that despite this difference, the depth to the neutral plane is the same for the two alternative distributions, disregarding the fact that in a real case, the toe resistances would not have been the same. Because the drag force is a force that has unloads the soil above the neutral plane and, then, re-loads it below the neutral plane, the drag force does not contribute to the settlement of the piles. That is, the settlement is only caused by the load applied to the pile head. (Simply expressed, down below, the soil ‘does not know’ that some of the overburden weight, making up the soil stress, in transferring down was routed through the piles for part of the way).

Graph "A" shows the load distribution, Graph "B" the settlement distribution, and Graph "C" the toe load-movement. The toe response is best measured in a test. If not obtained directly from a test, it can be calculated in a  $q$ - $z$  analysis (see Section 8.11.7). The dead load on the pile is 4,000 kN. With time, negative skin friction will develop, and the load in the pile will increase from the dead load value at the pile head down the pile to a maximum at the neutral plane force equilibrium. For Case I, the large soil settlement alternative, the neutral plane will develop at a depth of about 10.2 m. Below the neutral plane, the shaft shear against the pile acts in the positive direction, and the force at the pile toe for Case I is equal to the maximum toe load in the test. Graph “B” illustrates that for this toe movement (55 mm), and

considering the shortening of the pile and the shown interaction between forces and movement, the pile head will settle slightly more than 60 mm (" $S_I$ "). If on the other hand the soil settlement is small (Case II), then, the neutral plane is located higher up and the pile toe force is smaller, which only required a toe movement of 16 mm.

The heading of this section indicates the text will deal with "Neutral Plane and the Magnitude of the Drag Force". The foregoing couple of paragraphs demonstrate the two aspects cannot be separated from aspects of settlement and soil movement.

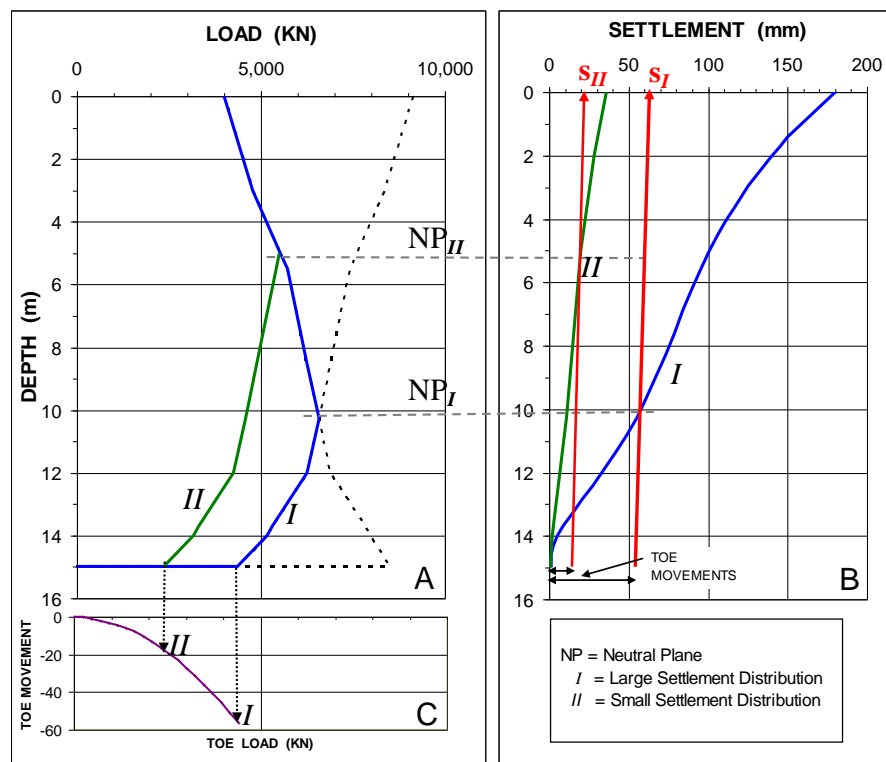


Fig. 7.19 Example of the mutual dependence of soil and pile settlement to load distribution

### 7.15 Unified Design Method for "Capacity", Drag Force, Settlement, and Downdrag.

The unified design of piled foundations (Fellenius 1984a, 1988, 2004) consists of the following steps.

1. Compile all soil data and perform a static analysis of the load-transfer.
2. Verify that the supported loads (dead and live) satisfy the code-required factor of safety, or load and resistance factors, when correlated to the ultimate pile resistance ("**capacity**") of the pile (the drag force must not be included in this calculation). This is a factor-of-safety or ultimate-limit state-design approach and the "factored-up" load is a load that induces a pile movement for which the foundation risk collapsing.
3. Verify that the maximum load in the pile, which is the sum of the dead load and the drag force, now unfactored, is adequately smaller than the unfactored **structural strength** of the pile by an appropriate factor of safety (usually 1.5), or that the strain resulting from the maximum load is limited to 1 millistrain (do not include the live load in this calculation). Note, the maximum load is a function of the location of the neutral plane, the degree of mobilization of the toe resistance, and the

length of the transition zone (the zone of transfer from fully mobilized negative skin friction to fully mobilized positive shaft resistance above and below the neutral plane, respectively). Moreover, the position of the neutral plane must be determined using unfactored forces.

4. Calculate the expected **settlement** profile including all aspects that can result in a change of effective stress at, below, or near the pile(s). Note, settlement due to the pile-supported loads (dead load) is mostly determined by load-transfer movements and further settlement due to the pile-supported load pertain to pile groups composed by more than 4 columns and 4 rows. Additional settlement can be caused by downdrag (settlement). Verify that the settlement does not exceed the maximum value permitted by the structural design with due consideration of permissible differential settlement. Note that the location of the neutral plane is a function of the pile toe movement. Using known (or test determined, or assumed) distributions of load and resistance, the location of the neutral plane is determined from the pile toe load-movement response ( $q$ - $z$  function) and requires that the design analysis establishes a fit between pile toe load and pile toe penetration onto the soil, as achieved by an iterative process searching for the balance between pile toe penetration, pile toe force, and neutral plane location. Of course, as it is a settlement analysis, the force must be unfactored.
5. Observe carefully the pile construction and verify that the work proceeds as anticipated. For driven piles, perform wave equation analysis to select the appropriate pile driving hammer and to decide on the driving and termination criteria (for driven piles). Document the observations (that is, keep complete and carefully prepared logs!).
6. When the factor of safety needs to be 2.5 or smaller, verify pile "capacity" by means of static or dynamic testing. N.B., with due consideration of the respective movements pertinent to the shaft and toe resistance responses for the pile.

Fig. 7.20 illustrates the analysis of the load-transfer curve for the shaft and toe resistances mobilized for a specific set of conditions, that is, as always, the shaft and toe resistances are correlated to a specific movement. The diagrams assume that above the neutral plane, the unit negative skin friction,  $q_n$ , and positive shaft resistance,  $r_s$ , are equal, an assumption on the safe side. Moreover, if the pile toe is located in a non-settling soil, the pile settlement and downdrag will be negligible. Notice, a key factor in the analysis is the estimate of the interaction of pile toe resistance and pile toe penetration. In order to show how the allowable load is determined, the figure assumes that the toe resistance has reached a specific penetration, say, the toe resistance mobilized in a static loading test. Moreover, the figure also assumes that this value is also that activated by the downdrag-imposed toe penetration. The figure further assumes that the soil movement relative to the pile near the neutral plane is large enough to ensure that the height of the transition zone is small, as shown in the figure. If, on the other hand, the soil-pile movement would be small, the transition zone will be longer and the pile toe movement smaller, i.e., the toe resistance will be smaller and the neutral plane will lie higher. Of course, this will not necessarily affect the allowable load if it is determined based on pile "capacity". The curve labeled " $Q_d = \Sigma |q_n|$ " is the load distribution starting from the applied dead load and the curve labeled " $Q_u - \Sigma R_s$ " is the resistance distribution starting at the "ultimate resistance", as determined one way or another. The intersection of the two curves is the location of the neutral plane.

Reducing the dead load on the pile has very little effect on the maximum load in the pile, as illustrated in the left side diagram of Fig. 7.21; the drag force would increase to make up for the reduction in the dead load. Obviously, if presence of drag force would be of concern, increasing the dead load would reduce the drag force! Clearly, the drag force is an environmental effect that should not be mistaken for something akin with the load from the supported structure.

The figure also shows a schematic illustration of the settlement in the soil and the downdrag for the pile. In the figure, the soil settlement curve is drawn assuming that there is soil settlement also below the pile

toe. The pile cap settlement is the soil settlement at the neutral plane plus the 'elastic' compression of the pile (pile shortening) for the load in the pile.

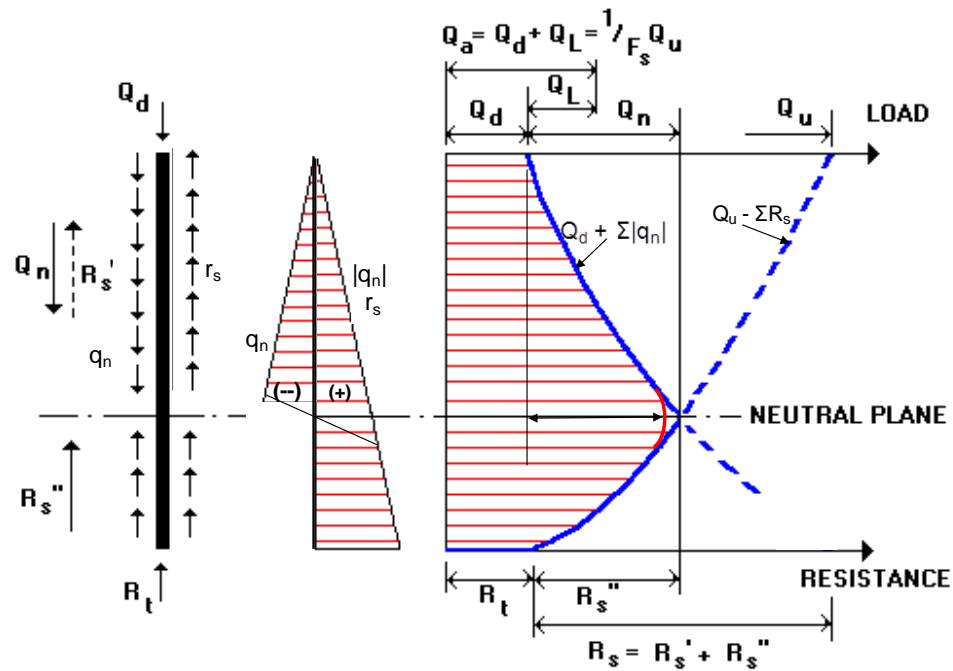


Fig. 7.20 Construing the Neutral Plane and Determining the Allowable Load

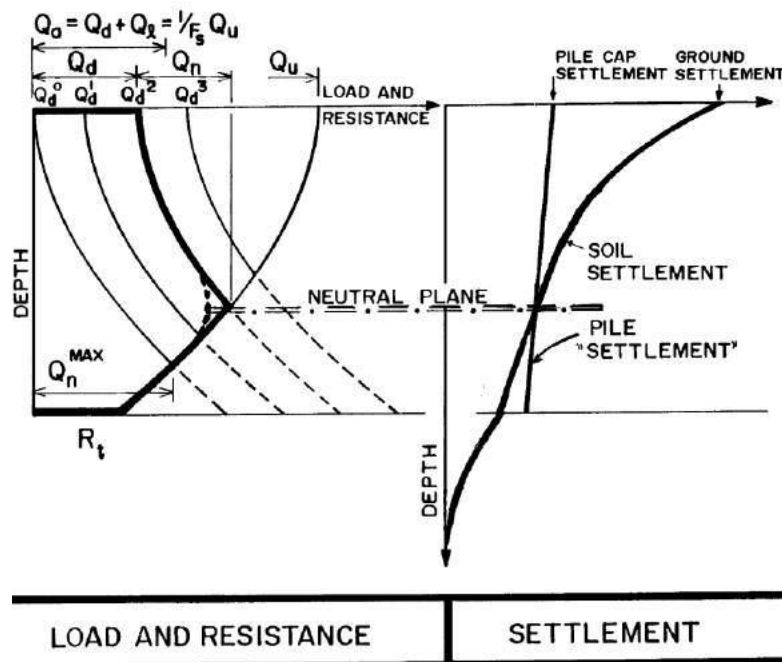


Fig. 7.21 Load-Transfer and Resistance Curves and Settlement Distribution

### 7.16.1 Drag Force

That negative skin friction develops where the soil settles around that pile is obvious. So is the fact that the negative skin friction accumulates to an axial force in the pile. Less obvious, but well-established in the many full-scale tests reported (Fellenius 2006 has compiled several of the case histories) is that the drag force develops primarily due to the fact that the pile and the soil are materials that have to function together despite their having very different stiffness (E-modulus) and, they therefore, react to the small movement always occurring in a soil body. Already movement no larger than a millimetre will cause shear forces to develop along the interface between the pile and the soil that will result in an equilibrium force between downward and upward acting accumulated shear. The force is called "drag force". Many still use the term "drag load", but this is a misnomer because it leads to the false idea that it somehow is similar to the load applied to the pile from the structure. Moreover, the drag force is not an independent entity, but an environmental force which development and magnitude depend on the pile toe response and the sustained (dead) load from the structure supported by the pile. The drag force is not to be included when considering the allowable load or the factored load. It is only important with regard to the axial strength of the pile. The reasons for this are discussed at length in Chapter 10.

### 7.16.2 A case history of applying the unified design method

Fellenius and Ochoa (2009) presented the results of testing and analysis of a 25 m long, strain-gage instrumented auger-cast pile constructed in sand and silty clay to bearing in a glacial till and designed according to the Unified Design Method. The spacing between the piles was large enough for the piles to act as single foundation-supporting piles. Fig. 7.22 shows the distributions of load and settlement for a typical pile, a test pile, at the site. For reference, an ultimate resistance ("capacity",  $R_{ult}$ ) is indicated in the figure. In the long-term, effective stress will increase due to a fill placed over the site, which will increase the shaft resistance along the pile. In addition, the fill will cause soil settlement, which will cause negative skin friction to develop. Consequently, the long-term load distribution will increase downward from the applied dead load to a maximum at the location where there is no relative movement between the pile and the soil—the neutral plane.

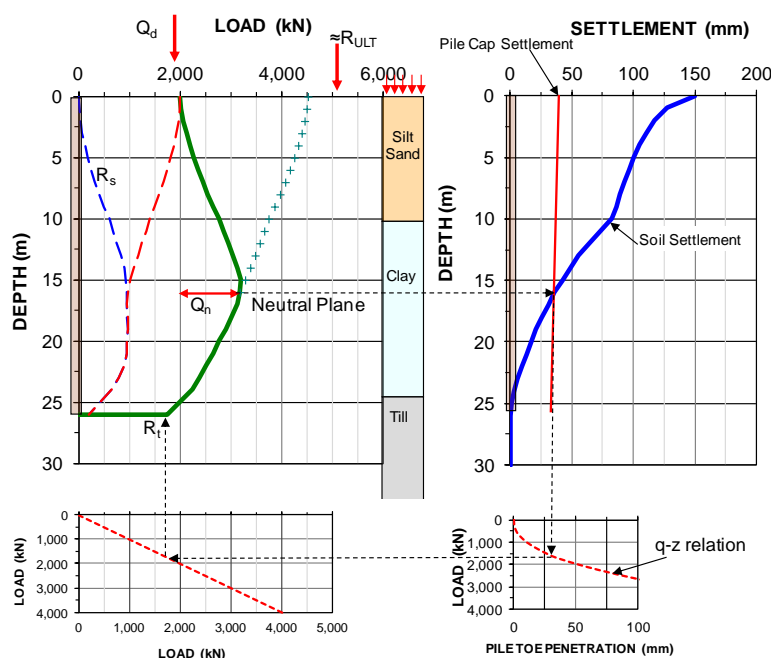


Fig. 7.22 The Unified Design Method and the correlation between pile toe penetration and pile toe load (Fellenius and Ochoa 2009)

The location of the neutral plane is determined by the requirement that the enforced toe movement generates the load at the pile toe that together with the shaft resistance distribution gives a location of the force-equilibrium neutral plane that is equal to the settlement-equilibrium neutral plane. The diagrams demonstrate that the applied load is increased or reduced, or, similarly, if the settlement is increased or reduced, the location of the neutral plane and, therefore, the penetration of the pile toe, will change, and, therefore, also pile toe load, which in turn will change the location of the force equilibrium, etc. Forces, settlement, and movements are interrelated and the design cannot simply be based on a factor of safety approach, but must consider all aspects.

Section 10.4 includes an additional numerical analysis of an example taken from the official Commentary on the Eurocode (Frank et al. 2004).

### 7.16.3 Piles in swelling soil

Piles in swelling soil are not subjected to negative skin friction, but to positive skin friction. The analysis of the distributions of shaft shear and load in the pile installed in swelling soil follows the same principles as for piles in settling soil, only the directions and signs are reversed. Figs. 7.23A and 7.23B illustrate the response of a pile installed through a swelling soil and some distance into a non-swelling soil. The pile is assumed to have a dead load of  $Q_d$  at the pile head. The solid and dashed lines in the Fig. 7.23A show the distribution of shaft shear in both negative and positive directions. The heavy blue line indicates the change-over from positive direction shaft shear (positive skin friction) caused by the swelling to negative direction shaft shear (negative shaft resistance) resisting the tension generated (Fig. 7.23B). The tension load in the pile is somewhat offset by the dead load,  $Q_d$  and reduces with depth due to the swelling. Note that the blue line in Fig. 7.27B, which starts at the applied load ( $Q_d$ ), is the load distribution in the pile. The intersection between the tension curve and the load distribution curve is where the neutral plane is located.

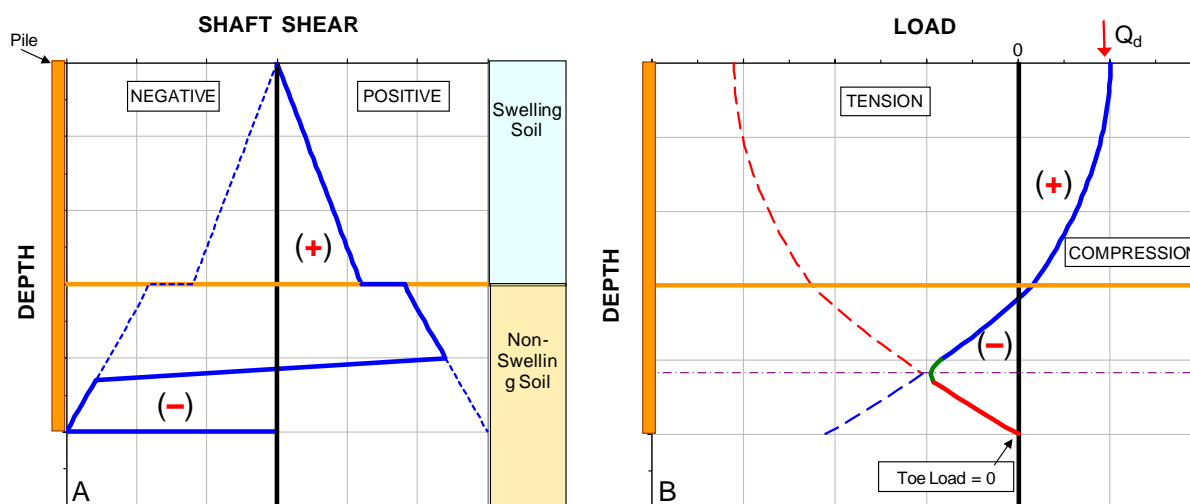


Fig. 7.23 Distributions of unit shaft shear and load for a pile in swelling soil

Fig. 7.24 shows the load distribution for the special condition of a pile installed through swelling soil layer and into a settling soil. The pile is assumed to be supporting a transmission tower, windmill pylon, or similar and, therefore, subjected to an uplift load. The distribution shows that although the pile is in tension throughout its length, it can still show a net settlement, as the neutral plane lies in the settling soil.

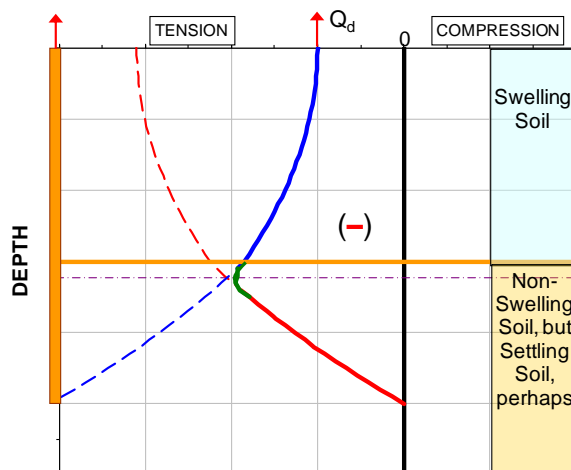


Fig. 7.24 Load distribution for a pile in swelling soil underlain by a settling soil

## 7.17 Settlement of a Piled Foundation

The primary aspect in the design of a piled foundation is determining—predicting—its settlement (Chapter 3). Settlement of a single pile or narrow piled foundation is caused by three factors. First, by the load-transfer movement, developing when the supported load is placed on the pile; second, by the increase of stress below the pile from the load supported by the piled foundation, and, third, by downdrag due to changes of soil effective stress due to other aspects than the pile load, e.g. fill, other loaded areas, groundwater lowering, etc.

### 7.17.1 Load-Transfer Movement of single piles

Mobilizing the shaft resistance requires only a small movement, frequently no more than a few millimetre. When the load from the supported structure is first applied to the pile, only a very small portion, if any, will reach the pile toe. As negative skin friction develops along the pile, additional pile shortening will occur and gradually the pile toe will be engaged. The toe movement is a function of toe stiffness response. Moreover, before applying the sustained load to the pile head, residual force may be present in the pile. If so, this preexisting 'locked-in' force will need to be considered in determining the load-transfer movement.

The procedure of determining the settlement due to load-transfer movement for a single pile or a narrow pile group is carried out in the following two interrelated steps.

1. Calculate and plot the distribution of the shaft resistance and determine (make an assumption for) the magnitude of toe resistance and toe movement that result from applying the dead load to the pile—the load-transfer movement for the load from the structure. This requires estimating pile compression for the load distribution and applying a  $t$ - $z$  relation to the pile element immediately above the pile toe and a  $q$ - $z$  relation for the pile-toe load-movement. (The  $t$ - $z$  and  $q$ - $z$  relations can either be theoretical or be obtained from a static loading test that shows the relations. Few head-down tests measure pile-toe load-movement, but most bidirectional tests do; see Section 8.15). The load distribution that might have developed before the sustained load (dead load) was placed on the pile needs here to be taken into account. The load-transfer movement is the sum of the pile shortening and the pile toe movement due to the pile toe load and includes the shaft movement necessary to mobilize the shaft resistance for the element immediately above the pile toe, which also is equal to the beginning (initial) pile toe movement. The additional pile toe movement is caused by the load beyond the total shaft resistance reaching the pile toe.



2. Assume now that the soil settles around the pile and a force equilibrium—neutral plane—develops between the dead load applied to the pile head and the drag force versus the positive shaft resistance and toe resistance. The process will cause an increased pile toe resistance, which magnitude can be estimated in an iterative procedure matching toe resistance and toe movement according to the  $q$ - $z$  relation applied. The calculation will result in additional pile shortening. The additional shortening and the increase of toe movement is additional to the values determined per Point 1. The magnitude of the drag force depends on the assumed height (or length) of the transition zone, as do therefore, the calculated pile shortening. The height has no influence on the location of the neutral plane, however, nor on the magnitude of the pile toe movement. In determining the location of the neutral plane, the settlement below the pile toe level can be left out of the analysis of the depth to the neutral plane, because the only thing that matters for the location of the neutral plane is the interaction between the pile and the soil above and at the pile toe.

An obvious result of the development of the neutral plane is that, in service condition for a single pile or a narrow group of piles, no portion of the dead load is transferred to the soil directly from the pile cap—there is no contact stress. Unless, of course, the neutral plane lies right at the pile-cap base. Moreover, live loads do not cause settlement and neither does a drag force.

In a routine case, it is usually sufficient to just make sure that the neutral plane lies below a level which indicates a settlement that can be accepted—“the neutral plane lies in non-compressive soil”. However, when analyzing not just single piles or a few piles clustered together, but pile groups, matters can become more complicated, as then the compression of the soil below the pile toe level must be calculated as indicated in Clause 7.15. 2.

The Unified Design Method addressed here considers actual and acceptable settlements, as opposed to employing a pile “capacity” reduced by various factors of safety or resistance factors. A proper design should consider actually occurring loads, deformations, and movements, whereas the conventional “capacity-design” means considering forces only and, to boot, forces for an ultimate condition that supposedly will never develop. The main approach to the unified method was proposed more than 30 years ago (Fellenius 1984; 1988). However, many have still difficulty in taking the step from the conventional “capacity-reasoning” to the more rational “deformation-reasoning” of the unified method. The following notes aim to explain the basics of the unified design.

Consider a hypothetical case of a single 300 mm diameter, round, concrete pile installed through 25 m of clay and 5 m into an underlying sand. Fig.7.25 shows typical load-movement curves determined from a hypothetical static loading test on the pile calculated using the UniPile software (Goudreault and Fellenius 2014). The input data are from Case 9 of the examples in the software manual, although slightly simplified. The test is assumed to have been carried out in equal load increments (125 kN) until large significant pile toe movements were recorded. The pile head load-movement curve shows the load (1,400 kN) that corresponds to the Offset Limit (Section 8.2) and the load (1,600 kN) that gave a 30-mm pile toe movement. Coincidentally, the 30-mm toe movement is also 10 % of the pile toe diameter. (The load applied to the pile head that resulted in a movement equal to 10-% of the toe diameter is frequently used as a definition of capacity (see Section 8.1). This definition originates in a misconception of a recommendation by Terzaghi (Likins et al. 2011).

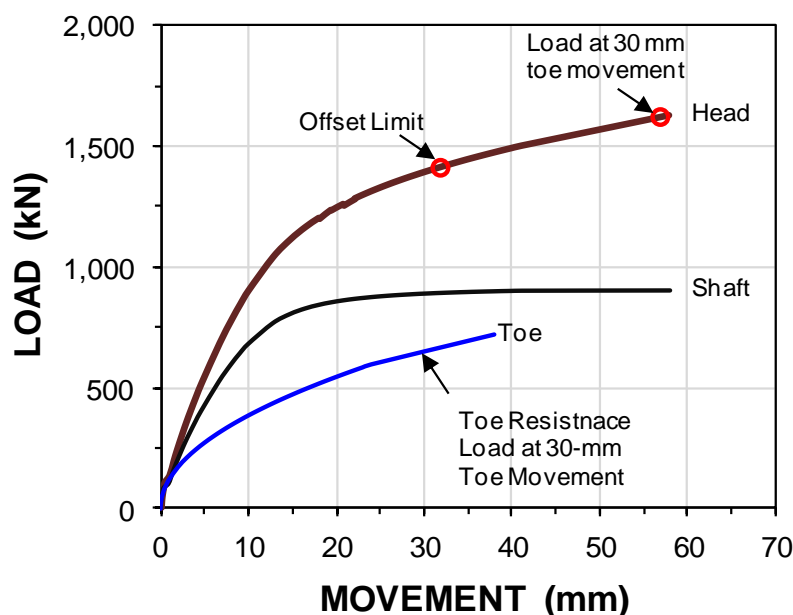


Fig. 7.25 Hypothetical case of results of a static loading test.

The hypothetical pile is assumed to have been instrumented for measuring the distribution of load down the pile during the static loading test. The hypothetically measured distributions for the applied loads are shown in Fig. 7.26, as calculated using UniPile. The assumed  $t$ - $z$  functions for the shaft (clay and sand) and  $q$ - $z$  function for the pile toe are indicated (Section 8.11). The figure also shows the hypothetical distribution of settlement at the site assumed to be caused by a small lowering of the groundwater table or by a similar change of effective stress triggering a consolidation process. Notice that the soil below the pile toe level was assumed sufficiently dense or stiff not to develop any appreciable settlement due to the groundwater table lowering or to the increase of stress from the load transferred to the soil below the pile toe level.

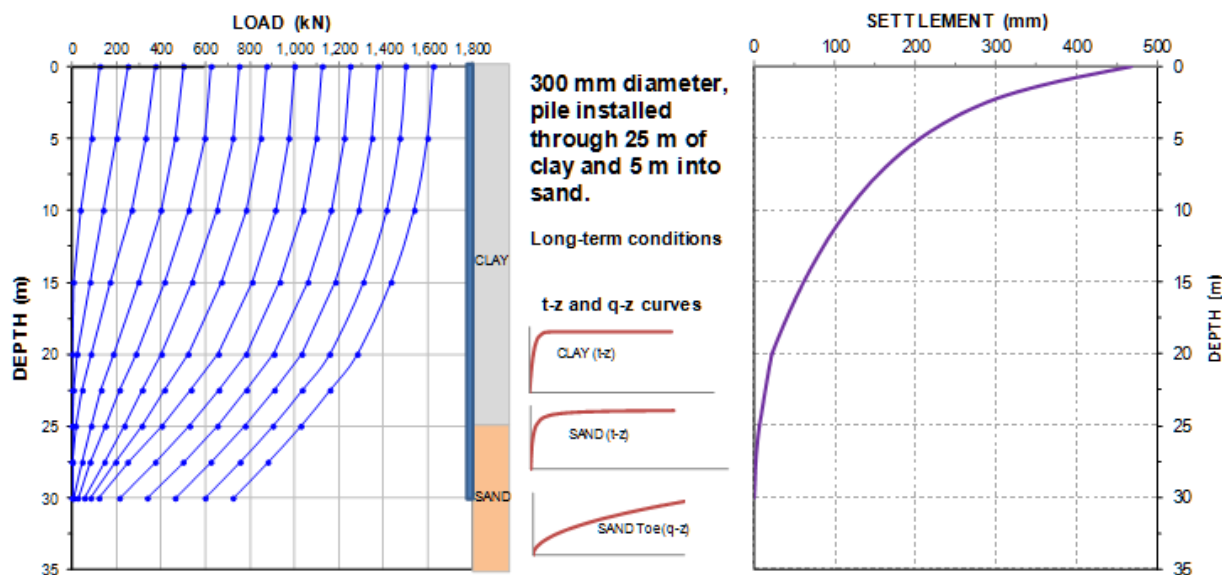


Fig. 7.26 Distributions of axial load in the pile and settlement of the soil around the pile.

The shaft resistance  $t$ - $z$  curves represent the shear-movement response of the soil along the pile. Depending on piles and soil, the response in any given case will differ from that of another case. Responses may exhibit large and small movement before a peak shear resistance, before continuing in a strain-hardening, strain-softening, or plastic mode. Normally, the shear it is not associated with volume change, although, it is conceivable that, on occasions, the soil nearest the pile surface can contract or dilate due to the shear movement, with corresponding slight effect on the single-pile  $t$ - $z$  curve.

At the pile toe, however, the downward movement of the pile (per  $q$ - $z$  function), displaces the soil both below the pile toe level, to the side, and—to a limited height—also up along the side of the pile. The  $q$ - $z$  function incorporates both effects and the  $q$ - $z$  curve combines the effects of soil being displaced and the soil volume being changed due to the shear forces that develop around the pile toe, where both compression and dilation can occur.

The conventional approach is to determine a "safe" working load by applying some definition of "capacity" to the pile head load-movement curve. (The definitions actually used in the engineering practice for what constitutes "capacity" differ widely). The working load is then determined by dividing the "capacity" with a factor of safety larger than unity or, in LRFD, multiplying it with a resistance factor smaller than unity. Conventionally, it is assumed that the service-ability (settlement aspect) of the piled foundation is ensured by this approach.

When the long-term settlement of the soil surrounding the pile is small, the approach usually results in a piled foundation that does not experience adverse deformations for the applied working load. On the other hand, when the soil, as in the subject case, settles around the pile, a drag force and a downdrag will develop. Some codes and standards, e.g., the AASHTO Specs and the Eurocode, add the calculated drag force to the working load, which is an incorrect and costly approach. When the drag force is accurately estimated (as opposed to underestimating it, which is a common mistake), this approach often results in that the pile, as originally designed, will seem to be unable to carry the desired working load and, therefore, the design is changed to employ larger, longer piles, and/or adding piles. More enlightened codes and standards, e.g., the Canadian Bridge Design Code, the Australian Building Code, US Corps of Engineers, etc., recognize that this approach is not just ignorant, but costly, and, that it yet does not ensure a safe foundation (Fellenius 2014a; 2016). The drag force is not the issue, the downdrag is, and the action of the settling soil has to be assessed in a settlement analysis.

The unified design considers the pile and soil deformations (settlement) and recognizes the fundamental reality that forces and movements are related and cannot be considered separately from each other. Thus, design of piled foundations according to the unified method involves matching the force and settlement interaction. A force equilibrium is determined as the location where the downward acting axial forces (dead load and drag force) are equal to the upward acting forces (positive shaft resistance below the equilibrium depth and toe resistance). The settlement equilibrium is determined as the location where the pile and the soil settle equally (the direction of shear forces along the pile changes from negative to positive at this location). When the shaft shear response is correctly identified, the two equilibriums occur at the same depth, called "neutral plane".

For the hypothetical case considered, as the supported structure is constructed, it will introduce a permanent working load (the dead or sustained load), say, 600 kN. The transient (live) load for the case is assumed to be about 100 kN. The loading test indicates that the load transfer movement due to the 600-kN load will be smaller than 10 mm. The purpose of the settlement analysis per the unified method is to determine the magnitude of the additional settlement that will develop in the long-term to follow the application of the load.

Fig. 7.27 repeats Fig. 7.26 and adds a curve to the load distribution diagram labeled "Increase of load due to negative skin friction", which mirrors the shaft resistance reduction of axial load with depth. The curve starts at the pile head at a load equal to the 600-kN permanent working load for the pile. Each intersection between the curve labeled "Increase of load due to negative skin friction" and the load distributions curves is a potential force-equilibrium neutral plane. A series of horizontal lines that intersect with the settlement curve has been added from each such intersection and each such intersection of these lines with the settlement distribution is a potential settlement-equilibrium neutral plane. At each potential settlement-equilibrium neutral plane, a slightly slanting line is drawn representing the pile shortening for the axial load in the pile. At the pile toe level, the distance between this line and the soil settlement at the pile toe level represents the pile toe penetration for the particular location of the settlement-equilibrium plane. Each intersection of the slanting lines with the line at the pile cap level indicates the settlement of the foundation. The task is to determine which of these would represent the long-term settlement of the supported foundation.

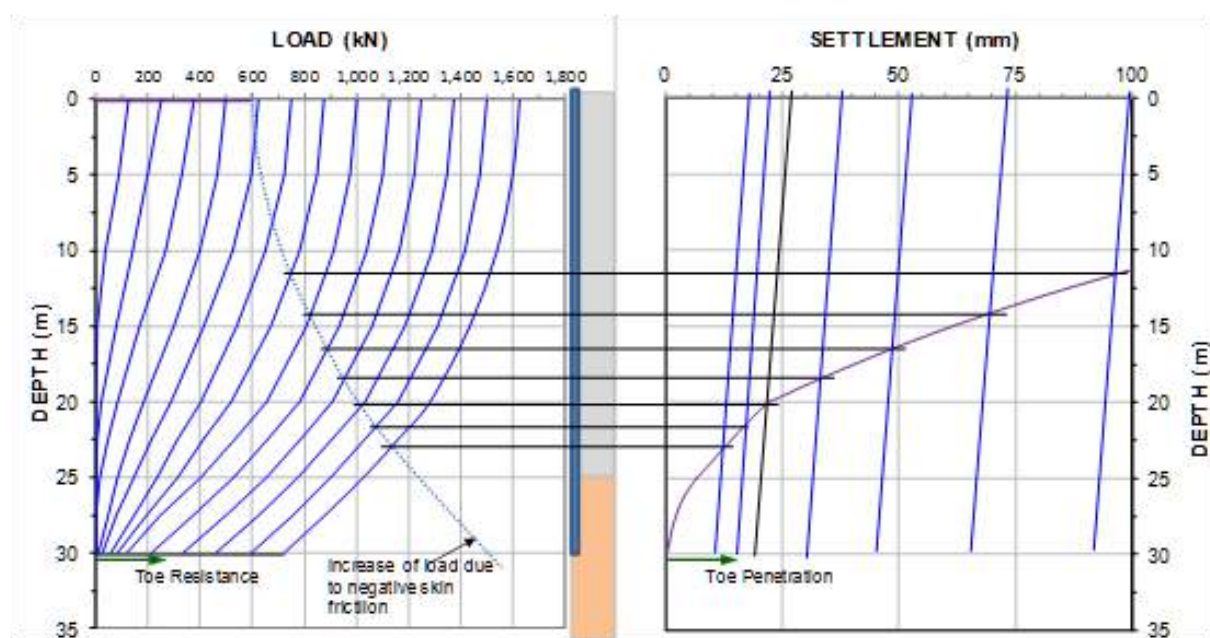


Fig. 7.27 Force and settlement equilibrium lines added to Fig. 7.21.

The figure shows several potential locations of force-equilibriums and settlement-equilibriums. However, there is only one location (depth) that is true, that is, only one location for which the pile toe force determines a location of the force-equilibrium that is at the same location (depth) as the settlement-equilibrium producing a pile toe penetration that, according to the pile toe load-movement curve, corresponds to the pile toe force in the load distribution diagram.

The true neutral plane location can be determined by trial-and-error as illustrated in Fig. 7.28. A first-attempt toe force is assumed, and the load distribution from this force is extended upward to intersection with the drag force curve. A horizontal line is then drawn to intersect with the settlement distribution curve. If this intersection is the settlement-equilibrium depth, then, the pile line will determine the pile toe penetration. The corresponding pile toe resistance is determined by correlation with the pile toe load-movement curve. As shown in the figure, this first-attempt resistance does not match the originally assumed toe force, the starting toe resistance. A new starting toe resistance is therefore selected and the process is repeated. After two or three attempts, a match, the closed (red) loop, is obtained as shown in Fig. 7.29.

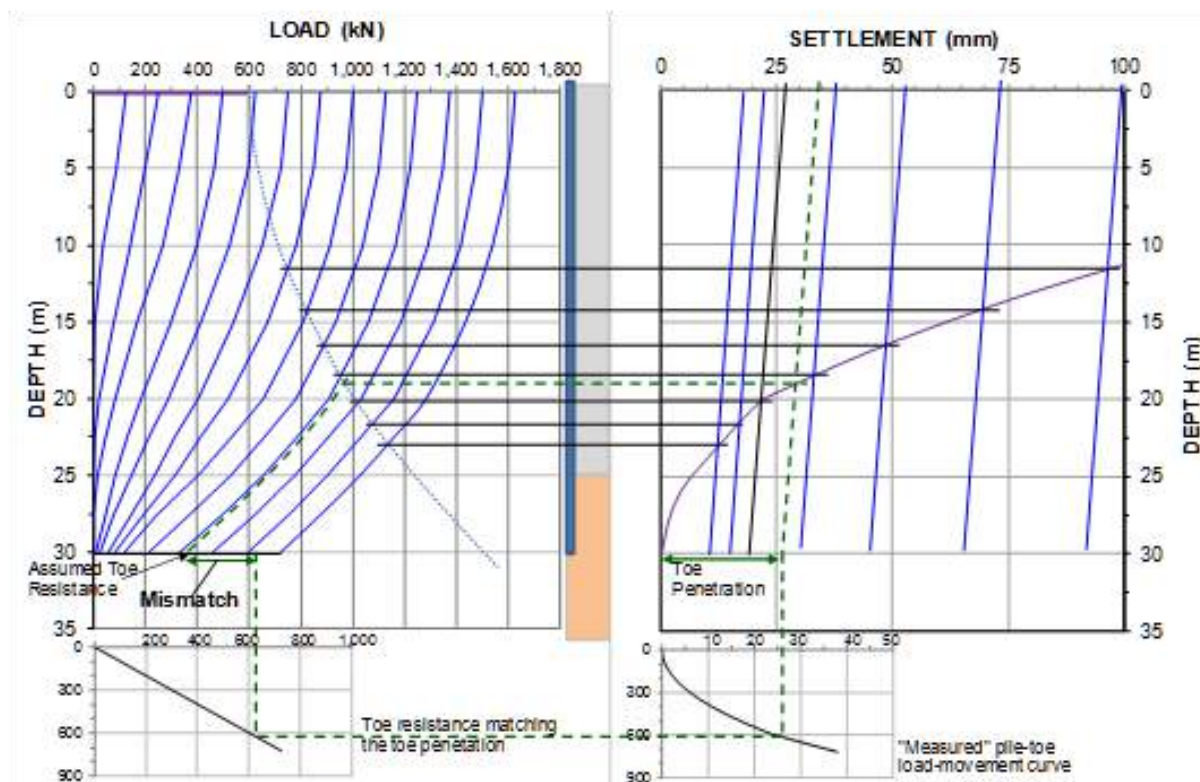


Fig. 7.28 First attempt to find the true neutral plane resulting in "mismatch".

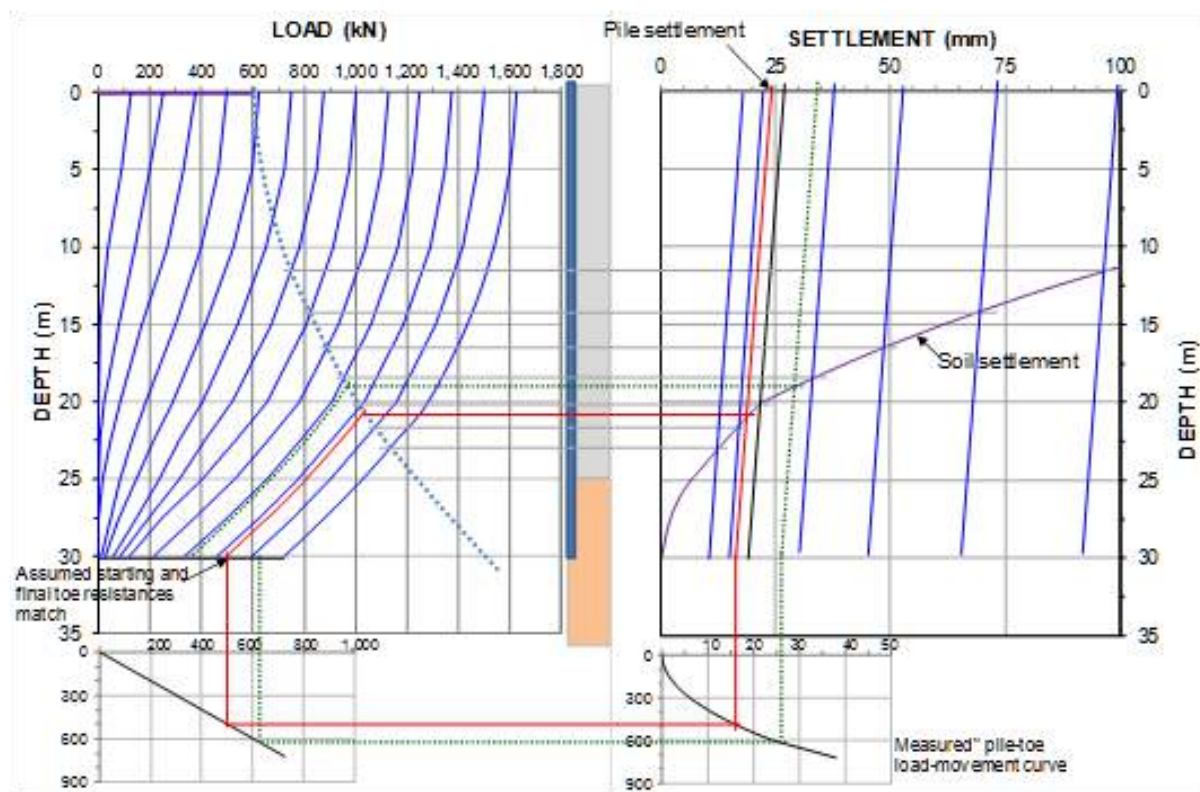


Fig. 7.29 Final match between starting and finished toe resistance and determining the pile settlement.



The purpose of matching the force-equilibrium and settlement-equilibrium to the pile toe movement and the pile toe force (never choose one without the other) is to determine—predict—the settlement of the single pile or small pile group. There is a misconception around that the movement measured for a specific applied load in a static loading test directly represents the settlement of a pile for the load. Note, however, that the static loading test does not measure settlement, but movement and, often, just the accumulated axial compression of the pile for the applied test load. Of course, knowing the movement response of a single pile for an applied load, in particular the pile-toe load-movement, is a vital part of determining the settlement for that pile, as illustrated in the foregoing.

The analysis shown produced a calculated pile head long-term settlement of about 25 mm, which is satisfactory for most piled foundations. Depending on the height of the transition zone (transition from negative to positive shaft shear directions), the drag force will amount to about 350 through 400 kN. It will prestress the pile and it will essentially be a beneficial load. The maximum axial load at the neutral plane will be about 1,000 kN, which is well within the pile structural strength. When, as in this case, the loads from the supported structure also includes transient (live) loads (here 100 kN), these will just replace a similar magnitude of drag force. There will be a small pile shortening, but it is recovered when the live load is gone and does not add to the long-term settlement.

#### **7.17.2 Settlement below the Pile Toe Level due to Consolidation and Secondary Compression**

For single piles and narrow pile groups—three or fewer rows or columns—because the stress increase in the soil layers below the pile toe level affects a limited volume (depth) of soil and the soil compressibility is usually small below the pile toe level, the settlement beyond or in addition to the load-transfer movement (the t-z and q-z relations) is usually small and negligible. However, for wider pile groups, the settlement of the pile group below the pile toe level due to the applied load can be substantial. It is best calculated as consolidation settlement below an assumed equivalent raft loaded with the dead load applied to the piled foundation. The equivalent raft approach addresses the overlap effect of the loads between the piles in the group, and it only applies to groups containing at least four to five rows or columns of piles in each direction<sup>5</sup>. The main amount of settlement occurs with time as the result of the stress change imposed by the applied load combined with other changes of the effective stress from, for example, fills, change of groundwater table and pore pressure distribution, unloading due to excavations, loads placed on adjacent foundations, etc.

It must be recognized that a pile group made up of a number of individual piles in a common cap may have different embedment lengths and toe resistance mobilized to different extent. The piles in the group have two things in common, however: They are connected to the same pile cap and, therefore, all pile heads move equally, and, although few in number, the piles must all have developed a neutral plane at the same depth somewhere down in the soil (long-term condition, of course). For the neutral plane to be the same (be common) for the piles in the group, with the mentioned variation of length, etc., the dead load applied to the pile head from the cap will differ between the piles, and where the conditions at the pile toe level varies for the piles, the mobilized pile toe resistance will also differ between the piles.

A pile in the narrow group with a longer embedment below the neutral plane, or one with a larger toe resistance as opposed to other piles, will carry a greater portion of the dead load applied to the group. On the other hand, a pile with a smaller toe resistance than the other piles in the group will carry a smaller

---

<sup>5</sup> The geotechnical literature includes many reports on tests involving groups of piles, mostly groups of no more than four to nine piles, total. Of course, depending on the pile spacing, a pile in a such group may differ in response compared to that of a single pile—more or less. However, the observations on such small groups, even if in full-scale, have little relevance to the response of wide pile groups.

portion of the dead load. If a pile is damaged at the toe, it is possible that the pile exerts a negative—pulling—force at the cap and thus actually increases the total load on the other piles (or the pile pulls out from the cap).

For a group of shaft-bearing piles in clay supporting a piled foundation, Terzaghi and Peck (1948) proposed that the settlement of the piled foundation could be calculated as that of an equivalent raft, having the same footprint as that of the piled foundation, located at the lower third point of the pile length, and loaded by the same load as the piled foundation. For the particular example they used, the lower third point happened to be close to the depth of the neutral plane (Section 7.2). Terzaghi and Peck (1948) suggested distributing the raft stress according the 2:1-method. Bjerrum et al. (1957) applied the equivalent raft method to two alternative placements of the raft: at the lower third point and at the pile toe depth, and distributed the stress underneath the center of the equivalent raft using the nomograms of Newmark (1942), i.e., the Boussinesq method. Fellenius (1984a) proposed (for narrow pile groups) that the equivalent raft should be placed at the neutral plane regardless of the depth to the lower third point and applied the settlement analysis of the so-placed equivalent raft to pile groups in all types of soils, which is the basis of the Unified Design Method of pile groups (Fellenius 1984a; 1988; 2004; 2011; 2016a). See also Section 7.17.3.

In determining the settlement of the equivalent raft at the neutral plane, the soil compressibility must include the stiffening effect of the "pile-reinforced" soil, and the settlement calculation of the equivalent raft and the piled foundation can be performed according to conventional calculations for change of effective stress, as well as more sophisticated methods. Because the "soil reinforcement effect" usually results in that only a very small settlement develops between the neutral plane and the pile toe level, the soil settlement between the neutral plane and the pile toe can normally be disregarded. The settlement between the neutral plane and the pile toe level is accounted for in the calculation of the pile shortening. (Of course, for calculation of the settlement outside the footprint of the piled foundation, no such stiffening effect due to the presence of the piles should be included).

The settlement caused by the change of effective stress due to the total load applied to the piles can simply be assumed as that caused by the change of effective stress due to load on an equivalent raft with a footprint located at the depth of the neutral plane equal to that of the pile group footprint,  $B$  and  $L$ . From here and to the pile toe depth, the stress is then transferred to the soil as a truncated cone to a projected equivalent raft with an accordingly larger width and length. For a wide pile group, the method for determining the size of the equivalent raft projected to the pile toe level is not applicable as the projected shaft resistance is only that experienced by the perimeter piles. The interior piles have little or no shaft resistance to spread out into the surrounding soil. For a narrow width pile group, however, the width and length of the equivalent raft to project to the pile toe from the pile group footprint at the neutral plane is important.

Because the foundation footprint stress at the neutral plane is not distributed out into the soil immediately below, but gradually along the length of pile between the neutral plane and the pile toe, a conventional Boussinesq or a 2(V):1(H) distribution from the neutral plane located results in too large a projected equivalent raft at the pile toe. A distribution using 5(V):1(H) provides more realistic stress distribution at the pile toe level. Therefore, I have proposed modifying the Unified Design Method for narrow pile groups, by calculating the settlement as that from an equivalent raft placed at the pile toe level and with a load spreading due to shaft resistance between the neutral plane and the pile toe (the distance, " $d$ ", below the neutral plane) calculated as that of raft with a width of  $B + 2d/5$  and length  $L + 2d/5$  as indicated in Fig. 7.30 (only one pile is shown). Below the projected equivalent raft at the pile toe, the stress distribution is calculated using Boussinesq distribution or by 2(V):1(H) for an average value. The Boussinesq method can consider differential settlement across the raft; pile rafts are typically flexible rafts.

The portion of the soil between the neutral plane and the pile toe depth is ‘reinforced’ with the piles—stiffened up—and, therefore, not very compressible. When calculating the soil settlement outside the piled foundation footprint, the reinforcing effect of the piles is disregarded, however. Thus, the difference in settlement calculated for a point right at the edge of the pile cap and one a small distance away will indicate the “hang-up” effect for the pile group—the difference of settlement between the piled foundation and the area around it.

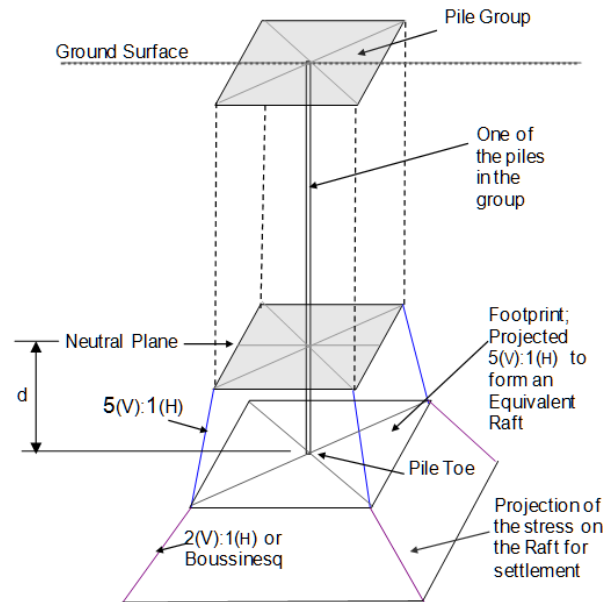


Fig. 7.30 Distribution of stress below the neutral plane for a narrow group of piles.

Be the piled foundation flexible or rigid, the average settlement below the equivalent raft is best calculated for the characteristic point defined in Chapter 1 (Sections 1.9 and 1.10). The “characteristic point” calculation of stress according to the Boussinesq method produces a settlement value quite close to that produced by the 2:1-method. For differential settlement within a piled foundation placed on a flexible raft—usually the case—the calculations need to employ the Boussinesq method.

### 7.17.3 Downdrag

Above the neutral plane, the soil moves down relative to the pile and, below the neutral plane, the pile moves down relative to the soil. At the neutral plane, the relative movement between the pile and the soil is zero. In other words, whatever the soil settlement occurring at the neutral plane, that settlement is equal to the settlement of the pile (the pile group). Between the pile head and the neutral plane, the settlement of the piled foundation is due to axial shortening of the pile as caused by the supported loads and the drag force and it is therefore small. Settlement of a piled foundation on a single pile or a small pile group is essentially the settlement of the soil at the neutral plane, i.e., the settlement of the soil at the intersection of the settlement curve and the neutral plane (which now is the **settlement equilibrium**). The amount of that settlement that is in addition to the load transfer movement and settlement due to the load supported by the piled foundation and to other causes in the soil below the pile toe level is called downdrag.

Note that the location of the neutral plane (as **force equilibrium**) must be in balance with the pile toe force and the pile toe movement (i.e., its penetration into the soil). That penetration is equal to the difference in settlement between the neutral plane and the pile toe adjusted for the pile shortening for the average axial load between the neutral plane and the pile toe.



The magnitude of the downdrag is determined by the stress changes and compressibility of the soil below the pile toe level and, to some extent, also the downdrag-enforced penetration of the pile toe into the soil when it is "dragged down" by the interactive process of soil settlement and pile toe penetration.

Note that most of the various software and methods purporting to calculate pile settlement are in fact calculating the load-transfer movement of the pile for an applied load, such as that measured in a short-term static loading test, which rarely reflects the long-term settlement of the piled foundation and usually correlates poorly to pile group settlement.

### 7.18 Wide Piled Foundations

The response of a wide piled foundation, a piled raft, is different to that of a single pile or a narrow piled foundation. Unfortunately, only a few case histories are available on response of wide pile groups to load. Hansbo (1984; 1993) and Hansbo and Jendebý (1998), reported a most educational case on long-term response of two adjacent four-storey buildings in Göteborg, Sweden, supported on piles in a thick deposit of soft clay. One building was constructed on a grillage of beams (contact area was not reported) and the other on a raft. The nominal total average load over the building footprint corresponded to 66 kPa and 60 kPa, respectively, which are very similar values. The as-designed average axial working loads were 220 kN and 520 kN/pile, respectively, which are quite different values. The conservatively estimated pile "capacity" was 330 kN. At the end of construction, measured pile loads were about 150 and 300 kN, respectively, again, quite different values. The loads correspond to 45 and 35 kPa average stress over the each building footprint, and 70 and 60 %, respectively, of the total nominal loads for the buildings. The measurements showed that the buildings settled on average about the same amount, 44 and 41 mm, respectively over a 13 year period. It is interesting to see that the settlements correlated to average stress rather than pile load. Settlements below the pile toe level was small. The contact stress measured for Building 2 in three cells along the building perimeter ranged from 25 through 50 kPa.

Additional cases with valuable educational observations are by Russo and Viggiani (1995; 1997) and Mandolini et al. (2005), who presented a case history of a piled foundation of the main pier of a cable-stayed bridge over the Garigliano River in Southern Italy. Auxilla et al. 2009, who presented measurements of raft-soil interface (contact stress) for three 70 m tall cement silos. Yamashita et al. (2013, 2011a; 2011b), who reported observations of load and contact stress for a 54 m tall building on a continuous piled raft during construction and during one year afterward. Kakurai et al. (1987), who reported load 420 days of measurements of load and contact stress on 24 m embedment driven pipe piles under piled raft supporting a silo building. Liew et al. (2002), who reported measurements on a 17.5 wide tank raft supported on shaft bearing piles in soft compressible clay. Broms (1976), who compared settlement measured for two square embankments on a 15 m thick deposit of compressible soft clay, where one of the two embankments was supported on a grid of 500-mm diameter, 6 m deep cement-mix columns. Okabe (1977), who presented a remarkable case history of a bridge pier on 38 piles, measuring load in interior and perimeter piles.

The primary results of the case histories is that when converting the axial pile load and the soil stress to the E-modulus of the pile and soil, respectively, pile and soil have the same strain. That is, as no surprise, strain compatibility governs the response. The analogy to a reinforced concrete column is obvious. When load is applied to a column head, the resulting stress in the rebars and in the concrete develops in proportion to the moduli of the materials (steel and concrete) and their respective areas of the column cross section. If down the column, a crack exists cleanly across the section, then, all load will be in the rebars. Further down, when again the column is sound, the distribution of loads, stresses, and strains between the rebar and concrete is back in relation to the relative E-moduli of rebar to concrete.

The axial strain in a pile can easily be 100  $\mu\epsilon$  and more. With typical E-moduli of 200 GPa (steel), 30 GPa (reinforced concrete), or 5 GPa (wood), a 100  $\mu\epsilon$  strain represents significant axial pile stress. Strain compatibility requires that the strain in the soil is the same as the strain in the pile. For soil, the E-modulus is an order of magnitude or two smaller than that of a pile and the soil stress is, therefore, not large. There is little difference in this regard between conventional piled foundations with closely spaced piles, about 2.5 to 4 pile diameters, and "pile-enhanced footings", which are piled rafts with piles spaced 6 to 12 pile diameters apart. However, widely spaced piles leave a large raft area between the piles and, thus, the contact stress integrated over the contact area accumulates to a large load.

The settlement due to the load placed on a piled raft is a function of three main phenomena as detailed in Sections 7.17.1 through 7.17.3. The contact stress and distribution between the piles and the soil is addressed in Section 7.17.4. Section 7.17.5 discusses the distribution of load at the underside of the raft across the raft footprint.

### 7.18.1 Settlement due to compression of pile and soil body

Settlement of the pile-soil body can be determined as the compression of an equivalent pier with a E-modulus equal to that of the pile and soil combined. Eq. 32.

$$(7.32) \quad E_{\text{pile+soil}} = FR \times E_{\text{pile}} + (1 - FR) E_{\text{soil}} \approx FR \times E_{\text{pile}}$$

where

$$\begin{aligned} FR &= \text{Footprint Ratio} \\ E_{\text{pile}} &= \text{E-modulus of the pile} \\ E_{\text{soil}} &= \text{E-modulus of the soil} \end{aligned}$$

The compression contribution to the foundation settlement is then expressed in Eq. 7.33 as the shortening of a pier with height, H, when loaded by a total load, Q, and as a function of the Footprint Ratio.

$$(7.33) \quad \Delta L = \frac{Q H}{E_{\text{Pile+Soil}} A_{\text{Raft}}}$$

where

$$\begin{aligned} \Delta L &= \text{compression of the equivalent pier} \\ Q &= \text{load applied to the foundation raft} \\ H &= \text{height of equivalent pier (Length of piles)} \\ A_{\text{Raft}} &= \text{footprint area of the raft} \\ E_{\text{Pile+Soil}} &= \text{combined E-modulus, assumed representative for the average across the raft} \end{aligned}$$

The Footprint Ratio (FR) is the ratio between the total area of all piles over the footprint area of the pile group defined by the envelop around the piles. (N.B., the shape of the pile raft is irrelevant). The FR is depends mainly on the spacing and marginally on the pile shape being circular or square and the piles placed in equilateral or square grid. A group of circular piles placed symmetrically at a spacing of 3 pile diameters in a wide foundation (equilateral or triangular configuration) has an FR of 10.1 %, whereas the FR is 8.7 % for the piles placed at a 3 diameter spacing in a square grid. Fig. 7.31 shows the relation between Footprint Ratio and pile spacing for circular and square piles placed in equilateral and square grids. (On an aside, my experience is that when the Footprint Ratio exceeds 15 %, difficulties with the pile construction usually occur at the site. Best is to aim for a FR no larger than about 10 %. See also Section 7.19.1).

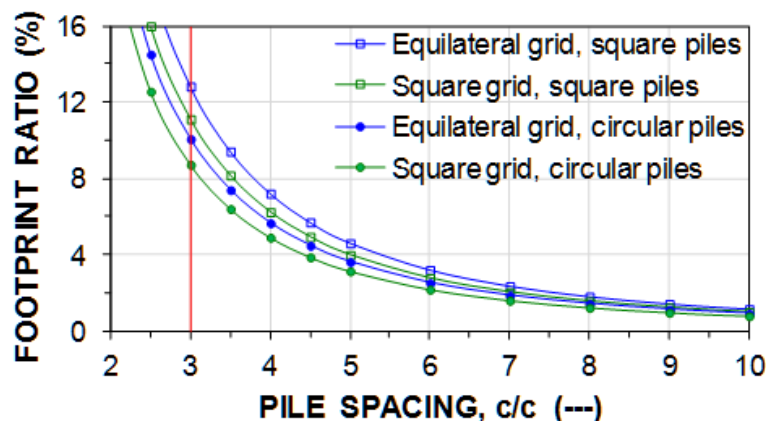


Fig. 7.31 Footprint Ratio as a function of grid type and pile size vs. pile spacing.

### 7.18.2 Settlement due to load transfer

The case records confirm the principle expressed by Franke 1991, who stated that "When load is applied to a group of piles, the shaft resistance is not mobilized the way it is in a single pile, from the head to the toe, but from the toe to the head"<sup>6</sup>. This applies to interior pile in a group and means that the load applied to the raft is unaffected by shaft resistance (and not increased by drag force). That is, provided that the relative stiffness pile to soil remains the same.

Going back to the analogy to the concrete column: If the column rests on a base softer than the rebar and the rebars protrude a small distance, all load is in the rebars. On loading the column, the rebars start to penetrate into the base and will do so until the penetration is equal to the rebar protrusion, which is when the concrete starts to experience stress unloading the rebars. Then, further penetration of the rebars might cease. If concrete—the matrix—would not be concrete but some soft material and the rebars not be protruding, then, they could still be pushed into the base, the floor as it were, provided that the matrix around the rebars would be compressed as much as the rebars are pushed into the base. The column is then a pile-soil body with the rebars as piles.

The pile toe resistance depends on the pile toe soil stiffness (load-penetration relations;  $q$ - $z$  functions, see Section 8.11) and, self-evidently, the toe penetration is equal to the distance the soil is pushed upward around the piles. The pile axial load is equal to the total load per pile and the toe resistance is equal to that load after the shaft resistance engaged by the soil in moving up along the pile has been subtracted. The toe penetration is the load-transfer movement of the piles for the applied load.

Fig. 7.32 describes the method for determining the toe penetration—the load-transfer movement of the raft—for a hypothetical case of a 1,400-kN average load/pile. The toe resistance curve was either measured in a static loading test or determined from a  $q$ - $z$  function representative for the pile-soil conditions. The curve "Total load minus shaft resistance mobilized above the pile toe" was calculated using representative input of shaft shear ( $t$ - $z$  function) and pile properties with reference to the total axial load in the pile. The process was carried out in UniPile for a range of lengths above the pile toe level assumed affected by shaft resistance and each result was subtracted from the total axial load in the pile for a movement equal to the movement calculated for each length. The intersection of this curve with the pile toe curve, determined the equilibrium and the pile toe penetration that represents the load transfer settlement.

<sup>6</sup> Franke (1991) actually said "... from top to tip and from tip to top" making this statement the single context I know where using the terms "top" and "tip" do sound good and well.

The calculation should be for the full average load per pile, disregarding any reduction due to soil stress because any such transfer can be assumed compensated for by the contribution to the load-transfer movement from the initial compression of the soil below the raft when applying the load to the raft.

When the toe penetration is short (small), i.e., large toe resistance, the length of pile above the pile toe with shaft resistance is short. For piles in soft soils, the matrix compression can be large and, therefore, result in a long length of pile with shaft resistance. In particular for shaft bearing piles with minimal toe resistance.

The piles inside a pile group will interact, much like the interaction and interplay of stress between the reinforcement and the concrete in a reinforced concrete element. However, any axial load that is shed to the soil is then transferred from the soil to a neighboring pile that, in turn sends some of its own load to the first pile or to other piles. Caputo and Viggiani (1984) showed that in performing a static loading test on a pile, the adjacent, and the not so adjacent, piles, moved, too, demonstrating the interaction from pile to pile.

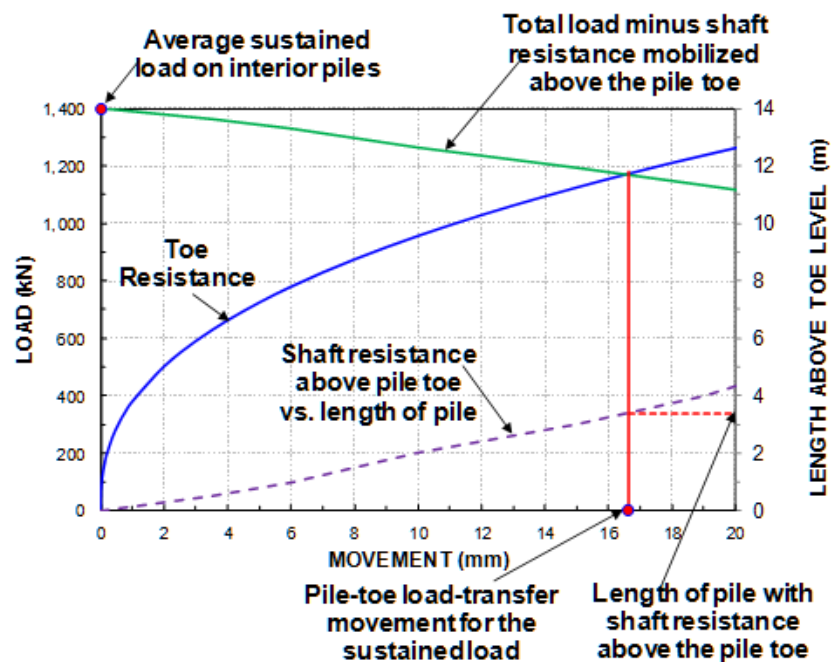


Fig. 7.32. The process for determining the load-transfer movement.

### 7.18.3 Settlement due to compression of the soil below the pile toe level

Settlement due to compression of the soils below the pile toe level can be determined as that of an equivalent flexible raft at the pile toe level loaded with the load applied to the pile raft as summarized in Fig. 7.33. Note that all contributions to the effective stress below the equivalent raft needs to be included in the calculation. The Boussinesq stress distribution means that the raft settlement will vary across the raft diameter; be largest in the center and smallest along the sides. That is, the equivalent raft will "dish", less so than a flexible raft placed level with the ground, but still significant. (An infinitely rigid raft would not dish). The stress and settlement calculated for the characteristic point (See Section 1.9) are conventionally considered to be independent of the raft degree of flexibility and are, therefore, considered to be the average values for the raft—flexible or rigid.

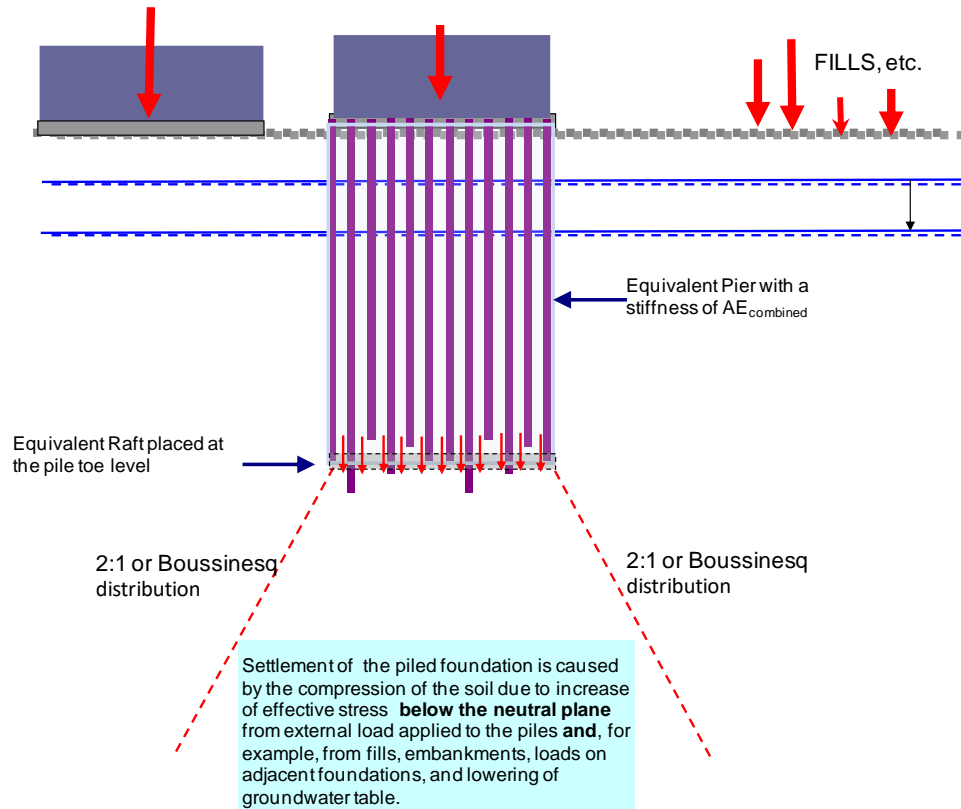


Fig. 7.33. The equivalent raft for calculation of settlement below the pile toe level.

#### 7.18.4 Contact stress

Just like the rebars and the concrete in the reinforced concrete column, the distribution of the raft load to the piles and to contact stress is according to the respective E-moduli of the piles and the soil and to the respective areas of pile and soil. Ordinarily, the strain introduced in the pile is in the range of 100 to 200 microstrain, which, for a 400 mm diameter square concrete pile correlates to about 400 to 800 kN load range. Most soils surrounding a pile would have a modulus that is one or more orders of magnitude smaller than the modulus of the pile material. A 200 microstrain soil-strain combined with, say, a soil E-modulus of 50 MPa, will amount to 10 kPa contact stress. At, say, a 5-m<sup>2</sup>, footprint area per pile, this correlates to a 50 kN load—"contact raft load"—from the raft to the soil over the pile footprint area from the raft. Coincidentally, the contact stress is about equal to the "wet load" of the concrete raft.

This does not mean that the contact raft load can be assumed be load subtracted from the pile as compared to a case of the same total raft load applied to a raft elevated from the ground. Strain compatibility requires, for example, that, if deeper down, the soil matrix is very compressible (say, the pile goes through a layer of soft clay), some of the load is transferred to the piles increasing the strain in the pile and reducing the load in the soil until its new compatibility value. (The soil strain will also increase as it must stay the same as that in the pile). Then, in the, say, stiff soils further down, the reverse happens: load is transferred from the pile to the soil until a new equilibrium is established. These changes occur with minimum of relative movement between the pile and the soil. In other words, assuming that the piled raft can be enhanced by some of the load being independently carried by the soil as contact stress is a delusion. It is simply not possible to assign a working load for the piles, whether a "safe" load or one close to the pile "capacity" and expecting the pile load to be the actual load and that contact stress will make up additional resistance margin to a satisfactory total factor of safety.

### **7.18.5 Load distribution across the raft and between piles**

This section is being updated



### 7.19 Piled Raft and Piled Pad Foundations

The oldest form of piled foundations were not rafts, but a group of piles with soil compacted around and above the pile heads to form a pad on which the structure was placed. Structurally, there are advantages in connection the pile head to the a structural raft when the load is uniformly distributed over the footprint. The old technique has therefore been revived in the modern "piled pad foundation", which is similar to a piled raft foundation<sup>7)</sup>, but with piles are not connected to the raft. The foundation is analyzed as a conventional footing cast on the compacted fill above the pile-reinforced soil with the footing stress distributed out into the soil from the pile toe level, not from the footing base.

In Scandinavian countries, piles have since long been used to support road embankments without being connected to any structural element. A recent modern application of a piled pad foundation is the foundations for the Rion-Antirion bridge piers (Pecker 2004, Dobry et al. 2007, Paniagua 2007). Another is the foundations of the piers supporting the Golden Ears Bridge in Vancouver, BC, illustrated in Fig. 7.35 (Sampaco et al. 2008), which piles consist of 350 mm diameter (square), 36 m long prestressed concrete piles reinforcing the silty clay at the site to reduce settlement. To provide lateral resistance in a seismic event, the footing on the pad is supplied with 900 mm diameter, 5 m long bored piles connected to the footing and pile cap. The latter piles will not add any bearing to the foundation, but actually add a small load due to transfer of the drag force that will be developing along the full 5 m length.

With regard to the soil response to vertical loads of the foundation, the difference between a piled raft and a piled pad is small (though the structural design of the concrete of concrete raft and the footing will be different). For both the piled raft and the piled pad foundations, the piles are designed to a factor of safety of unity or smaller. The main difference between the raft and the pad approaches lies with regard to the response of the foundations to horizontal loading, seismic events, and later spreading and absence of stress concentrations for the raft. Cases of actual earth quake impacting pile-pad foundations show that the pile pad foundation provides the structure with a beneficial cushioning effect during a seismic event (Yamashita et al 2011b and Yamashita et al. 2013).

The piles for a piled raft foundation are connected through the raft and this will minimize the effect of any lateral spreading. Resistance to horizontal loading by a piled raft foundation is obtained by means of pile response to horizontal load. A piled pad foundation provides little resistance to either lateral spreading or horizontal loads. The potential of lateral soil-spreading under the foundation can be offset by having the pile group area larger than the area (footprint) of the footing on the pad, incorporating horizontal soil reinforcement in the pad, minimizing the lateral spreading by incorporating vertical drains (wick drains, see Chapter 4) to suitable depths, etc.

---

<sup>7)</sup> The pile pad foundation is sometimes called "column-supported embankment foundation", "inclusion piled foundation", or "disconnected footing concept"; none of which is a good term.



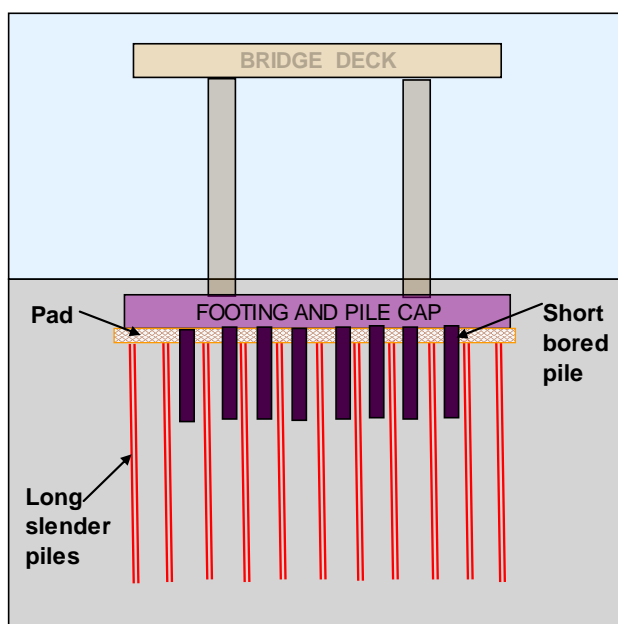


Fig. 7.35 Piled pad foundations for the Golden Ears Bridge piers.  
(After Sampaco et al. 2008).

Perhaps the largest difference between the piled raft and piled pad foundation, as opposed to a conventional piled foundation lies in that the former are soil improvement methods to be analyzed from the view of deformation (vertical and horizontal), whereas the conventional foundation also needs, or so some codes state, to be analyzed from a bearing "capacity" view with due application of factor-of-safety to the pile "capacity". N.B., if the latter indicates "safe" condition, this does not mean that the foundation is adequate. In contrast, if the former analysis shows satisfactory conditions, the foundation is satisfactory.

## 7.20. A Few Related Comments on Pile Groups

### 7.20.1 Pile Spacing

Determining the size of the pile cap is a part of the design. The size is decided by the pile diameter, of course, and the number of piles in the pile group. The decisive parameter, however, is the spacing between the piles. Pile caps are not cheap, therefore, piles are often placed close together at center-to-center spacings of only 2.5 to 3 pile diameters. A c/c spacing of 2.5 diameters can be considered O.K. for short toe-bearing piles, but it is too close for long shaft-bearing piles. The longer the pile, the larger the risk for physical interference between the piles during the installation, be the piles driven or bored. Therefore, the criterion for minimum pile spacing must be a function of the pile length. A suggestion is given in Eq. 7.30.

$$(7.30) \quad c/c = 2.5b + 0.02D$$

where

$c/c$	=	minimum center-to-center pile spacing
$b$	=	pile diameter (face to face for non circular pile section)
$D$	=	pile embedment length

The pile spacing for a group of long piles can become large and result in expensive pile caps. For example, Eq. 7.30 requires a spacing of 1.75 m (3.5 diameter) for a group of nine 0.5 m diameter, 50 m long piles. If necessary, the spacing at the pile head can be appreciably reduced, if the outer row(s) of piles are inclined outward by a small amount, say, 1(V):10(H) or even 1(V):20(H).

Still, the spacing is not an absolute. Piles can be placed very close to each other, indeed, even touching. For example, when used to serve as a retaining wall around a basement, as well as a support of a future wall. An interesting recent development is replacing a large diameter bored pile with several smaller diameter piles essentially covering the same footprint. Fig. 7.36A illustrates four about 1.2-m diameter CFA piles replaced a 2.5-m diameter bored pile for a tall building Florida, USA (Baquerizo 2015). The sketch to the right shows the approximately clover leaf shape of the final "new" pile. The not grouted center is not shown. Fig. 7.36B shows an about 3.6 m long and 1.2 m wide barrette was replaced by twelve 0.6-m diameter CFA piles. Static loading tests on special test piles proved that the approach worked.

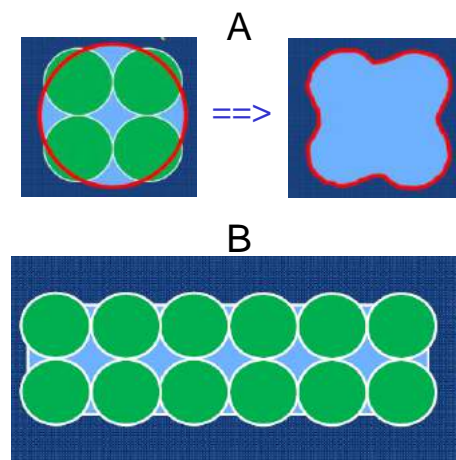


Fig. 7.36 Four piles replacing a single pile and twelve piles replacing a barrette (after Baquerizo 2015)

### 7.20.2 Pile Size

The equipment available to the foundation industry in the past limited the size of the piles that could be constructed. However, during the past decade or so, means to construct very large diameter piles have been developed and piles several metre in diameter can be constructed, indeed, even piles with rectangular cross section, so-called barrettes, that can be several metre in side length; i.e., so large that it could be a matter of definition whether the pile is a pile or a wall. This development has gone hand in hand with the development of taller and taller buildings and larger loads concentrated to a small area. The result is that large load do not any more need to be supported on wide pile groups made up of many piles, but can rely on a single large diameter pile; in effect, a heavy loaded column can continue as a large diameter pile, which saves much money otherwise spent on a pile cap. However, large diameter piles are frequently used also for heavy loaded wide pile groups (pile groups comprising several rows and columns at a pile spacing of 2 to 3 pile diameters) notwithstanding that smaller diameter piles (at an acceptable new spacing) within about the same size pile cap (footprint) might support the same total load, require less thick pile raft, and be considerably less costly to construct. Not to mention that the bidding for the foundation contract will be of interest also to smaller contractors that would not bid on the large-pile-diameter project due to their not having the capital allowing them to obtain the large equipment. Smaller diameter piles are usually cheaper and require thinner (and cheaper) pile caps. The construction is faster, verifying pile "capacity" and integrity is less costly, and distributing the loads on a larger number of points reduces risk.

### 7.20.3 Design of Piles for Horizontal Loading

Because foundation loads act in many different directions, depending on the load combination, piles are rarely loaded in true axial direction only. Therefore, a more or less significant lateral component of the total pile load always acts in combination with an axial load. The imposed lateral component is resisted by the bending stiffness of the pile, the degree of pile fixity, and the shear resistance mobilized in the soil surrounding the upper length of the pile.

An imposed horizontal load can also be carried by means of inclined piles, if the horizontal component of the axial pile load is at least equal to and acting in the opposite direction to the imposed horizontal load. Obviously, this approach has its limits as the inclination cannot be impractically large. It should, preferably, not be greater than 4(vertical) to 1(horizontal). Also, only one load combination can provide the optimal lateral resistance.

In general, it is not correct to resist lateral loads by means of combining the soil resistance for the piles (inclined as well as vertical) with the lateral component of the vertical load for the inclined piles. The reason is that resisting an imposed lateral load by means of soil shear requires the pile to move against the soil. The pile will rotate due to such movement and an inclined pile will then either push up against or pull down from the pile cap, which will substantially change the axial load in the pile.

Buried pile caps and foundation walls can often contribute considerably to the lateral resistance (Mokwa and Duncan 2001). The compaction and stiffness response of the backfill and natural soil then becomes an important issue.

In design of vertical piles installed in a homogeneous soil and subjected to horizontal loads, an approximate and usually conservative approach is to assume that each pile can sustain a horizontal load equal to the passive earth pressure acting on an equivalent wall with depth of  $6b$  and width  $3b$ , where  $b$  is the pile diameter, or face-to-face distance.

Similarly, the lateral resistance of a pile group may be approximated by the soil resistance on the group calculated as the passive earth pressure over an equivalent wall with depth equal to  $6b$  and width equal to as indicated in Eq. 7.31 (CFEM 1985).

$$(7.31) \quad L_e = L + 2B$$

where  $L_e$  = Equivalent Wall Width  
 $L$  = the width of the pile group in the plan perpendicular  
to the direction of the imposed loads  
 $B$  = the width of the pile group in a plane parallel  
to the direction of the imposed loads

The lateral resistance calculated according to Eq. 7.31 must not exceed the sum of the lateral resistance of the individual piles in the group. That is, for a group of  $n$  piles, the equivalent width of the group,  $L_e$ , must be smaller than  $n$  times the equivalent width of the individual pile,  $3b$ . For an imposed load not parallel to a side of the group, calculate for two cases, applying the components of the imposed load that are parallel to the sides.

The very simplified approach expressed above does not give any indication of movement. Neither does it differentiate between piles with fixed heads and those with heads free to rotate, that is, no consideration is given to the influence of pile bending stiffness. Because the governing design aspect with regard to lateral response of piles is lateral displacement, and the lateral "capacity" or ultimate resistance is of secondary importance, the usefulness of the simplified approach is very limited in engineering practice.

The analysis of lateral behavior of piles must consider two main aspects: First, the pile response: the bending stiffness of the pile, how the head is connected (free head, or fully or partially restrained head) and, second, the soil response: the input in the analysis must include the soil resistance as a function of the magnitude of lateral movement.

The first aspect is modeled by treating the pile as a beam on an "elastic" foundation, which is done by solving a fourth-degree differential equation with input of axial load on the pile, material properties of the pile, and the soil resistance as a nonlinear function of the pile displacement.

The derivation of lateral stress may make use of a simple concept called "coefficient of subgrade reaction" having the dimension of force per volume (Terzaghi, 1955). The coefficient is a function of the soil density or strength, the depth below the ground surface, and the diameter (side-to-side) of the pile. In cohesionless soils, the following relation is used:

$$(7.32) \quad k_s = n_h \frac{z}{b}$$

where  $k_s$  = coefficient of horizontal subgrade reaction  
 $n_h$  = coefficient related to soil density  
 $z$  = depth  
 $b$  = pile diameter

The intensity of the lateral stress,  $p_z$ , mobilized on the pile at Depth  $z$  follows a "p-y" curve (Eq. 7.33).

$$(7.33) \quad p_z = k_s y_z b$$

where  $y_z$  = the horizontal displacement of the pile at Depth  $z$

Combining Eqs. 7.32 and 7.33:

$$(7.34) \quad p_z = n_h y_z z$$

The fourth-order relation governing the behavior of a laterally loaded pile is then as follows:

$$(7.35) \quad Q_h = EI \frac{d^4 y}{dx^4} + Q_v \frac{d^2 y}{dx^2} - p_z$$

where  $Q_h$  = lateral load on the pile  
 $EI$  = bending stiffness (flexural rigidity) (Note, for concrete piles, the bending stiffness reduces with bending moment)  
 $Q_v$  = axial load on the pile

Design charts have been developed that, for an input of imposed load, basic pile data, and soil coefficients, provide values of displacement and bending moment. See, for instance, the Canadian Foundation Engineering Manual (CFEM 1985; 1992). The software LPILE by Ensoft Inc. is a most useful program for analysis lateral response of piles and its manual provides a solid background to the topic. Duncan et al. (1992) provides more in-depth discussion and recommendations.

The CFEM design charts cannot consider all the many variations possible in an actual case. For instance, the p-y curve can be a smooth rising curve, can have an ideal elastic-plastic shape, or can be decaying after a peak value, much like a t-z curve (See Section 8.12). As an analysis without simplifying shortcuts is very tedious and time-consuming, resorting to charts was necessary in the past. However, with the advent of the personal computer, special software has been developed, which makes the calculations easy and fast. In fact, as in the case of pile driving analysis and wave equation programs, engineering design today has no need for computational simplifications. Exact solutions can be obtained as easily as approximate ones. Several proprietary and public-domain programs are available for analysis of laterally loaded piles.

One must not be led to believe that, because an analysis is theoretically correct, the results also describe the true behavior of the pile or pile group. The results must be correlated to pertinent experience, and, lacking this, to a full-scale test at the site. If the experience is limited and funds are lacking for a full-scale correlation test, then, a prudent choice of input data is necessary, as well as of wide margins and large margins of safety.

Designing and analyzing a lateral test is much more complex than for the case of axial response of piles. In service, a laterally loaded pile in a group of piles almost always has a fixed head (restrained-head) condition. However, a fixed-head test is more difficult and costly to perform as opposed to a free-head test. A lateral test without inclusion of measurement of lateral deflection down the pile (bending) is of limited value. While an axial test should not include unloading cycles, a lateral test should be a cyclic test and include a large number of cycles at different load levels. The laterally tested pile is much more sensitive to the influence of neighboring piles than is the axially tested pile. Finally, the analysis of the test results is complex and requires the use of a computer and appropriate software.

#### **7.20.4 Seismic Design of Lateral Pile Behavior**

A seismic wave appears to a piled foundation as a soil movement forcing the piles to move with the soil, and a horizontal force develops in the foundation, starting it to move in the direction of the wave. The movement is resisted by the pile cap (depending on the structure supported); bending and shear are induced in the piles. A half period later, the soil swings back, but the pile cap is still moving in the first direction, so the forces increase. This situation is not the same as one originated by a static force.

Seismic lateral pile design consists of determining the probable amplitude and frequency of the seismic wave as well as the natural frequency of the foundation and structure supported by the piles. The first requirement is, as in all seismic design, that the natural frequency of the foundation and structure must not be the same as that of the seismic wave (a phenomenon called "resonance"). Then, the probable maximum displacement, bending, and shear induced at the pile cap are estimated. Finally, the pile connection and the pile cap are designed to resist the induced forces.

In the past, seismic design consisted of assigning a horizontal force equal to a quasi-static load as a percentage of the gravity load from the supported structure, e.g., 10 %, proceeding to do a static design. Often this approach resulted in installing some of the piles as inclined piles to resist the load by the horizontal component of the axial force in the inclined piles. This is not just very arbitrary, it is also wrong. The earthquake does not produce a load, but a movement, a horizontal displacement. The force is simply the result of that movement and its magnitude is a function of the flexural stiffness of the pile and its connection to the pile cap. The stiffer and stronger the stiffness, the larger the horizontal load. Moreover, while a vertical pile in the group will move sideways and the force mainly be a shear force at the connection of the piles to the pile cap, the inclined pile will rotate and to the extent the movement is parallel to the inclination plane and in the direction of the inclination, the pile will try to rise. As the pile

cap prevents the rise, the pile will have to compress, causing the axial force to increase. As a result of the increased load, the pile could be pushed down. Moreover, the pile will take a larger share of the total load on the group. The pile inclined in the other direction will have to become longer to stay in the pile cap and its load will reduce — the pile could be pulled up or, in the extreme, be torn apart. Then, when the seismic action swings back, the roles of the two inclined piles will reverse. After a few cycles of seismic action, the inclined piles will have punched through the pile cap, developed cracks, become disconnected from the pile cap, lost bearing "capacity"—essentially, the foundation could be left with only the vertical piles to carry the structure, which might be too much for them. If this worst scenario would not occur, at least the foundation will be impaired and the structure suffer differential movements. Inclined piles are not suitable for resisting seismic forces. If a piled foundation is expected to have to resist horizontal forces, it is normally better to do this by means other than inclined piles.

An analysis of seismic horizontal loads on vertical piles can be made by pseudo-static analysis. However, one should realize that the so-determined horizontal force on the pile and its connection to the pile cap is not a force causing a movement, but one resulting from an induced movement—the seismic displacement.

### **7.20.5 Pile Testing**

A pile design should consider the need and/or value of a pile test. A "routine static loading test", one involving only loading the pile head in eight steps to twice the allowable load and recording the pile head movement, is essentially only justified if performed for proof-testing reasons. The only information attainable from such a test is that the pile "capacity" was not reached. If it was reached, its exact value is difficult to determine and the test gives no information on the load-transfer and portion of shaft and toe resistance. It is, therefore, rarely worth the money and effort, especially if the loading procedure involves just a few (eight or so) load increments of different duration and/or an unloading sequence or two before the maximum load.

In contrast, a static loading test performed by building up the applied load by a good number of equal load increments with constant duration, no unloading/reloading, to a maximum load at least equal to twice the allowable load and on an instrumented pile (designed to determine the load-transfer) will be very advantageous for most projects. If performed during the design phase, the results can provide significant benefits to a project. When embarking on the design of a piling project, the designer should always take into account that a properly designed and executed pile test can save money and time as well as improve safety. A bidirectional-cell test is superior to a conventional head-down test. A dynamic test with proper analysis (PDA with CAPWAP) will also provide valuable information on load-transfer, pile hammer behavior, and provide the benefit of testing more than one pile.

For detailed information on pile testing and analysis of static loading tests, see Chapter 8. For pile dynamics, see Chapter 9.

### **7.20.6 Pile Jetting**

Where dense soil or limitations of the pile driving hammer hamper the installation of a pile, or just to speed up the driving, the construction often resorts to water jetting. The water jet serves to cut the soil ahead of the pile toe. For hollow piles, pipe piles and cylinder piles, the spoils are left to flow up inside the pile. When the flow is along the outside of the pile, the effect is a reduction of the shaft resistance, sometimes to the point of the pile sinking into the void created by the jet. The objective of the jetting may range from the cutting of the dense soil ahead of the pile toe or just to obtain the lubricating flow along the pile shaft. When the objective is to cut the soil, a large water pressure combined with small diameter jet nozzle is needed to obtain a large velocity water jet. When the objective is to obtain a "lubricating" flow, the jet nozzle must be large enough to provide for the needed flow of water. It is necessary to watch the flow so the water flowing up along the pile does not become so large that the soil near the surface

erodes causing a crater that would make the pile lose lateral support. It is also necessary to ensure that the jet cutting ahead is symmetrical so that the pile will not drift to the side. To limit the risk of sideways shifting ("pile walking"), outside placement of jetting pipes is risky as opposed to inside jet placement, say, in a center hole cast in a concrete pile.

Water pumps for jetting are large-volume, large-pressure pumps able of providing small flow at large pressure and large flow at small pressure. The pumps are usually rated for 200 gal/min to 400 gal/min, i.e., 0.01 m<sup>3</sup>/s to 0.02 m<sup>3</sup>/s to account for the significant energy loss occurring in the pipes and nozzle during jetting. The flow is simply measured by a flow meter. However, to measure the pump pressure is difficult and to measure it at the nozzle is practically impossible. The flow rate (volume/time) at the pump and out through the jet nozzle and at any point in the system is the same. However, the pressure at the jet nozzle is significantly smaller than the pump pressure due to energy losses. The governing pressure value is the pressure at the jet nozzle, of course. It can quite easily be estimated from simple relations represented by Eq. 7.36 (Torricelli's relation) and Eq. 7.37 (Bernoulli's relation) combined into Eq. 7.38. The relations are used to design the jet nozzle as appropriate for the requirements of volume (flow) and jetting pressure in the specific case.

$$(7.36) \quad Q = \mu A v$$

where

$Q$	=	flow rate (m <sup>3</sup> /s)
$\mu$	=	jetting coefficient $\approx 0.8$
$A$	=	cross sectional area of nozzle
$v$	=	velocity (m/s)

$$(7.37) \quad \frac{v^2}{2g} = \frac{p}{\gamma} \quad \text{which converts to: Eq. 7.37a} \quad v^2 = \frac{2p}{\rho}$$

where

$v$	=	velocity (m/s)
$g$	=	gravity constant (m/s <sup>2</sup> )
$p$	=	pressure difference between inside jet pipe at nozzle and in soil outside
$\gamma$	=	unit weight of water (kN/m <sup>3</sup> )
$\rho$	=	unit density of water (kg/m <sup>3</sup> )

$$(7.38) \quad A = \frac{Q\sqrt{\rho}}{\mu\sqrt{2p}}$$

where

$A$	=	cross sectional area of nozzle
$Q$	=	flow rate (m <sup>3</sup> /s)
$\mu$	=	jetting coefficient $\approx 0.8$
$\rho$	=	unit density of water (kg/m <sup>3</sup> ); $\approx 1,000$ kg/m <sup>3</sup>
$p$	=	pressure; difference between inside jet pipe at nozzle and in soil outside

When inserting the values (0.8 and 1,000) for  $\mu$  and  $\rho$  into Eq. 7.38, produces Eq. 7.39.

$$(7.39) \quad A = 28 \frac{Q}{\sqrt{p}}$$

For example, to obtain a cutting jet with a flow of 1 L/s (0.001 m<sup>3</sup>/s; 16 us gallons/minute) combined with a jet pressure of 1.4 kPa (~200 psi), the cross sectional area of the jet nozzle need to be 7 cm<sup>2</sup>. That is, the diameter of the nozzle needs to be 30 mm (1.2 inch).

During jetting and after end of jetting, a pile will have very small toe resistance. Driving of the pile must proceed with caution to make sure that damaging tensile reflections do not occur in the pile.

The shaft resistance in the jetted zone is not just reduced during the jetting, the shaft resistance will also be smaller after the jetting as opposed to the conditions without jetting. Driving the pile, "re-driving", after finished jetting will not restore the original shaft resistance.

### **7.20.7 Bitumen Coating**

When the drag force (plus dead load) is expected to be larger than the pile structural strength can accept, or the soil settlement at the neutral plane (settlement equilibrium) is larger than the structure can tolerate, the drag force (the negative skin friction) can be reduced by means of applying a coat of bitumen (asphalt) to the pile surface. Resorting to such reduction of shaft shear is messy, costly, and time-consuming. In most cases, it is also not necessary, when the long-term conditions for the piles and the piled foundation are properly analyzed. Moreover, other solutions may show to be more efficient and useful. However, bitumen coating is efficient in reducing negative skin friction and the drag force, as well as in lowering the neutral plane. Note, a bitumen coat will equally well reduce the positive shaft resistance and, hence, lower the pile "capacity".

A bitumen coat can be quite thin, a layer of 1 mm to 2 mm will reduce the negative skin friction to values from of 25 % down to 10 % of the value for the uncoated pile. The primary concern lies with making sure that the bitumen is not scraped off or spalls off in driving the pile. The bitumen is usually heated and brushed on to the pile. In a cold climate, the coat can spall off, i.e., loosen and fall off in sheets "sailing" down from the piles like sheets of glass. The potential injury to people and damage to property down below is considerable. In a hot climate, the coat may flow off the pile before the pile is driven. A dusty pile surface—be the pile a concrete pile or a steel pile—may have to be primed by "painting" the surface with very thin layer of heated, hard bitumen before applying the shear layer. Fig. 7.37 illustrates brushing the shear layer onto a primed surface of a concrete pile. Fig. 7.38 shows the coated pile when driven through a protective casing. Note that the bitumen has flowed and formed a belly under the pile after the coating was applied.

A functional bitumen coat on a pile to reduce shaft resistance can be obtained from a regular bitumen supplier. The same bitumen as used for road payment can be used. Be careful about roofing bitumen as often some fibers have been added to make it flow less. Note also, that driving through coarse soil will scrape off the bitumen coat—even a "thick one"—and preboring, or driving through a pre-installed casing, or another means to protect the bitumen, may be necessary. Moreover, in hot weather, it may be necessary to employ a two-layer bitumen coat to ensure that the bitumen will not flow off between coating the pile and driving it. The inner coat is the about 1 mm to 2 mm "slip coat" and an outer coat of about the same thickness of very stiff bitumen is then apply to cover the inner coat to keep it in place.

The range of bitumen to use depends on the climate of the site location. The ground temperature is about equal to the average annual temperature of the site. Therefore, a harder bitumen is recommended for use in tropical climate than in a cold climate. For most sites, a bitumen of penetration 80/100 (ASTM D946) is suitable (Fellenius 1975a; 1979).





Fig. 7.37 View of applying a bitumen coat to a concrete pile



Fig. 7.38 View of a bitumen-coated pile driven through a protective casing  
The left side of the pile was the pile underside in storage

#### 7.20.8 Pile Buckling

Buckling of piles is often thought to be a design condition, and in very soft, organic soils, buckling could be an issue. However, even the softest inorganic soil is able to confine a pile and prevent buckling. The corollary to the fact that the soil support is always sufficient to prevent a pile from moving toward or into it, is that when the soils moves, the pile has no option other than to move right along. Therefore, piles in

slopes and near excavations, where the soil moves, will move with the soil. Fig. 7.39 is a 1979 photo from Port of Seattle, WA, and shows how 24-inch prestressed concrete piles supporting a dock broke when a hydraulic fill of very soft silt flowed against the piles.



Fig. 7.39 View of the consequence of a hydraulic fill of fine silt flowing against 24-inch piles.

#### **7.20.9 Plugging of Open-Toe Pipe Piles and in-between Flanges of H-piles**

Plugging of the inside of a pipe pile driven open-toe is a common occurrence. If a definite plug has formed that moves down with the pile, the pile acts as a closed-toe pile. The soil mass inside the pile will be of importance for the driving, but not for the static shaft resistance under service conditions. For design, it is a matter of whether to trust that the resistance of the plug will act as toe resistance available in the long-term. In case of an open-toe pipe driven through soft or loose soil and into a competent dense soil therein forming a base, the so-obtained toe resistance can be trusted in most conditions. In contrast, when driving a pipe pile with an inside column—a "core"—, the pipe slides over the column and shaft resistance is mobilized both outside and inside the pipe. That is, inside shaft resistance will occur along the entire length of the soil column. However, when the pile is loaded statically, the core will combine with the pipe and only its lowest length will be affected. The "static resistance" determined by dynamic measurements (Chapter 9) will therefore be larger than the static resistance determined in a subsequent static loading test. Fig. 7.40 taken from Fellenius (2015) illustrates that static condition. The figure exaggerates the length ("height") of the core portion engaged by shaft shear and compression movement.

Paik et al. (2003) and Ko and Jeong (2015) performed static loading tests on double-walled pipe piles separating outside and inside shaft shear, showing that the inside soil column was only affected a distance up from the pile toe corresponding to the compression of the core for the load acting at the pile toe.

No leap of imagination is needed to realize that the core can be modeled as a pile turned upside down and tested from below. The key point to realize is that a such core-pile is soft in relation to a real pile. Its axial deformation modulus,  $E$ , is about equal to that of soil, albeit compressed under confined condition. The stiffness of the core is, therefore, about 3 to 4 order-of-magnitudes smaller than that of a real pile of the same diameter. Moreover, as indicated by O'Neill and Raines (1991), the effective stress in the core is constant (uniform material is assumed). Therefore, the ultimate unit shear resistance between the core and the inside of the pipe is more or less constant and modeling the shear force distribution along the core should be by means of average shear force; by total stress analysis so to speak. (In contrast, the shaft resistance along the outer pipe, of course, must be modeled using effective stress principles).

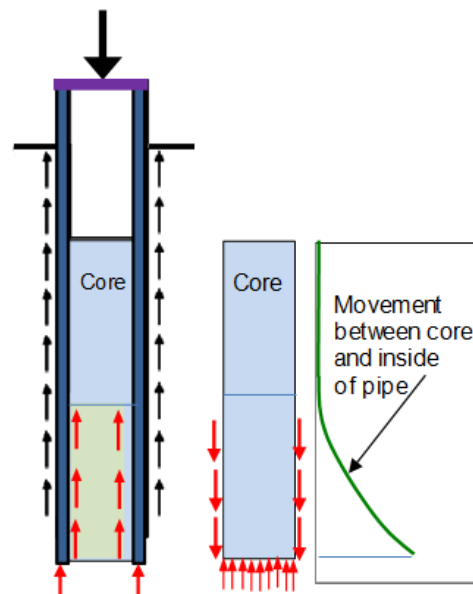


Fig. 7.40 Force vectors in static loading of an open-toe pipe pile with inside soil column, a "core".

In modeling the core as a soft pile pushed upward a distance equal to that of the pile toe movement in a static loading test, with the toe force compressing the core, we can appreciate that the imposed movement can never result in a large force at the bottom of the soft core and that the force on the core base will have been "spent" within a short distance up from the core bottom. The force-movement response of the core—unit shear resistance along the inside of the pipe—is more or less an elastic-plastic response, combined with the gradual mobilization of the core length, the response is similar to a pile toe response, i.e., an almost linear or relatively gently curving, force-movement of a pile toe. The difference is the magnitude of toe force and the stiffness, i.e., the slope of the curve.

Fellenius (2015) presented simulations shown in Fig. 7.41 of the response to static loading of simulations of the response to static loading of two pipe piles, one open-toe and one closed-toe, pipe pile with OD 711 mm, wall 7 mm, and length 11 m driven into a sand similar to the test piles employed by Paik et al. (2003). The simulation is made using an average beta-coefficient of 0.40 along the outside of the pipe and a toe resistance of 2 MPa. The shaft response is described by a hyperbolic function with the 0.40 beta-coefficient shaft resistance mobilized at a relative movement of 5 mm between the shaft and the soil (Chapter 8). The toe resistance is described by a ratio function with an exponent of 0.600 and the 2 MPa toe-resistance mobilized at 30-mm toe movement.

The simulated load-movement curves for the pile driven open-toe assumes that a soil core exists inside the full length of the pipe after the driving. The outer shaft resistance is the same as that for the closed-toe case. Moreover, I have assumed that the shear force between the core and the pipe has been activated along a 2.5 m length, that the average shear force is 40 kPa, and that the core has an E-modulus of 50 MPa. This establishes that, for a toe movement of 30 mm, the toe force is about 200 kN. With a bit of allowance for the force on the steel wall (the 7-mm annulus of the pipe; the steel cross section), this is the toe resistance of the open-toe pile at that toe movement.

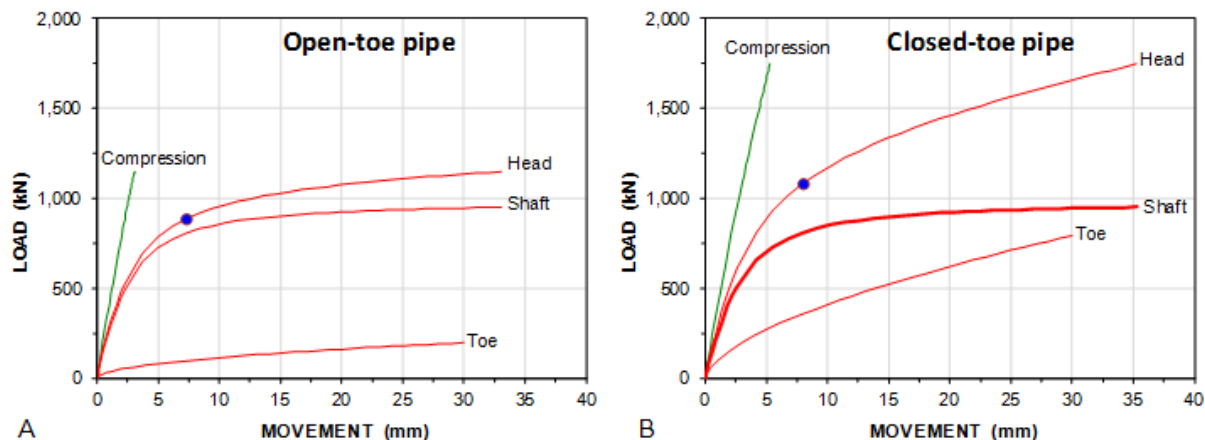


Fig. 7.41 Load-movement curves for a static loading test on a pipe pile  
A. Test an open-toe pipe pile and B. Test on a closed-toe pipe pile.

While the shaft shear between the core and the pile is assumed to be almost elastic-plastic, the gradual increase of force against the core base is best described by gently rising ratio function, as established in an analysis of the core for the mentioned assumptions using the upward response of the core in a bidirectional test. This is indicated in the toe curve in the figures.

An ultimate resistance can always be established from the pile head load-movement curve by some definition or other. However, a pile is composed of a series of individual elements, therefore, ultimate resistances for the complete pile as determined from the pile head load-movement curve, and that for the pile elements occur at different stages of the test. Whatever the definition based on the pile head load-movement, it has little relevance to the difference in response between the pile driven closed-toe as opposed to that driven open-toe. A useful relation in practice is the load at the pile head that results in a certain pile toe movement. The circles in Figs. 7.40A and 7.40B indicate the pile head load for a 5 mm toe movement of the simulated pile, which is usually a safe value of "allowable load". It includes an allowance for group effects that can increase the toe movement during long-term service, and, therefore, the piled foundation settlement, as well as for moderate amount of future downdrag. Note that, although the difference in toe resistance at the end-of-test 30-mm toe movement between the response of the open- and closed-toe pipe piles is about 600 kN, at the more moderate 5 mm toe movement, the difference is only about 200 kN.

In back-calculating the results of an actual static loading test on an open-toe pipe pile with a soil core and modeling the forces measured in various locations along the pile, the core effect cannot be treated as an ultimate toe resistance, but needs to be considered as an add-on movement-dependent resistance along a lower length of the core. This add-on shaft shear can be obtained by modeling the core effect separately, simulating its response as if were tested upward in a bidirectional test. While the core base (pile toe) movement is easily measured, the unit shaft shear along the core and the core stiffness will have to be assumed or determined in special tests.

When driving an open-toe pipe pile, the question is will the pile develop a rigid plug and, therefore, start responding like a closed-toe pile, and, as an inside soil core develops, what will the soil resistance response to the driving be? Then, for the design of service conditions, the follow-up question is will the long-term static response be of the rigid plug or the soil column? Answer to the service condition question will come from reference to results of static loading tests on full-scale pipe piles of different diameters and length with measured core response and back-analysis of the static load-movement measurements of the pile and the core as suggested above.

Plugging can also occur in-between the flanges of an H-pile. Whether plugged or not, for static response, the shaft resistance up along the pile should be calculated on the "square" because the shear resistance will act on the smallest circumferential area. The shear surface will only be the "H" if the shear force for soil to steel contact is much smaller than that at soil to soil. If "plugged" at the toe, the effect of the soil "core" inside the flanges can be analyzed in the same manner as indicated for the inside core of the pipe pile, i.e., by adding the "pile-head response" of a soft, "upside-down" pile at the H-pile toe to the toe resistance of the "H" steel section. It would have a marginal effect, only, on the pile toe load-movement response.

Analyzing an H-pile in driving is harder than analyzing the open-toe pipe pile, because the plug/column can occur along different length of the pile. Indeed, also at different times during the short interval of the driving impact.

### **7.20.10 Sweeping and Bending of Piles**

Practically all piles, particularly when driven, are more or less out of design alignment, and a perfectly straight pile is a theoretical concept, seldom achieved in practice. It should be recognized that the deviation from alignment of a deep foundation unit has little influence on its response to load either with regard to settlement or to "capacity". It may be of importance for the structure supported on the pile, however. Therefore, assigning a specific tolerance value of deviation, say, a percentage of inclination change, only applies to the pile at the pile cap or cut-off location (as does a specific deviation of location).

When long piles are driven into any type of soil, or shorter piles driven through soils containing obstructions, the piles can bend, dogleg, and even break, without this being recognized by usual inspection means after the driving. Pipe piles, and cylinder concrete piles, that are closed at the toe provide the possibility of inspection of the curvature and integrity given by the open pipe. An open-toe pile that was filled with soil during the driving can be cleaned out to provide access to the inside of the pile. It is normally not possible to inspect a precast concrete pile or an H-pile for bending. However, by casting a center tube in the precast concrete pile and a small diameter pipe to the flanges of the H-pile before it is driven, access is provided for inspection down the pile after driving.

The location of a pile and its curvature can be determined from lowering an inclinometer down the pile, if access is provided by the open pipe or through a center pipe (Fellenius 1972). Fig. 7.42 shows an example of deviations between the pile head and pile toe locations for a group of 60 m (200 ft) long, vertically driven prestressed concrete piles in soft soil (Keehi Interchange, Hawaii). The piles were made from two segments spliced with a mechanical splice. The main cause of the deviations was found to be that the piles were cast with the pile segment ends not being square with the pile. When this was corrected, the piles drove with only small deviations.

For a pipe pile, inspection down the open pile is often only carried out by lowering a flashlight into the pipe, or center tube, to check that the pile is sound, which it is considered to be if the flash light can reach the bottom of the pile while still being seen from above. However, dust and water can obstruct the light, and if the light disappears because the pile is bent, there is no possibility to determine from this fact whether the pile is just gently sweeping, which is of little concern, or whether the pile is severely bent, or doglegged. In such a case, a specially designed, but simple, curvature probe can be used to vindicate undamaged piles, and to provide data for aid in judging and evaluating a suspect pile.



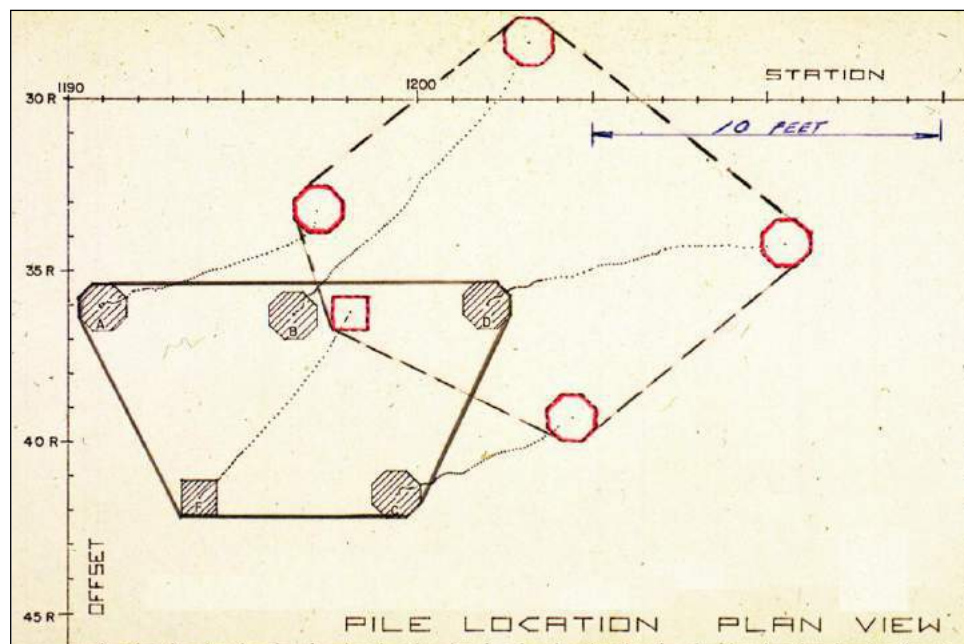


Fig. 7.42 Example of deviations determined by inclinometer measurements in 60 m long prestressed piles.

The curvature probe consists of a stiff, straight pipe of dimensions so chosen that it, theoretically, will 'jam' inside the pipe, or center tube, at a predetermined limiting bending radius expressed in Eq. 7.40 (Fellenius 1972). The principle of the use of the curvature probe are illustrated in Fig. 7.43.

$$(7.40) \quad R = \frac{L^2}{8t} = \frac{L^2}{8(D_1 - D_2)}$$

Where

- R = Bending radius
- L = Probe length
- t = Annulus  $D_1 - D_2$
- $D_1$  = Inside diameter of the pile or center tube
- $D_2$  = Outside diameter of the curvature probe

For obvious reasons, both the probe and the center tube should be made from standard pipe sizes. The probe must be stiff, that is, be a heavy-wall pipe. The length of a probe for use in steel pipe piles can be determined from selecting a probe with diameter (outside) that is about 80 % of the inside diameter of the pipe.

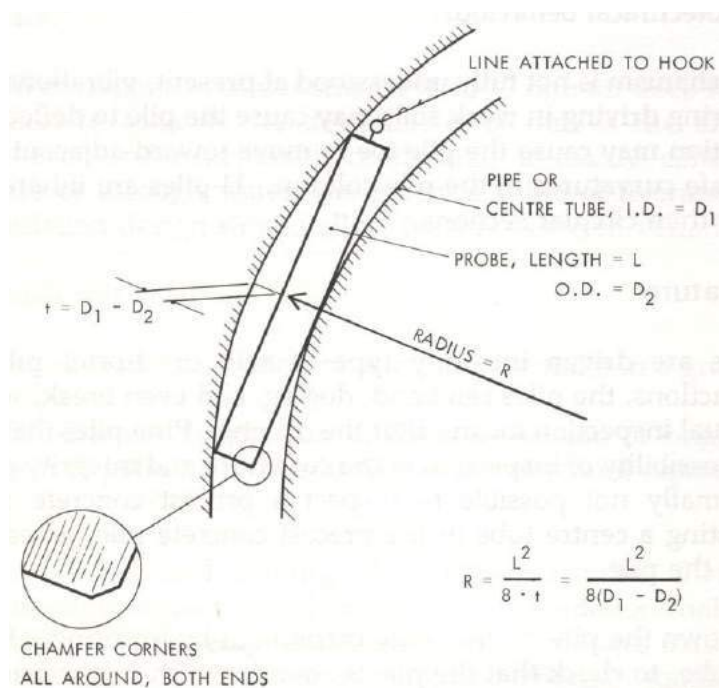


Fig. 7.43 Principle of the curvature probe

The passage of the curvature probe down the pile is affected by numerous imprecisions, such as ovality of the shape of the pipe, diameter tolerances of pipe, unavoidable 'snaking' of the center tube cast in a concrete pile, offsets when splicing pile, etc. However, the curvature is not intended to be an exact instrument for determining bending. (If exact measurement is desired, lower an inclinometer down the pile). Instead, the curvature probe is a refinement of the slow, crude, and imprecise inspection by eye and flashlight. Its main purpose is to vindicate piles, which otherwise may have to be rejected. Consequently, in deciding the limiting bending radius, one should not base the design on calculations of the bending moment ( $M$ ) and fiber stress (the radius determined from the relation:  $M = EI/R$ ). Such calculations imply a non-existent exact relation and will suggest that the limiting radius be about 400 m, and more. Probes designed according to such strict values are impractical and cause more difficulties than they solve. Practice has shown that the most suitable probes are those designed for limiting radii of 200 m and 100 m, the 100-m probe being used only if the 200-m probe 'jams'. Any 'jamming' (inability of the probe to reach the bottom of the pile) would then be evaluated, considering location of the 'stop', pile driving records, results from probing neighboring piles, intended use of the pile, etc.

A center pipe for placement in a precast concrete pile usually consists of small diameter, 1.5-inch (40 mm) steel tubing cast concentrically in the pile. Sometimes, for purpose of special testing, such as telltale instrumentation in combination with inclinometer measurements, larger diameter center pipes are used. Up to 6 inches (150 mm) pipes have been used in practice in 16-inch (400 mm) piles. For cost reasons, the larger center pipes often consist of PVC-pipes. (When center pipes larger than 6 inches are used, the pile is more to be considered a hollow pile, or a hollow-core cylinder pile, with a certain wall thickness).

A suitable size of center tube in precast concrete piles is 1.5 inch schedule 40 (inside diameter 40.9 mm), with a corresponding size of pipe for the curvature probe of 1.0 inch schedule 80 (33.4 mm outside diameter).

It is important that the splicing of the center pipe in the casting form is made without lips or burrs on the inside, obstructing the pipe. The splicing of the tubes must be made square and with outside couplings to ensure that no inside lips or edges are obstructing the passage of the probe. Center tubes made of PVC are cheaper than made from steel, but they are more apt to snake laterally, to float in the fresh concrete, and to be dislocated by the vibrator. Steel center tubes are preferred, as they are stiffer and heavier. When using PVC-pipes, it must be considered that the PVC exhibits an appreciable thermal expansion and contraction from the heat generated during the hydration of the concrete. Conical connections (splicing) must therefore not be used. Naturally, all PVC-couplings must be almost water tight to prevent the cement solution from entering the tubes.

In mechanically spliced piles, the center pipe is taken through the splices by means of a special standard arrangement, which supports the center pipe through the splicing plates and ensures that it is truly perpendicular to the plates. The splicing plates must be equipped with o-ring seals. Otherwise, due to the very large pore pressures generated and the remolding of the soil nearest the pile surface during the pile driving, soil would enter the center pipe and costly cleaning work would be required after the driving. That the seal is properly designed and arranged is essential. For instance, I have observed that the center pipe in 200 ft (60 m) long spliced pile filled completely with clay due to a faulty o-ring in one of the splices.

To ensure a straight center tube, it must be supported in the casting form and tied to the longitudinal reinforcement. A center tube is considered straight in the casting form before pouring the concrete, if the maximum deviation of the tube, as measured over a distance of 4 metre is 5 mm. This deviation tolerance corresponds to a calculated bending radius of 400 m. The limit is quite liberal. Practice has shown that there is no difficulty in having the tubes cast within this tolerance.

Piles with center tubes are usually also equipped with pile shoes. Where that is the case, it is necessary to supply the base plate of the shoes with a receiving pipe to center the tube in the pile, and to ensure positively that the tube at the toe of the pile (the zone of particular importance in the inspection) is straight.

If splices are used in the pile, a similar centering of the tube is necessary to enable the probe to pass through the splices without encountering difficulties due to offset of centers, 'knees', etc.

It is advisable to check that the tubes are straight and unobstructed after casting by pushing the probe into and through the center tube, while the pile lies on the ground in the casting yard (the probe has to be attached to the end of a standard pipe of small diameter, or pulled through by a line blown ahead through the tube). Fig. 7.44 shows such a test in progress on an about 30 m (100 ft) long prestressed concrete pile segment. Bending was induced in the pile segment to verify the practicality of the bending radius assigned to the curvature probe.

Adding a center pipe to precast concrete piles increases in-place cost per unit length of the pile by about 10 percent. However, properly handled, the total costs are reduced. The tremendous assurance gained by adding center pipes to the pile and carrying out a qualified inspection through these, will in almost every case justify an increase of the design load and reduction in the number of piles for the project. I have experienced projects, where, if the center pipes in the piles had not been used, a reduction of the recommended safe allowable load would have been necessary, whereas having the center pipes resulted in a recommendation to use increased allowable loads.





Fig. 7.44 Verifying the principle of the curvature probe

Center pipes have additional advantageous uses. For instance, providing a center pipe in a pile selected for a static loading test lends itself very obviously, and very cheaply, to accommodate a telltale rod to the bottom of the pipe. This rod is then used to record the pile toe movements during the loading test.

Center pipes provide the possibility of jetting a pile through dense soil layers in order to reduce driving time, increase penetration, and/or reduce bending.

Standard arrangements are available for pile shoes and driving plates, which will allow the jetting through the soil, when required. The practical advantage is that standard pile segments are used. Therefore, if jetting is found to be advisable at a site, this can be resorted to without much cost increase or delay, provided the piles are already equipped with center pipes.

Again, with a slight change of pile shoe design, the center pipe can be used to insert a drill rod through the pile and to drill beyond the pile toe for grouting a soil or rock anchor into the ground, when in need of an increased tensile "capacity". Or in the case of a pile driven to sloping bedrock, when the pile-toe support even when using rock shoes is doubtful, a steel rod can be dropped through the center pipe and beyond the pile toe into a drilled hole and grouted to provide the desired fixity of the pile toe.

#### 7.20.11 Influence on Adjacent Foundations

Driving a pile group produces heave and lateral movements, as well as pore pressures, which displace the soil upward and outward and increase pore pressures within and around the footprint of the pile group. When driving in soft clay near already existing foundation—shallow or deep—the movements and pore pressures can adversely affect the existing foundations. Bozozuk et al. (1978) found that the effect of driving a group of piles was that the piles created a heave within the pile group corresponding to about 50 % of the total pile volume and the remaining volume could be represented by a line from the heave at the edge of the group to intersection with a line rising at 2(V):(1H) from the pile toe level to the ground surface as illustrated in Fig. 7.45. The horizontal displacement of the soil outside the group can be estimated as proportional to the horizontally displaced soil at the various depths within the shaded area.

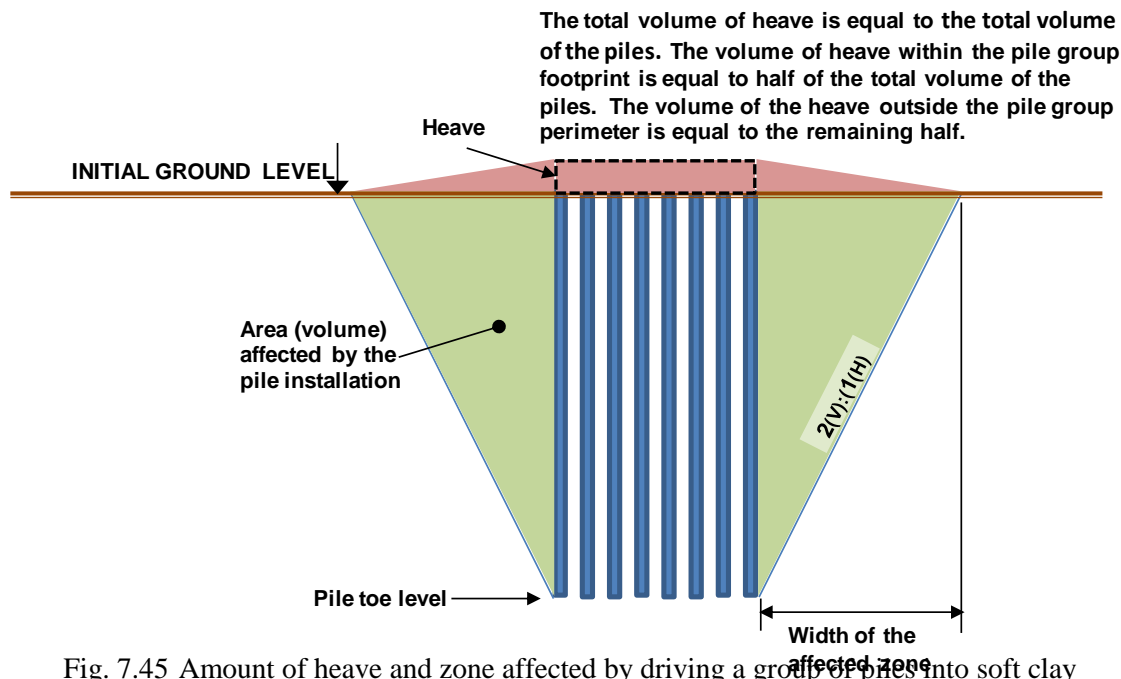


Fig. 7.45 Amount of heave and zone affected by driving a group of piles into soft clay

Undesirable settlement can also result from driving piles in sand. Chapter 9, Section 9.15 addresses this aspect.

## 7.20 "Capacity" as a function of time

Capacity is thought of as being a given quantity. Once determined, that's it, right! Of course, we all accept that a capacity determined in a theoretical analysis may not agree fully with the capacity found in a static loading test and we may have to adjust our parameters once we have test data. However, while our analysis of the test results does not usually consider the effect of time, Nature always considers time. It is not irrelevant whether or not we test a pile two weeks, a month, half a year, or longer after it was driven or constructed. "Capacity" will change with time—usually increase. ("Capacity" decreasing with time is a phenomenon associated with resistance due to temporary pore pressure decrease and a subsequent return of pore pressure and it usually occurs during the first hour or sooner after construction).

"Capacity" increase with time is not something limited to small diameter piles, it is a reality for all sizes and lengths of pile. Fig. 7.46 shows the full-length pile shaft resistance determined in static loading tests on two "companion" strain-gage instrumented piles, one tested 42 days after construction and one tested 31 days later, 72 days after construction (Teparaksa 2015). Both piles were 1.2 m times 3.0 m barrettes constructed under bentonite slurry in a Bangkok, Thailand, with 67 m embedment into about 22 m of soft clay deposited on about 28 m of medium dense to dense silt and sand followed at 50 m depth by layers hard clay and very dense sand. The data indicate that, at this site, a significant increase of soil shear stiffness developed also after the initial 43-day wait between construction and testing. Movement data for the case are estimates from the pile head movement and the larger movement required to reach the peak value for test Pile TP-2 may be an exaggeration. For Pile TP-1, a 60 kPa average ultimate shaft resistance could be defined to have been reached at an average movement of about 5 mm. Defining the ultimate average shaft resistance for Pile TP-2 at the resistance reached at the same movement indicates 75 kPa, whereas the peak resistance appears to have required an about 15-mm movement (pile compression was small).

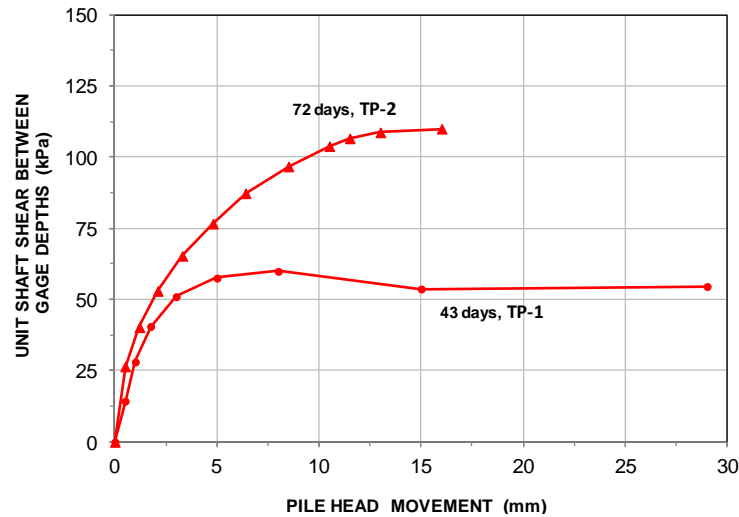


Fig. 7.46 Shaft resistance vs. average gage movement at two times after construction  
(Data from Teparaska 2015)

Pile "capacity" usually includes the also the pile toe response. However, pile toe "capacity" does not exist in reality other than as a "declared" value. Of course, in many instances, the stiffness of a pile toe response does increase with time. However, the mechanisms involved at the toe are not the same as those involved along the shaft. Nevertheless, overlooking the variations due to difference definition of pile "capacity" as based on the pile-head load-movement curve, a large number of tests on different pile in different geologies do show increasing values with time. Fig. 7.47 shows the capacities determined at three sites plotted versus days in logarithmic scale. The "Sandpoint" case is from a test on a 400-mm diameter, 45 m long concrete-filled steel tube driven in soft clay (Fellenius et. al. 2004) with a dynamic test performed 1 hour, a static loading test 48 days later, and a dynamic test 8 years after the end of driving. The "Paddle River" case is from static loading tests on two 324-mm diameter, steel pipe piles driven in stiff till clay near Edmonton, Alberta, one 16 m long and one 20 m (Fellenius 2008). The "Konrad-Roy" case (Konrad and Roy 1981) is from static loading tests on a 200-mm diameter, 7.6 m long steel pipe pile driven in soft clay (the "capacity" values are scaled up by a factor of 10).

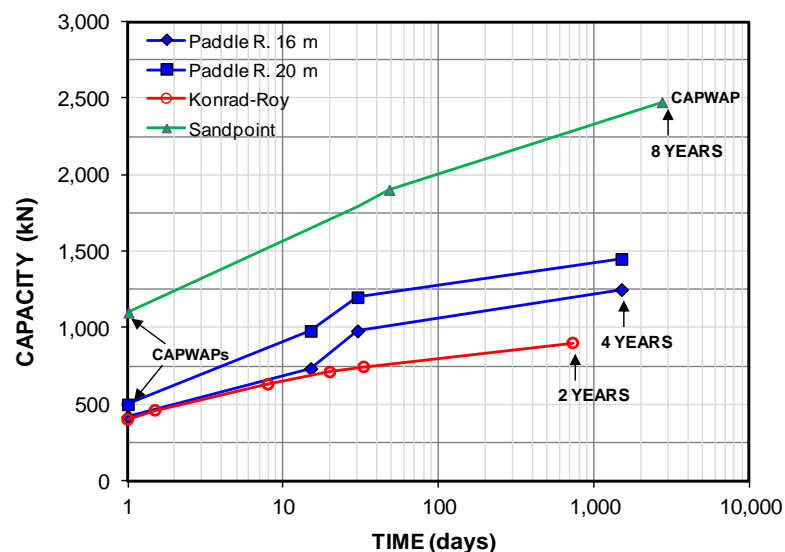


Fig. 7.47 "Capacity" determined at days after driving

The "capacity" increase is a function of increase of effective stress due to dissipation of the excess pore pressures created during the construction and, also, of aging. When studying the increase over a short time after the construction, the trend appears to be linear in a logarithmic time scale. However, beyond about 100 days, when most of the excess pore pressures can be assumed to have dissipated, the trend is different and the "capacity" growth rate to reduce. Fig 7.48 shows two linear trends (the same data plotted normalized to "capacity" of 100 % or that at 100 days). One for the days during the pore pressure dissipation time and one for the small growth after the pore pressure dissipation. Another word for pore pressure dissipation is consolidation. There is a tempting analogy with the settlement theory for clays consisting of a "primary" process during the dissipation (consolidation) and a "secondary" process thereafter (as in secondary compression).

The gradual reduction of the "capacity" increase during the "secondary" process makes a lot of sense. In a way, it is a parallel to the gradual decrease of the increase in settlement due to secondary compression after the end of the consolidation period.

Indeed, "capacity" is a very subjective value already before we take the time development into account. So, why is it that it is the main value, sometimes the only value, that our Codes and Standards have us base our piled foundation design on?

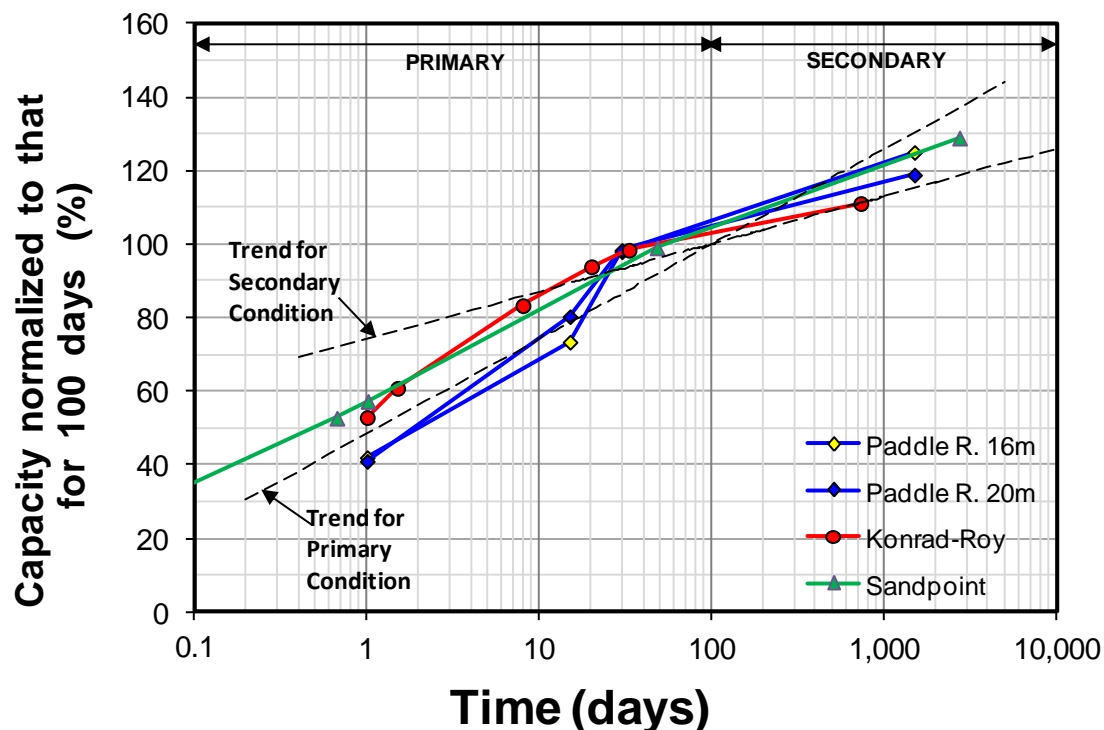


Fig. 7.48 Capacities normalized to 100 % of 100-day values

## 7.21 Scour

Scour is the term for "Nature's excavation" resulting from rapid water action, e.g., the Hurricane Sandy ravaging the US East coast in 2013 causing collapse of several bridge foundations—piled foundations. The effect of wave and flowing water is not just to remove the bottom sediment over a wide area around the foundations (general scour), but also to create a hole around the foundations (local scour). The latter removes the contact between the piles and the soil to some depth. More important, the over a wide area

general scour and the local scour remove overburden, which reduces the effective stress around the length of pile still in contact with the soil, i.e., the shaft resistance is reduced also for the length of pile below the bottom of the scoured hole.

The FHWA manual (Hanningan et al. 2006) recommends that potential scour around piled foundations be estimated by two components. First, the depth of the general scour and then a local scour determined as an inverted cone to a certain depth,  $Z_s$ , determined from scour depth analysis and/or observations of past events (Fig. 7.49). The slope of the scour sides are estimated to be 2(H): 1(V). That is, the cone diameter at the new sea or river bed to be 4 times the depth.

The FHWA manual recommends the obvious that shaft resistance (and lateral resistance) only be considered for the length of pile below the scour hole bottom. However, the additional recommendation that the effect of the unloading of the soil due to the general and local scour below the scoured hole be disregarded is incorrect on the unsafe side. The unloading will have a significant effect on the effective overburden stress and the shaft resistance along the remaining embedment length. Indeed, it also has a small reducing effect on the toe resistance (stiffness, rather). For that matter, it is not particularly onerous to include the unloading in an effective stress analysis. of the "after-scour" conditions.

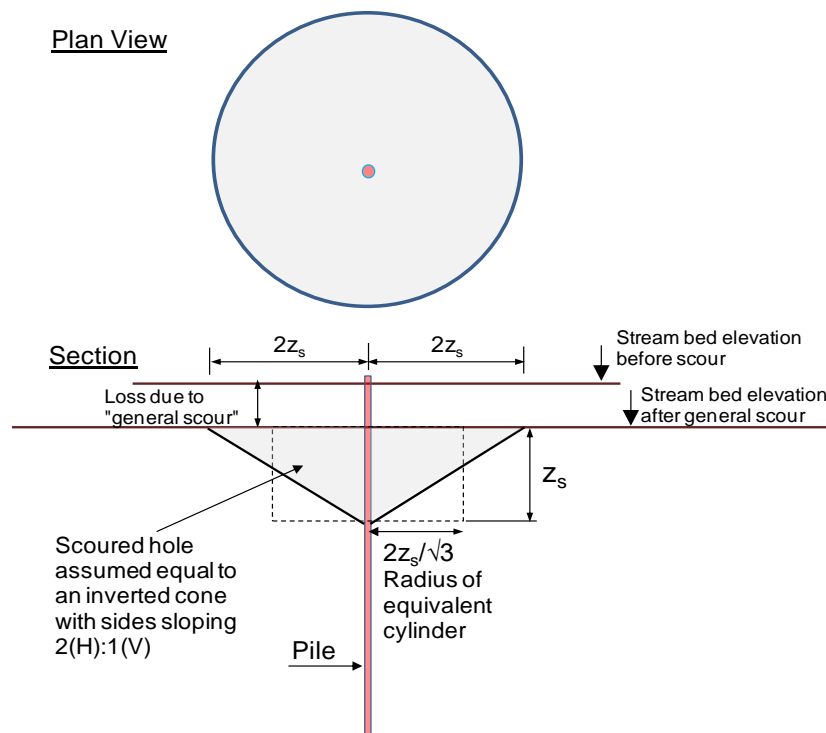


Fig. 7.49. Scour configuration according to the FHWA Manual

Fig. 7.50 shows the load distributions for before and during a scour event (per calculations performed using customary US units) for a driven 36-inch square, 80 ft long concrete pile. The general scour depth is 15 ft and the local scour depth is 18 ft. The before- and after-scour conditions are determined in an effective stress analysis using the beta-coefficients as listed in to the right of the figure. The toe resistance is simply assigned a value of 1,000 kips and assumed to not change due to the unloading by the scour. In order to simplify the calculations, the unloading effect of the local scour hole is calculated as the reduced stress due to a cylinder with a radius equal to  $2/\sqrt{3}$  times  $Z_s$  (equal mass).

The load distribution before scour is determined from effective stress analysis of test results. The scoured-out hole is assumed to be an inverted cone with a circular base approximated to a cylinder. To avoid cluttering up the graph, the toe resistance is assumed unchanged. In reality, the toe resistance will reduce somewhat due to the loss of overburden stress.

The pile bearing "capacity" and load distribution (the beta-coefficients) are assumed to have been determined in testing (static loading tests or dynamic with PDA/CAPWAP) during the construction of the piled foundations calibrating the response to load. The figure presumes that the desired working load is 700 kips and the required factor of safety during a scour event is 2.0, i.e., the desired "capacity" is 1,400 kips. The calibration of the conditions, the assigned scour conditions indicate the design results: the piles need to be driven to 80 ft depth and to a "capacity" of close to 2,000 kips.

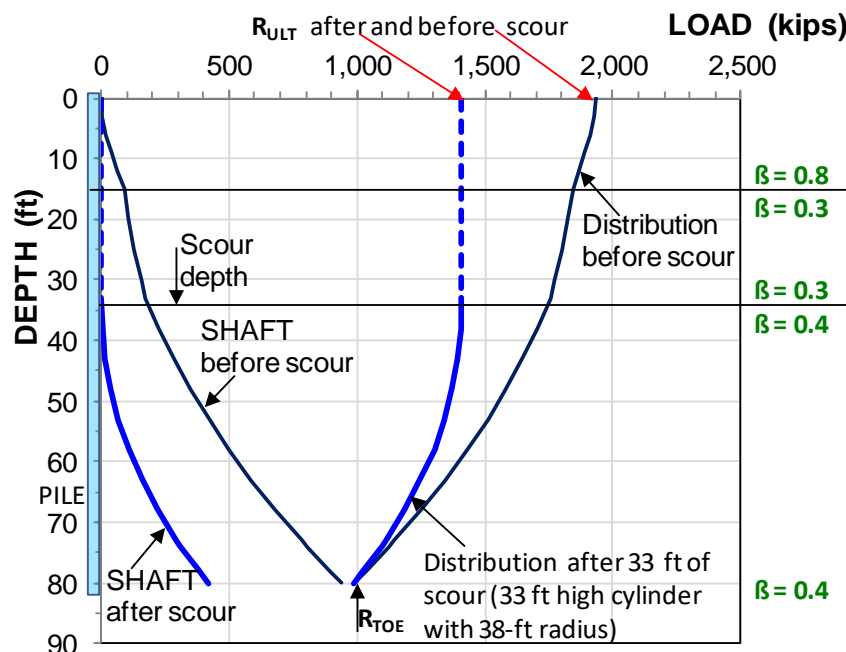


Fig. 7.50 Load distributions at "capacity" before and after-scour

## 7.22 A piled foundation example

To expound the procedures of the Unified Method, the method is applied to a typical example of a wide piled foundation, say, a storage tank, as follows. A hypothetical site comprises a 15 m thick layer of soft compressible clay followed by 25 m of dense silt and sand on hard soil at 40 m depth. The clay layer is subject to a gradual regional subsidence. A structure imposing a 64 MN sustained load (no live load), will be constructed at the site. The foundation consists of a hexagonal piled raft with a 3.0 m side-to-side distance. The designers have decided to use 91 round precast concrete piles with 300 mm diameter, placed at a 3.0 diameter center-to-center equilateral spacing. Fig. 7.51 shows the raft footprint and the soil profile.

To assist the hypothetical design, four test piles are assumed installed to embedment lengths of 30, 25, 20, and 15 m. Fig. 7.52 shows the hypothetical pile-head load-movement curves of the tests. The pile-toe response was assumed to be the same for all four tests and the pile-toe load-movement curve is included in the figure. The tests were terminated when the pile toe movement was 30 mm.

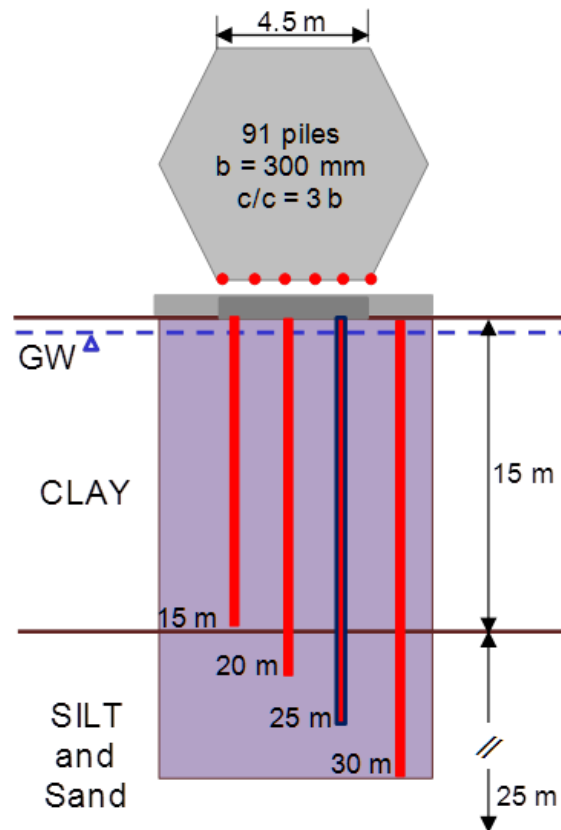


Fig. 7.51. The raft footprint and soil profile with alternative pile lengths.

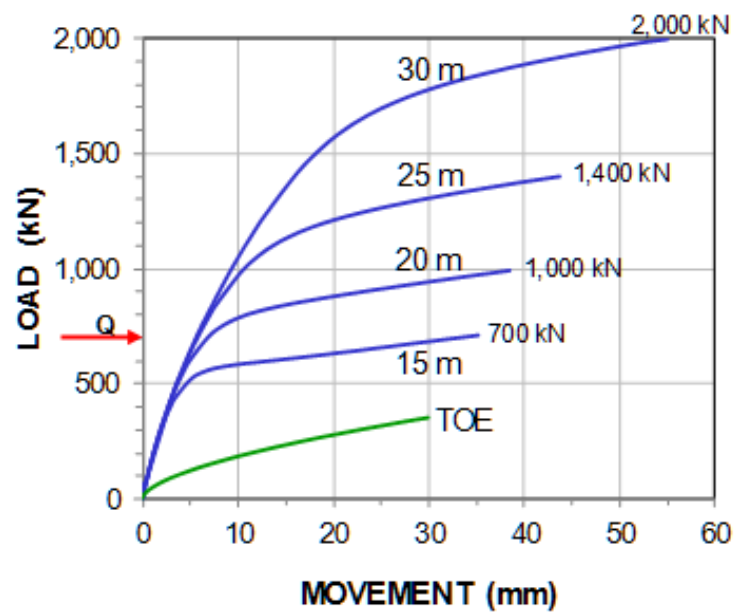


Fig. 7.52. Hypothetical load-movement curves



Storage tanks frequently have outside appurtenances that need to be supported on single piles and small pile groups. If the working load ( $Q$ ) applied to such piles outside the raft is the same as that applied to the average raft pile, i.e.  $Q = 700$  kN, then, the required pile length appears to be 25 m. Not because the "capacity" of the 25-m pile appears to be around twice the working load, but because the long-term settlement is acceptable, as indicated by the results of the unified-method analysis shown in Fig. 7.53 (only showing the load distribution for the match of the toe force and toe movement).

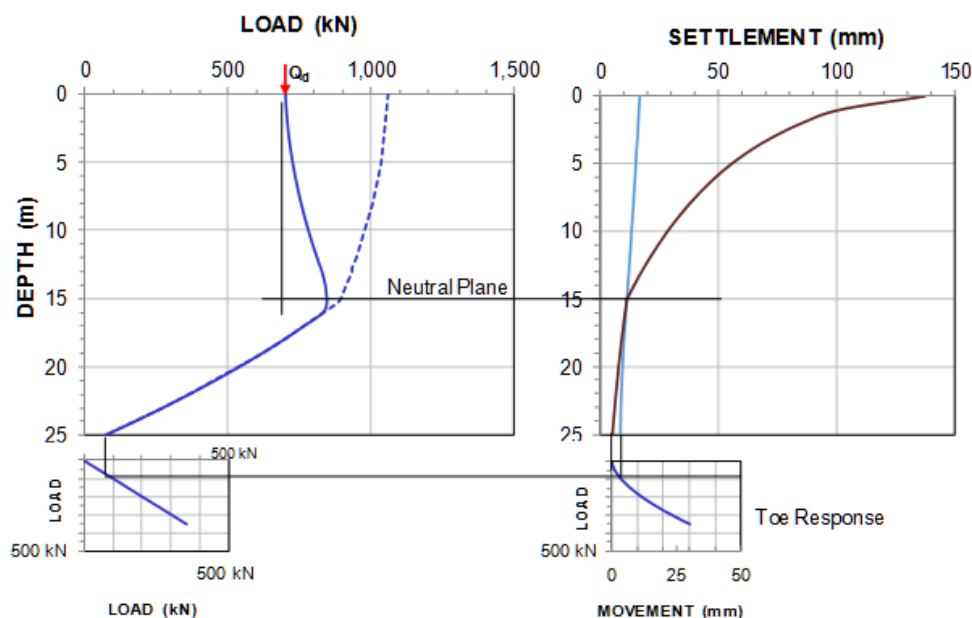


Fig. 7.53. Load distribution and match between toe resistance and settlement.

The piles would be subjected to a drag force of about 150 kN, which would be of no consequence. The drag force would be smaller for a shorter pile, but that pile would have the neutral plane up in the settling clay and suffer excessive downdrag and, therefore, be unsuitable. A longer pile would be spending more money than warranted.

The various methods employing analysis and relations would provide estimates of the long-term settlements for the pile raft. Eqs. 7.32 and 7.33 determine the pier settlement response. (The Footprint Ratio is 12 % and the pile modulus is assumed to be 30 GPa). The height of the equivalent pier is the pile length and, thus, the calculated compressions of the equivalent piers for the 15, 20, 25, and 30 m pile lengths are 5, 6, 8, and 10 mm, respectively.

The dominant settlement is that developing in the silt and sand layer below the pile toe level and it is a function of the compressibility of that layer. I made use of the effortless freedom of a hypothetical example and simply selected the compressibility that gave a 25 mm total settlement for the piled raft supported on 25 m long piles (using UniSettle, Goudreault and Fellenius 2011). I then calculated, employing the same compressibility, the settlement of equivalent rafts placed at the other three depths. Fig. 7.54 shows, as a function of pile length, the settlements calculated for the compression of the equivalent pier, the equivalent raft, and the two combined, i.e., the total settlement for the piled raft. The equivalent raft values are shown as a bar, where the center of the bar is the settlement calculated for the characteristic point, which is representative for a rigid raft. The left and right ends of the bar are settlements calculated (using UniSettle) for the raft side and center, respectively, for the Boussinesq stress distribution, which is considered representative for a flexible raft. Thus, the bar indicates the range of the differential settlement of the flexible equivalent raft, and, therefore, also of a flexible piled raft.



Two results are evident from the figure. First, the settlement contributed by the equivalent raft for the example below the pile toe level is larger than that of the compression of the equivalent pier. Second, designing the piled foundation on shorter piles, 15 m length) appears to result in very small additional settlement, 5 mm, beyond those of the 25-m "pure" piled foundation. Obviously, were it possible to use fewer piles, potential savings could be realized. For example, if the spacing would be increased to 3.75 pile diameters, while keeping the dimensions of the raft, the number of piles needed would reduce to 61. The corresponding reduction of the FR to 8 % would result in an about 30 % increased calculated pier compression, a moderate value. The settlement of the equivalent raft would be the same. The total settlement for such an enhanced piled raft would increase to about 30 mm from the about 25 mm value for the "pure" option.

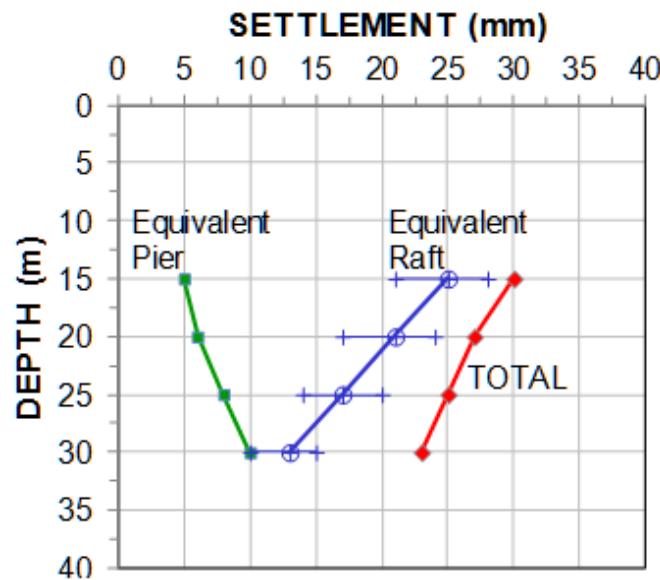


Fig. 7.54. Settlements versus pile depth.

### 7.23 Conclusions

For design of a pile group, some consider "capacity" of the group as the sum of the single piles times a reduction factor, a "group efficiency factor". However, the response of a group, such as the example case, is by load-movement and settlement. Estimating "capacity" by applying a group efficiency coefficient is not meaningful.

I cannot emphasize enough that pile design is design for settlement. Design of piles to sound bedrock is easy, the structural strength of the pile governs. Design of piles bearing in competent, low-compressibility soil is similarly easy—the load-movement response at the pile toe will govern (along with pile structural strength; the neutral plane will be at the pile toe or slightly above). For single piles and narrow groups, where the soils at the pile toe are less competent, the neutral plane will be higher up in the soil, and the settlement at the neutral plane will govern. For a group where inner rows are shielded by outer rows, i.e., a wide group, the design is governed by the settlement at the pile toe elevation. The simplest analysis is then to calculate the settlement for an equivalent raft placed at the pile toe elevation.

A foundation design should always be directed toward determining settlement letting "capacity" reasoning take second place. The unified method satisfies the requirement by employing interaction of forces and movements to determine the short- and long-term settlements for a single pile or a narrow pile group.

Note, pile design requires that the site investigation is geared to determine the compressibility characteristic in the deeper soil layers, so a settlement analysis can be made. A design based on *"the capacity is with a factor of safety of two or better, so we will have no settlement"* is an inadequate approach as many have learnt to their peril. Note, the settlement is only partially caused by the load on the piles. Unless the pile group is very large, the bothersome settlement is that caused by other factors than the pile loads, such as, fills, groundwater table lowering, neighboring structures, regional subsidence, etc. The statement that *"once capacity is shown to be OK, settlement will be OK, too"* is not valid. However, the inverse statement *"once settlement is shown to be OK, capacity will be OK, too"* is valid.

Design for "capacity" is a "belt and braces" approach. "Capacity" is the belt, and however fancy it is and how strong it seems to be, its success in preventing the pants from sliding down depends not just on the strength, many other aspects may control: e.g., the size of a proverbial beer belly in relation to the hip, so-to-speak. Settlement is the braces. If strong enough, then be they ugly or silly, be the belly wide or not, the braces will prevent excessive downward movement. A piled foundation may fail, and many have (as shown by developing excessive movement) despite the factor of safety of the individual piles shown to have been larger than 2 and 3. No piled foundation responding adequately regarding pile movement and foundation settlement has ever 'failed'.

The adequacy of the design calculations is not a function of the sophistication of the model or the computer program employed, but of (1) the adequacy of the soil information and (2) the quality and representativeness of the parameters used as input to the analyses. Both are somewhat lacking in the state-of-the-practice of foundation design.

Moreover, when a theory involves more than one or two parameters, before it can be stated that it truly represents actual response so as to be useful to predict a response, i.e., be used in the design of a foundation, the calibration of the method applied to the model per measured response must also include measurements of the relevant input parameters of the model.

Calling a calculation "a prediction" does not make it one. If the analysis model depends on pile-soil interaction, it is not sufficient to just measure axial load distribution in the piles. The soil forces and soil deformations must also be recorded and the model verifies against the observations

To improve the reliability of the design of piled foundations, research building up case histories must include instrumentation and monitoring of response to load applied to a pile group and single piles, including recording not just the settlement of the pile cap, but also:

- the movements between the pile and the soil at depths, in particular at the pile toe level
- the distribution of strain and movement in the soil with depth
- the earth stress against the piles
- the axial load distribution both in perimeter and interior piles
- the pile toe penetration into the soil and this compared to that of a single pile
- the settlement below the pile toe level

It is not financially possible to carry out a stand-alone research project on a wide piled foundation, but detailed instrumentation and monitoring of actual, well-defined projects (e.g., wide tanks) are needed. Direct research will have to be satisfied by studying small piled foundations.

## CHAPTER 8

### ANALYSIS OF RESULTS FROM THE STATIC AXIAL LOADING TEST

#### 8.1 Introduction

For piled foundation projects, it is usually necessary to confirm that the response of the piles to the loads from the supported structure agrees with the assumptions of the design. The most common such effort is by means of a static loading test and, normally, determining "capacity" is the primary purpose of the test. The capacity is understood to be the load—the "ultimate load"—applied to the pile when the movement measured at the pile head occurs under a sustained load or for only a slight increase of the applied load—the pile plunges. This definition is inadequate, however, because large movements are required for a pile to plunge and the ultimate load then reached in the test is often governed less by the capacity of the pile-soil system and more of the man-pump system. On most occasions, a distinct plunging ultimate load is not obtained in the test and, therefore, the ultimate load must be determined by some definition based on the load-movement data recorded in the test. (As this chapter defines capacity, I have refrained from placing the term inside quotation marks).

An old definition of capacity, originating in a misinterpretation of a statement by Terzaghi (1942), is that capacity is the load for which the pile head movement is 10 % of the diameter of the pile. However, Terzaghi stated that determining the capacity of a pile from analysis of records of a static loading test should not be undertaken unless the pile (a 12-inch diameter pile was the subject of the discussion) had moved at least 10 % of the pile toe diameter, which is quite a different matter; his statement was not to claim that capacity would be a function of pile diameter—he knew better—but to make clear that to derive a capacity from a test requires that the pile has moved a reasonable length against the soil (Likins et al. 2012).

If we consider unit resistance rather than total, a capacity, whether for shaft resistance or toe resistance, is irrelevant of pile diameter or curvature of the pile shaft. Just think of how the resistance along the side of a barrette could be governed by the width of the barrette. In regard to a pile toe, the observations of the footing tests reported in Section 6.10, for example, show that an ultimate resistance, i.e., capacity, does not exist. It is regrettable that the misconception of the 10-% statement has crept into several standards and codes, e.g., the Eurocode.

Of old, Canadian practice was to define capacity as the test load that resulted in a 1.5-inch pile head movement. Such definitions do not consider the elastic shortening of the pile, which can be substantial for long piles, while it is negligible for short piles. In reality, a movement limit does not have anything to do with a specific ultimate resistance of a pile as related to the soil response to the loads applied to the pile in a static loading test, only to a movement allowed by the superstructure to be supported by the pile. This, of course, makes it the most important definition of all, a movement limit is a key part of a pile design, but it does not define capacity in the 'ultimate sense' of the word.

Sometimes, the pile capacity is defined as the load at the intersection of two straight lines, approximating an initial pseudo-elastic portion of the load-movement curve and a final pseudo-plastic portion, as eyeballed from the graph. This definition results in interpreted capacity values that depend greatly on judgment and, above all, on the scale of the graph. Change the scales and the perceived capacity value changes also. The interpretation of a loading test is influenced by many occurrences, but the draughting manner should not be one of them.

Without a proper definition, interpretation becomes a meaningless venture. To be useful, a definition of pile capacity from the load-movement curve must be based on some mathematical rule and generate a

repeatable value that is independent of scale relations, a judgment call, or the eye-balling ability of the individual interpreter. Furthermore, it has to consider shape of the load-movement curve, or, if not, it must consider the length of the pile (which the shape of the curve indirectly does).

Fellenius (1975; 1980) presented nine different definitions of pile capacity evaluated from load-movement records of a static loading test. Six of these have particular interest, namely, the Davisson Offset Limit, the Hansen 80-% criterion, Hansen 90-% criterion, the Chin-Kondner Extrapolation, the Decourt Extrapolation, and the DeBeer Interception. A seventh limit could be the Maximum Curvature Point, although it is overly dependent on the accuracy of measurements and, therefore impractical. All are detailed in the following section, Section 8.2. The algorithms of the Hansen 80-% criterion and the Chin-Kondner extrapolation methods are useful for load-transfer analysis (Section 8.11).

There is more to a static loading test than analysis of the data obtained. As a minimum requirement, the test should be performed and reported in accordance with the ASTM guidelines (D 1143 and D 3689) for axial loading (compression and tension, respectively), keeping in mind that the guidelines refer to routine testing. Tests for special purposes may well need stricter performance rules.

Two of the most common errors in performing a static loading test are to include unloading/reloading cycles and to let the load-holding duration vary between load increments. As I will demonstrate in this chapter, for an instrumented test, unloading/reloading and differing load-holding durations will make it next to impossible to get reliable evaluation from the strain-gage data (see Section 8.16.5). If unloading/reloading cycles are thought needed, complete the primary test first and then carry out cyclic testing by a series of load cycles between selected values of load. Moreover, don't confuse a single or a couple of unload/reload events with cyclic testing. In cyclic testing, a large number of cycles are applied between two load values, usually at least 20, sometimes up to 100 (for information and comments on cyclic testing methods, see Fellenius 1975).

Believing that holding a load at a certain magnitude constant for a longer time (24 hours is a common length of the long load-holding time), or at several such load magnitudes, would provide direct information for predicting settlement of a piled foundation, is a very much misconceived belief. Such interspersed load-holding events have little relevance to analysis or prediction of settlement. However, they do mess up the means for a reliable analysis and interpretation of the results of the test, including using the test results for a settlement analysis. A proper and useful static loading test should consist of load increments that are equal in magnitude, applied at equal intervals, and held for equal length of time. If the test aims to evaluate a pile "capacity", the number of increments should be about 20 or more. The load-holding duration can be short, some maintain that 5 minutes are enough, or long, some maintain that 60 minutes are required. The common point is that the durations must be equal. Appreciating the value of redundancy of readings, I usually choose a load-holding time of 10 or 15 minutes, and I apply a total number of increments of about 5 % or less of the maximum test load. Thus, a test requiring 24 increments applied every 10 or 15 minutes will be over in four or six hours, respectively.

The two errors mentioned—unloading/reloading and differing load-holding duration—originate in old practice from before we had the concept of ultimate resistance and factor of safety, and before we had the means to test and the understanding of what we do when we test. Piles were simply tested by assessing movements at load levels of working load and multiples of working load. Assessment was by the net and gross movements as well as slope of load-movement between the unload/reload points. All utterly meaningless and long since discarded by those who know how piles respond to load and how design of piled foundations should be carried out and verified in tests. Unloading and reloading steps are vestigial items that must be purged from any modern practice that aims to follow sound, up-to-date, and knowledgeable engineering principles. Retaining the old practice of unloading/reloading and holding the load "still" for varying durations is akin to attempting to grow a tail as extension to one's vestigial tailbone.

Tests on uninstrumented piles are usually a waste of money. If a test is considered necessary, the pile must be instrumented so that the load distribution can be determined (see Section 8.13). The minimum instrumentation is telltales (or similar) to measure pile toe movement. A reasonably short pile no more than about, say, 15 m in a one or two-layer soil profile tested by means of a bidirectional test arrangement (Section 8.15) does not need any other instrumentation than to measure the imposed movements (using, say, telltales).

## 8.2 Davisson Offset Limit

The Offset Limit Method proposed by Davisson (1972) is presented in Figure 8.1, showing the load-movement results of a static loading test performed on a 112 ft (34 m) long, 12-inch (300 mm) precast concrete pile. The Davisson limit load, “the offset limit load”, is defined as the load corresponding to the movement which exceeds the elastic compression of the pile by a value of 0.15 inch (4 mm) plus a factor equal to the diameter of the pile divided by 120 (Eqs. 8.1a and 8.1b). For the 12-inch diameter example pile, the offset value is 0.25 inch (6 mm) and the offset is 0.8 inch (20 mm). The intersection with the load-movement curve is the offset limit load; 375 kips (1,670 kN).

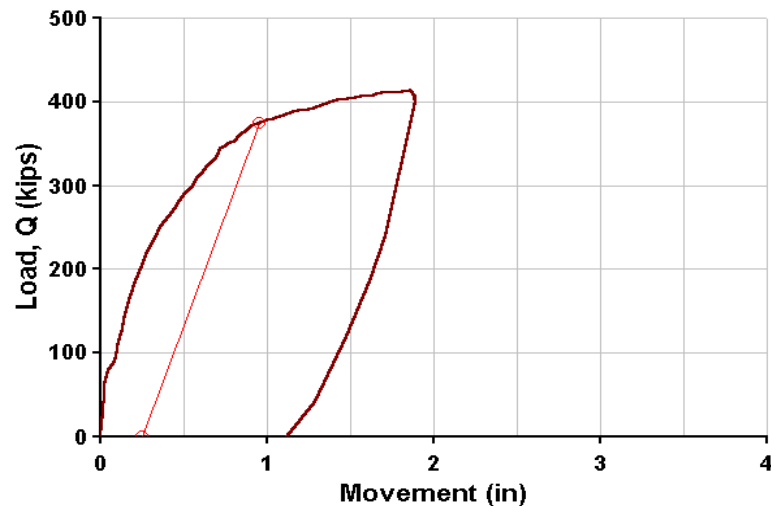


Fig. 8.1 The Offset Limit Method

$$\text{(Eq. 8.1a)} \quad \text{OFFSET (inches)} = 0.15 + b/120$$

$$\text{(Eq. 8.1b)} \quad \text{OFFSET (SI-units—mm)} = 4 + b/120$$

where  $b$  = pile diameter (inch or mm, respectively)

The offset distance is by some thought to be the pile toe movement produced by the load applied to the pile head load equal to the offset limit. This is incorrect.

Notice that the Offset Limit Load is not necessarily the ultimate load. The method is based on the assumption that a perceived "capacity" is reached at a certain small toe movement and tries to estimate that movement by adjusting it to the stiffness of the pile which is a function of material, length, and diameter. It was developed by correlating subjectively-considered pile-capacity values for a large number of pile loading tests to one single criterion. It is primarily intended for test results from small diameter driven piles tested according to “quick” methods and it has gained a widespread use in phase with the increasing popularity of wave equation analysis of driven piles and dynamic measurements.

### 8.3 Hansen 80-% and 90-% Criteria

#### 8.3.1 Hansen 80-% Criterion

Hansen (1963) proposed a definition for pile capacity as the load,  $Q_u$ , for which the measured load-movement curve starts to be four times the movement of the pile head as obtained for 80 % of that load, that is, the  $0.80Q_u/0.25\delta_u$  point lies on the curve. The method applies to tests on piles in a strain-softening soil and determines the peak resistance in the test from which the resistance then reduces due to soil strain-softening. The ‘80%- criterion’ can be estimated directly from the load-movement curve, but it is more accurately determined in a plot of the square root of each movement value divided by its load value and plotted against the movement. Figure 8.2 shows the plot of  $\sqrt{(Q/\delta)}$  **square root of movement over load versus pile head movement** for the same example as used for the Davisson construction (with the load and movement values of the example converted to SI-units). The 80-% pile-head **load-movement** curve constructed per Eq. 8.2 has been added for reference as measured and as constructed from the assumption of the curve satisfying the 80-% criterion for every measured movement (along with the 90-% curve, see Section 8.3.2). The dashed curve shown in Fig. 8.2 for the 80-% can also be manually constructed by taking a pile-head-load,  $Q_n$  (say, the maximum load applied) and its movement,  $\delta_n$ , and setting the immediately preceding load-movement pair,  $Q_{n-1}/\delta_{n-1}$ , as  $Q_{n-1} = 0.9Q_n$  and  $\delta_{n-1} = 0.5\delta_n$ , etc., until the movement becomes insignificant.

Normally, the 80%-criterion agrees well with the intuitively perceived “plunging failure” of the pile. The following simple relations are derived for use in computing the capacity or ultimate resistance,  $Q_u$ , according to the Hansen 80%-criterion:

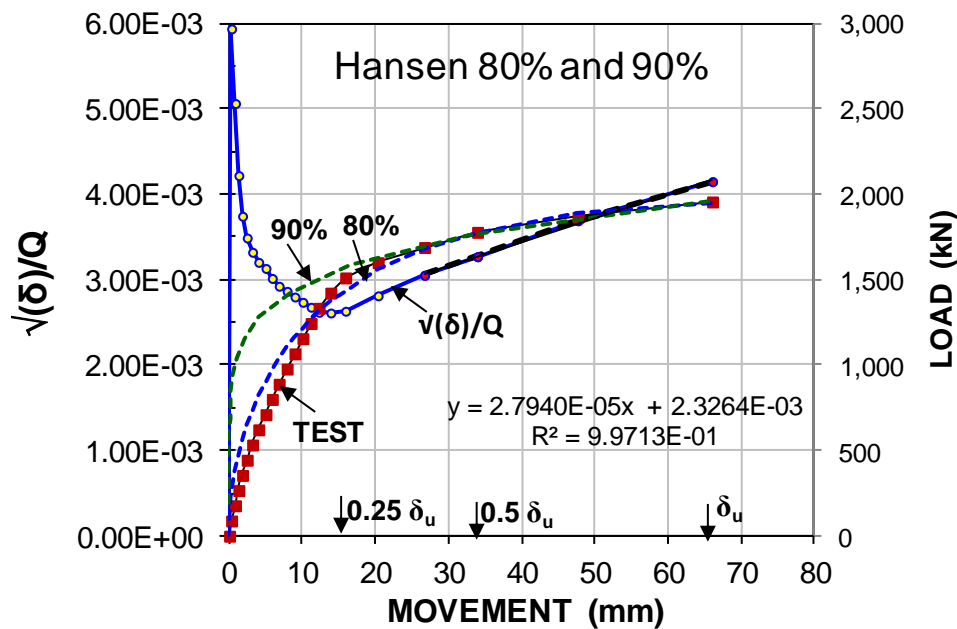


Fig. 8.2 Hansen's Plot for the 80 and 90 percent criteria

The 80-% criterion determines the load-movement curve for which the Hansen plot is a straight line throughout. Eq. 8.2 is the equation for the straight portion, which slope,  $C_1$ , and Y-intercept,  $C_2$ , can be determined by linear regression of the straight portion of the Hansen plotted line. Eq. 8.2 is the relation for the ‘ideal’ curve, shown as a dashed line in Figure 8.2. Eq. 8.3 expresses the ultimate resistance,  $Q_u$ , as a function of  $C_1$  and  $C_2$ . Eq. 8.4 expresses the movement,  $\delta_u$ , for the peak resistance,  $Q_u$ .

$$(Eq. 8.2) \quad Q = \frac{\sqrt{\delta}}{C_1\delta + C_2}$$

$$(Eq. 8.3) \quad Q_u = \frac{1}{2\sqrt{C_1 C_2}}$$

$$(Eq. 8.4) \quad \delta_u = \frac{C_2}{C_1}$$

Where

- $Q$  = any applied load
- $\delta$  = the movement associated with Load  $Q$
- $Q_u$  = peak load or ultimate load
- $\delta_u$  = movement at the peak load
- $C_1$  = slope of the straight line in the  $\sqrt{\delta}/Q$  versus movement diagram
- $C_2$  = y-intercept of the straight line in the  $\sqrt{\delta}/Q$  versus movement diagram

For the example shown in Fig. 8.2, Eq. 8.2 indicates, coincidentally, that the Hansen Ultimate Load is equal to the 1,960-kN maximum test load applied to the pile head. Eq. 8.4 indicates that the peak was reached at  $\delta_u = 83$  mm. Beyond the 83-mm movement, theoretically, the resistance reduces (strain-softens), notwithstanding the appearance in the figure of a plastic response for movements beyond about 40 mm.

When using the Hansen 80%-criterion, it is important to check that the point  $0.80 Q_u/0.25 \delta_u$  indeed lies on or near the measured load-movement curve. The relevance of evaluation can be reviewed by superimposing the load-movement curve according to Eq. 8.2 on the observed load-movement curve. The two curves should be more or less overlapping from the load equal to about 80 % of the ultimate load,  $Q_u$ , per the Hansen 80-% criterion at  $0.25 \delta_u$ .

### 8.3.2 Hansen 90-% Criterion

Hansen (1963) also proposed a 90-% criterion, which defines pile capacity as the load,  $Q_u$ , for which the measured load-movement curve starts to be twice the movement of the pile head as obtained for 90 % of that load, the  $0.90Q_u/0.5\delta_u$  point on the curve. This definition of capacity was adopted by the Swedish Pile Commission (1970) and has had some acceptance in the Scandinavian countries. The dashed curve shown in Fig. 8.2 is the load-movement curve determined by manual construction from the capacity taken as the maximum load applied to the pile in the test,  $Q_n$ , and its movement,  $\delta_n$ , where the immediate preceding load-movement pair,  $Q_{n-1}/\delta_{n-1}$ , is determined as  $Q_{n-1} = 0.9Q_n$  and  $\delta_{n-1} = 0.5\delta_n$ , etc. until the movement becomes insignificant.

A curve that mathematically satisfies the 90-% criterion at every point is a power function expressed in Eq. 8.5. However, it is faster and simpler to check for  $Q_u$  directly on the load-movement curve.

$$(Eq. 8.5) \quad Q = Q_u \left( \frac{\delta}{\delta_u} \right)^{0.152}$$

Where

$Q$	=	any applied load
$\delta$	=	movement associated with Load $Q$
$Q_u$	=	ultimate load
$\delta_u$	=	movement at $Q_u$

The principle behind the Hansen 90%-criterion is that the point  $0.90 Q_u/0.5 \delta_u$  indeed lies on the measured load-movement curve. The relevance of this for a tests is obtained by superimposing a calculated load-movement curve according to Eq. 8.5 (or a manually constructed curve) on the observed load-movement curve. The two curves should be more or less overlapping from the load equal to about 80 % of the Hansen-80% ultimate load at  $0.25 \delta_u$  to the load,  $Q_u$ , considered as the ultimate load or "the capacity".

A load movement curve constructed as an extrapolation of the Hansen 90-% criterion will show increasing load with increasing movement *ad infinitum*. That is, the 90-% relation does not have a true  $Q_u$  or a true  $Q_{inf}$  value. It is not a useful definition. In fact, it is nothing but a Ratio Curve (Gwizdala 1996; see Section 8.11.1) with an exponent,  $\theta$ , equal to 0.152. In a given case, it could be possible that a calculated load-movement curve using a different  $\theta$  could show to be fitting the actual curve over a longer movement and load range and/or for a different choice of  $Q_u$ -value.

## 8.4 Chin-Kondner Extrapolation

Figure 8.3 gives a method proposed by Chin (1970; 1971) for piles (in applying the general work by Kondner 1963). To apply the Chin-Kondner method, divide each movement with its corresponding load and plot the resulting value against the movement. As shown in the figure, after some initial variation, the plotted values fall on a straight line. The inverse slope of this line is the Chin-Kondner Extrapolation of the ultimate load. The method is essentially a fit and extension of the test to a hyperbolic shape. The maximum or ultimate load is the load reached asymptotically at infinitely large movement. It is, therefore, always an extrapolation of the test. The method can be used to extrapolate a trend to a final value. However, a primary principle and requirement of a capacity evaluated from a static loading test and combined with a factor of safety or resistance factor, is that it must not be larger than the maximum load applied in the test. An extrapolated capacity can only be combined with an assigned factor of safety or resistance factor considered for use with a capacity determined in a well-supported theoretical analysis, i.e., a larger factor than that used for a load applied within the test. The Chin-Kondner relation has an ultimate load, but it occurs at an infinitely large movement, asymptotically, and, again, as no capacity should be used that has a larger movement than the maximum movement of the static loading test, the application of the Chin-Kondner method is limited.

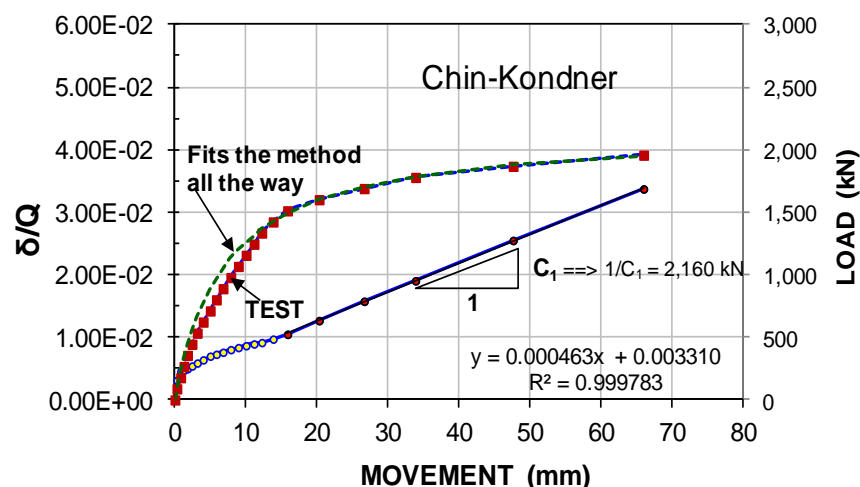


Fig. 8.3 Chin-Kondner Extrapolation method



$$(Eq. 8.5) \quad Q_u = \frac{1}{C_1}$$

Where  $Q_u$  = capacity or ultimate load (i.e., load at infinite movement;  $\delta \rightarrow \infty$ )  
 $C_1$  = slope of the straight line in the  $\delta/Q$  versus movement diagram

The inverse slope of the straight line (Eq. 8.5) for the example indicates a Chin-Kondner Extrapolation Limit of 2,160 kN, a value exceeding the 1,960-kN maximum test load applied to the pile head. Although some indeed use the Chin-Kondner Extrapolation Limit as the pile capacity established in the test (with an appropriately large factor of safety), this approach is not advisable. This rather restricts the usefulness of the method.

The criterion determines the load-movement curve for which the Chin-Kondner plot,  $Q/\delta$  vs.  $\delta$ , is a straight line throughout. The equation for this 'ideal' curve is shown as a dashed line in Figure 8.3 and the Eq. 8.6 gives the relation for the curve. With the measured movement values as input, Eq. 8.6 is the "hyperbolic" fit to the test data and, if larger than measured values are input, the continued plot becomes the "hyperbolic extrapolation" of the test data.

$$(Eq. 8.6) \quad Q = \frac{\delta}{C_1\delta + C_2}$$

$$(Eq. 8.7) \quad \delta = \frac{QC_2}{1 - QC_1}$$

Where  $Q$  = applied load  
 $\delta$  = movement associated with Load  $Q$   
 $C_1$  = slope of the straight line in the  $\delta/Q$  versus movement diagram  
 $C_2$  = y-intercept of the straight line in the  $\delta/Q$  versus movement diagram

Chin (1978) proposed to use the Chin-Kondner method to check the consistency of a pile response to a test process. Thus, if during the progress of a static loading test, a weakness in the pile would develop in the pile, the Chin-Kondner line would show a kink. Therefore, there is considerable merit in plotting the readings per the Chin-Kondner method as the test progresses. Moreover, the Chin-Kondner limit load is of interest when judging the results of a static loading test, particularly in conjunction with the values determined according to the other two methods mentioned.

Generally speaking, two points will determine a line and third point on the same line confirms the line. However, it is very easy to arrive at a false Chin-Kondner value if applied too early in the test. Normally, the correct straight line does not start to materialize until the test load has passed the Davisson Offset Limit. As an approximate rule, the Chin-Kondner Extrapolation load is about 20 % to 40 % greater than the Offset limit. When this is not a case, it is advisable to take a closer look at all the test data.

The Chin-Kondner method is applicable on both quick and slow tests, provided constant time intervals between load increments are used. Procedures that include unloading/reloading cycles and/or unequal load increments are therefore not applicable.

## 8.5 Decourt Extrapolation

Decourt (1999; 2008) proposed a method, which construction is similar to those used in Chin-Kondner and Hansen methods. To apply the method, divide each load with its corresponding movement and plot the resulting value against the applied load. The results are shown in the left of the two diagrams of Figure 8.4, a curve that tends to a line for which the extrapolation intersects with the abscissa (units are customary US-units). A linear regression over the apparent line (last five points in the example case) determines the line. The Decourt extrapolation load limit is the value of load at the intersection, 474 kips (2,110 kN) in this case. As shown in the right diagram of Figure 8.4, similarly to the Chin-Kondner and Hansen methods, an ‘ideal’ curve can be calculated and compared to the actual load-movement curve of the test.

The Decourt extrapolation load limit is equal to the ratio between the y-intercept and the slope of the line as given in Eq. 8.6A. The equation of the ‘ideal’ curve is given in Eq. 8.6B.

$$(Eq. 8.8) \quad Q_u = \frac{C_2}{C_1}$$

$$(Eq. 8.9) \quad Q = \frac{C_2 \delta}{1 - C_1 \delta}$$

Where

- $Q$  = applied load
- $Q_u$  = capacity or ultimate load
- $\delta$  = movement for  $Q$
- $C_1$  = slope of the straight line in the  $Q/\delta$  versus movement diagram
- $C_2$  = y-intercept of the straight line in the  $Q/\delta$  versus movement diagram

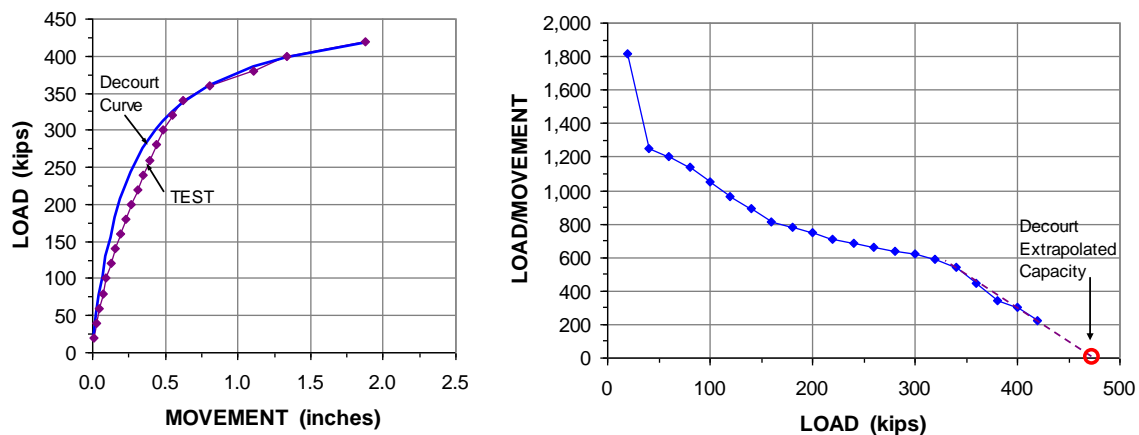


Fig. 8.4 Decourt Extrapolation method

Results from using the Decourt method are very similar to those of the Chin-Kondner method because both methods assume the load-movement to be hyperbolic. The Decourt method has the advantage that a plot prepared while the static loading test is in progress will allow the User to ‘eyeball’ the projected ultimate resistance once a straight line plot starts to develop. The limitations of the Decourt method are the same as those for the Chin-Kondner method.

## 8.6 DeBeer Intersection Load

If a trend is difficult to discern when analyzing data, a well known trick is to plot the data to logarithmic scale rather than to linear scale. Then, provided the data spread is an order of magnitude or two, all relations become linear, i.e., they show a clear trend. (Determining the slope and axis intercept of the line and using this for some 'mathematical truths' is not advisable; such "truths" rarely serve other purpose than that of fooling oneself).

DeBeer (1968) and DeBeer and Walays (1972) made use of the logarithmic linearity. Not by creating a "mathematical truth", but by letting the linearity demonstrate where a change had occurred in the test. They therefore plotted the load-movement data in a double-logarithmic diagram. If the load-movement log-log plot shows (with some approximation) two different lines connecting the data before and after a certain point, this "point of intersection" is the ultimate load (provided the number of points allow the linear trends to develop). DeBeer called the load at the intersection the "yield load". Figure 8.5 shows that the intersection occurs at a load of 360 kips (1,600 kN) for the example test.

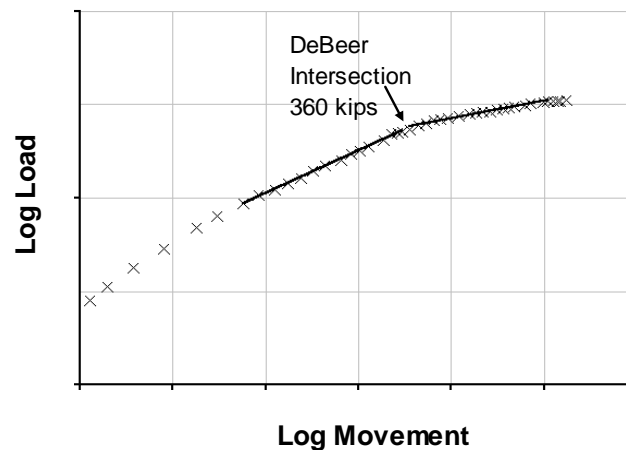


Fig. 8.5 DeBeer's double-logarithmic plot of load-movement data

## 8.7 The Creep Method

For loading tests applying equal increments of load applied at equal intervals of time, Housel (1956) proposed that the movement of the pile head during the later part of each load duration be plotted against the applied total load. These "creep" movements would plot along two straight lines, which intersection is termed the "creep load". For examples of the Creep Method, see Stoll (1961). The example used in the foregoing, being taken from a constant-rate-of-penetration, CRP, test, is not applicable to the Creep Method. To illustrate the creep method, data are taken from a test where the quick maintained-load method was used with increments applied every ten minutes. The "creep" measured between the six-minute and ten-minute readings is plotted in Figure 8.6. The intersection between the two trends indicates a Creep Limit of 550 kips. For reference to the test, the small diagram beside Figure 8.6 shows the load-movement diagram of the test and the Offset Limit Load.

If the "creep load" is to be considered in a test evaluation, it is important that no unloading/reloading cycles and/or that all load holding durations are equal. Then when a kink, similar to that shown in Fig. 8.6 appears, it is usually a sign of the shaft resistance having been fully mobilized and the pile toe has started to receive load and to move; information better obtained by means of a toe telltale and other instrumentation.

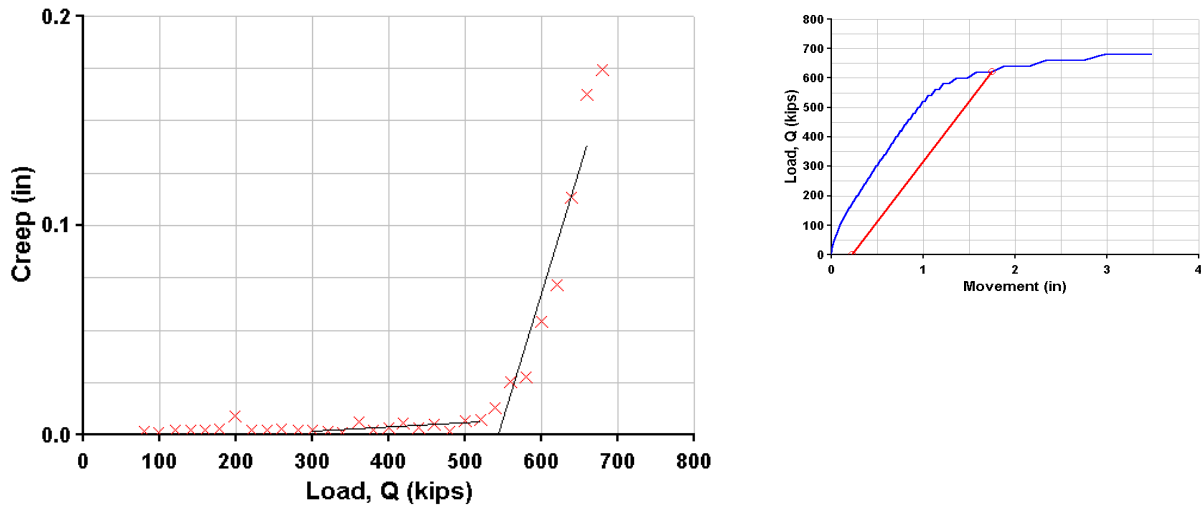


Fig. 8.6 Plot for determining the creep limit

### 8.8 Load at Maximum Curvature

When applying increments of load to the pile head, the movement increases progressively with the increasing load until the ultimate resistance is reached, say, as a state of continued movement for no increase of load—i.e., plastic deformation. Of course, plastic deformation develops progressively. Eventually the plastic deformation becomes the dominate feature of the curve. At loads smaller than that load, the curvature of the load-movement curve increases progressively. Beyond the load, the curve becomes more of a straight line. This response occurs at the point of maximum curvature of the load-movement curve. Provided that the increments are reasonably small so that the load-movement curve is built from a number of closely spaced points, the location of maximum curvature can usually be “eyeballed” to determine the limit load.

Shen and Niu (1991) proposed to determine the curvature by its mathematical definition and to plot the curvature of the load-movement curve against the applied load, as shown in Figure 8.7. Their mathematical treatment is quoted below. (Shen and Niu state that the third derivative is the curvature, which is not quite correct. Moreover, there is no merit in studying the third derivative instead of the curvature of the load-movement curve). Initially, this plot shows a constant value or a small gradual increase until a peak is obtained followed by troughs and peaks. The first peak is defined as the yield load. Shen and Niu defined the first peak to occur as the Yield Limit Load and claimed that the second peak occurs at the ultimate load.

First, the slope,  $K$ , of the load-movement curve is determined:

$$(Eq. 8.10) \quad K = \frac{\Delta \delta}{\Delta Q} = \frac{\delta_i - \delta_{i-1}}{Q_i - Q_{i-1}}$$

Eq. 8.11 then shows the change of slope for a change of load

$$(Eq. 8.11) \quad \Delta K = \frac{\Delta K}{\Delta Q} = \frac{K_{i+1} - K_i}{Q_{i+1} - Q_i}$$

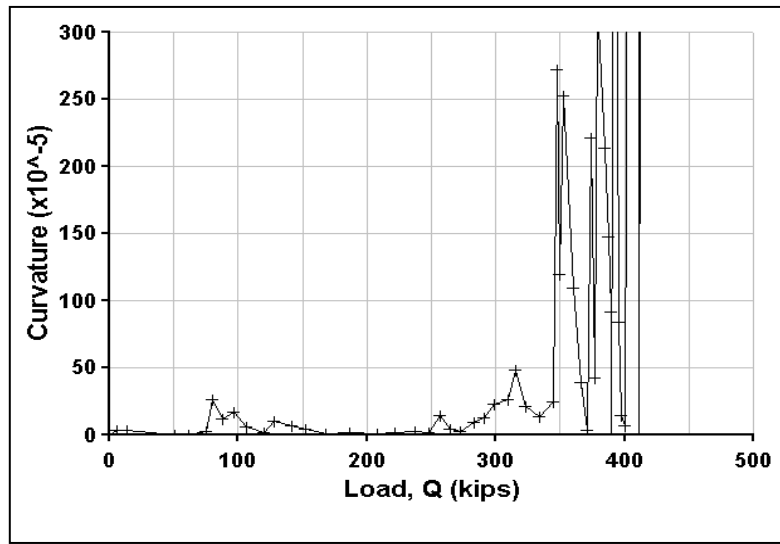


Fig. 8.7 Plot for determining the load-movement curve maximum curvature

$$(Eq. 8.12) \quad \Delta^2 K = \frac{\Delta^2 K}{\Delta Q^2} = \frac{\Delta K_{i+1} - \Delta K_i}{\Delta Q_{i+1} - \Delta Q_i}$$

and the third derivative is

$$(Eq. 8.13) \quad \Delta^3 K = \frac{\Delta^3 K}{\Delta Q^3} = \frac{\Delta^2 K_{i+1} - \Delta^2 K_i}{\Delta Q_{i+1}^2 - \Delta Q_i^2}$$

Strictly, the curvature,  $\rho$ , is

$$(Eq. 8.14) \quad \rho = \frac{\Delta^2 K}{(1 + K^2)^{3/2}}$$

The primary condition for the Shen-Niu yield-load method to be useful is that all load increments are equal and accurately determined. Even a small variation in magnitude of the load increments or irregular movement values will result in a hodgepodge of peaks to appear in the curvature graph, or, even, in a false yield load. It is then more practical to eyeball the point of maximum curvature from the load-movement curve.

## 8.9 Factor of Safety

To determine the allowable load on a pile, pile capacity evaluated from the load-movement curve of a static loading test is normally divided by a factor of safety (or multiplied by a resistance factor in ULS design or LRFD). The factor of safety is not a singular value applicable at all times. The value to use depends on the desired avoidance of unacceptable consequence of a failure, as well as on the level of knowledge and control of the aspects influencing the variation of capacity at the site. Not least important are, one, the method used to determine or define the ultimate load from the test results and, two, how representative the test is for the site. For piled foundations, practice has developed toward using a range

of factors. See also the discussion on Factor-of-Safety presented in Chapter 10.

In a testing programme performed early in the design work and testing piles that are not necessarily the same type, size, or length as those which will be used for the final project, it is common to apply a safety factor of at least 2.5 to the capacity evaluated from the test results—often applied without too much thought placed on what definition of capacity that was employed. In the case of testing during a final design phase, when the loading test occurs under conditions well representative for the project, the safety factor is usually 2.0 or 2.2, again, applied to a rather ambiguously determined capacity. When a test is performed for purpose of verifying the final design, testing a pile that is installed by the actual piling contractor and intended for the actual project, the factor commonly applied is 2.0. Well into the project, when testing is carried out for purpose of proof testing and conditions are favorable, the factor may be further reduced and become 1.8. A reduced safety factor may also be warranted when limited variability is confirmed by means of combining the design with detailed site investigation and control procedures of high quality. One must also consider the number of tests performed and the scatter of results between tests. Not to forget the assurance gained by means of incorporating dynamic methods for controlling hammer performance and capacity determination alongside the static methods of testing and analysis.

However, the value of the factor of safety to apply depends, as mentioned, on the method used to determine the capacity. A conservative method, such as the Davisson Offset Limit Load, warrants the use of a smaller factor as opposed to when applying a method such as the Hansen 80%-criterion. It is good practice to apply more than one method for defining the capacity and to apply to each method its own factor of safety letting the smallest allowable load govern the design. That is, the different analysis methods define lower and upper boundaries of the ultimate resistance. Moreover, the lower boundary does not have to be the Offset Limit. It can be defined as the load on the pile when the load-moment curve starts to fit (becomes close to) the “ideal” Hansen, Chin-Kondner, or Decourt load-movement curves. All criteria should be coupled with an assessment of the maximum movement associated with an applied load equal to the evaluated capacity.

In **factored design** (LRFD—Load and Resistance Factor Design or ULS design—Ultimate Limit States Design), a “resistance factor” is applied to the capacity and a “load factor” is applied to the load. Considering both the fact that factored design must always be coupled with a serviceability limit state design (SLS—Serviceability Limit States Design, or unfactored design), it has been proposed that the pile capacity should be determined by a method closer to the plunging limit load, that is, the Hansen 80 %-criterion would preferred over the Offset Limit Load. Note, that the serviceability limit state addresses settlement. Therefore, the load-transfer distribution determined in an instrumented static loading test is tremendously valuable, indeed necessary, when assessing settlement of a piled foundation. Moreover, it should be remembered that, while there are many piled foundations that have failed to support a structure adequately despite a customary factor of safety applied to a capacity value, there are no such unacceptable foundations where the design correctly assessed the settlement aspects.

## 8.10 Choice of Criterion

It is difficult to make a rational choice of the best capacity criterion to use, because the preferred criterion depends heavily on one's past experience and conception of what constitutes the ultimate resistance of a pile. One of the main reasons for having a strict criterion is, after all, to enable compatible reference cases to be established.

The Davisson Offset Limit is very sensitive to errors in the measurements of load and movement and requires well maintained equipment and accurate measurements. No static loading test should rely on the jack pressure for determining the applied load. A load-cell must be used at all times (Fellenius 1984). In a sense, the Offset Limit is a modification of the 1.5 inch movement, the “gross movement”, criterion of the

past. Moreover, the Offset-Limit method is an empirical method that does not really consider the shape of the load-movement curve and the actual transfer of the applied load to the soil. However, it is easy to apply and has gained a wide acceptance, because it has the merit of allowing the engineer, when proof-testing a pile for a certain allowable load, to determine in advance the maximum allowable movement for this load with consideration of the length and size of the pile. Thus, as proposed by Fellenius (1975), contract specifications can be drawn up including an acceptance criterion for piles proof tested according to quick testing methods. The specifications can simply call for a test to at least twice the design load, as usual, and declare that at a test load equal to a factor,  $F$ , times the design load, the movement shall be smaller than the elastic column compression of the pile, plus 0.15 inch (4 mm), plus a value equal to the diameter divided by 120. The factor  $F$  is a safety factor and should be chosen according to circumstances in each case. The usual range is 1.8 through 2.0.

The Hansen 80%-criterion is often close to what one subjectively accepts as the true ultimate resistance determined from the load-movement curve of the static loading test. This may occur even if the soil is not truly strain-softening or the peak resistance has not been reached. The value is then smaller than the Chin-Kondner or Decourt extrapolated values. Note, however, that the Hansen 80-% method is more sensitive to inaccuracies of the test data than are the Chin-Kondner and Decourt methods.

In contrast to the Hansen 80-% criterion, the Hansen 90-% criterion is not useful and could give misleading results. It is only mentioned here because it is in use in some places, so a reference is needed. If required for curve fitting, the ratio function (Gwizdala 1996) is more convenient.

The Chin-Kondner Extrapolation method and the Decourt Extrapolation method, allow continuous check on the test, if a plot is made as the test proceeds, and an extrapolating prediction of the maximum load that will be applied during the test. Sudden kinks or slope changes in the Chin-Kondner line indicate that something is amiss with either the pile or with the test arrangement (Chin 1978).

The Hansen's 80%, and the Chin-Kondner and Decourt methods allow the later part of the load-movement curve to be plotted according to a mathematical relation, and, which is often very tempting, they make possible an "exact" extrapolation of the curve. That is, it is easy to fool oneself and believe that the extrapolated part of the curve is as true as the measured. As mentioned earlier, whatever one's preferred mathematical criterion, the pile capacity value intended for use in design of a pile foundation must not be higher than the maximum load applied to the pile in the test.

The shape of the pile-head load-movement curve is influenced by the length of the pile (i.e., by the amount of pile shortening) and whether or not the pile is affected by residual force. Moreover, piles are used in order to control and limit the amount of settlement of the supported foundation. What settlement to consider acceptable is a function of the response of the structure, not of the piles directly. Personally, I find that a useful definition for "pile capacity" is the pile head load in the test that produced a 30 mm toe movement. Then, after applying an appropriately conservative factor of safety (working stress) or resistance factor (ULS design or LRFD) to the capacity, the issue becomes whether or not the settlement of the foundation for the so-determined sustained portion of working load (unfactored) is acceptable, i.e., if it is smaller than the upper limit of what is acceptable for the structure. In many cases, the assigned working load will have to be reduced or the pile be installed deeper in order to ensure that the settlement is smaller than the assigned limit. In other cases, the settlement analysis can show that the load can be increased or the piles be installed to a more shallow depth.

Be the choice of capacity definition difficult or not, most current standards and code presuppose if not outright require, that a capacity be determined from a pile loading test. Indeed, most of the time, the reason for at all carrying out a loading test is to determine the capacity of the test pile. I have since long been interested in seeing how this is reflected in the practice. On occasion, I have, therefore, disseminated pile-head load-movement curves to individuals active in design of piled foundations and asked them to

send me back what capacity the curves would represent in their opinion and by their preferred method, e.g., Fellenius 2013; 2017. Figure 8.8 shows the results from one such event, the capacity values determined by 94 individual participants in analyzing a static loading test pile-head load-movement curve on a 600-mm diameter, 10 m long bored pile in silty sand. N.B. the capacities are not predictions. They are assessed and determined from the actual load-movement curve. The variation between capacity values is not unique, but found in several similar studies.

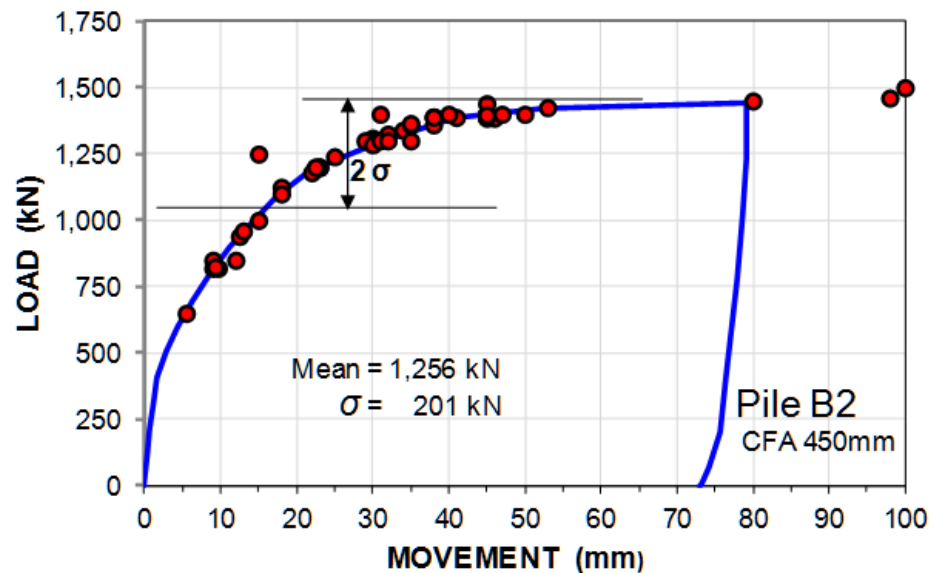


Fig. 8.8 54 capacities determined from an actual pile-head load-movement curve as assessed by 94 participants (Fellenius 2017).

It is obvious that the profession does not have a common approach to determining a pile capacity from a static loading test. I have on other occasions pursued similar studies asking participants to tell me what factor of safety (or what resistance factor) they would apply to their capacity values. The factor of safety values received have ranged from a low of 1.8 and a high of 2.5. The resistance factor have ranged between 0.65 and 0.7, a much closer span, which is because most codes encompassing the limit states design, or LRFD, do indicate the factor to apply to the capacity of a static loading test. However, the same codes do not indicate how to determine the capacity itself!

By any appreciation of the state-of-the-practice, the situation is scary. Some comfort is by the fact that, as indicated in Section 7.23, settlement is the primary aspect for a piled foundation design. Capacity is rather irrelevant and, mainly, only in the context of load-transfer.

### 8.11 Loading Test Simulation

The resistance of a pile to the load applied in a static loading test is a function of the relative movement between the pile and the soil. When calculating the capacity of a pile from the pile-head load-movement curve, the movement necessary to mobilize the ultimate resistance of the pile is not considered. However, a resistance is always coupled to a movement. In fact, to perform a static loading test, instead of applying a series of load increments, one can just as well apply a series of predetermined increments of movement and record the subsequent increases of load. For example, this is actually how the constant-rate-of-penetration test is performed. Usually, however, a test is performed by adding predetermined increments of load to a pile head and recording the subsequent pile head movement.



In a head-down static loading test, the resistance in the upper regions of the soil profile is engaged (mobilized) first. That is, the shaft resistance is engaged progressively from the pile head and down the pile. The first increment of load only engages a short upper portion of the pile. The actual length is determined by the length necessary to reach an equilibrium between the applied load and the shaft resistance (mobilized as the pile head is moved down). The movement is the 'elastic' shortening (compression) of the length of pile active in the transfer of the load from the pile to the soil. The pile toe does not receive any load until all the soil along the pile shaft has become engaged. Up till that time, the movement of the pile head is the accumulated 'elastic' shortenings of the pile. Note that the moment necessary for mobilizing shaft resistance is very much smaller than the movement necessary for mobilizing the toe resistance. If the soil has a strain-softening response, which is common, the shaft resistance may be reducing along some of the upper length even before the pile toe is engaged (See Section 7.3).

While the shaft resistance normally has a clear maximum value, the toe resistance continues to increase with increasing movement. Figure 8.9 shows a few typical shapes of resistance versus movement curves. They are not assumed to be from the same pile.

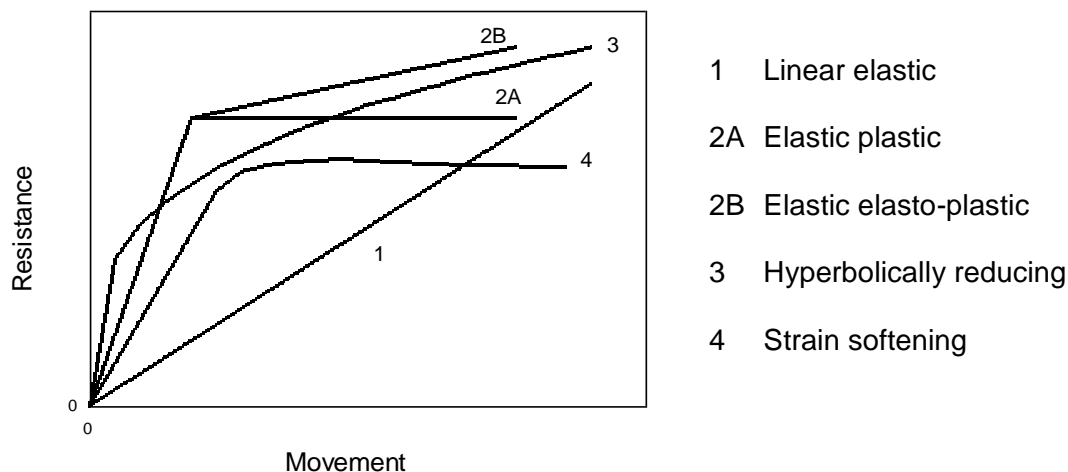


Fig. 8.9 Typical resistance versus movement curves

Resistance versus movement curves (load-movement curves) for shaft and toe resistances are called  $t$ - $z$  function for shaft resistance and  $q$ - $z$  function for toe resistance. The  $t$ - $z$  function is thought to represent the shaft resistance response of a short element along the pile, i.e., unit shaft resistance vs. movement. A  $t$ - $z$  function should be applied to the response of an element. The process has little meaning if applied to a longer length of a pile, indeed the full pile length.

The following are  $t$ - $z$ / $q$ - $z$  functions governed by a known values of ultimate unit resistance,  $r_u$ , and an assumed movement for that resistance,  $\delta_u$ , plus one additional parameter particular to the  $t$ - $z$ / $q$ - $z$  function considered. When a value of  $r_u$  has been determined in a calculation or from measurements, and a movement,  $\delta_u$ , for that value has also been either measured, or assumed, then, each of the functions will only depend on that additional parameter. In using the  $t$ - $z$ / $q$ - $z$  functions it is convenient to normalize the load to 100 % of a target load and all other measured loads set to a ratio (%) of the target load,  $r_{trg}$ .

I have compiled the various  $t$ - $z$  and  $q$ - $z$  functions in an Excel template "cribsheet" (Fellenius 2016c) that can be used to back-calculate load-movement records for a pile element and determine a suitable  $t$ - $z$ / $q$ - $z$  function as based on a single "function coefficient".

### 8.11.1 The Gwizdala (Ratio) Function

A t-z or q-z curve can be defined by Eq. 8.15 as the ratio of two resistances equal to the ratio of the respective movements raised to an exponent (Gwizdala 1996, Fellenius 1999). The function is also called the Ratio function.

$$\text{Eq. 8.15} \quad \frac{r_1}{r_2} = \left( \frac{\delta_1}{\delta_2} \right)^\theta$$

where

- $r_1$  = Resistance 1
- $r_2$  = Resistance 2
- $\delta_1$  = movement mobilized at  $r_1$
- $\delta_2$  = movement mobilized at  $r_2$
- $\theta$  = function coefficient;  $0 \leq \theta \leq 1$

Although the stress at infinite movement,  $\delta_{\text{inf}}$ , is infinitely large, an ultimate, or target, value can be defined as the load occurring at any definite or specific movement. When a target resistance and target movement are known or assumed, the shape of the t-z/q-z curve is governed by the  $\theta$ -exponent, as illustrated in Fig 8.10, showing the resistance and the movement in percent of target resistance and target movement. Notice, a custom t-z/q-z curve can be computed for resistance and movement larger than the target value.

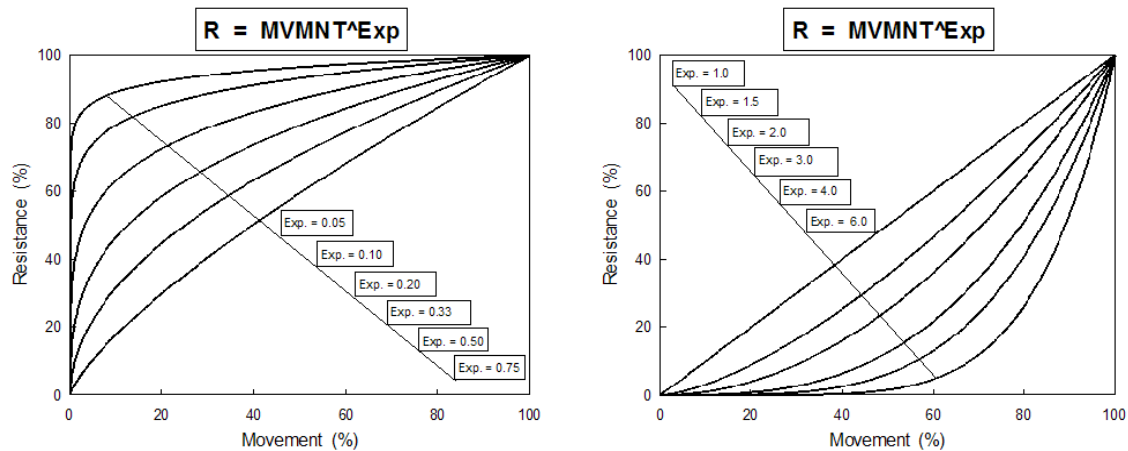


Fig. 8.109 Shape of t-z and q-z curves for a range of exponents

The Gwizdala Function t-z curve for shaft resistance and the q-z curves for toe resistance usually take different  $\theta$ -exponents. A curve with the exponent ranging from 0.05 through 0.30 is typical for a shaft resistance, while toe resistance response is closer to curves with exponents between 0.4 and 1.0. A resistance curve, shaft or toe, conforming to an exponent larger than 1.0 would be extraordinary. For toe resistance, it could be used to model a pile with a gap, or some softened zone, below the pile toe that has to be closed or densified before the soil resistance can be fully engaged. Gwizdala (1996) has suggested several relations for the  $\theta$ -exponent as a function of soil and pile type.

The symbols in Eq. 8.15 can be modified, as follows: the pair  $r_1/\delta_1$  can be set to a variable pair,  $r/\delta$ , and  $r_2/\delta_2$  be set to a "target pair",  $r_{\text{trg}}/\delta_{\text{trg}}$ . Eq. 8.15 then becomes Eq. 8.16 and shows the equation for unit resistance—shaft or toe—at a certain movement according to the Ratio Function in relation to the target resistance and target movement.

$$\text{Eq. 8.16} \quad r = r_{trg} \left( \frac{\delta}{\delta_{trg}} \right)^{\Theta}$$

where  $r$  = force variable (shaft resistance or toe stress)  
 $r_{trg}$  = target resistance  
 $\delta$  = movement variable  
 $\delta_{trg}$  = movement at  $r_{trg}$   
 $\Theta$  = function coefficient;  $0 \leq \Theta \leq 1$

(Note,  $r_{trg}$  and  $\delta_{trg}$  can be from any point on the curve, as long as they are from the same pair).

The concept of a "target", i.e., a specific value of stress and movement, is useful when matching a contiguous stress-movement response to a t-z function. Figure 8.11 shows t-z curves plotted from Eq. 8.16 assuming a Ratio Exponent,  $\Theta$ , ranging from 0.15 through 1.00 and that the curve must have a load or stress,  $r_{trg}$ , equal to 100 % of the stress that results in a movement,  $\delta_{trg}$ , set equal to 100 % of some specific movement. The two make for a  $r_{trg}/\delta_{trg}$  load/movement pair. That is, the variable is the function coefficient. Different coefficients will result in different shapes of the t-z curve, but they will all go through the target point,  $r_{trg}/\delta_{trg}$  load/movement. An coefficient of 1.0 makes the curve appear as a straight line through the target point.

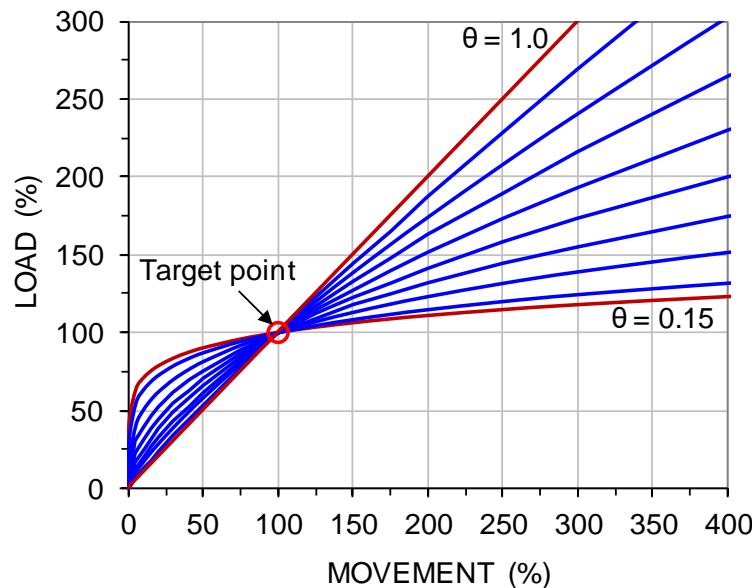


Fig. 8.11 Ratio Function for t-z shaft shear force vs. movement

### 8.11.2 The Hyperbolic Function

It is very common to find that actual test records fit a Chin-Kondner hyperbolic function (see Section 8.4) as expressed by Eq. 8.17a through 8.17c.

$$\text{Eq. 8.17a} \quad r = \frac{\delta}{C_1 \delta + C_2}$$

$$\text{8.17b} \quad C_1 = \frac{1}{r_{inf}}$$

$$\text{8.17c} \quad C_2 = \delta_1 \left( \frac{1}{r_1} - \frac{1}{r_{inf}} \right)$$

where  $r$  = shaft shear force variable (or toe stress)  
 $\delta$  = movement variable  
 $C_1$  = the slope of the line in a  $r/\delta$  vs.  $\delta$  diagram; the Chin-Kondner plot  
 $C_2$  = ordinate intercept the  $r/\delta$  vs.  $\delta$  diagram  
 $r_1/\delta_1$  = any stress/movement pair, usually a "target" pair,  $r_{trg}/\delta_{trg}$   
 $r_{inf}$  = ultimate resistance, occurring at infinite movement, which then is the  $1/C_1$ -value.

When the extrapolation to  $r_{inf}$  is less than obvious, both the  $C_1$  and  $C_2$  are best determined by plotting, from the measured data, the  $\delta/r$  values versus the measured movements,  $\delta$ , and then select an appropriate part of the plot for a linear regression calculation, which directly provides  $C_1$  and  $C_2$ , as the respective values of the slope and intercept of the regressed line. Note that  $C_2$  can be set as a function of  $C_1$  and the target pair,  $r_1/\delta_1$ . In effect, once  $C_1$  is chosen,  $C_2$  is determined (Eq. 8.17c).

Figure 8.12 shows hyperbolic t-z curves for a  $r_{trg} = 100\%$  occurring for a movement of 100 % ( $\delta_{trg}$ ) for  $C_1$ -coefficients ranging from 0.001 through 0.009 for resistances at infinite movement ( $\delta_{inf}$ ) of ten and 1.11 times that at the target resistance, respectively. That is, the input of  $C_1$  is the Chin-Kondner function coefficient and it decides the shape of the curve for the chosen 100-% target resistance and 100-% target movement.

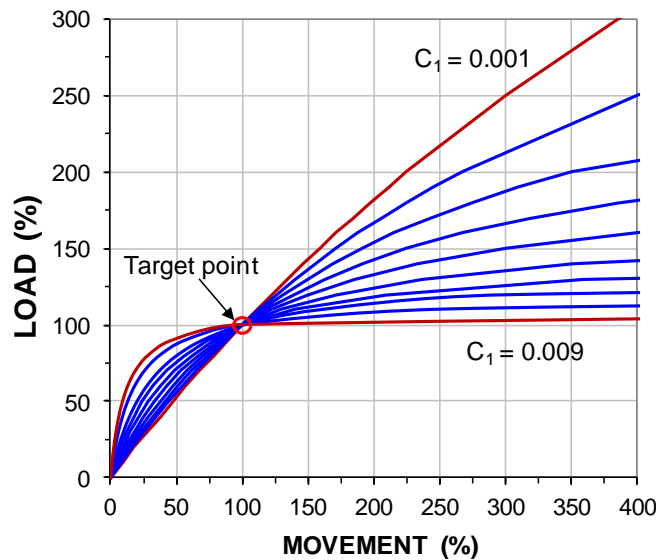


Fig. 8.12 The hyperbolic function for t-z shaft shear force vs. movement

### 8.11.3 The Van der Veen (Exponential) Function

When fitting measured stress-movement values to an elastic-plastic t-z response, sometimes the kink occurring at the change from the initial straight, sloping line (the 'elastic' line) and the final horizontal straight line (the 'plastic' line) can be disturbing. Then, the exponential fit can show to be more suitable, as given by Eq. 8.18 (Van der Veen 1953), as it provides a more rational elasto-plasto curve having a curved transition from sloping linear to horizontal linear.

$$\text{Eq. 8.18} \quad r = r_{inf}(1 - e^{-b\delta})$$

where  $r$  = shaft shear force variable (or toe stress)  
 $r_{inf.}$  = shaft shear force (or toe stress) at infinite movement  
 $\delta$  = movement variable  
 $b$  = function coefficient  
 $e$  = base of the natural logarithm = 2.718

If an infinite target resistance,  $r_{trg}$ , of 100 % is desired at and beyond a specific target movement,  $\delta_{trg}$ , then, a fit to this pair is achieved by varying the function coefficient ( $b$ ) until the curve just about reaches this target pair,  $r_{trg}/\delta_{trg}$ .

Figure 8.13 shows a t-z stress-movement curve plotted from Eq. 8.18 with the exponent,  $b$ , equal to 0.54, which will cause the curve to cross reach the 100-% target stress or load,  $r_{trg}$ , at the target movement,  $\delta_{trg}$ , of 100 %. Note, by choosing a  $C_1$ -coefficient of 0.0098 or 0.0099, the hyperbolic function can be made to show a similar almost elastic-plastic shape.

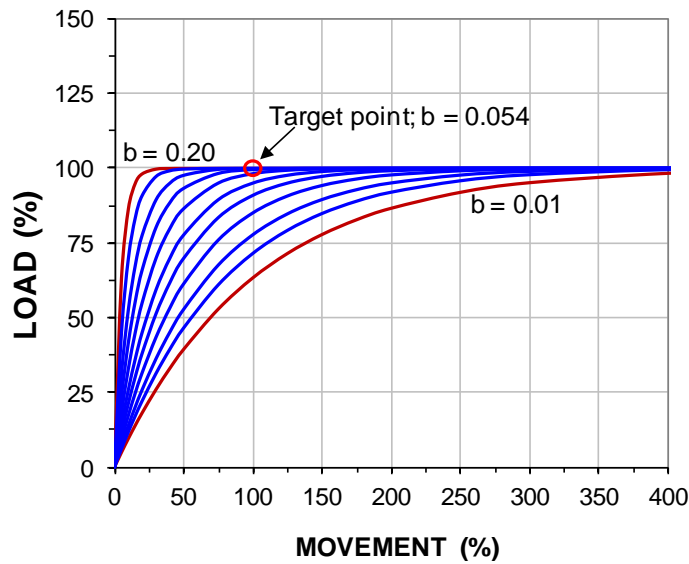


Fig. 8.13 Van derVeen exponential function for t-z shaft shear force vs. movement

#### 8.11.4 The Hansen 80-% Function

Shaft resistance often shows a strain-softening post-peak response, that is, after reaching a peak value,  $r_{peak}$ , which is the “ultimate” resistance, the resistance reduces with further movement. The Gwizdala (Ratio), Chin-Kondner (Hyperbolic), and Van der Veen (Exponential) functions are less suitable for simulating the response to the applied load for piles exhibiting strain-softening. However, the Hansen 80-% function (See Section 8.3) enables a strain-softening response to be modeled. The Hansen 80-% function is expressed in Eqs. 8.19a through 8.19e.

$$\begin{aligned}
 8.19a \quad r &= \frac{\sqrt{\delta}}{C_1 \delta + C_2} & 8.19b \quad C_1 &= \frac{1}{2r_{peak} \sqrt{\delta_{peak}}} & 8.19c \quad C_2 &= \frac{\sqrt{\delta_{peak}}}{2r_{peak}} \\
 8.19d \quad r_{peak} &= \frac{1}{2\sqrt{C_1 C_2}} & 8.19e \quad \delta_{peak} &= \frac{C_2}{C_1}
 \end{aligned}$$

where  $r$  = shaft shear force variable (or toe stress)  
 $\delta$  = movement variable  
 $C_1$  = the slope of the straight line in the  $\sqrt{\delta}/r$  versus movement ( $\delta$ ) diagram  
 $C_2$  = ordinate intercept of the straight line in the  $\sqrt{\delta}/r$  versus movement ( $\delta$ ) diagram  
 $r_{\text{peak}}$  = peak resistance, often taken as the target resistance  
 $\delta_{\text{peak}}$  = movement at the peak resistance, often taken as the target movement

Figure 8.14 shows a stress-movement curve plotted from Eq. 8.19a on the assumption that  $r_{\text{peak}} = 100\%$  is the peak stress and occurs at movement set to 100 %. ( $\delta_{\text{trg}} = \delta_{\text{peak}}$ ). This result was achieved for a  $C_1$ -coefficient equal to 0.0005 (the  $C_2$ -intercept is a function of  $C_1$  as given by Eq. 8.19c).

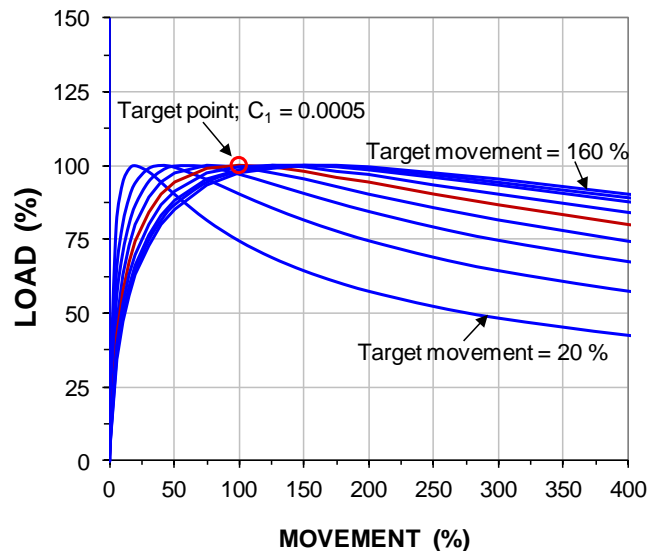


Fig. 8.14 Hansen 80-% function for t-z shaft shear force vs. movement

An input of  $r_{\text{peak}} = r_{\text{trg}} = 100\%$  and an associated movement determines the Hansen 80-% Function, that is, any target pair input fixes the shape of the curve. Therefore, the Hansen 80-% Function has a limited use with regard to fitting measured load-movement unless the target movement,  $\delta_{\text{trg}}$ , is equal to the movement for the measured peak and results in a simulated shape that is similar to that of the shape of the measured load-movement, in particular for the strain-softening part (movement beyond the target movement).

### 8.11.5 The Zhang Function

Zhang and Zhang (2012) presented an additional strain-softening function, a function leading up to a peak and reducing thereafter with increased movement, as expressed in Eqs. 8.17a through 8.17f. The  $a$ -,  $b$ - and  $c$ -coefficients are interrelated and Eqs. 8.17e and 8.17f express 'b' and 'c' as functions of 'a'.

$$8.17a \quad r = \frac{\delta(a + c\delta)}{(a + b\delta)^2}$$

$$8.17b \quad r_u = \frac{1}{4(b - c)}$$

$$8.17c \quad \delta_u = \frac{a}{b - 2c}$$

$$8.17d \quad r_{\text{inf}} = \frac{c}{r_u b^2}$$

$$8.17e \quad b = \frac{1}{2r_{\text{peak}}} - \frac{a}{\delta_{\text{peak}}}$$

$$8.17f \quad c = \frac{1}{4r_{\text{peak}}} - \frac{a}{\delta_{\text{peak}}}$$

where

$r$	=	shaft shear force variable (or toe stress)
$\delta$	=	movement variable
$r_{peak}$	=	peak resistance
$\delta_{peak}$	=	movement at peak resistance
$a, b, \text{ and } c$	=	coefficients (“ $b$ ” and “ $c$ ” are functions of “ $a$ ”)
$r_{inf}$	=	resistance at infinitely large movement (must always be $\geq 0$ )

A fit to a measured force-movement curve can be found by defining the target pair as the values of peak resistance and movement at the ultimate resistance, and fine-tuning for the ‘ $a$ ’-coefficient, letting the ‘ $b$ ’- and ‘ $c$ ’-coefficients be determined by the ‘ $a$ ’-coefficient and the target  $r_{peak}$  and  $\delta_{peak}$  values until a fit to the measured curve is achieved. In contrast to the Hansen 80-% strain-softening conditions, any target pair can be input as long as the resistance at infinite movement is larger than zero ( $r_{inf} \geq 0$ ).

Figure 8.15 shows a load-movement curve plotted from Eqs. 8.17a through 8.17f on the assumption that  $r_{peak}$  is equal to 100 % load and occurs at a movement set to 100 %. The ‘ $a$ ’-coefficient can range from 0 through 0.100. The curve with ‘ $a$ ’ = 0 is a no strain-softening case and an unrealistic case, as it would indicate a totally plastic soil response. An ‘ $a$ ’-coefficient of 0.01 represents softening to zero resistance at infinite movement. A softening to 50 % of the peak resistance ( $r_{peak}$ ) at infinite movement would be obtained using an ‘ $a$ ’-coefficient of 0.009 and its shape would then be similar to the Hansen 80%-curve shown in Fig. 8.13 (and this also beyond the 10 mm limit of the movement axis).

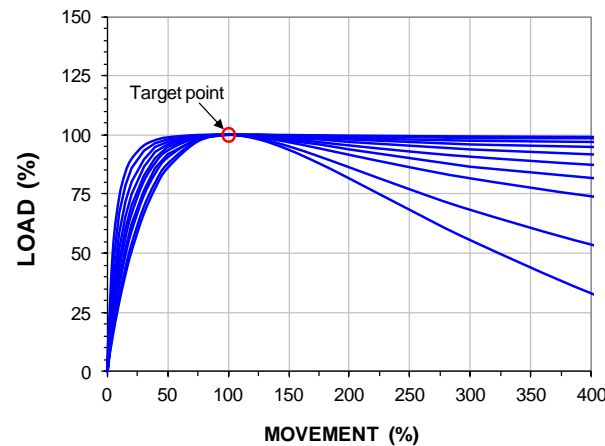


Fig. 8.15 Zhang function for t-z shaft shear force vs. movement

The shape of the Zhang Function is controlled by input of the ‘ $a$ ’-coefficient. The larger the ‘ $a$ ’, the more pronounced the strain-softening after the peak. However, the  $r_{inf}$  cannot become smaller than zero, which determines the largest acceptable input of ‘ $a$ ’ for different target movements,  $\delta_{trg}$ . Thus, for a range of target movements ranging from 1 mm through 80 mm, the ‘ $a$ ’-coefficient must be smaller than the values listed in Table 8.1. A value smaller than that listed for the particular target movement,  $\delta_{trg}$ , would infer a negative  $r_{inf}$ .

**TABLE 8.1 The upper limit of the ‘ $a$ ’-coefficient as a function of the target movement,  $\delta_{trg}$**

$\delta_{trg}$ (mm)	1	2	3	4	5	6	7	8	9	10
$a$	0.0025	0.0050	0.0075	0.0100	0.0125	0.0150	0.0175	0.0200	0.0225	0.0250
$\delta_{trg}$ (mm)	12	15	20	25	30	40	50	60	70	80
$a$	0.0300	0.0375	0.0500	0.0625	0.0750	0.1000	0.1250	0.1500	0.1750	0.2000

### 8.11.6 The Vijayvergiya Function

Vijayvergiya (1977) presented the function expressed in Eq. 8.20, which also represents a strain-softening curve. Figure 8.16 shows a series of curves per the Vijayvergiya function. When the curve is set to go through a target point, a V-coefficient is equal to 2 will make the peak force equal to the target force at the target movement. The use in practice of the Vijayvergiya function is to assume the peak stress or load is equal to the ultimate resistance and to assign a V-coefficient of 2. This disregards the fact that the function implies a strain-softening after the peak stress as opposed to a plastic (ultimate) value. Moreover, it fixes the shape and in effect claims that "one size fits all".

$$8.20 \quad r = r_{trg} \left( V \sqrt{\frac{\delta}{\delta_{trg}}} - (V-1) \frac{\delta}{\delta_{trg}} \right)$$

where

- $r$  = shaft shear force variable (or toe stress)
- $\delta$  = movement variable
- $r_{trg}$  = target resistance
- $\delta_{trg}$  = movement at target resistance
- V and N = coefficients
- N = resistance at infinitely large movement (must always be  $\geq 0$ ).

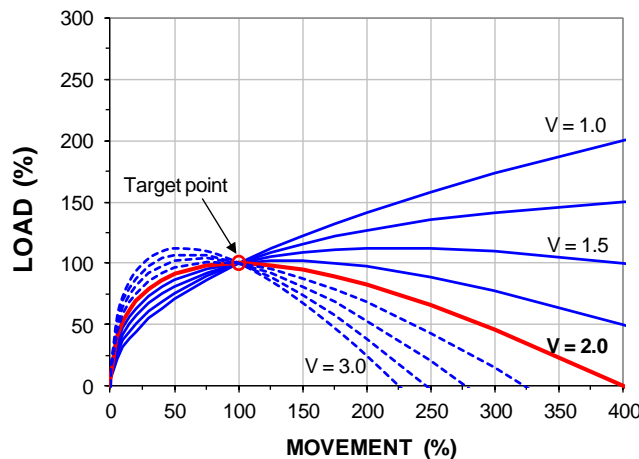


Fig. 8.16 Vijayvergiya function for t-z shaft shear force vs. movement

### 8.11.7 The Six Function Curves Compiled

Figure 8.17 shows the six function curves fitted to a measured pile-element load-movement curve. All curves are calculated using a target pair that resulted in the closest fit to the measured test data. But for the Ratio function, the target point was similar for the curves. The initial part of all six show a reasonably good fit to the test data. The best fit for the test results was obtained by the Hyperbolic (Chin-Kondner) and the Van derVeen Functions.

The Ratio Function has the built-in assumption that the resistance continues to increase with movement beyond the value perceived as the ultimate resistance, and the Hyperbolic Function implies a finite ultimate resistance, but one that occurs at an infinitely large movement. The Hyperbolic and Hansen 80-% Functions are particularly well suited for shaft resistance response. As a pile toe resistance does not show any tendency to ultimate resistance, to model its load-movement response, I have found the Gwizdala Ratio Function most fitting. Note that the fitting to a pile head-movement is rarely the same as that fitted to the individual pile elements (See Section 7.3, Fig. 7.7. Indeed, there is little sense in using load-transfer functions to back-calculate the pile-head load-movement response.



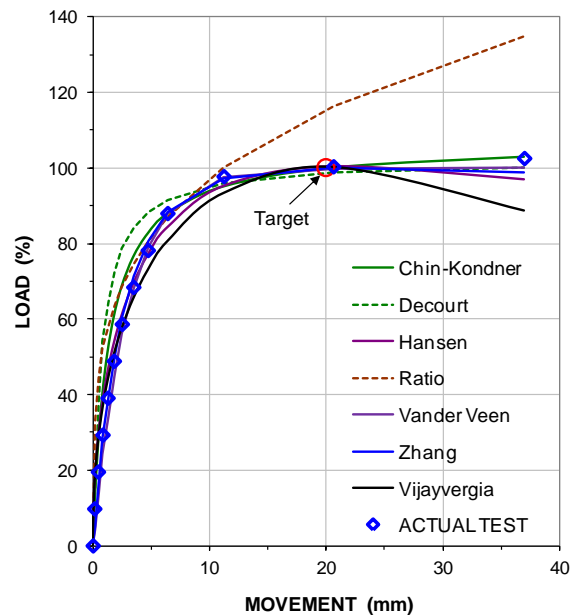


Fig. 8.17 Example of six t-z functions fitted to a load-movement curve measured for a pile element (gage location).

For shaft resistance, the t-z curve is a shear-dependent concept. Therefore, other than due to the fact that different construction procedures may have made the soil response different for small diameter piles as opposed to large diameter piles, the shaft resistance, and, therefore, also the t-z curve is qualitatively independent of the pile diameter, that is, the unit shaft resistance,  $r_s$ , and the movement,  $\delta$ , are independent of the pile diameter. However, for toe resistance, the q-z response is a deformation concept and the movement,  $\delta$ , is proportional to the pile diameter (increases with the pile diameter) for the same unit stress (see Sections 6.2 and 7.2), but its normalized value is independent of the diameter. Estimating pile toe movement by calculating it as a case of settlement of a footing in a soil of appropriate compressibility can be helpful in finding what function and function coefficient to use (the Ratio usually).

#### 8.11.8 Procedure for Fitting a Simulated Test Curve to a Measured Using t-z and q-z Functions

There is more to analyzing results of a static loading test than just determining a "capacity". A pile can be perceived as a string of short elements, each located in a soil for which the interaction of shear forces mobilized by movement follows one of the t-z functions described above and, for the pile-toe element, also a q-z function. For a routine head-down test, usually only the pile head load-movement is available for fitting a simulation to. Sometimes, the test includes a toe-telltale that indicates the toe movement albeit no pile toe force. In case of a strain-gage instrumented pile, each strain gage location (i.e., a pile element) will provide a load, but no movement (unless the instrumentation is by Glostrex system, see Section 8.14). The most useful test method for detailed analysis is the bidirectional test, because it either separates shaft resistance from toe resistance or separates the shaft resistance along the upper length of the pile (above the cell assembly) from the combined shaft and toe resistances of the lower length of the pile (below the cell assembly).

Bidirectional tests on long test piles normally include strain-gage and telltale instrumentation. Whether just from a routine head-down test or all the way to a bidirectional instrumented test, the measured load-movement response (or responses) is the primary reference to matching the simulated to measured curves in the analysis.

The analysis can be produced in a regular spreadsheet template prepared with pertinent t-z and q-z functions. However, this effort can be quite time-consuming. I have the advantage of using UniPile (Goudreault and Fellenius 2014), a commercially available software ([www.unisoftGS.com](http://www.unisoftGS.com)), and the following pertains to the use of this software.

(1) Take note of (choose) a point, a reference or a "target" load-movement pair, on the measured load-movement curve. The load-movement curve can be that of the pile head, or the upward or downward loading direction of a bidirectional cell (Section 8.15), or a strain-gage determined or telltale determined load-movement pair. There is usually a distinct level of load and movement that you feel is where the pile entered a "failure" mode. It usually would not be for the maximum test load, i.e., not the last load-movement pair; a load-movement pair from where the movements are very large is rarely the best target to use in a fitting of a simulation to the test curve.

(2) Start the analysis by building a UniPile file with the appropriate pile details, the soil profile (soil layer thickness and densities), groundwater table (pore pressure distribution also, if non-hydrostatic), and other factors, such as loads and excavations, which influence the effective overburden stress distribution near the test pile. Then, apply an effective stress to find what beta-coefficient(s) or unit shear value(s) that will fit (return) the chosen target load (Chapter 7). The analysis results in the load distribution, i.e., the axial load versus depth for the chosen target load. The relevance of the various beta-coefficients or unit stress values that gave the fit depends on the complexity of the soil profile and the relevance of the input parameters. The procedure applies also to total analysis, but because total stress analysis does not consider important aspects, such as effect of excavated or filled areas and pore pressure distribution, it is less realistic and, therefore, best avoided.

(3) Choose the target movements for the pile elements considering the movement of the measured (the reference) target pair and the fact that the movements reduce with the distance from the load generator, the hydraulic jack. That is, the movement of target pair of the considered pile element may be smaller than that of the reference target pair on the pile-head load-movement curve. Then, choose a t-z function and let the software simulate the reference load-movement curve. The software assumes that the target force is always 100 % of the force calculated for the input beta-coefficient that gave the load-distribution fit for the string of pile elements. However, this calls for a special twist when using the Van der Veen Function (the Exponential). The analysis presupposes that the resistance target value,  $r_{trg}$ , is 100 %. But, if the input of target movement,  $\delta_{trg}$ , is chosen to, say, 4 mm, the initial rise of the exponential curve becomes unrealistically steep. To alleviate this, i.e., to simulate a less steep initial rise, it is advisable to input a larger target movement. At 4 mm movement, the load will still be very close to the 100-% value.

The actual fitting to the load movement curve is done by choosing t-z and q-z functions (curves) and assigning them to the soil layers by trial and error. The effort can be quite time-consuming. However, a fit to the target pair on the reference load-movement curve is relatively quickly obtained by astute selections of distribution of beta-coefficients for the different soil layers and pile-toe stress and, foremost, suitable t-z and q-z functions. Once that is achieved, take note of one or two points on the measured curve and see what t-z and q-z function to choose and what of the various shape-determining coefficients to input. Through a series of trial-and-error runs a good fit between the simulated load-movement curve and the measured reference curve will eventually be achieved. The larger the number of soil layers and the length of the pile, the more time-consuming the effort. A piece of advice: when you change a function input, **change only one parameter at a time** and check the results in a trial run before attempting the next change.

When the fit is established, the software can estimate the residual force considered present in the pile before the test and allow make adjustment for this to be made in calculating the pile-toe load-movement.

### 8.12 Effect and Mechanism of Residual Force

The load-movement of a pile head consists of three components: the load-movement of the shaft resistance, the compression of the pile, and the load-movement of the pile toe. The combined load-movement responses reflects the relative magnitude of the three. Moreover, only the shaft resistance may exhibit an ultimate resistance. The compression of the pile is a more or less linear response to the applied load and does not have an ultimate value (disregarding a structural failure were the load to reach the strength of the pile material). However, the load-movement of the pile toe is also a more or less linear response to the load and has no failure value. Therefore, the concept of an ultimate load, a failure load or capacity is really a fallacy and a design based on the ultimate load is a quasi concept, and of uncertain relevance for the assessment of the suitability of a piled foundation design.

The above statement is illustrated in Figure 8.18 which presents the results from a test on a 15 m long, 600 mm diameter, jacked-in concrete pile (Fellenius 2014). The test included measuring the total shaft and the toe resistances versus the movement in a heads-down static loading test (all axial loads in the pile were assumed zero at the start of the test). The test reached a peak load (6,500 kN) at an about 20-mm movement of the pile head and then test was continued in a plunging mode. The maximum toe movement was 60 mm. Because the installation was by jacking, a considerable residual force was present in the pile at the start of the static test. At the peak load, the shaft resistance response (as assumed induced in the test) and the load at the pile toe were 5,300 kN and 1,200 kN, respectively. Figure 8.19 shows the load-movement curve that would have been measured had the pile not had any residual force. The Davisson Offset Limit and the pile head movement for a 30-mm toe movement are indicated in both figures. Both simulation alternatives are obtained using the UniPile software (Goudreault and Fellenius 2013).

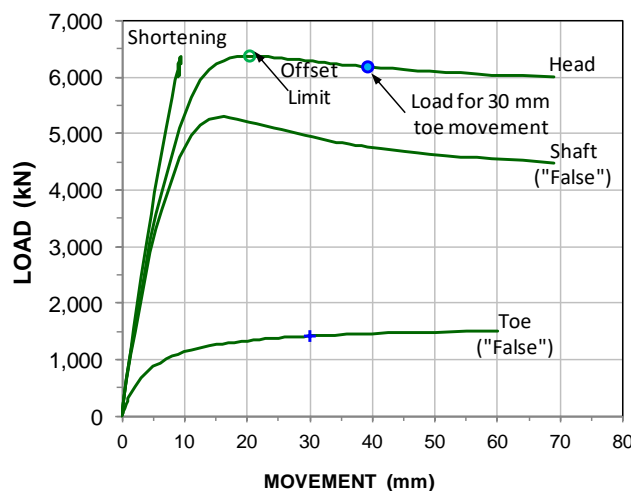


Fig. 8.18 Pile with residual force

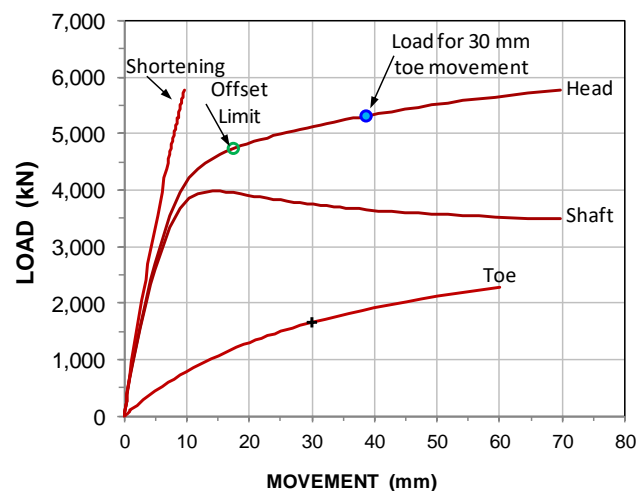


Fig. 8.19 Same pile without residual force

For a pile where the shaft resistance response is strain-softening, the ultimate shaft resistance for each pile element is the same whether or not there is any residual force. The larger shaft resistance shown in the first figure is just apparent—indeed "false". For the toe resistance, the measurements do not include the residual toe force, which means that the measured pile toe load-movement is too small and "false". The second diagram shows the "true" shaft and toe resistance curves. By whatever definition of capacity, the residual force will have had the effect of indicating a larger capacity than that found if the residual force would not be present, or be accounted for in the test evaluation.

Generally, presence of residual force will result in an overestimation of pile capacity, overestimation of shaft resistance, and a corresponding underestimation of the toe resistance. Indeed, the residual force can even cause the records to indicate—falsely so—a tendency for ultimate toe resistance!

The pile toe load-movement response is an obvious enhancement of the test results. However, this response must recognize that some residual force will always develop in a pile, a driven pile in particular. Therefore, at the start of the static loading test, the pile toe is already subjected to load and the toe load-movement curve will display an initial, steep reloading portion. Depending on the magnitude of the residual force, the measured toe response can vary considerably. For examples and discussion, see Fellenius (1999).

A static loading test on a pile that has developed residual force is subjected to negative skin friction along the upper length of the pile. The loads applied to the pile head in the test will begin by reducing the negative skin friction and, then, start mobilizing positive shaft resistance. The mechanism is a part of a shaft hysteresis loop illustrated in Figure 8.20 showing the mobilized shaft shear versus the movement between the pile and the soil. When no residual force is present in the pile at the start of the test, the starting point is the origin, O, and the shaft shear is mobilized along Path O-B and on to C. Residual force develops as negative skin friction along Path D-A (Point D is assumed to be the origin of the onset of residual force). In a subsequent static loading test, the shaft shear is mobilized along Path A-O-B. However, if the presence of residual force is not recognized, the path will be thought to be along the dashed path A-B. If Point B represents fully mobilized shaft resistance, then, the assumption of no residual force in the pile will indicate a "false" resistance that is twice as large as the "true" resistance. The relative movement will be only slightly larger than the virgin movement would have been. Note that the unloading along Path B-D is given the same shape as the unloading along Path A-O; one is the inverse of the other. Similarly, the loading along Path D-A has the same shape as the loading along Path O-B; again, one is the inverse of the other. In a real case, these shapes need not be fully identical.

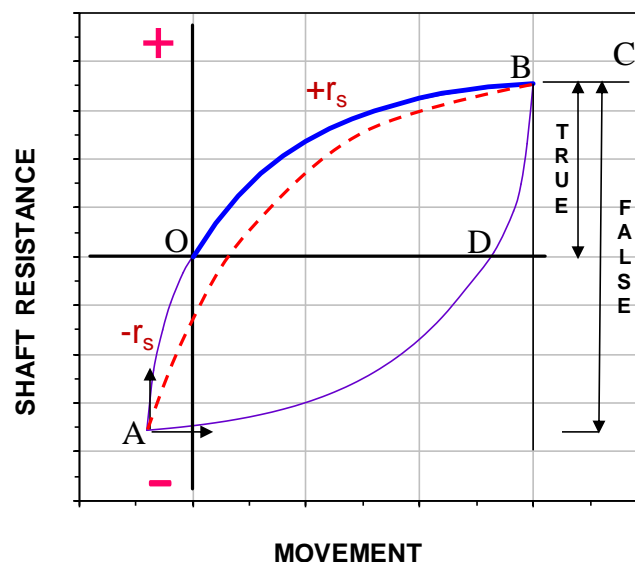


Fig. 8.20 Hysteresis loop for the shaft resistance mobilized in a static loading test

The figure makes it clear that not recognizing that residual force is present in the test pile, will lead the analysis to obtain a larger than true shaft resistance for the test pile. It should be noted that an advantage of performing a bidirectional test as opposed to a head-down test is that the loads determined in a bidirectional test will be "true" loads, that is, the values determined by the bidirectional cell are independent of any presence of residual force.

Figure 8.21 illustrates the typical the pile toe response. Similar to the shaft resistance development, when no residual force is present, the mobilization of the toe resistance is along Path O-B and on to C. When the pile construction has involved an unloading, say, at Point B, per the Path B-D'-A, the reloading in the static loading test will be along Path A-D-B-C. Unloading of toe load can occur for driven piles and jacked-in piles, but is not usually expected to occur for bored piles (drilled shafts). However, it has been observed also in bored piles, in particular for test piles which have had additional piles constructed around (near) them and for full-displacement piles. If the presence of residual toe force is not recognized, the reloading path will be thought to represent the pile toe response and not only will the toe resistance be underestimated, the shape of the toe load-movement response—the q-z curve—will be misinterpreted. For example, the break in the reloading curve at Point B can easily be mistaken for a failure load and be so stated.

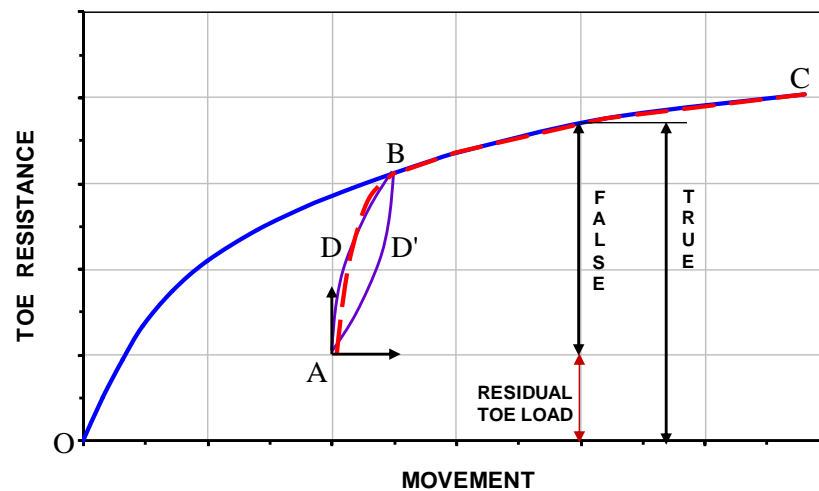


Fig. 8.21 Pile toe response in unloading and reloading in a static loading test

### 8.13 Instrumented Tests

Our profession is gradually realizing that a conventional static "head-down" loading test on a pile provides limited information. While the load-movement measured at the pile head does establish the "capacity" of the pile (per one definition or other), it gives no quantitative information on the load-transfer mechanism (magnitude of the toe resistance and the distribution of shaft resistance). Yet, this information is what the designer often needs in order to complete or verify a safe and economical design. Therefore, frequently, the conventional test arrangement is expanded to include instrumentation to obtain the required information. Instrumentation can consist of telltales and strain-gages.

#### 8.13.1 Telltale Instrumentation

The oldest and simplest, but not always the cheapest, method of instrumenting a test pile is to place one or several telltales to measure the shortening of the pile during the test. The measurements can be used to determine the average load in the pile. Two telltales placed with tips at different depths in the pile provide three values of average load: each gives an average load over its length and the third value is the shortening over the distance between the two telltale tips (as the difference between the two full-length values). Similarly, three telltales provide six values. The most important telltale is the one that has its tip placed at the pile toe, because it provides the pile toe movement (by subtracting the shortening of the pile from the pile head movement).

To emphasize, when using a telltale value for determining average load, the shortening must be measured directly and not be determined as the difference between movement of telltale tip and pile head

movement. This is because extraneous small movements of the reference beam always occur and they result in large errors of the shortening values. If you do not measure shortening directly, forget about using the telltale data to estimate average load.

Telltale rods are usually small diameter rods installed inside guide pipes. Installing such telltales properly is not a simple task. There must be no friction along the length because the friction will cause random shortening of the telltale adversely affecting the measurements. This means that the guide pipe must be straight. Friction can be reduced by having the annulus between the telltale and the guide pipe filled with oil. When installing the telltale, it should be installed by one rod at a time spliced onto the rod string as the telltale is lowered. The telltale must not be assembled on the ground and then hoisted above the pile for insertion, as this will invariably cause kinks in the telltale and make the telltale rod push against the guide pipe with undesirable friction adversely affecting the records.

The simplest telltale addition to a test is a single telltale to the pile toe to record the pile toe movement, which is an addition to a static test that greatly enhances its value. A modern type of telltale system is to use an anchor at the pile toe connected with tensioned wires which elongation or shortening is recorded using a vibrating-wire sensor. Of course, neither the rod telltale nor the anchor extensometer is restricted to being the only such in a test pile.

Telltale rods should always be installed to measure pile shortening directly. When two telltales are installed to different depths in a pile, the induced strain is obtained by calculating the difference in shortening between the two telltales and dividing this with the length between them and the pile cross sectional area to obtain the average strain at between the two telltale points (tips). Then, provided the telltale length considered is at least 5 m, the commonly used 0.001 inch or 0.01 mm dial-gage reading gradation usually results in an acceptable value of strain over the telltale length. It is futile to try to expect that telltale measurements can be accurately converted to load in the pile. However, they can serve as back-up records.

Fig 8.22 presents the results of a static loading test performed on a 20 m long pile instrumented with a telltale to the pile toe for measuring the pile toe movement. The pile toe load was not measured. The figure includes the pile compression (“COMPR.”). The load-movement diagram for the pile head shows that the pile clearly has reached an ultimate load. In fact, the pile “plunged”. Judging by the curve showing the applied load versus the pile toe movement, it would appear that also the pile toe reached an ultimate resistance—in other words, the toe bearing capacity was reached. However, this is not the case.

Most of the shaft resistance was probably mobilized at or before a toe movement of about 2 mm to 3 mm, that is, at an applied load of about 2,500 kN. At an applied load beyond about 3,300 kN, where the movements start to increase progressively, the shaft resistance might even have started to deteriorate (strain softening). Thus, approximately between pile toe movements of about 3 mm to about 10 mm, the shaft resistance can be assumed to be fully mobilized and, conservatively assumed, be approximately constant. An adjacent test indicated that the ultimate shaft resistance of the pile was about 2,000 kN. When subtracting the 2,000 kN from the total load over this range of the measured toe movement, the toe load can be estimated. This is shown in Figure 8.23, which also shows an extrapolation of the toe load-movement curve beyond the 10-mm movement, implying a strain softening behavior of the pile shaft resistance. Extrapolating the toe curve toward the ordinate indicates the existence of a residual force in the pile prior to the start of the static loading test.

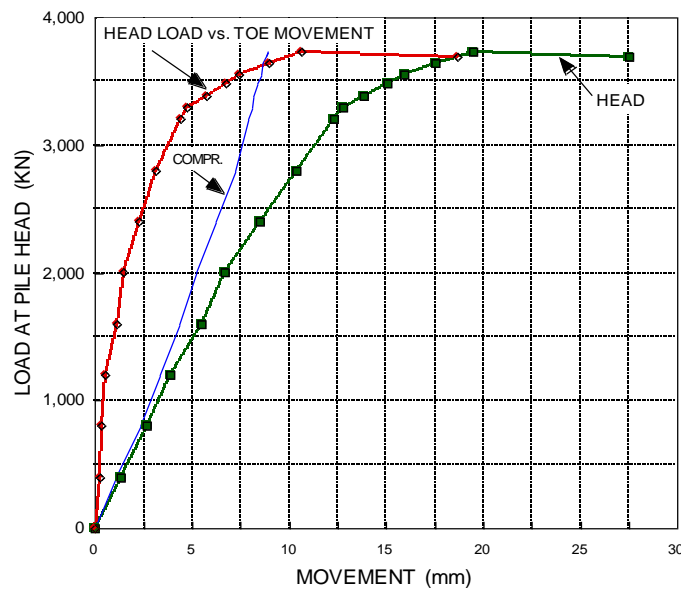


Fig. 8.22 Load-movement diagram of a static loading test on a 20 m long, 450 mm diameter closed-toe pipe pile in compact sand with telltale measurements of toe movement (Fellenius 1999)

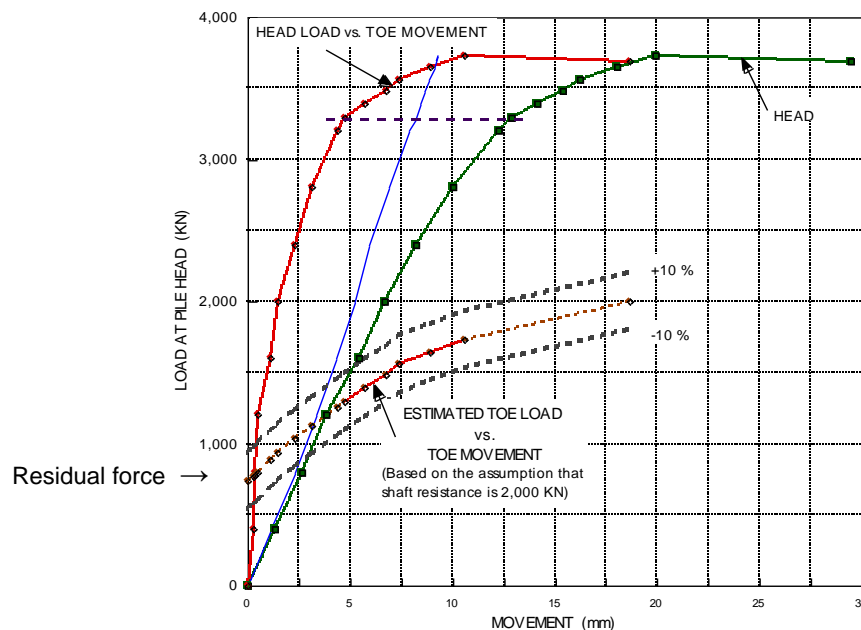


Fig. 8.23 The same test data shown in Fig. 8.22 with the results of analysis of the load-movement of the pile toe. The results from a static loading test on an adjacent pile instrumented with strain-gages indicated that the shaft resistance would be about 2,000 kN (Fellenius 1999).

### 8.13.2 Determining Load Distribution from Telltale Measurements

The main use of the average load in a pile calculated from a telltale, or the average loads if several telltales are placed in the pile, is to produce a load distribution diagram for the pile. The shortening caused by the applied load divided by the telltale length is the induced strain. That strain multiplied with the pile

stiffness,  $EA$ , is the average load over the telltale length. The distribution diagram is determined by drawing a line from the plotted value of load applied to the pile head through plots of each value of average load calculated for that applied load. Case history papers reporting load distribution resulting from the analysis of telltale-instrumented pile loading tests invariably plot the average loads at the mid-point of each telltale length considered. But, is that really correct?

Although several telltales are usually placed in the pile, even with only one telltale in the pile (provided it goes to the pile toe), we can determine an axial load distribution line or curve for each load applied to the pile head. As the toe telltale supplies the pile toe movement for each such distribution, the data establish the pile toe load-movement curve, which is more useful than the pile head load-movement curve.

If the average load is determined in a pile that has no shaft resistance—it acts as a free-standing column—it the load distribution is a vertical line down from the applied load; the applied load goes undiminished down to the pile toe. In a pile, however, the load reduces with depth due to shaft resistance. Assuming that the unit shaft resistance is constant and equal to a value, " $a$ ", along the pile, then, the total shaft distribution increases linearly down the pile and the load distribution is a straight line from the load applied the pile head down to the pile toe, as shown by the three diagrams in Figure 8.24 for a telltale with length, " $h$ ".

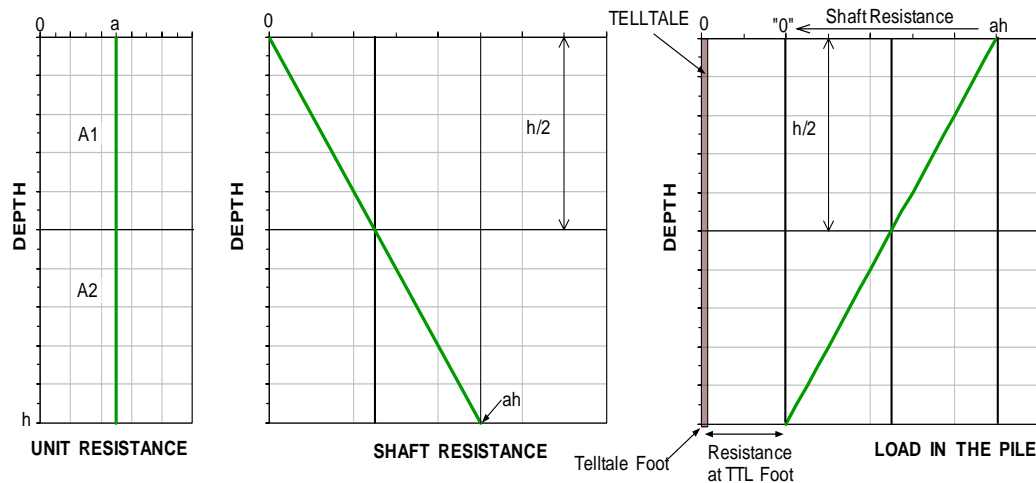


Fig. 8.24 Load distribution for constant unit shaft resistance

The straight-line load distribution line crosses a vertical line drawn through the average load at mid height of the telltale (or the mid height of the pile). The two areas,  $A_1$  and  $A_2$ , separating by a line are equal and the average load should be plotted at mid height of the telltale length.

Let us assume a more realistic distribution of the unit shaft resistance, one that increases linearly with depth, such as a unit shaft resistance proportional to the effective overburden stress. Figure 8.25 shows the same three types of diagrams as in the previous figure, one with unit shaft resistance ( $a_z$ ) versus depth ( $z$ ), one with total shaft resistance increasing to  $ah^2/2$ , and one showing the load distribution versus depth. For reference, the diagrams include the lines, dashed, for constant unit shaft resistance. The unit shaft resistance is a line proportional to the effective overburden stress and the shaft resistance and load distribution curves are the result of the integration of the unit shaft resistance. As in the previous figure, the two areas,  $A_1$  and  $A_2$ , are equal and, therefore the total shaft resistance represented by the two areas must be equal, which determines the depth to where the applied load has reduced to half—the definition of average load. The depth is at  $1/\sqrt{2}$  of the telltale length,  $h$ . That the average value should be plotted at the point  $h/\sqrt{2} = 0.70h$  is not trite matter. The incorrect representation of the average load entails more shaft resistance in the upper portion of a pile and less in the lower portion. The error has contributed to the “critical depth” fallacy.



As indicated in the load distribution diagrams of the two figures, for a telltale starting from the pile head, the applied load minus two times the difference to the average load represents the load at the telltale foot regardless of the unit shaft resistance being assumed constant or linearly increasing. Thus, a single telltale from the pile head will indicate two load values in the pile: one for the average value and one at the telltale foot. Combined with the telltale-determined movement of the pile toe, the toe telltale provides the pile-toe load-movement response, a very useful record for the analysis of the pile response.

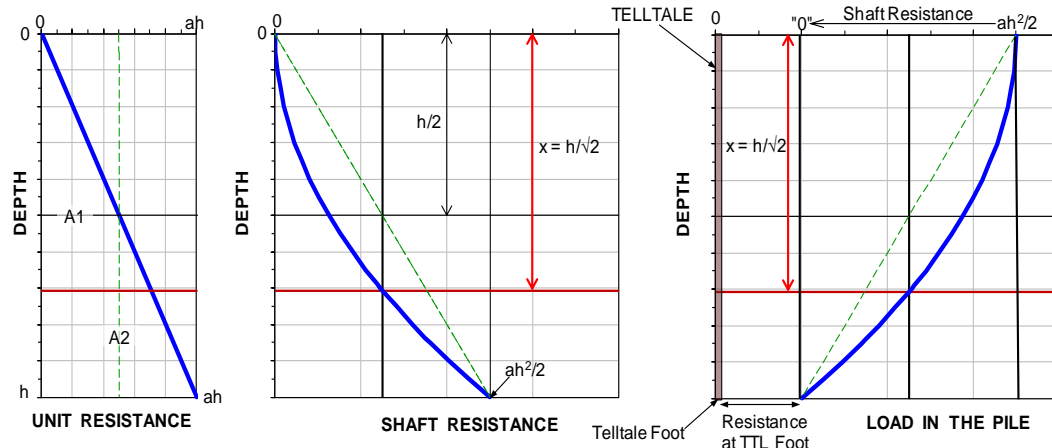


Fig. 8.25 Linearly increasing unit shaft resistance and the resulting non-linear load distribution

If two (or more) telltales (different lengths) are used, the difference in shortening between the two telltales represents the shortening of the length (e.g., "d") between the shorter telltale foot and the longer telltale foot. The load calculated from the shortening difference should be plotted at  $d/\sqrt{2}$  distance below the foot of the shorter telltale. Note, however, that a telltale measurement always includes an error. The error in the calculated load is normally small in relation to the measured shortening. However, as also the difference of shortening between values from two telltales can sometimes be small, the error that was negligible for the single value can then become large for the combined value.

The possibility, and often also the probability, of the data having been incorrectly plotted and analyzed is a good thing to keep in mind when consulting old case histories. When producing results to go into new case histories, use vibrating wire strain gages or extensometers rather than telltales rods for determining load. A telltale rod to the pile toe is always good to include, however.

As mentioned, these days, telltales consist of extensometers attached to anchors rather than telltale rods. Such gages provide better accuracy and enable more reliable values. Records from two or more extensometer anchors can be combined, as used in the Glostrex system (see Figure 8.26), which combines several anchors in a string so that the shortening (and, therefore, both strain and load) are measured between anchor points at short distances distributed down the pile (Hanifah and Lee 2006).



Fig. 8.26 A Glostrex anchor placed down in a cylinder pile (Hanifah and Lee 2006; with permission)

### 8.13.3 Brief Notes on Strain-Gage Instrumentation

Most instrumentation in a test pile comprise a system consisting of vibrating-wire strain-gages or electrical resistance gages. Attaching single-level gages to a rod that is connected to a reinforcing cage placed in the pile before concrete is placed or a rod pushed into the concrete immediately after it is poured makes for an inadequate instrumentation; one not suitable for detailed analysis. That is, not unless it can be assured that each gage is placed exactly in the center of the pile, e.g., by means of a Glostrex anchor system in pipe pile or a cylinder pile, or in a center pipe carefully cast into a prestressed concrete pile. A gage level must have a pair of gages placed diametrically opposed at equal radial distance from the center in order to compensate for axial bending of the pile—unavoidable and with significant effect even when small. If one of the two gages making up a pair is damaged, then the other one is not useful and must be discarded.

Having three gages, all functioning well, at each gage level would seem to improve accuracy of measurements. Yes, it does, however, the improvement is only marginal. It would also seem to add redundancy to the measurements, but that is incorrect. If one of the three gages would "die", then the other two cannot be trusted and their measurements must be discarded. Thus adding a third gage has reduced the redundancy. If redundancy is desired, then, use two pairs at each gage level, not three single gages.

Figure 8.27 illustrates how bending can affect strain-gage measurements during a static loading test and shows the importance of always discarding the "surviving" gage of a pair where one of the pair has "died". The records are shown as applied load plotted versus measured strain as taken from a gage level comprising two gage pairs, Pair A and C and Pair B and D. The gages of each pair were placed diametrically opposed in a bored test pile. Both pairs functioned well in the test. As indicated, the average of Pairs A&C and B&D, as well as of all four gages gave essentially the same average load-curve. However, if we assume that Gage B "died", then the average of the "surviving" gages, A&C and D, is quite off the true curve, about  $100 \mu\epsilon$  at the maximum load, as would the records showing the average of Gages A&C and B had Gage D been the gage that died, instead, but 'the other way'. And, had the average been taken by combining one "surviving" gage in each pair, the resulting error would have been even larger. The magnitude of the about  $100 \mu\epsilon$  error for the illustrated case should be considered in the light of the fact that the average strain for the maximum load was about  $400 \mu\epsilon$ .

Vibrating wire strain-gages are designed with a wire tensioned between two supports attached to a common base. When the base elongates due to an outside force, the wire tension changes, which changes the frequency of the wire. A magnet is placed close to the wire and can be excited to "pluck" the string and then to pick up the frequency of the vibrations. The vibrations are calibrated to the strain in the base letting the frequency reading tell the strain change imposed. To function properly, the metal of the string and of the supports and the base must have the same thermal coefficient, which makes the gage insensitive to temperature as long as the temperature is the same over the entire gage. To further ensure maximum precision, the last step in the manufacture is annealing the gage to remove potential internal stresses. Temperature insensitivity is very important for gages placed in a concrete pile as the temperature in the ground before the pile is installed is usually quite different to that in the ground. Moreover, the hydration of the concrete can raise the temperature to close to the boiling point, and the subsequent cooling can take many weeks and may not have completed before the static test starts. Because concrete and steel have dissimilar thermal coefficients (for concrete, the coefficient depends on the type of mineral used for the ballast portion), the cooling may introduce strain in the gages that has no relation to a shear strain between the pile and the soil. The reading precision of a vibration wire gage is  $1 \mu\epsilon$ , which means that any error of load calculated from strain measurements depend on other factors than the gage performance, such as unknown pile modulus and pile area as well as error in the value of the applied external load. Note also that strain-gage measurements, although not the gage itself, are affected by presence of residual force.

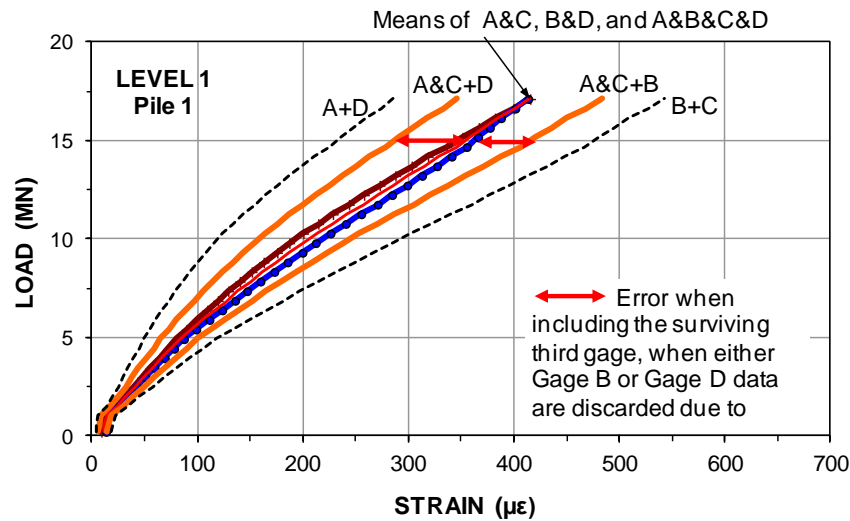


Fig. 8.27 Strains measured in four strain-gages—two pairs—with averages of the pairs and of all four gages (from Fellenius and Tan 2012)

The vibrating wire is commonly supplied as a "sister bar" which is the name used for a gage (factory-attached) to a small diameter, about 1 m long rebar that can be properly tied to a reinforcement cage to ensure that the gage will not tilt during the construction. Attaching the actual vibrating wire gage, an about 50 to 100 mm long piece, directly to the reinforcing cage provides much less assurance of avoiding tilting of the gage. Actually, if a tilt occurs, it will result in the gage records being significantly off and the evaluation of the records can become rather misleading.

#### 8.14 The Bidirectional Test

It is difficult to determine the magnitude of the portion of the applied test load that reaches the pile toe. Even when a strain-gage pair is placed at the pile toe and a telltale is used to measure the pile toe movement, interpretation of the data from a conventional "head-down" test is complex. While the portion of the applied load reaching the pile toe ostensibly can be determined from the strain-gage measurement, the actual load is often not known due to a residual force present at the pile toe already before the start of the static loading test. Then, the pile cross section and the E-modulus of the pile at the gage location may not be known correctly, which will throw off the load evaluation.

The difficulty associated with wanting to know the pile-toe load-movement response, but only knowing the pile-head load-movement response, is overcome in the bidirectional test, which incorporates one or more sacrificial hydraulic jack-like device(s) placed at or near the toe (base) of the pile to be tested (be it a driven pile, augercast pile, drilled-shaft pile, precast pile, pipe pile, full-displacement pile, H-pile, or a barrette). Early bidirectional testing was performed by Gibson and Devenny (1973), Amir (1983), and Horvath et al., (1983). About the same time, an independent development took place in Brazil (Elisio 1983; 1986), which led to an industrial production offered commercially by Arcos Egenharia Ltda., Brazil, to the piling industry. In the late 1980s, Dr. Jorj Osterberg also saw the need for and use of a test employing a hydraulic jack arrangement placed at or near the pile toe (Osterberg 1998) and established a US corporation called Loadtest Inc. to pursue the bidirectional technique. When Dr. Osterberg in 1988 learnt about the existence and availability of the Brazilian device, initially, the US and Brazilian companies collaborated. Outside Brazil, the bidirectional test is now called the "Osterberg Cell test" or the "O-cell test". During the about 30 years of commercial application, Loadtest Inc. has developed a practice of strain-gage instrumentation in conjunction with the bidirectional test, which has vastly contributed to the international knowledge and state-of-the-art of pile response to load.

Figure 8.28 shows a schematic picture of the bidirectional test. The hydraulic system is filled with water. When hydraulic pressure is applied to the cell—the hydraulic jack—it expands, pushing the shaft upward and the toe downward. In addition to the cell pressure, which is calibrated to applied load, the test incorporates movement measurements: telltales extending from the cell top plate to the ground surface to measure the shortening of the pile above the cell, and, when adjusted to the upward movement of the pile head, the measurements provide the upward movement of the cell top plate in relation to the soil. The separation of the top and bottom cell plates is measured by displacement transducers placed between the plates. The downward movement of the cell base plate is obtained as the difference between the upward movement of the top plate and the cell plate separation. Finally, an additional set of telltales measures the pile toe movement.

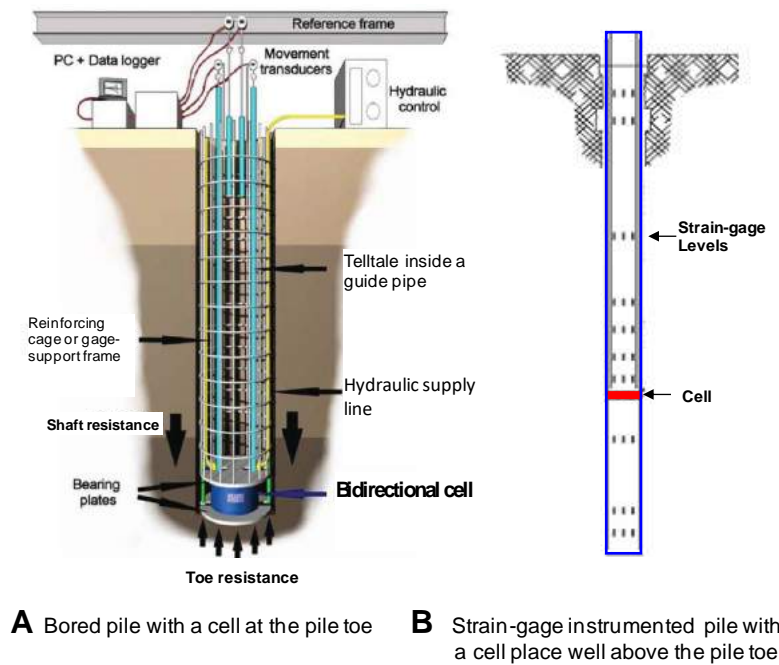


Fig. 8.28 Pile with bidirectional cell (from Loadtest Inc. flier with permission)

The test consists of applying load increments to the pile by means of incrementally increasing pressure in the cell and recording the resulting plate separation, toe movement, and pile head movement. The upward and downward load-movements do not represent equal response to the applied load. The upward load-movement is governed by the shear resistance characteristics of the soil along the shaft, whereas the downward load-movement is governed by the compressibility of the soil below the pile toe (for a cell placed near the pile toe). The fact that in a conventional “head-down” test the shaft moves downward, while in the bidirectional test it moves upward, is of no consequence for the determination of the shaft resistance. Shaft resistances in the upward or the downward (positive and negative) directions are equal.

The cell assembly is built with an internal bond between the plates, the cell cover is welded to the bottom plate, construction feature that enables the cell assembly to be attached to the reinforcing cage and lowered with it into the pile. At the test start, pressure is applied to the cell to break the bond and, also, to create a horizontal fracture zone that separates the pile into an upper and lower length, which, respectively, are pushed upward and downward by the cell pressure applied in the test. The bond-breaking pressure (load) is usually small, only affecting the pile and soil nearest the bidirectional cell level. Theoretically, when the water pressure gets to affect the pile cross section at the cell level, the strain gages should react to the so imposed hydraulic force. The force is usually too small to result in any appreciable strain change, however.

At the start of the test, the pressure in the cell is zero and the axial load (“pre-existing” load) in the pile at the cell level consists of the buoyant weight of the pile plus any residual force in the pile. This load is carried structurally by the cell assembly and the pile structure. The first pressure increments transfer the “pre-existing” axial load to pressure in the cell hydraulic fluid. The completed transfer of this load to the cell pressure is when the cell top and bottom plates start to separate, opening the cell.

The cell system is saturated by supplying water to the cell-pressure pipe (water is normally the hydraulic fluid used for the test). The water in the cell-pressure pipe results in a hydrostatic pressure at the footprint area of the cell portion of the cross section. A water-filled pipe from the ground surface to the cell level ensures that the hydrostatic pressure (pore pressure) acts on the cross section of the pile outside the cell area as soon as the two plates have separated by a minute distance. The phreatic height of the pore water in the soil at the cell level is usually not significantly different to the distance to the groundwater table and, therefore, before the start of the test, the water pressure in the cell is about the same as the pore pressure in the ground at the cell level.

For a strain-gage instrumented pile, there are three sets of key readings to obtain and document in the test report. The first set is the reading of all gages including telltales, usually considered the “zero” reading, taken immediately before adding any pressure to the cell. The second set is the readings—several—taken during the breaking the bond (the seal) between the cell plates. The third set is the readings—several—during and after unloading from the bond breaking, if now the pile is unloaded after the breaking of the bond, as opposed to going to the first load step (increment) directly.

Before the cell pressure can impose a change of the load in the pile, the weight of the pile must be transferred to the load cell. Moreover, on breaking the bond and obtaining the minute first separation of the cell plate, the pile becomes subjected to a hydraulic force, equal to the pore pressure at the cell location and equal in the upward and downward direction. For the upward directed force, the hydraulic force is combined with the pile weight into the buoyant pile weight which is subtracted from the cell load in determining the load that is moving the pile upward and engaging the pile shaft resistance. For the downward directed force, the water force can be considered as an addition to the cell load. (It can be assumed acting on the full cross section of the pile, i.e., the area of the cell assembly is included, because the cell pressure manometer is usually up on the ground and the pressure at the cell level includes the hydrostatic pressure of the water column between the pressure gage and the cell level). However, the water force is countered by the pore pressure at the pile toe exerting an upward similar force. The water force should therefore be included in determining the actual downward force in the pile.

Theoretically, the cell load minus the pile buoyant weight versus the upward movement is the load-movement curve of the pile shaft. However, similar to the case of a conventional head-down test, compensation for the pile weight is usually not taken into account in the analysis for shaft resistance and pile capacity—a debatable fact for both types of test. The cell load versus the downward movement is the load-movement curve of the cell bottom plate, that is of the pile toe, if the bidirectional cell would be located at or near the pile toe (strictly, it is the load-movement of the shaft length below the cell level and the pile toe in combination). The advantage of measuring load-movement response of the pile shaft separately from that of the pile toe is not available for a conventional, head-down, static loading test.

If residual force is present in the pile, it affects the initial shape of the upward and downward load-movement curves. It does not affect the peak force of the curve. The measured cell load includes the residual force (if any is present). However, when the pile is instrumented with strain gages, the gage values only show the loads imposed in the pile over and above those already there at the start of the test. When evaluating gage records, therefore, the potential presence of residual force needs to be taken into account in order to establish the true distribution of load in the pile from the gages. (The method of adjusting records for presence of residual force is addressed in Section 8.13).

If the cell is located near the pile toe, the shaft resistance below the cell can be disregarded and the measured cell plate downward movement is approximately equal to the pile toe movement. An additional cell level can be placed anywhere along the pile shaft to determine separately shaft resistance along a so-established upper and a lower length of the shaft above the lower cell level.

When the full “pre-existing” load in the pile has been transferred to pressure in the cell, a further increase of pressure expands the cell, that is, the top plate moves upward and the bottom plate moves downward. The separation of the cell plates result in an opening of a space (a void) in the soil. This results in tension in the soil near the cell level. Usually, for an cell-assembly located near the pile toe, this has only marginal effect on the response. However, for a cell-assembly located up in the pile, it could affect the shaft shear forces within a small zone above and below the cell. More important is that the cell load will not be evenly distributed as axial load in the pile near the cell location. Therefore, for the strain-gages measurements to accurately represent the average stress distribution, they should be placed no closer than about two pile diameters above and/or below the cell.

Figure 8.29 presents typical results of a bidirectional cell test (performed in Brazil as early as 1981) on a 520-mm diameter, 13 m long, bored pile in silty sand (Elisio 1983).. The diagram shows the downward and upward movements of the pile as measured at the location of the bidirectional cell place 2.0 m above the pile toe.

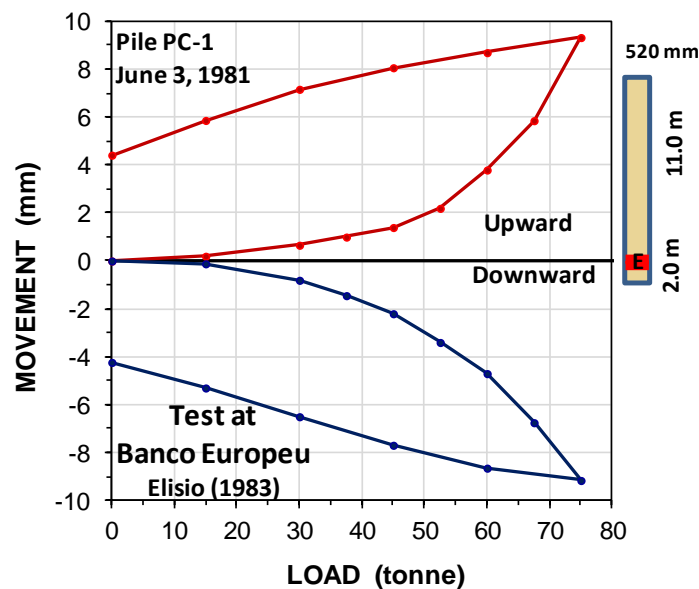


Fig. 8.29 Illustration of the main results of a bidirectional cell test: Upward and downward load-movements measured in a test on a 520-mm diameter, 13 m long pile (data from Elisio 1983).

An additional example of results from a bidirectional cell test is shown in Figure 8.30. The test was carried out on a strain-gage instrumented, 1,200 mm diameter, 40 m long bored pile (Loadtest 2002) for a bridge foundation. The soil profile consisted of about 10 m of clayey silt, on about 15 m of sandy silt deposited at about 25 m depth on dense to very dense sand with gravel. The depth to the groundwater table was 4.0 m. A 540-mm diameter bidirectional cell was placed at 35 m depth, 5 m above the pile toe. The test was terminated at a maximum cell load of about 8,000 kN, when the upward response of the shaft was in an ultimate resistance mode. The maximum upward and downward movements were 100 mm and 60 mm, respectively. The test procedure was a quick test in fourteen increments, each held for 10 minutes. No unloading/reloading cycles that would have disturbed the test were included. The figure shows the measured upward and downward curves for the applied bidirectional-cell loads, including a simulation of the curves (as discussed below) produced by the UniPile software (Goudreault and Fellenius 2014).

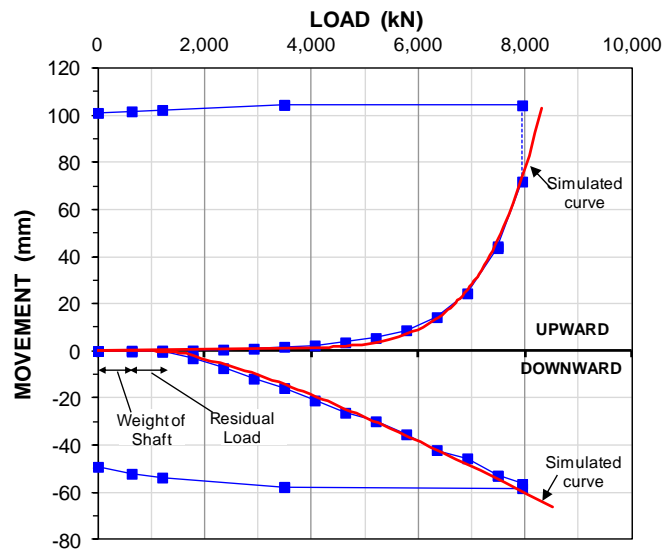


Fig. 8.30 Results of a bidirectional test on a 1,200 mm diameter, 40 m long bored pile

The strain-gage instrumentation was at four levels: 9 m, 17 m, 23 m, and 29 m depths. The strain records were used to determine the pile stiffness relation,  $EA$ , and the load distribution in the pile at the gage levels. The results of the evaluations are shown as load distributions in Figure 8.31 for the applied cell loads and the loads evaluated from the strain records. The curve to the right is the **equivalent head-down load-distribution** for the final load applied as obtained by “flipping over”—mirroring—the distribution of the maximum cell load as evaluated from the strain-gage records, thus providing the distribution of an equivalent head-down test encountering the same maximum shaft shear and toe responses as the cell test. The cell loads and the head-down distribution are adjusted for the pile buoyant weight and, for this case, also the downward water pressure at the cell. An effective stress back-calculation of the load distribution at the maximum load was fitted to the equivalent head-down distribution and the fit to the maximum applied load indicated the beta-coefficients shown to the right. (An effective-stress back-analysis should always be carried out on the results of a static loading test—bidirectional or conventional head-down).

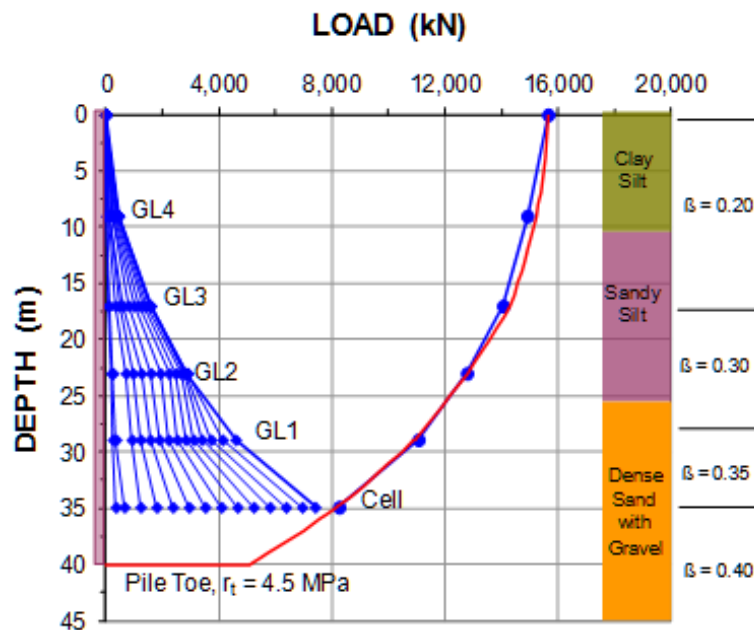


Fig. 8.31 Measured load distribution and the equivalent head-down load-distribution for the last maximum cell load ( $r_t$  = toe resistance)



The results from a bidirectional cell test can also be used to produce an **equivalent head-down load-movement** curve, which can be constructed by a direct method adding the upward and downward loads measured for equal movements with adjustment to the larger pile compression obtained in a head-down test as opposed to a test (reflecting the fact that, in a head-down test, the pile axial 'elastic' shortening is larger than that measured in a bidirectional cell test because, in a head-down test, the loads at the pile toe are conveyed through the shaft, compressing it). This method does not consider the fact that the upward load-movement in the bidirectional test “starts” by operating against the larger resistance at depth and engages the smaller resistance at shallow depth toward the end of the test. Therefore, the so-produced equivalent head-down load-movement curve will usually show a stiffer beginning and a softer ending as opposed to the conventional head-down test curves.

Once a fit to the measured upward and downward records is established (c.f., Figure 8.30), the UniPile software can determine the equivalent head-down curves using the so-calibrated soil response. Figure 8.32 shows equivalent pile-head load-movement curve along with the simulated equivalent shaft and toe resistances curves. The equivalent pile-head curve manually produced from the test data is also included. The slight difference between the directly calculated curve and the simulation is considered due to the that the manual method used for construing the equivalent head-down curve from the test records does not include the effect of the head-down test engaging the upper soil layers before the lower.

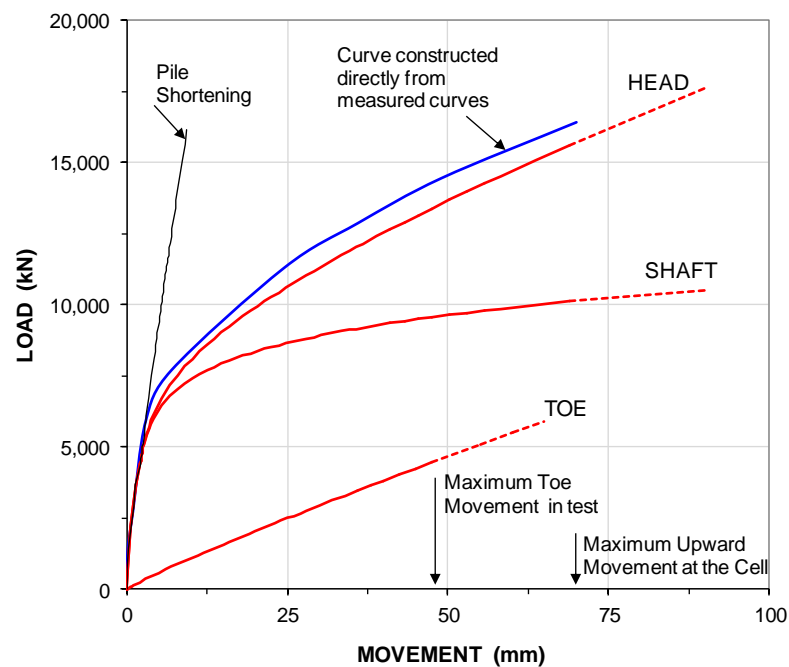


Fig. 8.32 The equivalent pile-head load-movement curves of the bidirectional test.

Be it a conventional head-down test or a bidirectional cell test, the conventional capacity evaluation is of little relevance to the pile assessment. However, in contrast to a head-down test, the bidirectional test is not limited to just a capacity analysis, but it also supports the far more important analysis of the settlement of the piled foundation. This is because the bidirectional test provides the distribution of resistance along the pile, which is central to determining the settlement of the pile or, rather, of the structure founded on the piled foundation.

When, as often is the case, a project involves settlement concerns, the load-distribution curve from a bidirectional test allows a detailed analysis of the movement response of the pile for the applied load from the supported structure coupled with the effect of the settlement in the surrounding soil.



### 8.15 Residual Force in an Instrumented Pile

As mentioned, the cell loads obtained in the bidirectional cell test include the residual force (if any) in the pile. In contrast, the results of conventional “head-down” static loading tests on instrumented piles do not provide the residual force directly. Pile instrumentation consists of strain gages, and the load in the pile at the gage location is determined from the change of strain, induced by a load applied to the pile head, by multiplying it with the pile material modulus and cross sectional area. The change of strain is the strain reading minus the “zero reading” of the gage, i.e., the reading when no outside axial load is applied to (or along) the pile. In a driven pile, the zero reading is ideally taken immediately before the driving of the pile. However, the “zero” value of strain in a pile can change due to the driving—particularly for a steel pile. Moreover, even if the gages are insensitive to temperature change, the pile material is not and the cooler environment in the ground will have some effect on the “zero level” of strain in the pile.

The concrete in a concreted pipe pile or a precast pile is affected by aging and time-dependent changes. In case of a prestressed pile, some change of the zero strain introduced by the release of the strands continues for days after their release. For an instrumented bored pile, the value of “zero strain” is not that clearly defined in the first place—is the “zero” before concreting or immediately after, or, perhaps, at a specific time later? In fact, the “zero reading” of a gage is not one value but several, and all need to be considered (and included in an engineering report of the test results). For example, in case of a driven prestressed concrete pile, the first zero reading is the factory zero reading. Second is the reading taken immediately before placing the gages in the casting forms. Third is the reading after the release of the strands and removal of the piles from the form. Fourth is the reading before placing the pile in the leads to start driving. Fifth is the reading immediately after completion of driving. Sixth is the reading immediately before starting the test. The principle is that a gage readings should be taken immediately before (and after) every event of the piling work and not just during the actual loading test. A similar sequence of readings applies to other pile types. The evaluation of the gage records is obviously greatly assisted if the test on the instrumented pile is a bidirectional cell test, as this test method provides the load-response independently of residual force.

#### 8.15.1 Case History of Residual Force and Other Influences

Strains may develop that have no connection to the average axial strain in a pile due to applying load to the pile. An example of this is the elongation of the reinforcing bars (with strain gage attached) due to the temperature rise at the outset of the grouting of a pile shown in Figure 8.33: measurements of temperature and strain during the 5 first days after the driving and grouting. The records are from a strain-gage instrumented 600 mm diameter, 35 m long spun-pile driven through clay and silt into sand near Busan, Korea. The about 300 mm annulus was grouted after the driving (Fellenius et al. 2009).

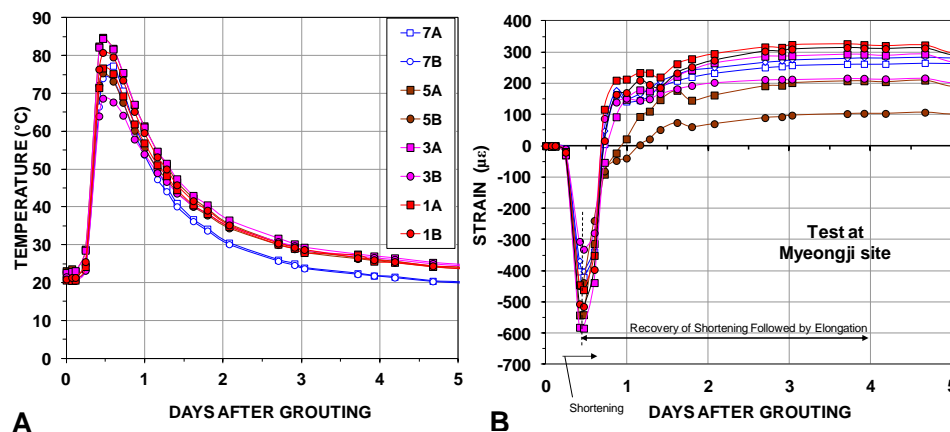


Fig. 8.33 Development of temperature and strain in a 35 m long spun-pile pile during first 5 days after grouting (reducing strain indicates compression/shortening) (Fellenius et al. 2009)

Over the initial about 12 h of increasing temperature from the hydration, the peak temperature reached almost boiling point. The thermal elongation of the bars was partially prevented by the grout stiffness resulting in an imposing significant of stress (negative strain) in the pile. When the pile started to cool after having reached the peak temperature, the records indicated a reversal of the strain to tension, as also caused by the grout partially preventing the shortening of the gage bar. After about three days of cooling, the further strain change was small because further change of temperature was small. The gages now indicated a net tension which does not correspond to any development of shear forces along the pile. (The vibrating wire gages are insensitive the temperature change). The evaluation of the gage records include correction for difference in thermal coefficient between the grout/concrete and the steel. by applying the known difference in thermal coefficient. However, before the grout/concrete fully interacted with the steel, the two materials were partially able to elongate/shorten independently), which effect is not adjusted in the following cooling phase.

Figure 8.34 shows that after about 5 to 10 days, the temperature of the gages, but for the gage pair nearest the ground surface (SG7A and 7B) had reached a near constant value, the soil temperature (which is the average annual temperature in the area of the site). However, but for the SG7A and 7B gage pair, the strain in the pile continued to decrease over the next about 40 days. As discussed by Fellenius et al. (2009) and Kim et al. (2011), the pile is affected by build-up of residual force creating compression in the pile and swelling due to absorption of water from the ground creating tension strain. Near the ground surface, the build-up is small and the strain change is almost entirely caused by swelling.

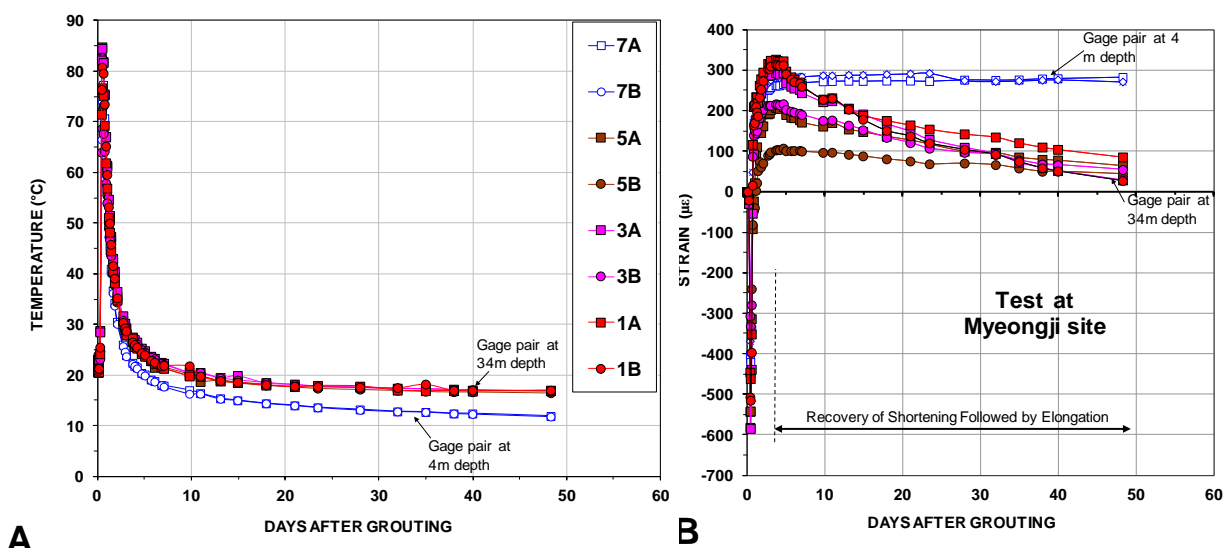


Fig. 8.34 Development of temperature and strain in a 35 m long spun-pile pile during 50 days after grouting (Fellenius et al. 2009)

### 8.15.2 Case History on Calculation True Load Distribution

The following is an example for determining the distribution of residual force from measurements of distribution of imposed load. The case is from a CAPWAP-determined resistance distribution. Figure 8.35A shows a cone stress,  $q_c$ , diagram from a CPTU sounding close to the test pile. The sand is loose to compact. Figure 8.35B shows the load distribution, which is from the CAPWAP determined distribution for the first blow of restrike on the pile 216 days after the initial driving.

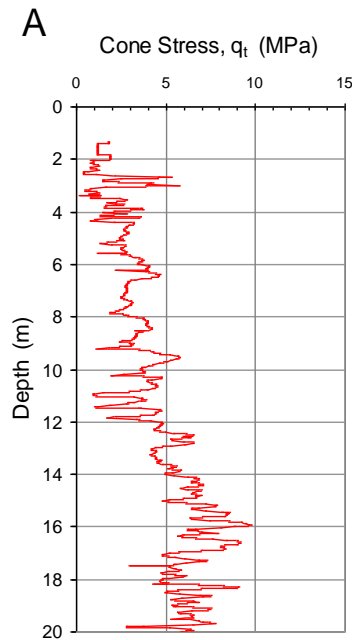


Fig. 8.35A CPT profile

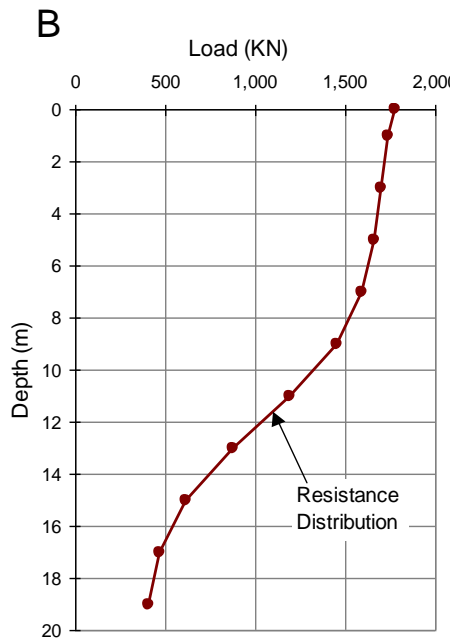


Fig. 8.35 B CAPWAP determined load-distribution

The pile is a 235 mm side square precast concrete pile driven 19 m into a sand deposit (Axelsson 2000). As described in Chapter 9, CAPWAP analysis makes use of strain and acceleration measured for an impact with a pile driving hammer. The analysis delivers amongst other results the static resistance mobilized by the impact. In the calculation, the pile is simulated as a series of many short elements and the results are presented element per element, as had measurements been made at many equally spaced gage levels along the pile. The CAPWAP program allows an adjustment of the wave-trace matching for locked-in load due to the immediately preceding impact, if the pile is subjected to residual force. However, the CAPWAP analysis does not determine a resistance distribution due to the residual force any more than the strain-gage measurements in a static loading test on an instrumented pile do.

Determining the distribution of residual force and adjusting the load distribution from “false” to “true” is an action simple in principle. Figures 8.36 and 8.37 indicate the procedure, which builds on the assumption that at and near the ground surface, the residual force is the result of fully mobilized negative skin friction that deeper down changes to partially mobilized and, then, at the neutral plane, switches over to partially mobilized positive shaft resistance and, perhaps, near the pile toe, to fully mobilized positive shaft resistance. If this sounds similar to the development of drag force and a neutral plane in a pile, it is because the two phenomena are essentially one-and-the-same. When the subject is the load locked-in in a pile just before the start of a static loading test, the term is “residual force”. When the subject is the long-term distribution after a structure has been built, the term is “drag force”.

The CAPWAP determined ultimate resistance is 1,770 kN. The total shaft resistance is 1,360 kN and the toe resistance is 410 kN. The CAPWAP distribution has an “S-shape indicating that the unit shaft resistance increases with depth to a depth of about 13 m. However, below this depth, the distribution curve indicates that the unit shaft resistance is progressively becoming smaller with depth. From a depth of about 15 m, the unit shaft resistance is very small. This distribution is not consistent with the soil profile established by the CPT sounding. Instead, the resistance distribution is consistent with a pile subjected to residual force. Because the soil is relatively homogeneous—an important condition—the data can be used to determine the distribution of residual force as well as the resistance distribution unaffected by the residual force, the “true” ultimate resistance.

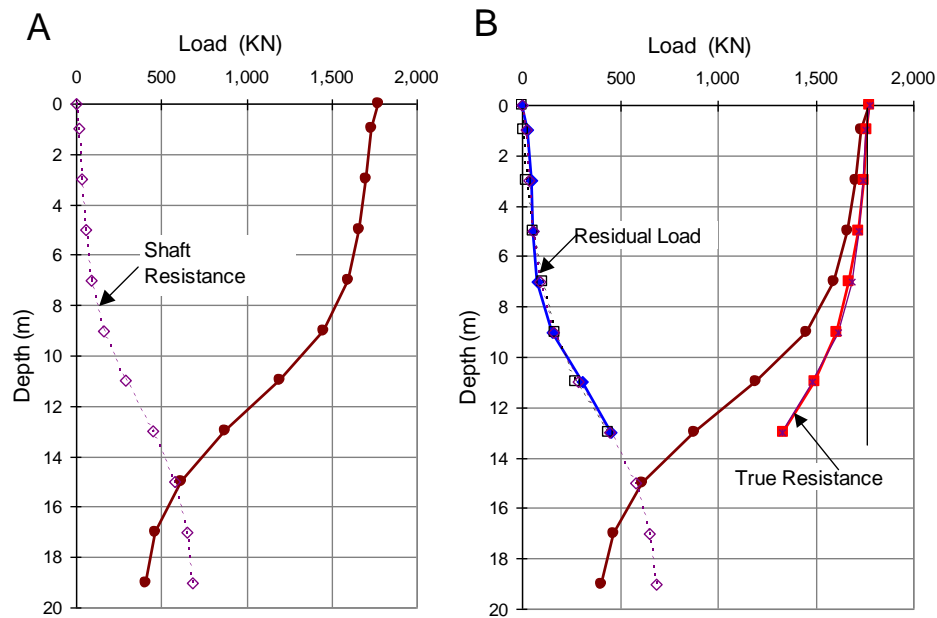


Fig. 8.36 Procedure for determining the distribution of residual force and “true” resistance

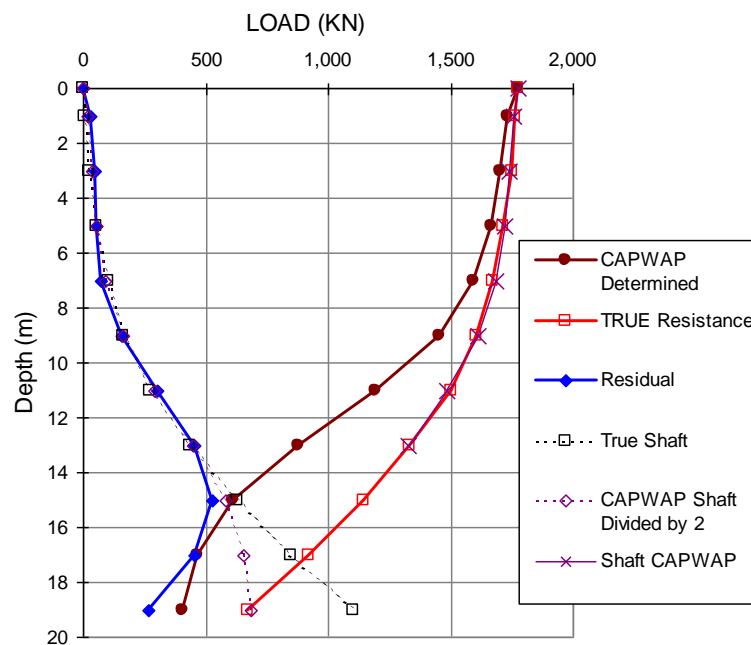


Fig. 8.37 Final results: Measured load, residual force, and true resistance

The analysis procedure is based on the assumption that the negative skin friction is fully mobilized and equal to the positive shaft resistance mobilized by the impact (“applied test load”). Thus, where the residual force is built up from fully mobilized negative skin friction, the “true” shaft resistance (positive or negative direction of shear) is half of that determined directly from the test data. The figure (8.34 above) demonstrates the procedure. A curve has been added that shows half the CAPWAP determined shaft resistance: Starting at the ground surface and to a depth of 13 m, the curvature increases progressively. To this depth, it represents the distribution of the residual force and, also, of the true shaft resistance. The progressive increase indicates proportionally to the effective overburden stress. A back-calculation of the shaft resistance shows that the beta-coefficient (the proportionality factor in the effective stress analysis) is about 0.6.

Below the 13-m depth, however, the “half-curve” bends off. The depth is where the transition from negative skin friction to positive toe resistance starts and the assumption of fully mobilized negative skin friction is no longer valid. To extend the residual-force distribution curve beyond the 13 m depth, one has to resort to the assumption that the beta-coefficient found in the upper soil layers applies also to the soil layers below 13 m depth and calculate the continuation of the true resistance distribution. The continuation of the distribution of the residual force is then obtained as the difference between the true resistance and the CAPWAP determined distribution. The results of this calculation show that the residual pile toe force was about 230 kN, which means that the test toe load of 410 kN in reality was 640 kN.

The objective of the analysis procedure is to obtain a more representative distribution of resistance for the test pile. The CAPWAP determined resistance distribution misrepresents the condition unless the distribution is corrected for residual force. The corrected shaft and toe resistances are about 1,100 kN and 640 kN as opposed the direct values of 1,360 kN and 410 kN. Significant effect of residual force on CAPWAP-determined distributions is rare. In the example, the long wait time between end-of-driving, EOD and beginning-of-restrike, BOR, is probably the reason for the obvious presence of residual force.

However, most piles will to a larger or smaller extent be affected by residual force, that is, most load distributions evaluated from a static loading test will show presence of residual force. If the pile is a bored pile tested relatively soon after its construction, the amount residual force is often found to be insignificant, even negligible. For driven piles, residual force is a common occurrence.

To further illustrate the effect of residual force on the evaluation of test data, the following fictional example assumes to be test data from a bidirectional cell test with the cell placed at the pile toe of a pile similar to the foregoing test pile. The bidirectional cell test is assumed to be pursued until the shaft failed and the toe load would then have been equal to the shaft resistance, 1,130 kN. Considering the water pressure effect for the upward and downward loads of about 10 kN and the total pile weight of about 25 kN, bidirectional test would have been carried to a cell load of 1,145 kN and an equivalent head-down load would be 2,275 kN.

Figure 8.38 shows the load distributions of the fictional bidirectional cell test (BDC). The effect on the results of the bidirectional test of the residual force is an apparent zero shaft resistance above about 15 m depth. The figure shows the “flipped” distribution of the test results, that is, the equivalent head-down load distribution of the bidirectional test ‘false’ data. Moreover, the figure shows, qualitatively, that the cell test ‘false’ curve plots to the right of the ‘true’ load distribution curve, i.e., on the opposite side of the case for the conventional ‘false’ head down curve. Note, also, that the cell load does show the true load, which the implied instrumentation gages do not.

## **8.16 Modulus of ‘Elasticity’ of the Instrumented Pile**

### **8.16.1 Aspects to consider**

In arranging for instrumentation of a pile, several aspects must be considered. The gages must be placed in the correct location in the pile cross section to eliminate influence of bending moment. If the gages are installed in a concrete pile, a key point is how to ensure that the gages survive the installation—a strain-gage often finds the visit from a vibrator a most traumatic experience, for example. We need the assistance of specialists for this work. The survival of gages and cables during the installation of the pile is no less important. Therefore, the knowledge and interested participation and collaboration of the piling contractor, or, more precisely, his field crew, is vital.

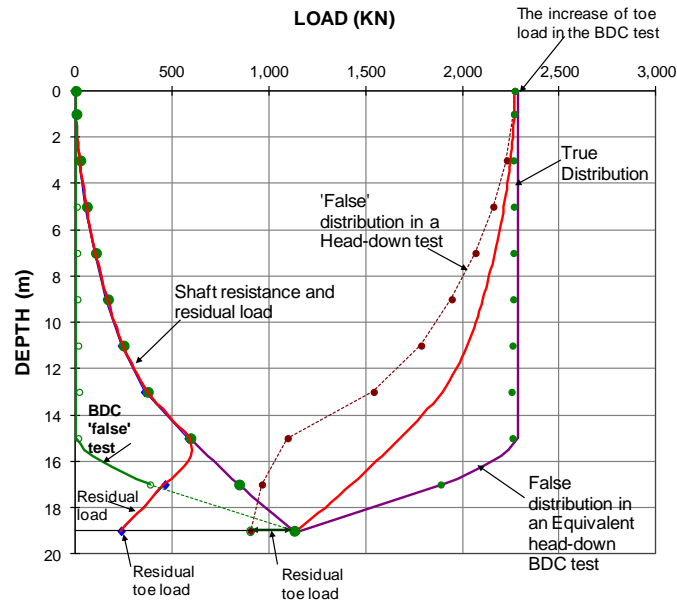


Fig. 8.38 Comparison of ‘true’ and ‘false’ load-distributions for a conventional head down test to the equivalent head-down distributions derived from a bidirectional cell test

Once the gages have survived the pile manufacture and installation—or most of the gages, a certain redundancy is advised—the test can proceed and all should be well. That is, provided we have ensured the participation of a specialist having experience in arranging the data acquisition system and the recording of the readings. Then, however, the geotechnical engineer often relaxes in the false security of having all these knowledgeable friends to rely on. He fails to realize that the reason for why the friends do not interfere with the testing programme and testing method is not that they trust the geotechnical engineer’s superior knowledge, but because advising on the programme and method is not their mandate.

The information obtained from a static loading test on an instrumented pile can easily be distorted by unloading events, uneven load-level durations, and/or uneven magnitude of load increments. Therefore, a static loading test for determining load transfer should be carried through in one continuous direction of movement and load without disruptions or unloading. Maintain all load levels an equal length of time—an occasional extended load holding will adversely affect the interpretation of the results while providing nothing useful in return.

So, once all the thoughts, know-how, planning, and hands-on have gone into the testing and the test data are secured, the rest is straightforward, is it not? No, this is where the fun starts. This step is how to turn strain into load, a detail that is surprisingly often overlooked in the data evaluation of the test results.

### 8.16.2 Converting Strain to Load Using the Pile Modulus

Strain gages are usually vibrating-wire gages. The gages provide values of strain, not load, which difference many think is trivial. Load is just strain multiplied by the area and the elastic modulus, right?

The measured strain data are transferred to load by use of the Young’s modulus of the pile material and of the pile cross sectional area. For steel piles, this is normally no problem (cross sectional changes, guide pipes, etc. can throw a “monkey-wrench” into a best laid plan, however). In case of precast concrete piles, prestressed concrete piles, and concreted pipe piles, the modulus is a combined modulus of the steel and concrete, normally proportional to area and modulus, as shown in Eq. 8.21.

$$(8.21) \quad E_{comb} = \frac{E_s A_s + E_c A_c}{A_s + A_c}$$

where

$E_{comb}$	=	combined modulus
$E_s$	=	modulus for steel
$A_s$	=	area of steel
$E_c$	=	modulus for concrete
$A_c$	=	area of concrete

The modulus of steel is known accurately. It is a constant value (about  $29.5 \times 10^6$  ksi or 205 GPa). In contrast, not only can the concrete modulus have many values, the concrete modulus is also a function of the applied stress or strain. Common relations for its calculation, such as the relation between the modulus and the cylinder strength, are not reliable enough. A steel pile is only an all-steel pile in driving—during the test, it is often a concrete-filled steel pipe. The modulus to use in determining the load is the combined value of the steel and concrete moduli. By the way, in calculating the concrete modulus in a concrete-filled steel pipe, would you choose the unconfined or the confined condition?

Were the records from loading a free-standing pile (like a column), the slope of a plot of load versus strain would indeed represent the stiffness,  $EA$ , of the column. In contrast to a column, however, for a pile, the axial load is not constant, but diminishes with the distance from the load application (at the pile head or at the bidirectional cell). Therefore, before the shaft resistance is fully mobilized, the slope of the load-versus-strain curve is steeper than that of its equivalent column, i.e., the apparent stiffness is larger than the true stiffness of the pile. Once the shaft resistance is fully mobilized and assuming that the continued response is plastic, the slope is equal to the true stiffness of the pile. However, if also the continued shaft resistance would be strain-hardening, the slope would still show a slope that is steeper than true, and, if the continued shaft resistance would be strain-softening, the slope would indicate a stiffness that is smaller than the true.

Usually, the modulus reduces with increasing stress or strain. This means that when load is applied to a pile or a column, the load-movement follows a curve, not a straight line. Some years ago, I presented a method (explained below) for determining the strain-dependency from test data based on the assumption that the curved line is a second degree function (Fellenius 1989). The second degree relation means that the change of stress divided by the strain and plotted against the strain is a straight, but sloping line for the column. For the pile, the equivalent plot will only show the straight line when all shaft resistance is mobilized and the applied increment of load goes unreduced to the pile toe.

Well, the question of what modulus value to use is simple, one would think. Just place a gage level near the pile head where the load in the pile is the same as the load applied to the pile head, and let the data calibrate themselves, as it were, to find the concrete modulus. However, in contrast to the elastic modulus of steel, the elastic modulus of concrete is not a constant, but a function of the imposed load, or better stated, of the imposed strain.

Over the large stress range imposed during a static loading test, the difference between the initial and the final moduli for a concrete pile can be substantial. This is because the load-movement relationship (stress-strain, rather) of the tested pile, taken as a free-standing column, is not a straight line. Approximating the curve to a straight line may introduce significant error in the load evaluation from the strain measurement. However, the stress-strain curve can with sufficient accuracy be assumed to follow a second-degree line:  $y = ax^2 + bx + c$ , where  $y$  is stress and  $x$  is strain (Fellenius, 1989). The trick is to determine the constants  $a$  and  $b$  (the constant  $c$  is zero).

The approach builds on the fact that the stress,  $y$ , can be taken as equal to **the secant modulus** multiplied by the strain,  $\epsilon$ . The secant modulus, or the secant stiffness, rather, is the applied load ( $Q$ ) divided by the measured strain ( $\epsilon$ ) and it is a function of strain. It can be determined directly from the load-strain data **obtained at a gage located near the pile head**, as illustrated in Figure 8.39, presenting records from a static loading test on a 1.83 m diameter, open toe, strain gage instrumented, driven, steel pipe pile with a 38 mm thick wall. The pile was not concreted. The uppermost strain-gage level was 1.8 m (1.0 pile diameter) below the pile head and 1.2 m below the ground surface. The static loading test was a quick test with 23 equal increments of 1,100 kN applied every 10 minutes to a maximum load of 25,500 kN, when bearing failure developed. The loads were measured using a separate load cell. As should be the case, the stiffness,  $EA$ , of the steel pile is constant. (The amount of steel was not precisely known, but it can, if desired, now be established from the relation for the secant modulus). Note that the first two values are a bit off. The deviation is inconsequential, but a small load adjustment will remove it, if desired.

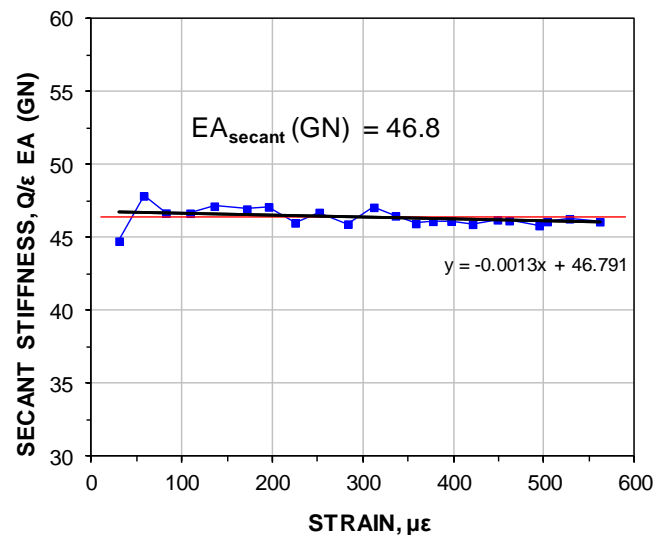


Fig. 8.39 Secant stiffness vs. measured strain for a not-concreted steel pipe pile (Fellenius 2012)

For a concreted pipe pile or for a concrete pile—driven or bored—the relation may be linear, but concrete is usually strain-dependent, as illustrated in Figure 8.40, showing secant stiffness for a near-pile-head gage level records of a 600-mm diameter spun pile.

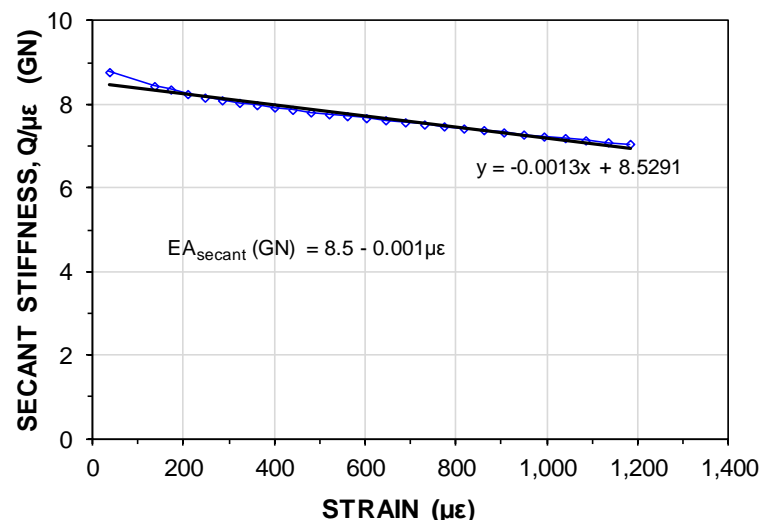


Fig. 8.40 Secant stiffness vs. measured strain for a 600-mm spun pile (Fellenius 2012)



The straight-line response is not immediately apparent and the initial uncertainty will be much greater if the pile has been even partially loaded before the start of the test. Indeed, the accurate relation for the EA is almost totally lost if the test included unloading/reloading cycles. The initial uncertainty is illustrated in Figure 8.41, which is from a test on a 400-mm diameter concentered pipe pile (taken from a gage level about 1.5 m below the ground surface) and Figure 8.42 which is from a test on a 900-mm diameter bored pile taken from a gage at the ground surface. As shown, the initial deviation from the straight-line secant relationship could be "corrected" by adding a mere  $8 \mu\epsilon$  of strain to each of the measured values to remove the "false" zero value from the records. (For information on the "Tangent Stiffness" trend line, see Section 8.16.3)

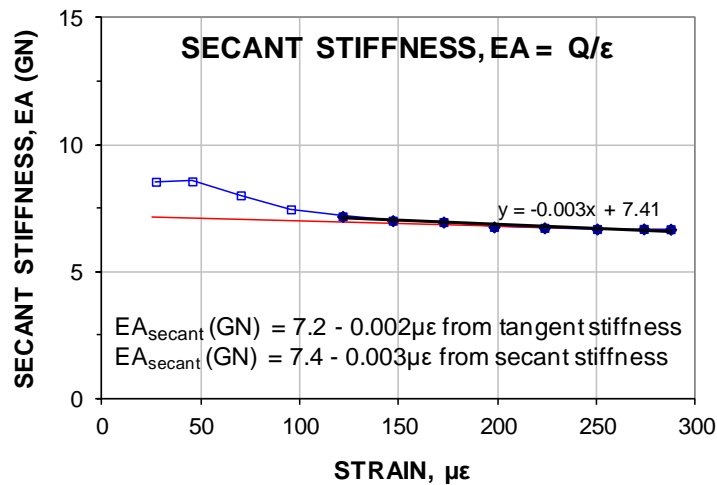


Fig. 8.41 Secant stiffness ( $Q/\mu\epsilon$ ) vs. measured strain for a 400-mm concentered steel pipe pile (Fellenius 2012)

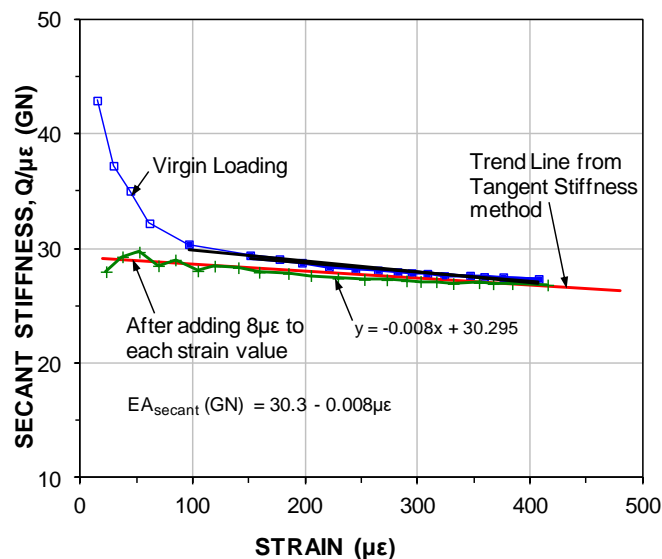


Fig. 8.42 Secant stiffness ( $Q/\mu\epsilon$ ) vs. measured strain for a 900-mm bored pile (Fellenius 2012)

The initial uncertainty can be removed by instead checking the incremental stiffness (tangent modulus), which is independent of any incorrect zero value and **can be applied to strain data from any depth in the pile**. The construction of the tangent modulus (change of load over change of strain vs. strain) is similar to that of the secant modulus (change of load over strain vs. strain). To numerically convert a tangent modulus relation to a secant modulus relation is simple.

### 8.16.3 Mathematics of the Tangent Modulus Method

For a pile taken as a free-standing column (case of no shaft resistance), the tangent modulus of the composite material is a straight line sloping from a larger tangent modulus to a smaller. Every measured strain value can then be converted to stress via its corresponding strain-dependent secant modulus.

The equation for the tangent modulus  $M_t$ , is:

$$(8.22) \quad M_t = \left( \frac{d\sigma}{d\varepsilon} \right) = a\varepsilon + b$$

which can be integrated to:

$$(8.23) \quad \sigma = \left( \frac{a}{2} \right) \varepsilon^2 + b\varepsilon$$

Eq. 8.24 provides an alternative way of calculating the stress

$$(8.24) \quad \sigma = E_s \varepsilon$$

Therefore, combining Eqs. 8.23 and 8.24:

$$(8.25) \quad \sigma = E_s \varepsilon = 0.5a\varepsilon^2 + b\varepsilon \quad \text{and} \quad E_s = 0.5a\varepsilon + b$$

where

$M_t$	=	tangent modulus of composite pile material
$E_s$	=	secant modulus of composite pile material
$\sigma$	=	stress (load divided by cross section area)
$d\sigma$	=	$(\sigma_{n+1} - \sigma_1)$ = change of stress from one load increment to the next
$a$	=	slope of the tangent modulus line
$\varepsilon$	=	measured strain
$d\varepsilon$	=	$(\varepsilon_{n+1} - \varepsilon_1)$ = change of strain from one load increment to the next
$b$	=	y-intercept of the tangent modulus line (i.e., initial tangent modulus)

With knowledge of the strain-dependent, composite, secant modulus relation, the measured strain values are converted to the stress in the pile at the gage location. The load at the gage is then obtained by multiplying the stress by the pile cross sectional area.

**Procedure.** When data reduction is completed, the evaluation of the test data starts by plotting the measured tangent modulus versus strain for each load increment (the values of change of load or stress divided by change of strain are plotted versus the measured strain). For a gage located near the pile head (in particular, if above the ground surface), the modulus calculated for each increment is unaffected by shaft resistance and the calculated tangent modulus is the actual modulus. For gages located further down the pile, the first load increments are substantially reduced by shaft resistance along the pile above the gage location and a linear relation will not develop until the shaft resistance is fully mobilized at and above the gage location. Initially, therefore, the tangent modulus values calculated from the full load increment divided by the measured strain will be large. However, as the shaft resistance is being mobilized down the pile, the strain increments become larger and the calculated modulus values become smaller. When all shaft resistance above a gage location is mobilized, the calculated modulus values for the subsequent increases in load at that gage location are the computed tangent modulus values of the pile cross section at the gage location. (N.B., provided that the soil is neither strain-hardening nor -softening).

For a gage located down the pile, shaft resistance above the gage will make the tangent modulus line plot above the modulus line for an equivalent free-standing column—giving the line a translation to the left. The larger the shaft resistance, the higher the line. However, the slope of the line is unaffected by the amount of shaft resistance above the gage location. The lowering of the line is not normally significant. For a pile affected by residual force, strains will exist in the pile before the start of the test. Such strains will result in a lowering of the line—a translation to the right—offsetting the shaft resistance effect.

It is a good rule, therefore, always to determine the tangent modulus line by placing one or two gage levels near the pile head where the strain is unaffected by shaft resistance. An additional reason for having a reference gage level located at or above the ground surface is that such a placement will also eliminate any influence from strain-softening of the shaft resistance. If the shaft resistance exhibits strain-softening, the calculated modulus values will become smaller and infer a steeper slope than the true slope of the modulus line. If the softening is not gradual, but suddenly reducing to a more or less constant post-peak value, a kink or a spike will appear in the diagram.

**Tangent Modulus Example.** To illustrate the approach, Figure 8.43 shows the results of a static loading test on a 20 m long Monotube pile will be used. The pile is a thin-wall steel pipe pile, tapered over the lowest 8.6 m length. (For complete information on the test, see Fellenius et al., 2000).

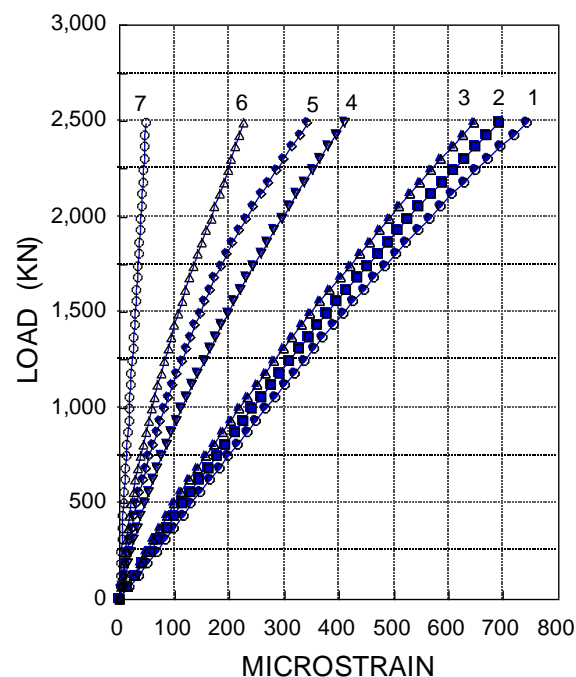


Fig. 8.43 Strain measured at Gage Levels 1 through 7

The soil consisted of compact sand. Vibrating wire strain gages were placed at seven levels, with Gage Level 1 at the ground surface. Gage Levels 2 through 5 were placed at depths of about 2, 4, 9, and 12 m, respectively. Gage Level 6 was placed in the middle of the tapered portion of the pile, and Gage Level 7 was placed at the pile toe.

Figure 8.44 shows curves of applied load and measured strain for the seven gages levels in the pile. Because the load-strain curves of Gage Levels 1, 2, and 3 are very similar, it is obvious that not much shaft resistance developed above the Gage Level 3. The figure shows that tangent modulus values for the five gages placed in the straight upper length of the pile, Gages Levels 1 through 5. The values converge to a straight line represented by the “Best Fit Line”.

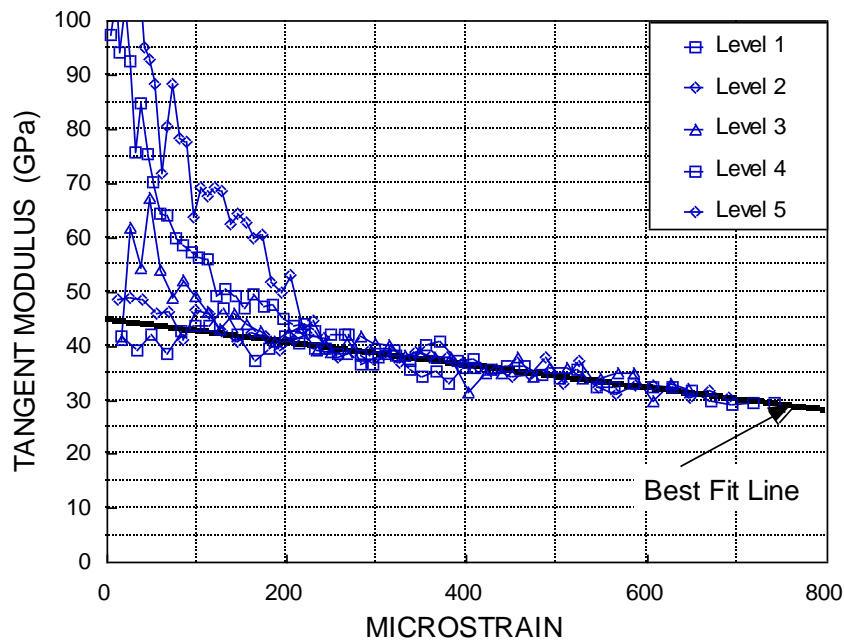


Fig. 8.44 Tangent modulus diagram

Linear regression of the slope of the tangent-modulus line indicates that the initial tangent modulus is 44.8 GPa (the constant “b” in the equations). The slope of the line (coefficient “a” in the equations) is -0.021 GPa per microstrain ( $\mu\epsilon$ ). The resulting secant moduli are 40.5 GPa, 36.3 GPa, 32.0 GPa, and 27.7 GPa at strain values of 200  $\mu\epsilon$ , 400  $\mu\epsilon$ , 600  $\mu\epsilon$ , and 800  $\mu\epsilon$ , respectively.

The pile cross sectional area as well as the proportion of concrete and steel change in the tapered length of the pile. The load-strain relation must be corrected for the changes before the loads can be calculated from the measured strains. This is simple to do when realizing that the tangent modulus relation (the “Best Fit Line”) is composed of the area-weighted steel and concrete moduli. Conventional calculation using the known steel modulus provides the value of the concrete tangent modulus. The so-determined concrete modulus is then used as input to a calculation of the combined modulus for the composite cross sections at the locations of Gage Levels 6 and 7, respectively, in the tapered pile portion.

Figure 8.45 presents the strain gage readings converted to load, and plotted against depth to show the load distribution in the pile as evaluated from the measurements of strain using Eq. 8.24. The figure presents the distribution of the loads actually applied to the pile in the test. Note, however, that the strain values measured in the static loading test do not include the strain in the pile that existed before the start of the test due to residual force. Where residual force exists, the values of applied load must be adjusted for the residual force before the true load distribution can be established.

When determining the load distribution in an instrumented pile subjected to a static loading test, one usually assumes that the loads are linearly proportional to the measured strains and multiplies the strains with a constant—the elastic modulus. However, only the modulus of steel is constant. The modulus of a concrete can vary within a wide range and is also a function of the imposed load. Over the large stress range imposed during a static loading test, the difference between the initial and the final tangent moduli for the pile material can be substantial. While the secant modulus follows a curved line in the load range, in contrast, the tangent modulus of the composite material is a straight line. The line can be determined and used to establish the expression for the secant elastic modulus curve. Every measured strain value can therefore be converted to stress and load via its corresponding strain-dependent secant modulus.

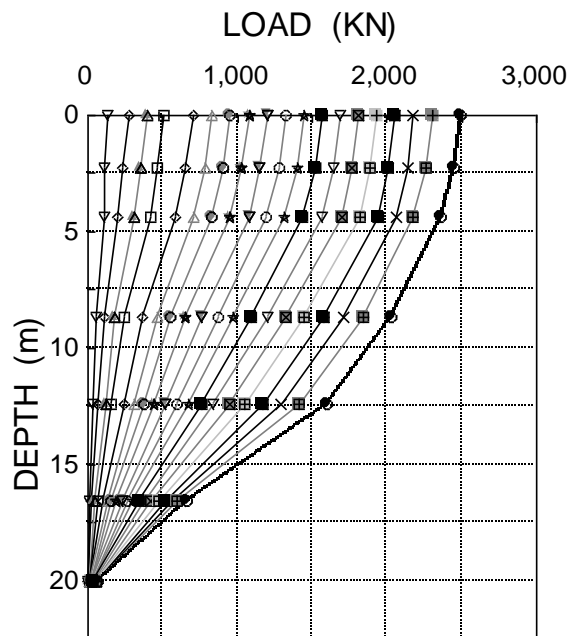


Fig. 8.45 Load distribution for each load applied to the pile head

For a gage located near the pile head (in particular, if above the ground surface, the tangent modulus calculated for each increment is unaffected by shaft resistance and it is the true modulus (the load increment divided by the measured strain). For gages located further down the pile, the first load increments are substantially reduced by shaft resistance along the pile above the gage location. Initially, therefore, the tangent modulus values will be large. However, as the shaft resistance is being mobilized down the pile, the strain increments become larger and the calculated modulus values become smaller. When all shaft resistance above a gage level is mobilized, the calculated modulus values for the subsequent increases in load at that gage location are the tangent modulus values of the pile cross section.

Note, the incremental stiffness method (tangent modulus method) requires that the test data are from a properly performed test where all increments are equal and held for equal length of time, and where no unloading/reloading cycles have been included. If not, the gage evaluation will be adversely affected, possibly show to be useless without significant wishful guesswork.

**By the way.** The example of determining the measured values of load presented in the foregoing is only the starting point of the analysis. Next comes assessing whether or not the pile is subjected to residual force. Figure 8.46 presents the final result for the Monotube pile after adjustment to residual force according to the procedure given in Section 8.15.

#### 8.16.4 Comparison between Secant Modulus Determined Directly and from Tangent Modulus

When a strain-gage level lies close to the pile head, a direct method for determining the secant modulus can be applied. Figure 8.47 shows a tangent stiffness (incremental stiffness) plot of strain-gage records from a head-down static loading test on a concrete-filled pipe pile driven at Sandpoint, Idaho (Fellenius et al. 2002). The gage was placed close to the head of the pile and the data are the same as those used for the Figure 8.39 secant stiffness plot.

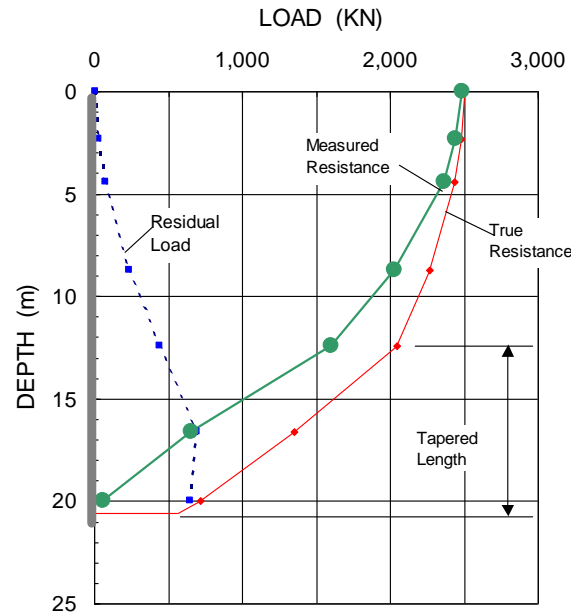


Fig. 8.46 The example case with measured load, residual force, and true resistance

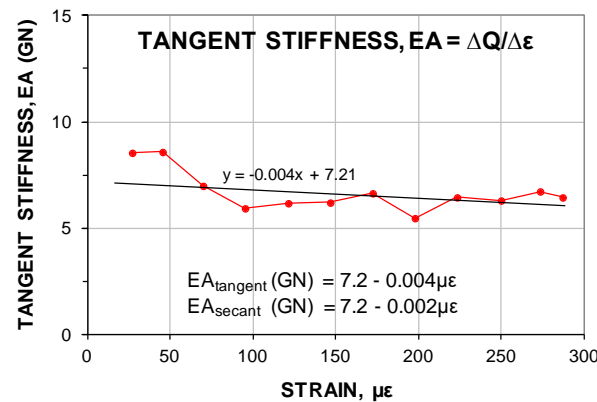


Fig. 8.47 Comparison between stiffness determined from tangent and secant modulus approaches

The secant stiffness trend is not fully established before the imposed strain has reached about 200  $\mu\epsilon$ . This is because in the beginning of a test, the pile head and the gage located close to the pile head are often influenced by random effects such as bending and sideways movements. Such effects are eliminated for the tangent stiffness plot. However, the tangent plot shows a bit of a scatter—differentiation will exaggerate small variations in the data. The secant modulus plot is less sensitive to such variations and produces a smoother curve, but requires a well-established zero-level.

### 8.16.5 The Adverse Effect on Strain-gage Records from Unloading/Reloading Cycles

Unloading and reloading cycles have a strong adverse effect on the interpretation of strain-gage records, as illustrated in the following. Figure 8.48 shows the results of a head-down static loading test on a strain-gage instrumented, 600-mm diameter, 56 m embedment depth, cylinder pile with the central void grouted after the driving (Kim et al. 2011). At an applied load of about 8,400 kN, a hydraulic leak developed that necessitated unloading the pile. After repairs, the test started anew and reached a load of about 9,000 kN at which the pile started plunging. The label "1L" indicates the virgin loading records of the pile and "2L" indicates the re-loading.

Before the secant and tangent methods (the secant and incremental stiffness methods) were developed, it was common to evaluate the pile stiffness,  $EA$ , from a plot of load versus strain, as shown in Figure 8.49. The red line is sloping at a stiffness ( $EA$ ) equal to 7.0 GN, which appears to be suitable for both load cycles. For a simple plot of distribution of load versus depth calculated from the strains measured at various strain-gage pairs down the pile, this could often be sufficient for the calculations. However, not so for any precise analysis or further detailing of the test results.

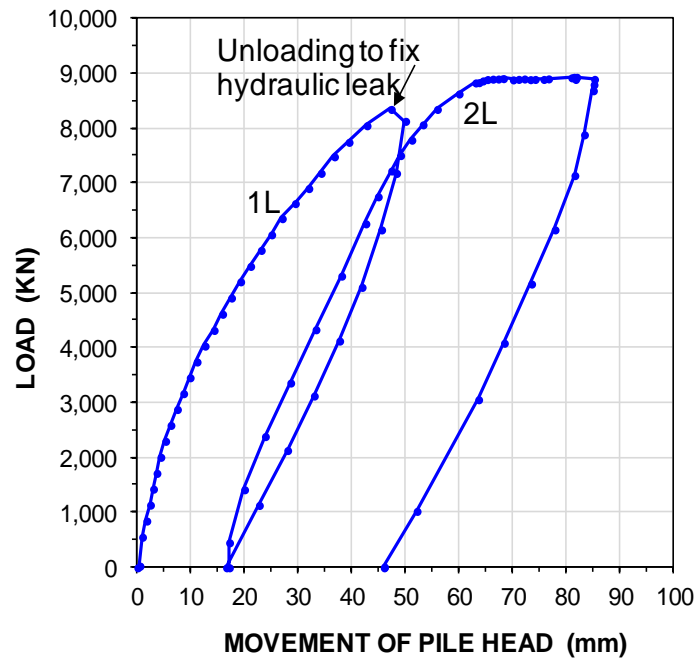


Fig. 8.48 Pile-head load-movement for the 600-mm cylinder pile.

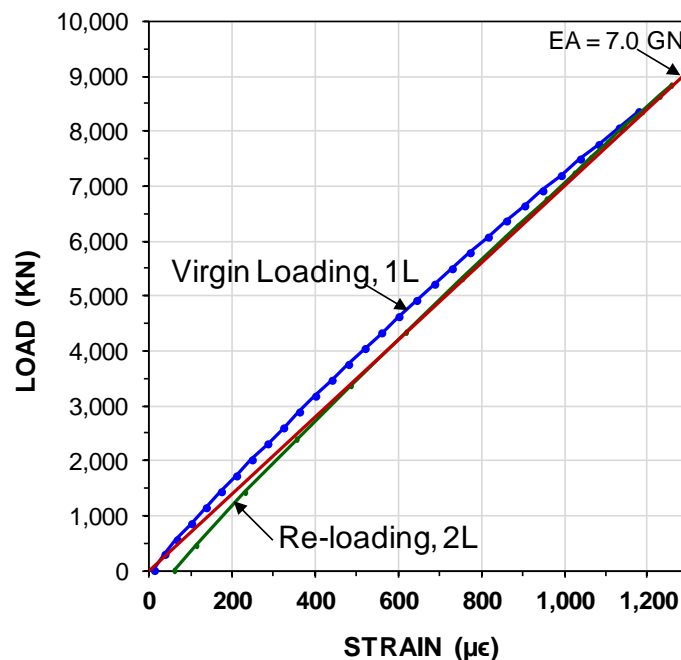


Fig. 8.49 Load-strain plot for virgin loading and re-loading with approximate stiffness line ( $EA = 7.0 \text{ GN}$ )

The axial stiffness of a concrete pile is a function of the imposed strain, and for a gage level close to the pile head (i.e., a gage located where the pile is not influenced by soil resistance), plotting the "secant modulus" (load/strain) will show the secant stiffness if the pile has essentially zero prior strain. That is, if the loading is for virgin conditions (Cycle 1L). Figure 8.50 shows for the example case how the secant modulus is obtained from a linear regression of the 1L-secant line (See also Section 8.16.2 and Figure 8.38 illustrating the results of a test on a similar pile). The secant method worked well for the virgin plot. However, the strain records from the reloading (Cycle 2L) are very much affected by the strains imposed by the preceding test. As indicated, an attempt to correct the records by subtracting a fixed value of strain from each record does some improvement, but the re-loading relation still deviates considerably.

The direct secant method is not applicable to the gage records from further down the pile. For those, the evaluation of the pile stiffness needs to be performed by the incremental stiffness (tangent modulus) method, as shown in Figure 8.51 (the plot is from the records of the same gage; the records used for the preceding graph). The incremental method applied to the reloading records (Cycle 2L) does not show a similar trend as that for the virgin records (Cycle 1L). Because the incremental stiffness method relies on differentiation, a "correction" similar to that attempted for the secant method is not possible and the reloading has adversely, and irreparably, affected the strain-gage evaluation possibilities.

The accidental unloading occurred very near the maximum load, so, fortuitously, the test results were still suitable for the particular project.

Figure 8.52 shows an example of a bidirectional test on a 1.85 m diameter, 65 m long bored pile, for which, again, an accidental hydraulic leak necessitated an unloading and reloading cycle (Thurber Engineering Inc., Edmonton; personal communication 2016). The pile constructed with a 8.7-m length in clay shale and siltstone below the bidirectional cell level. The figure shows the downward load-movement cell records.

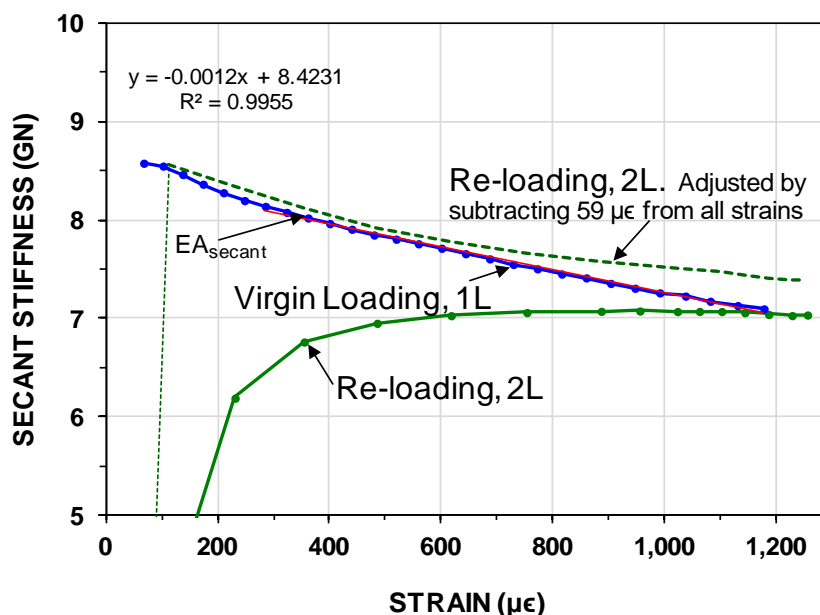


Fig. 8.50 Secant modulus plot of the from the near-the pile-head gage records



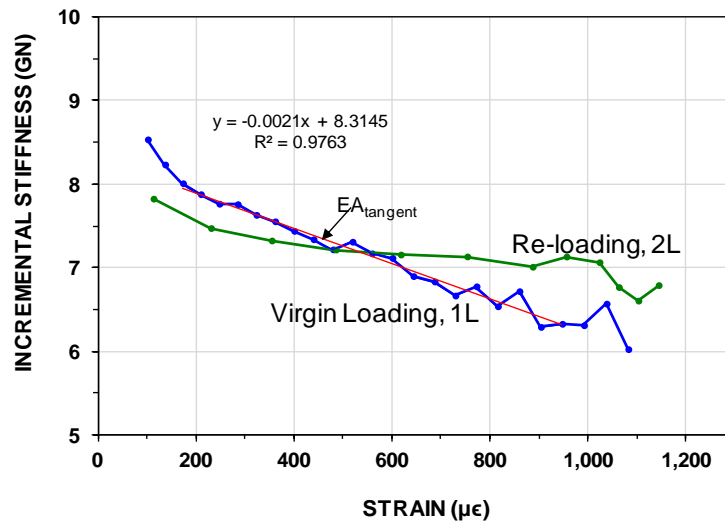


Fig. 8.51 Incremental stiffness ("tangent modulus") for virgin loading and re-loading.

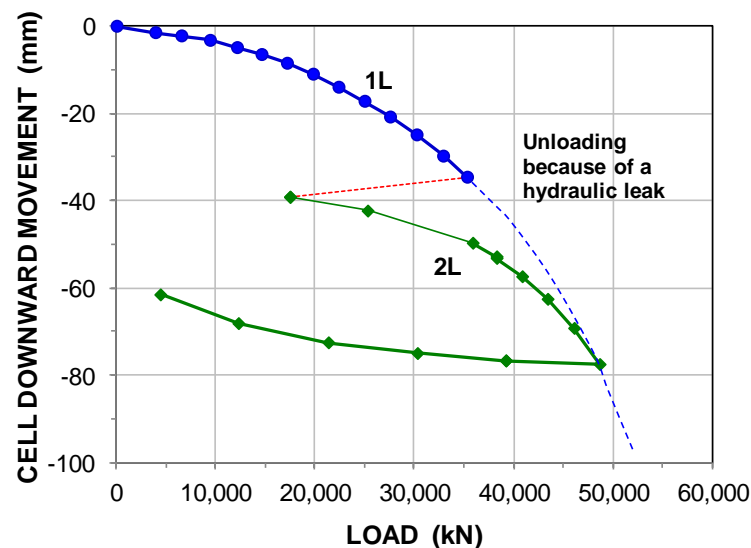


Fig. 8.52 Cell load versus downward movement for the 1,850-m diameter bored pile

Figure 8.53 shows the load versus strain diagram for the two cycles as measured by strain-gage SGL2. placed about half way between the bidirectional cell level and the pile toe. Again, it would seem that the unloading/reloading did not have much adverse effect of the results. However, Figure 8.54 shows that plotting the data in an incremental stiffness diagram that the effect of the unloading/reloading has eliminated the suitability of using the re-loading records for detailed analysis of the strain-gage records of Cycle 2L.

Similar to the test on the cylinder pile, the records before the accidental unloading were sufficient for the test records to meet the design objectives of the test for the particular project.

The two case histories are from unintentional and undesirable unloading/reloading events. They do show that to intentionally include such events in a test programme is unadvisable and regrettable.

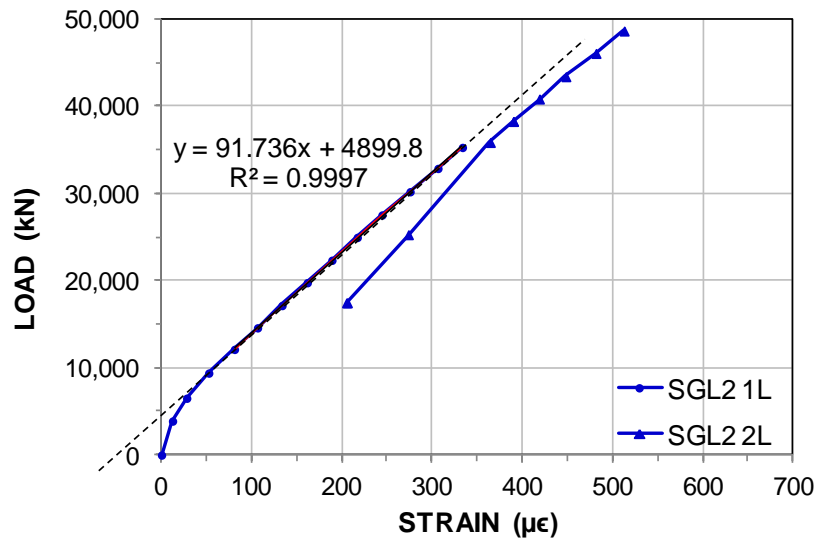


Fig. 8.53 Pile-head load-movement for the 1.85-m bored pile

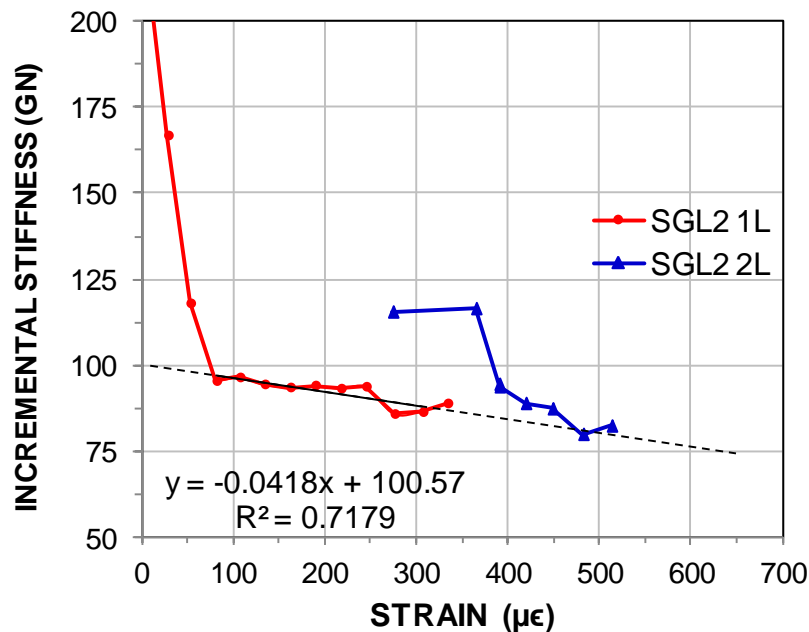


Fig. 8.54 Incremental stiffness ("tangent modulus) for virgin loading and re-loading

### 8.17 Concluding Remarks

Be the test a simple proof test or an elaborate instrumented test, a careful analysis of the recorded data is necessary. Continuing the test until the ultimate resistance is reached and combining full-scale field tests with analysis using basic soil mechanics principles of effective stress and load-transfer mechanism will optimize the information for the pile. Moreover, such analysis is necessary for any meaningful transfer of the test result to other piles for the same project as well as for gaining insight of general validity. Notice, forgetting that piles are subjected to residual force throws the most elaborate instrumentation and analysis scheme to the wind.

As indicated in the foregoing, the concept of ultimate resistance (capacity) does not apply to the pile toe. When accounting for residual force in an analysis, a pile toe does not develop a capacity failure, but shows only a line curving due to experiencing a moderately larger movement for each additional load increment. For most piles used in current practice, the failure load inferred from the pile head load-movement curve occurs at a pile toe movement (additional to that introduced by the residual force) in the range of 5 mm through 15 mm, about 10 mm on average. In a test performed for reasons beyond simple proof testing, as a minimum, a toe telltale should be included in the test and the analysis of the test results include establishing the q-z curve for the pile toe and the residual force. Moreover, the test should continue until a pile toe movement of at least 30 mm. The data and analysis will then enable estimating the long-term pile toe movement and pile toe load, which information is necessary for locating the neutral plane, determining the maximum load in the pile, and verifying the long-term settlement of the pile group.

It is often more advantageous to perform a bidirectional cell test rather than a conventional head-down test, because the cell test will provide separation of the shaft and toe resistances, the pile-toe load-movement behavior, and the residual force in the pile (at the location of the cell).

A small or moderate size project can normally only afford one static loading test. For driven piles, the pile driving can become a part of a dynamic test by means of the Pile Driving Analyzer and the analysis of measured strain and acceleration in the Analyzer and by means of CAPWAP and WEAP analysis (See Chapter 9). Dynamic testing is often also for bored piles. The dynamic test has the advantage of low cost and the possibility of testing several piles at the site to identify variations and ranges of results. It determines the adequacy of the pile driving equipment and enables the engineers to put capacity into context with the installation procedures. A CAPWAP analysis also produces the distribution of shaft resistance along the pile and determines the pile toe resistance. Notice, however, also the dynamic test may be affected by residual force, which results in the analysis exaggerating the shaft resistance and underestimating the toe resistance correspondingly. By testing and analyzing records from initial driving and from restrike after some time (letting set-up develop along with increased residual force), as well as testing a slightly shorter pile not driven to full toe resistance, engineering analysis will assist the analyses at very moderate extra cost.

When applying the results of a static loading test on a single pile to the design of a foundation supported by a group of piles, it quickly becomes obvious that the "capacity" of the single pile and the associated factor of safety are not always appropriate for the design of the piled foundation. Do not let the effort toward evaluating the pile capacity and factor of safety overshadow the fact that, in the end, it is the pile settlement that governs. The serviceability of a structure is the key aspect of a design.

To assess the settlement issue, the analysis of the loading test should produce information on the load distribution along a pile, the location of the neutral plane, and the anticipated settlement of the soils around the piles. When the results of even a routine test performed with no instrumentation are combined with a well-established soil profile and a static analysis (Chapter 7), reasonably representative load and resistance distributions can sometimes be derived even when the test is limited to just the pile-head load-movement records. The more important the project, the more information needs to be made available. The more detailed and representative the analysis of the pile behavior—for which a static loading test is only a part of the overall design effort—the more weight the settlement analysis gets and the less the "capacity" and the factor of safety govern the design.

It is important to realize that the analysis of the results of a static loading test is never better than the test allows. The so-called "standard test procedure" of loading up the pile in eight increments waiting for "zero movement" to occur at each load level and then keeping the maximum load on the pile for 24 hours is the worst possible test. Of course, if the pile capacity is larger than twice the allowable load (the usual maximum load applied in a routine pile loading test), the results of the test according to this method are very well able to prove this. However, a test by this method gives no information on what the margin

might be, and, therefore, gives no information on any savings of efforts, such as relaxing of pile depths, pile construction method, and pile driving termination criteria, etc. On the other hand, if the pile capacity is inadequate so that the pile fails before the maximum load, the “standard test procedure” provides very little information to use for determining the actual pile capacity (it probably occurred somewhere when adding the last increment, or when trying to do so). Nothing is so bad, however, that it cannot be made worse. Some “engineers”, some codes, even, incorporate, at one or two load levels, unloading and reloading of the pile and/or extra load-holding period, ensuring that the test results are practically useless for informed engineering decisions.

Frankly, the “standard 8-increment, 24- to 72-hour duration, test procedure” is only good for when the pile is good and not when it isn’t, and it is therefore a rather useless method.

The method that provides the best data for analysis of capacity and load-transfer is a test performed by means of several small increments applied at constant short time intervals. For example, the test should aim for applying a series of a minimum of 20 to 25 increments to at least twice the working load, each increment applied exactly after a specific duration, usually every 10 or 15 minutes. If the pile has not reached capacity and if the reaction system allows it, a few more increments can be applied, enhancing the value of the test at no cost. After the maximum load has been on the pile for the 10- or 15-minute increment duration, the pile should be unloaded in about six or eight steps with each held constant for no more than 2 minutes.

Notice, once a test is started with a certain increment magnitude and duration, do not change this at any time during the test. It is a common mistake to reduce the load increment size when the movement of the pile starts to increase. So, don’t. Start out with small enough increments, instead. And, notice, the response of the pile in the early part of the test is quite important for the analysis of the overall test results. As are a series of “zero” records before starting the test, which should include records during at least an hour with no load applied to the pile.

For some special cases, cyclic testing may provide useful information. However, the cyclic loading should not be combined with the test for load-transfer and capacity, but must be performed separately and after completion of the regular test. And, note, a simple unloading and reloading makes no cyclic test. A useful cyclic test requires many cycles, usually 20 to 50, and the sequence should be designed to fit the actual conditions of interest.

The absolutely best test for obtaining an optimum of information to use in the design of a piled foundation is to first carry out a bidirectional cell test and, thereafter, carry out a head-down test with the cell open so that all pile toe resistance is eliminated from the test. Such a test will not only allow for determination of the unknowns of the soil response to the pile load, but also provide the means for assessing the unknown unknowns that invariably pop up in the course of the design and construction work. It is important to recognize, however, that the head-down test will be a test on a pile with residual forces built in from the preceding bidirectional test, which fact and effect will have to be incorporated in the analysis of the test data.

A static loading test must be performed using a jack pump able to automatic pressure-holding and mechanical increase of pressure to generate the next load. Manual activation of the pump to hold the load and manual pumping to raise the load to the next level is a thing of the past and has no place in today’s world where higher quality of the engineering work is required and expected. The load actually applied to the pile must be monitored by a separate load cell, not the jack pressure gage. A common mistake in recording the test measurements is to take note of the load that was intended to be applied to the pile head instead of the load that the load cell shows was applied. By all means let the jack pressure guide you to the load to apply, but let the data logger record it from the separate load cell (along with the jack pressure).

The days of manually reading the gages and noting down the values are long since gone. A static loading test must have all readings obtained by a data logger (data acquisition system). Moreover, the data logger must be able to record all records with reference to a common date-time stamp. Do not try to save costs by having two separate data loggers and believe that the records can be reliable "married" via the date-time stamp for each set of records. My experience is that ever so often a line shift is made and a "divorce" occurs before the marriage is completed.

If someone balks at the quality requirements, rather arguing about the cost of the purchase of the equipment, point out that omitting the use of the data logger and load cell is rather dim-witted in light of, first, the fact that the costs are minimal compared to the costs of the tests and, second, not including proper equipment might jeopardize much of the value of the test. The argument that "***we have never needed this before***" is hardly worth a comment; someone from the stone age cannot comprehend much of it anyway. But, ignorance and learning aversion is no excuse.

After the test is concluded, the records must be reviewed and analyzed. There is not much one can do with a conventional routine test involving only the pile-head load-movement records. Instrumented tests need some work, of course. First, reduce the strain records to show the change of strain as the test progressed. However, always include with the test data the zero-strain from the factory calibration, the readings after having attached the gages (sister bars) to the reinforcing cage (or similar), the readings immediately after lowering the instrumented reinforcing cage in the pile, the readings immediate before and after concreting (grouting) the pile, and frequently during the wait time before the start of the static loading test (more frequently during the first 48 hours). Strain-gages are equipped with a temperature sensor, so record also the temperature.

After compiling the test records in a spread sheet table:

- 1) Verify the relevance of all records by plotting and reviewing for all gages the applied load versus the individually measured strains and the average of each gage.
- 2) For a head-down test, plot the secant stiffness ( $Q/\mu\epsilon$ ) versus the average strain for the gage pair closest to the pile head.
- 3) Plot for all gage pairs, the tangent stiffness ( $\Delta Q/\Delta\mu\epsilon$ ) versus the average strain and use the plot to obtain the secant stiffness, EA, relation(s). A judgment call will show what stiffness to use for all gage records or if to apply different values to different gage levels.
- 4) Use the values of secant EA-stiffness to calculate (multiply EA and measured values of average strain) and plot the results in a load-distribution graph.
- 5) Select one or more suitable load-distributions to use as target for an effective stress simulation (using UniPile) and have the software compute the load-movement for the pile head and the pile toe in static loading test as well as the individual load-movement or stress-movement for the gage levels. Compare the latter to the measured gage loads and estimates of the gage movements. If using the Glostrex system, the movements are part of the measuring system.
- 6) Review the results. You will always learn something new from each test.

The Case I bidirectional test reported in Section 8.16.5 was balanced, that is, the test established both the shaft and toe resistance responses. Had the results been unbalanced, that is, had the results only showed a good response of the pile the upper length (upward response) or of the lower length (downward response), then, combining a bidirectional cell test with a conventional head-down test and performing the

bidirectional test first would have provided a test determining both responses. Then, had the "weakest" part of the pile been to toe response, the subsequent head-down test would have established the shaft response. If, instead, the shaft response had been the "weakest" part, the add-on resistance provided by a head-down arrangement would have enable the bidirectional test to determine the toe response in a repeat test. The combination is obtained at low-cost because the head-down load will be small. In fact, performing a head-down test after the bidirectional cell test will always optimize and enhance the value of the bidirectional test. Note, however, that if the pile is a bored pile with some bulges along its length, these will introduce resistance points in the first test. In the second test, which now reverses the direction of movement, these resistance points will not engage the soil appreciably until the "reverse direction" movement becomes about the same as that of the first. The difference will imply a less stiff initial response to the applied loads for the second test. Moreover, the strain records of the repeated loading will be affected by locked-in strains and not be fully suitable for detailed analysis of the load distribution.

*In spite of their obvious deficiencies and unreliability, pile driving formulas still enjoy great popularity among practicing engineers, because the use of these formulas reduces the design of pile foundations to a very simple procedure. The price one pays for this artificial simplification is very high.* Karl Terzaghi (1942); Also stated in Terzaghi (1943) Theoretical Soil Mechanics. John Wiley & Sons, New York.

## CHAPTER 9

### PILE DYNAMICS

#### 9.1 Introduction

The development of the wave equation analysis from the pre-computer era of the fifties (Smith 1960) to the advent of a computer version in the mid-seventies was a quantum leap in foundation engineering. For the first time, a design could consider the entire pile driving system, such as wave propagation characteristics, particle-velocity dependent aspects (damping), soil deformation characteristics, soil resistance (total as well as its distribution of resistance along the pile shaft and between the pile shaft and the pile toe), hammer behavior, and hammer cushion and pile cushion parameters.

The full power of the wave equation analysis is first realized when combined with dynamic monitoring of the pile during driving. The dynamic monitoring consists in principle of recording and analyzing the strain and acceleration induced in the pile by the hammer impact. It was developed in the USA by Drs. G.G. Goble and F. Rausche, and co-workers at Case Western University in the late 1960s and early 1970s. It has since evolved further and, as of the early 1980s, it was accepted all over the world as a viable tool in geotechnical engineering practice.

Pile driving consists of forcing a pile to penetrate into the ground by means of a series of short duration impacts. The impact force has to be greater than the static soil resistance, because a portion of the force is needed to overcome the dynamic resistance to the pile penetration (the dynamic resistance is a function of the particle velocity of the pile). Mass of the ram (hammer), ram impact velocity, specifics of the pile helmet and of cushioning element such as hammer and pile cushions, as well as cross section of the ram, and cross section and length of the pile are all important factors to consider in an analysis of a specific pile driving situation. Of course, also the soil parameters, such as strength, shaft resistance including its distribution along the pile, toe resistance, and dynamic soil parameters, must be included in the analysis. It is obvious that for an analysis to be relevant requires that information used as input to the analysis correctly represents the conditions at the site. It a complex undertaking. Just because a computer program allows input of many parameters does not mean that the analysis results are true to the situation analyzed.

The soil resistance acting against a driven pile is based on the same mechanics as the resistance developed from a static load on the pile. That is, the resistance is governed by the principle of effective stress. Therefore, to estimate in the design stage how a pile will behave during driving at a specific site requires reliable information on the soil conditions including the location of the groundwater table and the pore pressure distribution. For method and details of the static analysis procedures, refer to Chapter 7.

The design of piles for support of a structure is directed toward the site conditions prevailing during the life of the structure. However, the conditions during the pile installation can differ substantially from those of the service situation—invariably and considerably. The installation may be represented by the initial driving conditions, while the service situation may be represented by the restrrike conditions.

Questions of importance at the outset of the pile driving are the site conditions, including soil profile and details such as the following: will the piles be driven in an excavation or from the existing ground surface, is there a fill on the ground near the piles, and where is the groundwater table and what is the pore pressure distribution? Additional important questions are: will the soils be remolded by the driving and develop excess pore pressures? Is there a risk for the opposite, that is, dilating conditions, which may impart a false resistance? Could the soils become densified during the continued pile installation and cause the conditions to change as the pile driving progresses? To properly analyze the pile driving conditions and select the pile driving hammer requires the answers to questions such as these.

In restriking, the pore pressure distribution, and, therefore, the resistance distribution is very different to that developing during the initial driving. For this reason, a pile construction project normally involves restriking of piles for verification of capacity. Usually, the restrike observation indicates that a set-up has occurred. (Notice, it is not possible to quantify the amount of soil set-up unless the hammer is able to move the pile). On occasions, the restrike will show that relaxation, i.e., diminishing capacity, the opposite to soil set-up, may have occurred, instead.

As is the case for so much in engineering design and analysis, the last few decades have produced immense gains in the understanding of “how things are and how they behave”. Thus, the complexity of pile driving in combination with the complexity of the transfer of the loads from the structure to a pile can now be addressed by rational analysis. In the past, analysis of pile driving was simply a matter of applying a so-called pile driving formula to combine “blow count” and capacity. Several hundred such formulae exist. They are all fundamentally flawed and lack proper empirical support. Their continued use is strongly discouraged.<sup>1</sup>

## 9.2. Principles of Hammer Function and Performance

Rather simplistically expressed, a pile can be installed by means of a static force, i.e. a load, which forces the pile into the soil until it will not advance further. Such installation techniques exist and the piles are called “jacked-in piles”, see for example Yang et al. (2006) and Fellenius (2015). The jacked load is then about equal to the static capacity of the pile. However, for most piles and conditions, the magnitude of the static load needs to be so large as to make it impractical to use a static load to install a pile other than under special conditions.

---

<sup>1</sup> In the past, when an engineer applied a “proven” formula — “proven” by the engineer through years of well-thought-through experience from the actual pile type and geology of the experience — the use of a dynamic formula could be defended. It did not matter what formula the engineer preferred to use, the engineer’s ability was the decisive aspect. That solid experience is vital is of course true also when applying modern methods. The engineers of today, however, can lessen the learning pain and save much trouble and costs by relating their experience to the modern methods. Sadly, despite all the advances, dynamic formulae are still in use. For example, some Transportation Authorities and their engineers even include nomograms of the Hiley formula in the contract specifications, refusing to take notice of the advances in technology and practice! Well, each generation has its share of die-hards. A couple of centuries or so ago, they, or their counterpart of the days, claimed that the Earth was round, that ships made of iron could not float, that the future could be predicted by looking at the color of the innards of a freshly killed chicken, etc., rejecting all evidence to the contrary. Let’s make it absolutely clear, basing a pile design today on a dynamic formula shows unacceptable ignorance and demonstrates incompetence. Note, however, that the use of the most sophisticated computer program does not provide any better results unless coupled with experience and good judgment.



In driving a pile, one is faced with the question of what portion of the applied dynamic force is effective in overcoming the capacity (that is, the “useful” static soil resistance) and what portion is used-up to overcome the resistance to the pile movement, or, rather, its velocity of penetration. This velocity dependent resistance is called damping. In principle, a pile is driven by placing a small weight some distance over the pile head and releasing it to fall. In falling, the weight picks up velocity, and, on impacting the pile head, it slows down before bouncing off the pile head. The weight’s change of velocity, that is, this deceleration, creates a force between the hammer and the pile during the short soil, overcoming static resistance, inertia of the masses involved, as well as overcoming resistance due to duration of the contact. Even a relatively light weight impacting at a certain significant velocity can give rise to a considerable force in the pile, which then causes the pile to penetrate a short distance into the velocity of penetration. Accumulation of impacts and consequential individual penetrations make up the pile installation.

The impact duration is so short, typically 0.05 seconds, that although the peak penetration velocity lies in the range of several metre/second, the net penetration for a blow is often no more than about a millimetre or two. (Considering ‘elastic’ response of pile and soil, the gross penetration per blow can be about 20 times larger). In contrast to forcing the pile down using a static force, when driving a pile, the damping force is often considerable. For this reason, the driving force must be much larger than the desired pile capacity.<sup>2)</sup>

The ratio between the mass of the impacting weight and the mass of the pile (or, rather, its cross section and total mass) and its velocity on impact will govern the magnitude of the impact force (impact stress) and the duration of the impact event. A light weight impacting at high velocity can create a large local stress, but the duration may be very short. A low-velocity impact from a heavy weight may have a long duration, but the force may not be enough to overcome the soil resistance. The impact velocity of a ram and the duration of a blow are, in a sense, measures of force and energy, respectively.

The force generated during the impact is not constant. It first builds up very rapidly to a peak and, then, decays at a lesser rate. The peak force can be very large, but be of such short duration that it results in no pile penetration. Yet, it could be larger than the strength of the pile material, which, of course, would result in damage to the pile head. By inserting a cushioning pad between the pile head and the impacting weight (the hammer or ram), this peak force is reduced and the impact duration is lengthened, thus both keeping the maximum force below damaging values and making it work longer, i.e., increasing the penetration per blow.

The effect of a hammer impact is a complex combination of factors, such as the velocity at impact of the hammer, the weight of the hammer (impacting mass) and the weight of the pile, the cross section of the hammer and the cross section of the pile, the various cushions in the system between the hammer and the pile, and the condition of the impact surfaces (for example, a damage to the pile head would have a subsequent cushioning effect on the impact, undesirable as it reduces the ability of the hammer to drive the pile), the weight of the supporting system involved (for example, the weight of the pile driving helmet), and last, but not least, the soil resistance, how much of the resistance is toe resistance and how much is shaft resistance, as well as the distribution of the shaft resistance. All these must be considered when selecting a hammer for a specific situation to achieve the desired results, that is, a pile installed the pile to a certain depth and/or capacity, quickly and without damage.

---

<sup>2</sup> This seemingly obvious statement is far from always true. The allowable load relates to the pile capacity after the disturbance from the pile driving has dissipated. In the process, the pile will often gain capacity due to set-up (see Chapter 7).

Old rules-of-thumb, e.g., that the pile weight to ram weight ratio should be ‘at least 2 for an air/steam hammer’ and ‘at least 4 for a diesel hammer’ are still frequently quoted. These rules, however, only address one of the multitudes of influencing aspects. They are also very inaccurate and have no general validity.

The hammer energy, or rather, the hammer “**rated energy**” is frequently used to indicate the size of a hammer and its suitability for driving a certain pile. The rated energy is the weight of the ram times its travel length and it is, thus, the same as the “positional” energy of the hammer. The rated or positional energy is a rather diffuse term to use, because it has little reference to the energy actually delivered to the pile and, therefore, it says very little about the hammer performance. By an old rule-of-thumb, for example, for steel piles, the rated energy of a hammer was referenced to the cross section of the pile as  $6 \text{ MJ/m}^2$ . This rule has little merit and leads often to an incorrect choice of hammer. (In English units, the rule was 3 ft-kips per square inch of steel).

A more useful reference for pile driving energy is the “**transferred energy**”, which is energy actually transferred to a pile and, therefore, useful for the driving. It can be determined from measurements of acceleration and strain near the pile head during actual pile driving obtained by means of the Pile Driving Analyzer (see Section 9.7). The transferred energy value is determined after losses of energy have occurred (such as losses before the ram impacts the pile, impact losses, losses in the helmet, and between helmet and pile head).

Although, no single definition for hammer selection includes all aspects of the pile driving, energy is one of the more important aspects. Energy is addressed in more than one term, as explained in the following.

The term “**energy ratio**” is also commonly used to characterize a hammer function. The energy ratio is the ratio between the transferred energy and the rated energy. This value is highly variable as evidenced in the frequency chart shown in Fig. 9.1. The measurements shown in the diagram were from properly functioning hammer and the variations are representative for variation that can occur in the field.

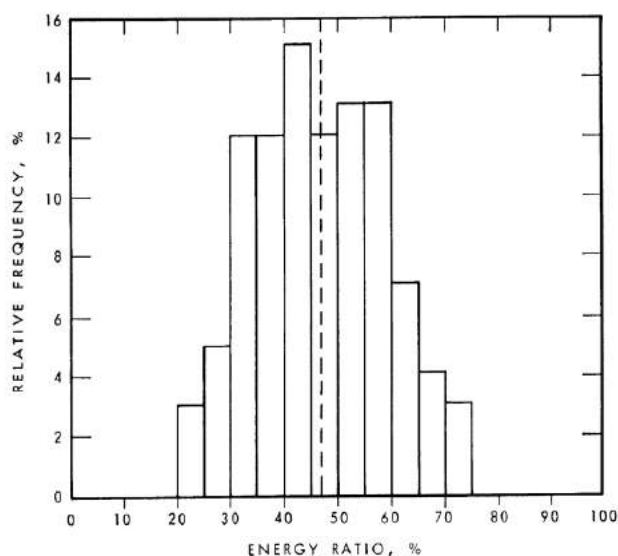


Fig. 9.1 Energy ratio

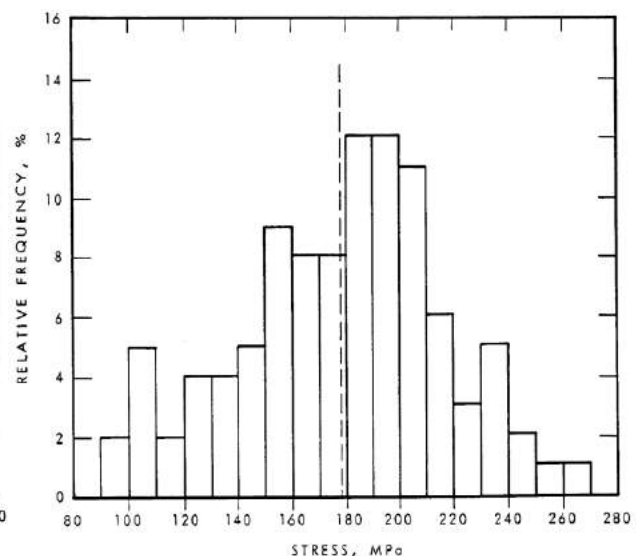


Fig. 9.2 Impact stress

From measurements on 226 steel piles (data from Fellenius et al. 1978)

For example, the term “**hammer efficiency**”. Hammer efficiency is defined as the ratio between the kinetic energy of the ram at impact to the ideal kinetic energy, which is a function of the ram velocity. A 100 % efficiency corresponds to ideal kinetic energy: the velocity the ram would be the same as the ram would have had in free fall in vacuum with no losses. Notice, the hammer efficiency does not consider the influence of cushioning and losses in the helmet, the helmet components, and the pile head.

Obviously, energy alone is not a sufficient measure of the characteristic of an impact. Knowledge of the magnitude of the impact force is also required and it is actually the more important parameter. However, as the frequency chart presented in Fig. 9.2 demonstrates, field measurements indicate that also the impact stress varies considerably.

The reasons for the variations of energy and stress are only partly due to a variation of hammer size, hammer cushion characteristics, and hammer performance. The variations are also due to factors such as pile size (diameter and cross sectional area), pile length, and soil characteristics. As will be explained below, these factors can be taken into account in a wave equation analysis.

### 9.3. Hammer Types

The oldest pile driving hammer is the conventional “**drop hammer**”. Its essential function was described already by Caesar 2,000 years ago in an account of a Roman campaign against some Germanic tribe (building a bridge, no less). The drop hammer is still commonly used. As technology advanced, hammers that operate on steam power came into use around the turn of the century. Today, steam power is replaced by air power from compressors and the common term is now “**air/steam hammer**”. Hammers operating on diesel power, “**diesel hammers**”, were developed during the 1930s. An advancement of the air/steam hammer is the “**hydraulic hammer**”, which uses air pressure in addition to lifting the ram, accelerate it downward to a large impact velocity after a small travel length. Electric power is used to operate “**vibratory hammers**”, which function on a principle very different to that of impact hammers. Commonly used hammers are described below.

#### 9.3.1 Drop Hammers

The conventional drop hammer consists chiefly of a weight that is hoisted to a distance above the pile head by means of a cable going up to a pulley on top of the leads and down to be wound up on a rotating drum in the pile driver machine. When released, the weight falls by gravity pulling the cable along and spinning the drum where the excess cable length is stored. The presence of the cable influences the efficiency of the hammer.<sup>3)</sup> The influence depends on total cable length (i.e., mass) as well as the length of cable on the drum, the length between the drum and the top of the leads, and the length of cable between the leads and the drop weight. This means, that the efficiency of the hammer operating near the top of the leads differs from when it operates near the ground. The amount of friction between the ram weight and the guides in the leads also influences the hammer operation and its efficiency. Whether the pile is vertical or inclined is another factor affecting the frictional losses during the “fall” and, therefore, the hammer efficiency. In addition, to minimize the bouncing and rattling of the weight, the operator usually tries to catch the hammer on the bounce, engaging the reversal of the drum before the impact. In the process, the cable is often tightened just before the impact, which results in a slowing down of the falling ram weight just before the impact, significantly reducing the efficiency of the impact.

---

<sup>3</sup> Note, as indicated above, hammer efficiency is a defined ratio of kinetic energy and the term must not be used loosely to imply something unspecified but essentially good and desirable about the hammer.

### 9.3.2 Air/Steam Hammers

The air/steam hammer operates on compressed air from a compressor or steam from a boiler, which is fed to the hammer through a hose. Fig. 9.3 illustrates the working principle of the single-acting air/steam hammer. (The figure is schematic and does not show assembly details such as slide bar, striker plate helmet items, etc.). At the start of the upstroke, a valve opens letting the air (or steam) into a cylinder and a piston, which hoists the ram. The air pressure and the volume of air getting into the cylinder controls the upward velocity of the ram. After a certain length of travel (the upward stroke), the ram passes an exhaust port and the exhaust valve opens (by a slide bar activating a cam), which vents the pressure in the cylinder and allows the ram to fall by gravity to impact the hammer cushion and helmet anvil. At the end of the downward stroke, another cam is activated which opens the inlet valve starting the cycle anew. The positional, nominal, or rated energy of the hammer is the stroke times the weight of the ram with its parts such as piston rod, keys, and slide bar.

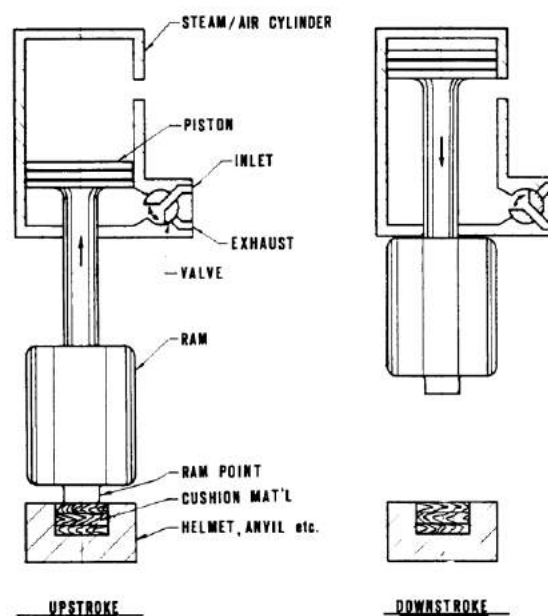


Fig. 9.3 The single-acting air/steam hammer (DFI 1979; used with permission)

As in the case of the drop hammer, the efficiency of the impact is reduced by friction acting against the downward moving ram. However, two very important aspects specific to the air/steam hammer can be of greater importance for the hammer efficiency. First, the inlet valve is always activated shortly before the impact, creating a small pre-admission of the air. If, however, the release cam is so placed that the valve opens too soon, the air that then is forced into the cylinder will slow the fall of the weight and reduce the hammer efficiency. The design of modern air/steam hammers is such as to trap some air in above the ram piston, which cushions the upward impact of the piston and gives the downward travel an initial “push”. The purpose of the “push” is also to compensate for the pre-admission at impact. For more details, see the hammer guidelines published by Deep Foundations Institute (DFI 1979).

When the air pressure of the compressor (or boiler) is high, it can accelerate the upward movement of the ram to a significant velocity at the opening of the exhaust port. If so, the inertia of the weight will make it overshoot and travel an additional distance before starting to fall (or increase the “push” pressure in the “trap”), which will add to the ram travel and seemingly increase the efficiency.

For the double-acting air/steam hammer, air (steam) is also introduced above the piston to accelerate the down stroke, as illustrated in Fig. 9.4. The effect of this is to increase the impact rate, that is, the number of blows per minute. A single-acting hammer may perform at a rate of about 60 blows/minute, and a double acting may perform at twice this rate. The rated energy of the double-acting hammer is more difficult to determine. It is normally determined as the ram stroke times the sum of the weights and the area of the piston head multiplied by the downward acting air pressure. The actual efficiency is quite variable between hammers, even between hammers of the same model and type. Where the ram velocity at impact is measured, this determines the kinetic energy that then is used in lieu of rated energy.

A double-acting air/steam hammer is closed to its environment and can be operated submerged.

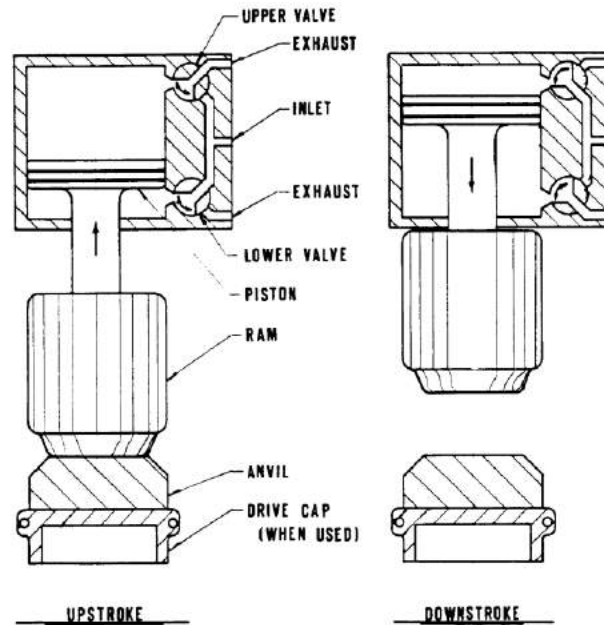


Fig. 9.4 The double-acting air/steam hammer (Deep Foundations Institute 1979)

### 9.3.3 Diesel Hammers

A diesel hammer consists in principle of a single cylinder engine. A diesel hammer is smaller and lighter than an air/steam hammer of similar capability. Fig. 9.5 illustrates the working principle of a liquid injection **single-acting open-end diesel hammer**. The hammer is started by raising the ram with a lifting mechanism. At the upper end of its travel, the lifting mechanism releases the ram to descend under the action of gravity. When the lower end of the ram passes the exhaust ports, a certain volume of air is trapped, compressed, and, therefore, heated. Some time before impact, a certain amount of fuel is squirted into the cylinder onto the impact block. When the ram end impacts the impact block, the fuel splatters into the heated compressed air, and the combustion is initiated. There is a small combustion delay due to the time required for the fuel to mix with the hot air and to ignite. More volatile fuels have a shorter combustion delay as opposed to heavier fuels. This means, for example, that if winter fuel would be used in the summer, pre-ignition may result. Pre-ignition is combustion occurring before impact and can be caused by the wrong fuel type or an overheated hammer. Pre-ignition is usually undesirable.

The rebound of the pile and the combustion pressure push the ram upward. When the exhaust ports are cleared, some of the combustion products are exhausted leaving in the cylinder a volume of burned gases at ambient pressures. As the ram continues to travel upward, fresh air, drawn in through the exhaust ports, mixes with the remaining burned gases.

The ram will rise to a height (stroke) that depends on the reaction of the pile and soil combination to the impact and to the energy provided by the combustion. It then descends under the action of gravity to start a new cycle. The nominal or rated energy of the hammer is the potential energy of the weight of the ram times its travel length. It has been claimed that the energy released in the combustion should be added to the potential energy. That approach, however, neglects the loss of energy due to the compression of the air in the combustion chamber.

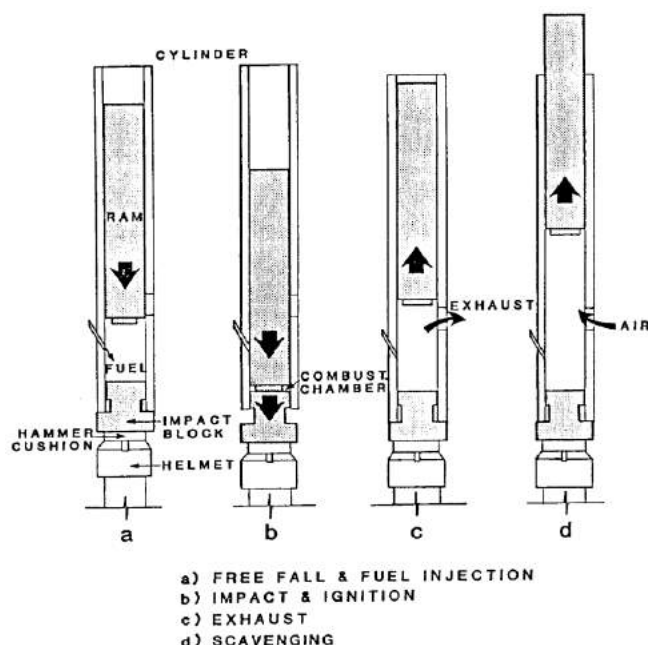


Fig. 9.5 Working principle of the liquid injection, open-end diesel hammer (GRL 2002)

The sequence of the combustion in the diesel hammer is illustrated in Fig. 9.6 showing the pressure in the chamber from the time the exhaust port closes, during the precompression, at impact, and for the combustion duration, and until the exhaust port opens. The diagram illustrates how the pressure in the combustion chamber changes from the atmospheric pressure just before the exhaust port closes, during the compression of the air and the combustion process until the port again opens as triggered by the ram upstroke. During the sequence, the volume of the combustion chamber changes approximately in reverse proportion to the pressure. Different hammers follow different combustion paths and the effect on the pile of the combustion, therefore, differs between different hammers.

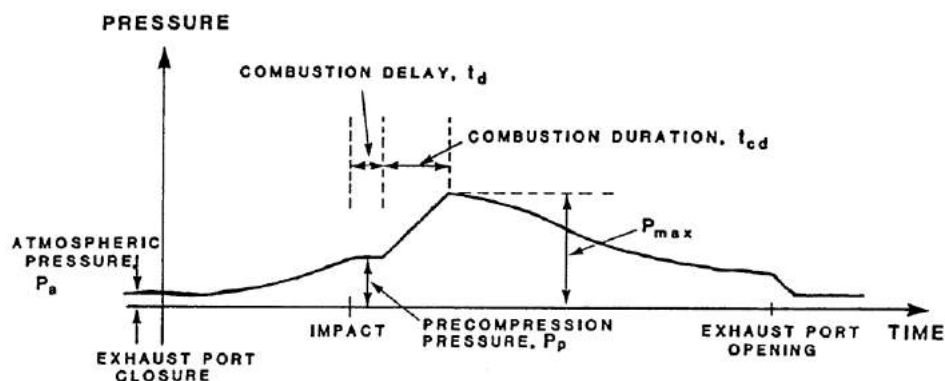


Fig. 9.6 Liquid injection diesel hammer: pressure in combustion chamber versus time (GRL 2002)

The pressure in the chamber can be reduced if the cylinder or impact block rings allow pressure to leak off resulting in poor compression and inadequate ram rise, that is, reduced efficiency. Other reasons for low ram rise is excessive friction between the ram and the cylinder wall, which may be due to inadequate lubrication or worn parts, or a poorly functioning fuel pump injecting too little fuel into the combustion chamber.

The reason for a low hammer rise lies usually not in a poorly functioning hammer. More common causes are “soft or spongy soils” or long flexible piles, which do not allow the combustion pressure to build up. The hammer rise (ram travel) of a single-acting diesel hammer is a function of the blow-rate, as shown in Eq. 9.1 (derived from the basic relations Acceleration =  $g$ ; Velocity =  $gt$ ; Distance =  $gt^2/2$  and recognizing that for each impact, the hammer travels the height-of-fall twice).

$$(9.1) \quad H = \frac{g}{8f^2}$$

where  $H$  = hammer stroke (m)  
 $g$  = gravity constant ( $m/s^2$ )  
 $f$  = frequency (blows/second)

In practice, however, the hammer blow rate is considered in blows per minute, BPM, and the expression for the hammer rise in metre is shown by Eq. 9.2 (English units—rise in feet—are given in Eq. 9.2a). The hammer rise (ft) as a function of the blow rate (blows/min) expressed by Eq. 9.2a is shown in Fig. 9.7.

$$(9.2) \quad H = \frac{4,400}{BPM^2}$$

$$(9.2a) \quad H = \frac{14,400}{BPM^2}$$

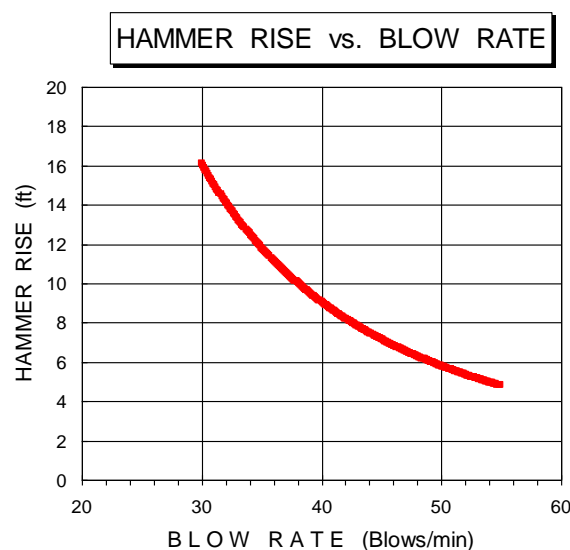


Fig. 9.7 Hammer rise (ft) as a function of blow-rate (BPM). Single-acting diesel hammer. Effect of friction in ram cylinder is not included)

Eqs. 9.2 and 9.2a provide a simple means of determining the hammer rise in the field. The ram travel value so determined is more accurate than sighting against a bar to physically see the hammer rise against a marked stripe.

For some types of hammers, which are called **atomized injection hammers**, the fuel is injected at high pressure when the ram has descended to within a small distance of the impact block. The high pressure injection mixes the fuel with the hot compressed air, and combustion starts almost instantaneously. Injection then lasts until some time after impact, at which time the ram has traveled a certain distance up from the impact block. The times from the start of injection to impact and then to the end of combustion depend on the velocity of the ram. The higher the ram velocity, the shorter the time periods between ignition, impact, and end of combustion.

Similar to the drop hammer and air/steam hammer, on and during impact of a diesel hammer ram, the impact block, hammer cushion, and pile head move rapidly downward leaving cylinder with no support. Thus, it starts to descend by gravity and when it encounters the rebounding pile head, a secondary impact to the pile results called “**assembly drop**”.

**Closed-end diesel hammers** are very similar to open end diesel hammers, except for the addition of a bounce chamber at the top of the cylinder. The bounce chamber has ports which, when open, allow the pressure inside the chamber to equalize with atmospheric pressure. As the ram moves toward the cylinder top, it passes these ports and closes them. Once these ports are closed, the pressure in the bounce chamber increases rapidly, stops the ram, and prevents a metal to metal impact between ram and cylinder top. This pressure can increase only until it is in balance with the weight and inertial force of the cylinder itself. If the ram still has an upward velocity, uplift of the entire cylinder will result in noisy rattling and vibrations of the system, so-called “racking”. Racking of the hammer must not be tolerated as it can lead both to an unstable driving condition and to the destruction of the hammer. For this reason, the fuel amount, and hence maximum combustion chamber pressure, has to be reduced so that there is only a very slight “lift-off” or none at all.

#### 9.3.4 Direct-Drive Hammers

A recent modification of the atomized injection hammer is to replace the hammer cushion with a striker plate and to exchange the pile helmet for a lighter “direct drive housing”. This change, and other structural changes made necessary by the modification, improves the alignment between the hammer and the pile and reduces energy loss in the drive system. These modified hammers are called “direct drive hammers” and measurements have indicated the normally beneficial results that both impact force and transferred energy have increased due to the modification.

#### 9.3.5 Vibratory Hammers

The vibratory hammer is a mechanical sine wave oscillator with two weights rotating eccentrically in opposite directions so that their centripetal actions combine in the vertical direction (pile axis direction), but cancel out in the horizontal. The effect of the vibrations is an oscillating vertical force classified to frequency and amplitude.

Vibratory hammers work by eliminating soil resistance acting on the pile. The vibrations generate pore pressures which reduce the effective stress in the soil and, therefore, the soil shear strength. The process is more effective along the pile shaft as opposed to the pile toe and works best in loose to compact silty sandy soils, which do not dilate and where the pore pressure induced by the cyclic loading can accumulate (draining off is not immediate).



The pile penetrates by force of its own weight plus that of the hammer weight plus the vertical force (a function of the amplitude of the pulse) exerted by the hammer. Two types of drivers exist: drivers working at high frequency, and drivers working at a low frequency in resonance with the natural frequency of the soil. For details, see Massarsch (2004; 2005) and Section 9.14.

Because the fundamental effect of the vibratory hammer is to reduce or remove soil resistance, the capacity cannot be estimated from observations of pile penetration combined with hammer data, such as amplitude and frequency. This is because the static resistance ('capacity') of the pile during the driving is much smaller than the resistance (capacity) of the pile after the driving and only the resistance during the driving can be estimated from observations during the driving. The resistance removed by the vibrations is usually the larger portion and it is not known from any observation.

Several case histories have indicated that vibratorily driven piles have smaller shaft resistance as opposed to impact driven piles. This is of importance for tension piles. Note, however, that the difference between the two types of installation may be less in regard to cyclically loaded piles, for example, in the case of an earthquake, where the advantage of the impact driven pile may disappear.

## 9.4 Basic Concepts

When a hammer impacts on a pile head, the force, or stress, transferred to the pile builds progressively to a peak value and then decays to zero. The entire event is over within a few hundreds of a second. During this time, the transfer initiates a compression strain wave that propagates down the pile at the speed of sound (which speed is a function of the pile material—steel, concrete, or wood). At the pile toe, the wave is reflected back toward to the pile head. If the pile toe is located in dense soil, the reflected wave is in compression. If the pile toe is located in soft soil, the reflection is in tension. Hard driving on concrete piles in soft soil can cause the tension forces to become so large that the pile may be torn apart, for example<sup>4)</sup>.

That pile driving must be analyzed by means of the theory of wave propagation in long rods has been known since the 1930s. The basics of the mathematical approach was presented by E.A. Smith in the late 1950s. When the computer came into common use in the early 1970s, wave equation analysis of pile driving was developed at the Texas A&M University, College Station, and at the Case Western Reserve University, Cleveland. Computer software for wave equation analysis has been available to the profession since 1976.

During the past two decades, a continuous development has taken place in the ease of use and, more important, the accuracy and representativeness of the wave equation analysis. Several generations of programs are in use as developed by different groups. The most versatile and generally accepted program is the GRLWEAP (2002).

---

<sup>4)</sup> What driving tension to accept or permit in precast concrete piles is often mismanaged, be the piles ordinary reinforced or prestressed. Most standards and codes indicate the limit tension to be a percentage of the steel yield plus a portion of the concrete tension strength. For prestressed pile, the limit for the steel reinforcement (the strands) is often set to the net prestress value for the pile (leading some to believe that ordinary reinforced precast piles, having no net prestress, cannot accept driving tension!). However, the unacceptable level of driving tension will occur where the pile has developed a crack and where then only the reinforcement is left to resist the tension and hold the pile together. Therefore, no contribution can be counted on from the concrete tension strength—it may be a definite feature everywhere else in the pile, but not in that crack. The allowable driving tension is simply the steel yield divided by a factor of safety, usually about 1.5, which is applicable to ordinary reinforced as well as prestressed pile alike. Incidentally, the net prestress is usually about  $\approx 70\%$  of the strand yield point, that is about  $1/1.5$ , which makes the net prestress a good value for what tension value to accept, though the fact of the prestressing is not the relevant point in this context.

Axial wave propagation occurs in a uniform, homogeneous rod—a pile—is governed by Eq. 9.3.

$$(9.3) \quad \sigma = \frac{E}{c} v \quad \text{derived from the "Wave Equation":} \quad \rho \frac{\partial^2 u}{\partial t^2} = E \frac{\partial^2 u}{\partial x^2}$$

where

$\sigma$	=	stress	
$E$	=	Young's modulus	
$c$	=	wave propagation speed	$c = \sqrt{\frac{E}{\rho}}$
$v$	=	particle velocity	

The wave equation analysis starts the pile driving simulation by letting the hammer ram impact the pile at a certain velocity, which is imparted to the pile head over a large number of small time increments. The analysis calculates the response of the pile and the soil. The hammer and the pile are simulated as a series of short infinitely stiff elements connected by weightless elastic springs. Below the ground surface, each pile element is affected by the soil resistance defined as having elastic and plastic response to movement and a damping (viscous) response to velocity. Thus, a 20 metre long pile driven at an embedment depth of 15 metre may be simulated as consisting of 20 pile elements and 15 soil elements. The time increments for the computation are set approximately equal to the time for the strain wave to travel the length of half a pile element. Considering that the speed of travel in a pile is in the range of about 3,000 m/s through 5,000+ m/s, each time increment is a fraction of a millisecond and the analysis of the full event involves more than a thousand calculations. During the first few increments, the momentum and kinetic energy of the ram is imparted to the pile accelerating the helmet, cushions, and pile head. As the calculation progresses, more and more pile elements become engaged. The computer keeps track of the development and can output how the pile elements move relative to each other and to the original position, as well as the velocities of each element and the forces and stresses developing in the pile.

The **damping** or viscous response of the soil is a linear function of the velocity of the pile element penetration (considering both downward and upward direction of pile movement). The damping response to the velocity of the pile is a crucial aspect of the wave equation simulation, because only by knowing the damping can the static resistance be separated from the total resistance to the driving. Parametric studies have indicated that in most cases, a linear function of velocity will result in acceptable agreement with actual behavior. Sometimes, an additional damping called radial damping is considered, which is dissipation of energy radially away from the pile as the strain wave travels down the pile.

The material constant, **impedance, Z**, is very important for the wave propagation. It is a function of pile modulus, cross section, and wave propagation speed in the pile as given in Eq. 9.4.

$$(9.4) \quad Z_p = \frac{E_p A_p}{c_p}$$

where

$Z_p$	=	pile impedance
$E_p$	=	Young's modulus of the pile material
$A_p$	=	pile cross section area
$c_p$	=	wave propagation speed (= speed of sound in the pile)

Combining Eqs. 9.3 and 9.4 yields Eq. 9.5 and shows that the force is equal to impedance times pile velocity. Or, in other words, force and wave speed in a pile are proportional to impedance. This fact is a key aspect of the study of force and velocity measurements obtained by means of the Pile Driving Analyzer (see Section 9.7).

$$(9.5) \quad \sigma A = F = Z_P v_P$$

where  $\sigma$  = axial stress in the pile  
 $A$  = pile cross section area  
 $F$  = force in the pile  
 $Z_P$  = pile impedance  
 $v_P$  = pile particle velocity

Eqs. 9.4 and 9.5 can be used to calculate the axial impact force in a pile during driving, as based on measurement of the pile particle velocity (also called "physical velocity"). Immediately before impact, the particle velocity of the hammer is  $v_0$ , while the particle velocity of the pile head is zero. When the hammer strikes the pile, a compression wave will be generated simultaneously in the pile and in the hammer. The hammer starts to slows down, by a velocity change denoted  $v_H$ , while the pile head starts to accelerate, gaining a velocity of  $v_P$ . (The pile head velocity before impact is zero, the velocity change at the pile head is the pile head velocity). Since the force between the hammer and the pile must be equal, applying Eq. 9.3 yields the relationship expressed in Eq. 9.6.

$$(9.6) \quad Z_H v_H = Z_P v_P$$

where  $Z_H$  = impedance of impact hammer  
 $Z_P$  = impedance of pile  
 $v_H$  = particle velocity of wave reflected up the hammer  
 $v_P$  = particle velocity of pile

At the contact surface, the velocity of the hammer — decreasing — and the velocity of the pile head — increasing — are equal, as expressed in Eq. 9.7. Note, the change of hammer particle velocity is directed upward, while the velocity direction of the pile head is downward (gravity hammer is assumed).

$$(9.7) \quad v_0 - v_H = v_P$$

where  $v_0$  = particle velocity of the hammer immediately before impact  
 $v_H$  = particle velocity of wave reflected up the hammer  
 $v_P$  = particle velocity of pile

Combining Eqs. 9.6 and 9.7 and rearranging the terms, yields Eq. 9.8.

$$(9.8) \quad v_P = \frac{v_0}{1 + \frac{Z_P}{Z_H}}$$

where  $v_P$  = particle velocity of pile  
 $v_0$  = particle velocity of the hammer immediately before impact  
 $Z_H$  = impedance of hammer  
 $Z_P$  = impedance of pile

Inserting  $Z_H = Z_P$ , into Eq. 9.8 yields Eq. 9.9, which shows that when the impedances of the hammer and the piles are equal, the particle velocity of the pile,  $v_P$ , in the pile behind the wave front will be half the hammer impact velocity,  $v_0$  (the velocity immediately before touching the pile head).

$$(9.9) \quad v_P = 0.5 v_0$$

where  $v_P$  = particle velocity of pile  
 $v_0$  = particle velocity of the hammer immediately before impact

Combining Eqs. 9.3, 9.5, and 9.9, yields Eq. 9.10 which expresses the magnitude of the impact force,  $F_i$ , at the pile head for equal impedance of hammer and pile.

$$(9.10) \quad F_i = 0.5 v_0 Z_P$$

where  $F_i$  = force in pile  
 $Z_P$  = impedance of pile  
 $v_0$  = particle velocity of the hammer immediately before impact

The **duration of the impact**,  $t_0$ , that is, the time for when the pile and the hammer are in contact, is the time it takes for the strain wave to travel the length of the hammer,  $L_H$ , twice, i.e., from the top of the hammer to the bottom and back up to the top as expressed in Eq. 9.11a. Then, if the impedances of the hammer and the pile are equal, during the same time interval, the wave travels the length,  $L_W$ , as expressed in Eq. 9.11b. — Note, equal impedances do not mean that the wave velocities in hammer and pile are equal — Combining Eqs. 9.11a and 9.11b provides the **length of the stress wave** (or strain wave) in the pile as expressed by Eq. 9.11c.

$$(9.11a) \quad t_0 = \frac{2L_H}{c_H} \quad (9.11b) \quad t_0 = \frac{2L_W}{c_P} \quad (9.11c) \quad L_W = 2L_H \frac{c_P}{c_H}$$

where  $t_0$  = duration of impact (i.e., duration of contact between hammer and pile head)  
 $L_H$  = length of hammer  
 $L_W$  = length of the compression wave in pile  
 $c_H$  = velocity compression wave in hammer  
 $c_P$  = velocity of compression wave in pile

When a hammer impacts a pile, the force generated in the pile slows down the motion of the hammer and a stress wave ("particle velocity wave") is generated that propagates down the pile. After quickly reaching a peak velocity (and force) — immediately if the pile head is infinitely rigid — the pile head starts moving slower, i.e., the generated particle velocity becomes smaller, and the impact force decays exponentially according to Eq. 9.12a, which expresses the **pile head force**. Combining Eqs. 9.3, 9.5, and 9.12a yields to show that, together with the impact velocity, the ratio between the ram impedance and the pile impedance governs the force a hammer develops in a pile. (For hammer and pile of same material, e.g., steel, the ratio is equal to the ratio of the cross sectional areas). A ram must always have an impedance larger than that of the pile or the hammer will do little else than bounce on the pile head.

$$(9.12a) \quad F = F_i e^{-\frac{Z_P}{M_H} t}$$

$$(9.12b) \quad F = F_i e^{-\frac{M_P L_E}{M_H c_P}}$$

where

$F$	=	force at pile head	and	$F_i$	=	force at impact
$M_H$	=	mass of hammer element	and	$M_P$	=	mass of pile element
$e$	=	base of the natural logarithm (= 2.718)				
$Z_P$	=	impedance of the pile cross section				
$L_E$	=	length of pile element				
$t$	=	time				

If the pile is of non-uniform cross section, every change of impedance change will result in reflections. If the impedance of the upper pile portion is smaller than that of the lower, the pile will not drive well. When the reverse is the case, that is, the impedance of the upper pile portion is larger than that of the lower, a tension wave will reflect from the cross section change. For example, in marine projects, sometimes a concrete pile is extended by an H-pile, a "stinger". The impedances of the concrete segment and the steel H-pile segment should, ideally, be equal. However, the H-pile size (weight) is usually such that the impedance of the H-pile is smaller than that of the concrete pile. Therefore, a tensile wave will reflect from the cross section change (for a discussion, see Section 8, below). If the impedance change is too large, the reflected tension can damage the concrete portion of the pile, and if the change is substantial, such as in the case of an impedance ratio close to 2 or greater, the tension may exceed the tensile strength of the concrete pile. (A case history of the use of stinger piles is described in Section 9.11, Case 4).

As an important practical rule, the impedance of the lower section must never be smaller than half of the upper section. That it at all can work, is due to that the concrete pile end (i.e., where the two segments are joined) is not normally a free end, but is in contact with soil, which reduces the suddenness of the impedance change. However, this problem is compounded by that the purpose of the stinger is usually to achieve a better seating into dense competent soil. As the stinger is in contact with this soil, a strong compression wave may be reflected from the stinger toe and result in an increasing incident wave, which will result in that the tensile reflection from where the section are joined—where the impedance change occurred. If the concrete end is located in soft soil, damage may result.

When a pile has to be driven below the ground surface or below a water surface, a **follower** is often used. The same impedance aspects that governed the driving response of a pile governs also that of a follower. Ideally, a follower should have the same impedance as the pile. Usually, though, it designed for a somewhat larger impedance, because it must never ever have a smaller impedance than the pile, or the achievable capacity of the pile may reduce considerably as compared to the pile driven without a follower. Indeed, a too small follower may be doing little more than chipping away on the pile head.

A parameter of substantial importance for the drivability of the pile is the so-called **quake**, which is the movement between the pile and the soil required to mobilize full plastic resistance (see Fig. 9.8). In other words, the quake is the zone of pile movement relative to the soil where elastic resistance governs the load transfer.

Along the pile shaft, the quake is usually small, about 2 mm to 3 mm or less. The value depends on the soil type and is independent of the size of the pile (diameter). In contrast, at the pile toe, the quake is a function of the pile diameter and, usually, about 1 % of the diameter. However, the range of values can be large; values of about 10 % of the diameter have been observed. The larger the quake, the more energy is required to move the pile and the less is available for overcoming the soil static resistance. For example, measurements and analyses have indicated that a hammer driving a pile into a soil where the quake was

about 3 mm (0.1 inch) could achieve a final capacity of 3,000 kN (600 kips), but if the quake is 10 mm (0.4 inch), it could not even drive the pile beyond a capacity of 1,500 kN (300 kips) (Authier and Fellenius 1980).

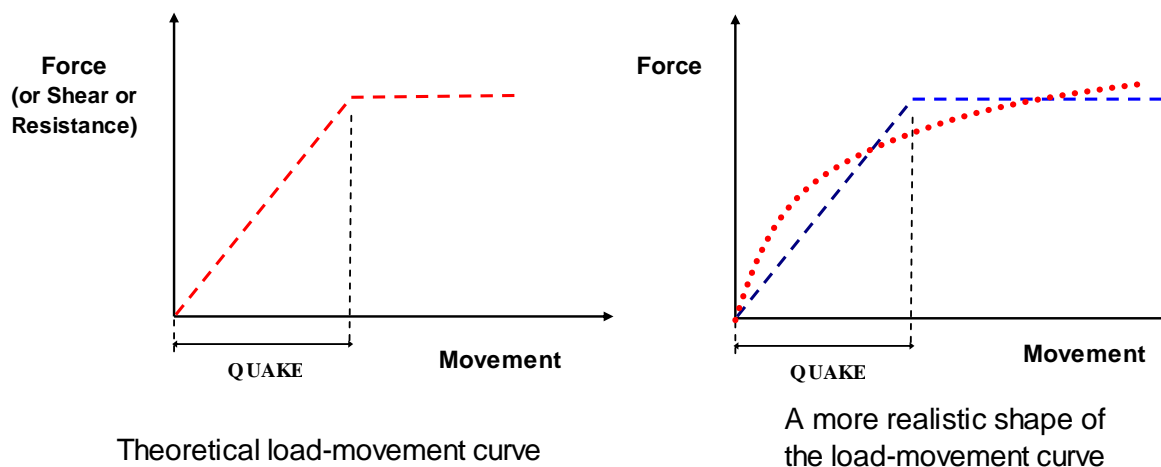


Fig. 9.8 Development of soil resistance to pile movement (q-z curves).

Aspects which sometimes can be important to include in an analysis are the effect of a soil adhering to the pile, particularly as a **plug** inside an open-end pipe pile or between the flanges of an H-pile. The plug will impart a toe resistance (Fellenius 2002). Similarly, the resistance from a soil column inside a pipe pile that has not plugged will add to the shaft resistance along the outside of the pile.

The **stiffness, k**, of the pile is an additional important parameter to consider in the analysis. The stiffness of an element is defined in Eq. 9.13. The stiffness of the pile is usually well known. The stiffness of details such as the hammer and pile cushions is often more difficult to determine. Cushion stiffness is particularly important for evaluating driving stresses. For example, a new pile cushion intended for driving a concrete pile can start out at a thickness of 150 mm of wood with a modulus of 300 MPa. Typically, after some hundred blows, the thickness has reduced to half and the modulus has increased five times. Consequently, the cushion stiffness has increased ten times.

$$(9.13) \quad k = \frac{EA}{L}$$

where

- $k$  = stiffness
- $E$  = Young's modulus of the pile material
- $A$  = pile cross sectional area
- $L$  = element length

A parameter related to the stiffness is the **coefficient of restitution, e**, which indicates the difference expressed in Eq. 9.14 between stiffness in loading (increasing stress) as opposed to in unloading (decreasing stress). A coefficient of restitution equal to unity only applies to ideal materials, although steel and concrete are normally assigned a value of unity. Cushion material have coefficients ranging from 0.5 through 0.8. For information on how to determine the coefficient of restitution see GRL (2002).

$$(9.14) \quad e = \sqrt{\frac{k_1}{k_2}}$$

where  $e$  = coefficient of restitution  
 $k_1$  = stiffness for increasing stress  
 $k_2$  = stiffness for decreasing stress

When the initial compression wave with the force  $F_i(t)$  reaches the pile toe, the toe starts to move. The **pile toe force** is expressed by Eq. 9.15.

$$(9.15) \quad F_p(t) = F_i(t) + F_r(t)$$

where  $F_p(t)$  = force in pile at toe at Time  $t$   
 $F_i(t)$  = force of initial wave at pile toe  
 $F_r(t)$  = force of reflected wave at pile toe

If the material below the pile is infinitely rigid,  $F_r = F_i$ , and Eq. 9.15 shows that  $F_p = 2F_i$ . If so, the strain wave will be reflected undiminished back up the pile and the stress at the pile toe will theoretically double. When the soil at the pile toe is less than infinitely rigid, the reflected wave at the pile toe,  $F_r(t)$ , is smaller, of course. The magnitude is governed by the stiffness of the soil. If the force in the pile represented by the downward propagating compression wave rises more slowly than the soil resistance increases due to the imposed toe movement, the reflected wave is in compression indicating a toe resistance. If the force in the compression wave rises faster than the soil resistance increases due to the imposed toe movement, the reflected wave is in tension. However, the force sent down and out into the soil from the pile toe will be a compression wave for both cases.

In this context and to illustrate the limitation of the dynamic formulae, the driving of two piles will be considered. Both piles are driven with the same potential ("positional") energy. First, assume that the on pile is driven with a hammer having a mass of 4,000 kg and is used at a height-of-fall of 1 m, representing a positional energy of 40 KJ. The impact velocity,  $v_0$ , is independent of the mass of the hammer and a function of gravity and height-of-fall, ( $v = \sqrt{2gh}$ ). Thus, the free-fall impact velocity is 4.3 m/s. If instead a 2,000 kg hammer is used at a height-of-fall of 2 m, the positional energy is the same, but the free-fall impact velocity is 6.3 m/s and the force generated in the pile overcoming the soil resistance will be larger. The stress in the pile at impact can be calculated from Eq. 9.16, as derived from Eqs. 9.3 - 9.5.

$$(9.16) \quad \sigma_p = \frac{E_p}{c_p} v_p$$

where  $\sigma_p$  = stress in the pile  
 $E_p$  = pile elastic modulus  
 $c_p$  = propagation speed of compression wave in the pile  
 $v_p$  = particle velocity in the pile

The impact stress in piles composed of steel, concrete, or wood can be calculated from the material parameters given in Table 9.1. In the case of a concrete pile and assuming equal potential energy, but at heights-of-fall of 1 m and 2 m, the calculated stresses in the pile are 44 MPa and 63 MPa, respectively. In

case of a pile cross section of, say, 300 mm and area about 0.09 m<sup>2</sup>, the values correspond to theoretical impact forces are 4,000 kN and 5,600 kN. Allowing for losses down the pile due to reflections and damping, the maximum soil forces the impact wave could be expected to mobilize are about a third or a half of the theoretical impact force, i.e., about 2,000 to 3,000 kN for the "heavy" and "light" hammers, respectively. Moreover, because the lighter hammer generates a shorter stress-wave, its large stress may decay faster than the smaller stress generated by the heavier hammer and, therefore, the lighter hammer may be unable to drive a long a pile as the heavier hammer can. Where in the soil a resistance occur is also a factor. For example, a pile essentially subjected to toe resistance will benefit from a high stress level, as generated by the higher impact, whereas a pile driven against shaft resistance drives better when the stress-wave is longer and less apt to dampen out along the pile. A number of influencing factor are left out, but the comparison is an illustration of why the dynamic formulae, which are based on positional energy relations, are inadvisable for use in calculating pile bearing capacity.

**Table 9.1 Typical Values**

Material	Density, $\rho$ (kg/m <sup>3</sup> )	Modulus, E (GPa)	Wave speed, c (m/s)
Steel	7,850	210	5,120
Concrete	2,450	40	4,000
Wood fresh or wet	1,000	16	3,300

The **maximum stress** in a pile that can be accepted and propagated is related to the maximum dynamic force that can be mobilized in the pile. The peak stress developed in an impact is expressed in Eq. 9.17, as developed from Eq. 9.16.

$$(9.17) \quad \sigma_p = \frac{E_p}{c_p} \sqrt{2gh}$$

where  $\sigma_p$  = stress in the pile  
 $E_p$  = pile elastic modulus  
 $c_p$  = propagation speed of the stress wave in pile; wave speed  
 $g$  = gravity constant  
 $h$  = critical height-of-fall

Transforming Eq. 9.17 into Eq. 9.18 yields an expression for a height that causes a stress equal to the strength of the pile material.

$$(9.18) \quad h_{\sigma} = \frac{\sigma_{p, \text{mk}}^2}{2g\rho E_p}$$



where	$h_{cr}$	=	critical height-of-fall
	$\sigma_{P, max}$	=	maximum stress in the pile $\leq$ strength of the pile material
	$E_P$	=	pile elastic modulus
	$g$	=	gravity constant
	$\rho$	=	density of pile material

For a concrete pile with cylinder strength ranging between 30 MPa and 60 MPa and the material parameters listed in Table 9.1, the critical height-of-fall ranges between 0.5 m and 2.0 m (disregarding losses, usually assumed to amount to an approximately 20 % reduction of impact velocity). In the case of a steel pile with a material yield strength of 300 MPa, the critical height-of-fall becomes 2.8 m. (Note, no factor of safety is included and it is not recommended to specify the calculated limits of height-of-fall for a specific pile driving project).

The above brief discussion demonstrates that stress wave propagation during pile driving is affected by several factors, such as hammer weight, hammer impact velocity, and pile impedance. It is therefore not surprising that a single parameter, driving energy, cannot describe the pile driving operation correctly.

The total soil resistance  $R_{tot}$  during pile driving is composed of a movement-dependent (static) component,  $R_{stat}$ , and a velocity-dependent (dynamic) component,  $R_{dyn}$ , as expressed in Eq. 9.19.

$$(9.19) \quad R_{tot} = R_{stat} + R_{dyn}$$

where	$R_{tot}$	=	total pile capacity
	$R_{stat}$	=	static pile capacity
	$R_{dyn}$	=	dynamic pile capacity

The soil resistances can be modeled as a spring with a certain stiffness and a slider representing the static resistance plus a dashpot representing dynamic resistance—damping — as illustrated in Fig. 9.9. (Note that the figure illustrates also when the direction of pile movement has reversed). For small movements, the static resistance is essentially a linear function of the movement of the pile relative the soil. The damping is a function of the velocity of the pile. Smith (1960) assumed that the damping force is proportional to the static soil resistance times pile velocity by a damping factor,  $J_s$ , with the dimension of inverse velocity. Goble et al. (1980) assumed that the damping force is proportional to the pile impedance times pile velocity by a dimensionless damping factor,  $J_c$ , called viscous damping factor, as expressed in Eq. 9.20.

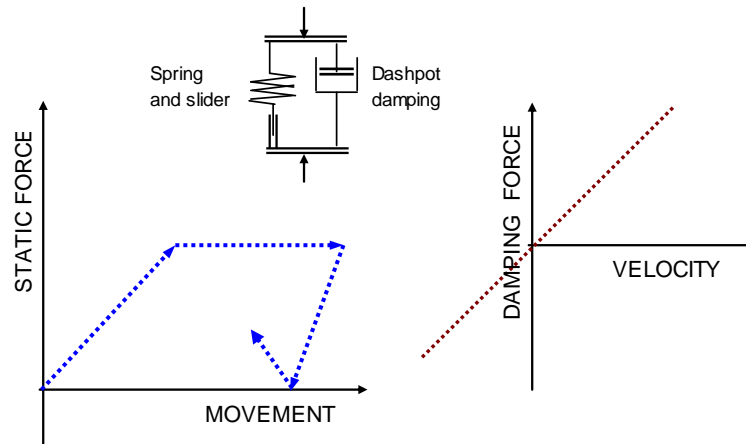


Fig. 9.9 Model and principles of soil resistance — elastic and plastic and damping

$$(9.20) \quad R_{dyn} = J_c Z_p v_p$$

where

- $R_{dyn}$  = dynamic pile resistance
- $J_c$  = a viscous damping factor
- $Z_p$  = impedance of pile
- $v_p$  = particle velocity of pile

Typical and usually representative ranges of viscous damping factors are given in Table 9.2.

**Table 9.2.** Damping factors for different soils (Rausche et al. 1985).

Soil Type	$J_c$
Clay	0.60 – 1.10
Silty clay and clayey silt	0.40 – 0.70
Silt	0.20 – 0.45
Silty sand and sandy silt	0.15 – 0.30
Sand	0.05 – 0.20

It is generally assumed that  $J_c$  depends only on the dynamic soil properties. However, as shown by Massarsch and Fellenius (2008) and Fellenius and Massarsch (2008), in practice, measurements on different size and different material piles in the same soil do show different values of  $J_c$ . Iwanowski and Bodare (1988) derived the damping factor analytically, employing the model of a vibrating circular plate in an infinite elastic body to show that the damping factor depends not just on the soil type but also on the ratio between the impedance of the soil at the pile toe and the impedance of the pile. They arrived at the relationship expressed in Eq. 9.21, which is applicable to the conditions at the pile toe.

$$(9.21) \quad J_c = 2 \frac{\rho_t c_s A_t}{\rho_p c_p A_c} = 2 \frac{Z_s A_t}{Z_p A_c}$$

where

- $J_c$  = dimensionless damping factor
- $\rho_t$  = soil total (bulk) density of the soil
- $\rho_p$  = density of the pile material
- $c_s$  = shear wave speed in the soil
- $c_p$  = speed of the compression wave in the pile
- $A_t$  = pile area at pile toe in contact with soil
- $A_c$  = pile cross-sectional area
- $Z_s$  = impedance of the soil (determined from P-wave velocity)
- $Z_p$  = impedance of the pile at the pile toe

The equation shows that the damping factor,  $J_c$  depends on the ratio of the soil impedance to the pile impedance and of the ratio of pile cross section area and pile toe area. The latter aspect is particularly important in the case of closed-toe or "plugged" pipe piles. Table 9.3 compiles  $J_c$  damping values calculated according to Eq. 9.21 for pile with an average soil density of  $\rho_t = 1,800 \text{ kg/m}^3$  and material parameters taken from Table 9.1. For the steel piles, a ratio between the pile toe area and the pile cross sectional area of 10 was assumed. Table 9.3 shows the results for soil compression wave velocities ranging from 250 m/s to 1,500 m/s. Where the actual soil compression wave speed can be determined, for example, from cross-hole tests, or seismic CPT soundings, Eq. 9.21 indicates a means for employing the soil compression wave speed to estimate  $J_c$  -factors for the piles of different sizes, geometries, and materials to be driven at a site.

**Table 9.3.** Values of viscous damping factor,  $J_c$ , for different pile materials and wave speeds

Material	Compression wave speed at pile toe, $c_p$ (m/s)					
	250	500	750	1,000	1,250	1,500
Steel	0.02	0.04	0.07	0.09	0.11	0.13
Concrete	0.09	0.18	0.28	<u>0.37</u>	0.46	0.55
Wood	0.27	0.55	0.82	1.09	1.36	1.64

## 9.5 Wave Equation Analysis of Pile Driving

The GRLWEAP program includes files that contain all basic information on hammers available in the industry. To perform an analysis of a pile driven with a specific hammer, the hammer is selected by its file number. Of course, when the analysis is for piles driven with drop hammers, or with special hammers that are not included in the software files, the particular data must be entered separately.

The GRLWEAP can perform a drivability analysis with output consisting of estimated penetration resistance (driving log), maximum compression and tension stresses induced during the driving, and many other factors of importance when selecting a pile driving hammer. The program also contains numerous other non-routine useful options. For additional information, see Hannigan (1990).

The most common routine output from a wave equation analysis consists of a bearing graph (ultimate resistance curve plotted versus the penetration resistance—often simply called "blow-count"<sup>5</sup>) and diagrams showing impact stress and transferred energy as a function of penetration resistance. Fig. 9.10 presents a Bearing Graph showing the relation between the static soil resistance (pile capacity;  $R_{ULT}$ ) versus the pile penetration resistance (PRES) at initial driving as the number of blows required for 25 mm penetration of the pile into the soil. The relation is shown as a band rather than as one curve, because natural variations in the soil, hammer performance, cushion characteristics, etc. make it impossible to expect a specific combination of hammer, pile, and soil at a specific site to give the response represented by a single curve. The WEAP analysis results should therefore normally be shown in a band with upper and lower boundaries of expected behavior. The band shown may appear narrow, but as is illustrated in the following, the band may not be narrow enough.

<sup>5</sup> Penetration resistance is number of blows per a unit of penetration, e. g., 25 mm, 0.3 m, or 1.0 m. Blow count is the actual number of blows counted for a specific penetration, or the inverse of this: a penetration for a specific number of blows. For example, on termination of the driving, an 11 mm penetration may be determined for 8 blows. That is, the blow count is 8 blows/11 mm, but the penetration resistance is 18 blows/25 mm. Sometimes the distinction is made clear by using the term "equivalent penetration resistance". Note, the "pile **driving** resistance" refers to force. But it is an ambiguous term that is best not used.

The Bearing Graph is produced from assumed pile capacity values. For this reason, the WEAP analysis alone cannot be used for determining the capacity of a pile without being coupled to observed penetration resistance (and reliable static analysis). WEAP analysis is a design tool for predicting expected pile driving behavior (and for judging suitability of a hammer, etc.), not for determining capacity. For the case illustrated in Fig. 9.10, the desired capacity (at End-of-Initial-Driving, EOID) ranges from 1,900 kN through 2,150 kN. The Bearing Graph indicates that the expected PRES values for this case range from 4 bl./25 mm through 16 bl./25 mm. Obviously, the WEAP analysis *alone* is not a very exact tool to use. It must be coupled with a good deal of experience and judgment, and field observations.

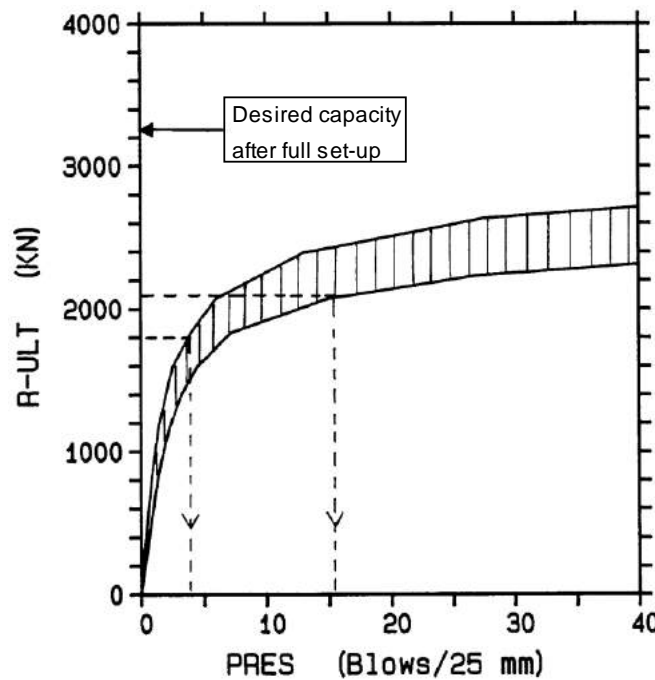


Fig. 9.10 WEAP Bearing Graph (Fellenius 1984)

The desired long-term capacity of the pile is 3,150 kN. However, the Bearing Graph shows that, for the particular case and when considering a reasonable penetration resistance (PRES), the hammer cannot drive the pile against a resistance (i.e., to a capacity) greater than about 2,500 kN. Or, in other words, the WEAP analysis shows that the hammer cannot drive the pile to a capacity of 3,150 kN. Is the hammer no good? The answer lies in that the Bearing Graph in Fig. 9.10 pertains, as mentioned, to the capacity of a pile at initial driving. With time after the initial driving, the soil gains strength and the pile capacity increases due to soil set-up. Of course, if the designer considers and takes advantage of the set-up, the hammer does not have to drive the pile to the desired final capacity at the end-of-initial-driving, only to a capacity that when set-up is added the capacity becomes equal to the desired final value. For the case illustrated, the set-up was expected to range from about 1,000 kN through 1,200 kN and as the analysis shows the hammer capable of driving the piles to a capacity of about 2,000 kN at a reasonable PRES value, the hammer was accepted.

Generally, if initial driving is to a capacity near the upper limit of the ability of the hammer, the magnitude of the set-up cannot be proven by restriking the pile with the same hammer. For the case illustrated, the hammer is too light to mobilize the expected at least capacity of 3,150 kN, and the restriking would be meaningless and only show a small penetration per blow, i.e., a high PRES value.

## 9.6 Hammer Selection by Means of Wave Equation Analysis

The procedure of hammer selection for a given pile starts with a compilation of available experience from previous similar projects in the vicinity of the site and a list of hammers available amongst contractors who can be assumed interested in the project. This effort can be more or less elaborate, depending on the project at hand. Next comes performing a wave equation analysis of the pile driving at the site, as suggested below. Notice, there are many potential error sources. It is important to verify that assumed and actual field conditions are in agreement.

### Before start of construction

- Compile the information on the soils at the project site and the pile data. The soil data consist of thickness and horizontal extent of the soil layers and information on the location of the groundwater table and the pore pressure distribution. The pile data consist of the pile geometry and material parameters, supplemented with the estimated pile embedment depth and desired final capacity.
- Calculate the static capacity of the pile at final conditions as well as during initial driving. For conditions during the initial driving, establish the extent of remolding and development of excess pore pressure along the pile. Establish also the capacity and resistance distribution at restrike conditions after the soil has reconsolidated and "set-up", and all excess pore pressures have dissipated.
- Establish a short list of hammers to be considered for the project. Sometimes, the hammer choice is obvious, sometimes, a range of hammers needs to be considered.
- For each hammer considered, perform a wave equation analysis to obtain a Bearing Graph for the end-of-initial-driving and restrike conditions with input of the static soil resistances and pile data as established earlier. For input of hammer data and soil damping and quake data, use the default values available in the program. This analysis is to serve a reference to the upper boundary conditions—the program default values are optimistic. Many soils exhibit damping and quake values that are higher than the default values. Furthermore, the hammer efficiency used as default in the program is for a well-functioning hammer and the actual hammer to be used for the project may be worn, in need of maintenance service, etc. Hence, its efficiency value is usually smaller than the default value. Repeat, therefore, the analysis with best estimate of actual hammer efficiency and dynamic soil parameters. This analysis will establish the more representative Bearing Graph for the case.
- A third Bearing Graph analysis with a pessimistic, or conservative, input of values is always advisable. It will establish the low boundary conditions at the site and together with the previous two analyses form a band that indicates the expected behavior.
- When a suitable hammer has been identified, perform a Drivability Analysis to verify that the pile can be driven to the depth and capacity desired. Also this analysis should be made with a range of input values to establish the upper and lower boundaries of the piling conditions at the site.
- Determine from the results of the analysis what hammer model and size and hammer performance to specify for the project. Hammers should not be specified as to rated energy, but to the what they will develop in the pile under the conditions prevailing at the site. That is, the specifications need to give required values of impact stress and transferred energy for the hammer, pile, and soil system. Suggested phrasings are given in Chapter 11.

### **During construction**

- For most projects, at the start of the pile driving, dynamic monitoring with the Pile Driving Analyzer (PDA; Section 9.8 should be performed. The PDA measurements combined with CAPWAP analyses (Section 9.11) will serve to show whether or not the hammer is performing as per the specifications. The measurements will also serve to confirm the relevance of the theoretical calculations (static and dynamic analyses) and, when appropriate, indicate the need for amendments. Although the primary purpose is to verify the pile capacity, other PDA deliverables are hammer performance, transferred energy, pile stresses, soil set-up, etc.
- It is important that the conditions assumed in the analyses are related to the actual conditions. Check actual pile size, length, and material and verify that cushions and helmets as to size, material type, and condition. Then, ascertain that the hammer runs according to the manufacturer's specifications as to blow rate (blows/minute) and that the correct fuel is used. Request records from recent hammer maintenance.
- Depending on size of project, degree of difficulty, and other factors, additional PDA monitoring and analysis may be necessary during the construction work. If questions or difficulties arise during the continued work, new measurements and analysis will provide answers when correlated to the initial measurement results.

### **9.7 Aspects to Consider When Reviewing Results of Wave Equation Analysis**

- Check the pile stresses to verify that a safe pile installation is possible.
- If the desired capacity requires excessive penetration resistance (PRES values greater than 800 blows/metre—200 blows/foot), re-analyze with a more powerful hammer (pertinent to piles bearing in dense soil; piles driven to bedrock can be considered for larger PRES values if these can be expected to be met after a limited number of blows).
- If the penetration resistance is acceptable but compressive stresses are unacceptably high, re-analyze with either a reduced stroke (if hammer is adjustable) or an increased cushion thickness.
- If (for concrete piles) the penetration resistance is low but tension stresses are too high, either increase the cushion thickness or decrease the stroke or, possibly, use a hammer with a heavier ram, and then re-analyze.
- If both penetration resistance and compressive stresses are excessive, consider the use of not just a different hammer, but also a different pile.

### **9.8 High-Strain Dynamic Testing of Piles Using the Pile Driving Analyzer, PDA**

Dynamic monitoring consists in principle of attaching gages to the pile shortly below the pile head, measuring force and acceleration induced in the pile by the hammer impact (see Fig. 9.11). The dynamic measurements are collected by a data acquisition unit called the Pile Driving Analyzer, PDA. A detailed guide for the performance of the PDA testing is given in ASTM Designation D4945-89.

### 9.8.1 Wave Traces

The PDA data are usually presented in the form of PDA "wave traces", which show the measured force and wave speed developments drawn against time as illustrated in Fig. 9.12. The time indicated as  $0 L/c$ , is when the peak impact force occurs, and Time  $2 L/c$  is when the peak force has traveled down to the pile toe, been reflected there, and again appears at the gages at the pile head. The wave has traveled a distance of  $2 L$  at a wave speed of  $c$  (ranges from about 3,500 m/s in concrete through about 5,100 m/s in steel—12,500 ft/s and 16,700 ft/s, respectively). Peak force divided by the pile cross sectional area at the gage location is the impact stress. The acceleration integrated to pile physical velocity is simply called "velocity".

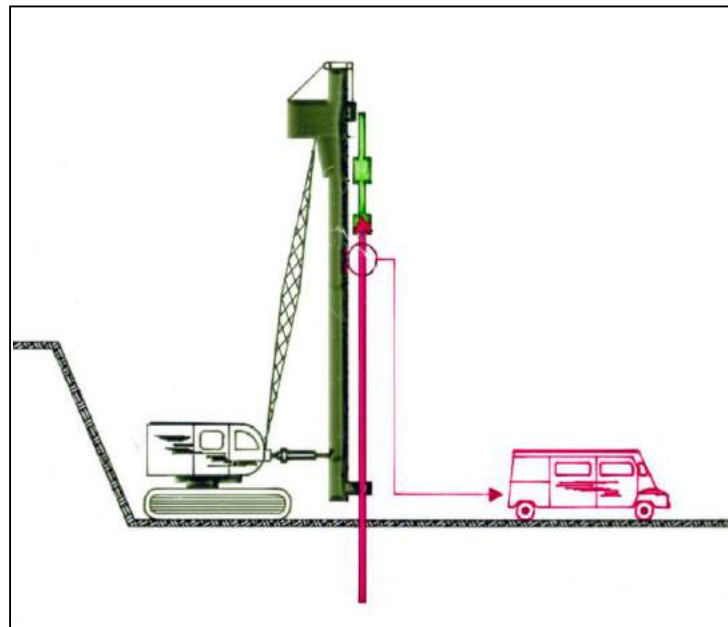


Fig. 9.11 Typical arrangement of dynamic monitoring with the Pile Driving Analyzer (PDA). The two pairs of PDA gages, the accelerometer and the strain-gage, are usually attached shortly below the pile head.

Notice that Fig. 9.12 shows the force and velocity traces as initially overlapping. This is no coincidence. Force and velocity introduced by an impact are proportional by the impedance,  $Z = EA/c$ . ("c" is wave propagation speed; see Eq. 9.4, above). The most fundamental aspect of the wave traces lies in how they react to reflections from the soil, when the traces no longer overlap. When the stress wave on its way down the pile encounters a soil resistance, say at a distance "A" below the gage location, a reflected wave is sent back up the pile. This wave reaches the gages at Time  $2A/c$ . At that time, force is still being transferred from the hammer to the pile and the gages are still recording the force and physical velocity. The reflected stress-wave superimposes the downward wave and the gages now measure the combination of the waves. The reflected force will be a compression wave and this compression will add to the measured force, that is, the force wave will rise. At the same time, the resistance in the soil slows down the pile, that is, the measured velocity wave gets smaller—the trace dips. The consequence is a separation of the traces. The larger this separation, the greater the soil resistance. Soil resistance encountered by the pile toe has usually the most pronounced effect. It is evidenced by a sharp increase of the force wave and a decrease of the velocity wave, usually even a negative velocity—the pile rebounds.

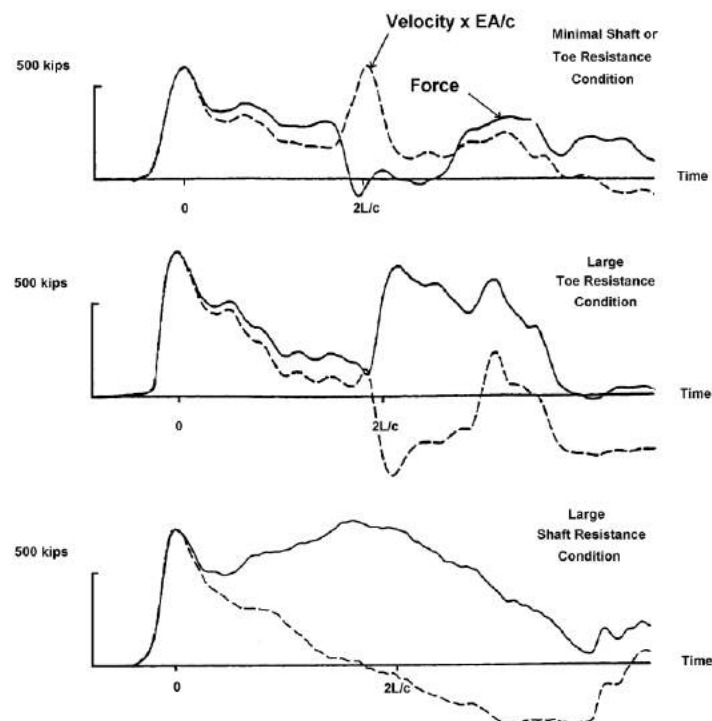


Fig. 9.12 Force and Velocity Wave Traces recorded during initial driving and restriking (Hannigan 1990; used with permission)

When dynamic measurements first started to be made in the 1950s, force could be measured by either an accelerometer or a strain gage. At the time, strain gages were prone to malfunction due to moisture and were more laborious to attach, as opposed to accelerometers. The latter were also more accurate, and could be (should be) attached at a single point. However, they were more prone to damage. Depending on preference, either gage type was used. It was not until Dr. Goble and co-workers attached both gage types to the test pile at the same time that the tremendous benefit became apparent of comparing the force determined from measured strain to the force determined from measured and integrated acceleration. The purpose of attaching both gages was that it was hypothesized that the pile capacity would be equal to the force (from the strain gage) when the pile velocity (from the integrated acceleration) was zero and no damping would exist. However, when the velocity at the pile head is zero, the velocity down the pile will not be zero, so the approach did not work and it was abandoned. The practice of using both gage types was retained, of course.

For a pile of length “L” below the gages, reflection from the pile toe will arrive to the gage location at Time  $2L/c$ . This is why the wave traces are always presented in the “L/c scale”. The full length of the pile ‘in time’ is  $2L/c$  and the time of the arrival of a reflection in relation to the  $2L/c$  length is also a direct indication of where in the pile the resistance was encountered.

A resistance along the pile shaft will, as indicated, reflect a compression wave. So will a definite toe resistance as illustrated in the middle wave traces diagram of Fig. 9.12, where the compression trace increases and the velocity trace decreases. Again, the larger the toe resistance, the larger the separation of the two traces. Indeed, the compression stress in the pile at the pile head at Time  $2L/c$  may turn out to be larger than the impacting wave at Time  $0L/c$ . This is because the toe reflection overlaps the incident wave which is still being transferred to the pile head from the hammer. In those cases, the maximum compression stress occurs at the pile toe not at the pile head.



A drop hammer does not bounce off the pile head on its impacting the pile head, only when the compression wave originating at the pile toe reaches the ram (if the pile toe is in contact with dense and competent soil). In case of a diesel hammer, its ram lifts off the anvil as a result of the combustion. However, a strong compression wave reflected from the pile toe will increase the upward velocity of the ram and it will reach higher than before. For the next blow, the fall be longer and, therefore, the impact velocity will be higher resulting in a stronger impact wave, which will generate a stronger reflected compression wave, which will send the ram even higher, and . . . If the operator is not quick in reducing the fuel setting, either the diesel hammer or the pile or both can become damaged.

If the soil at the pile toe is soft and unable to offer much resistance to the pile, the reflected wave will be a tensile wave. When the tensile wave reaches the gage location, the gages will record a reduction in the compression wave and an increase in the tensile wave. If the tensile wave is large (very little or no resistance at the pile toe, the pile head may lose contact with the pile driving helmet (temporarily, of course) which will be evidenced by the force trace dropping to the zero line and the velocity trace showing a pronounced peak. The magnitude of the tensile force is directly proportional to the impact wave. A large increase in the velocity trace at Time  $2L/c$  is a visual warning for excessive tension in the pile. This is of particular importance for concrete piles, which piles have limited tension strength.

Whether a tension or a compression wave will be reflected from the pile toe is not just a function of the strength of the soil at the pile toe. Strength is the ultimate resistance after a movement has occurred. In brief, if the force in the pile at the pile toe rises faster than the increase of resistance due to the pile toe penetration, a tension wave is reflected. If, instead, the soil resistance increases at the faster rate, then, a compression wave results. Ordinarily, the quake is small, about 1 % of the pile diameter or 2 mm to 4 mm, and the acceleration of the pile toe is such that the pile toe resistance is mobilized faster than the rise of the force in the pile. However, some soils, for example some silty glacial tills and highly organic soils, demonstrate large quake values, e. g., 20 mm to 50 mm. Yet, these soils may have considerable strength once the pile toe has moved the distance of the quake. When driving piles in such soils, the pile toe will at first experience little resistance. When the pile toe movement is larger than the quake, the pile toe works against the full soil resistance. Dynamic measurements from piles driven in such soils, will show a tensile reflection at  $2L/c$  followed by a compression reflection. The sharper the rise of the impact wave, the clearer the picture. If the conditions are such that the peak of the impact wave has reached the pile toe before the pile toe has moved the distance of the quake, the full toe resistance will not be mobilized and the penetration resistance becomes large without this being ‘reflected’ by a corresponding pile capacity. Simply expressed, a large quake will zap the efficacy of the driving (Fellenius and Authier 1980).

The visual message contained in the force and velocity records will provide the experienced PDA operator with much qualitative information on where in the soil the resistance originates—shaft bearing versus toe bearing, or combination of both—consistency in the response of the soil as well as in the behavior of the hammer, and many other aspects useful the assessment of a pile foundation. For example, it may be difficult to tell whether an earlier-than-expected-stopping-up of a pile is due to a malfunctioning hammer producing too small force or little energy, or if it is due to fuel pre-ignition. The PDA measurements of hammer transferred energy and impact force will serve as indisputable fact to determine whether or not a hammer is functioning as expected.

Included with routine display of PDA traces are Wave-Down and Wave-Up traces. The Wave-Down trace is produced by displaying the average of the velocity and force traces, thus eliminating the influence of the reflected wave and, as the name implies, obtaining a trace showing what the hammer is sending down into the pile. Similarly, half the difference between the two traces displays the reflected wave called Wave-Up, which is the soil response to the impact. Fig. 9.13 shows an example of a routine display of the wave traces (see below for explanation of the Movement and Energy traces).

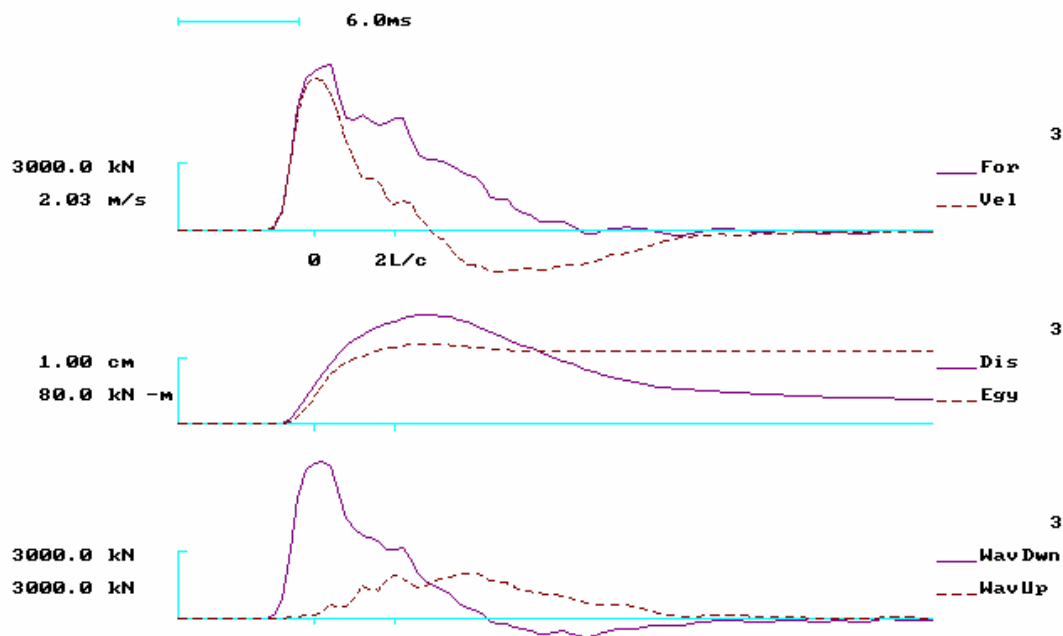


Fig. 9.13 Routine Display of PDA Wave Traces  
Force and Velocity, Movement ("Dis.") and Transferred Energy ("Egy."), and Wave Down and Wave Up

Comparing wave traces from different blows will often provide important information. For example, the discussion above referring to the strong compression wave reflecting from the pile toe is illustrated in Fig. 9.14 by two blows recorded from the initial driving of a steel pile through soft and loose silty soil to contact with a very dense glacial till. The pile toe was brought to contact with the glacial till between Blow 55 and Blow 65. The increased toe resistance resulted in a small increase of the impact force (from a stress of about 150 MPa to 170 MPa), which values are well within acceptable levels. However, for Blow 65 at Time  $2L/c$ , which is when the toe reflection reaches the pile head, a stress of 280 MPa was measured. This stress is very close to the steel yield for the pile material (reported to be 300 MPa). No surprise then that several of the pile were subsequently found to have considerable toe damage). Compounding the problem is the very small shaft resistance and a larger than usual toe quake. This is also obvious from the wave traces by the small separation of the traces and the "blip" immediately before Time  $2L/c$ .

### 9.8.2 Transferred Energy

The energy transferred from the hammer to the pile can be determined from PDA data as the integral of force times velocity times impedance. Its maximum value, called EMX, is usually referred to as the Transferred Energy. In assessing a hammer based on the transferred energy, it should be recognized that the values should be obtained during moderate penetration resistance and from when the maximum value does not occur much earlier than Time  $2L/c$ . Neither should a hammer be assessed by energy values determined from very easy driving. The consistency of the values of transferred energy is sometimes more important than the actual number.

### 9.8.3 Movement

A double integration of the acceleration produces a pile movement (displacement) trace, displaying the maximum and net penetration of the pile. An example is shown in the middle graph of Fig. 9.13, above.

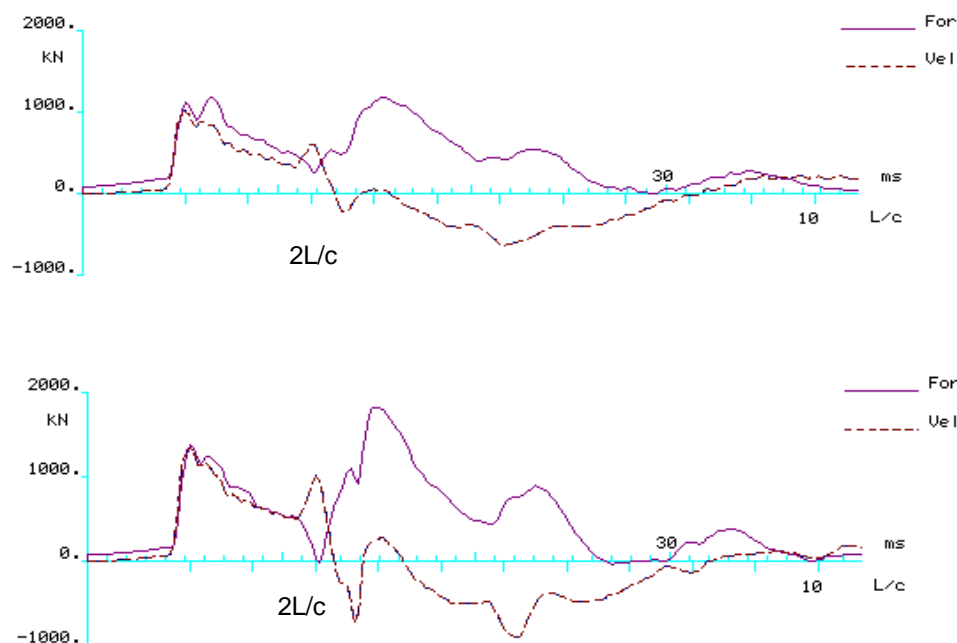


Fig. 9.14 Two Force and Velocity Wave Traces compared

## 9.9. Pile Integrity

### 9.9.1 Integrity Determined from High-strain Testing

In a free-standing, uniform rod, no reflections will appear before Time  $2L/c$ . For a pile, no sudden changes of shaft resistance normally occur along the pile. Therefore, the separation of the force and velocity traces caused by the shaft resistance is normally relatively gradual before Time  $2L/c$ . However, a sudden impedance reduction, for example, the intentional change of an H-Pile stinger at the end of a concrete section, will result in an increase of the velocity trace and a decrease of the force wave, a “blip” in the records. The magnitude of the “blip” is a sign of the magnitude of the impedance change. A partially broken length of a concrete pile is also an impedance change and will show up as a blip. The location along the time scale will indicate the location of the crack. A crack may be harder to distinguish, unless it is across a substantial part of the cross section. Rausche and Goble (1979) developed how the “blip” can be analyzed to produce a quantified value, called “beta” for the extent of the damage in the pile. The beta value corresponds approximately to the ratio of the reduced cross sectional area to the original undamaged cross sectional area. Beta values close to unity do not necessarily indicate a damage pile. However, a beta value smaller than 0.7 would in most cases indicate a damaged pile. Beta-values between 0.7 and 0.9 may indicate a change in the pile integrity, or impedance, but do not necessarily indicate damage. It must be recognized that an anomaly in the records does not necessarily indicate a defect in the pile. See also Salem et al. (1995) and Bullock (2012). Fig. 9.15 shows an example.

### 9.9.2 Integrity Determined from Low-strain Testing

The purpose of performing low-strain testing is to assess the structural integrity of driven or cast-in-place concrete piles, drilled-shafts, and wood piles, and to determine the length of different types piles including sheet piles where length records are missing or in doubt. A detailed guide for the performance of low-strain integrity testing is given in ASTM Designation D 5882-96.

The work consists of field measurements followed by data processing and interpretation. The measurements consists of hitting the pile with a hand-held hammer and recording the resulting signal with a sensitive accelerometer connected to a special field data collector (PIT Collector). The collector can display the signal (a velocity trace integrated from the measured acceleration) , process the data, and send the trace to a printer or transfer all the data to a computer. Special computer programs are used for data processing and analysis.

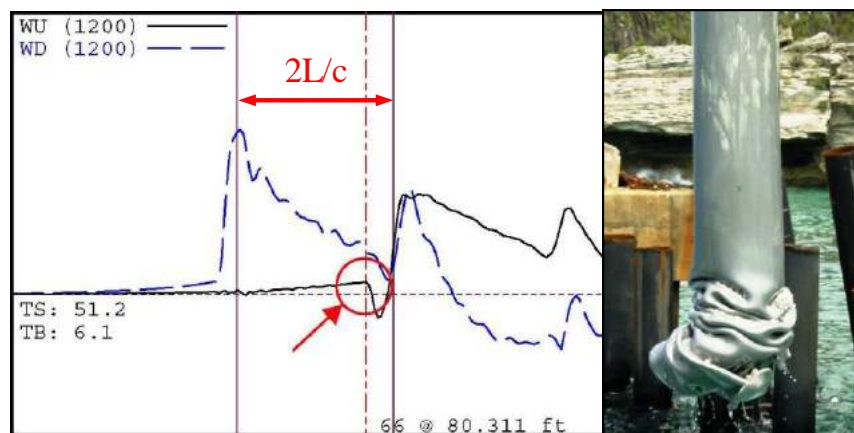


Fig. 9.15 Wave traces revealing damage to the pipe pile (later extracted).  
From Bullock (2012; used with permission).

Fig. 9.16 shows schematically the principle of low-strain testing—collecting the pulse echo of signals generated by impacting the pile head with a hand-held hammer. The “motion sensor” transmits signals to a unit called the PIT Collector. The PIT Collector is equipped with a processor, and display and storage units. The stored processed data will be transferred to a PC for further processing and interpretation.

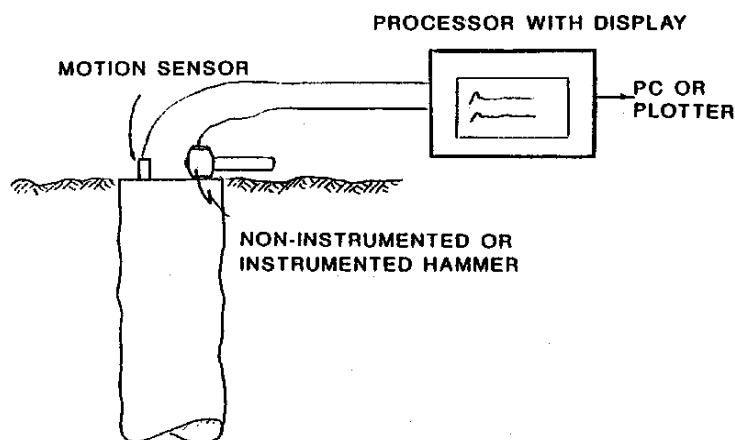


Fig. 9.16 Schematics of low-strain testing arrangement

The measurements are evaluated on site for preliminary assessment of the pile integrity. Questionable piles, if any, are identified and subjected to detailed analysis. The detailed analysis assists in identifying magnitude and location of structural concerns along the pile.

### 9.10 Case Method Estimate of Capacity

The data recorded by the PDA are displayed in real time (blow by blow) in the form of wave traces. Routinely, they are also treated analytically and values of stress, energy, etc., are displayed to the operator. The values include an estimate of pile capacity called the Case Method Estimate, CMES. The CMES method uses force and velocity measured at Times 0  $L/c$  and 2  $L/c$  to calculate the total (static and dynamic) resistance, RTL, as shown in Eq. 9.22.

$$(9.22) \quad RTL = \frac{F_{(t1)} + F_{(t1+2L/c)}}{2} + \frac{M c}{2L} (V_{(t1)} + V_{(t1+2L/c)})$$

where:

- $RTL$  = Total resistance
- $F_{(t1)}$  = Force measured at the time of maximum pile head velocity
- $F_{(t1+2L/c)}$  = Force measured at the return of the stress wave from the pile toe
- $M$  = Pile mass
- $c$  = Wave speed in the pile
- $L$  = Length of pile below gage location
- $V_{(t1)}$  = Pile velocity measured at the time of maximum pile head velocity
- $V_{(t1+2L/c)}$  = Pile velocity measured at the return of the stress wave from the pile toe

The total resistance is greater than the static bearing capacity and the difference is the damping force. Damping force is proportional to pile toe velocity and calculated as indicated in Eq. 9.23. (When velocity is zero just at the time when the pile starts to rebound ("unloads"), the total resistance (RTL) is a function of static resistance only. Initially in the development of the method of analysis of dynamic measurements, it was thought that the pile static capacity could be determined from this concept. However, the pile velocity is not zero all along the pile, so the approach was shown to be inapplicable (Goble et al. 1980). It was revived for the "long duration impulse testing method as indicated in Section 9.13).

$$(9.23) \quad R_d = J \frac{M c}{L} V_{(toe)} = J (F_{(t1)} + \frac{M c}{L} V_{(t1)} - RTL)$$

where

- $R_d$  = Damping force
- $J$  = Case damping factor
- $M$  = Pile mass
- $V_{toe}$  = Pile toe velocity
- $c$  = Wave speed in the pile
- $L$  = Length of pile below gage location
- $F_{(t1)}$  = Force measured at the time of maximum pile head velocity
- $V_{(t1)}$  = Pile velocity measured at the time of maximum pile head velocity
- $RTL$  = Total resistance

The PDA includes several CMES methods, some of which are damping-dependent and some are damping-independent. The damping-dependent methods evaluate the CMES value by subtracting the damping force,  $R_d$ , from the CMES value of total dynamic capacity (RTL). As shown in Eq. 9.23, the damping force is proportional to the measured pile physical velocity,  $V_{toe}$ .

The Case Damping factor ranges from zero to unity with the smaller values usually considered to represent damping in coarse-grained soil and the higher in fine-grained soils. The factor is only supposedly a soil parameter, however. Different piles driven at the same site may have different J-factors and a change of hammer may require a reassessment of the J-factor to apply (Fellenius et al. 1989). Therefore, what J-factor to apply to a certain combination of hammer, pile, and soil pile is far from a simple task, but one that requires calibration to actual static capacity and experience. A factor determined for EOID conditions may show to be off considerably for the restrike (RSTR) condition, for example. It is always advisable to calibrate the CMES method capacity to the results of a CAPWAP analysis (Section 9.10).

The most common damping-dependent CMES methods are called RSP, RMX, and RSU. There is also a damping-independent method called RAU.

The **RSP** value is the CMES RTL value calculated from the force and velocity measurements recorded at Times 0 L/c and 2 L/c and applying a Case Damping factor, J, ranging from zero to unity. Typically, a CMES value indicated as RS6 is determined for a J = 0.6.

The **RMX** value is the maximum RSP value occurring in a 30 ms interval after Time 0 L/c, while keeping the 2 L/c distance constant. In case of hard driven piles, the RMX value is often more consistent than the RSP value. For details, see Hannigan (1990). Typically, a CMES value indicated as RX6 is determined for a J = 0.6. The RMX method is the most commonly applied method. Routinely, the output of RMX values will list the capacities for a range of J-factors, implying an upper and lower boundary of capacity.

The **RSU** value may be applied to long shaft bearing piles where most of the movement is in the form of elastic response of the pile to the imposed forces. Often, for such piles, the velocity trace has a tendency to become negative (pile is rebounding) well before Time 2 L/c. This is associated with the length of the stress wave. As the wave progresses down the long pile and the peak of the wave passes, the force in the pile reduces. In response to the reduced force, the pile elongates. The soil resistance, which initially acts in the positive direction, becomes negative along the upper rebounding portion of the pile, working in the opposite direction to the static resistance mobilized along the lower portion of the pile (which still is moving downward). In the RSU method, the shaft resistance along the unloading length of the pile is determined, and then, half this value is added to the RSP value computed for the blow. For long shaft bearing piles, the RSU value, may provide the more representative capacity value. However, the RSU is very sensitive to the Case damping factor and should be used with caution.

The damping-independent **RAU** method consists of the RSP method applied to the results at the time when the toe velocity is zero (the Case J-factor is irrelevant for the results). The RAU method is intended for toe-bearing piles and, for such piles, it may sometimes show more consistent results than the RMX method. It also should be applied with considerable caution.

Although the CMES capacity is derived from wave theory, the values depend so much on choosing the proper J-factor and method, and, indeed, the representative blow record, that their use requires a good deal of experience and engineering judgment. This is not meant as a denigration of the CMES method, of course. There is much experience available and the methods have the advantage of being produced in real time blow for blow. When considered together with the measurements of impact force and transferred energy with due consideration to the soil conditions, and with calibration of a representative record to a signal-matching analysis (CAPWAP; see below), an experienced engineer can usually produce reliable estimates of capacity for every pile tested.

The estimate of capacity makes use of the wave reflected from the soil. It is often overlooked that the soil can never send back up to the gages any more than the hammer has sent down in the first place. Simply, the analysis of the record postulates that the full soil resistance is indeed mobilized. If the hammer is not able to move the pile, the full resistance of the pile is not mobilized. The PDA will then not be able to accurately determine the pile capacity, but will deliver a “lower-bound” value. When the capacity is not fully mobilized, the capacity value is more subjected to operator judgment and, on occasions, the operator may actually overestimate the capacity and produce analysis results of dubious relevance.

Moreover, the capacity determined is the capacity at the time of the testing. If the pile is tested before set-up has developed, the capacity will be smaller than the one determined in a static loading test some time later. A test at RSTR (if the pile moves for the blow) is more representative for the long-term performance of a pile under load than is the test at EOID. (Provided now that the pile has been let to rest during the period between the initial driving and the restrike: no intermediate restriking and no other pile driven in the immediate vicinity).

A restrike will sometimes break down the bond between the pile and the soil and although in time the bond will be recovered this process is often slower than the rate of recovery (set-up) starting from the EOID condition. This is because a restrike does not introduce the any lateral displacement of the soil, while the initial driving introduces a considerable lateral displacement of the soil even in the case of so-called low-displacement piles such as H-piles.

Restriking is usually performed by giving the pile a certain small number of blows or the number necessary to for achieving a certain penetration. The pile capacity reduces with the number of blows given, because the restrike driving disturbs the bond between the pile and the soil and increases pore pressure around the pile. Therefore, the analysis for capacity is normally performed on one of the very first restrike blows, as analysis for one of the later blows would produce a smaller capacity. Normally, the disturbance effect disappears within a few hours or days. However, a static test immediately following the completion of the restrike event may show a smaller capacity value than that determined in the analysis of the PDA data from an early restrike blow. Moreover, a static test is less traumatic for a pile than a dynamic restrike test. For this reason, when comparing dynamic and static test results on a pile, it is preferable to perform the static loading test first.

Performing the static test first is not a trivial recommendation, because when restriking the pile after a set-up period, it would normally have an adequate stick-up to accommodate the monitoring gages. Because a static test is normally performed with a minimum stick-up above ground (the pile is cut off before the test), attaching the gages after a static test may not be straight-forward and require hand excavation around the pile to provide access for placing the gages.

### **9.11. CAPWAP Determined Pile Capacity**

The two traces, force and velocity, are mutually independent records. By taking one trace, say the velocity, as an input to a wave equation computer program called CAPWAP, a force-trace can be calculated (Rausche et al. 1985).. The shape of this calculated force trace depends on the actual hammer input given to the pile as represented by the measured velocity trace and on the distribution of static resistance and dynamic soil parameters used as input in the analysis. Because the latter are assumed values, at first the calculated force-trace will appear very different from the measured force-trace. However, by adjusting the latter data, the calculated and measured force traces can be made to agree better and the match quality is improved. Ultimately, after a few iteration runs on the computer, the calculated force-trace is made to agree well with the measured trace. An agreement, ‘a good signal match’, means that the soil data (such as quake, damping, and ultimate shaft and toe resistance values) are

close to those of the soil into which the pile was driven. In other words, the CAPWAP signal match has determined the static capacity of the pile and its distribution along the pile (as the sum of the resistances assigned to the analysis). Fig. 9.17 presents an example of the results of a CAPWAP signal matching along with the wave traces and PDA data and is an example of a routine report sheet summarizing the data from one blow. When several piles have been tested, it is of value to compile all the PDA and CAPWAP results in a table, separating the basic measured values from the analyzed (computed) values.

**PDA Data Table**

EMAX (kJ)	Energy ratio (%)	Impact force (kN)	Max. force (kN)	Impact stress (MPa)	CSX (MPa)	CSB (MPa)	PRES (bl/25mm)	CASE Method Estimate (kN)			
								RX4	RX5	RX6	RA2
17.4	30.5	2,830	2,830	169	169	122	12	2,060	1,816	1,571	721

Emax: Maximum transferred energy

CSX: Maximum compressive stress

CSB: Maximum compressive stress, toe

RMJ: Case Method Estimate with a J-factor=J

RA2: Case Method Estimate, damping independent

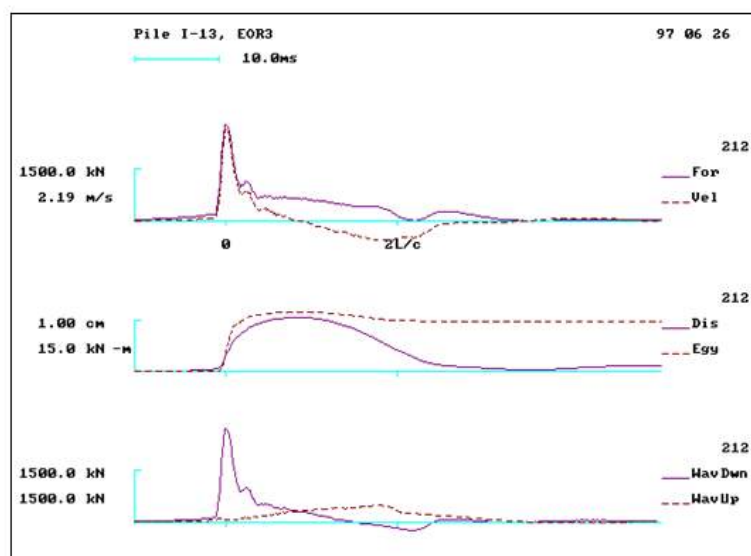
PRES: Penetration resistance

Energy Ratio: Ratio between transferred and rated energy (57 kJ)

**CAPWAP Table**

Mobilized Static Resistance (kN)			Max. Stress (MPa)		Smith Damping (s/m)		Quake (mm)	
Total	Shaft	Toe	Compression	Tension	Shaft	Toe	Shaft	Toe
1,724	1,686	38	168	10	0.244	-	2.000	1.700

PDA Wave Traces



CAPWAP Signal Match and Resistance Distribution

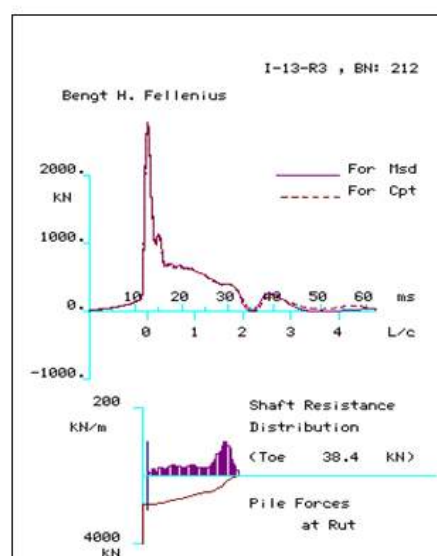


Fig. 9.17 Example of a routine PDA and CAPWAP summary sheet: Table and graph

The CAPWAP determined capacity is usually close to the capacity determined in a static loading test. This does not mean that it is identical to the value obtained from a static test. After all, the capacity of a test pile as evaluated from a static loading test can vary by 20 percent with the definition of failure load applied. Also, only very few static loading tests can be performed with an accuracy of 5 percent on load values. Moreover, the error in the load measurement in the static loading test is usually about 10 percent of the value, sometimes even greater.



A CAPWAP analysis performed on measurements taken when a pile penetrates at about 5 blows to 12 blows per inch will provide values of capacity, which are reliable and representative for the static behavior of the pile at the time of the driving. Provided that the static test is equally well performed (not always the case), the two values of static capacity are normally within about 15 percent of each other. For all practical engineering purposes, this can be taken as complete agreement between the results considering that two different methods of testing are used.

In practice, engineers employing dynamic testing and CAPWAP analysis limit the analysis to the last impact given to the test pile at initial driving and the first (if possible) of the impacts given in restriking the test pile. They treat the dynamic tests as so much of a lesser cost static test. However, this is losing the full benefit of the dynamic test. Often at the end of initial driving, the full resistance is not mobilized (the pile is being driven at the maximum ability of the hammer to advance the pile) and the CAPWAP-determined distribution may not be determined at the optimum use of the method. Therefore, also records of a blow from before the end of initial driving, say, from a foot above termination, should be subjected to a CAPWAP analysis and the results compared and discussed. Similarly, at restrike, also a record from the end of restrike, say the fifth or tenth blow should be analyzed. The latter analysis will often show a larger toe resistance than the analysis for very first restrike record (because the restriking has reduced the set-up and the shaft resistance being smaller allows more force and energy to reach the pile toe. Of course, an extra couple of CAPWAP analyses cost money—but so what, it is cheap money for the value obtained.

A CAPWAP analysis uses as input the speed of wave propagation,  $c$ , in the pile. Eqs. 9.11 through 9.17 show the importance and interdependence of the material density, impedance, and elastic modulus. The proper selection of the input parameters will govern the correct location of the soil and pile response (reflections) and of particular importance is the use of a correct wave speed for determining the elastic modulus. For a concrete pile, minute cracks—hairline fissures—can develop and together they could have the effect of slowing down the wave and require a smaller modulus to be input for the correct analysis results. The elastic modulus is usually determined from the time for the wave to reach the pile toe and be reflected up to the gage location at the pile head, Time  $2L/c$ . Also the evaluation of the impact force makes use of the elastic modulus. However, where hair line fissures have slowed down the wave speed and indicated a reduced modulus, no such reduction occurs at the gage location. In such cases, using the E-modulus input from the " $2L/c$ " time is not correct and a unreduced modulus applies.

It is important that the blow selected for CAPWAP analysis is from where the maximum pile movement is larger than the quake resulting from the analysis. However, the pile movement should not be too much larger than the quake. The shape of the simulated load-movement curve, particularly for the pile toe, becomes less representative beyond the quake movement. When using the PDA/CAPWAP for reasons similar to performing a routine static loading test, or as a replacement for such, as a part of a field verification process where many piles are tested, the main purpose of the test and analysis is to establish a reliable level of at-least capacity. However, when issues of load distribution, set-up also are a part of the study, then using a blow with a "perfect" record becomes vital. Often, running a CAPWAP on a couple of contiguous blows assists the final assessment. Doing an additional analysis on a blows recorded when the pile was a foot higher up is a prudent measure that may resolve many questions. Indeed, relying on the results from a single blow frequently insufficient and, because the blow record already exists, doing a second blow judiciously chosen is a reassurances obtained at a very low cost.

Aoki (2000) proposed a Dynamic Increasing Energy test, DIET, consisting of a succession of blows from a special free-falling drop hammer, while monitoring the induced acceleration and strain with the Pile Driving Analyzer. Each blow to be analyzed by means of the CAPWAP program. The DIET test assumes that CAPWAP-determined static load-movement curves represent a series of loading-unloading, and reloading of the pile as in a static loading test to a progressively larger maximum applied load. The curve from the first blow represents virgin condition and the following blows represent reloading condition.

Fellenius (2014) presented a case history from Sao Paulo, Brazil (as reported Oliveira et al. 2008), where DIET tests were performed with four blows on a 700-mm diameter, 12 m long, CFA pile 66 days after constructing the pile. The results were verified by carrying out a static loading test 31 days after the dynamic test. Figure 9.18 shows the DIET load-movement curves for the pile head, shaft, and toe, and for the static loading test, all plotted in sequence of event. The dashed curves are back-calculated curves applying UniPile and t-z and q-z functions.

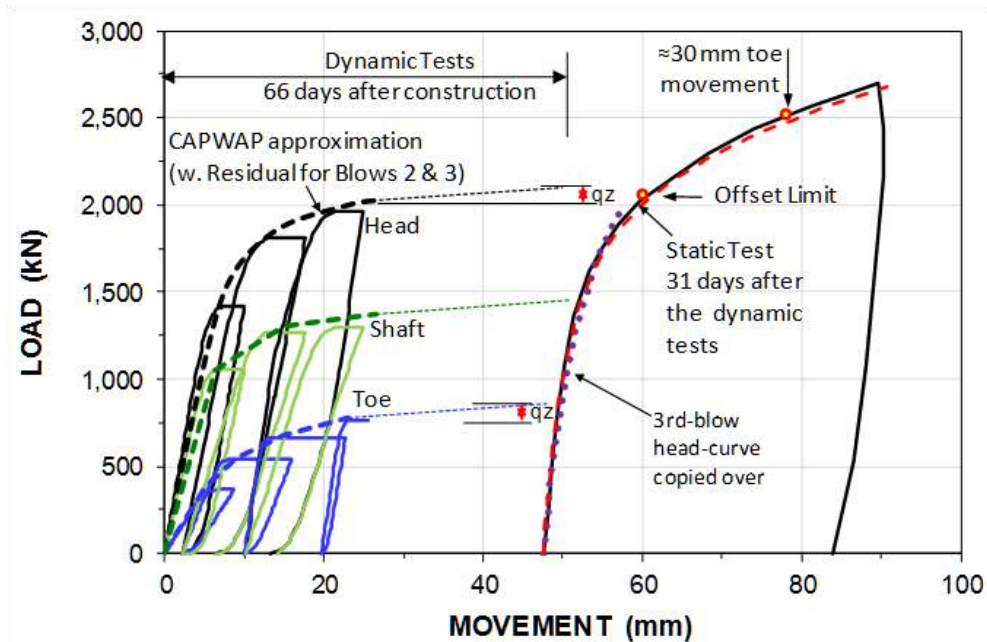


Figure 9.18 Load-movement curves for CAPWAP analyses and the static loading test (Fellenius 2014)

The results show that the CAPWAP-determined pile capacity agreed very well with the capacity of the static loading test, when defined by the offset limit (Section 8). The results also show that the dynamic tests stiffened up the pile giving an increase of the capacity determined from the load-movement of the static loading test. The increase was about 200 kN or 10 %. Indeed, The DIET method (dynamic testing and combining a series of blows with increasing force and CAPWAP analysis) provides results that more closely resemble those of a static loading test than does a single CAPWAP.

### 9.12. Results of a PDA Test

The cost of one conventional static test equals the costs of ten to twenty dynamic tests and analyses, sometimes more. Therefore, the savings realized by the use of dynamic testing can be considerable, even when several dynamic tests are performed to replace one static loading test. Moreover, pile capacity can vary considerably from one pile to the next and the single pile chosen for a static loading test may not be fully representative for the other piles at the site. The low cost of the dynamic test means that for relatively little money, when using dynamic testing, the capacity of several piles can be determined. Establishing the capacity of several piles gives a greater confidence in the adequacy of the pile foundation, as opposed to determining it for only one pile. Therefore, the PDA/CAPWAP applied to a driven pile project ensures a greater assurance for the job.

The CAPWAP results include a set of parameters to use as input to a wave equation analysis, which allows the wave equation can be used with confidence to simulate the continued pile driving at the site, even when changes are made to pile lengths, hammer, and pile size, etc.

The limitations mentioned above for when the full resistance is not mobilized apply also to the CAPWAP analysis, although the risk for overestimation of the capacity is smaller.

The distribution of the capacity on shaft and the toe resistances is determined with less accuracy as opposed to the total capacity. The reason lies in that a pile is always to a smaller or larger degree subjected to residual force and the residual force cannot be fully considered in the CAPWAP analysis. The effect of residual force present in a test pile is an overestimation of the resistance along the upper length of the pile (shaft resistance) and an underestimation along the lower length (toe resistance). It has no effect on the total capacity, of course. (It is not always appreciated that the sensitivity of the analysis results to residual force is equally great for the results of a static loading test).

A pile test will unavoidably change—disturb—the pile response to load. A dynamic test more so than a static test. It is not irrelevant, therefore, when comparing static and dynamic tests, for the best compatibility, the static loading test should "go first", as indicated in Fellenius (2008). This is not a trivial recommendation, because a dynamic test requires a stick-up of the pile head above ground, whereas a static loading test is preferably performed with a minimum stick-up.

Some preliminary results of the PDA testing will be available immediately after the test, indeed, even as the pile is being driven. For example, the transferred energy, the impact and maximum stresses in the pile, and a preliminary estimate of capacity according to the CMES method. The following is reported following processing in the office.

- Selected representative blow records including a graphic display of traces showing Force and Velocity, Transferred Energy and Pile Head Movement, and Wave Up and Wave Down.
- Blow data processed presented in tables showing a series of measured data for assessment of the pile driving hammer and pile.
- CAPWAP results showing for each analyzed blow the results in a CAPWAP diagram and the quantified results in tables.
- Complete pile driving diagram encompassing all dynamic data (Fig 9.17)

Figs. 9.19 and 9.20 show examples of the measurements presented in a PDA diagram. The PDA diagram can be used to study how transferred energy, forces and stresses, hammer stroke, and penetration resistance vary with depth. When the PDA monitoring is performed not just for to serve as a simple routine test but to finalize a design, establish criteria for contract specifications, etc., then, a PDA diagram is of great value and assistance to the engineer's assessment of the piling.

The foregoing should make it quite clear that relying on a dynamic formula, that is, on essentially only the "blow-count" to determine capacity is a dangerous approach. Salem et al. 2008, present a case history where the blow count was considerably misleading, as was established in dynamic testing and CAPWAP analysis.

Lately, it has been stated that measurements on long, 10 to 20 feet (3 to 6 m) diameter, offshore piles have shown that the wave speed in these piles is faster than in other steel piles. These piles may have a 3/4 inch (20 mm) and more wall thickness, which would seem to be a thick wall. However, scaling down the diameter to that of a pile 12 to 24-inch pile diameter (0.3 to 0.6 m), the proportional wall thickness becomes about 2 mm, which would make for a very flimsy pile. When such a pile is long, that is, longer than about 30 pile diameters, then, the toe of the thin-wall pile vibrates laterally like the end of a tuning fork, and if the toe is in a soft easily disturbed soil, liquefaction of the soil and loss of all shaft resistance near the pile toe will entail. On encountering that zone, the stress wave sends a tension reflection that can

be interpreted as an indication of pile toe damage and/or loss of pile length, if the wave interpretation applies the conventional steel modulus. Field measurements have shown the indication to be false. Inputting a larger wave speed moves the origin of the reflection to below the pile toe, which removes the damage indication and lets the tension reflection be interpreted as a large-quake soil. When the pile toe reaches deeper located, more competent soil layers, the "damage" reflection may disappear, but, then, the wave speed is already established. It has been suggested that the large diameter piles are fabricated from different steel to that in smaller diameter piles (because similarly large wave speeds have not been reported from the smaller diameter piles) and that may be true. However, because the result of the calculation using the larger wave speed is a larger CAPWAP-determined capacity. I suggest that whether the damage indication is true or false should first be ascertained by other means than modifying the elastic modulus of the steel.

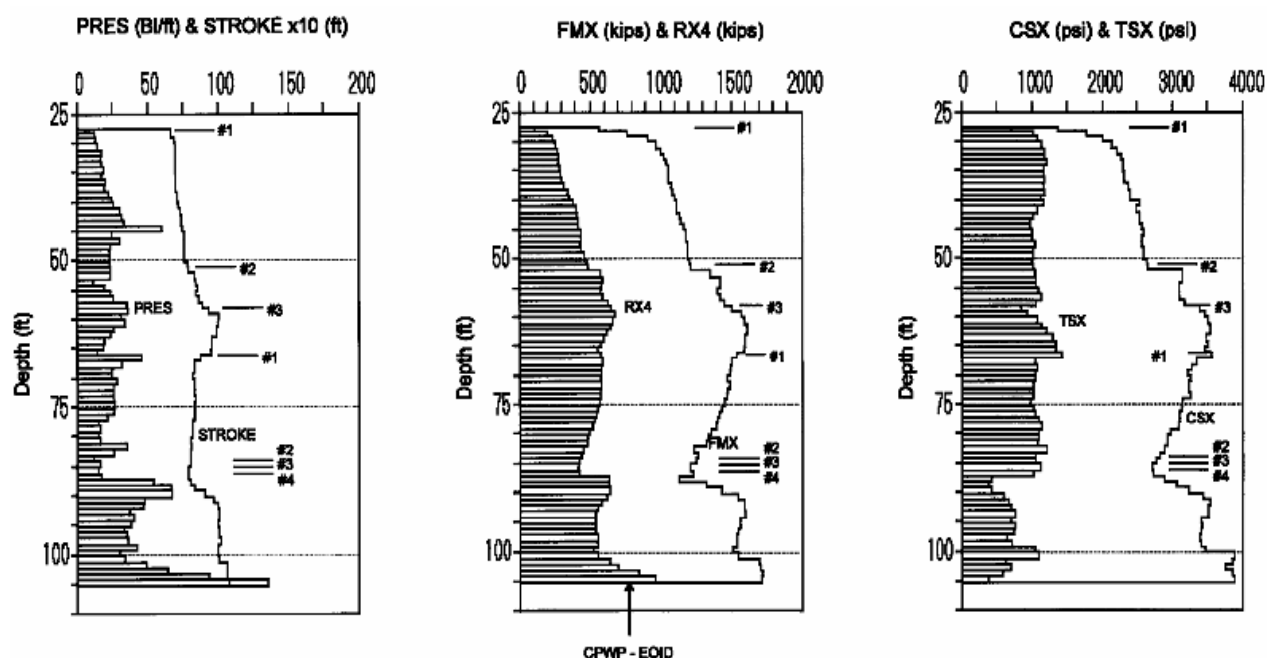


Fig. 9.19 Example of PDA Diagrams from the driving of a concrete pile  
(Labels #1 through #4 indicate hammer fuel setting)

### 9.13. Long Duration Impulse Testing Method—The Statnamic and Fundex Methods

In the conventional dynamic test, the imparted stress-wave has a steep rise and an intensity that changes along the pile length. That is, when the impact peak reaches the pile toe and the entire pile is engaged by the blow, force from the pile hammer transmitted to the pile varies and is superimposed by numerous reflections. The force in the pile varies considerable between the pile head and the pile toe. The steep rise of the stress-wave and the reflections are indeed the condition for the analysis. When the impact is "soft" and the rise, therefore, is less steep, it becomes difficult to determine in the analysis just from where the reflections originate and how large they are. However, in the 1990s, an alternative dynamic method of testing was developed, called Statnamic, here denoted "*long duration impulse method*" consisting of giving the pile just this soft-rising, almost constant force. The method is usually called "rapid loading test" and consists of impacting the pile in a way where the rise of force is much softer than in the pile driving impact, and the impulse (a better word than "impact") was of a much longer duration. The long duration impulse usually makes the pile move as a rigid body, that is, the pile velocity at the pile head is the same as the velocity at the pile toe. This aspect made possible an analysis method, called the "*unloading point method*" for determining the pile capacity (Middendorp et al. 1992).

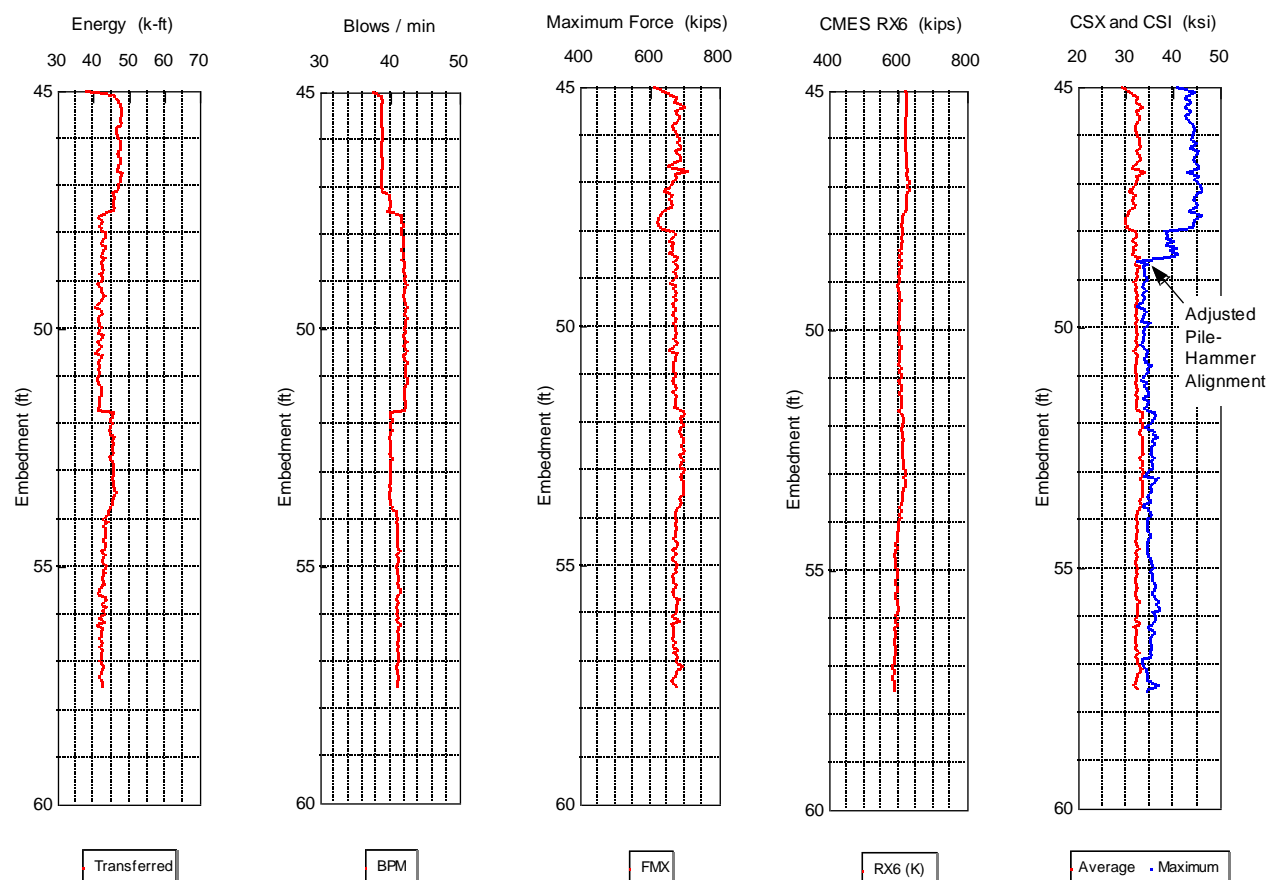


Fig. 9.20 Example of PDA Diagrams from the driving of a steel pile

The long duration impulse method is a dynamic method. However, the transfer of the force to the piles, the impulse, can take 100 to 200 milliseconds, i.e., five to twenty times longer time than the time for a pile driving impact. The stress-wave velocity in the pile is the same, however. This means that the sharp changes of force experienced in the pile driving are absent and that the pile moves more or less as a rigid body. Although the ram travel is long, the peak force is reduced by that the impact velocity has been reduced. As a large ram mass is used, a large energy is still transferred to the pile. The key to the long duration impulse method lies in this slowing down of the transfer of the force from the impacting hammer to the pile. In method employed by a Dutch company, Fundex, this is achieved by letting the ram impact a series of plate springs which compression requires the hammer to move much more than required in case of the ordinary hammer and pile cushions, and thus reduce the kinetic energy in the transfer to the pile. The Statnamic method, developed by Berminghammer in Canada, achieves the effect in the pile in a radically different way, using a propellant to send a weight up in the air above the pile, in the process creating a downward force on the pile according to Newton's third law.

The measurements consist of force, movement, acceleration, and time. The most important display of the results consists of a load-movement curve, as illustrated in Figure 9.21.

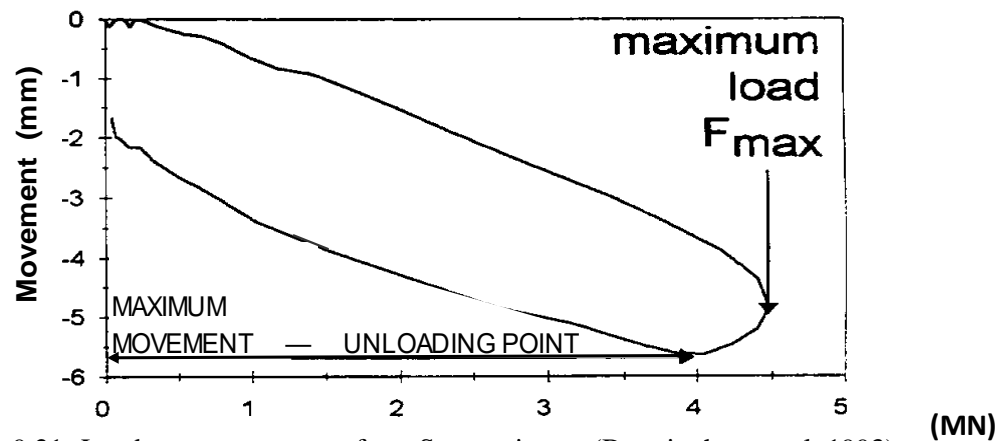


Fig. 9.21 Load-movement curve from Statnamic test (Bermingham et al. 1993)

Load, movement, velocity, and acceleration versus time are important records of the test. An example of these records are presented in Figure 9.22 (same test as in Figure 9.21). The maximum movement (about 4 mm in the example case) is where the pile direction changes from downward to upward, i.e., the pile rebounds, is called the "Unloading Point", "P-point" for short. The maximum load applied to the pile by the ram impulse (about 4.5 kN in the example case) occurs a short while (about 3 ms in the example case) before the pile reaches the maximum movement. Most important to realize is that the pile velocity is zero at the unloading point, while the acceleration (upward) is at its maximum. Shortly before and after the maximum force imposed, the velocity of the pile head and the pile toe are considered to be essentially equal, that is, no wave action occurs in the pile. This is assumed true beyond the point of maximum movement of the pile.

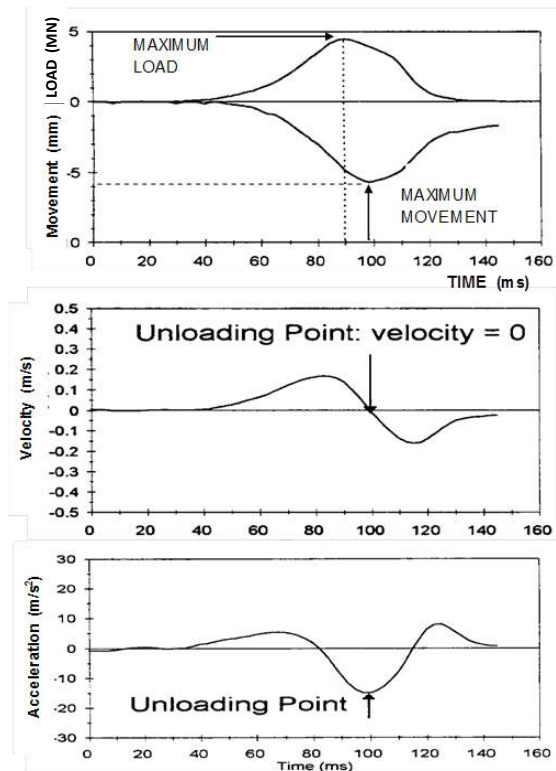


Fig. 9.22 Load, movement, velocity, and acceleration versus time from a Statnamic test (Bermingham et al. 1993; used with permission)

In the pile-driving dynamic test, the methods of analysis of the force and velocity measured in a dynamic test includes a separation of the damping portion (the velocity dependent portion) of the dynamic resistance. Inertia forces are considered negligible. In contrast, in the long duration impulse method, the velocity of the pile is zero at the unloading point, which means that damping is not present. However, the acceleration is large at this point and, therefore, inertia is a significant portion of the measured force. The equilibrium between the measured force and the other forces acting on the pile at any time is described by Eq. 9.24 (Middendorp et al. 1992).

$$(9.24) \quad F = ma + cv + ku$$

where

$F$	=	measured force (downward)
$m$	=	mass of pile
$a$	=	acceleration (upward)
$c$	=	damping factor
$v$	=	velocity
$k$	=	modulus
$u$	=	movement

The two unknowns in Eq. 9.24 are the damping factor,  $c$ , and the modulus,  $k$ . The other values are either known or measured. As mentioned, at the unloading point, the velocity is zero along the full length of the pile. This becomes less true as the pile length increases, but for piles shorter than about 40 m, observations and research have shown the statement to be valid (Middendorp et al. 1998; Nishimura et al. 1998).

At the time of zero velocity, the damping component of Eq. 9.24 is zero, because the velocity is zero. This determines the static resistance at the unloading point, because the force and acceleration are measured quantities and the mass is known. Thus, the static resistance acting on the pile at the unloading point is obtained according to Eq. 9.25 as the value of measured force plus the inertia (note acceleration is upward—negative).

$$(9.25) \quad R_p = (F_p - ma_p)$$

where

$R_p$	=	static resistance at the UPM-point
$F_p$	=	force measured force at the UPM-point
$m$	=	mass of pile
$a_p$	=	acceleration measured at the UPM-Point

In the range between the maximum measured force and the unloading point, the load decreases (the pile decelerates; acceleration is negative) while the movement is still increasing, and the pile has a velocity (downward and reducing toward zero at the unloading point, which means that damping is present). These quantities are measured. Moreover, it is assumed that at the maximum force, the pile has mobilized the ultimate shaft resistance and the continued soil response is plastic until the unloading point is reached. That is, the static resistance is known and equal to the value determined by Eq. 9.25. This is the primary assumption of the Unloading Point Method for determining the pile capacity (Middendorp et al. 1992).

Eq. 9.24 can be rearranged to Eq. 9.26 indicating the solution for the damping factor.

$$(9.26) \quad c = \frac{F - ma - R_p}{v}$$

where

- $c$  = damping factor
- $F$  = measured force (downward)
- $m$  = mass of pile
- $a$  = acceleration (upward)
- $R_P$  = static resistance at the UPM-point
- $v$  = velocity

The value of the damping factor,  $c$ , in Eq. 9.26 is calculated for each instant in time between the maximum measured force and the unloading point. For the Statnamic test, the number of data points depends on the magnitude of movement of the pile after the maximum Statnamic force is reached. Typically, the number of data points collected in this range is 50 to 200. The  $c$  values are averaged and taken to represent the damping factor acting on the pile throughout the test. The measured force and acceleration plus the pile mass then determine the static load-movement curve according to Eq. 9.27.

$$(9.27) \quad R_P = F - ma - c_{avg} v$$

where

- $R_P$  = static resistance at the UPM-point
- $F$  = measured force (downward)
- $m$  = mass of pile
- $a$  = acceleration (upward)
- $c_{avg}$  = average damping factor between the maximum force and the P-point
- $v$  = velocity

Figure 9.23 illustrates the results of the analysis for a 9 m long, 910 mm diameter bored pile in clay (Justason and Fellenius 2001).

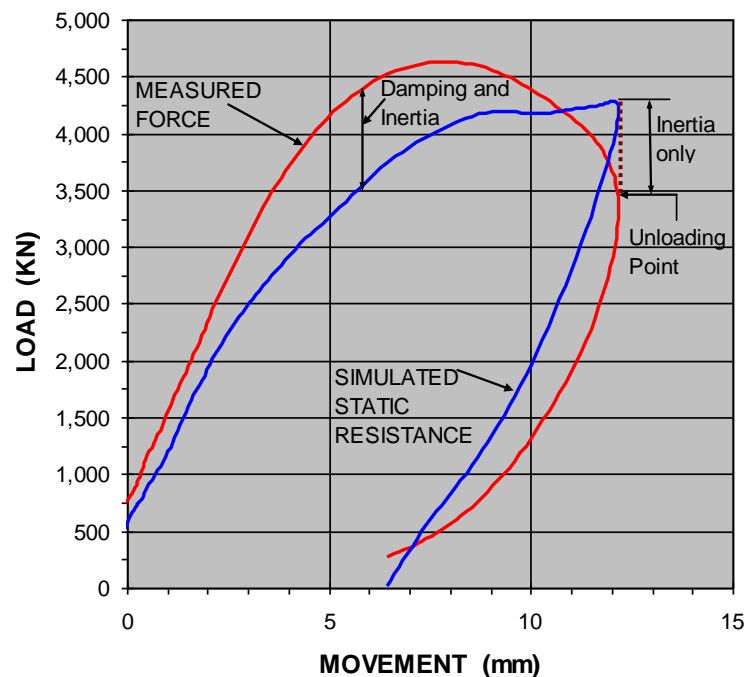


Fig. 9.23 Example of measured force-movement curve and simulated static load-movement curve Data from Justason and Fellenius (2001)



Lately, several papers have been published reporting case histories on capacity determined in a Statnamic test according to the Unloading Point Method, UPM (e.g., Middendorp et al. 2008; Brown and Hyde 2008). The papers show that the method considerably overestimates the capacity determined on the same pile in a static loading test. In clay, the overestimation has been as large as close to a factor of two. The referenced papers hypothesize that the capacity overestimation is a result of the velocity of the pile and associated dynamic effects, notwithstanding that the UPM capacity is determined at zero velocity—non-dynamic condition—and recommend that a correction factor be applied to the UPM-determined capacity. Such correction factors can never be general factors associated with the method, and it appears necessary to calibrate the Long Duration Impulse Testing Methods to a static loading test before relying on a UPM-determined response for a specific site and project.

#### 9.14. Vibratory Pile Driving

The information in this section draws primarily from research and results presented by K.R. Massarsch (Massarsch 2000, 2002, 2004).

Vibratory driving is a common method for installing or extracting sheet piles and piles. Vibratory pile driving causes oscillating horizontal ground vibrations in coarse-grained soils. It can be shown that these horizontal vibrations reduce the shaft resistance during driving. The process results in the permanent increase of horizontal effective stress which causes arching around the vibrated pile. The most important parameters are vibration frequency, vibration amplitude, and eccentric moment. These parameters govern vibratory driving and, in particular, the soil resistance at the toe and along the shaft of a pile. The resonance frequency of the vibrator-pile-soil system, significantly affects pile penetration and emission of ground vibrations. At resonance of the vibrator-pile-soil system, the vertical vibration velocity in the soil reaches a maximum and pile penetration becomes very slow, whereas, beyond resonance, the vibration velocity decreases and the pile penetration is fast. (Resonance cannot occur in a direction perpendicular to the pile, i.e., the horizontal direction). Field monitoring of the vibratory driving process can be used to optimize vibratory pile driving.

Vibratory excitation affects a pile in a different way than does impact driving. In the case of vibratory driving, the pile is rigidly connected to the vibrator, resulting in minimal energy loss in transfer from the vibrator to the pile. The vibration frequency is relatively low, typically below 40 Hz (2,400 rpm) and the wave length propagating down the pile is much longer than in the case of impact driving. It is generally recognized that vibratory driving is most effective in coarse-grained (frictional) soil and less efficient in fine-grained (cohesive) soil.

Modern vibrators are hydraulically driven, which allows continuous variation of the vibrator frequency during operation. The vertical oscillation of the vibrator is generated by counter-rotating eccentric masses.

The peak value of the centrifugal force acting in the vertical direction depends on the eccentric moment and the circular frequency of the rotating eccentric masses, as expressed in Eq. 9.28.

$$(9.28) \quad F_v = M_e \omega^2$$

where  $F_v$  = centrifugal force  
 $M_e$  = eccentric moment  
 $\omega$  = circular frequency ( $\omega = 2\pi f$ ; )

Many modern vibrators with variable eccentric moment and frequency enable the centrifugal force to be adjusted continuously during operation. The driving ability of the vibrator is determined by the vertical displacement amplitude (single amplitude) as a function of the eccentric moment and the total dynamic mass as expressed in Eq. 9.29. The total dynamic mass is the sum of all masses accelerated by the vibrator. This includes the rotating eccentric units, the pile, and the vibrator clamp. Note that most equipment manufacturers express the displacement amplitude as peak-to-peak ("double") amplitude.

$$(9.29) \quad s = \frac{M_e}{m_t}$$

where     $s$     =    displacement amplitude (single)  
           $M_e$    =    eccentric moment  
           $m_t$    =    total dynamic mass

One important parameter that affects the penetration resistance during pile driving and during vibratory compaction is the operating frequency of the vibrator. Resonance vibration of the vibrator-pile-soil system is a function of several parameters with the shear wave speed (and therefore the shear modulus) being one of the most important. For most practical applications, the shear wave speed of undisturbed medium dense sand ranges between 150 and 250 m/s. However, in the presence of uninterrupted strong ground vibrations, the shear wave speed may reduce due to strain-softening effects. For most cases, the resonance frequency is in the range of 15 to 25 Hz and decreases with increasing pile length (and ratio of vibrator to pile mass). Note that the eccentric moment does not influence the resonance frequency.

An important such aspect of vibratory pile (or sheet pile) driving (or extraction) is that at-or close to-resonance, the penetration speed of the pile slows down dramatically, as the soil and pile (sheet pile) vibrate in phase. Vertical ground vibrations reach a peak at the resonance frequency of the vibrator-pile-soil system and the vertical vibration velocity is about 5 to 10 times larger than at the maximum vibration frequency. At resonance, shaft resistance builds up along the pile-soil interface, which enhances the transfer of vibration energy to the soil. This effect reduces penetration speed and can cause vibration problems during the operation. With increasing vibration frequency, the relative displacement between the pile and the soil increases, resulting in a reduction of shaft friction. Therefore, piles should be vibrated at a frequency of at least 1.5 times the resonance frequency in order to achieve efficient pile penetration and to minimize vibration emission.

Horizontal ground vibrations are significantly lower than the vertical. At frequencies below resonance, the relative movement between the pile and the soil is small, resulting in an almost static pile-soil interaction.

Eq. 9.28 that the displacement amplitude,  $s$ , is independent of the vibration frequency,  $f$ . In order to maximize the displacement amplitude, the total dynamic mass,  $m_t$ , should be kept as small as possible. Vibrators with variable eccentric moment allow the machine operator to start up and shut down the vibrator at zero vibration amplitude, thereby reducing the risk of vibration amplification due to resonance.

The resistance of the soil along the pile consists of two components, pile shaft resistance and pile toe resistance.

\

#### **9.14.1    Pile Shaft Resistance**

In the case of impact driving, the inertia of the pile and the static resistance along the pile-soil interface must be overcome in order to achieve a net pile penetration. At the end of each impact, the pile penetration slows down and static conditions return along the pile. In contrast, in the case of vibratory

driving, the pile is kept axially (usually vertically) oscillating during the entire driving phase and the shaft resistance developing in vibratory driving is considerably smaller than that encountered in impact driving. Liquefaction is mentioned in the geotechnical literature as a possible cause of reduced shaft friction (permanent and/or temporary). However, liquefaction only develops in saturated soil and, yet, vibratory driving works well also in dry soil. Other causes mentioned are “rolling friction” and “material degradation”. However, these terms are mainly descriptive and, therefore, difficult to quantify.

A more rational explanation can be based on the cyclic forces generated during vibratory driving. Field measurements of ground vibrations during vibratory driving have shown that the vertically oscillating force creates—due to shaft resistance—also a horizontally oscillating force with a frequency that is twice the vertical vibration frequency. The horizontally oscillating wave field builds up pulsating horizontal stresses which reach a maximum at the end of each downward and upward end of the vibration cycle and the shaft resistance of a pile is temporarily reduced. The soil is compressed horizontally, building up high horizontal effective stresses and, indeed, preconsolidates the soil adjacent to the pile.

In fine-grained (cohesive) soils, shaft resistance decreases due to strain and the number of vibration cycles (remolding) occurring when the relative displacement between the pile and the soil exceeds about 5 to 10 mm. The magnitude of the eccentric moment of the vibrator is therefore important for vibratory driving of piles in cohesive soils, as it determines the relative displacement between the pile and the soil (Eq. 9.28).

#### **9.14.2 Pile Toe Resistance**

During a vibration cycle, when the pile has completed a downward motion and starts the upward rebound movement of the cycle, the soil below the pile toe will first follow the upward movement in an elastic response. Soon, however, during the continued upward movement, the contact force between the pile toe and the soil is reduced to zero and there is a separation of the pile toe from the underlying soil that increases if the upward movement continues. This causes causing a suction (“cavitation”) between the pile toe and the soil below the toe, which is important because the suction can result in a remolding and/or loosening of the soil below the pile toe—even result in a net separation of the pile toe from the underlying soil and leave a gap below the pile toe. The toe resistance during the following cycle depends on the loosening and potential gap due to the preceding vibration cycle. The larger the amplitude, the larger the potential effect on toe bearing. For this reason, it is advantageous to reduce the vibration (displacement) amplitude gradually over a minute or two at the end of driving toe-bearing piles, as opposed to a sudden vibration turn-off and end of driving.

#### **9.14.3 Vibrator Performance Parameters**

During the last two decades, vibrators have experienced a rapid development in terms of power, range of operating parameters (eccentric moment and frequency) and monitoring of the driving and extraction process. (Initially, before 1990, most hydraulic vibrators had fixed eccentric moment, with a typical operating frequency of 22 to 30 Hz. These vibrators were mostly used for driving and extracting sheet piles).

The introduction of vibrators with variable frequency and amplitude allowed the resonance-free starting and shut-down of vibratory driving. Such vibrators allow the operating frequency and eccentric moment (and thus amplitude) to be varied according to driving requirements and soil conditions. The vibrator operation is computer-controlled and programmable.

The vibration amplitude given by vibrator manufacturers is usually in terms of double-amplitude and refer to a freely suspended vibrator (without clamp and pile/sheet pile). However, the vibration amplitude is an

important parameter and must take into account the mass of also the clamping device and the pile. Note as indicated by Eq. 9.34, the displacement amplitude is not affected by the vibrator operating frequency.

An additional parameter to consider is the amplitude of the relative displacement between the pile and the soil, as it is important in regard to overcoming the toe resistance in coarse-grained soil and for the shaft resistance in cohesive soils. The larger the relative displacement between the pile and the soil, the more effective the driving process will be. The displacement amplitude depends on the total dynamic mass which must be accelerated by the vibrator and the eccentric moment. Therefore, if a pile is to be driven into clayey soil, a large eccentric moment will result in better driving performance.

With modern computerized equipment it is possible to acquire, display, and record information from a range of sensors, which can be mounted on the pile, the vibrator, the power pack, and the ground. Monitoring the vibratory driving process and the response of the ground and/or of adjacent structures is an important aspect of modern vibratory works. For instance, in the case of vibratory driving in the vicinity of vibration-sensitive buildings or equipment, the maximum vibration intensity needs to be controlled in order to ensure that specified limiting values are not exceeded. The monitoring usually consists of recording the following parameters:

- Position of pile
- Recording intervals (at least one reading per second)
- Depth of sheet pile during penetration or extraction (penetration speed)
- Operating frequency of vibrator
- Acceleration of vibrator
- Static force applied to the pile (pushing or lifting force affecting the vibrator weight)
- Hydraulic pressure of vibrator/power pack
- Vibration velocity on ground (geophones or accelerometers)
- Eccentric moment
- Centrifugal force
- Displacement amplitude (prior to and during the driving)

When piles or sheet piles are to be installed with vibratory driving equipment, the selection of the equipment and the installation process must be based on sound information obtained from geotechnical investigations. Having to replace an unsuitable vibrator will not only result in project delays and incur additional costs, the use of an unsuitable vibrator can, under unfavorable conditions, also produce damaging ground vibrations. The required vibrator capacity can be estimated based on soils information which includes records of CPT soundings, and results of field trials. With this proposed concept, it is possible to develop a correlation between penetration resistance and pile penetration speed for different vibrator types and pile sizes.

#### **9.14.4 Vibratory Driving Planned from Penetration Tests**

Rational design of a vibratory driving project requires site information that includes a well-established soil profile with soil description. The most reliable geotechnical information can be obtained from a continuous record of soil layering and density, such as provided by a CPTU sounding.

Unless past experience is available from vibratory driving in similar geology and comparable equipment, field trials are the best way of estimating the vibratory driving resistance of piles or sheet piles. During the driving test, it is important that the vibrator rests on the pile and is not held back by the machine operator, which would affect the penetration speed.

Vibratory driving of piles and sheet piles can be carried out with minimum environmental adverse effects, such as ground vibrations, noise, and soil disturbance. As the operating frequency of the vibrator has a strong influence on vibrations emitted from the vibrating pile, the highest risk of ground vibrations occurs when the vibrator is operated at the resonance frequency of the vibrator-pile-soil system. It is also when the pile penetration progress is the smallest.

### 9.15. Vibration Caused by Pile Driving

The information in this section draws primarily from research and results presented by K.R. Massarsch (Massarsch 1992; 2000; 2004 2008; and Massarsch and Fellenius 2014; 2014).

During driving, energy is transmitted from the pile hammer to the pile, and, as the pile penetrates into the soil, both static and velocity-dependent (dynamic) dynamic resistances are generated. The dynamic soil resistance gives rise to ground vibrations which are transmitted through the soil, potentially, causing settlement in some soils, or adversely affecting nearby installations or structures on or in the ground. In this context, the process is more complex than realized by many, but the theoretical format is quite simple, as will be shown below. Based on work by Massarsch 2002; 2004, Massarsch and Fellenius (2008; 2014) discussed the interactive nature of the pile impedance and the soil impedance which can be used to assess the vibration effect of pile driving. The fact that the damping factor is a function of the ratio between the pile impedance and the soil impedance for P-waves is verified by a reanalysis of vibration measurements reported by Heckman and Hagerty (1978), who measured the intensity of ground vibrations at different distances away from piles being driven. The piles were of different type, size, and material. Heckman and Hagerty (1978) determined a 'k'-factor, expressed in Eq. 9.30, which governs the ground vibration intensity. The vibration velocity, also called peak particle velocity, PPV, is the standard measure of vibration intensity and reference to risk for vibration settlement due to pile driving.

$$(9.30) \quad v = k \frac{\sqrt{W}}{r}$$

where

$v$	=	vibration velocity (m/s)
$W$	=	energy input at source (J)
$k$	=	an empirical vibration factor ( $\text{m}^2/\text{s}\sqrt{\text{J}}$ )
$r$	=	distance from pile (m)

The vibration velocity in Eq. 9.30 is not defined in terms of direction of measurement (vertical, horizontal, or resultant of components). Moreover, the empirical factor,  $k$ , is not dimensionless, which has caused some confusion in the literature. Figure 9.24 presents the  $k$ -factor values of Heckman and Hagerty (1978) as a function of pile impedance and measurements of pile impedance.

The measurements were taken at different horizontal distances away from piles of different types and sizes driven with hammers of different rated energies. Unfortunately, the paper by Heckman and Hagerty (1978) is somewhat short on details regarding the driving method, ground conditions, and vibration measurements and, therefore, the data also include effects of ground vibration attenuation and, possibly, also effects of vibration amplification in soil layers. Yet, as shown in Figure 9.25, a strong correlation exists between the pile impedance and the  $k$ -factor, as the ground vibrations increased markedly when the impedance of the pile decreased. In fact, ground vibrations can be ten times larger in the case of a pile with low impedance, as opposed to vibrations generated at the same distance from the driving of a pile with high impedance (Massarsch 1992; Massarsch and Fellenius 2008; Fellenius and Massarsch 2008).

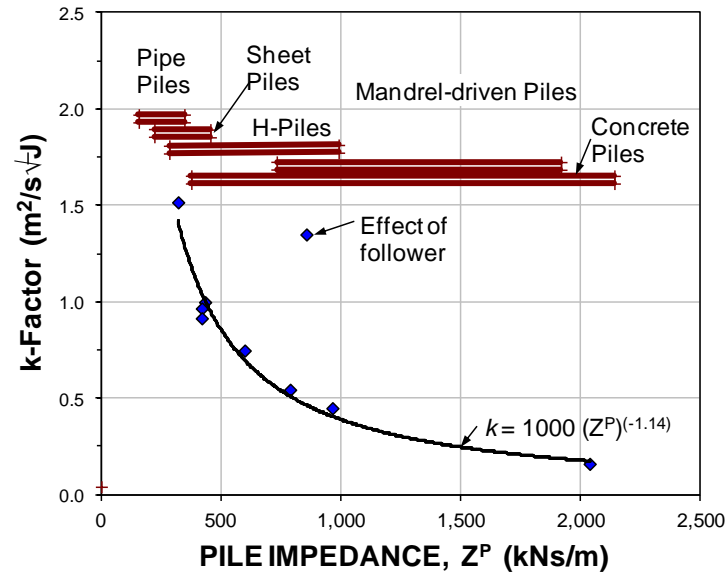


Fig. 9.24 Influence of pile impedance on the vibration factor,  $k$  (Eq. 9.30).  
(Data from Heckman and Hagerty 1978).

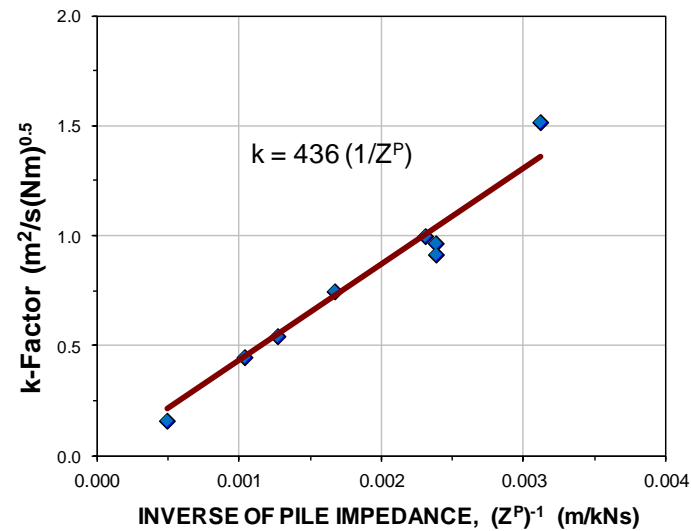


Fig. 9.25 Relationship between  $k$ -factor and inverse of pile impedance. Data from Figure 9.24 replotted.

The correlation shown in Figures 9.23 and 9.24 is surprisingly good, considering that the measurements were taken in different soil conditions. The data provided by Heckman and Hagerty (1978) indicate that ground vibrations in the reported cases mainly originated from the pile toe. Indeed, the data confirm that the energy transmission efficacy correctly reflects the vibration emission from the pile to the surrounding soil layers.

Combining Eqs. (9.4) and (9.30) results in Eq. (9.31), which can be used for estimation of ground vibration from pile driving (Massarsch and Fellenius 2014).

$$(9.31) \quad v = \frac{436}{Z^P} \frac{\sqrt{F^H W_0}}{r}$$

where

- $v$  = vibration velocity (a physical velocity)
- $Z_P$  = pile impedance
- $F^H$  = pile driving efficacy factor
- $W_0$  = nominal energy
- $(F^H W_0)$  = transferred energy obtained from dynamic measurements

Nilsson (1989) reports vibration velocity measurements from the driving of 270-mm diameter concrete piles through fill and overburden soils to dense glacial till at 25 m depth. Massarsch and Fellenius (2008; 2014) reanalyzed data using the relation expressed in Eq. 9.31, as shown in Figure 9.26.

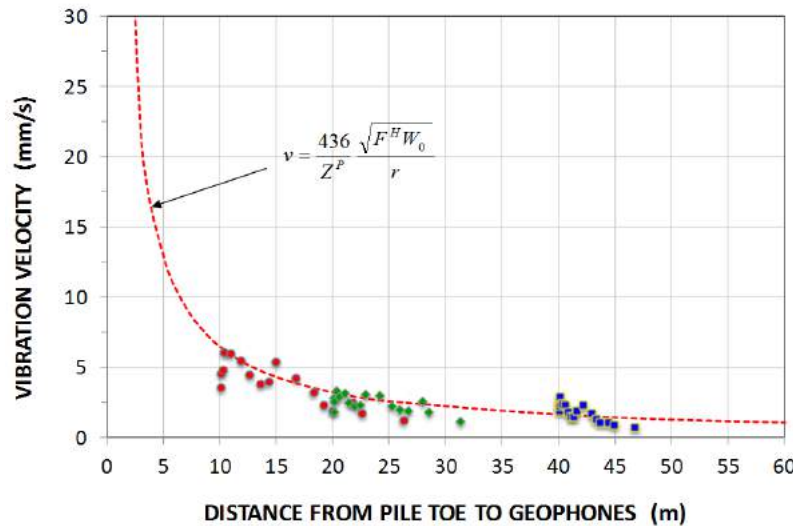


Fig. 9.26 Vibration velocity per Eq. 9.30 plotted with measurements of vibration velocity. (Data from Nilsson 1989, as presented by Massarsch and Fellenius 2014).

Under unfavorable conditions, the installation of piles or sheet piles can cause damage to buildings or other structures on the ground. Frequently, such damage is attributed to vibrations of the structure itself.

In the case of impact pile driving, the frequency content of ground vibrations cannot be controlled by changing the pile driving process. In contrast, during vibratory driving, the pile or sheet pile is rigidly attached to the vibrator, which oscillates vertically at a frequency, which can be chosen and modified by the operator. The operating frequency and amplitude of modern vibrators can be adjusted in order to achieve optimal driving while minimizing environmental impact. However, if a vibrator is operated at or near the resonance frequency of buildings or building elements, strong vibrations can be generated. This effect can be used to increase the efficiency of deep vibratory compaction systems, such as “resonance compaction” (Massarsch and Fellenius 2005).

When a pile penetrates easily into the ground, the intensity of transmitted vibrations will be low. However, vibrations increase when denser soil layers are encountered and pile penetration speed

decreases. Ground vibrations depend thus on the geotechnical conditions which need to be considered in the risk assessment. During the initial phase of pile penetration, the source of vibrations will be located close to the ground surface. However, when the pile penetrates deeper into the ground, the source of vibrations becomes more complex. Vibrations can be emitted from the toe of the pile, but also along the pile shaft. Therefore, geotechnical conditions are of great importance when trying to predict the intensity of ground vibrations and. It is important that the location is known of stiff soil layers, through which the pile shall be driven and which can give rise to strong ground vibrations. Massarsch and Fellenius (2008) present an in-depth discussion of factors influencing ground vibrations due to pile driving.

Building damage due to pile driving vibrations can be caused by settlement in the ground below an adjacent building foundation. The risk of settlement due to ground vibrations exists primarily in loose sand and silt. In other soils, such as soft clays, vibrations can contribute to, but are rarely the main source of settlement.

It is possible to determine critical vibration levels, which are based on the shear strain level generated by ground vibrations. When vibrations pass through material, strain is induced, which can be calculated, if the particle velocity and the wave speed of the pile are known. Soil strain caused by propagation of a compression wave (P-wave) can be determined from Eq. 9.32.

$$(9.32) \quad \varepsilon = \frac{v_p}{c_p}$$

where  $\varepsilon$  = induced strain  
 $v_p$  = particle velocity measured in the direction  
parallel to the wave propagation  
 $c_p$  = wave speed in the direction  
parallel to the wave propagation

Similarly, as shown in Eq. 9.33, the shear strain,  $\gamma$ , can be calculated by dividing the particle velocity measured perpendicularly to the direction of wave propagation with the shear wave speed.

$$(9.33) \quad \gamma = \frac{v_s}{c_s}$$

where  $\gamma$  = shear strain  
 $v_s$  = particle velocity measured in the direction  
perpendicular to the wave propagation  
 $c_s$  = shear-wave speed the direction  
parallel to the wave propagation

Determining shear wave speed is routine part of a CPTU sounding (Chapter 2, Section 2.9).

Shear strain is an important parameter when assessing the risk of settlement in granular soils or disturbance of cohesive soils. A threshold strain level,  $\gamma_t$ , exists below which it is unlikely that any rearrangement of soil particles can occur and, therefore, the vibrations will not generate an increase of pore water pressure in water-saturated sands. At a shear strain smaller than  $\gamma_t \approx 0.001\%$  ( $10 \mu\varepsilon$ ) the risk for settlement is low. When this level is exceeded, the risk of particle rearrangement and, therefore, settlement increases. At a shear strain level of  $\approx 0.010\%$  ( $100 \mu\varepsilon$ ), vibrations can start to cause settlement. Significant risk of settlements exists when the shear strain level exceeds  $\approx 0.100\%$  ( $1,000 \mu\varepsilon$ ).



It is important to note that shear modulus and shear wave speed are affected by shear strain. Massarsch (2004) showed that the shear wave speed decreases with increasing shear strain and that this reduction depends on the fines content (plasticity index) of the soil. The reduction of shear wave speed is more pronounced in gravel and sand than in silt and is even smaller in clay. The effect must be appraised when determining the shear wave speed at a given strain level. Based on Eq. 9.32, and taking into account the reduction in shear wave speed with shear strain level, Massarsch (2002) proposed a simple chart (Figure 9.27) showing the relationship between vibration velocity (particle velocity) and shear wave speed due to ground vibrations for three different levels of shear strain in relation to the risk for settlement in sand.

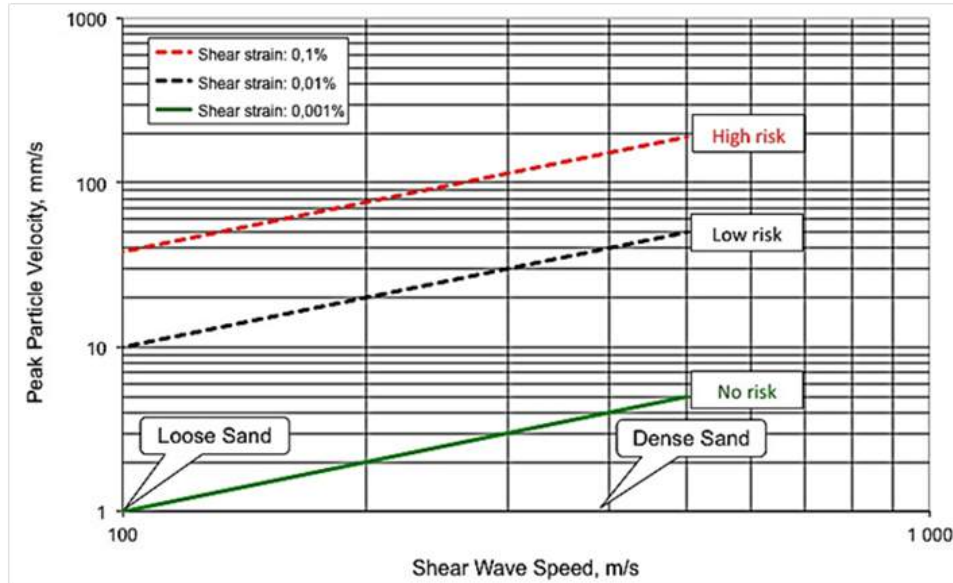


Fig. 9.27 Assessment of settlement risk in sand as function of amplitudes of shear-wave speed, shear strain, and vibration velocity (Massarsch 2008)

### 9.16. Settlement, Compaction, and Densification Caused by Pile Driving Vibrations

The information in this section draws primarily from research and results presented by K.R. Massarsch (Massarsch 2000 and Massarsch and Fellenius 2014).

The magnitude of settlement due to pile driving vibrations depends on several factors, such as soil type and stratification, groundwater conditions (degree of saturation), pile type, and method of pile installation (driving energy). For estimating settlements in a homogeneous sand deposit adjacent to a single pile, Massarsch (2004) proposed the basic procedure, illustrated in Figure 9.28, which shows that the most significant densification due to pile driving occurs within a zone corresponding to three pile diameters around the pile being driven. The volume reduction resulting from ground vibrations will cause significant settlements in a cone with an inclination 2(V):1(H), with its apex at a depth of 6 pile diameters below the pile toe. Thus, the settlement trough will extend a distance of  $3D + L/2$  from the centre of the pile, with maximum settlement at the centre of the pile. Maximum and average settlements, can be estimated using the Eq. 9.34 relationship, for an appropriate value of the soil compression factor,  $\alpha$ .

$$(9.34) \quad s_{\max} = \alpha(D + b); \quad s_{\text{avg}} = \frac{\alpha(D + 6b)}{3}$$

where

$s_{max}$	=	maximum settlement
$\alpha$	=	soil compression factor
$D$	=	pile embedment
$b$	=	pile diameter

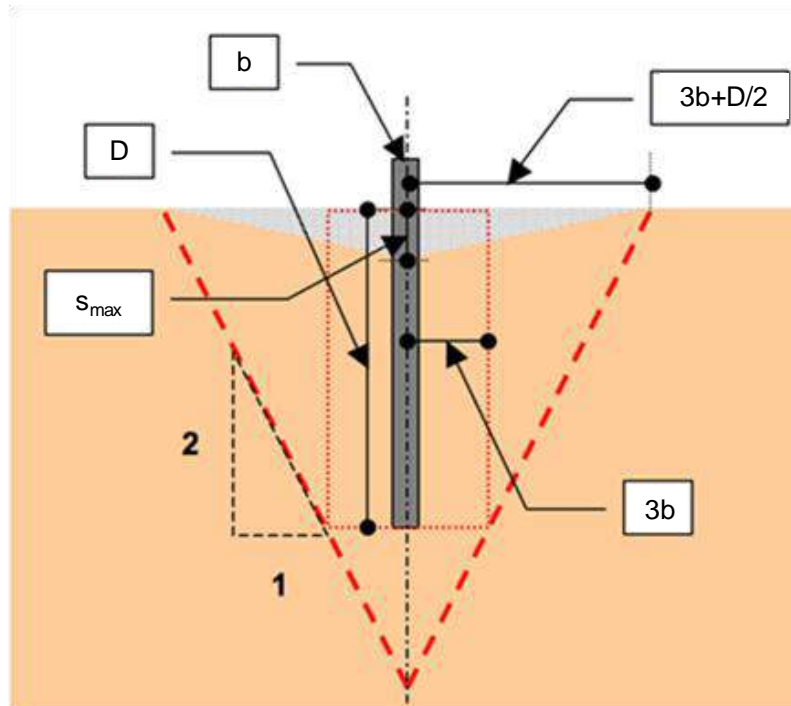


Fig. 9.28 Basic method of estimating settlements adjacent to a single pile in homogeneous sand (after Massarsch 2004)

Table 9.4 shows compression factors applicable to driving in very loose to very dense sand at driving energy ranging from low to high.

**TABLE 9.4** Compression factor,  $\alpha$ , for sand based on soil density and level of driving energy (Massarsch 2004)

Energy: ==>	Low	Average	High
Soil Compactness	- - - Compression factor $\alpha$		
Very loose	0.02	0.03	0.04
Loose	0.01	0.02	0.03
Medium	0.005	0.01	0.02
Dense	0.00	0.005	0.01
Very dense	0.00	0.00	0.005

Assume that a concrete pile with diameter  $b = 300$  mm and an embedment length  $D = 10$  m is installed in a deposit of medium dense sand. The pile is driven using an impact hammer and pile penetration is normal (stiff layers requiring high driving energy are assumed not to be present). The compression value,

$\alpha$ , for medium dense sand and average driving energy according to Table 9.4 is  $\alpha = 0.010$ . According to Eq. 9.33, the maximum settlement adjacent to the pile and the average surface settlement of the cone base are 118 mm and 39 mm, respectively. The radius of the settlement cone of the ground surface footprint is 5.9 m, resulting in an average surface slope of 1:50 (0.118/5.90).

Vibrations from construction activities, such as pile driving, are normally not likely to cause damage to buildings or building elements. Only in the case of very sensitive buildings with poor foundation conditions may settlements be initiated or existing cracking aggravated, e.g., foundations on loose to very loose sand. This aspect is not included in most vibration standards, which were primarily developed for blasting applications.

The Hong Kong Buildings Department has issued a Practice Note, APP-137 “Ground-borne Vibrations and Ground Settlements Arising from Pile Driving and Similar Operations” which provides guidelines on the control of ground-borne vibrations and ground settlements generated from pile driving or similar operations with a view to minimizing possible damage to adjacent properties and streets. This standard is the only one which suggests limiting values with regard to ground settlement and ground distortion. The Hong Kong acceptance limits for settlement is referenced to the vibration velocity as shown in Table 9.5 (quoted from Massarsch and Fellenius 2014).

Table 9.5. Empirical guidelines according to HK Practice

Instrument	Criterion	Alert	Alarm	Action
Ground settlement	Total settlement	12 mm	18 mm	25 mm
Service settlement	Total settlement or angular distortion	12 mm or 1:600	18 mm or 1:450	25 mm or 1:300
Building tilting	Angular distortion	1:1000	1:750	1:500

Ground settlements should be considered on a case-by-case basis with respect to the integrity, stability, and functionality of the affected ground and structures.

Damage to building due to pile driving vibration (in shaking the building structure) is a separate issue outside the purpose of this chapter. For more information, see Massarsch 2002; 2004, 2008.

### 9.17. Vibratory Compaction

The information in this section draws primarily from research and results presented by K.R. Massarsch (Massarsch 1991; 1994; 2002, and Massarsch and Fellenius 2014).

The density of sand placed under water (subaqueous fill) is generally lower than when placed above the ground water (subaerial fill). For a hydraulic fill, the weakest zone is generally located just beneath the water level. The range of densities achievable by hydraulic placement of sand are typically at the boundary between values giving acceptable performance and those resulting in unacceptable performance. In most cases, compaction of sand fill is required to reduce total and differential settlements.

Sand fill can be assumed to be essentially normally consolidated. This important aspect offers the opportunity to assess more accurately the in-situ stress conditions prior to and post compaction, including determining the degree of required compaction.

A variety of sand compaction methods can be used to meet the design requirements. One method, which has found increasing application, is resonance compaction (Massarsch 1991) using a powerful, hydraulic vibrator with variable operating frequency is mounted on top of a purpose-built "compaction probe" as shown in Figure 9.29. The cross-section of the probe has a double-Y shape. An important aspect is that the weight of the probe is significantly reduced by the incorporation of circular openings in the probe walls. The openings also increase the interaction between the oscillating probe and the surrounding soil, that is, the efficiency of the vibration emissions from the compaction probe to the surrounding soil.

The resonance compaction method uses the vibration amplification effect which is created when the operating frequency of the vibrator is adjusted to the resonance frequency of the vibrator-probe-soil system.

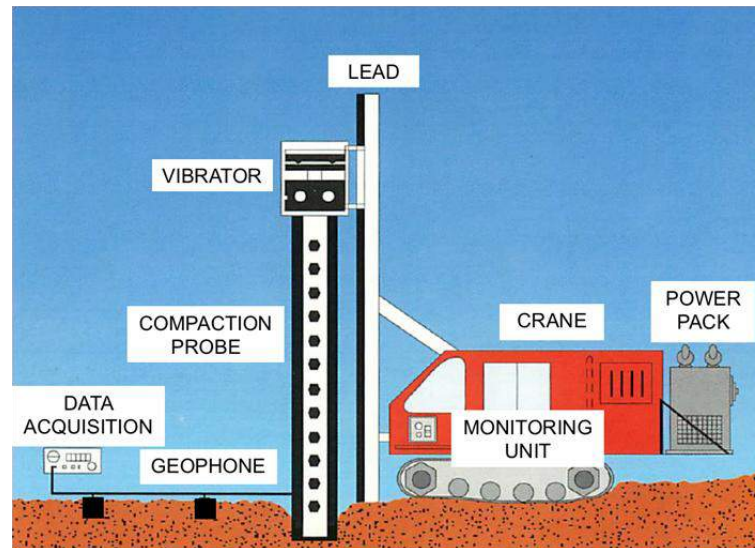


Fig. 9.29. Principles of equipment used for resonance compaction

The cone penetrometer, CPTU, is a very suitable tool for assessing whether or not a soil deposit is compactable by means of resonance compaction. Figure 9.30 shows a delineated of compactable, marginally compactable, and not compactable delineated in two CPTU Eslami-Fellenius classification charts (see Section 2.2) depicting the zones in different axis scales.

When using the resonance compaction unit, geophones measuring vibration velocity are placed on the ground surface, typically at a distance of 4 m from the compaction point. The vibration measurements are fed into a data acquisition system, together with other compaction parameters, such as probe penetration depth, vibrator acceleration, operating frequency, and hydraulic pressure of the vibratory system (power-pack). The system principles have been described by Massarsch and Fellenius (2005).

A fundamental aspect of resonance compaction is the variation of vibrator frequency. In granular soil, when the probe is operated at a high frequency (approximately  $>35$  Hz) substantially higher than the resonance frequency of the vibrator-probe-soil system, surface friction along the compaction probe is effectively reduced and the main resistance originates at the toe of the compaction probe. In loose granular soil, the probe sinks into the ground at high penetration speed and ground vibrations are low. Most of the vibration energy is then dissipated as heat along the probe surface. Thus, the penetration speed of the probe (when excited at high frequency) reflects the soil resistance at the toe of the probe. Provided that the probe penetrates freely and is not held back, the penetration speed can be related to the cone stress measured by the CPT. Or, conversely, the cone stress can be used on a site-specific basis in estimating the efficiency of a forthcoming compaction effort in terms of probe penetration speed.

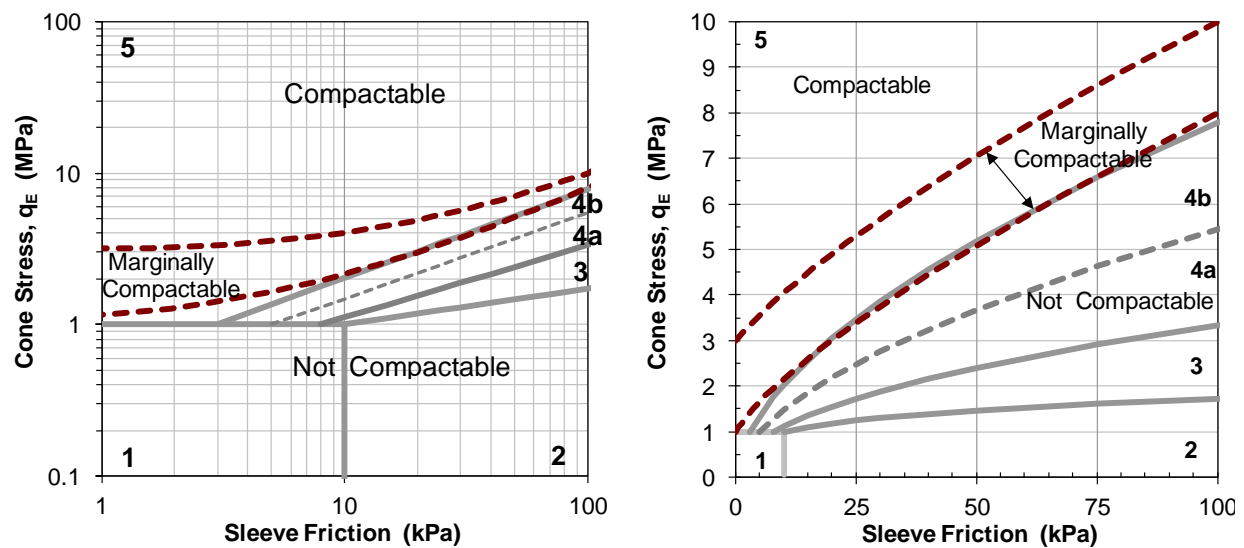


Fig. 9.30 Classification of compactable zone as delineated in an Eslami-Fellenius chart (data from Massarsch and Fellenius 2002)

When the vibrator frequency is gradually reduced, two distinct phenomena can be observed: the probe penetration speed slows down and the intensity of ground vibration increases. When the operating frequency of the vibrator reaches the resonance frequency of the vibrator-probe-soil system, the probe more or less ceases to penetrate; at the same time, ground vibrations reach a maximum. At this stage, the vibrator energy is efficiently transmitted to the soil along the probe surface and vibration compaction is most effective. The energy transfer to the surrounding soil is enhanced by the small dynamic impedance of the probe due to the large openings in the probe wall.

In loose to medium dense, water-saturated granular soil, resonance can cause liquefaction. The probe then oscillates in the liquefied soil (acting as a heavy liquid) and no ground vibrations are transmitted to the soil as little or no friction exists along the probe. As the vibration continues, the excess pore water pressure dissipates, effective stress builds up and friction between the probe surface and the surrounding soil increases again along the probe. The end result is a reduction of the soil volume (compaction), an increase in soil density (modulus) and a permanent densification that can be correlated to a reduced compressibility (Janbu modulus number) and preconsolidation margin.

Settlement is often the critical parameter for assessing the need for and the results of vibratory compaction. Sections 2.10 and 2.20 describe the use of cone penetration test to determine the compressibility before and after compaction. More information is available in Massarsch and Fellenius (2012).

As mentioned (Clause 9.14.1), the vertically oscillating probe induces high horizontal stresses. As a result of the strong, horizontal stress pulses caused by the vertically oscillating probe, permanent horizontal stresses are created in the ground resulting in a permanent preconsolidation effect. It can be assumed that sand fill prior to compaction is normally consolidated. This preconsolidation effect can be estimated from the increase in sleeve friction prior to and after compaction. From the increase in lateral earth stress, the overconsolidation ratio (and preconsolidation margin) can be estimated. The preconsolidation effect needs to be taken into account in the settlement analysis in order to obtain representative results.



## CHAPTER 10

### WORKING STRESS AND LOAD AND RESISTANCE FACTOR DESIGN

#### 10.1 Introduction

Of old, people designed for expected settlement. Full-scale tests were rare. When performed, a loading test usually aimed to reveal information on settlement response to load, rather than the ultimate resistance (capacity) of the tested foundation. The concept of capacity was introduced when, first, Stanton in 1859 and, then, Wellington in 1893 (Chellis 1951) presented the Stanton and Engineering News formulas, respectively, which proposed a ratio between intended load and pile capacity (of driven piles), that is, the factor of safety,  $F_s$ , (Likins et al. 2012). About 1900, a Swedish pioneer Ernst Wendel, published results of full-scale, static loading tests on piles in clay and discussed the  $F_s$ -concept. At that time, however, the response of other foundations, such as footings, was still considered in terms of expected settlement, and there was no theoretical calculation of capacity of footings.

In the 1910s, Wolmar Fellenius completed slope stability analysis to incorporate cohesive and friction strengths simultaneously and brought forward the  $F_s$ -concept as a ratio between induced rotating moment to the rotating moment that would occur in failure of the embankment (see Massarsch and Fellenius 2012). Less known is that he also developed a calculation method for bearing capacity of footings based on the circular/cylindrical rotation analysis employing shear strength friction and cohesion and defining a factor of safety as the ratio between the calculated bearing capacity and the working load applied to the footing (Fellenius 1926). In 1943, Terzaghi presented his bearing capacity theory (the “triple N” formula, Eq. 6.1a) and adopted the same definition of the safety factor. Since then, everybody have used the  $F_s$ -concept. Settlement analysis is these days often not included—many assume that, if the factor of safety is good, settlement will not be of concern for the foundation. A mistaken assumption associated with many structural failures due to excessive foundation movements.

Indeed, settlement is the governing aspect of a foundation design. Note, in contrast to the case of the old days, we do now know how to do a settlement analysis and do not need to continue relying on applying a quasi  $F_s$ -value to a perceived “capacity”. Besides, the bearing capacity theory for footings is totally wrong (Section 6.10). And, while we can determine—by some definition—the bearing capacity of a pile, again, it is the settlement of the pile, or pile group, that governs and that settlement is more due to what occurs around the pile than to the load applied to the pile (see Chapter 7).

With regard to piled foundations, while foundations on single piles or just a few piles need to satisfy a  $F_s$ -criterion, this is not necessarily so for groups of piles. Piled foundations on groups of piles need primarily, and definitely, to be designed for settlement. On occasions, the piles are not even connected to the foundation structure (Section 7.5) and, therefore, pile capacity and  $F_s$  is not an issue, but settlement always is. It is time to return to the design principles of the long past.

Of course, footings can experience a bearing capacity type failure. Figure 10.1 shows a hypothetical case of a footing loaded to the point of a bearing capacity failure illustrated by a slip circle. If the footing is placed on clay and the load,  $Q$ , is brought on in one sudden shot, this is what well could happen. A practical case is loading a silo or a storage tank. However, if the load on a full size footing supporting sustained loads would be placed gradually and concentrically (no tilting) and, if the load is larger than suitable for the conditions, although the foundation settlement will become so large that the structure supported on the footing will fail one way or another, no bearing capacity failure of the footing

foundation will occur. The exception being if the soil is made up of a highly overconsolidated clay that, at first, reacts to the load by reduction of the pore pressure, thus “fooling” the construction to believe that the footing can take more load than it actually can. In time, the pore pressures will return to the original level and the footing will fail. One may call this a case of a “delayed sudden failure”. However, no such case (nor any other) can be realistically analyzed with the “triple N” formula, Eq. 6.1a.

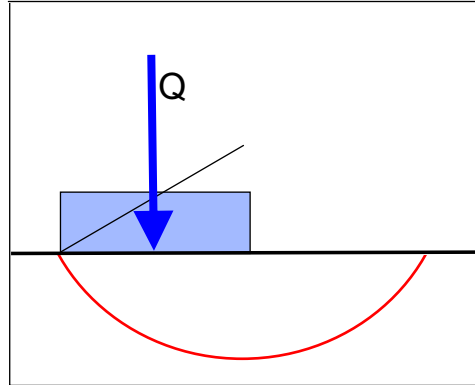


Fig. 10.1 Hypothetical case of bearing capacity failure analysis of a footing

If a footing is loaded by an off-center inclined load, the soil may become overstressed along one side and the settlement will be larger along that side than along the opposing side. The resulting tilt of the structure will move the resultant closer to the side and increase the stress along that side, which will increase the tilt yet again. Eventually, a progressive failure can occur in overturning as the resultant goes beyond the middle third and non-linear and non-constant static stress distribution response develops as the resultant keeps moving toward the edge (Section 6.6). Figure 10.2 shows a hypothetical such case. Assuming that the footing is reinforced concrete, or has other means to resist cracking in two, the stability benefits from the horizontal force,  $R_H$ , a tension force in the footing slab. However, **if the load is from an uneven fill instead**, there is no  $R_H$  helpful force. Instead, the fill will generate a force due to earth stress as indicated by the light shaded triangle in the figure that the sliding resistance may not be able to resist.

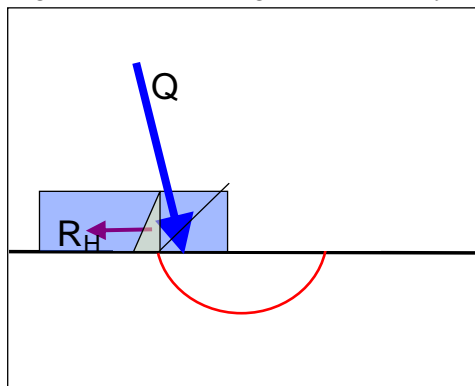


Fig. 10.2 Hypothetical case of bearing capacity failure of a footing with off-center and inclined load

In other words, bearing capacity may be of concern also for footings, and a design will need to address and analyze this. However, not by the triple-N formula and not by looking at an off-center and inclined loading as a case that can be separated from a straightforward the vertical load. In most cases, if a settlement analysis shows that the settlement will be within acceptable limits, “capacity” is more than adequate. If the analysis instead would show that the settlement instead is unacceptably large, would anyone care about what the capacity value could be?



## 10.2 The Factor of Safety

All engineering designs must include a margin of safety against failure. In most geotechnical applications, this margin is achieved by applying a factor of safety defined as the available soil strength divided by the mobilized shear resistance. The available strength is either cohesion ( $c$ ) or friction ( $\tan \phi$ ), or both combined. (Notice that friction is not the friction angle,  $\phi$ , but its tangent,  $\tan \phi$ ). For bearing capacity of footings, the factor of safety is not defined as a ratio between strength and mobilized resistance, but as given by Eq. 10.1.

$$(10.1) \quad F_s = \frac{r_u - q'}{q_{allow}} \quad \text{or, alternatively} \quad F_s = \frac{r_u}{q_{allow}}$$

where

$F_s$	=	factor of safety
$r_u$	=	ultimate unit resistance (unit bearing capacity)
$q'$	=	overburden effective stress at the foundation level
$q_{allow}$	=	the allowable bearing stress (contact stress)

Geotechnical engineering practice is to use the bearing capacity formula and apply a factor of safety of 3.0 to the capacity is based on analysis, i.e., calculations using soil parameters. For footings, there is some confusion whether, in calculating the bearing capacity according to the "triple-N" formula (Eq. 6.1), the relation  $(N_q - 1)$  should be used in lieu of  $N_q$ . Moreover, subtracting the overburden stress,  $q'$ , from  $r_u$  is also in some contention. That is, whether or not the factor of safety should apply to a "net" stress. The Canadian Foundation Engineering Manual (1992) omits the  $q'$  part, that is, uses the second alternative of Eq. 10.1. The difference has little practical importance, however. In coarse-grained soils, for example, the friction angle,  $\phi'$ , normally exceeds a value of  $33^\circ$  and the corresponding  $N_q$ -value exceeds 25, that is, when also considering the effect of  $N_\gamma$ , the "error" is no greater than a percentage point or two. In terms of the effect on the friction angle, the difference amounts to about  $0.2^\circ$ , which is too small to have any practical relevance.

More important, as mentioned, the definition of factor of safety given by Eq. 10.1 is very different from the definition when the factor of safety is applied to the shear strength value in the bearing capacity formula. This is because the ultimate resistance determined by the bearing capacity formula (Eq. 6.1) includes several aspects other than soil shear strength. Particularly so for foundations on soil having a substantial friction component. Depending on the particulars of each case, a value of 3 to 4 for the factor of safety defined by Eq. 10.1 corresponds, very approximately, to a factor of safety on shear strength in the range of 1.5 through 2.0 (Fellenius 1994).

In fact, the bearing capacity formula is wrought with much uncertainty and the factor of safety, be it 3 or 4, applied to a bearing capacity formula is really a "*factor of ignorance*" and does not always ensure an adequate footing foundation. Therefore, in the design of footings, be it in clays or sands, the settlement analysis should be given priority over the bearing capacity calculation.

The ultimate resistance according to the bearing capacity formula (Eq. 6.1), assumes a relatively incompressible subsoil. For footings placed on compressible soils, Vesic (1973; 1975) adjusted the formula by a rigidity factor, which considered soil compressibility resulting in a reduction of the calculated ultimate resistance,  $r_u$ . Where the soil is compressible enough to warrant such adjustment, settlement analysis, not bearing capacity analysis, should be let to govern the limiting (allowable) stress. Notice, it is equally important to consider stability against sliding and to limit the load eccentricity. Either of the three may prove to govern a design.

### 10.3 Development of Limit States and Load and Resistance Factor Designs

The global factor to apply is an empirically determined function of the type of load—dead or live, common or exceptional. Initially, practice was to let those distinctions be taken care of by applying coefficients to the load values. From this basis, starting in Europe some years ago, a full “partial factor of safety approach” has grown, in which each component, load as well as resistance, is assigned its own uncertainty and importance. The design requirement is that the sum of factored resistances must be larger than the sum of factored loads.

The working stress approach to geotechnical design, WSD, consists of establishing the soil strength and determining the allowable shear by dividing the strength with a factor of safety—“global factor of safety approach”. The particular value of the factor of safety to apply depends on the type of foundation problem as guided by experience and ranges from a low of about 1.3 applied to problems of slope stability of embankments to a high of 4 applied to bearing capacity equations for footings, while a factor of safety of about 2 is applied to pile capacity determined in a loading test and 3 to capacity determined by analysis.. As mentioned, the capacity expressed by the bearing capacity equation does not just depend on soil strength values (cohesion and friction), other aspects are also included in the equation.

The partial factor of safety approach combines load factors, which increase the values of the various loads on a structure and its components, with resistance factors, which reduce the ultimate resistance or strength of the resisting components. This design approach is called Ultimate Limit States, ULS, or Load and Resistance Factor Design, LRFD.

Several countries and regions are currently preparing for a forthcoming shift of the foundation design approach from the working stress design, WSD, to a Limit States Design, LSD, or a Load and Resistance Factor Design, LRFD. New limit states codes have been enacted or proposed in Canada, USA, and Europe. Several Far Eastern countries are in a similar process. The Canadian efforts are contained in the Ontario Highway Bridge Design Code (OHBDC 1983; 1994) by the Ministry of Transportation and Communication, Ontario, MTO. A further development of this code to a Canadian National Code was published in 2006 by the Canadian Standards Association, CSA. The US development is led by the Federal Highway Administration, FHWA, and a report has been published by Barker et al. (1991). The American Association of State Highway and Transportation Officials, AASHTO, has a Specification that applies LRFD rules to structural components as well as to the geotechnical design. The European Community, EC, has developed a limit states foundation code, Eurocode 7, which is being accepted as a National Code by all countries of the European Community.

Initially, Canadian geotechnical engineers were rather unwilling to consider changing to a ULS design approach as it applies to soils and foundations. However, in 1983, a committee formed by the Ontario Ministry of Transportation, MTO, produced a limit states design code for foundations of bridges and substructures. The 1983 Code very closely adopted the Danish system of partial factors of safety, where all factors are larger than or equal to unity (loads and other ‘undesirable’ effects are multiplied and resistances and other ‘beneficial’ effects, are divided by the respective factors). However, in the Canadian version, all factors were multipliers larger than unity and the resistance factors were smaller than unity. Because the load factors were essentially already determined (the same values as applied to the superstructure were used), the code committee was left with determining what values to assign to the resistance factors. Notice the importance distinction that these resistance factors were applied to the soil strength, only.

Soil strength in classical soil mechanics is governed by cohesion,  $c$ , and friction,  $\tan \phi$ . After some comparison calculations between the final design according to the WSD and ULS (LRFD) approaches, a

process known as ‘calibration’, the MTO committee adopted the reductions used in the Danish Code of applying resistance factors to cohesion and friction equal to 0.5 and 0.8, respectively. However, the calibration calculations showed considerable differences in the design end product between the ‘old’ and the ‘new’. A ‘fudge’ factor was therefore imposed called “resistance modification factor” to improve the calibration agreement. The idea was that once a calibration was established, the presumed benefits of the ULS approach as opposed to the WSD approach would let the profession advance the state-of-the-art. Such advancement was apparently not considered to be possible within the ‘old’ system. Details of the approach used in the MTO 1983 Code are presented in the 2nd edition of the Canadian Foundation Engineering Manual (CFEM 1985).

Very soon after implementation of the 1983 Code, the industry voiced considerable criticism against the new approach, claiming that designs according to the WSD and the ULS agreed poorly in many projects, in particular for more complicated design situations, such as certain high retaining walls and large pile groups. It is my impression that many in the industry, to overcome the difficulties, continued to design the frequent simple cases according to the WSD method and, thereafter—resorting to a one-to-one calibration—determined what the ULS values shear force parameters should be in the individual cases and reported these as the design values! Hardly a situation inspiring confidence in the new code. The root to the difficulty in establishing a transition from the WSD to the ULS lied in the strict application of fixed values of the strength factors to fit all foundation cases, ignoring the existing practice of adjusting the factor-of-safety to the specific type of foundation problem and method of analysis. It soon became very obvious that the to-all-cases-applicable-one-value-resistance-modification-factor approach was not workable. For the same reason, neither is the partial-factor-of-safety approach (favored in the European code).

In 1988, the Ministry decided to revise the 1983 Code. A foundation code committee reviewed the experience thus far and came to the conclusion that the partial-factor-of-safety approach with fixed values on cohesion and friction should be abandoned. Of course, the Code could not be returned to the WSD approach, nor would this be desirable. Instead, it was decided to apply resistance factors to the ultimate resistance of a foundation rather than to the soil strength and to differentiate between types of foundations and methods of determining the capacity of the foundation. In 1992, it was decided that the MTO Ontario code should be further developed into a National Code on foundations under the auspices of the Canadian Standards Association, CSA, which work resulted in the 2006 National Standard of Canada, Canadian Highway Bridge Design Code, CAN/CSA-S6-06.

The 2006 Code specifies numerous loads and load factors, such as permanent (dead), transient (live), and exceptional loads; making differences between loads due to weight of building materials, earth stress, earth fill, wind, earthquake, collision, stream flow, etc., with consideration given to the effect of various load combinations, and providing minimum and maximum ranges for the load factors. The factors combine and it is not easy to come up with an estimated average factor; the average value for a typical design appears to hover around 1.25 on dead load and 1.40 on live load. The examples of unit weights of the soil backfill material, such as sandy soil, rock fill, and glacial till, are all given with values that assume that they are fully saturated. Because most backfills are drained, and therefore not fully saturated, this is an assumption on the safe side.

Independently of the MTO, a US Committee working on a contract from the US Federal Highway Administration, FHWA, developed a limit states design manual for bridge foundations (Barker et al. 1991) employing the same approach as that used by the MTO second committee. (Because the Eurocode has stayed with the partial factor-of-safety approach, there exists now a fundamental difference between the Eurocode and the Canadian and US approaches).

The Load and Resistance Factor Design as well as the Ultimate Limit states design for footings have one major thing in common with the Working Stress Design of old. All presume that bearing capacity is a reality and that it can be quantified and therefore be assigned a safety factor (partial factor or resistance factor, as the case may be). This is a fallacy, because, while bearing capacity exists as a concept, it does not exist in reality. What matters to a structure is the movement of its foundation and that this movement be no larger than the structure can accept<sup>1</sup>.

Deformation of the structure and its components is determined in an unfactored analysis (all factors are equal to unity)<sup>2</sup> and the resulting values are compared to what reasonably can be accepted without impairing the use of the structure, that is, its serviceability. This design approach is called Serviceability Limit States, SLS. e.g., the Canadian Highway Bridge Design Code, CAN/CSA-S6-06. Indeed, the serviceability approach, i.e., settlement and movement calculations, is the only approach that has a rational base.

Be it working stress or limit state design, the approach with regard to footings is straight-forward. Analytically, the triple N-formula prevails and for 'bearing capacity' little distinction is made between live loads and sustained (permanent, dead) loads (other than in choosing the safety factor or the resistance factor). However, for piled foundations the situation is more complex.

The pile design must distinguish between the design for **bearing capacity** (Eq. 7.3) and design for structural strength. The capacity is determined considering positive shaft resistance developed along the full length of the pile plus full toe resistance. The loads in reference to capacity consist of dead and live load, but no drag force (the drag force does not affect the bearing capacity of the pile; drag force is of structural concern, not geotechnical; see Section 7.17).

If design is based on only theoretical analysis, the usual factor of safety is about 3.0 in working stress design (WSD) and the usually applied resistance factor in limit states design (ULS) is about 0.4. If the analysis is supported by the results of a loading test, static or dynamic, the factor of safety is reduced (or the resistance factor is increased), depending on the level of reliance on and confidence in the capacity value, number of tests, and the particular importance and sensitivity of the structure to foundation deformations.

A static analysis is often considered uncertain enough to warrant a factor-of-safety of 3.0 in determining the safe embedment depth. This depth only too often becomes the installation depth for the design. Yet, the uncertainty can just as well hit the other way and not only hide that much shorter piles will do, the 'designed safe' installation depth may be totally unattainable. Blindly imposing a factor-of-safety is not a safe approach. See also Section 7.13.

Design of foundations should be with a "belt and braces" approach, where the "belt" represents the capacity analysis and the "braces" the settlement analysis. Far too many piled foundation designs omit the settlement analysis. However, when fretting about accidentally dropping one's pants due to a fault in the belt, strengthening the "belt" buckle will not likely make the "braces" redundant.

---

<sup>1</sup> This notwithstanding that in the special case of a footing in clay subjected to rapid loading, bearing capacity failure may occur. The latter is a situation where pore pressure dissipation is an issue and it may affect the design of silos and storage tanks. However, simple bearing capacity analysis of such cases can then not be used to model the soil response because the foundation response to load is complex and a design based on 'simple' bearing capacity calculation is rarely satisfactory.

<sup>2</sup> As prevailing in some codes, the serviceability consist of a capacity reasoning with "resistance" factors other than those applied in an ULS approach. This is a quasi and illogical approach that does not properly address the settlement issue.

## 10.4 Factor of Safety and Resistance Factors for Piled Foundations

The principles of the Unified Design as outlined in Section 7.17 is accepted in several standards and codes, e.g., the Canadian Highway Bridge Design Code, the Australian Piling Standard, the Hong Kong Geo Guidelines, the FHWA Pile Manual, the US Corps of Engineers Manual, to mention a few. However, two major codes, the Eurocode 7 and the AASHTO Specs, deviate considerably from those principles. The two will be discussed in the following.

### 10.4.1 The Eurocode

The Eurocode requirements for piled foundations are best demonstrated by review of two commentaries (guidelines) on the Eurocode 7 (Simpson and Driscoll 1998, Frank et al. 2004) presenting a design example comprised of a 300-mm diameter bored (circular) pile installed to 16.5 m depth through 5 m of soft clay above a thick layer of stiff clay (the two documents use the same example). The unfactored dead load assigned to the pile is 300 kN. Live load is not included.

The example information is summarized in Figure 10.3. The guidelines state that the pile shaft resistances are determined in an effective stress analysis that results in an average unit shaft resistance in the "soft clay" of 20 kPa and in the "stiff clay" of 50 kPa (50 kPa is right at the borderline between firm and stiff consistency). The toe resistance is assumed to be zero. The shaft resistances in the two layers are 94 kN and 543 kN, respectively, combining to a total capacity of 637 kN. A surcharge will be placed over the site, generating consolidation settlement. The specific surcharge stress is not mentioned. Nor is the location of the groundwater table indicated.

Eurocode Guide , Example 7.4 (Bored 0.3 m diameter pile)

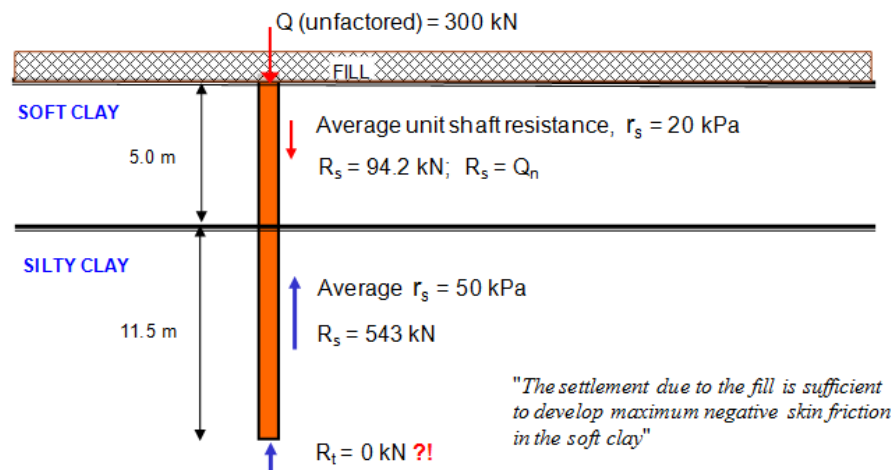


Fig. 10.3 Example 7.4 according to Simpson and Driscoll (1998) and Frank et al. (2004)

A back-calculation for the condition of the guidelines example (for long-term and when full consolidation has developed from the surcharge placed on the ground surface), applying the stated unit shaft resistance values, shows that the surcharge stress is 30 kPa, the groundwater table lies at the ground surface and the pore pressure is hydrostatically distributed with depth, the total density of the soft clay layer is  $1,800 \text{ kg/m}^3$  ( $w_n = 40\%$ ;  $e_0 = 1.09$ ) and  $1,960 \text{ kg/m}^3$  ( $w_n = 28\%$ ;  $e_0 = 0.74$ ) in the stiff clay layer, and the effective stress proportionality coefficient,  $\beta$ , is 0.40 in both clay layers. A beta-coefficient of 0.40 is very large for a soft clay and large for a stiff clay unless it would be a clay till or similar. However, as the stated purpose of the example is to demonstrate the Eurocode handling of negative skin friction, selecting realistic coefficients is not essential to the example.

It is likely that the piles are constructed before the surcharge is placed or before any appreciable consolidation from the surcharge has developed, which represents a short-term condition. Applying the same beta-coefficients, the effective stress calculation show the shaft resistance along the full length of the pile to be 450 kN for the short-term condition.

Checking the conditions for a conventional global factor of safety design, the factor of safety on the stated long-term capacity shows to be 2.1. Conventionally, a factor of safety of 3.0 applies to the design calculations based on theoretical static analysis. Thus, the "design" appears to be short on capacity. Had the 637-kN capacity been determined in a static loading test, the 2.1 factor of safety would have been acceptable in a conventional global factor of safety design. The factor of safety calculated for the short-term condition is 1.5, which by the conventional approach would be inadequate even if the capacity would have been determined in a static loading test!

Checking the conditions for a ULS design according to the Canadian Highway Code, the factored load is  $300 \times 1.25 = 375$  kN and the factored resistance is  $637 \times 0.4 = 255$  kN. Thus, the design is inadequate also in a ULS design.

According to Frank et al. (2004), the Eurocode considers the drag force to be a permanent load acting on the pile much the same way as the load applied to the pile head. Moreover, the assumption is made that the settlement due to the surcharge only causes negative skin friction in the soft clay (94 kN drag force) and no negative skin friction and no settlement develops in the lower layer, the stiff clay—but full positive shaft resistance does develop in that layer. Moreover, the Eurocode disregards the contribution from the shaft resistance in the soft clay layer allowing support only from the 543-kN shaft resistance in the stiff clay layer (as mentioned, the toe resistance is assumed to be zero).

Note that the original distribution of load and drag force combine to a total downward acting load of 394 kN and an upward acting force of 543 kN. That is, an unbalanced force of 147 kN. The pile should be shooting up from the ground!

The Eurocode applies the principles of ultimate limit states, ULS, for analysis of capacity (geotechnical strength), that is, factoring resistances and loads separately, requiring the sum of the factored resistances to be equal to or larger than the sum of the factored loads.

The guidelines apply two approaches to the design of the example pile. According to the Eurocode DA-1, Combination 2, ("normally considered first"), the load and resistance factors applicable to the design calculations for the dead load applied to the pile is 1.00 and the load factor for the drag force is 1.25. The resistance factor on the shaft resistance ("design resistance") is 0.77 (actually, this is the inverse of the partial factor safety, 1.30, that the Eurocode applies to shaft resistance). For the long-term condition, the sum of the factored loads is  $1 \times 300 + 1.25 \times 94 = 417$  kN and the factored resistance is  $0.77 \times 543 = 418$  kN. According to the Eurocode, therefore, the long-term condition is acceptable.

In the alternative approach, the Eurocode DA-1, Combination 1, the load factor for the dead load applied to the pile is 1.35 and the same load factor is applied to the drag force. The resistance factor on the shaft resistance is 1.00. Per the guidelines, the factored load is  $1.35 \times (300 + 94) = 532$  kN, and the factored resistance is  $1.00 \times 543 = 543$  kN. Thus, also for this approach, according to the guidelines, the long-term condition is acceptable.

For the short-term condition, it can be assumed that no drag force would have developed and, therefore, the guidelines would employ shaft resistance acting along the full length of the pile. With no surcharge effect on the effective stress distribution, short-term pile capacity is 450 kN and the short-term factor of safety is only 1.5. According to Eurocode DA-1, Combination 2, the factored load and the factored

resistance are  $1.00 \times 300 = 300$  kN and  $0.77 \times 450 = 347$  kN, respectively. Thus, the Eurocode would find the pile design results acceptable also for the short-term condition. According to Combination 1, the factored load and the factored resistance are  $1.35 \times 300 = 405$  kN and  $1.00 \times 450 = 450$  kN, respectively, again showing the short-term conditions acceptable.

The foregoing is how the design approach is presented in the Simpson and Driscoll (1998) and Frank et al. (2004) commentaries (I have added the aspects of the short-term condition). In my opinion, the Eurocode approach, as presented in the two commentaries, is quite wrong—tending to be on the dangerous side. As mentioned, the guidelines state that negative skin friction only develops in the soft clay and imply that no settlement will develop in the stiff clay. This is hardly realistic. Why would negative skin friction not develop in the stiff clay? Numerous full-scale tests in different soils have shown that fully mobilized shaft shear—in the negative as well as in the positive direction—requires only a very small movement between the pile shaft and the soil. Possibly, the authors of the example had in mind that the settlement in the stiff clay is much smaller than in the soft clay and such small settlement might be of negligible concern for the structure supported on the pile(s), but that is an issue for the settlement of the foundation supported on the pile(s) and not for the development of negative skin friction and drag force. If positive direction shaft shear along the pile can be relied on during the development toward the long-term (ongoing consolidation), then, surely, the same "ability" must be assumed to be available also for the negative direction shaft shear.

In my opinion, typical and reasonable compressibility parameters for the two clay layers would be Janbu virgin modulus numbers,  $m$ , of 15 (optimistically) and 40, respectively, and re-loading modulus numbers,  $m_r$ , of 150 and 400, respectively. The virgin modulus numbers correlate to virgin compression indices,  $C_c$ , of 0.32 and 0.10, respectively (the corresponding void ratios are mentioned above). Moreover, it would be reasonable to assume that both layers are somewhat overconsolidated, and I have assumed preconsolidation margins of 5 kPa and 20 kPa, respectively. These values characterize the soft clay as compressible and the stiff clay as a soil of low compressibility. I also assume that the stiff clay layer is 15 m thick and deposited on a firm layer of minimal compressibility, e.g., a very dense glacial till.

Figure 10.4A shows the condition for the more realistic load distribution for the long-term condition when the consolidation process has developed an equilibrium between the downward acting forces and the upward acting resistances. No toe resistance is indicated because the guidelines state that this is the case for the example.

The calculations of load distributions and settlement for the guidelines example and the modified example are performed using the UniPile program (Goudreault and Fellenius 2013). The analysis follows generally accepted principles of effective stress analysis as detailed in Fellenius (2012).

Fig. 10.4B shows the calculated distribution of the long-term settlement of the soil and the pile. I have assumed that the pile is a single pile for which, then, the load applied to the pile will not cause any appreciable consolidation settlement below the pile toe.

Some pile head movement (settlement) will develop due to load transfer of the 300 kN dead load to the soil during the construction of the structure. It will be limited to the compression of the pile for the imposed axial load and the small load-transfer movement of the pile element nearest the pile toe. It is not included in the 35-mm long-term settlement of the pile, which is due to downdrag, i.e., settlement due to imposed pile toe movement and a small amount from additional compression as the axial load in the pile increases.

The settlement distribution shown in the figure is that assumed developed at 90-% degree of consolidation, say, 30 years after placing the surcharge. Secondary compression would add about 10

to 20 mm of settlement to the 30-year value and then increase slightly with time. I would expect that the settlement after the first about 20 years after construction will be about 80 % of the values shown in the figure.

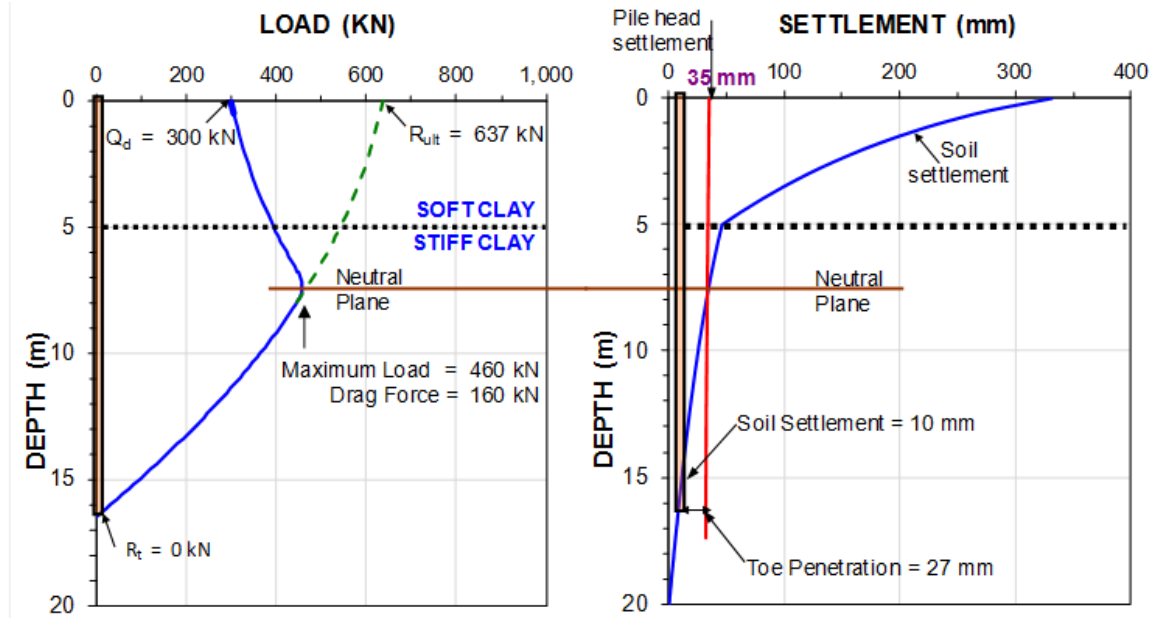


Fig. 10.4A Load distribution

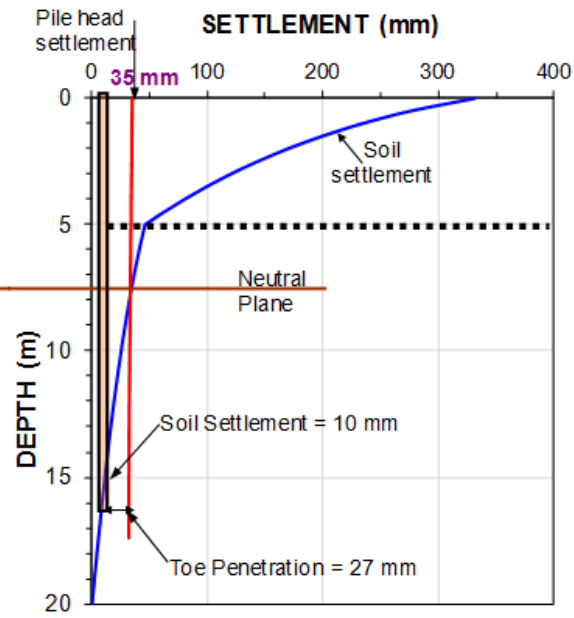


Fig. 10.4B Settlement distribution

In the long-term, the soil settlement will result in negative skin friction along the pile that will accumulate to a drag force. The drag force plus the dead load from the structure supported on the pile will always be in equilibrium with the positive direction forces. Eventually, a stationary force equilibrium will develop at a depth called "neutral plane" ("equilibrium plane" might be the better term). For the guidelines example, as illustrated in Figure 10.4A, the neutral plane will be at a depth of 7.4 m. There is always a transition zone from negative to positive direction of shear along the pile and a small transition zone is indicated by the curved change from increasing load to decreasing. When the soil settlement relative to the pile is large, the height of the transition zone is small, when the settlement is small, the height is large. In the latter case, the drag force is smaller than in the former case. However, the location of the neutral plane is approximately the same, be the settlement small or large.

As indicated in Figure 10.4A, the drag force is 160 kN and the maximum load will be 460 kN. Below the neutral plane, in the what some call the "stable zone" (the soil is no less stable above, however), the accumulated positive shaft resistance is equal to the dead load plus the drag force, i.e., 460 kN—of course, this is what the force equilibrium means. However, the total ultimate shaft resistance is 637 kN, and after subtracting the 160-kN drag force, the remaining shaft resistance, the resistance below the neutral plane, is 477 kN, not 460 kN. The explanation to this discrepancy lies in the assumed transition zone. For example, if the transition zone is longer than the length indicated in Figure 10.4A, the drag force might reduce to, say, 100 kN, and the maximum load would become 400 kN. It would then seem as if the shaft resistance below the neutral plane, because of the equilibrium condition would be 400 kN, significantly smaller than 477 kN. The incongruity is due to comparing two mechanically conflicting conditions: when the pile responds to changing movement—is in flux—and when it is in a stationary condition.

The location of the force-equilibrium neutral plane is always the same as the location of the settlement equilibrium neutral plane, which is where there is no relative movement between the pile and the soil, i.e., where the soil and the pile(s) settle equally. This condition determines the settlement of the pile head after



due consideration of the compression of the pile for the load between the pile head and the neutral plane. As mentioned, when the pile settlement is due to the soil dragging the pile down, it is termed "downdrag".

If one would argue that my assumed values of compressibility of the stiff clay are too conservative, and, quite optimistically, apply values resulting in much smaller consolidation settlement than shown in Figure 10.4B, then, the long-term soil settlement would still be sufficient to mobilize fully the negative skin friction and the positive shaft resistance. Indeed, were the piles to be constructed after the full consolidation had taken place, the distribution of load would still be the same as illustrated in Figure 10.4A, the final state would just take a longer time to develop. The long-term settlement would be small, of course. The transition height would therefore be longer.

Now, were the Eurocode principles applied with the correctly determined distribution of forces along the pile, the analysis would result in a factored load of  $1 \times 300 + 1.25 \times 160 = 500$  kN versus a factored resistance of  $0.77 \times 460 = 354$  kN, and the design would no longer be acceptable according to the Eurocode.

For a real case, it is likely that the stiff clay would provide some toe resistance. For example, if a 100-kN toe resistance would be included in the analysis, I think most would agree that the margin against failure of the pile would have improved. However, improvement would not be recognized in an analysis applying the Eurocode principles, because the location of the neutral plane would have moved down, the drag force would have increased by about 50 kN, and the positive shaft resistance, below the neutral plane would have decreased with the same amount. Despite the increase of capacity, the factored resistance would have become smaller by the amount of  $0.77 \times 50 = 38$  kN, and the increase of drag force would have added  $1.35 \times 50 = 68$  kN to the factored load. In effect, providing toe resistance to the pile would actually have made the Eurocode indicate that the adequacy of the pile design had gone down!

I strongly disagree with the Eurocode design principles. The magnitude of the maximum load in the pile (consisting of the dead load plus the drag force) is only of concern for the axial structural strength of the pile. In contrast, when assessing a design for bearing capacity (geotechnical strength), the drag force must not be lumped in with the load from the structure. The main requirement or premise of design for bearing capacity is the adequacy of the margin against the possibility of the loads applied to the pile could exceed total resistance of the pile, i.e., resistance acting along the entire length of the pile. The safety factors (resistance factors) are chosen to ensure a margin against that possibility. Drag force will develop only when the chosen factors are successful in providing that margin. If the factors are inadequate, the pile will start to fail, and, then, there is no negative skin friction and no drag force—nonetheless, the pile, most undesirably, fails. To avoid this misfortune, a proper design applies margins to the load and resistances. When considering the margin against failure—against the geotechnical response, i.e., capacity—the design must not add-in the drag force, which is a load that *a priori* assumes absence of failure. Indeed, the larger the drag force on a pile, the larger the margin against failure of the pile (provided the axial strength of the pile is not exceeded).

Consider a pile, similar to the guidelines example, installed in a uniform soft soil that is undergoing consolidation and has minimal toe resistance. (Such piles are often called floating piles). Assume further that the shaft resistance is about two to three times larger than the load to be applied to the pile—which would seem to be an adequate design. Eventually, a force equilibrium will develop between the downward direction loads (dead load plus drag force), and the upward direction shaft resistance with a neutral plane located somewhere below the mid-point of the pile. However, applying the Eurocode principles, the factored loads would be larger than the factored resistance. Actually, even if no dead load would be applied, the Eurocode would show that the pile would not even be adequate to support its own drag force. Indeed, when the geotechnical response is correctly analyzed, a mainly shaft bearing pile can never meet the requirements of the Eurocode.

Assume now that the pile would have a significant toe resistance, say, just about equal to the total shaft resistance and the capacity would be doubled to four to six times the applied load. Now, the neutral plane would lie deeper and the provision that all contribution to "bearing" above the neutral plane would be disregarded and instead be applied as load (drag force) would show this pile to be inadequate to support any load according to the Eurocode! In effect, the Eurocode lumping-in the drag force with the loads from the structure in assessing geotechnical pile response is absurd and leads to large unnecessary foundation costs.

I must point out that my criticism is for the Eurocode and not for the authors of the guidelines, who simply report how the code treats the design example, claiming it neither to be right nor wrong.

The guidelines example only includes a permanent load. The Eurocode recognizes that live load and drag force do not act together—a pile element cannot have shaft shear in both the negative and positive directions at the same time. I assume that as long as the factored live load is smaller than the factored drag force, the Eurocode just leaves out live load from the analysis.

As mentioned, the objective of the guidelines example was to illustrate the principles of the Eurocode for analysis of a pile subjected to negative skin friction from settlements of the surrounding soil. It is, however, of interest to compare the settlement for the single pile to that of a group of piles. Let's assume that the example pile is one of a group of 64 piles in circular configuration at a center-to-center spacing of 4 pile diameters with a footprint of 130 m<sup>2</sup>. Because of the large pile spacing, the piles inside the group would not have any appreciably reduced drag force compared to the single pile. (Drag force is limited by the buoyant weight of the soil in between the piles. Therefore, a small spacing means that full drag force is reduced compared to that of the single pile). Moreover, because the piles reinforce the soil, the downdrag (settlement at the neutral plane) is significantly reduced. However, the load (64 x 300 kN) from the structure on the pile group will add stress (about 150 kPa) to the soil below the pile toe level, which will result in consolidation settlement between the pile toe level and the bearing, non-settling layer at 20 m depth. Calculations applying the method (See Chapter 7) show that the pile group will settle close to about 80 mm in the long term.

#### **10.4.2 The AASHTO Specs**

The AASHTO LRFD Specifications (AASHTO 2012) is very similar to Eurocode 7 in regard to principles, although the selection of factors is different. The "Specs" pertain to transportation projects, e.g., bridge foundations. It is the only Limits States geotechnical code in the USA although several guidelines, such as the FHWA Manual (2006), addressing LRFD exist that are by many taken as equal to codes. The AASHTO Code is therefore often also applied to foundations for buildings. For the most common load combination, called Strength Limit I, the AASHTO code applies a load factor of 1.25 to dead load. The load factor for drag force is 1.25. The AASHTO code specifies total stress analysis for piles in "clay", i.e., the  $\alpha$  method with, usually, a constant unit shaft resistance with depth, reserving effective stress analysis, the  $\beta$  method, for piles in "sand". The stated resistance factors for shaft and toe resistance in "clay" are 0.45 and 0.40, and in "sand" 0.55 and 0.50, respectively, as recommended by O'Neill and Reese (1999). The AASHTO code applies the same approach to the drag force as the Eurocode, i.e., the drag force is considered a load similar to the dead load on the pile and no shaft resistance contribution is allowed from the soil above the neutral plane.

According to the AASHTO Specs, a design according to the guidelines example is not acceptable.

The AASHTO code is usually interpreted to require live load and drag force to act simultaneously. That is, the drag force is added to the applied dead load and live load on the pile in assessing the pile for

bearing capacity (the Eurocode does not lump in the live load with the dead load). This notwithstanding that Article 3.11.8 of AASHTO states that *“If transient loads act to reduce the magnitude of downdrag forces and this reduction is considered in the design of the pile or shaft, the reduction shall not exceed that portion of transient load equal to the downdrag force”*. The commentary to this clause does not make the intent of the article more clear in stating that *“Transient loads can act to reduce the downdrag because they cause a downward movement of the pile resulting in a temporary reduction or elimination of the downdrag force. It is conservative to include the transient loads together with the downdrag”*. The latter is not "conservative", combining forces working in opposite directions is irrational and, therefore, including the drag force is simply "wrong".

The AASHTO Specs is now the only US Code that considers the drag force to be a load similar to that from the structure. The two other dominant piled foundation codes in the US, the FHWA (2016) and the Corps of Engineers (Greenfield and Filtz 2009), both recommend the unified method with the main "negative skin friction" issue being downdrag and the drag force is only of concern for the axial pile strength.

### 10.5 Serviceability Limit States

All designs must also consider the Serviceability Limit State, SLS; normally the state that develops in the long-term. It represents the stationary state for which the distance to the neutral plane and the load distribution stay essentially unchanged over time. (In contrast, design for ULS conditions considers the state where soil failure occurs and the pile is in flux—is moving fully mobilizing shaft resistance (along the entire length) and toe resistance).

Note, for the stationary condition—SLS—, the "assumed" values of toe resistance and toe penetration cannot be chosen independently of each other because they are interconnected by their  $q$ - $z$  function. If the toe resistance would be assumed to be zero, this would only be possible if the  $q$ - $z$  relation states that the toe resistance is zero regardless of toe penetration (such as for the guidelines example—a floating pile in soft clay might have next to no toe resistance). Most piles, however, will exhibit a toe resistance that is proportional to the imposed toe movement. The upper limit of toe resistance would be to assume that the neutral plane is at the pile toe level, which would result in a large toe resistance. However, in soils that would require a large toe penetration, as opposed to on bedrock, large toe resistance is not normally possible unless the downdrag is exceedingly large. In fact, for every distribution of settlement and every  $q$ - $z$  relation, there is only one location of the neutral plane and only one value of mobilized toe resistance. That is, three interdependent parameters govern the condition and any two of them determine the third.

The objective of serviceability limit states design, SLS, for a piled foundation is to combine the geotechnical response to the dead load placed on the pile (load distribution) and the settlement distribution around the pile. This will determine the stationary conditions for the pile.

SLS is design for deformation—settlement—of the piled foundation, and it applies neither load factors nor resistance factors. The designer assesses the calculated settlement in relation to the settlement that can be tolerated by the structure. Of course, there has got to be a suitable margin between the calculated settlement and the maximum settlement the foundation can tolerate. This margin is not achieved by imposing a certain ratio between the two settlement values. Instead, in calculations using unfactored loads and resistances and applies realistically chosen values for resistances, a conservative  $q$ - $z$  relation, and conservative values for compressibility parameters, etc., to determine the location of the neutral plane location and the downdrag. The so determined settlement must have a suitable margin to the maximum tolerable for the particular foundation and structure.

The analyses must include a realistic depth to the location of the neutral plane. The upper boundary settlement will then represent sufficiently improbable outcome of the design; "improbable", yes, but still mechanically possible.

## 10.6 Concluding Remarks

The design for geotechnical strength, the ULS condition, addresses a non-stationary failure process—the pile is moving down relative to the soil. By applying a factor of safety, or load and resistance factors to increase load and reduce the resistances, the designer ensures that the design has backed-off sufficiently from the possibility of the ULS condition. The premise is still that the pile would be failing! To include drag force in this scenario is a violation of principles because the pile approaches a failure condition, there is no longer any drag force present. To yet include it, perhaps defended by saying that "in a negative skin friction scenario, it is good to have some extra margin", is nothing other than design by ignorance. Why not instead boost the load factors and reduce the resistance factors? That would at least aim the ignorance toward the correct target.

The fact is that the phenomenon of negative skin friction, NSF, resulting in drag force plus dead load in balance with positive direction forces occurs for every pile—eventually. In ultimate limit states, ULS design, whether the settlement is small or large, the NSF issue is limited to checking the adequacy of the pile axial strength, which could be a deciding factor for sites where the depth to the neutral plane is more than about 80 to 100 times the pile diameter. Design of single piles and small pile groups must include assessing the expected settlement of the soil surrounding the pile and the downdrag of the pile, i.e., the settlement of the soil—and the pile—at the neutral plane in serviceability limit states, SLS. Indeed, for serviceability design, be the pile long or short, therefore, the issue is the downdrag, not the drag force. For pile groups, the settlement of the soil layers below the pile toe levels may show to be critical.

Addressing the ULS design for a NSF issue is not modeled by adding the drag force to the load from the structure. If a calculations model does not relate the depth to the neutral plane to a pertinent force equilibrium, the model would have little relevance to the actual conditions. Moreover, the tendency for many is to assume that the drag force only develops in soil that settles significantly in relation to the pile—a limit of 10 mm is often mentioned. Thus, the analysis returns a drag force conveniently small and of little bearing (pun intended) on the design calculations. In reality, long, mainly toe-bearing piles, even in soil exhibiting settlement much smaller than 10 mm, will be subjected to large drag force (which is only of concern for the axial strength of the pile). When the correct drag force and location of the neutral plane are applied, adding the drag force to the loads from the structure will result in a mechanically impossible design.

The serviceability, SLS, design must be based on a settlement analysis incorporating the pile (or piles or pile group) response to unfactored loads and unfactored responses of primarily the pile toe and the settlement of the soils as affected by the stress changes at the pile location. For a margin to represent uncertainty, the design can apply a pessimistic approach to compressibility of the soil used in the settlement analysis and the estimate of the stiffness response of the pile toe.

There is a large lack of consistency in our practice for determining what really is the capacity of the pile. Yet, the practice seems to treat capacity as an assured number, proceeding to specify decimals for the various factors with no respect to how capacity was determined, the extent of the soils investigation, the number of static tests, the risks involved (i.e., the consequence of being wrong), the change with time, etc. Most codes do either not address settlement of piled foundations or address them only very cursorily. The practice seems to assume that if the capacity has "plenty of FOS", or similar, the settlement issue is taken care of. This is far from the truth. I personally know of several projects where capacity was more than

adequate with regard to geotechnical strength—the literature includes several additional cases—yet, the foundations suffered such severe distress that the structures had to be demolished.

A major weakness of most codes is that they refer to a "capacity" without properly defining what the capacity is, or not defining it by an acceptable method.

The movements measured in a static test are from 'elastic' compression of the pile (shortening), from build-up of shaft resistance that may exhibit an ultimate—plastic—response, but more often a response that is either post-peak-softening or a strain-hardening, and from pile toe movement increasing as a function of the pile toe stiffness. There is no ultimate resistance for a pile toe! Indeed, the search for a pile capacity definition is charged with modeling the response to load by an elastic-plastic condition, when two of the three components definitely do not exhibit anything remotely like an elastic-plastic response and the third only rarely so.

As if the difficulty in choosing a suitable definition of capacity by itself would not cause enough uncertainty for applying the ULS code requirements, the practice employs a variety of definitions ranging from the Offset limit to the Chin-Kondner extrapolation (Sections 8.2 through 8.8). Basing a design on geotechnical strength—the capacity—be it by theoretical analysis or interpretation of results from a static loading test, is fraught with large uncertainty, hardly covered by the relatively small range of suggested factors of safety or resistance factors.

In answer to the requirement of the ULS condition, I prefer to recognize that what the structure supported on the piles is concerned with is the actual movement or settlement of the of the pile head, which is governed by the movement of the pile toe and soil settlement at the pile toe level, not by the shape of the load-movement curve or a value based on a pile diameter. The analyses leading up to assessing the SLS condition is the key to a successful design. Or more simply put: a large factor of safety does not ensure that the settlements will be small. However, an SLS analysis showing the settlements to be small does ensure that the capacity of the pile(s) is adequate. I am not suggesting we cease carrying out a ULS analysis, but we definitely need to improve how we do it and we need to pay more attention to the SLS.

If the Eurocode and AASHTO Specs would be combined with correct understanding of the short -term and long-term response of piled foundations, it would quickly be realized that the two codes are very wrong. Unfortunately, as they are usually applied without that understanding, they are the cause of large extra foundation costs and, yet, do not provide safe foundations. It is most urgent that the two codes be revised.

To repeat, the geotechnical designer could do well to recognize that, regardless of magnitude of safety factor and or load and resistance factors, a design based on capacity is a rather inadequate approach. Whether or not the foundation response is acceptable to a structure depends on deformation and settlement. The design should therefore foremost concentrate on establishing settlement. If settlement is not acceptable, capacity is not an issue. On the other hand, an acceptable safety against a calculated capacity does not guarantee that a foundation will not settle excessively.



# CHAPTER 11

## SLOPE STABILITY

### 11.1 Introduction

Wherever the ground is sloping, shear forces are induced that tend to cause soil movements. The movements can be large and, in the extreme, sudden. We then talk about slope failure and slope instability. The effect of water in the process is very important, in particular, when the water pressure changes or seepage is introduced.

Early on, analysis of slope stability was made assuming interaction of soil bodies delineated by plane surface boundaries. For example, the sliding of a wedge of soil at a river bank sketched in Figure 11.1, which can be analyzed—optimized—considering the force vectors involved for different wedge sizes. Or, similarly, the retained slope in Figure 11.2, showing earth stress acting against a retaining wall, which alternatively is analyzed using Coulomb-Rankine principles of earth stress. The force vectors shown in the figures are generated by the downward movement of the wedges. Failure occurs for the river bank when the movement has mobilized a shear resistance,  $\tau$ , equal to the soil shear strength. For the wall, the shear force along the sloping shear plane governs the force,  $P$ , which can be of a magnitude that the retaining wall can accept without 'failure' (i.e., being pushed outward); the shear resistance,  $\tau$ , can then be smaller than or be at the strength limit.

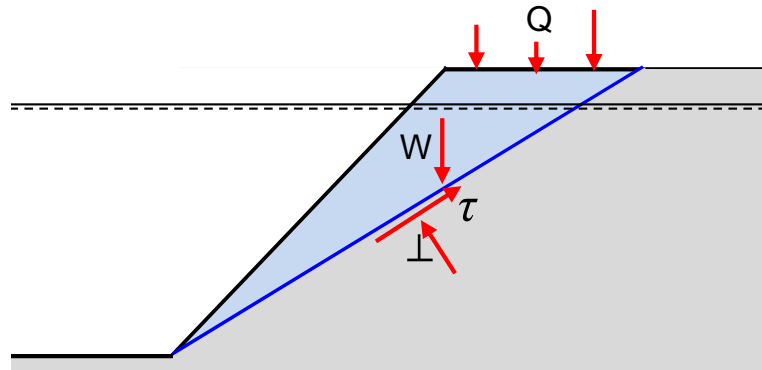


Fig. 11.1 A sliding soil wedge at a river bank held fast by shear resistance,  $\tau$ , along a failure plane

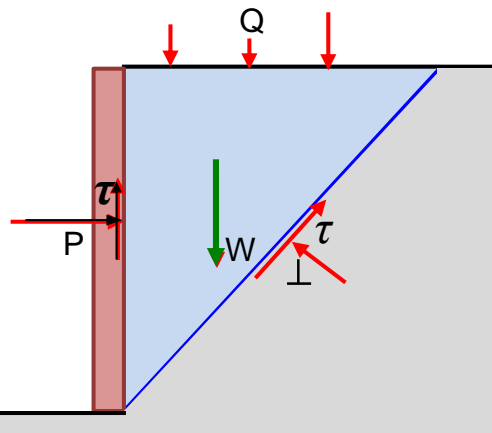


Fig. 11.2 Earth Stress; a sliding soil wedge retained by a wall

As the 1800s turned into the 1900s, industrial development and railway construction in Sweden necessitated extending the harbor of the Western Swedish city of Gothenburg (Göteborg). In 1905, the Harbor authorities established a design and construction department headed by W. Fellenius. In the years following, several large docks that could accommodate deep-draught ships were constructed. Amongst them, the Stigberg Quay (Stigbergskajen). In March 1916, this dock failed. The dock, a reinforced concrete structure on relatively short wood piles, a new approach at the time, had been constructed along the shoreline over a thick deposit of marine postglacial, soft clay. The design had been made applying slope stability analysis using friction along plane slip surfaces, which was the common method in these days. However, K. Petterson, an engineer and T. Hultin, chief engineer at the Harbor design and construction department, noticed that the failure surface was not plane but curved. Petterson and Hultin subsequently back-calculated the slide employing circular failure surfaces, still assuming the soil resistance to be friction,  $\tan \phi$ , and this method was used in the design of the replacement dock (Bjerrum and Flodin 1960).

W. Fellenius (1918; 1926; 1927; 1936) advanced the slip-circle method to include cohesion in combination with friction and developed analytical methods for the calculations—the Method of Slices—as well as nomograms and charts to simplify the rather elaborate and time-consuming effort necessary to establish the most dangerous slip circle—called "the probable" in a back-analysis of an actual slope failure—representing a cross section through a soil cylinder body. He also initiated the definition of factor of safety as the ratio of resisting rotational moment of the forces to the forcing (overturning) rotational moment of forces, the "total factor of safety" for the design analysis of slopes.

The Swedish Geotechnical Commission (1922) established methods for determining the shear strength of cohesive soil, which made it possible for the profession to apply the slip-circle method in design employing shear strength values determined on soil samples in a  $\phi = 0^\circ$  approach. Fellenius (1929) also developed the slip-circle method for "bearing capacity" design of footings and vertical loads on horizontal ground, applying the mentioned definition of factor of safety, and applied the Friction Circle method for determining the earth stress on a retaining wall.

Fig. 11.3 shows the basic principle of the method-of-slices. The sliding soil body is split up into vertical slices and the forces on each slice are determined from the soil input available to determine for each slice its increments of resisting and overturning rotational moments. Note, the angle  $\phi'$  is the angle of rotation of the tangentially and perpendicularly oriented forces acting against the surface of the arc at the bottom of the slice. That angle cannot be larger than the internal friction angle of the soil. The angle  $\alpha$  is the angle between the arc at the bottom of the slice to the horizontal. By leaving out the influence of horizontal slice forces, the analysis is statically determinate. The factor of safety,  $F_s$ , for the analyzed circle is the ratio of the sum of  $M_{\text{RESISTING}}$  to the sum of  $M_{\text{OVERTURNING}}$  as shown in Eq. 11.1.

$$(11.1) \quad F_s = \frac{M_{\text{RESISTING}}}{M_{\text{OVERTURNING}}}$$

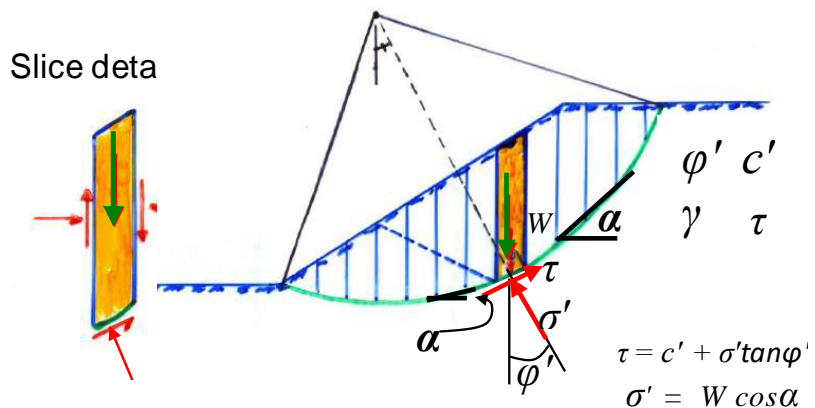


Fig. 11.3 The basic principle of the Method of Slices



Later research, e.g., Bishop 1955, developed slip-circle methods that included slice-forces interaction ("interslice forces") and showed that such analysis usually produced  $F_s$ -values that are a few percentage points smaller than the "Swedish slip-circle analysis".

Figure 11.4 shows the  $c$ '- $\phi$ ' circle used by W. Fellenius (1926) in analyzing the Stigberg Quay failure. The text is in Swedish, the same figure was used with German text in 1927 (Fellenius 1927). The circle marked "FK" is stated to be "Most dangerous (i.e., critical) slip circle calculated applying cohesion and friction through Point D" (the land-side start of the failure zone)". The "friction circle" is explained in Section 11.3

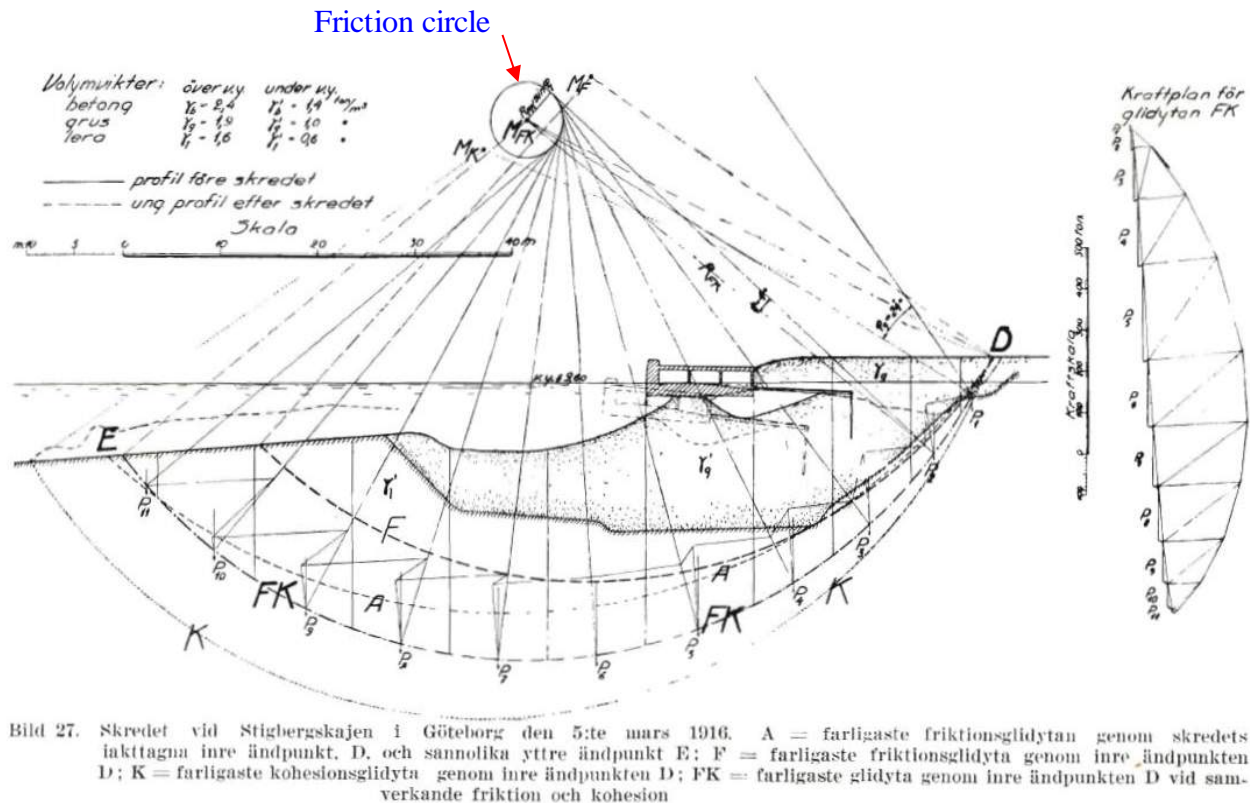


Figure 11.4 Original slip circle for one section of the Stigberg Quay (W. Fellenius 1926; 1927)

W. Fellenius (1926; 1927) applied the slip circle analysis for determining earth stress as an alternative to the usual Coulomb method. Figure 11.5 is copied from the report and shows an example of earth stress (load/length of wall) calculation applying the friction circle for  $c$ '- $\phi$ ' conditions in a graphic force-vector method. The "E" indicates the total earth-load against the wall (per metre length of wall).

To perform a slip circle analysis according to the methods of slices, the rotating cylinder is divided in a number of vertical slices. However, for simple geometries, uniform soil conditions, and when interslice forces can be disregarded, delineating the slope body into distinct parts, "slices", each providing forces and/or resistances, can be simplified, as illustrated in Fig. 11.6. As mentioned, the disregard of the interslice forces usually results in a safety factor,  $F_s$ , that is slightly larger than that resulting from the calculation that includes these forces, i.e., disregarding the slice forces means "erring" on the safe side.

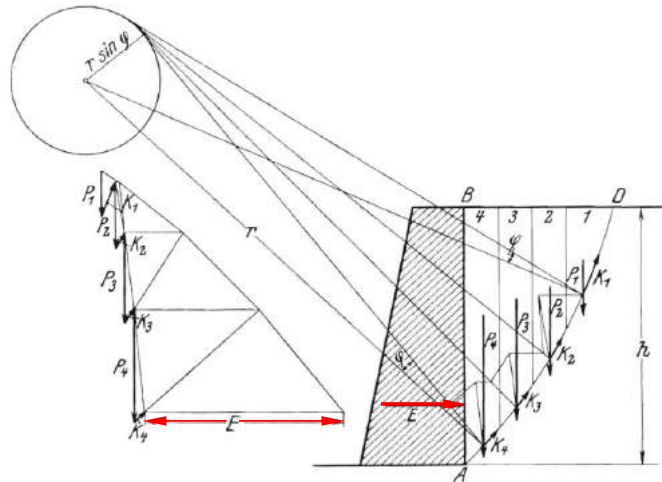


Figure 11.5 The method of slices applied to the calculation of earth stress against a wall (W. Fellenius 1926; 1927)

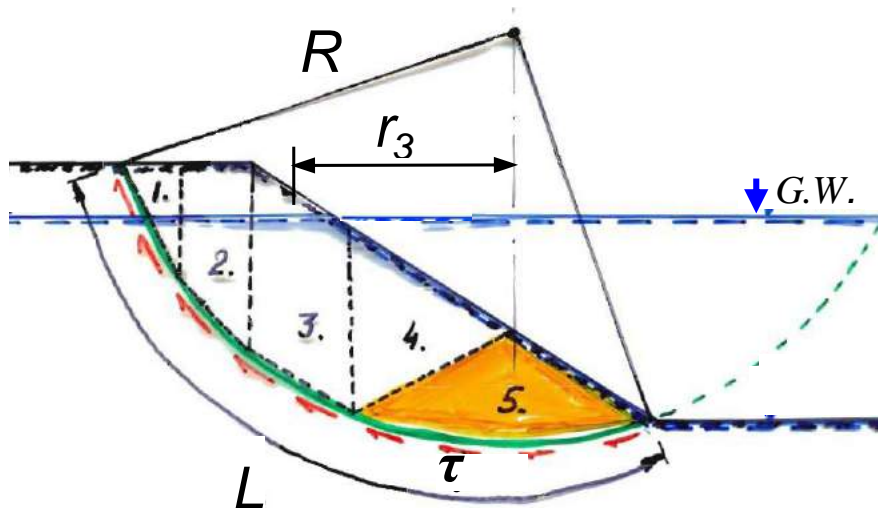


Figure 11.6 Simplified delineation of the "slices" for  $\phi=0$  and disregarding interslice forces

## 11.2 Example of Slip Circle Analysis

Figure 11.7 shows a cross section of a canal dug in a homogeneous clay layer having a total density of  $1,700 \text{ kg/m}^3$  and an undrained shear strength,  $\tau$ , of  $20 \text{ kPa}$ . The water level in the canal and the groundwater table in the clay is at Elev.  $+9.0 \text{ m}$ . The clay is fissured above Elev.  $+9.0 \text{ m}$  and a  $10\text{-kPa}$  uniform load acts on the horizontal ground surface along the canal. A potential slip circle is indicated, representing a cross section through a cylindrical soil body along the canal.

- Use total stress parameters to calculate the factor of safety of the canal slope for the indicated slip circle in a  $\phi = 0$  analysis.
- How would the factor of safety be affected if the water level in the canal is increased or lowered?
- The indicated toe circle is not the one with the lowest factor of safety. Search out the most critical circle.

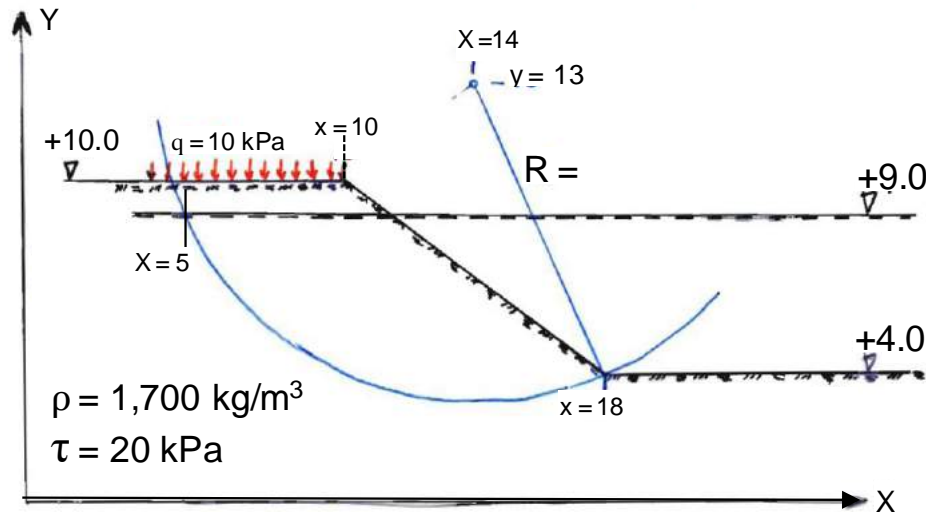


Figure 11.7 Example of  $\phi=0$  stability calculation for a canal dug in clay

Figure 11.8 shows a simple division into parts, Areas #1 through #6, active in the overturning moment. Area #7 has no lever arm for the rotation and Area #8 is too small to have any effect.

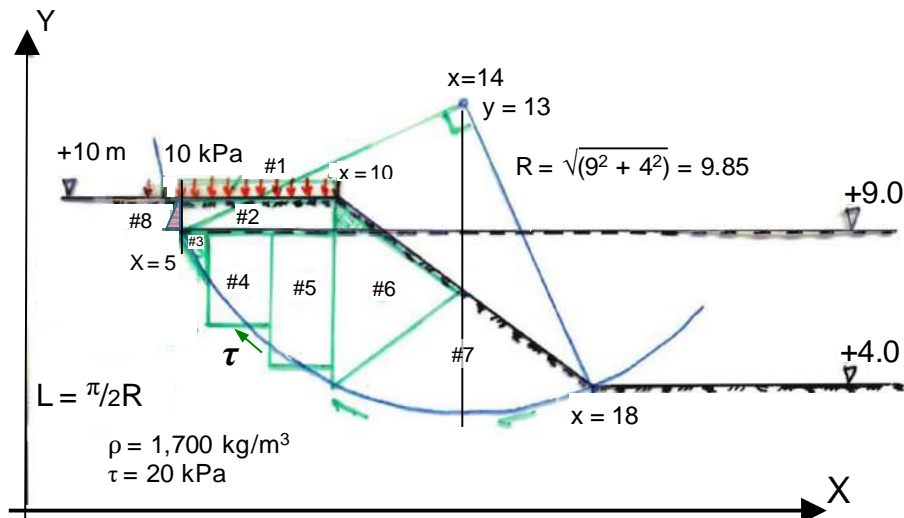


Figure 11.8 Division in Areas #1 through #8 (all distances are in metre)

The rotation moments are simply calculated as the areas times unit weight times lever arm, as follows.

#### Water level at Elev. +9.0 m

1.	$5.0 \times 10(5/2 + 4)$	=	325		
2.	$5.0 \times 1 \times 17(5/2 + 4)$	=	553		
3.	$0.5 \times 1 \times 1.5 \times 7(1/3 + 4 + 4)$	=	44		
4.	$2 \times 3 \times 7(1 + 2 + 4)$	=	294	$\Sigma M_{\text{Forcing}}$	= 1,720 kNm/m
5.	$2 \times 4 \times 7(1 + 4)$	=	280	$M_{\text{Resisting}} = \tau L R = \tau (\pi/2) R^2$	= 3,047 kNm/m
6.	$0.5 \times 4 \times 6 \times 7(2/3 \times 4)$	=	224	$F_s = 3,047/1,720$	= 1.77
7.	balances out	=	0		

What is the  $F_s$  for a sudden drop of GW to Elev. 4.0 m? First, the unit weight to use in the calculations would be  $17 \text{ kN/m}^3$ , throughout, which would result in  $M_{\text{Forcing}}$  increasing to  $2,923 \text{ kNm/m}$ , and  $F_s$  reducing to 1.04. The "sudden" lowering would also remove the balancing water pressure in the canal, but the water pressure in the soil along the slip surface (circle arc) would remain, however, which would add a horizontal force and create an overturning moment of about  $1,000 \text{ kNm/m}$ . (The lowering would constitute a condition called "rapid drawdown"). The canal slope would fail even before the water level had dropped to Elev.+4.0 m.

Because of the fissures in the uppermost 1.0 m thick layer, no benefit of shear resistance is considered in this zone. Instead, a vertical fissure in the crust can be assumed to exist rising up right at the spot where the circle cuts the 1.0-m depth. This defines the width of the fill and size of uppermost soil areas, Areas #1 and #2, active as forcing load (it also defines the "fortuitous" 90-degree angle of the slip circle). Area #2 lies above the groundwater table and its weight is calculated using the total unit weight of the clay. For Areas, #3 through #6, the buoyant unit weight is used. For Area #6, the fact that a small triangular part of Area 6 actually lies above the water table is neglected.

The fissure delineating Area #2 could be filled with water and the pore pressure would then result in a horizontal overturning force, as indicated by Area #8. Indeed, the fissure could even be closed, which would result in an extension of the slip circle through the upper 1.0-m layer and require adding the net effect of the shear resistance along the circle extension and the overturning force from the soil stress and the surcharge. For the example case, this has minimal effect and is simply disregarded in the analysis. However, disregarding the effect of a surficial layer, typically embankment fill, on a soft ground is often not advisable. For example, Figure 11.9 shows a case of an embankment on soft ground with a  $\phi=0$  circle through the soft ground and the slip surface continuing as a plane surface through the  $\phi>0$  embankment. The rotational moment from the embankment is simply calculated as active earth stress (plus water pressure when appropriate) acting against the vertical from the bottom of the embankment.

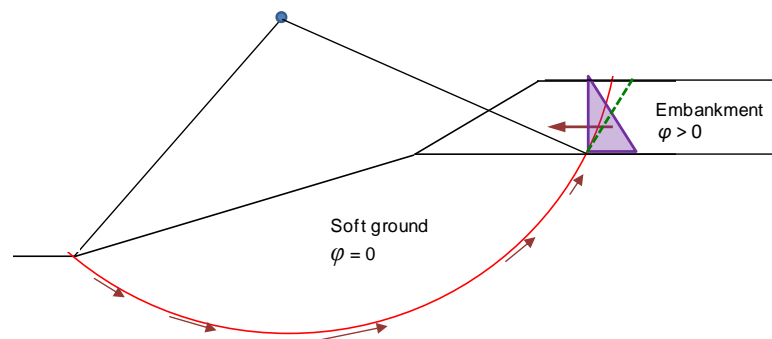


Figure 11.9 Combining a slip circle through  $\phi = 0$  soil with a plane surface through  $\phi > 0$  soil

### 11.3 The Friction Circle — $c = 0$ and $\phi > 0$ Analysis

When a soil body, e.g., a cylinder of soil, rotates and its surface slides against another soil body, the movement causes the perpendicular stress against the boundary surface to rotate around the contact point. The maximum angle of the latter rotation is equal to the soil friction angle,  $\phi$ . For a uniform soil and a constant friction angle, all stresses will be tangent to a circle concentric to the slip circle and with the radius equal to  $\sin \phi$  times the circle radius,  $R$  (W. Fellenius 1926; 1927, Taylor 1948). The resultant to all the stresses is vertical and lies at a distance from the slip circle center equal to  $KR \sin \phi$ , where "K" depends on the central angle of the circle and the distribution of the stresses against the circle arc. Taylor (1948) indicated that for most cases "K" is rather small, about 1.05. Figure 11.10 illustrates the principle of the Friction Circle.

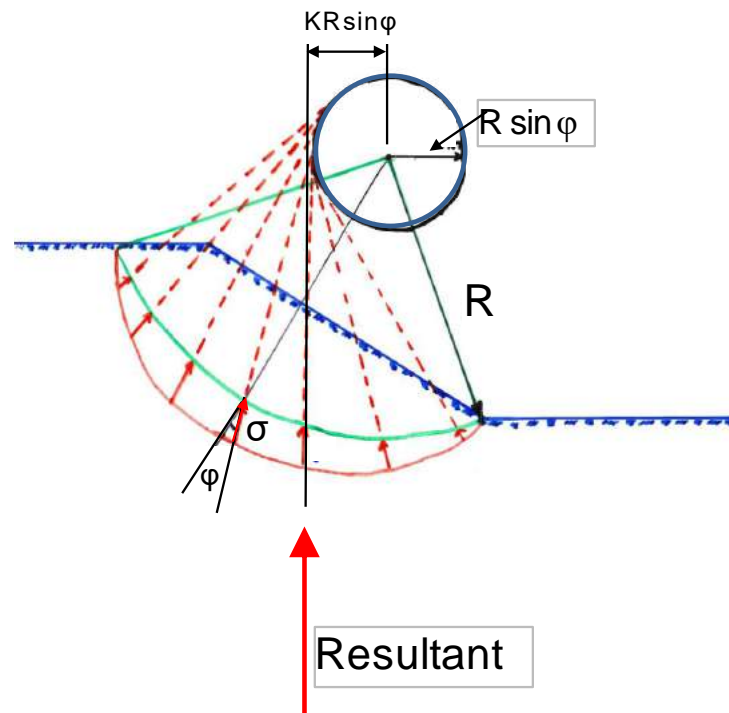


Figure 11.10 The Friction Circle

**Example** Figure 11.11 shows a slope in a coarse-grained formation with a strip footing placed at the crest of the slope. The footing stress is 100 kPa. The water table is located well below the lowest point of the circle. Determine the factor of safety of the slope and footing system.

Q:	$100 \times 4$	=	400	$M_Q$	=	3,600 kNm/m
$W_1$ :	$20 \times \frac{1}{2} \times 8 \times 10$	=	800	$M_{W1}$	=	6,100 kNm/m
$W_2$ :	$20 \times \frac{1}{2} \times 10 \times 10$	=	1,000	$M_{W2}$	=	1,700 kNm/m
$W_3$ :	$20 \times 10 \times 1$	=	200	$M_{W3}$	=	0 kNm/m
$\Sigma$		=	2,400 kN/m	$\Sigma$	=	11,400 kNm/m

The resultant's lever arm is  $11,400/2,400 = 4.75$  m  $= KR \sin \phi_{\text{mobilized}}$

$$\phi_{\text{mobilized}} = \sin^{-1}(4.75/(1.05 \times 11)) = 24^\circ$$

Factor of safety,  $F_s = \tan \phi' / \tan \phi_{\text{mobilized}} = 0.577 / 0.451 = 1.28$

A factor of safety of 1.3 is usually accepted value in a slope stability analysis. However, before it is accepted, it must be verified that another location of the circle center does not produce a smaller value.

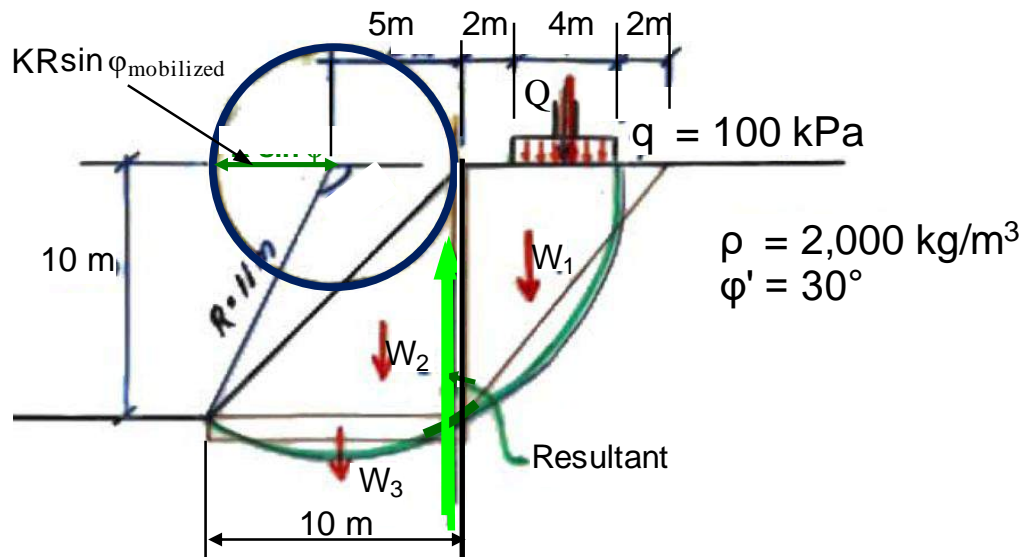


Figure 11.11 A slope in coarse-grained soil with a footing load at the crest of the slope

#### 11.4 Logarithmic Spiral — $c = 0$ and $\phi > 0$ Analysis

The logarithmic spiral is a curve for which the radius ("vector radius"),  $r$ , increases continuously and the normal in any point of the spiral has a constant angle,  $\phi$ , to the radius at that point. The equation for the spiral radius is given in Eq. 11.2 and is a function of a conveniently chosen "zero" radius,  $r_0$ , and the angle of rotation variable,  $\alpha$ , measured between  $r_0$  and  $r$ , and of  $\phi$ . Figure 11.12 shows a logarithmic spiral cutting the toe and the crest of a slope at the outside of a footing placed on the crest. If the resultant to all forces, i.e., to  $Q$ ,  $W_1$ , and  $W_2$ , goes through the center of the spiral, then, the resistance and forcing rotational moments are equal and the value of  $\phi$  in the spiral equation is the friction angle mobilized for the slope condition. The factor of safety is  $\tan \phi_{\text{spiral}} / \tan \phi_{\text{soil strength}}$ .

$$(11.2) \quad r = r_0 e^{\alpha \tan \phi}$$

where

- $r$  = radius in any point
- $r_0$  = radius at the starting point
- $\alpha$  = angle of rotation from  $r_0$  through  $r$
- $\phi$  = angle between the normal and the radius at any point; a constant

Slope stability analysis by the logarithmic spiral is time-consuming if pursued by hand. However, it is not difficult to prepare a spreadsheet-type computer calculation. Enter first the slope configuration into an  $x$   $y$  diagram, then, choose the coordinates for the spiral center and let the spreadsheet calculate the radial distances to the slope toe and one other point at the crest through which the spiral is thought to go. This will determine the  $r_0$ -distance (assumed to be horizontal line pointing to the left of the center as shown in Figure 11.12). Every and all input of  $\phi$ , will show a spiral going through the slope toe and chosen crest point. The spreadsheet can be written to calculate the weights to the left and the right of the spiral center and to determine the  $x$ -coordinate of the resultant. There will be one  $\phi$ -value for which this coordinate is close to the  $x$ -coordinate of the spiral center. Repeating the process for another spiral center location will give a new such  $\phi$ -value. In an iterative process, the location of the center that results in the lowest  $\phi$ -value represents the end result, the  $\phi_{\text{spiral}}$  for the case, and, as before,  $\tan \phi_{\text{spiral}} / \tan \phi_{\text{soil}}$  is the factor of safety.



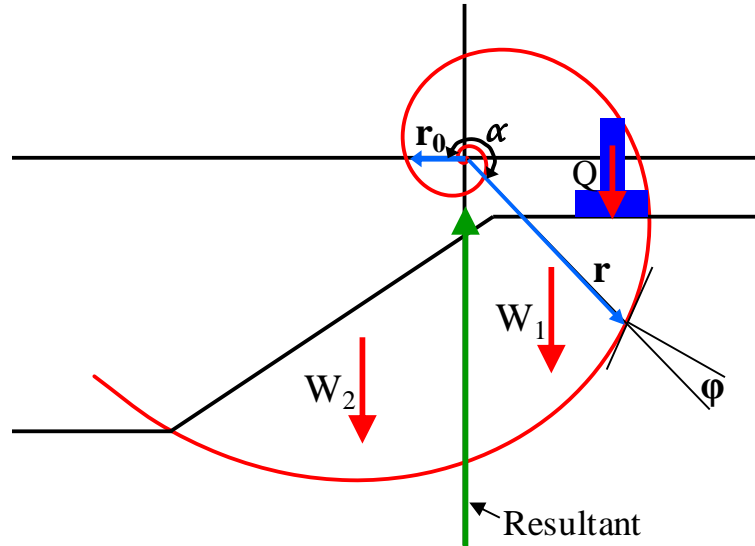


Figure 11.12 A logarithmic spiral fitted to a slope with a footing load on the crest level.

The length,  $s$ , of the arc of a spiral from  $r_0$  through  $r$  is given in Eq. 11.3, i.e., the length of the spiral for the angle of rotation,  $\alpha$ .

$$(11.3) \quad s = r_0 \frac{e^{\alpha \tan \phi} - 1}{\sin \phi}$$

where  $s$  = length of arc from  $r_0$  through  $r$   
 $\alpha$  = angle of rotation from  $r_0$  through  $r$   
 $\phi$  = angle between the normal and the radius at any point; a constant

The arc length,  $s_2 - s_1$ , between two points defined by  $r_2$  and  $\alpha_2$  and  $r_1$  and  $\alpha_1$ , respectively, is then easily obtained.

### 11.5 Analysis for $c'$ - $\phi'$ Conditions

Reanalyze the example in Section 11.2 in a  $c'$   $\phi'$  analysis with an effective cohesion,  $c'$ , of 8 kPa and an effective internal friction angle,  $\phi'_{\text{soil strength}}$ , of  $21^\circ$  at conditions with the water level at Elev.+9.0 m.

The resisting moment due to the cohesion,  $c' = 8$  kPa, is  $\tau L R = 8 (\pi/2) 97 = 1,219$  kNm/m

The sum of Areas #1 through #6 vertical forces is  $50 + 85 + 16 + 42 + 56 + 84 = 333$  kN/m. Area #7 must now be included, adding  $8 \times 3 \times \frac{1}{2} \times 7 = 84$  kN/m and making the total = 417 kN/m.

The total overturning moment,  $M_{\text{Forcing}}$  is still 1,720 kNm/m, which means that the net moment for the friction to resist is  $1,720 - 1,219 = 501$  kNm/m.

The lever arm is  $501/417 = 1.209$  m =  $KR \sin \phi_{\text{mobilized}}$

$\phi_{\text{mobilized}} = \sin^{-1}(1.209/1.05 \times 9.85) = 6.7^\circ$  and  $\tan \phi_{\text{mobilized}} \ll \tan 21^\circ$ .

But, the foregoing includes the erroneous presupposition that the cohesion can be fully mobilized at the same time as the friction is only partially mobilized. To avoid this conflict, one can perform a series of repeat analyses with different degree of mobilization of the effective cohesion,  $c'$ , and iteratively search for what that degree of mobilization of the  $c'$  will result in the same value for the ratio between  $\tan \phi_{\text{mobilized}}$  and  $\tan \phi'_{\text{soil strength}}$ , which ratio then would represent the degree of mobilization of the friction. The inverse of that degree is then the factor of safety for the slope. However, the movement necessary to mobilize a certain portion of the cohesion is not usually that necessary to mobilize the same portion of the internal friction. A similar conundrum exists if using the logarithmic spiral for the calculation of the  $c'$ - $\phi'$  condition.

Considering that some clays have distinct post-peak softening behavior and some soils, clay as well as sand, can be strain-hardening and the fact that soil profiles are built up of layers of different soils, once the case goes from the simple  $\phi = 0$  or  $c = 0$  and uniform soil profile to  $c'$ - $\phi'$  and variable soil profile, slope stability analysis becomes very complex.

## 11.6 Software

Before the computer became a universal tool for geotechnical engineers, stability analysis was performed by hand aided by the slide rule and graphic methods. As the calculation part of the analysis was time-consuming, thinking through the case to decide on the most probable location of the slip surface and the circle center was an investment in time well spent. In contrast, today's engineers have a host of slope stability software to choose between. Some are more sophisticated and complex than others, but every commercially available software will allow many more input options than engineers in the past would ever consider, or, rather, be able to consider. In fact, the analytical ability of the software goes much beyond the reliability of the input data. The ease of letting the computer do the work can lead to overlooking the dubiousity of the input, something that the engineers of old would not do as readily.

Commercially available software and some freeware range from simple limit equilibrium techniques through extensive numerical approaches. The engineer must fully understand the limitations of each method used by the software, as well as be able to appreciate if the method used correctly represents the probable failure mechanism. Most geotechnical general practitioners have limits in this regard and may need to seek the advice of the specialist. However, the project budget may have limits of funds to pay for the advice. A good help in resolving that predicament is to simplify the case to a level that can be analyzed using a "old-fashioned" hand calculation—a simple spreadsheet will often serve as a time saver, here. The analysis results may well show that the case is safe or can be made safe with little effort. NB, a large number of successful design were made before the advent of the computer program. If the hand calculation input shows a marginal stability and measures to alleviate this would be unacceptable for some reason, a well understood and performed computer simulation must be undertaken. The computer solution may then show a satisfactory stability level. However, if the difference between the hand calculation and the computer simulation is large, it may be well advised to review the input and method used for the computer analysis. In fact, having access to the results of a computer simulation does not remove the need for a thoughtful and thorough hand calculation using old and proven methods.



## CHAPTER 12

### SPECIFICATIONS AND DISPUTE AVOIDANCE

#### 12.1 Introduction and examples

Surprises costing money and causing delays occur frequently during the construction of foundation projects, and in particular for piling projects. The contract specifications often fail to spell out the responsibilities for such events and this omission invariably results in disputed claims that sometimes only can be resolved by litigation. Much of this can be avoided by careful wording of the specifications, expressing all quality requirements in quantifiable terms, and, in anticipating difficulties, setting out beforehand who is responsible.

When the unexpected occurs at a site and costs escalate and delays develop, the Contractor feels justified to submit a claim that the Owner may see little reason to accept. When the parties turn to the technical specifications for the rules of the contract, these often fuel the dispute instead of mitigating it, because the specifications are vague, unclear, unbalanced, and containing weasel clauses that help nobody in resolving the conflict. Rarely are specifications prepared for that deviations from the expected can occur.

Indeed, surprises occur frequently during the construction of foundation projects, and in particular in the case of piling projects. The surprises take many forms, but one aspect is shared between them: they invariably result in difficulties at the site and, more often than not, in disputes between the parties involved.

For example, the soil conditions sometimes turn out to differ substantially from what the contract documents indicate. On other occasions, the piles do not go down as easily as anticipated by the Owner's design engineers and/or by the Contractor's estimator. Or, they may go down more easily and become much longer than anticipated. Or, a proof test shows that the pile capacity is inadequate. Or, the piles do not meet a distinct "refusal" and, consequently, the stringent termination criterion in the specifications results in a very prolonged driving causing delays and excessive wear on the Contractor's equipment.

Quite often, the Contractor's equipment fails to do the job. Perhaps, the equipment required by the specifications is "misdirected". Perhaps, the Contractor is inexperienced and cannot perform well, or the equipment is poorly maintained and difficult to use. Whether or not the Contractor honestly believes that the subsequent delays, the inadequate capacity, the breakage, etc. are not his fault, he will submit a claim for compensation. Often, when the claim is disputed by the Owner, the Contractor nevertheless is awarded compensation by the court, because the contract specifications do not normally contain any specific or lucid requirement for the quality of the Contractor's equipment.

Or, the Contractor's leads are not straight and the helmet occasionally jams in the leads. However, are the leads out of the ordinary, after all, they are the same as used on the previous job—and, besides, although they are not straight can they really be called bent, or crooked?

Or, on looking down a pipe pile, the bottom of the pipe cannot be seen. Well, is then the pile bent and is it bent in excess?

Or, when the use of a water jet is required to aid the pile penetration, the pile does not advance or advances too quickly and drifts to the side or a crater opens up in the soil next to the side of the pile. The pump pressure and water flow are usually detailed in the specifications, but the size and length of the hose

and the size of the nozzle are rarely indicated. Yet, these details are vital to the performance of the jetting system, indeed, they govern the pressure and flow.

Frequently, sentences are used such as "in the Engineer's opinion", but with no specific reference to what the opinion would be based on. Such general "come-into-my-parlor" clauses do not hold much water in court, but they are the root of much controversy.

Be careful of the meaning of the terms used. For example, 'allowable load capacity' is a totally confusing set of words. A few years ago, I worked on a litigation case where the Engineer used the words 'allowable load capacity' to indicate the required working load of the piles. Unfortunately, the Contractor interpreted the words to refer to the capacity (in the proper sense of the term as "ultimate resistance") to which he had to drive the piles.

A similar confusion appeared on a more recent project (nothing really changes in this regard), where the engineer deliberately reduced the pile lengths to about half the usual length in order to avoid driving into a boulder layer existing at depth at the site. He also, appropriately, reduced the desired capacity and pile working load (50 tons), requiring a "capacity" of only 100 tons on piles normally accepted and installed to a 200 ton capacity, which is what the specs required. However, someone—it was never determined who—thought that plain 'capacity' sounded too casual and changed it to 'load capacity'. At the outset of the pile driving, the contractor asked what loads he was to drive to and was told that the loads were 100 tons. So, naturally, he drove to a capacity of twice the load, which meant that the piles had to be longer and, as the designer had expected, the piles were driven into the boulder layers. The results was much breakage, problems, delays, and costs. The claim for extra was \$300,000.

Indeed, jargon terms can be very costly. Incidentally, of all terms, "capacity" is most often misused. It simply means "ultimate resistance" and it does not require an adjective (other than "axial" as opposed to "lateral", for example). I once saw a DOT specs text—spell-checked—requiring the Contractor to achieve an "intimate capacity". I say, that is a daring term in these politically correct times!

On the topic of using jargon: The word "set" is not a synonym for "blow-count" (the blows per a certain penetration length). "Set" is the penetration for one blow or, possibly for a series of blows. Its origin is an abbreviation of "settlement" meaning the penetration for one blow. I have one example of what "set" can cause: specifications stated that the Contractor was to drive the piles (concrete piles of limited strength concrete) "*to a very small set and the Contractor was cautioned not to overdrive the piles*". Of course, the Contractor took care not to damage the piles by driving them too hard, which is what "overdriving" means. In fact, the driving turned out to be very easy and several of the piles drove much deeper than the plans and drawings indicated. Unfortunately, in writing the sentence I just quoted, the spec-writer meant to warn the Contractor that the number of blows per unit of penetration (e.g., blows per foot) was expected to be very small and that the piles, therefore, could easily drive too deep. Talk about diametrically opposed interpretations. And predictable surprises. In this case, the Engineers insisted that their intended interpretation was the right one and a costly claim and litigation ensued (which the Contractor won). The word "set" is frequently misconstrued to be a synonym for "termination criterion", which, incidentally, is not the same as "blow count". As the industry has such a vague understanding of the proper meaning of the term "set", avoid using it in any context.

The jargon confusion does not get any better by shifting from "set" to "refusal". Although most people have a qualitative understanding of the meanings, one person's refusal can still be another person's promise. "Refusal" is an absolute term. It would imply that one just cannot drive the piles deeper having exhausts all means to do so. A Contractor claiming this, is not believed. Then, specifications suggesting "a refusal of 6 blows/foot sounds not only silly, but implies a spec writer with a poor command of language. "Termination criterion" is a neutral term that states exactly what is meant. Use it!

What about “battered”? It is a term that separates the men from the boys, or people experienced in — or at least exposed to — piling from people who are not. The latter group includes lawyers, judges, and people serving as jury members in jury trials. I once assisted a contractor who had to go to court to recover costs. This contractor had quite an uphill battle once the judge realized that the contractor had battered the piles, because the judge had experience of battered housewives and children, but he had no knowledge and little appreciation of that the term would have a discrete meaning for piling people. When the matter was made clear to him, he was quite annoyed by that a group of professionals would use a jargon term that had a perfectly suitable every-day English term available, i.e., “inclined”. I agreed then and I agree now. Please, stop using “batter”. My cry in the wilderness; It is getting worse instead of better. I recently read a journal paper where the term was used to characterize a leaning structure!

In another court case, where the term “load test” was used, the judge wondered why it was needed to test the loads: “are they not known before the construction?” he asked. When educated that the term applies to testing a pile by adding loads to it, he requested the lawyers to use the term “loading test” to more correctly refer to what was dealt with. I have followed his admonition ever since, as you can see in Chapter 8.

Most specifications only identify a required pile driving hammer by the manufacturer's rated energy. However, the rated energy says very little of what performance to expect from the hammer. The performance of hammers varies widely and depend on pile size, choice of helmet and cushions, soil behavior, hammer age and past use, hammer fuel, etc. Whether or not a hammer is “performing to specs” is one of the most common causes of discord at a site. The reason is that most specifications are very poor in defining the hammer.

In bidding, a Contractor undertakes to complete a design according to drawings and documents. Amongst these are the Technical Specifications, which purport to describe the requirements for the project in regard to codes, stresses, loads, and materials. Usually, however, only little is stated about the construction. Yet, in the case of a piling project, the conditions during the construction are very different to those during the service of the foundation, and the latter conditions depend very much on the former. When the project is similar to previous projects and the Contractor is experienced and knowledgeable, the technical specifications can be short and essentially only spell out what the end product should be. Such specifications are Performance Specifications. However, these are very difficult to write and can easily become very unbalanced, detailing some aspects and only cursorily mentioning others of equal importance. A specs text, be it for Performance Specifications or for Compliance Specifications (another name is Detailed Specifications), must spell out what is optional to the Contractor and what the Contractor must comply with. Even if the intent is that the specifications be Performance Specifications, and even if they so state, most specifications are actually written as Compliance Specifications. Government specifications are almost always Compliance Specifications.

When surprises arise and the Contractor as a consequence is slowed down, has to make changes to procedures and equipment, and generally loses time and money, then, disputes as to the interpretation of the specifications easily develop. Therefore, the writer of Specifications must strive to avoid loose statements when referring to quality and, instead, endeavor to quantify every aspect of importance. Do not just say that a pile must be straight, but define the limit for when it becomes bent! Do not just say that the pile shall have a certain capacity, but indicate how the capacity will be defined! Do not forget to give the maximum allowable driving stresses and how they will be measured, if measured! In short, take care not to include undefined or unquantified requirements. One of the most non-constructive situation is when the Engineer says that a pile is damaged, or bent, or too short, etc. and the Contractor says “no it ain’t”. The Engineer answers “it is, too!”, and before long whatever communication that existed is gone, the lawyers arrive, and everybody is a looser (well, perhaps not the lawyers).

You may enjoy the following direct quotes from contract specifications submitted by Government agencies.

1. Piles shall be driven to reach the design bearing pressures.
2. The minimum allowable pile penetration under any circumstance shall be 17 feet.
3. The Contracting Officer will determine the continued driving procedure to be followed if driving refusal occurs.
4. The hammer shall have a capacity equal to the weight of the pile and the character of the subsurface material to be encountered.
5. The hammer energy in foot-pounds shall be three times the weight of the pile in pounds.
6. Inefficient diesel, air, or steam hammers shall not be used.
7. Each pile shall be driven until the bearing power is equal to the design piles pressure.
8. All piles incorrectly driven as to be unsuitable as determined by the Contracting Officer shall be pulled and no payment will be made for furnishing, driving, or pulling such piles.
9. All piles determined to be unsuitable by the Contracting Officer shall be replaced by and at the expense of the Contractor.
10. The driving shall continue, using hammer falls of 150 mm to 200 mm in a series of 20 blows, until penetration of the pile has stopped. The height of the fall shall then be doubled and the pile again driven to refusal. This procedure shall be continued until the design load of the pile has been achieved.
11. The pile design load is defined as 1.5 times the working load. The design load will be deemed to have been achieved when the pile exhibits zero residual (=net?) set under 10 successive blows of the hammer, where each blow has a sufficient energy to cause elastic deformation of the pile at the ground level equal to the static shortening of the pile at design load, as calculated by Hooke's Law.
12. The piles shall be driven using a single-acting diesel hammer with a minimum rated hammer energy of 63 kJ or an equivalent hammer. *(Should the "equivalent hammer" have no more than 63 kJ rated energy or not less than 63 kJ?).*

Or have these requirements imposed on you?

- A. The hammer shall have a capacity equal to the weight of the pile and the character of the subsurface material to be encountered.
- B. Cut off portions of pile which are battered, split, warped, buckled, damaged, or imperfect.
- C. Piles shall be driven with a single-acting, partial double-acting, or double acting diesel, air, or steam hammer developing a driving energy of not less than 32,530 newton meters per blow with a minimum ram weight of 3,175 kilograms for an air or steam hammer and 454 kilograms for a diesel hammer.
- D. Where unwatering is required, the Contractor shall effect a dewatering scheme.
- E. The founding elevation shall be established by driving to a set (sic!) determined in accordance with the dynamic formula specified or by the application of the wave equation analysis procedure that verifies the pile resistance. When new conditions such as change in hammer size, change in pile size or change in soil material may occur, new sets shall be determined.

- F. Hammer performance shall be verified to ensure that the actual potential energy is not less than 90 % of the stated potential energy. (b) When the hammer performance is requested to be verified, all costs associated with this work will be included in the contract price when the energy delivered is less than 90 % of the stated potential energy specified in the submission. When the energy is greater than 90 % of the stated potential energy stated in the required submission, the costs will be paid as extra work.

I promise you that the above quotes are real and not made up by me for the occasion. I am sure that many of you have similar and worse examples to show. However, when you stop smiling, you should ponder what depths of ignorance and incompetence the eighteen quotes represent. And also ponder the consequence to Society of our industry having to function with such players in charge of the purse strings.

The following specs requirements I have not actually seen, but I would not be surprised if I were to find them or something similar to them one of these days:

- If the work is done without no extra expense to the Contractor, then the work will be taken down and done over again until the Contractor's expense is satisfactory to the Engineers.
- If something is drawn wrong, it shall be discovered, corrected, and done right with no extra expense to the Owner.
- The bid of any contractor walking around on the site with a smile on his face will be subjected to review.

## **12.2 A few special pointers**

Instead of specifying a pile driving hammer by its rated energy, specifications should specify a hammer by the energy transferred to the pile and the impact force delivered to the pile, which are well defined quantities. In the design phase, energy and force values are to be obtained by means of a wave equation analysis. The wave equation analysis will "marry" the hammer to the pile and soil and to the particular drivability conditions and desired capacity. Naturally, the Contractor has the right to expect that the values specified are correct.

More often than not, the analysis will show that theoretical analysis alone is not able to sufficiently accurately determine the hammer requirements. This is then not an argument against performing the analysis or for not specifying the values. It is an argument addressing the inadequacy of omitting hammer details or just giving a rated energy, which puts the risk onto the Contractor. It is also an argument demonstrating the Owner's obligation to find out ahead of time, or at the outset of a project, what the correct hammer values are. For example, by means of taking dynamic measurements with the Pile Driving Analyzer (PDA). PDA measurements are since many years routinely used to finalize a pile design in connection with test driving or during the Contractor's installation of index piles.

When the potential use of the Pile Driving Analyzer (PDA) is included in the technical specifications, then, if during the course of the piling work, reasons arise to question the hammer performance, the PDA can quickly and with a minimum of fuss be brought to the site and the hammer can be accepted or rejected as based on the agreement of the measurements with the specified values. Opinion may differ with regard to the adequacy of the specified values, but such differences are technical in nature and easily resolved without involving the lawyers.

Dynamic measurements may interfere with the Contractor's work, therefore, the general section of the specifications should contain a clause that outlines how the measurements are performed and what the responsibilities are for the parties involved, as well as how the work is going to be paid.

Dynamic measurements are also commonly carried out to determine pile capacity and integrity. Notice, the PDA measurements need analysis to be useful. Also, the data must be combined with conventional records of the pile installation.

Further, what is bent by bending and doglegging of a pile must be defined by a specific bending radius defining straightness, and out-of-location need to be defined by means of specific tolerances. For example, before driving piles must not be bent more than a specific arc of curvature over a certain distance. After driving the bending radius must not be smaller than a certain value. For pipe piles, this is readily determined by means of an inspection probe designed to jam in the pipe at this radius (Detailed in the Canadian Foundation Engineering Manual 1985, 1992). A pipe pile for which the bottom cannot be seen, but into which the probe reaches the bottom, is then by definition straight and acceptable.

The need for well written and well thought-through specifications is illustrated by the following summary of four cases of project disputes that went to litigation.

1. Overdriving of a group of steel piles. Several steel piles were to be driven into a dense sand to a predetermined embedment depth of 85 feet. Already at a depth of about 30 ft, penetration resistance values began to exceed 200 blows/foot. The 'Engineer' insisted that the Contractor drive the piles to the specified depth despite that driving required an excess of 1,000 blows/foot! A "post mortem" review of the records makes it quite clear that although the heads of the about 90 feet long piles were beaten into the specified 5-ft stick-up above the ground surface, the pile toes probably never went past a depth of 60 feet. The Contractor had planned for a two-week project in early Fall. In reality, it took almost three months. As the project was located north of the 60th parallel, one can perhaps realize that the subsequent claim for \$6,000,000 was justified. Incidentally, the Contractor could not get out of his obligation to drive the piles. His bond saw to that. However, he won the full amount of his claim from the Owner. The Owner later sued the Engineer for negligence and won. The Engineers went bankrupt.
2. Complete breakdown of communications between Contractor and Engineer. A Contractor got permission to use a heavy diesel hammer at an energy setting lower than the maximum which, according to the hammer manufacturer's notes would be equal to the rated energy for a smaller hammer given in the specifications for the project. At the outset of the piling, it became obvious that the piles drove very slowly at that setting, requiring more than 1,000 blows before the specified termination criterion (minimum depth) was reached. Static testing showed that the capacity was insufficient. The specifications included provision for jetting and the Engineer required this for all piles. Yet, it was clear that the pile could be driven down to the depths and capacities quickly and without jetting if the hammer was set to work at the maximum energy setting. Of course, this meant that the hammer energy was to be set at a values higher than that given in the specifications. The Engineers were willing to accept this change. However, the Contractor required extra payment for the deviation from the contract to do this, which the Engineer did not want to grant. One thing led to another. The Contractor continued to drive at reduced hammer setting and diligently worked to adhere to the smallest detail of the specification wordings. The Engineer refused to budge and required jetting and recorded everything the Contractor did to ensure that, as the Contractor now wanted to follow the specs to the letter, he was not to deviate from any of the details. Incidentally, the specifications called for outside jetting (rather than interior jetting) in silty soil, which resulted in drifting, bending, and breaking of piles. The final suit involved claims for compensation of more than \$10,000,000. The Contractor won about 40 % of the claim.

3. Specification for a near-shore piling project required piles to be driven flush with the sea bottom by means of a follower and stated that the follower should have 'sufficient impedance', but did not explained what this was and nobody checked the impedance of the follower. The Contractor drove the piles with a follower consisting of a steel pipe filled with wood chips. As the driving proceeded, the wood chips deteriorated and it became harder and harder to drive the piles. This was thought to be caused by densification of the sand at the site and the Contractor stated that the soil report failed to show that densifiable soils existed at the site and claimed compensation for changed soil conditions. The contract required that dynamic measurements be performed at the project, and they were. However, the results of the PDA measurements were not looked at by anyone! Eventually they were, of course, and it became obvious to all that the root of the problem was with the inadequate follower. Well, better late than never, but the delay certainly cost the parties a bundle of money.
4. Long prestressed piles were required to support a new dock for a port extension. The soil profile consisted of an about 35 m to 40 m very soft soil deposit with some dense sand layers of varying thickness and depth, followed by very dense gravel and sand with boulders. The depth to the bearing soil layer required piles of such length that they became heavier than the available equipment could handle. The piles problem was solved by building the piles as composite piles, the upper about 30 m long solid concrete section and a lower about 15 m long H pile section. The penetration into the dense soil was expected to vary because of the presence of the boulders. During driving through the soft soils, care was taken not to drive too hard as this would have induced damaging tension in the pile. However, when the pile toe reached the dense soil and the penetration resistance increased, the hammer was set to hit harder to build up capacity and to advance the H pile end into the bearing layer. Several piles broke already at moderate blow-count and others a few feet further into the very dense bearing layer during hard termination driving. Expressed reasons for the breakage ranged from poor quality of the piles through sudden barge movements and inadequate equipment and/or use of wrong pile cushions. Not until the case was before the courts was it established that the H pile extension was so light that the impact wave on reaching the end of the concrete section, which was in the very soft soil, a large portion of the wave was reflected as a tension wave. Because the pile toe was in the dense soil, when the remainder of the wave reached the pile toe, a strong compression wave was reflected. The low blow-count and good toe response made the hammer ram rise high and provide a strong impact to the pile. The tension from the end of the concrete section being proportional to the impact force, therefore, reached damaging levels. A study compiling driving logs showed that the breakage correlated well with the presence of soft soil at the bottom end of the concrete section. Dynamic measurements had been conducted for determining capacity early in the project. The 'post mortem' study of the records established that when the bottom end of the concrete section was in soft soil, tension reflections occurred that exceeded safe levels.

It is not possible to give too many details on projects that went to dispute, because space limitation precludes giving an adequately impartial background to the cases. An account giving some of the details could easily appear slanted toward one or the other of the various players, who may then be justified in feeling slighted. Therefore, only the above cursorily information is presented in these notes.

Lucid, comprehensive, and equitable specifications are necessary for successful projects. However, even when the specs are good, if the communication lines break down, the project may still end up keeping our fellow professionals in the legal field living well. However, it is my experience that rarely are the initial 'surprises' and difficulties such that the parties really need to go the full way of the courts. Instead of posturing and jockeying for legal position, if the parties show a bit of good intent and willingness to understand each other and make some effort toward finding out what really is happening and why so, litigation can often be avoided. When people keep talking to each other, an understanding can usually develop that the specs are unclear or special technical difficulties have indeed arisen, and that some common sense 'horse trading' may settle the money issues. Going to court should be a last resort.





## CHAPTER 13

### TERMINOLOGY AND STYLE

*Quote: English can be understood through tough thorough thought, though*

#### 13.1 Introduction and Basic Definitions

There is an abominable proliferation of terms, definitions, symbols, and units used in papers and engineering reports written by the geotechnical community. Not only do the terms vary between authors, many authors use several different words for the same thing, sometimes even in the same paper or report, which makes the material difficult to read and conveys an impression of poor professional quality. More important, poor use of terminology in an engineering report could cause errors in the design and construction process and be the root of a construction dispute, which, ultimately, the report writer may have to defend in litigation. Throughout this book, I have strived to employ a consistent terminology as summarized in this chapter.

Fig. 13.1 illustrates the main definitions and preferred piling terms, which subject area houses the greatest proliferation of muddled-up terms.

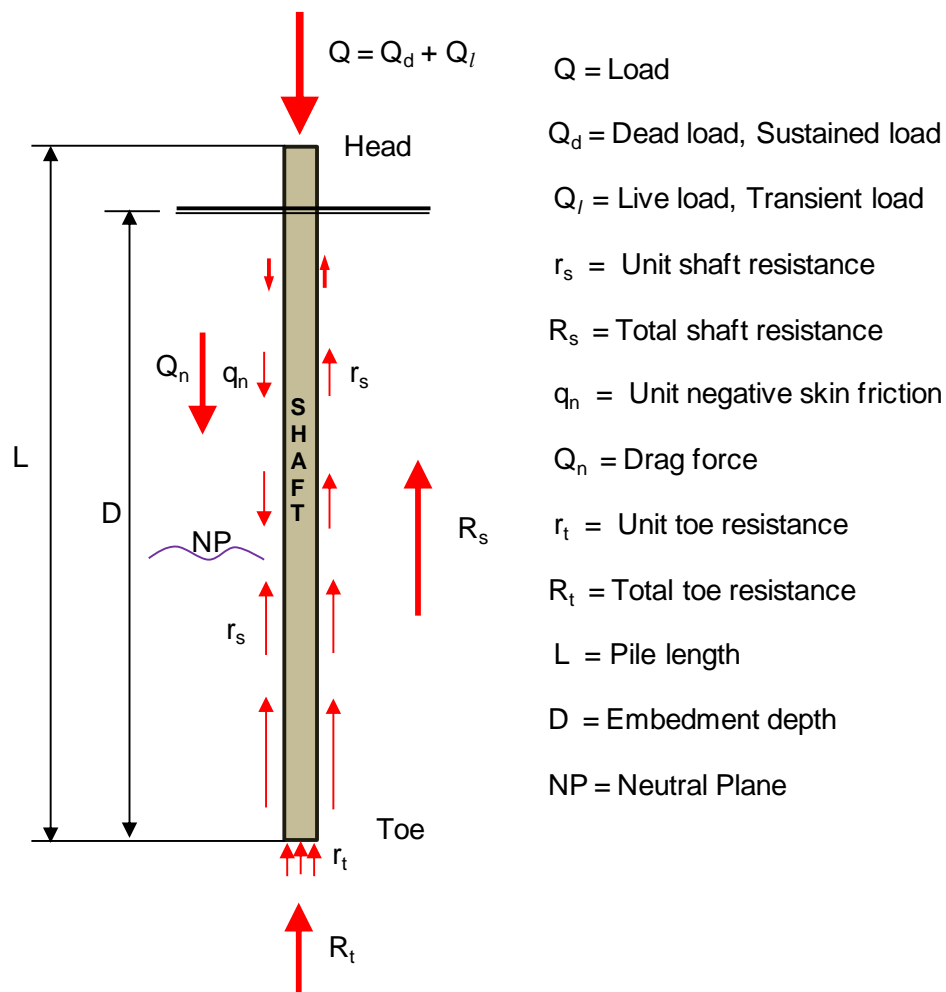


**Fig. 13.1. Definitions and Preferred Terms**

### Upper End of a Pile

One of the most abused terms is the name for the upper and lower ends of a pile. Terms in common use are, for the upper end, “top”, “butt”, and “head”, and for the lower end, “end”, “tip”, “base”, “point”, “bottom”, and “toe”.

The term “top” is not good, because, in case of wood piles, the top of the tree is not normally the 'top' of the pile, which can and has caused confusion. Also, what is meant by the word “top force”? Is it the force at the 'top of the pile' or the maximum (peak) force measured somewhere in the pile? “Butt” is essentially a wood-pile term. “**Head**” is the preferred term, as for example: “the forces were measured at the pile head”.

### Lower End of a Pile

With regard to the term for the lower end of a pile, the word “tip” is easily confused with “top”, should the latter term be used—the terms are but a typo apart. A case-in-point is provided by the 3rd edition (1992) of the Canadian Foundation Engineering Manual, Page 289, 2nd paragraph. More important, “tip” implies an uttermost end, usually a pointed end, and piles are usually blunt-ended.

The term “end” is not good for two reasons: the pile has two ends, not just one, and, more important, “end” has a connotation of time. Thus, “end resistance” implies a “final resistance”.

“Base” is not a bad term. However, it is used mainly for shallow footings, piers, and drilled-shafts. “Point” is often used for a separate rock-point, that is, a pile shoe with a hardened tip (see!) or point. Then, before driving, there is the point of the pile and on the ground next to the pile lies the separate rock-point, making a sum of two points. After driving, only one, the pile point, remains. Where did the other one go? And what is meant by “at a point in the pile”? Any point or just the one at the lower end?

The preferred term is “**toe**”, as it cannot be confused with any other term and it can, and is, easily be combined with other terms, such as “toe resistance”, “toe damping”, “toe quake”, etc.

Other than for a human connotation, the word “bottom” should be reserved for use as reference to the inside of a pile, for instance, when inspecting down a pipe pile, “the bottom of the hole”, and such.

### The Pile Shaft

Commonly used for the part of the pile in between the head and toe of the pile are the terms “side”, “skin”, “surface”, and “shaft”. The terms “skin” and “shaft” are about as frequent. “Side” is mostly reserved for stubby piers. “Surface”, although is used, the term is not in frequent use. The preferred term is “**shaft**” because “skin” is restricted to indicate an outer surface and, therefore, if using “skin”, a second term would be necessary when referring to the actual shaft of the pile.

### Other Preferred Piling Terms

A word often causing confusion is “capacity”, especially when it is combined with other words. “Capacity” of a unit, as in “lateral capacity”, “axial capacity”, “bearing capacity”, “uplift capacity”, “shaft capacity” and “toe capacity”, is the **ultimate resistance** of the unit. The term “ultimate capacity” is a tautology, a mixed metaphor to avoid, although it cannot be misunderstood. However, the meaningless and utterly confusing combination terms, such as “load capacity”, “design capacity”, “allowable capacity”, “carrying capacity”, “load carrying capacity”, even “failure capacity”, which can be found in many papers, should not be used. (I have experienced a court case where the single cause of the

\$300,000 dispute turned out to originate from the designer's use of the term "load capacity" to mean capacity, while the field people believed the designer's term to mean "allowable load". As a factor of safety of 2 was applied, the field people drove—attempted to drive—the piles to twice the capacity necessary with predictable results. Use "**capacity**" as a stand-alone term and as a synonym to "**ultimate resistance**".

Incidentally, the term "ultimate load" can be used as a substitute for "capacity" or "ultimate resistance", but it should be reserved for the capacity evaluated from the results of a static loading test.

As to the term "resistance", it can stand alone, or be modified to "ultimate resistance", "mobilized resistance", "shaft resistance", "toe resistance", "static resistance", "initial shaft resistance", "unit toe resistance", etc. Often, the term "response" can replace "resistance".

Obviously, combinations such as "skin friction and toe resistance" and "bearing of the pile toe" constitute poor language. They can be replaced with, for instance, "shaft and toe resistances", and "toe resistance" or "toe bearing", respectively. "Shaft bearing" is not commonly used, but it is an acceptable term.

Resistance develops when the pile forces the soil: "positive shaft resistance", when loading the pile in compression, and "negative shaft resistance", when loading in tension. The term "skin friction" by itself should not be used, but it may be combined with the 'directional' words "negative" and "positive": "Negative skin friction" is caused by settling soil and "positive skin friction" by swelling soil.

The terms "load test" and "loading test" are often thought to mean the same thing. However, the situation referred to is a test performed by loading a pile, not a test for finding out what load that is applied to a pile. Therefore, "**loading test**" is the semantically correct and the preferred term. Arguing for the term "loading test" as opposed to "load test" may suggest that I am a bit of a fusspot. I may call this favorite desserts of mine "iced cream", but most say "ice cream". In contrast, "iced tea" is the customary term for the thirst-quencher, and the semantically correct, and the normally used term for cream-deprived milk is "skimmed milk", not "skim milk". By any name, though, the calories are as many and a rose would smell as sweet. On the other hand, laymen, call them lawyers, judges, or first-year students, do subconsciously pick up on the true meaning of "load" as opposed to "loading" and are unnecessarily confused wondering why engineers desiring to determine the load that's going to be placed on a pile look down the soil instead of up the structure. So, why not use the term "loading test"?

While the terms "static loading test" "static testing" are good terms, do not use the term "dynamic load testing" or worse: "dynamic load test". Often a capacity determination is not even meant by these terms. Use "**dynamic test**" or "**dynamic testing**" and, when appropriate, "capacity determined by dynamic testing (or test)".

When presenting the results of a loading test, many authors write "load-settlement curve" and "settlement" of the pile. The terms should be "**load-movement curve**" and "**movement**". The term "settlement" must be reserved to refer to what occurs over long time under a more or less constant load smaller than the ultimate resistance. The term "displacement" should not be used as synonym for "movement", but preferably be reserved for where soil actually has been displaced, e.g., moved aside. The term "deflection" instead of "movement" is normally used for lateral deflection, but "displacement" is also used for this situation. "Compression", of course, is not a term to use instead of "movement" as it means "shortening".

In fact, as mentioned in Chapter 3, not just in piling terminology, but as a general rule, the terms "movement", "settlement", and "creep" all mean deformation. However, they are not synonyms and it is important not to confuse them.

When there is a perfectly good common term understandable by a layman, one should not use professional jargon. For example, for an inclined pile, the terms “raker pile” and “batter pile” are often used. But “a raker” is not normally a pile, but an inclined support of a retaining wall. As to the term “batter”, I have experienced the difficulty of explaining a situation to a judge whose prior contact with the word “batter” was with regard to “battered wives” and “battered children” and who thought, no, was convinced, that “to batter a pile” was to drive it abusively! The preferred term is “**inclined**”.

The word “set” is a short form of “settlement”, but means penetration for one blow, often penetration for a series of blows. Sometimes, “set” is thought to mean “termination criterion” and applied as blows/inch! The term “set” is avoidable jargon and should not be used. (See my expanded comment in Chapter 11).

The word “refusal” is another example of confusing jargon. It is really an absolute word. It is often used in combinations, such as “practical refusal” meaning the penetration resistance for when the pile cannot reasonably be driven deeper. However, “refusal” used in a combination such as “refusal criterion” means “the criterion for (practical) refusal”, whereas the author might have meant “**termination criterion**”, that is, the criterion for when to terminate the driving of the pile. Avoid the term “refusal” and use “penetration resistance” and “termination criterion”, instead. (See my expanded comment in Chapter 11).

Terms such as “penetration resistance”, “blow-count”, and “driving resistance”, are usually taken to mean the same thing, but they do not. “**Penetration resistance**” is the preferred term for the effort required to advance a pile and, when quantified, it is either the number of blows required for the pile to penetrate a certain distance, or the distance penetrated for a certain number of blows.

“**Blow-count**” is a casual term and should be used only when an actual count of blows is considered. For instance, if blows are counted by the foot, one cannot state that “the blow-count is so and so many inches per blow”, not even say that it is in blows/inch, unless inserting words such as: “which corresponds to a penetration resistance of. . .” Obviously, the term “equivalent blow-count” is a no-good term. In contrast, when the actual blow-count is 0.6 inch for 9 blows, the “equivalent penetration resistance” is 15 blows/inch.

“Driving resistance” is an ambiguous term, as it can be used to also refer to the resistance in terms of force and, therefore, it should be avoided.

Often, the terms “allowable load” and “service load” are taken to be equal. However, “allowable load” is the load obtained by dividing the capacity with a factor of safety. “Service load” or “working load” is the load actually applied to the pile. In most designs, it is smaller than the “allowable load”, and usually equal to “unfactored load”, a concept used in the LRFD approach. The term “design load” can be ambiguous — if using it, make sure to supply a clear definition.

The term for describing the effect of resistance increase with time after driving is “**set-up**” (soil set-up). Do not use the term “**freeze**” (soil freeze), as this term has a different meaning for persons working in cold regions of the world.

Soils can include water and be “moist”, “wet”, “damp”, and “saturated”. The measurement of the amount of water is the content of water in relation (percentage) of the weight of the solids, the dry weight. The term “moisture content” is sometimes used in the same sense as “**water content**”. However, the term “moisture content” is a spot-on example of an obfuscating jargon term to avoid. Most people, even geotechnical engineers, will consider that calling a soil “moist”, “damp”, or “wet” signifies three different conditions of the soils (though undefined). Moreover, a layman can understand what “water content” means, as well as the terms “moisture” and “content”, when encountered separately, but understanding

the meaning of the combination of “moisture” and “content” requires geotechnical training. It follows that laymen, read lawyers and judges, will believe and expect that “moisture content” is something different to “water content”, perhaps thinking that the former indicates a less than saturated soil. Yet, there is no difference. It is only that saying “moisture” instead of “water” implies, or intends to imply that the speaker possesses a greater degree of sophistication than conveyed by simply saying “water content” and, because the term is not immediately understood by the layman, it intends to send the message that the Speaker is in the “know”, a specialist of some stature. Don’t fall into that trap. Use “water content”. Jargon that has no other purpose than to make the subject matter incomprehensible for the uninitiated is bad technical writing and, remember, we should strive to use simple terms that laymen can understand.

Perhaps “moisture content” is used because it is perceived to make the author appear refined and a true expert. Would someone writing “humidity content” then look even more refined? Or, could “wetness content” perhaps elevate that lofty goal? Then, why not use the even more ‘refinedly’ sounding term: “wetness quotient”? Please, the word to use to modify “content” is “water”!

In this context, note that the terms “moist density” and “wet density” do not mean “saturated density”.

Avoid the term “timber pile”, use “wood pile” in conformity with the terms “steel pile” and “concrete pile”.

Do not use the term “reliability” unless presenting an analysis based on probabilistic principles.

Unlike many other languages, English provides the means to express the important fact that soil forces have direction whereas forces in water do not. Expressed differently, stress is a tensor, while pressure is isotropic. Therefore, it is fundamentally wrong to state that a certain load on a footing results in a certain “pressure”. The term to use is “stress”—there is no pressure between soil particles—and it is important to recognize the distinction between soil and water in response to force. Logically, therefore, the old terms “earth pressure” and “earth pressure coefficient” should be “earth stress” and “earth stress coefficient”. (However, it is probably futile to think that the profession would abandon using those strongly established “pressure” terms).

One of the silliest mistakes—unfortunately, also a very common one—is to use the word “predict” as a synonym to “calculate” or “compute”. Synonyms of “to predict” are “to forecast” or “to prophesy”. One does not “predict” the response of a pile from, say, pile test data. When a response is already known, one “calculates” or “computes”. “Prediction” is an absolute term, and it must only be used for a calculation that is truly a prediction of an expected behavior. A design is based on prediction from available data and calculation results. That is, the latter are themselves not predictions, but the use of them in a design is.

The terms “specific weight” and “specific gravity” were canceled as technical terms long ago, but they are still found in many professional papers. “Specific weight” was used to signify the weight of material for a unit volume. However, the proper terms are “**solid density**” and “**unit weight**” (the units are mass/volume and force/volume, respectively). The dimensionless term “specific gravity” was used to mean the ratio of the density of the material over the density of water. The internationally assigned term for this ratio is “relative density”, which term, unfortunately, conflicts with the geotechnical meaning of the term “relative density” as a classification of soil density with respect to its maximum and minimum density. For the latter, however, the internationally assigned term is “**density index**”.

### 13.2 Brief Compilation of Some Definitions and Terms

**Bored pile** - A pile that is constructed by methods other than driving, commonly called **drilled shaft**.

**Caisson** - A large, deep foundation unit other than a driven or bored pile. A caisson is sunk into the ground to carry a structural unit.

**Capacity** - The maximum or ultimate soil resistance mobilized by a foundation unit. A capacity must always be coupled to its associated movement. Note, modifiers such as "load capacity", "allowable capacity" "design capacity", etc. are misleading and false terms that should never be used.

**Capacity, bearing** - The maximum or ultimate soil resistance mobilized by a foundation unit subjected to downward loading.

**Capacity, geotechnical** - See **capacity, bearing**.

**Capacity, lateral** - The maximum or ultimate soil resistance mobilized by a foundation unit subjected to horizontal loading.

**Capacity, structural** - The maximum or ultimate strength of the foundation unit (a poor term to use).

**Capacity, tension** - The maximum or ultimate soil resistance mobilized by a foundation unit subjected to tension (upward) loading.

**Consolidation** - The dissipation of excess pore pressure in the soil.

**Creep** - Deformation continuing under constant shear force.

**Cushion, hammer** - The material placed in a pile driving helmet to cushion the impact (formerly called "capblock").

**Cushion, pile** - The material placed on a **pile head** to cushion the impact.

**Dead load** - See **Load, dead**.

**Direction** - Direction of soil movement along a pile; negative if downward and positive if upward. See **skin friction** and **shaft resistance**

**Downdrag** - The downward **settlement** of a deep foundation unit due to settlement at the **neutral plane** "dragging" the pile along; expressed in units of movement (mm or inch).

**Drag force** - The maximum force transferred to a deep foundation unit from accumulated **negative skin friction**.

**Drag load** - See **Drag force**. "Drag load" implies that the drag force would be similar to a working load and this *faux pas* is avoided by the term "force".

**Drilled shaft** - A bored pile.

**Dynamic method of analysis** - The determination of **capacity, impact force, transferred energy**, etc. of a driven **pile** using analysis of measured **stress-waves** induced by the driving of the pile.

**Dynamic monitoring** - The recording of strain and acceleration induced in a pile during driving and presentation of the data in terms of stress and **transferred energy** in the pile as well as of estimates of **capacity**.

**Factor of safety** - The ratio of maximum available resistance or of the **capacity** to the allowable or to the working stress or load.

**Foundation unit, deep** - A unit that provides support for a structure by transferring load or stress to the soil at depth considerably larger than the width of the unit. A **pile** is the most common type of deep foundation unit.

**Foundations** - A system or arrangement of structural members through which the loads are transferred to supporting soil or rock.

**Full displacement pile, FDP** - A bored pile where the soil has been displaced rather than excavated.

**Groundwater table** - The upper surface (boundary) of the zone of saturation in the ground.

**Impact force** - The peak force delivered by a pile driving hammer to the **pile head** as measured by means of **dynamic monitoring** (the peak force must not be influenced by soil resistance reflections).

**Kentledge** - Term for loaded platform serving as reaction to the load applied to a pile in a static loading test. Originally the term for the ballast placed in a ship to ensure stability. Sometimes, and incorrectly, used for other reaction arrangements. The term is unnecessary jargon to avoid. Best is to use "loaded platform".

**Live load** - See **Load, live**.

**Load, allowable** - The maximum load that may be safely applied to a **foundation unit** under expected loading and soil conditions and determined as the **capacity** divided by the **factor of safety**. When "allowable" is used as a modifier with a second adjective, it refers to a maximum notwithstanding that the actual **working load** could be smaller.

**Load, applied, or load, service, or load, working** - The load actually applied to a foundation unit.

**Load, dead, or load, sustained, or load, permanent** - The "always there" load applied to a foundation unit.

**Load, design** - A term that easily confuses and best avoided.

**Load factor** - A reduction factor applied to a **working load** always considered together with a "resistance factor" applied to the **ultimate resistance** of a foundation unit.

**Load, factored** - A load increased by multiplication with the appropriate **load factor**.

**Load, live, or load, transient, or load, temporary** - The "there today, gone tomorrow" load actually applied to a foundation unit. "Sustained live load" is a misnomer to avoid. It tries to recognize that some loads called live or transient loads in structural design are really functioning as permanent or dead loads in geotechnical design.

**Neutral plane** - The location where equilibrium exists between the sum of downward acting permanent load applied to the pile and **drag force** due to accumulated **negative skin friction** and the sum of upward acting **positive shaft resistance** and mobilized **toe resistance**. The neutral plane is also (always) where the relative movement between the pile and the soil is zero, i.e., the location of "settlement equilibrium".

**Pile** - A slender **deep foundation unit**, made of wood, steel, or concrete, or combinations thereof, which is either premanufactured and placed by driving, jacking, jetting, or screwing, or cast-in-situ in a hole formed by driving, excavating, or boring. A pile can be a non-displacement, a low-displacement, or displacement type.

**Pile head** - The uppermost end of a **pile**.

**Pile impedance** -  $Z = EA/c$ , a material property of a pile cross section determined as the product of the Young's modulus ( $E$ ) and area ( $A$ ) of the cross section divided by the **wave speed** ( $c$ ).

**Pile point** - A special type of **pile shoe**.

**Pile shaft** - The portion of the pile between the **pile head** and the **pile toe**.

**Pile shoe** - A separate reinforcement attached to the **pile toe** of a pile to facilitate driving, to protect the lower end of the pile, and/or to improve the toe resistance of the pile.

**Pile toe** - The lowermost end of a **pile**. (Use of terms such as pile tip, **pile point**, or pile end in the same sense as pile toe is discouraged).

**Pore pressure** - **Pressure** in the water and gas present in the voids between the soil grains minus the atmospheric pressure.

**Pore pressure, artesian** - **Pore pressure** in a confined body of water having a level of **hydrostatic pressure** (head) higher than the distance to the ground surface.

**Pore pressure, hydrostatic** - **Pore pressure** distribution as in a free-standing column of water (no gradient).

**Pore pressure elevation, phreatic** - The elevation of a **groundwater table** corresponding to a **hydrostatic pore pressure** equal to the actual **pore pressure**.

**Pore pressure gradient** - Non-hydrostatic pore pressure. The gradient can be upward or downward. At downward gradient, effective stress increases more than it would in a hydrostatic condition.

**Pressure** - Omnidirectional force per unit area. (Compare **stress**).

**Resistance factor** - A reduction factor applied to a the **ultimate resistance** of a foundation unit and always considered together with a **load factor**.

**Resistance, factored** - A resistance reduced by multiplication with the appropriate **resistance factor**.

**Resistance, ultimate** - Synonym to **capacity**.

**Secondary Compression** - **Settlement** continuing after end of primary consolidation. It should not be called "**creep**", as shear forces are not involved.

**Settlement** - The downward movement of a foundation unit or soil layer due to rapidly or slowly occurring compression of the soils located below the foundation unit or soil layer, usually requiring an increase of effective stress due to an applied load or lowering of pore pressure. When no change of effective stress occurs, the term is "**secondary compression**".

**Shaft resistance, negative** - Soil resistance acting downward along the pile shaft because of an applied uplift load.

**Shaft resistance, positive** - Soil resistance acting upward along the pile shaft because of an applied compressive load.

**Skin friction, negative** - Soil resistance acting downward along the pile shaft as a result of movement of the soil along the pile and inducing compression in the pile.



**Skin friction, positive** - Soil resistance acting upward along the pile shaft caused by swelling of the soil and inducing tension in the pile.

**Stress** - Unidirectional force per unit area. (Compare **pressure**).

**Stress, effective** - The total stress in a particular direction minus the **pore pressure**.

**Toe resistance** - soil resistance acting against the **pile toe**.

**Transferred energy** - The energy transferred to the pile head and determined as the integral over time of the product of force, velocity, and **pile impedance**.

**Wave speed** - The speed of strain propagation in a **pile**.

**Wave trace** - A graphic representation against time of a force or velocity measurement.

**Working load** - See **Load, working**.

### 13.3 Units

In the SI-system, all parameters such as length, volume, mass, force, etc. are to be inserted in a formula with the value given in its base unit. If a parameter value is given in a unit using a multiple of the base unit, e.g., 50 MN — 50 meganewton, the multiple is considered as an abbreviated number and inserted with the value, i.e., “mega” means million and the value is inserted into the formula as  $50 \cdot 10^6$ . Do not use a mongrel set of units, e.g., a certain stress as, say,  $34 \cdot 10^5$  kPa, must be written as 3.4 GPa. Moreover, while the kilogramme is written kg, it is really a single unit (base unit) although this is contradicted by the fact that its symbol, “kg”, is composed of two letters. For true multiple units, such as kilonewton and kilometre, the “kilo” is a prefix meaning 1,000<sup>1)</sup>.

Notice that the base units of hydraulic conductivity (permeability),  $k$ , and consolidation coefficient,  $c_v$ , are m/s and  $m^2/s$ , not cm/s or  $cm^2/s$ , and not  $m^2/year$  or  $m^2/hour$ , respectively. However, as indicated in Chapter 3, the “ $m^2/year$ ” is acceptable in practice.

When writing out SI-units, do not capitalize the unit. Write “67 newton, 15 pascal, 511 metre, 32° celcius, and 96 kilogramme. However, for these, it is better to simply write 67 N, 15 Pa, 511 m, 32 °C, and 96 kg.

If your text uses SI-units and the original work quoted from a paper used English, make sure to apply a soft conversion and avoid writing “30.48 metre”, when the original measure was “100 feet”, or maybe even “about 100 feet”. Similarly, “about one inch” is “about 20 mm” or “about 30 mm”, while a value of “2.27 inches” converts to “57.7 mm”.

When indicating length and distance in the SI-system, use the unit metre (m) and multiples millimetre (mm) or kilometre (km). Avoid using the unit centimetre (cm).

---

<sup>1)</sup> It is a pity that in developing the SI-system from the old metric systems, the cgs-system and MKSA-system, the unit for mass, the kilogramme, was not given a single symbol letter, e.g., “R” for “ram or ramirez”. Surely there must have been a Herr Doctor Ram or Señor Ramirez somewhere who could have been so honored. Then, the old unit “kg” would be “R”, and a tonne would be superfluous as a term as it would be replaced by “kR (or, preferably “KR”. I very much would like to have the convention of capitalizing the multiplying prefix also applied to “kilo”. A capital “K” is thought to conflict with the term “Kelvin”—the measure of temperature in degree celcius from the absolute lowest value of -273 °C—a weak point, I think, but, I have yielded to the convention).

For area, square centimeter ( $\text{cm}^2$ ) can be used when it is alone. However, never in combined terms (for example, when indicating stress). The unit for stress is multiple of newton/square metre or pascal ( $\text{N/m}^2$  or Pa). Combination units, such as  $\text{N/mm}^2$  and  $\text{MN/cm}^2$  violate the principle of the international system (SI) and can be the cause of errors of calculation. That is, prefixes, such as “M” and “m”, must only be used in the numerator and never in the denominator. Notice also that the units “bar” and “atmosphere” (1 bar = 100 kPa; 1 at = 98.1 kPa, 1 atm = 98.7 kPa,) are aberrations to avoid.

Notice, the abbreviated unit for “second” is “s”, not “sec”! — a very common and unnecessary mistake.

The units “newton”, “pascal”, “joule” etc. do not take plural ending. It is logical and acceptable to omit the plural ending for all other units in the SI-system.

For the time of the day, use 24-hour convention, not the 12-hour “am” and “pm” convention. Thus, fifteen minutes before three o'clock in the afternoon is 14:45h and twenty minutes after five o'clock morning time is 05:20h. Note that the letter “h” is always included.

Using the word “centigrade” to mean the unit for temperature is a far too common mistake. The correct term is “degree celsius” or just “celsius”, abbreviated “°C”, as in “a soil temperature of 14 °C”. Incidentally, the “centigrade” is an obsolete unit for the 400° circle (as opposed to 360°).

### 13.4 Spelling Rules and Special Aspects on Style

A design will invariably result in a written presentation of results and recommendations for a project. Even the best and most elaborate design resulting from a high standard engineering work can be totally shamed by poor report writing style. In the following a few suggestions are made on how to avoid some of the more frequent gaffes in report writing, and, for that matter, in writing up the work in a manuscript for professional dissemination.

Use either English or U.S. spelling: for example, English spelling includes the letter “u” in words such as “behaviour”, “colour”, “favour”, “harbour”, “labour”, “rumour”, “neighbouring”, “remould”, “gauge” and doubles the consonant in words such as “modelling”, “travelling”, “controlled”, “labelling”, “omitted”, “focussing”, and “referring”, “preferred”, and “occurring”, (but “offered” and “offering”, because the stress is on the first syllable). American spelling omits the “u” and does not double the consonant in these words. (“Occurring” and “occurred”, however, are written the same way by both conventions).

Write “z” instead of “s” such as “analyze”, “analyzing”, “analyzer”, “emphasize”, “organize”, “capitalize”, “idealize”, “rationalize”, “realize”, “specialize”, “summarize”, “symbolize”, and “horizontal”.

Use the spelling “to advise” and “to practise” and “the advice” and “the practice” (verb versus noun), and omit “e” before “able” in “arguable”, “drivability”, “desirable”, “lovable”, etc. However, the “e” is retained in “serviceability” and “noticeable” (to separate the consonant “c” from the vowel “a”).

A simple and useful distinction of meanings can be made by writing “metre” for distance and “meter” when referring to a measuring device. Similarly, the spelling “programme” as in “testing programme” keeps the meaning apart from “program” as in a “computer program”.

When using the verbs “centre” (English) or “center” (U.S.), use the correct tense forms: “centred” and “centered”, respectively.

Do not use loose contractions such as "don't" or "can't". Write "do not" and "cannot". Also, write "it is", not "it's" or "its". Besides, "its" is a possessive pronoun not to be written "it's".

Capitalize all months, days, and seasons.

Do not overuse nouns as adjectives. Four nouns in a row is an abomination. For instance, "the concrete pile toe capacity", which reads much better if changed to "the toe capacity of the concrete pile". In general emphasizing adjectives "much", "very", etc. are redundant, and "extremely", "absolutely" have no place in a thesis. If something is larger than something else, better than to say "much larger", quantify it and let the reader judge from the numbers.

Avoid "there are " constructions; write "two critical points are shown. . . ", not "there are two critical points shown...".

Avoid "of the"-phrases. Thus, write "the page length should be 100 mm" rather than "the length of the page should be 100 mm".

The first time a noun, e.g. "test", "measurement", "borehole", etc., is mentioned, avoid using definite article (i.e., "the"). Often, the text flows better if an indefinite article is used, i.e., "a", or no article.

Use plain English and common words rather than fancy ones, and be concise (on account of that sesquipedality does not result in perspicacity). Use short sentences and avoid lengthy or awkward constructions. If a sentence comes out to use more than three lines, it is usually better to split it into two.

Think of the literal meaning of words and expressions and avoid 'ear-sores' such as "up to a depth of ...".

Take care (proof read) not to leave a number alone at line end with its units at the next line, e.g., "16 MPa". Use a non-break space command between numerals and units for getting "16 MPa" to always be on the same line. Similarly, use the non break command to prevent a number from starting a line, i.e. the word immediately before the number should stay with the number.

When writing "Fig. 5", "Author B. C.", "i. e.", "e. g.", and other words using an abbreviation period, the automatic justification of the lines may result in too wide a space after the period, e. g., Fig. 5", "e. g., and Author B. C.". To avoid this, always follow such a period with a no-break-space command, or do not use a space. For names shown as only a first letter followed by a period, the space after the period between a series of such letters can be omitted.

Numerical values consisting of four or more digits can be difficult to read. Then, to improve clarity, separate each set of three digits with a comma, e.g., 7,312,940. (This is North American practice. European practice of separating the digits with a space for every three digits is less clear and can lead to mistakes in understanding).

Work on the interpunctuation and, in particular, the use of the comma. Commas are important for the understanding of the text and must not be neglected. Always place a comma before a conjunction introducing an independent clause. For example: "always remember, commas enhance the reader's

understanding of the message”. Also, ponder why the following two sentences have different meanings: “Also the professor may need assistance with regard to commas.” “Also, the professor may need assistance with regard to commas.” (Either meaning may require a bit of diplomacy in rendering the assistance). Finally, consider the life and death importance of whether Caesar's order about your execution or liberation reads "Execute, not liberate" or "Execute not, liberate".

Use always the convention of the "serial comma". Thus, write "red, white, and blue" with a comma separating each item in the series (of three or more items). That is, place a comma before the “and”, as well as before the “or” in a series of alternatives.

When the subject is the same for both sentence clauses and the connective is "but", a comma should be used after the word preceding “but”. Note, when the subject is the same for both clauses and the connective is "and", the comma should be omitted.

Notice that there is often a difference between similar words. For example, "alternate" and "alternative", where "alternate" refers to every second in a series, and "alternative" is one of two possibilities. "Alternate", but not "alternative" can sometimes mean "substitute". The word "substitute" is then preferred. And, do not confuse the meaning of the words "objective" and "object"—a common mistake.

You may want to indicate that a particular observation or item is more important than others, starting the sentence making this point as *"More important, the measurements show that ..."*. Do not write "importantly". The adverb of important, "importantly", is a synonym to "pompously". Similarly, when presenting items in order of importance, but you prefer not to use a bulleted or numbered list, do not write, "Firstly", "Secondly", "Thirdly", etc. Remove the "-ly" and write "First", "Second", "Third", etc.

Many times, the words “precision” and “accuracy” are improperly used. An example of “precision” is the reading precision of a gage, that is, the number of decimals given in the gage reading. “Accuracy” considers errors in the gage and in a combination of measurements and calculations. The following is a common error: “the accuracy of the prediction of capacity was 3 percent”. The text actually means to refer to an “agreement” between values. Besides, accuracy in prediction of pile capacity can never be as good as 3 percent!

Notice that a verbal message can be spoken or written, heard, or read. If you want to say that the message is spoken as opposed to written, say "oral". A non-verbal message is not necessarily non-spoken, but one not conveyed by words, but instead, for example, by grunts and gestures.

The word "anybody" means "anyone". "Any body" means "any corpse". Similarly, "any one" means "any single person".

The word "data" is a plural word and takes plural verbs. So are and do the words "criteria", "formulae", "media", "memoranda", "phenomena", as well as "strata". Therefore, the appertained verb must be in plural form. The corresponding singular words are "datum", "criterion", "formula", "medium", "memorandum", "phenomenon", and "stratum".

Words such as "usage", "finalized", etc. may look refined, but are examples of convoluted style. Use the simple versions: "use", or "final or finished", etc. Note, "utilization" refers to the manner or "using", and "utilize" is not a refined synonym to the word "use".

The words "order of magnitude" imply a relation of ten! Usually, the intended meaning is better expressed by plain "magnitude" or "size".

Puristically, "in-situ" should be written in italics, but hyphenating it provides sufficient distinction. Do not write "insitu", or "in situ".

The word "less" is overused. Whenever possible, replace it by its various equivalents, such as "fewer", "smaller", "lighter", "lower", "poorer", etc.

Do not use the ampersand symbol, "&", write "and".

Prefixes such as "pre-" are often unnecessary. For example, the word "predominant" can often be written "dominant" (and preferably be replaced by words such as "governing", "principal", "leading", etc.).

Limit each paragraph to a single message. Short paragraphs focus the reader's attention and assist understanding.

### **13.5 References and Bibliography**

All papers must include a section listing bibliographic information for works cited in the text called "References" (note the plural form). The format of the section varies between publications. For example, the Canadian Geotechnical Journal (CGJ) requires the author names to be capitalized, which is not how the ASCE Geotechnical and Environmental Journal (ASCE J.) wants it, for example. However, the latter puts the title of the paper inside quotation marks, which the CGJ does not. Both, as do most journals, require that a reference to a conference includes the dates and venue of the conference.

For publications cited in the text, use the author-date method. Note that the "al." in "et al." has an abbreviation period and that there is no comma between name and year. For example:

- "Terzaghi and Peck 1967 described..."
- "Terzaghi et al. 1996 preseted...."
- "Major papers on stability analyses (e.g., Bishop and Bjerrum 1960) are..."

The general format for listing references in alphabetical order in the References section is as follows.

- Last name and initials of all authors
- Year of publication (in parenthesis for the ASCE J., but no parenthesis for the CGJ)
- Title of paper, report or book chapter. (For a manuscript submitted to the ASCE placed the title inside quotation marks, but a manuscript intended for the CGJ has no quotation marks bracketing the title. The title should be in lower case letters but for the first letter of the first word)
- Title of journal, periodical, proceedings or book—often in italics

- Name and location of publisher (also for conference proceedings). Volume number followed without space by issue number in parenthesis and page numbers, or total number of pages<sup>1)</sup>
- For papers in conference proceedings indicate city (venue) and dates of conference

For author's first name initials, show only the first letter followed by a period. When more than one first name initial is used, the space after the period between a series of such letters should be omitted.

Use no line space between references, but employ a visual separation by an 8 mm (0.3 inch) hanging indent. Some journals may have different requirement in this regard.

### **13.6 Examples of referenced works from published books, journals, and hard-copy documents**

- Becker, D.E., Crooks, J.H.A., Been, K., and Jefferies, M.G., 1987. Work as a criterion for determining in-situ and yield stresses in clays. *Canadian Geotechnical J.* 24(4) 549-564.
- Begemann, H.K.S., 1965. The friction jacket cone as an aid in determining the soil profile. *Proc. of the 6th ICSMFE, Montreal, September 8-15, Univ. of Toronto Press, Vol. 2, 17-20.*
- Bjerrum L., Johannessen, I.J., and Eide, O., 1969. Reduction of negative skin friction on steel piles to rock. *Proc. 7th ICSMFE, Mexico City, August 25-29, Mexico Geotechnical Society, Vol. 2, 27-34.*
- Bruce, D.A., 2005. Glossary of grouting terminology. *ASCE J. Geotechnical and Geoenvironmental Engng.* 13(112) 1534-1542.
- Camp, W.M., 2004. Drilled and driven foundation behavior in a calcareous clay. *GeoSupport 2004, ASCE GSP124, ASCE, Reston, VA, 1-18.*
- Campanella, R.G. and Robertson, P.K., 1988. Current status of the piezocone test. *Penetration Testing 1988, Vol. 1, Balkema, Rotterdam, 93-116.*
- Crikey A.D., 2017. Exorbitant and extraneous finite extensions of alluvial fans in subservient geology. *Journal of Quaternary Geotechnique*, 13(2) 1-8.
- Fellenius, B.H., 2014. Basics of foundation design, a text book. Revised Electronic Edition, [www.Fellenius.net], 500 p.
- Germaine, J.T., 1982. Development of the directional shear cell for measuring cross-anisotropic clay properties. *ScD Thesis, Dept. of Civil Engineering, MIT, Cambridge, Mass, 569 p.*
- Holtz, R.D. and Kovacs, W.D., 1981. An introduction to geotechnical engineering. Prentice-Hall Inc., New York, 780 p.
- Holtz, R.D., Jamiolkowski, M. B., Lancelotta, R., and Peroni, R., 1991. Prefabricated vertical drains. Design and Performance. Construction Industry Research and Information Association, CIRIA, London, 131 p.
- Hong Kong Geo, 2006. Foundation design and construction. Hong Kong Geotechnical Control Office, No. 1/2006, 376 p.
- Massarsch, K.R., 1994. Settlement analysis of compacted fill. *Proceedings, 13th ICSMFE, New Delhi, January 5-10, Vol. 1, pp. 325-328.*
- Rausche, F., Moses, F., and Goble, G. 1972. Soil resistance predictions from pile dynamics. *American Society of Civil Engineers, J. for Soil Mechanics and Foundation Engineering*, 98(SM9) 917-937.
- Taylor, D.W., 1948. Fundamentals of soil mechanics. John Wiley & Sons, New York, 700 p.

---

<sup>1)</sup> In 2014, the ASCE Journal ceased page numbering, a senseless and regrettable change.

Westergaard, H.M., 1938. A problem of elasticity suggested by a problem in soil mechanics: A soft material reinforced by numerous strong horizontal sheets. In *Contributions to the Mechanics of Solids*, Stephen Timoshenko 60th Anniversary Volume, MacMillan, New York, 260-277 (as referenced by Holtz and Kovacs, 1981).

Data or facts taken from a company report or from personal communication should be referenced. Reference to personal communication is usually included to give due credit to an individual. For example:

Geotechnical Abundance Inc., 2010. Investigation for municipal works, East River, Project 09-10-7432, Report 2010-16, 64 p.

Zhining, B.C., 2010. Personal communication.

Below is the style for the referencing of a CD-type paper, which reference style is based on the Chicago Manual of Style format. No page numbers are needed, simply indicate that it is a CD-ROM.

Tamrakar, S. B., Mitachi, T., Toyosawa, Y., and Itoh, K., 2005. Development of a new soil tensile test apparatus. *Proc., Geo-Frontiers 2005, Site Characterization and Modeling*, ASCE Geotechnical Special Publication, GSP 138 (CD-ROM), ASCE, Reston, VA.

Citations to papers in the body of a manuscript or paper are listed in References section. Occasionally, an author wants to list also relevant papers that were not specifically mentioned in the body. Those are then placed in a separate section called "Bibliography".

There is no convention with regard to spelling out the full name of a journal, e.g., writing "Canadian Geotechnical Journal", or writing it "Can. Geot. J.", but the "American Society of Civil Engineering" is usually abbreviated to "ASCE". The ASCE Journal of Geotechnical and Geoenvironmental Engineering" is sometimes abbreviated to J. of Geot. a. Geoenv. Engng." Mostly, the extent and manner of the abbreviation comes down to whether or not it is necessary for saving a line of text in the Reference section.

### 13.7 Re-use of Figures and Data

The various journals and Editors are getting picky on the copyright issue. All re-used figures must have a copyright release submitted with the manuscript. This even if the "old" figure is from a paper by the author of the manuscript. To avoid this hassle, as it can be, the following is recommended: For your own previously used figures, replot them from your data with some appropriate adjustment to scale and symbols and then cite the source by writing "Data from ...". For figures from others, scan and digitize to extract the data, then, replot. Nobody will contest your use of the original figure, but, strictly, the copyright of the original figure is not fully removed. For that, you will have to add data points not included in the original. As to the citation, again, write: "*Data from ...*". Note while a Google map can be used freely, Google Earth does require a copyright release, which can be very time-consuming to obtain.

### 13.8 Some Useful Unit Conversions

1 millionth of a mouthwash = 1 microscope

The weight one evangelist carries with God = 1 billigram

Basic unit of laryngitis = 1 hoa

Half of a large intestine = 1 semicolon

1,000,000 aches = 1 megahurtz

365.25 days = 1 unicycle

1 million-million microphones = 1 megaphone

1 millionth of a fish = 1 microfiche

2 monograms = 1 diagram



## CHAPTER 14

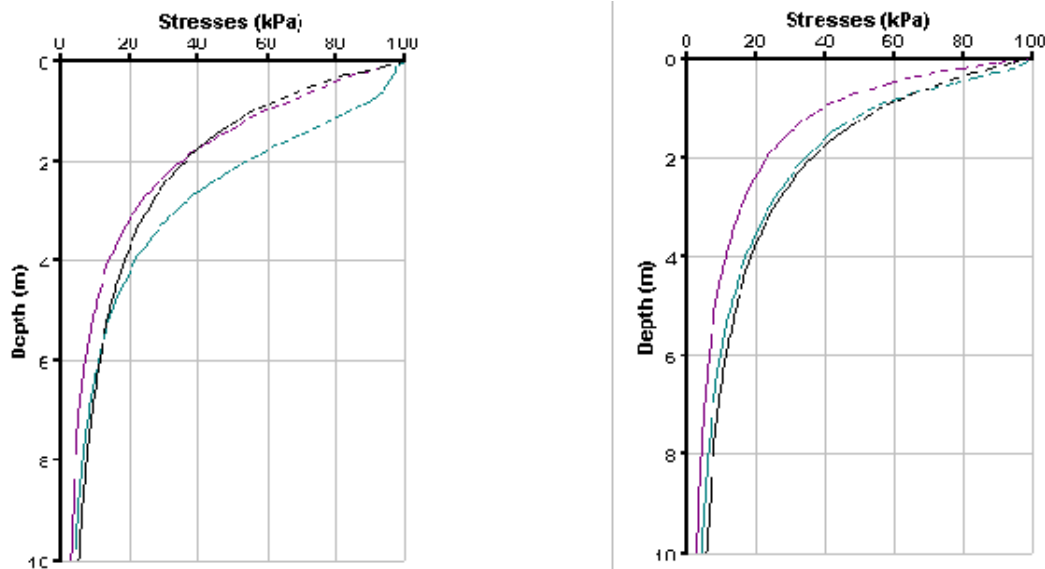
### EXAMPLES

#### 14.1 Introduction

This chapter offers a few examples to the analysis methods. A couple of these have been taken from the example section of the manuals of UniSettle and UniPile. A few have been prepared specially for this text. They can all be solved by hand or by the applicable UniSoft program.

#### 14.2 Stress Calculations

**Example 14.2-01.** Example 1 is intended for a comparison between stresses calculated using all three methods — Boussinesq, Westergaard, and 2:1 — for determining the stress distribution as applied to the center, the corner, and the characteristic point below a square 3.0 m footing loaded by a uniform stress of 40 kPa and placed on the surface of a soil of zero density. The UniSettle manual contains the example in the file called “Example 6 - Square.Unisettle4”. In the two diagrams below, the left diagram shows the stresses below the center of the footing and the right shows the stresses below the characteristic point.



Below the center of the footing, the stresses computed by the 2:1-method and the Westergaard method are very similar and somewhat smaller than the stresses computed by the Boussinesq method. For the stresses below the characteristic point, the stresses computed by the 2:1-method and the Boussinesq method are similar. Of course, the 2:1-method makes no distinction between the points of computation.

The example implies that for single areas, the 2:1-method is as good as the more elaborate methods. The 2:1-method is simple to use in hand calculation, but only rarely does the problem relate to the stresses underneath the footprint of a single area. Therefore, stress calculations in soils will need to be by Boussinesq or Westergaard methods of stress distribution. These days, however, nobody has the time for establishing the detail distribution at a point from several loaded areas using the conventional influence diagram and Newmark's chart (see the next example). A detailed calculation necessitates access to the UniSettle program.

**Example 14.2-2.** The soil profile at a site consists of a 4.0 m thick upper layer of medium sand with a saturated total density of  $2,000 \text{ kg/m}^3$ , which is followed by 8.0 m of clay (density  $1,700 \text{ kg/m}^3$ ). Below the clay, an 8 m thick sand layer (density  $2,100 \text{ kg/m}^3$ ) has been found overlying glacial till (density  $2,300 \text{ kg/m}^3$ ) deposited on bedrock at depth of 23.0 m. The bedrock is pervious. Two piezometers installed at depths of 18.0 m and 23.0 m, respectively, indicate phreatic pressure heights of 11.0 m and 25.0 m, respectively. There is a perched groundwater table in the upper sand layer at a depth of 1.5 m. The water content of the non-saturated sand above the perched groundwater table is 12.6 percent.

Determine the distribution of effective overburden stress and the pore pressure in the soil. (Assume stationary conditions—no consolidation occurs). Compare the distribution of effective stress for the case to stress values calculated for a case with no piezometers and an assumption of hydrostatic distribution below the perched groundwater table at 1.5 m depth.

The first step in the solution is to arrange a soil profile that lists all pertinent values, that is, the thickness and soil density of each layer, as well as the depth to the groundwater table and the pore pressures determined from the piezometer readings. The density of the non-saturated sand above the perched groundwater table is not given directly. However, knowing that the total density is  $2,000 \text{ kg/m}^3$ , and assuming that the solid density is  $2,670 \text{ kg/m}^3$ , phase system calculation will quickly provide the dry density value:  $1,600 \text{ kg/m}^3$  and that the total density for a water content of 12.6 % is  $1,800 \text{ kg/m}^3$ . Use the formulae in Chapter 1.2.

Five soil layers will describe the profile. The key to determining the distribution of effective stress in the soil is realizing that the pore pressure distribution is affected by the existence of three aquifers. First, the perched water in the upper sand, second, the aquifer in the lower sand, and, third, the artesian aquifer in the bedrock below the till. The clay and glacial till layers are impervious in relation to the lower sand layer, which is actually draining both layers resulting in a downward gradient in the clay and an upward in the till. In the sand layers, because of the higher hydraulic conductivity (permeability), the pore pressure distribution is hydrostatic (a gradient of unity). Because of the stationary conditions, the pore pressure distribution, although not hydrostatic, is linear in the clay and the till. Therefore, the information given determines the pore pressures at all layer boundaries and a linear interpolation within each layer makes the pore pressure known throughout the profile. The total stress, of course, is equally well known. Finally, the effective stresses are simply determined by subtracting the pore pressure from the total stress.

A stress calculation done by means of UniSettle, UniPile, or any custom-made spreadsheet program, provides the total and effective stresses and pore pressures at top and bottom of each layer. The calculation results are shown in the following table as “Initial Conditions”. For comparison, the “Final Conditions show the stresses if a hydrostatic distribution of pore pressures is assumed throughout the soil profile. The existence of pore pressure gradients in the soil and more than one aquifer is a common occurrence. Considering the considerable influence pore pressure gradients can bring to bear, it is a conundrum hard to explain why so many in the industry rarely bother about measuring pore pressures other than as the height of water in the borehole, assuming, inanely, hydrostatic conditions throughout the site and profile!

**Example 14.2.1. Results**

Depth (m)	Initial Conditions			Final Conditions		
	Total Stress (kPa)	Pore Stress (kPa)	Eff. Stress (kPa)	Total Stress (kPa)	Pore Stress (kPa)	Eff. Stress (kPa)
-----						
Layer 1	Non-sat Sand		1,800 kg/m <sup>3</sup>			
0.00	0.0	0.0	0.0	0.0	0.0	0.0
1.50	27.0	0.0	27.0	27.0	0.0	27.0
Layer 2	Sand		2,000 kg/m <sup>3</sup>			
GWT 1.50	27.0	0.0	27.0	27.0	0.0	27.0
4.00	77.0	25.0	52.0	77.0	25.0	52.0
Layer 3	Clay		1,700 kg/m <sup>3</sup>			
4.00	77.0	25.0	52.0	77.0	25.0	52.0
12.00	213.0	50.0	163.0	213.0	105.0	108.0
Layer 4	Sand		2,100 kg/m <sup>3</sup>			
12.00	213.0	50.0	163.0	213.0	105.0	108.0
20.00	381.0	130.0	251.0	381.0	185.0	196.0
Layer 5	Till		2,300 kg/m <sup>3</sup>			
20.00	381.0	130.0	251.0	381.0	185.0	196.0
23.00	450.0	250.0	200.0	450.0	215.0	235.0
-----End of data-----						

**Example 14.2-02.** A laboratory has carried out consolidation tests on a postglacial inorganic clay and reports the results as initial and final water contents ( $w_{\text{initial}}$  and  $w_{\text{final}}$ ) being 57.0 % and 50.0 %, respectively, an initial void ratio,  $e_0$ , of 1.44,  $S = 100$  %, and a total density,  $\rho_{\text{total}}$ , of 1,650 kg/m<sup>3</sup>. Do the values make sense?

Phase system calculations show that the values of  $w_{\text{initial}}$  of 57 % and the  $e_0$  of 1.44 combine only if the solid density of the material is 2,620 kg/m<sup>3</sup>, and the  $w_{\text{initial}}$  of 57 % and a void ratio of 1.44 combine only if the total density of 2,520 kg/m<sup>3</sup>. In reality, the solid density is more likely equal to 2,700 kg/m<sup>3</sup>. Then, a water content of 57 % corresponds to  $e_0 = 1.54$  and  $\rho_{\text{total}} = 1,670$  kg/m<sup>3</sup>.

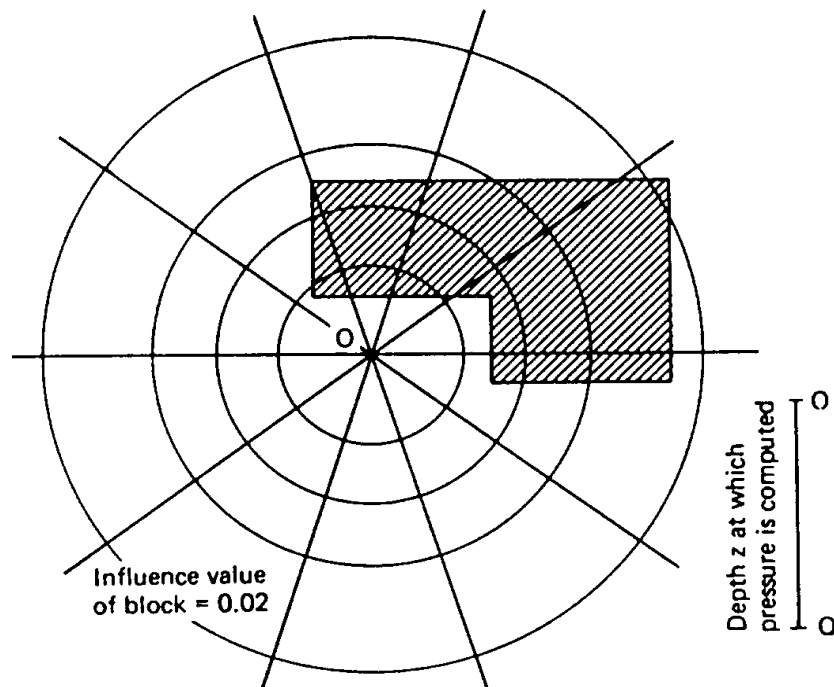
Are the errors significant? Well, the final water content of 50 % corresponds to a final void ratio of either 1.31 ( $\rho_s = 2,620$  kg/m<sup>3</sup>) or 1.35 ( $\rho_s = 2,700$  kg/m<sup>3</sup>). Adjusting the void ratio versus stress curve from the consolidation test, accordingly, changes the  $C_c$ -value from 0.80 to 1.25. This implies a significant error. However, the modulus number is equal to 7 (indicating a very compressible soil) whether based on the originally reported values or on the values adjusted to the proper value of solid density. In this case, the error in  $e_0$  compensates for the error in  $C_c$ .

The example is taken from a soil report produced by a reputable geotechnical engineering firm. Agreed, the errors are not significant. But they are nevertheless errors, and, while it never came about, it would have been a very uncomfortable experience for the responsible engineer under cross examination on the stand to try sound believable to the judge and jury in proclaiming that the errors ‘don’t matter’.

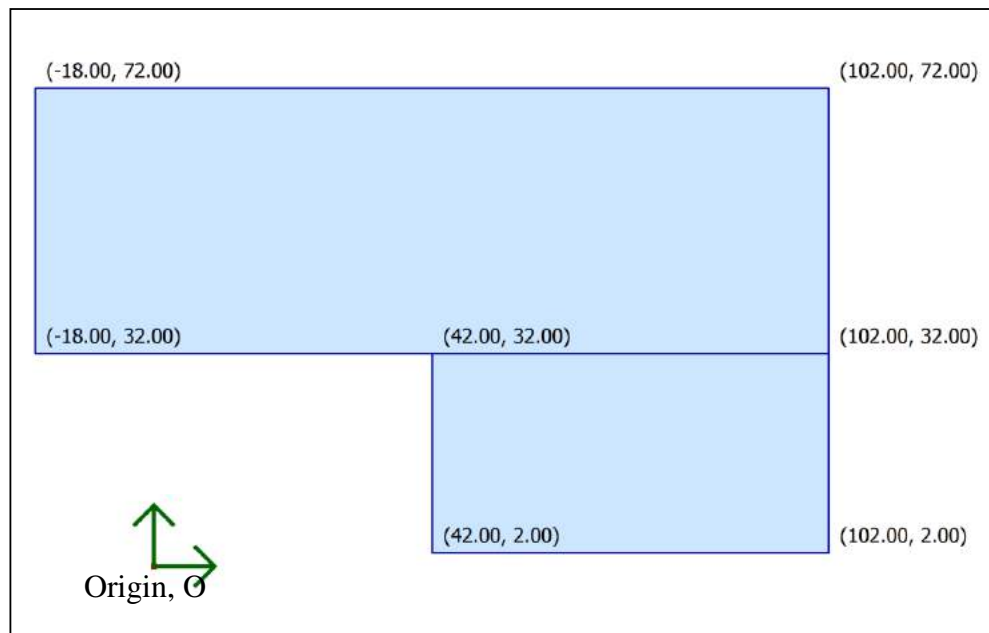
**Example 14.2.3.** Errors in the basic soil parameters are not unusual in geotechnical reports. For example, a laboratory report in my files produced by another company that deals with a sample of about the same type of clay as in Example 14.2.2 lists under the heading of “Determination of Density and Water Content” values of the weights of saturated and dry soil and dish etc., and, finally, the value of the water content as 50.8 % and also, although without showing calculations, the solid, total, and dry density values of  $2,600 \text{ kg/m}^3$ ,  $1,782 \text{ kg/m}^3$  and  $1,184 \text{ kg/m}^3$ , respectively. The two latter values match for calculations using an input of  $S = 100 \%$  and a solid density of  $2,960 \text{ kg/m}^3$ . With the slightly more plausible value of solid density of  $2,600 \text{ kg/m}^3$ , the total, and dry density values are  $1,690 \text{ kg/m}^3$  and  $1,120 \text{ kg/m}^3$ , respectively. Notice that the ratio of the dry density over the total density is 0.66, the same value as the ratio 100% over  $(100\% + 50.8\%)$ , implying accurate values. Yet, the value reported by the geotechnical laboratory for the total density is 5 % too large. Significant? Well, perhaps not very much, but it is a bad start of a foundation design.

**Example 14.2-03.** In illustrating Boussinesq stress distribution, Holtz and Kovacs (1981) borrowed (and converted to SI-units) an example by Newmark (1942): An L-shaped area is loaded by a uniform stress of 250 kPa. (The area is shown below with the dimensions indicated by x and y coordinates). The assignment is to calculate the stress induced at a point located 80 metre below Point O (coordinates  $x = 12 \text{ m}$ ;  $y = 2 \text{ m}$ ), a point well outside the loaded area. Back then, the effort involved using Newmark's nomograms and only one point could be calculated at a time. The plan view below shows the loaded area placed on the Newmark's influence diagram with Point O at the center of the diagram. A hand calculation documented by Holtz and Kovacs (1981), gives the results that the stress at Point O is 40 kPa.

The UniSettle4 manual contains the example in the file called “Example 1 - Newmark Diagram.UniSettle4”.



The following figure shows a plan view produced by UniSettle with the "O", at coordinates x=12; y=2.

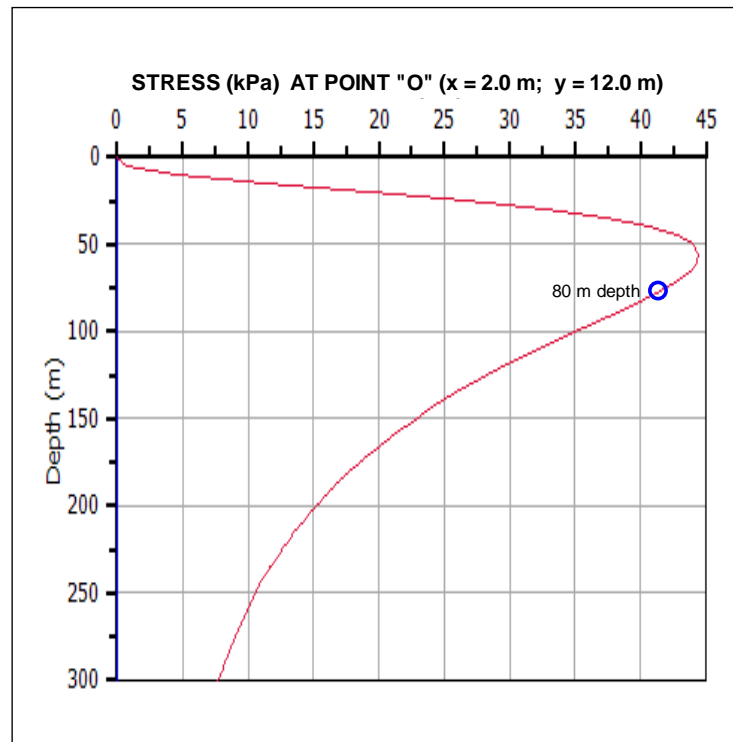


UniSettle shows that the hand calculation is correct; the calculated value of the stress is 40.6 kPa. The full results of the UniSettle calculations are presented in the table and diagram given below; in this case, the stresses at every 5 metre depth from 0 m to 200 m underneath Point O. (The table shows only the values for 75 m, 80 m, and 85 m).

**Stress Analysis - Boussinesq. ( 2 . 12. )**

Depth (m)	Initial Conditions			Final Conditions		
	Total Stress (kPa)	Pore Stress (kPa)	Eff. Stress (kPa)	Total Stress (kPa)	Pore Stress (kPa)	Eff. Stress (kPa)
75.00	0.0	0.0	0.0	41.8	0.0	41.8
80.00	0.0	0.0	0.0	40.6	0.0	40.6
85.00	0.0	0.0	0.0	39.2	0.0	39.2

The diagram presented below shows the vertical stress distribution underneath Point O according to Boussinesq as calculated by UniSettle.

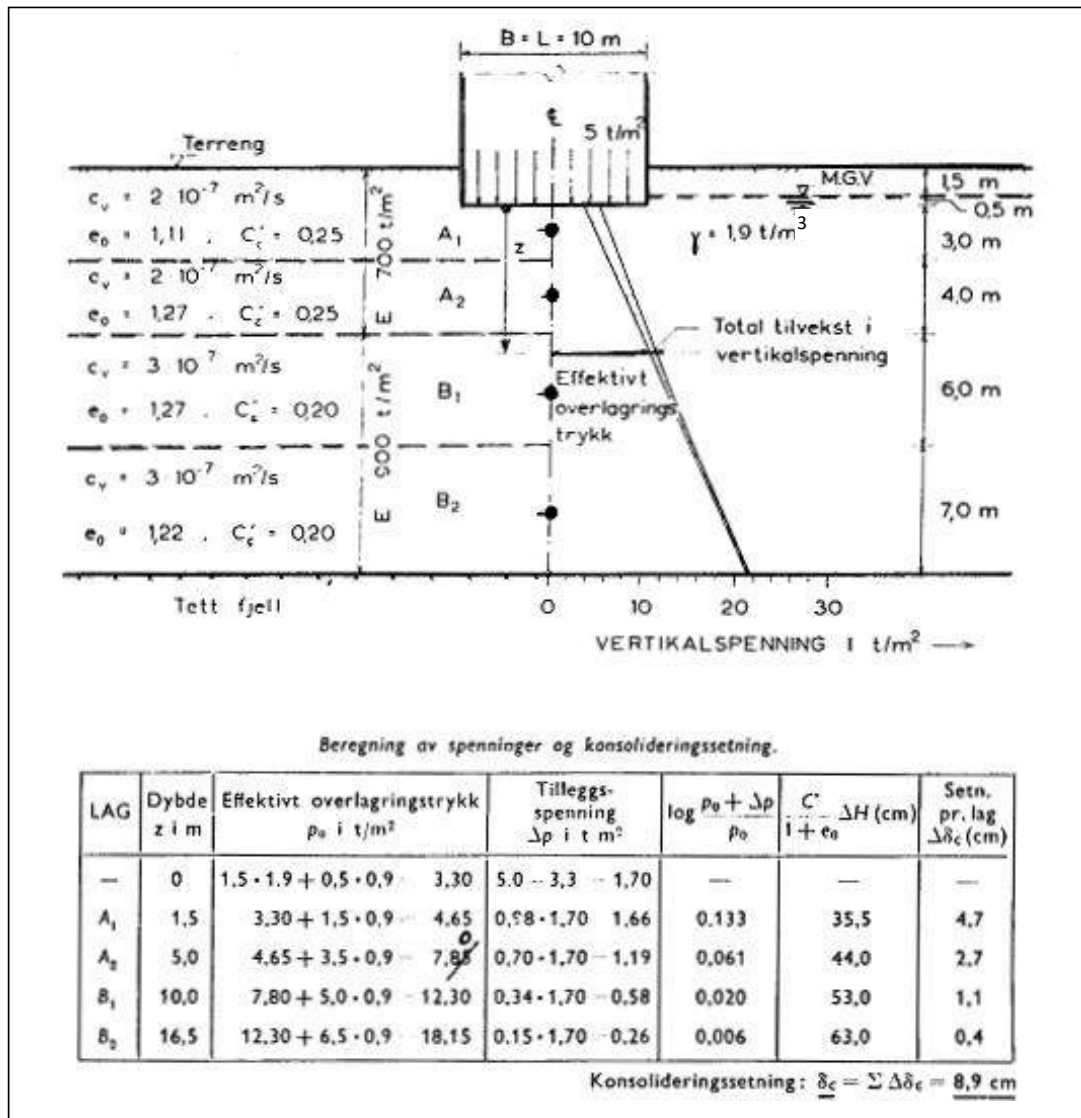


### 14.3 Settlement Calculations

**Example 14.3-01.** is taken from a classic geotechnical text: Norwegian Geotechnical Institute, Publication No. 16, Example 7, (Janbu et al., 1956): The example shows the results of calculations (pre-computer era, so by hand) of settlement for a structure with a footprint of 10 m by 10 m founded at a depth of 2.0 m on 22 m of an inorganic, normally consolidated clay deposited on bedrock, as shown below (copy of the original NGI 16 figure). Boussinesq stress distribution is assigned and the settlement is to be determined below the center of the structure. The initial groundwater table lies at a depth of 1.5 m and the distribution of pore water pressure is hydrostatic. The clay is built up of four layers with the parameters indicated in the below figure. The upper and the lower pair of layers are identical. The split into two pairs is made in NGI 16 to indicate that of the two main layers are split in two for the calculation process.

As a somewhat cheeky comment, a calculation by means of the phase system equations in Chapter 1 of the Red Book shows that the void ratio values of about 1.22 indicated in the figure are not compatible with the 1,900 kg/m<sup>3</sup> value indicated for the total saturated density unless the solid density of the clay particles is about 3,000 kg/m<sup>3</sup>, about ten percent higher than the probable value. The void ratio values combined with the more realistic value of solid density of 2,670 kg/m<sup>3</sup> require a saturated density of about 1,750 kg/m<sup>3</sup>. The 1,900 kg/m<sup>3</sup> value indicated in the figure has been retained in the following, however. (The Reader will have to excuse that also the Norwegian language has been retained; one does not tinker with the classics)!

The UniSettle4 manual contains the example in the file called "Example 2 - NGI 16.UniSettle4".



The original units in "old metric" shown in the figure have been converted to "new metric", i.e. SI units, and the net input of 17 kPa for the stress imposed by the structure (final conditions) has been replaced by an input stress of 50 kPa plus input of final excavation to the 2.0 m depth (i.e., a reduction by 33 kPa). (N.B., because the excavation has the same footprint as the structure, no difference is caused by separating input of load from input of excavation, as opposed to first reducing the imposed stress by the excavation equivalent). The soil layers in the figure are indicated as normally consolidated with compressibility parameters in the format of conventional  $C_c$   $e_0$  parameters. The NGI 16 publication was published in 1956, seven years before the advent of the Janbu tangent modulus approach. The modulus numbers for layers A1, A2, B1, and B2 are 19.4, 20.9, 26.1, and 25.5 (by soft conversion from the  $C_c$ - $e_0$  parameters; usually, modulus numbers are only used as whole numbers).

As given in the figure from NGI 16, settlement calculations result in 89 mm of consolidation settlement below the center of the foundation. The calculation using UniSettle results in 91 mm, which is practically the same. Assigning, say, 0.5 m thick sub layers and calculating using UniSettle reveals that no appreciable gain is achieved from using many sub layers: the settlement value is essentially the same, 93 mm.

The foundation for the structure is probably quite rigid. Therefore, the settlement calculated below the characteristic point ( $x = 3.7$  m;  $y = 3.7$  m) is more representative than below the center: In no time at all, UniSettle can calculate the consolidation settlement for the characteristic point, obtaining a value of 69 mm, about 25 % smaller than the value calculated for a point under the center of the structure (if assumed to be flexible).

Or, suppose that the structure would not be a rigid monolith, but a building with a basement. It is then very unlikely that the groundwater table stays at a depth of 1.5 m also inside the structure; most probably, the groundwater table is lowered at least to a depth of 2.0 m. After changing to a final groundwater table at 2.0 m and assuming hydrostatic distribution below this level, a re-calculation with UniSettle returns a settlement of 106 mm at the center and 91 mm at the characteristic point.

Well, perhaps the effect of lowering the groundwater table is not constant but changes linearly to the original value at bottom of the clay layer (22 m depth). UniSettle now calculates a settlement of 92 mm below the center of the structure and 77 mm at the characteristic point.

The NGI 16 text includes a separate calculation of the immediate settlement, a value of 22 mm is indicated to be added to the consolidation settlement of 89 mm for the example. Whether or not to include a calculation of immediate settlement in a case similar to the subject one can be argued. As can the method to use for its calculation: applying an elastic modulus, or adjusting the compressibility parameters; NGI 16 uses the elastic modulus approach with an E-value of 7,000 kPa for the two upper soil layers and 9,000 kPa for the two lower layers. UniSettle's calculation shows 20 mm for the original input values. (One might also question the magnitude of the immediate E-moduli, but is irrelevant to the example).

The NGI 16 figure also provides values of consolidation coefficient. With these values as input and indicating double-draining layers, then, about 90 % of the consolidation is completed after a year. However, a one-year duration of achieving a 90 % degree of consolidation is optimistic. Applying double drainage condition would mean that full drainage would occur at each clay layer boundary of the 4 to 7 m thick layers. That is, the layers would be assumed to drain into each other with no effect on the consolidation development! At best, the total 22-m soil thickness could be assumed double draining. This would mean that the consolidation time is not one year, but about  $(22/4)^2$  longer, i.e., 30 years. To calculate the development over time of the consolidation, because the upper and lower clay layer pairs are essentially equal, each pair should be turned into a single layer, which now would be single-drained. The assigned coefficients of consolidation now show that 90-% degree of consolidation would require 12 and 15 years, respectively, for the two soil layers. UniSettle calculates the settlement development over time over a hundred year duration. The maximum consolidation settlement is in most cases reached long before hundred years.

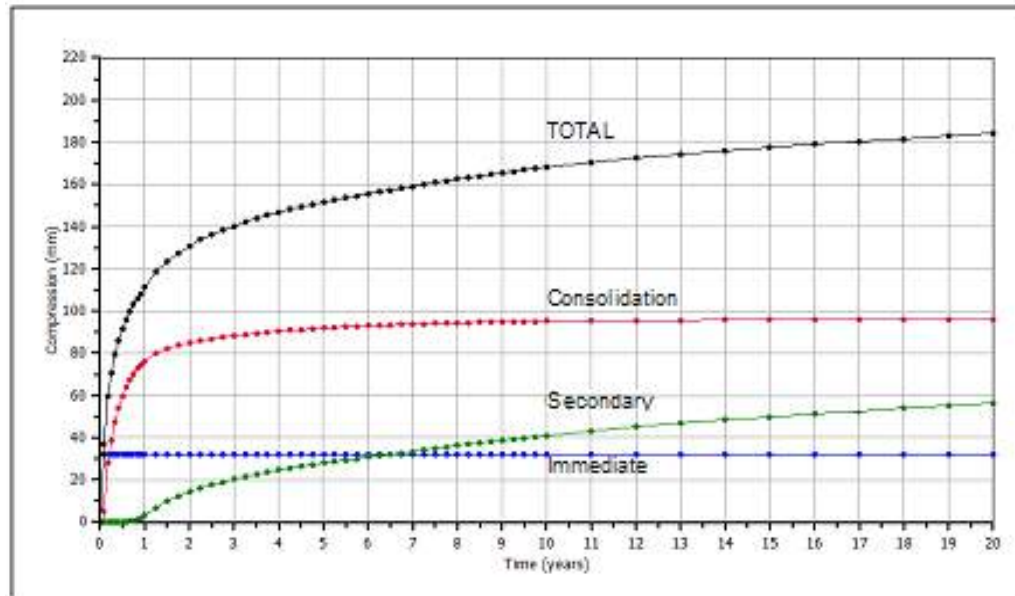
UniSettle calculates also the development over time of the secondary compression. The input required is the start of the consolidation, which is the time for when the first change (increase) occurred in the effective stress distribution, and the length of time for 90 % consolidation to develop. In contrast to the consolidation development, secondary compression continues indefinitely, albeit at a reducing rate. Therefore, UniSettle includes the option of eliminating the report period for the value of secondary compression to show in the results table. The user inputs the duration considered relevant, say 30 years.

The original example does not include values of secondary compression. The question is what coefficient of secondary compression,  $C_{\alpha}$ , to use as input. Some suggest that the coefficient should be in the range of 0.02, which gives a value of 0.005. Moreover, in an inorganic clay, a secondary compression that is larger than the immediate compression will not likely occur within the first about 30 years after the end of the consolidation. The 0.005 value meets this empirical condition.



The largest point of contention is when the secondary compression should be assumed to start. Does it start at the start of the consolidation or at the end of the consolidation? The modern consensus is that it starts when the consolidation is initiated. However, calculation practice is to let it start at the end of the consolidation.

The below figure shows the calculated immediate compression, consolidation settlement, secondary compression, and total settlement versus time for the original NGI 16 input calculated for the center of the excavation. The diagram is plotted after exporting the results to Excel and then plotting the data.



First 50 years of settlements for Example 2 at the center of the foundation

The above time-settlement diagram indicates the start of the secondary compression to be at the point of 90-consolidation. Because secondary compression is only of interest at a time long after the end of the consolidation, its initial portion is normally of little concern. However, a purist might find the initial horizontal portion of the secondary compression curve disturbing. UniSettle provides two ways of making the secondary compression start at the initiation of the consolidation. One "quick and dirty" approach is to input a very short time for the duration of the consolidation and adjust the coefficient so that, say, the 30-year compression is the same as the that for the actual duration. This approach, however, distorts initial portion of the curve. The second approach is to export the results to Excel and shift the secondary compression co

**Example 14.3-02** is also taken from the classic textbook (Terzaghi and Peck 1948): Examples in Chapter V, Articles 35 and 36 (Problems 3 and 1, respectively). The following is the verbatim quote from the book: *A building of very great length has a width of 120 ft. Its weight constitutes a practically uniform surcharge of 5.0 ksf on the ground surface. Between the depths of 70 and 90 ft, there is a layer of soft clay. The rest of the subsoil is dense sand. The soft clay has a natural water content of 45 %. The unit weight of the solids is 168.5 pcf and the total unit weight of the dense sand is 130 pcf. The free water level (groundwater table) is at the ground surface. From the results of consolidation tests, it has been ascertained that the compression index,  $C_c$ , is equal to 0.50.*

Problem 3 in Art 35: *Compute the intensity of vertical stress (using Newmark influence chart) due to the weight of the building at the following points located in a horizontal plane at mid-height of the compressible layer: directly below the edge of the building, 20 ft from the edge toward the center line, 40 ft from the edge toward the center line, and directly below the center line.*

*Answer: 2.30, 2.96, 3.43, 3.57 ksf}.*

Problem 1 in Art 36: *Compute settlements at the edge and center of the building.*

*Answer: 8.5 and 12.3 in.*

Using the information given in the problem texts, phase system calculation provides the void ratio,  $e_0$ , and saturated total density of the clay is determined to 1.21 and 110 pcf, respectively. The void ratio and compression index combine to a Janbu modulus number of 10.

Calculations of the stress using UniSettle returns the following values at the four locations: 2.28, 2.95, 3.40, and 3.56 ksf, respectively, i.e., the same answers as given in Problem 3. Calculations of settlement using UniSettle returns settlements values of 8.59 and 12.32 in., again a full agreement with the text book for Problem 1.

In a real case, it would be of interest to input also the compressibility of the dense sand, say, a modulus number of 300 (30 MPa or 4,350 ksf) and calculate the settlement in the sand. With that compressibility, UniSettle indicates that the sand contributes about an additional 6 inches of settlement. However, the settlement in the sand would develop during the construction and rather soon after its completion, i.e., be "immediate". It is easy to input suitable consolidation coefficients and divide the stress imposed by the building into components constructed at different times to model development of settlement with time. For example, one can model the sand settlement as immediate settlement with an immediate compression modulus,  $E_i$ , of 3,000 ksf, which incorporates also the 'consolidation' settlement of the sand. For completeness, an  $E_i$  of for the clay of 500 ksf is input. To model the consolidation development of the clay, a consolidation coefficient,  $c_v$ , is input as  $6 \times 10^{-8} \text{ m}^2/\text{s}$  ( $1.90 \text{ m}^2/\text{year}$ ;  $20.4 \text{ ft}^2/\text{year}$ ) for the clay. The building stress is modeled as four steps dividing the 5.0 ksf applied stress into four 1.25 ksf steps applied one month apart.

The UniSettle calculated development of settlement for the case is shown in Figure 12.3.2. Such compilations were rarely done in the 1940s. Indeed, they are rarely done today. While in the 1940s, the calculations would have taken a disproportionate amount of time, with UniSettle, all calculations results are now available after a minute or two of input. The UniSettle4 manual contains the example in the file called "Example 3 - Terzaghi-Peck.Uniset4".

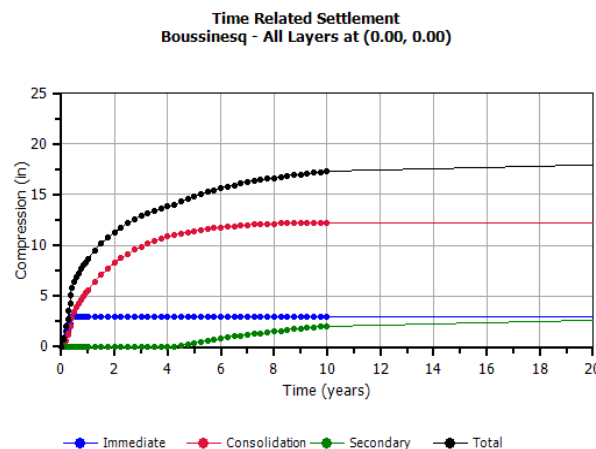
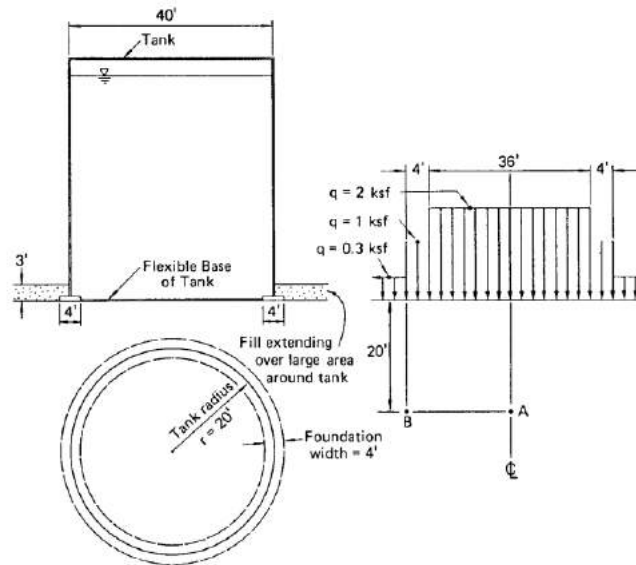
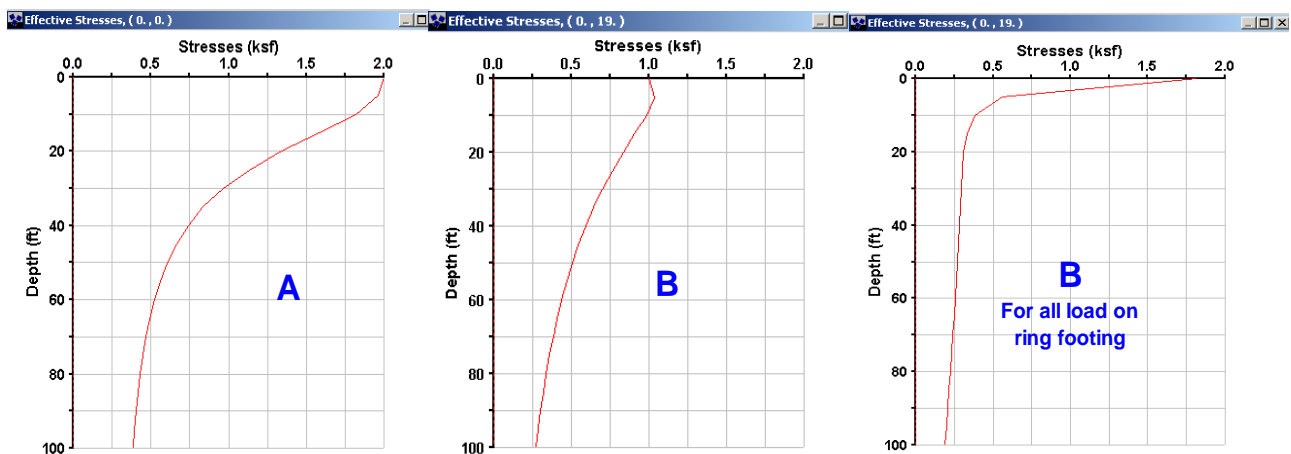


Fig. 14.3-02 Compilation of settlement development over time

**Example 14.3.3-07** is Example 4.4 in Chapter 4 of Perloff and Baron (1976) and presents a 40 feet wide circular water tank on a ring foundation, with fill placed outside the tank and with the tank bottom flexible and resting on the ground, as illustrated below. The assignment is to calculate Boussinesq stress at tank center (Point A) and at the ring at radius 20 ft (Point B) at a depth of 20 feet for both points. The input file shows the input of the stress from the surcharge and the tank as three overlapping areas. Area 1 is Surcharge of 0.3 ksf all over site, Area 2 is the 4 ft wide ring foundation for the tank structure with inside and outside radii of 18 ft and 22 ft with a uniform stress of 1.0 ksf. Area 3 is stress from the water inside the tank which has a radius of 18 ft and a uniform stress of 2.0 ksf. The stresses at the 20 ft depth calculated for A and B are 1.37 ksf and 0.84 ksf, respectively. The UniSettle4 manual contains the example in the file called “Example 4 - Ring Tank.Unisettle4”.



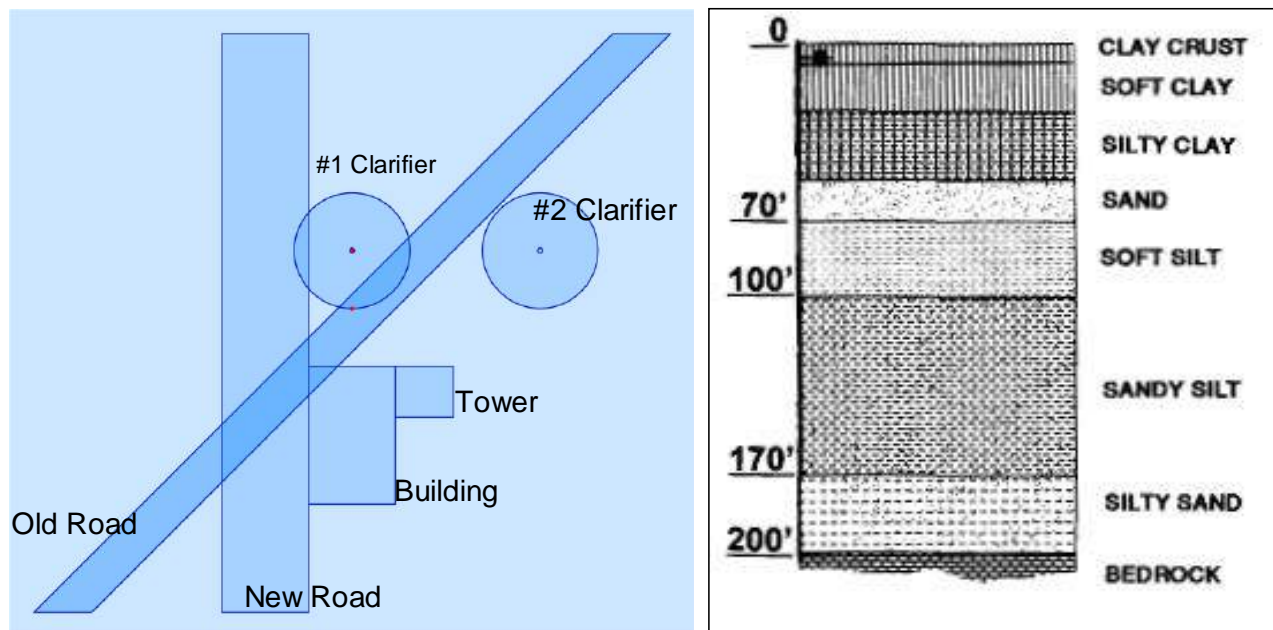
The example is interesting because it pertains to a realistic case and tempts to several what-if studies. So, what if the base of the tank would not flexible, but stiff so that all the tank loads go to the ring foundation (no surcharge is placed under the tank)? What then about the stresses at A and B? And, what about settlements? Make up a soil profile with suitable values of density and modulus numbers, etc. and try it out.



Well, the calculated settlement may actually not change much, but will the ring footing be stable?

**Example 14.3.4-08** This example is taken from the real world: A sewage treatment plant (or part of one) will be built in a low lying area, where the upper about 170 feet of soil is compressible. The clay soils are overconsolidated. The perched groundwater table will reduce following the construction, but the phreatic heads in the two aquifers will remain unchanged. One is slightly artesian, . An existing old road ( $q = 0.19$  ksf) crossing the area will be removed and replaced with a new road ( $q = 0.63$  ksf). The entire area will have to be raised about 1.5 ft by a general surcharge ( $q = 0.12$  ksf). The structures to build are two clarifiers ( $q = 1.8$  ksf), an administration building ( $q = 4.0$  ksf), and an office tower ( $q = 10.0$  ksf). The detailed soil profile is indicated on the borehole log. The UniSettle4 manual contains the example in the file called “Example 5 - Multi structures.Unisettle4”.

The task for the foundation design is to determine if the clarifiers can be placed on grade or not. The file is prepared for calculating the settlement in the center and edge of Clarifier No. 1. The calculation returns a total settlement of 4.8 in and a differential of 1.5 in. Depending on structural conditions and pipeline connections, etc., this much differential settlement can probably be accepted.



The building and the tower will require pile foundations. The question is how deep must the piles be installed to ensure that settlements will be no more than an inch? UniSettle can provide an immediate answer if the foundation depth of the building (and the tower, in turn) is changed from the 4 feet assigned in the file for a suitable depth for an equivalent footing. When details of the pile groups and loads have been decided (the UniPile program will be indispensable for this purpose), UniSettle can perform the necessary settlement calculations with full control of the contributory effects of the adjacent fill and structures.

Further calculation results are not presented here. The UniSettle file “Example 5 - Multi structures.Unisettle4” contains all the input and the User can phrase the relevant settlement questions and practice computing the answers. Notice that the general surcharge has been assigned a constant vertical stress distribution. Because its wide breadth and length, a Boussinesq distribution would have required a precision of about 1.0 ft to generate correct values, which would have required excessive computation time.

## 14.4 Earth Stress and Bearing Capacity of Retaining Walls

**Example 14.4-01** Taylor's unsurpassed textbook "Fundamentals of Soils" (Taylor, 1948) contains several illustrative examples on earth stress and bearing capacity of retaining walls. The first example quoted is a simple question of the difference in the earth stress coefficient when considering as opposed to disregarding that the ground surface behind a wall is sloping  $20^\circ$  (1(H):0.36(V)). The problem assumes Rankine earth stress (that is, wall friction angle is zero). Taylor writes: *"Determine the percentage error introduced by assuming a level fill when the slope angle actually equals 20 degrees. Assume a friction angle of 35 degrees and a vertical wall."* A computation using UniBear<sup>1</sup> shows that the earth stress coefficient,  $K_a$ , is 0.27 for the level backfill and 0.34 for the sloping backfill. The error in disregarding the slope is a 20 % underestimation of the magnitude of the earth stress.

**Example 14.4-02** Taylor (1948) includes an example asking for the difference in earth stress coefficient between a wall leaning away from the soil as opposed to leaning toward the soil. The leaning (inclination) is 2 inches per foot, the soil density is 100 pcf, the friction angle is 35 degrees, the ground surface is level, and there is no wall friction. Computation shows that the  $K_a$ -coefficient is 0.33 for an inclination away from the backfill soil and 0.18 for leaning toward the backfill. The  $K_a$ -coefficient for a vertical wall is 0.25. Obviously, the inclination of the wall should not be disregarded in a design analysis.

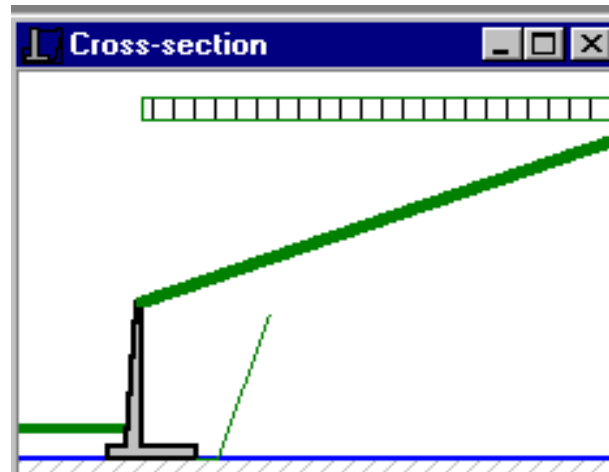
**Example 14.4-03** Taylor (1948) also deals with a 25 feet high concrete gravity wall (density 150 pcf) with a 4-foot width at the top. The inside face of the wall is vertical and the wall retains soil with a 35-degree friction angle and a density of 100 pcf. The wall friction angle is 30 degrees and the cohesion intercept is zero. Taylor asks for the required width of the wall if the resultant has to be located exactly in the third point of the base considering the case of (1) no wall friction and (2) wall friction included. He also asks for the base stresses and the safety against sliding. Taylor's text uses the Terzaghi original approach to the bearing capacity coefficients. A diagram in the book indicates that the  $N_q$ ,  $N_c$ , and  $N_\gamma$  coefficients are about 22, 37, and 21 for  $\phi = 30^\circ$ . According to the expressions by Meyerhof, the coefficients are 33, 36, and 44, respectively, and according to the expressions by Caquot and Kerisel, they are 33, 36, and 48, respectively. For the Caquot and Kerisel coefficients, for example, UniBear computes a necessary base width of 9.5 feet for the case of no wall friction on the condition that the resultant lies in the third point. The factor of safety on sliding is 2.09, which is adequate. However, the factor of safety for bearing is a mere 1.11, which is not adequate. Kind of a sly example, is it not?

The disregard of wall friction is not realistic, which perhaps is what Taylor intended to demonstrate. N.B., Taylor did not 'correct' for inclined load. When the wall friction is included, the numbers change considerably and even allow a reduction of the wall base width to 5 feet with adequate factors of safety for both sliding and bearing. As the wall has no footing, including wall friction is appropriate.

**Example 14.4-04** The following cantilever wall example is quoted from The Civil Engineering Handbook (Chen and McCarron, 1995): The wall is 7.6 m high and wall retains a sand soil with a  $\phi' = 35^\circ$  and a density of  $1,900 \text{ kg/m}^3$ . The wall friction is indicated as equal to the soil friction. The ground surface slopes upward and the slope is stated both as  $24^\circ$  and as 1 m over a distance of 2.8 m, that is, an angle of  $19.7^\circ$ . Both values are used in the calculations in the book. The applicable allowable bearing stress is stated to be 360 kPa. The location of the groundwater table is not mentioned in the book. It is therefore assumed to be well below the footing. A 0.6 m surcharge on the ground surface of soil with the same density as the backfill is included.

---

<sup>1</sup> Since 2009, the UniBear software, being inoperable under Windows 7 and later systems, is no longer marketed



The calculations in the book estimate  $K_a$  from the 24-degree slope combined with a nomogram based on logarithmic spiral calculations to be 0.38, as opposed to 0.33 according to the usual Coulomb relation.

The calculations by Chen and McCarron (1995) are made with some effort-saving minor simplifications and the book gives the total gravity force as 614 kN/m and the horizontal and vertical (wall friction component) earth stress forces as 301 kN/m and 211 kN/m. Computations using UniBear result in 669 kN/m, 315 kN/m, and 220 kN/m, respectively. A good agreement. The small difference lies in that UniBear allows including also the outside surcharge on the footing toe in the calculation of the gravity forces.

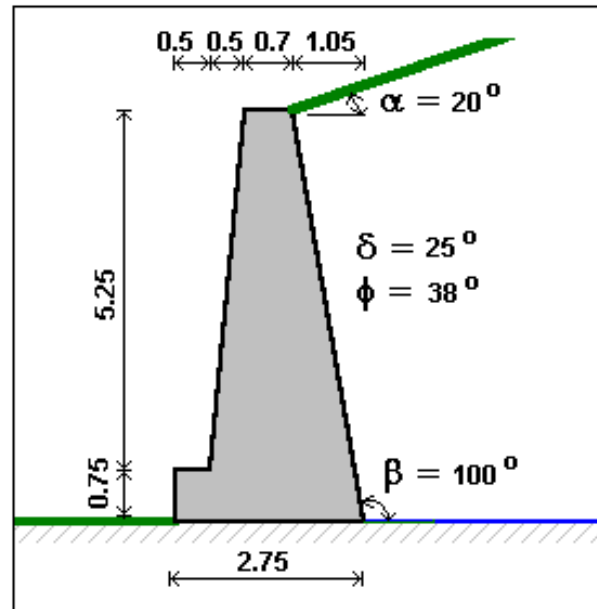
The book adds the gravity vertical force and the earth stress vertical forces to a total vertical force of 25 kN, and uses this value to calculate the sliding resistance to  $825 \text{ times } \tan 35^\circ = 578 \text{ kN/m}$ . UniBear calculates 890 kN/m and 670 kN/m, which are about the same values. The book gives an eccentricity of 0.25 m, UniBear 0.30 m. The book gives a sliding ratio of 1.9, UniBear 2.1. The differences are slight and the values would appear to indicate a safe situation.

However, it is principally incorrect to calculate the earth stress using full wall friction on a cantilever wall. A UniBear calculation applying a zero wall friction results in an eccentricity of 1.4 m and a sliding ratio of 1.3. Neither is acceptably safe.

A further difference is that the textbook determines a maximum edge stress of 245 kPa for the full base width without considering the eccentricity and compares this to the allowable bearing, 360 kPa (the 360 kPa-value must be including a factor of safety). In contrast, UniBear determines the average stress over the equivalent footing and compares this to the allowable stress (WSD design). The particulars of the bearing soil were not given. With the assumption that the soil under the base is the same as the backfill, that the groundwater table lies at the base, and that the Meyerhof coefficients apply, the computations result in a bearing resistances of 580 kPa and a factor of safety of only 1.4.

**Example 14.4.5.** Example 14.4.5 is quoted from a soil mechanics textbook (Craig 1992). The example consists of a simple gravity wall as illustrated below and the text asks for the sliding resistance and the maximum and minimum stresses underneath the footing. The densities of the wall and of the backfill are  $2,350 \text{ kg/m}^3$  and  $1,800 \text{ kg/m}^3$ , respectively. The soil has friction only and  $\phi'$  and  $\delta'$  are equal to  $38^\circ$  and  $25^\circ$ , respectively. The wall slope angle,  $\beta$ , is  $100^\circ$  and the ground slope angle,  $\alpha$ , is  $20^\circ$ .





The textbook indicates that the earth stress coefficient is 0.39, which is calculated assuming that the earth stress acts on the wall with full wall friction present. The calculated horizontal and vertical components of the earth stress are 103 kN/m and 72 kN/m, respectively. The weight of the structure is 221 kN/m and the resultant is located 0.98 m from the toe. The eccentricity is 0.40 m or about 15 % of the footing width. That is, the resultant lies within the middle third. The calculated sliding ratio is 1.33, which is somewhat low.

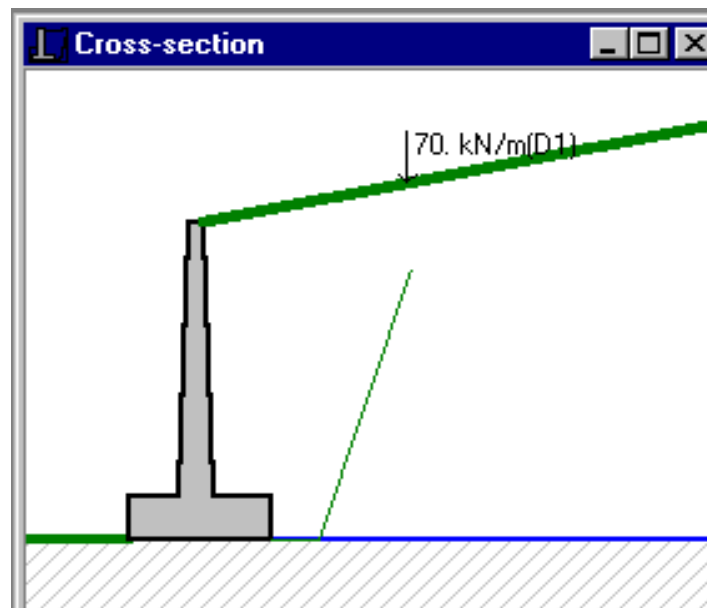
If the calculations are made for the earth stress acting against a normal rising from the heel of the footing and, therefore, with zero wall friction, an earth stress coefficient results of 0.29 and the horizontal component of the earth stress is 108 kN/m, which is close to the textbook's calculated value. The earth stress has no vertical component, but the weight of the backfill wedge on the wall (61 kN/m) is included in the analysis. It is about equal to the vertical component of the earth stress (72 kN/m) calculated by the textbook, so the new vertical force is essentially unchanged. The sliding ratio is 1.22, slightly smaller than before. A six-of-one-and-half-a-dozen-of-another case, is it? However, the resultant is not in the same location and the new eccentricity is 0.54 m or about 20 % of the footing width. That is, the resultant lies outside the middle third of the footing and this is not a safe situation. The UniBear approach is recommended for actual design situations.

The maximum and minimum stresses,  $q_{\max}$  and  $q_{\min}$  can be calculated from the following expression with input of the footing width,  $B$ , and eccentricity,  $e$ . For  $q_{\max}$  use the plus sign and for  $q_{\min}$  use the minus sign.

$$q_m = \frac{Q_v}{B} \left( 1 \pm \frac{6e}{B} \right)$$

Notice, the expression builds on that the stress distribution can be assumed to be linear. However, once the resultant lies outside the middle third, this is not a valid assumption.

**Example 14.4.6.** Example 14.4.6 demonstrates the influence of a line load. The case is taken from a text book by Bowles (1992) and presents a cantilever wall with a sloping ground surface and a 70-kN line load on the ground surface. The footing thickness and width are 1.0 m and 3.05 respectively (no information is given on the density of the wall, regular concrete density is assumed). The stem thickness is 0.73 m at the footing, 0.30 m at the top, and the stem height is 6.1 m. The ground surface slopes 5H:1V. The soil density is  $1,745 \text{ kg/m}^3$ , and the soil and wall friction angles are equal and  $35^\circ$ . The textbook requests the active earth stress and its point of application. The textbook gives the answer to the problem as "an earth stress of 164 kN/m acting  $58.6^\circ$  from the horizontal" (probably intending to say "vertical").



UniBear calculates a horizontal component of the backfill earth stress of 147 kN/m and the total horizontal stress from the line load of 31 kN/m, together 178 kN/m, not quite the value given in the textbook. However, these values are obtained using a wall friction of zero degrees, which as mentioned is recommended for cantilever walls. A calculation with the wall friction equal to the soil friction,  $35^\circ$ , results in horizontal and the vertical earth stress components of 112.5 kN/m and 78.75 kN/m, respectively. The sum of the horizontal components of the line load and earth stress is equal to 143.6 kN/m. The resultant to this load and the vertical earth stress is 164 kN, the same as given in the textbook. The angle between this load and the normal to the footing, the "vertical", is  $61^\circ$ , very similar to that given in the textbook.

Notice, that UniBear also calculated the vertical component of the line load that acts on the heel. For the subject example, it is 5 kN/m. Before UniBear, it was rather cumbersome to include this component and it was usually omitted. For reference to old analysis cases involving surface loads, some may desire to exclude the effect of this vertical component. This can be easily done by imposing a vertical line load on the footing that is equal on magnitude to the vertical component of the surface line load and which acts at the same distance from the toe but in the opposite direction.



## 14.5 Pile Capacity and Load-Transfer

**Example 14.5-01** In 1968, Hunter and Davisson presented an important paper on analysis of load transfer of piles in sand. The paper was the first to show measurements of residual forces in full-scale tests, and that such forces will greatly affect the load transfer evaluated from load measurements in a static loading test (as was postulated by Nordlund 1963). The case history demonstrates that residual force is not restricted to piles in clay but will develop also for piles in sand. The findings were later confirmed by the case history reported by Gregersen et al. (1973). Indeed, the two cases show that a drag force will also develop for piles in sand.

The tests were performed in a homogeneous deposit of “medium dense medium to fine sand” with SPT N indices ranging from 20 through 40 (mean value of 27) and a bulk saturated density of the sand of 124 pcf. The groundwater table was at a depth of 3 ft (hydrostatic pore pressure distribution can be assumed). Laboratory tests indicated an internal friction angle in the range of 31 degrees through 35 degrees. The friction angle for a steel surface sliding on the sand was determined to 25 degrees.

Static loading tests in push (compression test) followed by pull (tension test) were performed on six piles instrumented with strain gages and/or telltales. The piles were all installed an embedment depth of 53 ft and had a 2-foot stick-up above ground. The detailed test data are not included in the paper, only the total load and the evaluated toe loads (in both push and pull).

Pile #	Type	Shaft area (ft <sup>2</sup> /ft)	Toe area (ft <sup>2</sup> )	Installation manner
1	Pipe 12.75”	3.96	0.98	Driven; Vulcan 140C

The shaft cross section area includes the areas of guide pipes and instrumentation channels. The shaft surface area of the H-pile is given as the area of a square with a side equal to the flange width.

The paper does not include the load-movement curves from the static loading tests, only the evaluated ultimate resistances. The following table summarizes the ultimate resistances (pile capacities) and the toe resistances evaluated from the tests.

Pile #	Push Test			Pull Test		Adjusted Push	
	$R^{ult}$ (kips)	$R_s$ (kips)	$R_t$ (kips)	$R_s$ (kips)	‘ $R_t$ ’ (kips)	$R_s$ (kips)	$R_t$ (kips)
1	344	248	96	184	-74	174	170

The table data indicate that the piles were subjected to a negative (-74 kips) toe resistance during the pull test, which, of course, is not possible. (It would mean that there was someone down there holding on and pulling the other way). The negative toe resistance observed is due to residual force induced in the pile caused by the pile installation and the preceding push test. If the 184-kip resistance measured in the pull test is taken as the true shaft resistance, the true toe resistance would be 160 kips (344 - 184).

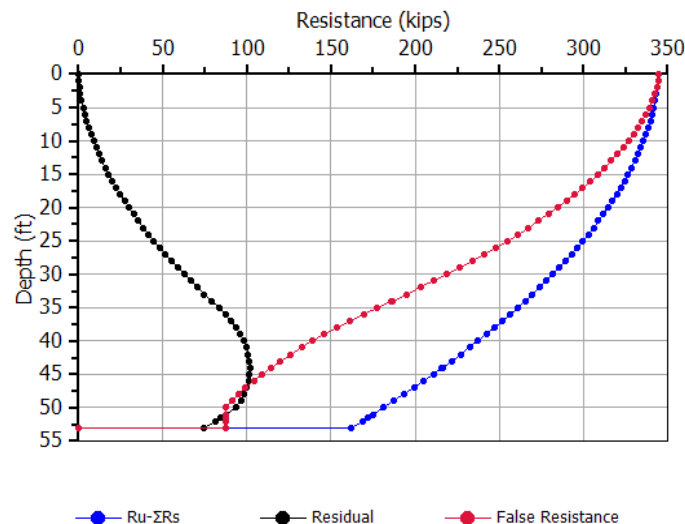
Hunter and Davisson (1969) adjusted the data for the push test by increasing the toe load by a value equal to the 74-kip apparent negative toe load of the pull test and decreasing the shaft resistance correspondingly— linearly to the pile head. The so adjusted values are shown in the two rightmost columns above.

The paper reports the effective stress parameters in a beta-analysis matched to the data. These data have been compiled in the table below and used as input to the UniPile program<sup>2)</sup> together with the soil and pile data as given above. The results of the UniPile computations are included in the table.

Pile #	Input Values		UniPile Analysis		
	$N_t$ (--)	$\beta$ (--)	$R^{ult}$ (kips)	$R_t$ (kips)	$R_s$ (kips)
1	53	0.50	377	194	183

The paper concludes that there is a difference in shaft resistance in push and pull as indicated by the different beta-coefficients evaluated from the push and pull tests. However, a review of the data suggest that the beta-coefficient determining the shaft resistance lies in the range of 0.45 through 0.52 for the piles and that the shaft resistance is about the same in push and pull. A “perfect” match to the 344-kip total resistance and the shaft and toe resistances of 184 and 160 kips (165-ksf), respectively, is achieved using a  $\beta$ -coefficient of 0.47 and an  $N_t$ -coefficient of 47. However, the purpose of this account is not to discuss the merits of details given in the paper, but to use the data to demonstrate the load-transfer analysis. The significance of the paper is the clear demonstration that the influence of residual forces must be included in the evaluation of pile test data.

The amount and distribution of residual force in a pile can be calculated by the same effective stress approach as used for matching the test data. A computation of Pile 1 with a residual force portion of 46 % of the toe resistance results in a computed residual toe resistance of 74 kips, which would mean that the “negative toe resistance” is close to what the authors reported in the paper. The corresponding “false shaft and toe resistances” are 258 and 88 kips, respectively. The diagram presents the push-test load transfer curves for the True Resistance, the Residual Force, and the False Resistance distribution curves as determined using the UniPile program.



<sup>2)</sup> For information on the program, visit <https://www.unisofltd.com>

**Example 14.5-02** Altaee et al., 1992 presented results and analysis of an instrumented 285 mm square precast concrete pile installed to an embedment of 11.0 m into a sand deposit. Three sequences of push (compression) testing were performed, each close to the ultimate resistance of the pile followed by a pull (tension) test. The instrumentation registered the loads in the pile during the static push testing, but did not provide accurate data during the pull test. During the push test, the groundwater table was at a depth of 6.2 m. During the pull test, it was at 5.0 m. The maximum load applied at the pile head was 1,000 kN, which value was very close the capacity of the pile. The pull test ultimate resistance was 580 kN.

The paper reports both the soil parameters and the magnitude of the residual loads affecting the test data. The effective stress parameters are as follows.

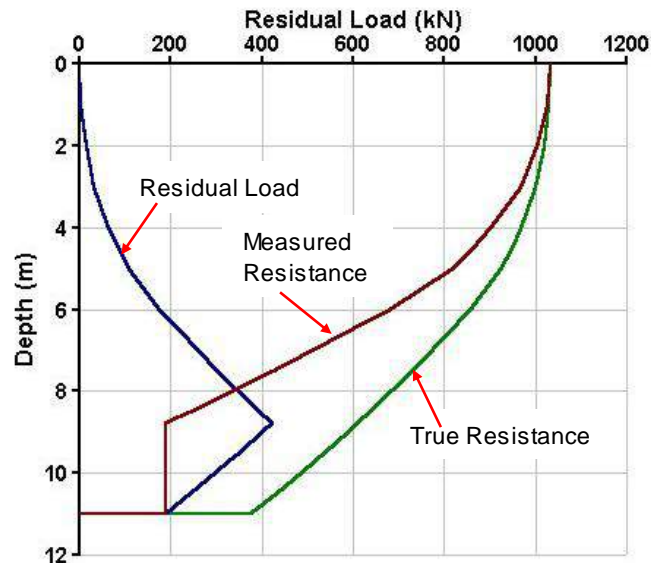
Layer	Depth	Total	$\beta$	$N_t$
--	(m)	Density (kg/m <sup>3</sup> )	--	--
Silt-Sand	0.0 - 3.0	1,600	0.40	--
Dry Sand	3.0 - 5.0	1,800	0.50	--
Moist Sand	5.0 - 6.5	1,900	0.65	--
Sat. Sand	6.5 - 11.0	2,000	0.65	30

The data have been used as input to a UniPile computation returning a capacity value of 1,034 kN, which is acceptably close to the measured load of 1,000 kN. The table below shows the computed results. The first column shows the computed resistance distribution (at ultimate resistance). The second column shows the results of a residual load computation with 50 % utilization of  $N_t$  (as matched to the data reported in the paper). The column headed "False Resistance" is obtained as the difference between the first two. A comparison with the recorded test data, shown in the far right column, indicates clearly that the data recorded during the test are affected by residual load. The small differences in agreement can easily be removed by inputting the soil parameters having the precision of an additional decimal.

DEPTH (m)	RES.DISTR. (kN)	RES.LOAD (kN)	FALSE RES. (kN)	TEST (kN)
0	1,034	0	1,034	1,000
4.5	948	85	863	848
6.0	856	177	679	646
7.5	732	302	430	431
9.0	591	(402)	~300	309
10.0	487	299		
10.5	433	245	188	191
11.0	376	188		

The computations assume that the change between increasing residual load (negative skin friction zone) to decreasing (positive shaft resistance zone) is abrupt (appearing as a 'kink' in the curve). In reality, however, the shift between the relative movement from negative and to positive directions occurs in a transition zone. For the tested pile, the analysis shows that this zone extends from about 1.0 m above the neutral plane (Depth 9.7 m) to about 1.0 m below the neutral plane. Therefore, the computed residual load at the Depth 9.0 m is overestimated, which is why it is given in parenthesis in the table. Instead, the residual load between 8.0 m and 12.5 m is approximately constant and about 300 kN. The about 2.0 m length of the transition zone corresponds to about 7 pile diameters in this case history.

The computed shaft resistance in the push test is 657 kN. Repeating the computation for “Final Conditions”, that is, with the groundwater at 5.0 m, the shaft resistance is 609 kN, again acceptably close the tested pull capacity (580 kN). Besides, the analysis of the test data indicates that a small degradation of the shaft resistance occurred during the push testing. Considering the degradation, the shaft resistances in push and pull are essentially of equal magnitude. The load-transfer curves are shown in the following diagram (the calculations do not include input of transition zone height).



**Example 14.5-03** The following example is a case history also obtained from the real world. However, in the dual interest of limiting the presentation and protecting the guilty, the case has been distorted beyond recognition. A small measure of poetic license has also been exercised. The example is from a foundation course that I used to give at University of Ottawa, where the students not only studied foundation analysis and design but also practiced presenting the results in engineering report. Therefore, the solution to the assignment was to be in the format of a consulting engineering letter report.

**Letter to Engineering Design and Perfection Inc. from Mr. So-So Trusting, P. Eng., of Municipal Waterworks in Anylittletown**

*Dear Sir: This letter will confirm our telephone conversation of this morning requesting your professional services for analysis of the subject piling project with regard to a review of integrity and proper installation procedure of the New Waterworks foundation piles.*

*The soil conditions at the site are described in the attached Summary of Borehole Records. These data were obtained before the site was excavated to a depth of 4.0 m. The piles are to support a uniformly loaded floor slab and consist of 305 mm (12 inch), square, prestressed concrete piles. The piles have been installed by driving to the predetermined depth below the original ground surface of 12.0 m (39 ft). The total number of piles is 700 and they have been placed at a spacing, center-to-center, of 2.0 m (6.5 ft) across the site.*

*An indicator pile-testing programme was carried out before the start of the construction. The testing programme included one static loading test of an instrumented test pile. Plunging failure of the test pile occurred at an applied load of 2,550 kN (287 tons) and the measured ultimate shaft resistance acting on the pile was 50 kN (6 tons) in the upper sand layer and 400 kN (45 tons) in the lower sand layer. The measured ultimate toe resistance was 2,100 kN (236 tons).*

*Relying on the results of the indicator test programme, our structural engineer, Mr. Just A. Textbookman, designed the piles for an allowable load of 1,000 kN incorporating a safety factor of 2.5 against the pile capacity taken as 2,500 kN (the 50-kN resistance in the upper sand layer was deducted because this layer was to be removed across the entire site after the pile driving).*

*The contractor installed the piles six weeks ago to the mentioned predetermined depth and before the site was excavated. The penetration resistance at termination of the driving was found to be about 130 blows/foot, the same value as found for the indicator piles.*

*After the completion of the pile driving and removal of the upper 4.0 m sand layer, our site inspector, Mr. Young But, requested the Contractor to restrike two piles. For both these piles, the blow count was a mere 4 blows for a penetration of 2 inches, i.e., equivalent to a penetration resistance of 24 blows/foot! A subsequent static loading test on one of the restruck piles reached failure in plunging when the load was being increased from 1,250 kN to 1,500 kN. We find it hard to believe that relaxation developed at the site reducing the pile capacity (and, therefore, also the penetration resistance) and we suspect that the piles have been broken by the contractor during the excavation work. As soon as we have completed the change-order negotiations with the contractor, we will restrike additional piles to verify the pile integrity. Meanwhile, we will appreciate your review of the records and your recommendations on how best to proceed.*

*Sincerely yours,*

*Mr. So-So Trusting, P. Eng.*

#### SUMMARY OF BOREHOLE RECORDS

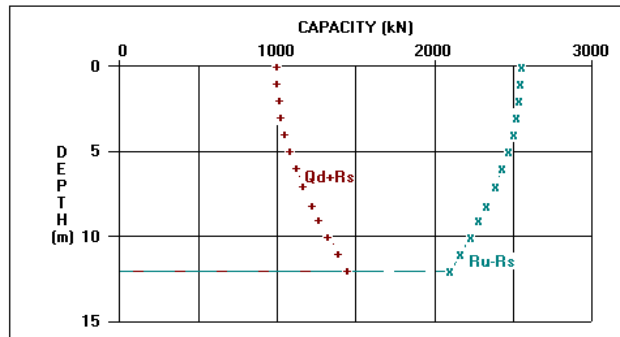
The soil consists of an upper layer of loose silty backfill of sand with a density of 1,700 kg/m<sup>3</sup> (112 pcf) to a depth of 4 m (13 ft) and placed over a wide area. The sand is followed by a thick deposit of compact to dense clean sand with a density of 2,000 kg/m<sup>3</sup> (125 pcf) changing to very dense sand at about 12.0 m (31 ft), probably ablation till. The groundwater table is encountered at a depth of 5.0 m (15 ft).

**Comments** Hidden in Mr. Trusting's letter is an omission which would cost the engineers in an ensuing litigation. The results of the two static tests were not analyzed! An effective stress analysis can easily be carried out on the records of the indicator pile test to show that the measured values of shaft resistance in the upper and lower sand layers correspond to beta ratios of 0.30 and 0.35, respectively and that the toe coefficient is 143 (the actual accuracy does not correspond to the precision of the numbers).

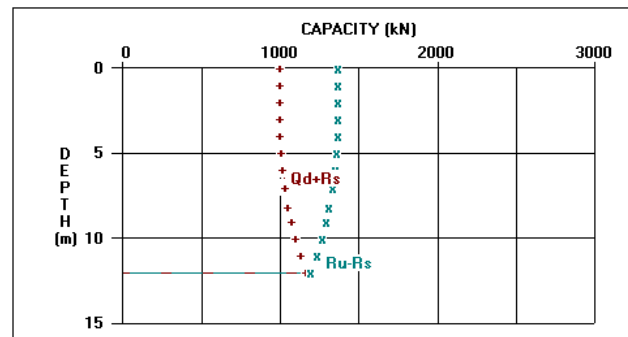
Had Mr. Trusting performed such an analysis, he would have realized that excavating the upper sand layer not only removed the small contribution to the shaft resistance in this layer, it also reduced the effective stress in the entire soil profile with a corresponding reduction of both shaft and toe resistance. In fact, applying the mentioned beta ratio and toe coefficient, the shaft and toe resistance values calculated after the excavation are 170 kN (19 tons) and 1200 kN (135 tons), respectively, to a total capacity of 1,366 kN (154 tons), a reduction to about half the original value. No wonder that the penetration resistance plummeted in restriking the piles! (Notice that the reduction of toe resistance is not strictly proportional to the change of effective overburden stress. Had the load-movement curve from the static loading test been analyzed to provide settlement parameters, a load-movement curve could have been determined for the post-excavation conditions. This would have resulted in an evaluated toe resistance being slightly larger toe resistance than the value mentioned above).

Obviously, there was no relaxation, no problem with the pile integrity, and the contractor had not damaged the piles when excavating the site. In the real case behind the story, the engineers came out of the litigation rather red-faced, but they had learnt the importance of not to exclude basic soil mechanics from their analyses and reports.

### BEFORE EXCAVATION



### AFTER EXCAVATION



**Example 14.5-04** The following problem deals with scour and it also originates in the real world. A couple of bridge piers are founded on groups of 18 inch (450 mm) pipe piles driven closed-toe through an upper 26 ft (8 m) thick layer of silty sand and 36 ft (11 m) into a thick deposit of compact sand. The dry-season groundwater table lies 6.5 ft (2 m) below the ground surface. During the construction work, a static loading test established that the pile capacity was 380 tons (3,400 kN), which corresponds to beta-coefficients of 0.35 and 0.50 in the silty sand and compact sand, respectively, and a toe bearing capacity coefficient of 60. The design load was 1,600 kN (180 tons), which indicates a factor of safety of 2.15—slightly more than adequate.

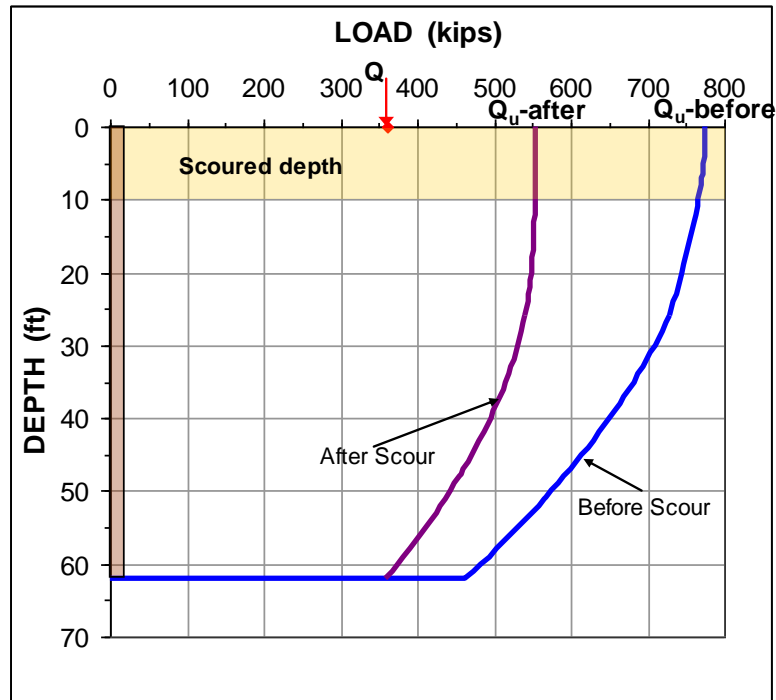
The static test had been performed during the dry season and a review was triggered when the question was raised whether the capacity would change during the wet season, when the groundwater table was expected to rise above the ground surface (bottom of the river). And, what would the effect be of scour? In the review, it was discovered that the upper 3 m (10 ft) of the soil could be lost to scour. However, in the design of the bridge, this had been thought to be inconsequential to the pile capacity.

A static analysis will answer the question about the effect on the pile capacity after scour. The distribution of pore water pressure is hydrostatic at the site and, in the Spring, when the groundwater table will rise to the ground surface (and go above), the effective overburden stress reduces. As a consequence of the change of the groundwater table, both pile shaft resistance and toe resistance reduce correspondingly and the new total resistance is 670 kips (3,000 kN). That is, the factor of safety is no longer 2.11, but the somewhat smaller value of 1.86—not quite adequate.

When the effect of scour is considered, the situation worsens. The scour can be estimated to remove the soil over a wide area around the piers, which will further reduce the effective overburden stress. The capacity now becomes 275 tons (2,460 kN) and the factor of safety is only 1.51. The two diagrams below show the resistance distribution curves for the condition of the static loading tests and for when the full effect of scour has occurred. (The load distribution curve,  $Q_d + R_s$ , is not shown).

Missing the consequence of reduced effective stress is not that uncommon. The TRUSTING case history in the foregoing is an additional example. Fortunately, in the subject scour case, the consequence was not so traumatic. Of course, the review results created some excitement. And had the site conditions been different, for example, had there been an intermediate layer of settling soil, there would have been cause

for some real concern. As it were, the load at the toe of the piles was considered to be smaller than the original ultimate toe resistance, and therefore, the reduced toe capacity due to reduced effective overburden stress would result in only small and acceptable pile toe penetration, that is, the settlement concerns could be laid to rest. In this case, therefore, it was decided to not carry out any remedial measures, but to keep a watchful eye on the scour conditions during the wet seasons to come. Well, a happy ending, but perhaps the solution was more political than technical.



**Example 14.5-05** The unified method for design of piled foundations was developed in the early 1980s. It combines capacity, drag force, settlement, and down drag in an interactive—unified—approach and was first published by Fellenius (1984). Fellenius (1988) advanced the approach and included a design example which was the first example of how to pursue a numerical analysis.

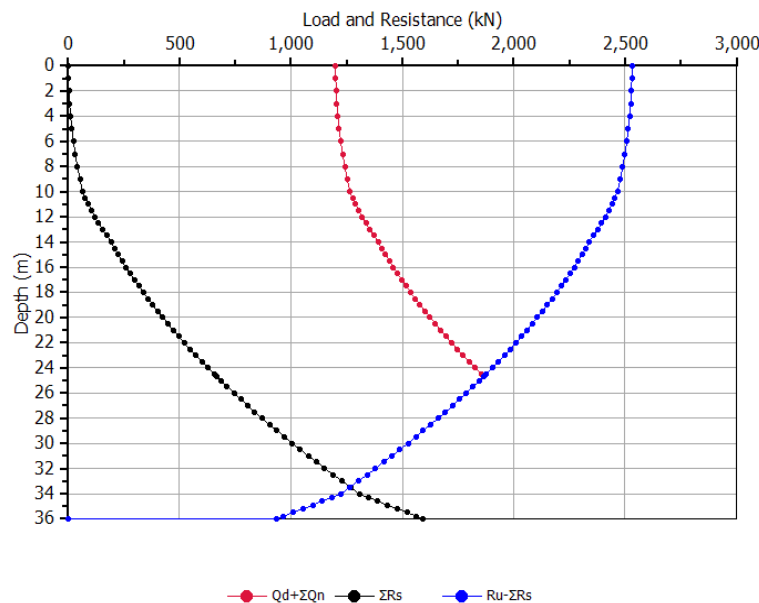
The design case presents a pile group consisting of 10 piles to be installed at the site, where the soil profile consisted of 10 m of soft or firm clay on a 4 m thick layer of sand. Below the sand lies a 20 m thick layer of slightly overconsolidated silty clay deposited on dense ablation till. The groundwater table is at the ground surface and the pore pressure is hydrostatically distributed. Some time after installing the piles and erecting the structure, a 2 m thick fill, causing a stress of 15 kPa is to be placed across the site.

Depth Range (m)	Type (--)	Density kg/m <sup>3</sup>	$\beta$ (---)	$m$ (---)	$m_r$ (---)	$j$ (---)	$\Delta\sigma'$ (kPa)
0 - 10	Clay	1,500	0.50	<u>20</u>	200	0	<u>20</u>
10 - 14	Sand	2,000	0.45	250	---	0.5	---
14 - 34	Clay	1,740	0.35	<u>80</u>	<u>400</u>	0	120
34 - --	Till	2,100	0.60	400	---	0.5	---

(The four underlined values were mistyped in the original Fellenius (1988) paper)

The 10 piles consist of 300 mm diameter pipe piles driven closed-toe to 36 m depth below the ground surface. The piles will be concrete-filled after driving and the intended allowable working load per pile is 1,400 kN of which 1,200 kN is dead load and 200 kN is live load. The maximum structurally allowable axial load at the neutral plane is 2,100 kN. The pile cap footprint is 3.5 m by 5.0 m, i.e., the area is 17.5 m<sup>2</sup> and the total 12,000 kN dead load corresponds to a 686-kN stress.

The calculated values of capacity and resistance distribution are shown in the figure. The curves differ slightly from the results given in the paper. This is because the original calculations were made before the advent of the personal computer which means that they include shortcuts and simplifications necessary for hand calculations. However, the differences are not large and the below plot looks identical to that in the paper. Similarly to the diagram in the paper, the figure disregards the effect of a transition zone.

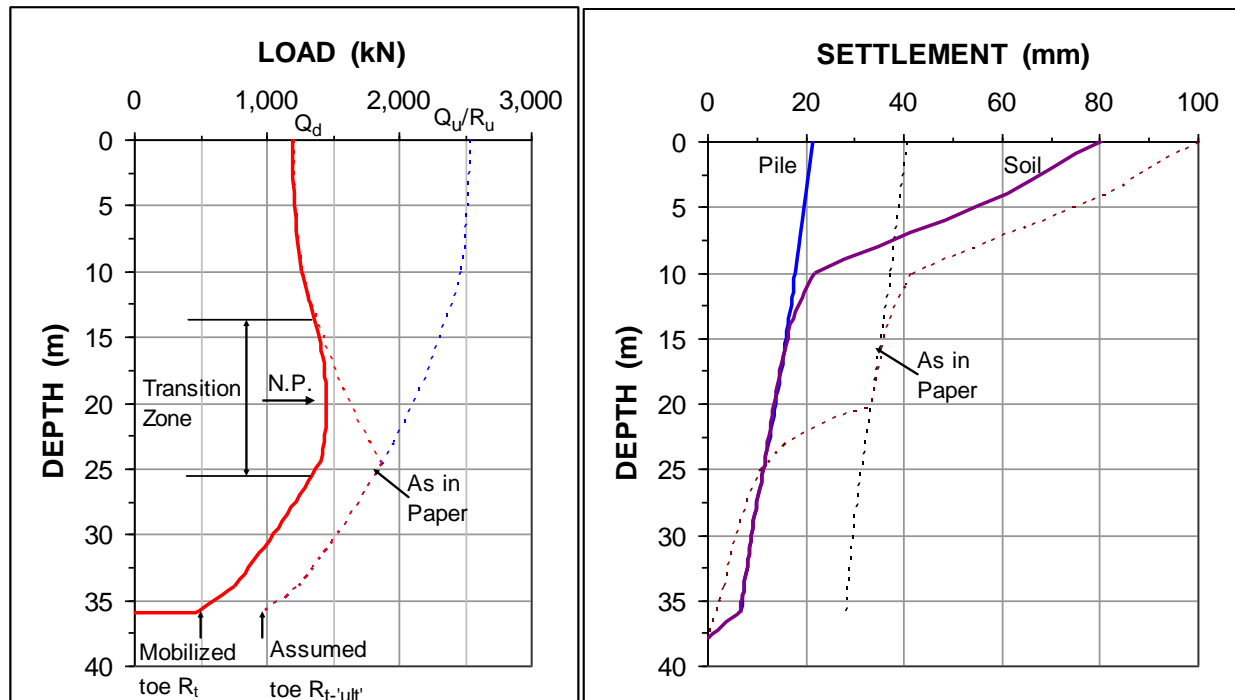


At the time when the paper was written, the fact that the pile toe load-movement relation is an essential part of the pile-soil response as well as of the location of the neutral plane was not fully understood. Moreover, neither was the necessity of considering the stiffness effect of a group piles on the compressibility of the soil between the neutral plane and the pile toe level. The settlement distribution presented in the paper was therefore larger than what an analysis would show today.

The below figure shows the load distribution from the dead load ( $Q_d$ ) assuming an 7-m height of the transition zone above the neutral plane and that only half the toe resistance ( $R_{u-ult}$ ) is mobilized. Moreover, the settlement calculation is for an equivalent raft placed at the pile toe (as opposed to the neutral plane). The load distribution presented in the paper is also shown (also shown in the preceding figure). The latter is the distribution when the ultimate resistance of the pile (the capacity) is mobilized as in a loading test. The figure also shows a diagram with the calculated pile group and soil settlements. The small relative movement between the pile shaft and the soil is what suggests using a long transition zone.

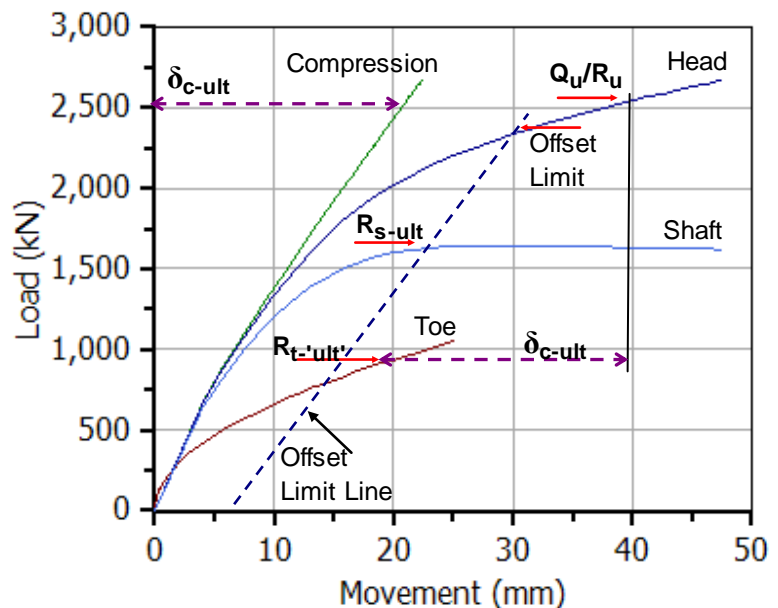
Adding the stiffening effect of the piles to the soil compressibility and considering that the downdrag enforced pile toe penetration into the till is small have caused the resistance mobilized by the pile toe to be much smaller than that assumed for the capacity calculation. As indicated in the below figure, this has resulted in a significantly smaller drag force and pile settlement than shown in the paper.





Twenty-five years ago, there was no easy way to simulate the load-movement results of a static loading test. However, with UniPile it is very simple. By selecting suitable  $t-z$  and  $q-z$  functions, UniPile applies the soil parameters and pile properties and calculates the loading test results illustrated in the below figure. Each soil layer was assumed to be governed by a different  $t-z$  function. As no actual test data are available to fit to the results, the only effort made was to select the movement values, particularly for the  $q-z$  function in the till so that the calculated capacity,  $Q_u/R_u$ , matches the ultimate shaft resistance,  $R_{s-ult}$ , and the calculated toe resistance,  $R_{t-ult}$ , mobilized in the test.

The curves have been supplemented with the "Offset Limit Line", which indicates an Offset Limit slightly lower than the assumed capacity. It would neither be time-consuming nor difficult to re-select the  $t-z$  and  $q-z$  curves to establish a "perfect" agreement between the capacity calculation and the Offset Limit capacity. However, as there are no actual test data to fit to, such effort would only be for cosmetic reasons.



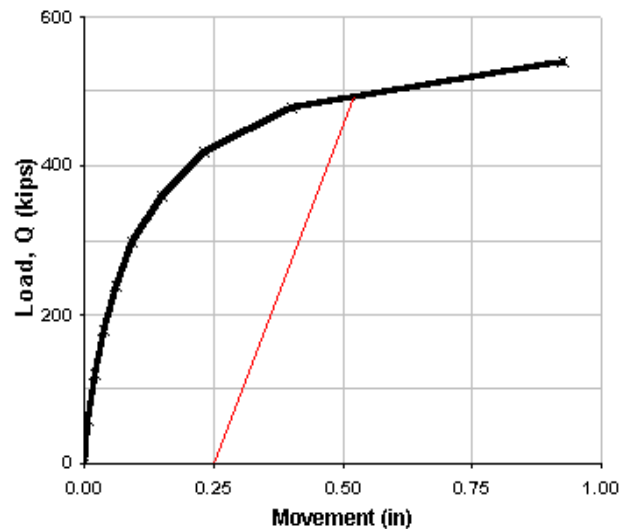
## 14.6 Analysis of Pile Loading Tests

**Example 14.6-01** Example 14.6.1 is from the testing of a 40 ft long H-pile. The pile description and the load-movement test data are as follows:

Head diameter, $b$	= 12.0 inches	Length, $L$	= 40.0 ft
Shaft area, $A_s$	= 4 ft <sup>2</sup> /ft	Embedment, $D$	= 38.0 ft
Section area, $A_{sz}$	= 0.208 ft <sup>2</sup>	Stick-up	= 2.0 ft
Toe diameter, $b$	= 12.0 inches	Toe area, $A_t$	= 1.0 ft <sup>2</sup>
Modulus, $E$	= 29,000 ksi	$EA/L$	= 1,810 kips/inch

The load-movement diagram indicates that the pile capacity cannot be eyeballed from the load-movement diagram (change the scales of the abscissa and ordinate and the eyeballed value will change too). The offset limit construction is indicated in the load-movement diagram. The Hansen, Chin-Kondner, and Decourt constructions are not shown, although these methods also work well for the case. However, neither the DeBeer nor the Curvature methods work very well for this case.

Row No.	Jack Load (kips)	Movement Average (inches)
1	0	0.000
2	60	0.007
3	120	0.019
4	180	0.036
5	240	0.061
6	300	0.093
7	360	0.149
8	420	0.230
9	480	0.399
10	540	0.926



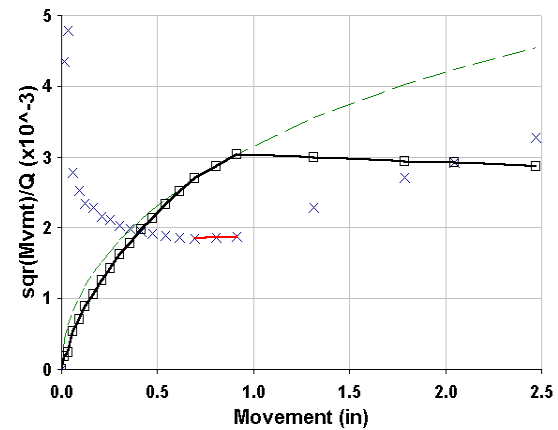
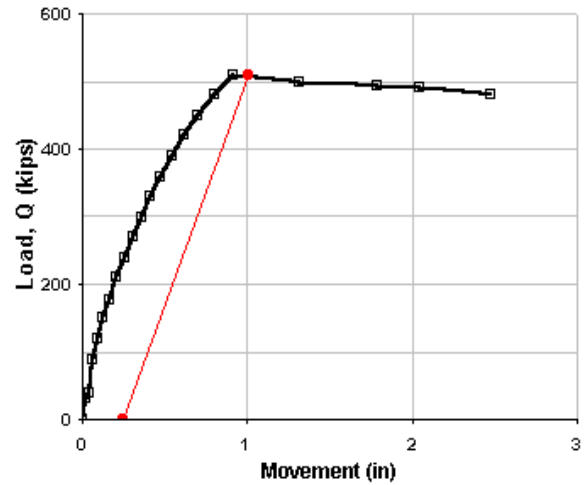
**Example 14.6-02** is from the testing of a hexagonal 12-inch diameter, 112 ft long precast concrete pile. As evidenced from the load-movement diagram shown below, the pile experienced a very sudden failure (soil failure was established) at the applied load of 480 kips. This loading test is an example of when the various interpretation methods are superfluous. Remember, the methods are intended for use when an obvious capacity value is not discernible in the test.

Head diameter, $b$	= 12.0 inches	Length, $L$	= 112 feet	Modulus, $E$	= 7,350 ksi
Shaft area, $A_s$	= 3.464 ft <sup>2</sup> /ft	Embedment, $D$	= 110 feet	$EA/L$	= 682 kips/inch
Section area, $A_{sz}$	= 0.866 ft <sup>2</sup>	Toe diameter, $b$	= 12.0 inches	Toe area, $A_t$	= 0.866 ft <sup>2</sup>
Stick-up	= 2 feet				

The test was aiming for a maximum load of 600 kips to prove out an allowable load of 260 kips with a factor of safety of 2.5. The 2nd diagram shows the Hansen construction and an extrapolation of the load-movement curve. Suppose the test had been halted at a maximum load at or slightly below the 480-kip

maximum load. It would then have been easy to state from looking at the curve that the pile capacity is “clearly” much greater than 480 kip and show that “probably” the allowable load is safe as designed. This test demonstrates the importance of not extrapolating to a capacity higher than the capacity established in the test.

Row No.	Jack Load (kips)	Movement Average (inches)
1	0.0	0.000
2	30.0	0.017
3	39.6	0.036
4	88.8	0.061
5	119.2	0.091
6	149.8	0.124
7	177.8	0.166
8	211.0	0.209
9	238.0	0.253
10	271.0	0.305
11	298.2	0.355
12	330.4	0.414
13	357.6	0.473
14	390.2	0.540
15	420.8	0.630
16	450.4	0.694
17	481.0	0.804
18	509.0	0.912
19	500.0	1.314
20	492.4	1.787
21	489.8	2.046
22	480.4	2.472





## CHAPTER 15

### PROBLEMS

#### 15.1 Introduction

The following offers problems to solve and practice the principles presented in the preceding chapters. The common aspect of the problems is that they require a careful assessment of the soil profile and, in particular, the pore pressure distribution. They can all be solved by hand, although the computer and the UniSoft programs will make the effort easier.

#### 15.2 Stress Distribution

**Problem 15.2.1.** At a construction site with ground surface at Elev. +115.5 m, the soil consists of an upper 6 metre thick compact sand layer, which at elevation +109.5 m is deposited on layer of soft, overconsolidated clay. Below the clay, lies a 5 metre thick very dense, sandy coarse silt layer, which at elevation +97.5 m is underlain by very dense glacial till followed by bedrock at elevation +91.5 m.

Borehole observations have revealed a perched groundwater table at elevation +113.5 m, and measurements in standpipe piezometer show the existence of an artesian water pressure in the silt layer with a phreatic elevation of +119.5 m. The piezometric head measured at the interface between the pervious bedrock and the glacial till is 15.0 m.

Laboratory studies have shown index values and physical parameters of the soil to be as follows.

Para- meter	Unit	Sand	Clay	Sandy Silt	Glacial till
$\rho_s$	$\text{kg/m}^3$	2,670	2,670	2,670	2,670
$\rho$	$\text{kg/m}^3$	2,050	1,600	2,100	2,300
$\phi'$	°	33	22	38	43
$k$	m/s	$1 \cdot 10^{-3}$	$1 \cdot 10^{-9}$	$1 \cdot 10^{-4}$	$1 \cdot 10^{-8}$
$\tau_u$	kPa	--	24	--	--
$c'$	kPa	0	0	0	0
$w_L$	--	--	0.75	--	--
$w_n$	%	22	67	19	11
$e_0$	--	0.59	1.79	0.51	0.29
$c_v$	$\text{m}^2/\text{s}$	-	$20 \cdot 10^{-8}$	--	--
$E_i$	MPa	100	10	120	>1,000
$m$	--	250	20	600	1,000
$m_r$	--	1,200	160	4,000	>10,000
$j$	--	1	0	0.5	1
$\Delta\sigma'$	kPa	--	50	100	1,000
OCR	--	3	--	--	--
$C_\alpha$					

- A. Calculate and tabulate the total stresses, the pore pressures, the effective stresses in the soil layers and **draw** (to scale) the corresponding pressure and stress diagrams.
- B. Verify that the values of water content,  $w_n$ , in the four soil layers agree with the values of density of the soil material assuming a solid density of  $2,670 \text{ kg/m}^3$  and a degree of saturation of 100 %
- C. Assume that the pore pressure in the lower sandy silt layer was let to rise. (Now, how would Mother Nature be able to do this)? How high (= to what elevation) could the phreatic elevation in the sand layer rise before an unstable situation would be at hand?

The table may seem to contain redundant information. This is true if considering only parameters useful to calculate stresses. However, the “redundant” parameters are helpful when considering which soil layers have hydrostatic pore pressure distribution and which have a pore pressure gradient. (Notice, as the conditions are stationary, all pore pressure distributions are linear).

**Problem 15.2.2.** A three metre deep excavation will be made in a homogeneous clay soil with a unit weight of  $16 \text{ kN/m}^3$ . Originally, the groundwater elevation is located at the ground surface and the pore pressure is hydrostatically distributed. As a consequence of the excavation, the groundwater table will be lowered to the bottom of the excavation and, in time, again be hydrostatically distributed over the general site area. There are three alternative ways of performing the excavation, as follows:

- A. First, excavate under water (add water to the hole as the excavation proceeds) and, then, pump out the water when the excavation is completed (1A and 1B).
- B. First, lower the water table to the bottom of the excavation (assume that it will become hydrostatically distributed in the soil below) and, then, excavate the soil (2A and 2B).

Calculate and tabulate the soil stresses for the original conditions and for the construction phases, Phases 1A and 1B, and 2A, and 2B at depths 0 m, 3 m, 5 m, and 7 m. Compare the calculated effective stresses of the construction phases with each other, in particular the end results Phases 1B and 2B. Comment on the difference.

**Problem 15.2.3.** The soil profile at a site consists of a 3 metre thick upper layer of medium sand (density  $1,800 \text{ kg/m}^3$ ) followed by 6 metre of clay (density  $1,600 \text{ kg/m}^3$ ) and 4 metre of sand (density  $2,000 \text{ kg/m}^3$ ) overlain dense glacial till (density  $2,250 \text{ kg/m}^3$ ). Pervious bedrock is encountered at a depth of 16 metre. A perched water table exists at a depth of 1.0 metre. Two piezometers are installed to depths of 7 metre and 16 metre, respectively, and the pore pressure readings indicate phreatic pressure heights of 10 metre and 11 metre, respectively. It can be assumed that the soil above the perched water table is saturated by capillary action. The area is surcharged by a widespread load of 10 kPa.

Draw-to scale and neatly-separate diagrams over effective overburden stress and pore pressures.

**Problem 15.2.4.** The soil profile at a site consists of a 4.0 m thick upper layer of medium sand (density  $1,800 \text{ kg/m}^3$ ), which is followed by 8.0 m of clay (density  $1,700 \text{ kg/m}^3$ ). Below the clay, a sand layer (density  $2,000 \text{ kg/m}^3$ ) has been found overlying glacial till (density  $2,100 \text{ kg/m}^3$ ) at a depth of 20.0 m deposited on bedrock at depth of 23.0 m. The bedrock is pervious. Two piezometers installed at depths of 18.0 m and 23.0 m, respectively, indicate phreatic pressure heights of 11.0 m and 19.0 m, respectively. There is a perched groundwater table in the upper sand layer at a depth of 1.5 m. The non-saturated but wet density of the sand above the perched groundwater table is  $1,600 \text{ kg/m}^3$ .

Draw-to scale and neatly-one diagram showing effective overburden stress and one separate diagram showing the pore pressure distribution in the soil.

**Problem 15.2.5.** The soil profile at a very level site consists of a 1 m thick upper layer of coarse sand (density  $1,900 \text{ kg/m}^3$ ) deposited on 5 m of soft clay (density  $1,600 \text{ kg/m}^3$ ). Below the clay, silty sand (density  $1,800 \text{ kg/m}^3$ ) is found. A piezometer installed to a depth of 8 m indicates a phreatic pressure height of 9 m. There is a seasonally occurring perched water table in the upper sand layer.

A very wide excavation will be carried out at the site to a depth of 4 m. Any water in the upper sand layer will be eliminated by means of pumping. The water pressure in the lower silty sand layer is difficult and costly to control. Therefore, it is decided not to try to lower it. Can the excavation be carried out to the planned depth? Your answer must be a "yes" or "no" and followed by a detailed rational supported by calculations.

**Problem 15.2.6.** The soil at a site consist of an upper 11 metre thick layer of soft, normally consolidated, compressible clay ( $c_v = 2 \cdot 10^{-8} \text{ m}^2/\text{s}$ , and unit weight  $= 16 \text{ kN/m}^3$ ) deposited on a 4 metre thick layer of overconsolidated, silty clay ( $c_v = 10 \cdot 10^{-8} \text{ m}^2/\text{s}$ , unit weight  $= 18 \text{ kN/m}^3$ , and a constant overconsolidation value of 20 kPa) which is followed by a thick layer of dense, pervious sand and gravel with a unit weight of  $20 \text{ kN/m}^3$ .

The groundwater table is located at a depth of 1.0 metre. The phreatic water elevation at the bottom of the soft clay layer is located 1.0 metre above the ground surface. At depth 16.0 metre, the pore water pressure is equal to 190 kPa.

In constructing an industrial building (area 20 by 30 metre) at the site, the area underneath the building is excavated to a depth of 1.0 metre. Thereafter, a 1.2 metre thick, compacted backfill (unit weight  $= 20 \text{ kN/m}^3$ ) is placed over a vast area surrounding the building area. The building itself subjects the soil to a contact stress of 80 kPa.

As a preparation for a settlement analysis, calculate and **draw** the effective stress distribution in the soil below the midpoint of the building. Notice, a settlement analysis requires knowledge of both the original effective stress and the final effective stress. Also, there is no need to carry the calculation deeper into the soil than where the change of effective stress ceases to result in settlement. Settlement in "dense sand and gravel" is negligible compared to settlement in clay and silt.

**Problem 15.2.7.** In sequence, a lake bottom profile consists of a 6 m thick layer of clayey mud (density  $= 1,700 \text{ kg/m}^3$ ), a 2 m thick layer of coarse sand (density  $= 2,000 \text{ kg/m}^3$ ), and a 3 m thick layer of glacial clay till (density  $= 2,200 \text{ kg/m}^3$ ) on pervious bedrock. The water depth in the lake is 3.0 m. Piezometer observations have discovered artesian pressure conditions in the sand layer: at a depth

of 7.0 m below the lake bottom the phreatic height is 12 m. Other piezometers have shown a phreatic height of 10 m in the interface between the till and the bedrock.

A circular embankment with a radius of 9 m and a height of 1.5 m (assume vertical sides) will be placed on the lake bottom. The fill material is coarse sand and it will be placed to a density of  $2,100 \text{ kg/m}^3$ .

Calculate and **draw** (in a combined diagram) the final effective stress and pore pressure profile from the embankment surface to the bedrock. Assume 2:1 distribution of the fill load.

**Problem 15.2.8.** A structure will be built in a lake where the water depth is 1.5 m and the lake bottom soils consist of an upper 1.5 m thick layer of pervious “muck” followed by 2.5 m layer of overconsolidated clayey silt deposited on a layer of overconsolidated coarse sand. Fractured bedrock is encountered at a depth of 16.0 m below the lake bottom. A soils investigation has established that the soil densities are  $1,500 \text{ kg/m}^3$ ,  $1,850 \text{ kg/m}^3$ , and  $2,100 \text{ kg/m}^3$ , respectively. Piezometers in the sand have shown an artesian head corresponding to a level of 2.0 m above the lake surface.

The structure will be placed on a series of widely spaced footings, each loaded by 1,500 kN dead load (which load includes the weight of the footing material; no live load exists). The footings are 3.0 m by 4.0 m in area and constructed immediately on the silt surface. Before constructing the footings, the muck is dredged out over an area of 6.0 m by 8.0 m, which area will not be back-filled.

Calculate the original and final (after full consolidation) effective stresses and the preconsolidation stresses in the soil underneath the mid-point of the footing.

### 15.3 Settlement Analysis

**Problem 15.3.1.** The soil at a site consists of an upper, 2 metre thick layer of sand having a density of  $1,900 \text{ kg/m}^3$  and a modulus number of 300. The sand layer is deposited on a very thick layer of clay having a density of  $1,600 \text{ kg/m}^3$  and a modulus number of 40. The groundwater table is located at the ground surface and is hydrostatically distributed.

A 3 metre wide, square footing supporting a permanent load of 900 kN is to be located at a depth of either 0.5 metre or 1.5 metre. Which foundation depth will result in the largest settlement? (During the construction, the groundwater table is temporarily lowered to prevent flooding. It is let to return afterward. Also, consider that backfill will be placed around the footing. You may assume that the footing is either very thin or that it is made of “concrete” having the density of soil).

**Problem 15.3.2.** The soil at a site consists of 2 metre thick layer of organic clay and silt with a density of  $1,900 \text{ kg/m}^3$  underlain by a layer of sand with a density of  $2,000 \text{ kg/m}^3$  deposited at the depth of 5 metre on a 4 metre thick layer of silty clay with a density of  $1,800 \text{ kg/m}^3$  followed by fractured bedrock. The groundwater table is located at a depth of 3.0 metre. The pressure head at the bedrock interface is 10 metre. The modulus number,  $m$ , of the clay and silt layer is 15. The sand layer can be considered overconsolidated by a constant value of 40 kPa and to have virgin modulus numbers,  $m$ , and reloading modulus numbers,  $m_r$ , of 120 and 250, respectively. Also the silty clay layer is overconsolidated, having an OCR-value of 2.0. Its virgin modulus and reloading modulus numbers are 30 and 140, respectively.

At the site, a building being 10 metre by 15 metre in plan area will be founded on a raft placed on top of the sand layer (after first excavating the soil). The load applied to the soil at the foundation level from the



building is 12 MN. Around the building, a fill having a density of  $1600 \text{ kg/m}^3$ , will be placed to a height of 1.25 metre over an area of 50 by 50 metre and concentric with the building. Simultaneously with the construction of the building, the pore pressure at the bedrock interface will lowered to a phreatic height of 6 metre.

Determine the settlement of the sand and the silty clay layers assuming that all construction activities take place simultaneously and very quickly. You must calculate the settlement based on the stress change for each metre of depth. What would the settlement be if the fill had been placed well in advance of the construction of the building?

**Problem 15.3.3.** A 2.0 m deep lake with a surface elevation at +110.0 m will be used for an industrial development. The lake bottom consists of a 4 m thick layer of soft clayey silt mud followed by a 3-m layer of loose sand deposited on a 1 m thick layer of very dense glacial till. The pore pressures at the site are hydrostatically distributed. The soil densities are  $1,600 \text{ kg/m}^3$ ,  $1,900 \text{ kg/m}^3$ , and  $2,300 \text{ kg/m}^3$ , respectively. The clay is slightly overconsolidated with an OCR of 1.2 and has virgin and reloading modulus numbers of 20 and 80. The sand OCR is 3.0 and the modulus numbers are 200 and 500. For the till,  $m = 1,000$ . To reclaim the area, the pore pressure in the sand layer will be reduced temporarily to a phreatic elevation of +107.0 m and a sand and gravel fill (density =  $2,000 \text{ kg/m}^3$ ) will be dumped in the lake over a wide area and to a height of 2.5 m above Elevation +108.0. Although the lake, the fill rather, will be drained, it is expected that a perched groundwater table will always exist at Elevation +109.0.

Calculate the elevation of the surface of the fill when the soil layers have consolidated.

**Problem 15.3.4.** Is anyone or are any of the following four soil profile descriptions in error? If so, which and why? Comment on all four descriptions and include an effective stress diagram for each of A through D.

- A. A 10 m thick clay layer is deposited on a pervious sand layer, the groundwater table lies at the ground surface, the clay is overconsolidated, and the pore water pressure is hydrostatically distributed.
- B. A 10 m thick clay layer is deposited on a pervious sand layer, the groundwater table lies at the ground surface, the clay is normally consolidated, and the pore water pressure is artesian.
- C. A 10 m thick clay layer is deposited on a pervious sand layer, the groundwater table lies at the ground surface, the clay is undergoing consolidation, and the pore water pressure is linearly distributed.
- D. A 10 m thick clay layer is deposited on a pervious sand layer, the groundwater table lies at the ground surface, the clay is preconsolidated, and the pore water pressure has a downward gradient.

**Problem 15.3.5.** The silt and sand layers in Problem 15.2-08 have modulus numbers ( $m$  and  $m_r$ ) 35 and 80, and 120 and 280, respectively, and the stress exponents are 0 and 0.5, respectively. The OCR in the silt is 2.5 and the sand is preconsolidated to a 40 kPa preconsolidation stress margin. Calculate the settlement of the footing assuming that all construction takes place at the same instant.

## 15.4 Earth Stress and Bearing Capacity of Shallow Foundations

**Problem 15.4.1.** An anchor-wall (used as dead-man for a retaining wall) consists of a 4 m wide and 3 m high wall (with an insignificant thickness) and is founded at a depth of 4 m in a non-cohesive soil having an effective friction angle of  $32^\circ$  and no cohesion intercept. The soil density is  $1,900 \text{ kg/m}^3$  above the groundwater table and  $2,100 \text{ kg/m}^3$  below. At times, the groundwater table will rise as high as to a depth of 2.0 m.

Calculate the ultimate resistance of the anchor wall to a horizontal pull and determine the allowable pulling load using a factor of safety of 2.5.

**Problem 15.4.2.** A trench in a deep soil deposit is excavated between two sheetpile rows installed to adequate depth and with horizontal support going across the trench. As the Engineer responsible for the design of the wall, you have calculated the earth stress acting against the sheetpile walls considering fully developed wall resistance, effective cohesion, and internal effective friction angle of the soil. You have also considered the weight of a wide body, heavy crawler rig traveling parallel and close to the trench by incorporating two line-loads of appropriate magnitude and location in your calculation. Your calculated factor of safety is low, but as you will be in charge of the inspection of the work and physically present at the site at all times, you feel that a low factor of safety is acceptable.

When visiting the site one day during the construction work, you notice that one track of the crawling rig travels on top of one of the sheetpile walls instead of on the ground next to the wall, as you had thought it would be. The load of the crawler track causes a slight, but noticeable downward movement of the so loaded sheetpile row.

Quickly, what are your immediate two decisions, if any? Then, explain, using text and clear sketches including force polygons, the qualitative effect—as to advantage or disadvantage—that the location of the crawler track has on the earth stress acting against the sheetpile wall.

**Problem 15.4.3.** As a part of a renewal project, a municipality is about to shore up a lake front property and, at the same time, reclaim some land for recreational use. To this end, a 6.0 m high L-shaped retaining wall will be built directly on top of the lake bottom and some distance away from the shore. Inside the wall, hydraulic sand fill will be placed with a horizontal surface level with the top of the wall. The wall is very pervious. The water depth in the lake is kept to 2.0 m. The lake bottom and the hydraulic fill soil parameters are density  $1,900 \text{ kg/m}^3$  and  $1,000 \text{ kg/m}^3$ , and effective friction angle  $37^\circ$  and  $35^\circ$ , respectively, and zero effective cohesion intercept.

Calculate the earth stress against the retaining wall.

**Problem 15.4.4.** The soil at a site consists of a thick layer of sand with a unit weight of  $18 \text{ kN/m}^3$  above the groundwater table and  $20 \text{ kN/m}^3$  below the groundwater table. The effective friction angle of the sand is  $34^\circ$  above the groundwater table and  $36^\circ$  below. At this site, a column is founded on a footing having a 3 m by 4 m plan area and its base at a depth of 2.1 m, which is also the depth to the groundwater table. Acting at the ground surface and at the center of the column, the column is loaded by a vertical load of 2,100 kN and a 300 kN horizontal load parallel to the short side of the footing. There is no horizontal load parallel to the long side. Neither is there any surcharge on the ground surface.

Calculate the factor of safety against bearing failure. In the calculations, assume that the column and footing have zero thickness and that the natural soil has been used to backfill around the footing to a density equal to that of the undisturbed soil.

Considering that the bearing capacity formula is a rather dubious model of the soil response to a load, verify the appropriateness of the footing load by calculating the footing settlement using assumed soil parameters typical for the sand.

**Problem 15.4.5.** A 3.0 m wide strip footing (“strip” = infinitely long) is subjected to a vertical load of 360 kN/linear-metre. Earth stress and wind cause horizontal loads and a recent check on the foundation conditions has revealed that, while the factors of safety concerning bearing capacity and sliding modes are more than adequate, the magnitude of the edge stress is right at the allowable limit. How large is the edge stress?

**Problem 15.4.6** A footing for a continuous wall supports a load of 2,000 kN per metre at a site where the soil has a density of  $1,900 \text{ kg/m}^3$ , an effective cohesion intercept of 25 kPa, and an effective friction angle of  $33^\circ$ . The footing is placed at a depth of 1.0 m which also is the depth to the groundwater table.

Determine the required width of the wall base (footing) to the nearest larger 0.5 m using a Global Factor of Safety of 3.0 and compare this width with the one required by the OHBDC in a ultimate limit states, ULS, design).

## 15.5 Deep Foundations

**Problem 15.5.1.** A group of 16 precast concrete piles, circular in shape with a diameter of 400 mm and concrete strength of 50 MPa, will be installed in a square configuration to an anticipated embedment depth of 15.0 m at a site where the soil consists of a 10 m thick upper layer of overconsolidated clay deposited on a thick layer of dense sand. The preconsolidation stress of the clay is 25 kPa above the existing effective stress. There is a groundwater table at the ground surface. The phreatic elevation in the sand layer lies 2.0 m above the ground surface. With time, it is expected to be lowered by 1.0 m.

The clay parameters are: density  $1,600 \text{ kg/m}^3$ , angle of effective friction 29 degrees, and the modulus numbers are 25 and 250, respectively. The sand parameters are: density  $2,000 \text{ kg/m}^3$ , angle of effective friction 38 degrees, and modulus number 250. The  $MK_s$ -ratio in the clay and in the sand are 0.6 and 1.0, respectively. The toe bearing capacity coefficient is 2.0 times the  $N_q$  coefficient. ( $\beta = MK_s \tan\phi'$ ).

The piles will be placed at a minimum center-to-center spacing of 2.5 times the pile diameter plus 2.0 % of the anticipated embedment length. The structurally allowable stress at the pile cap is 0.3 times the cylinder strength. It is the intent to apply to the pile group a dead load of 16 times the allowable dead load, 16 times 600 kN, and it can be assumed that this load is evenly distributed between the piles via a stiff pile cap cast directly on the ground.

An 1.0 m thick backfill will be placed around the pile cap to a very large width. The fill consists of granular material and its density is  $2,000 \text{ kg/m}^3$ .

- A. What is the allowable live load per pile for a global factor of safety of 2.5?
- B. Find the location of the neutral plane in a diagram drawn neatly and to scale and determine the future maximum load in the pile.
- C. Are the loads structurally acceptable?
- D. Estimate the settlement of the pile group.

**Problem 15.5.2.** An elevated road (a causeway) is to be built across a lake bay, where the water surface is at Elevation +10.0 and the water depth is 2.0 m. The lake bottom consists of a 12 m thick layer of compressible, normally consolidated silty clay deposited on a 40 m thick layer of sand on bedrock. The pore water pressure in the clay is hydrostatically distributed.

The causeway will be supported on a series of pile bents. Each bent will consist of a group of eight, 0.3 m square piles installed to Elevation -22.0 m in three equal rows at an equal spacing of 5 diameters (no pile in the center of the group). In both the clay and the sand layer, and for both positive and negative resistance, the value of  $MK_s$  is 0.6. The clay and the sand layers have unit weights of  $16 \text{ kN/m}^3$  and  $20 \text{ kN/m}^3$ , and friction angles of  $29^\circ$  and  $37^\circ$ , respectively. The effective cohesion intercept is zero for both layers. The modulus numbers and stress exponents are 50 and 280, and 0 and 0.5, respectively. The  $N_t$ -coefficient is 60. (Lead: calculate  $\beta = MK_s \tan\phi'$ ).

To provide lateral restraint for the piles, as well as establish a working platform above water, a sand fill is placed at the location of each bent. Thus, the sand fill will be permanent feature of each pile bent. The sand fill is 4.0 m thick and covers a 10 by 10 m square area. The sand fill has a saturated unit weight of  $20 \text{ kN/m}^3$ . Assume that the total unit weight of the sand fill is the same above as below the lake surface and that the shaft resistance in the fill can be neglected.

- A. Calculate and plot the distribution of the ultimate soil resistance along a single pile assuming that positive shaft resistance acts along the entire length of the pile and that all excess pore pressure induced by the pile driving and the placement of the sand fill have dissipated.
- B. Determine the allowable live load (for a single pile) acting simultaneously with a dead load of 900 kN and using a global factor of safety of 3.0.
- C. Calculate the consolidation settlement for the pile group. Then, draw the settlement distribution in the sand. (Assume that the fill has vertical sides).

**Problem 15.5.3.** Typically, a single pile in a specific large (many piles) pile group has a capacity of 200 tons, is assigned a toe resistance of 110 tons, and the allowable dead load is 80 tons. There is no live load acting on the pile group. The soil is homogeneous and large settlement is expected throughout the soil profile. The piles consist of pipes driven open-toe (open-end) into the soil and connected by means of a stiff pile cap. In driving, the inside of the pipe fills up with soil that afterward is drilled and cleaned out—of course, taking care not to disturb the soil at and below the pile toe. The pipe is then filled with concrete and the short column strength of the concreted pipe is 300 tons. By mistake, when cleaning one pile, the work was continued below the pile toe leaving a void right at the pile toe that was not discovered in time. The concreting did not close the void. The pile shaft was not affected, however, and the pile itself is structurally good. As the geotechnical engineer for the project, you must now analyze the misshapen pile and recommend an adjusted allowable load for this pile. Give your recommendation and justify it with a sketch and succinct explanations.

**Problem 15.5.4.** The Bearing Graph representative for the system (hammer, helmet cushion) used for driving a particular pile into a very homogeneous non-cohesive soil of a certain density at a site is given by the following data points: [600 kN/1; 1,000/2; 1,400/4; 1,600/6; 1,700/8; and 1,900/20 blows/inch—that is, ultimate resistance/penetration resistance]. The groundwater table at the site lies at the ground surface and the pore pressure distribution is hydrostatic. The pile is driven open-toe and can be assumed to have no toe resistance (no plug is formed). At the end-of-initial-driving, the penetration resistance is 3 blows/inch and, in restriking the pile a few days after the initial driving, the penetration resistance is 12 blows/inch. This difference is entirely due to pore pressures which were developed and present during initial driving, but which had dissipated at restriking. On assuming that the soil density is either  $2,000 \text{ kg/m}^3$  or  $1,800 \text{ kg/m}^3$  (i.e., two cases to analyze), determine the average excess pore pressure present during the initial driving in relation to (= in % of) the pore pressure acting during the restriking.

Notice, you will need to avail yourself of a carefully **drawn** bearing graph using adequately scaled axes.

**Problem 15.5.5.** Piles are being driven for a structure at a site where the soils consist of fine sand to large depth. The density of the sand is  $2,000 \text{ kg/m}^3$  and the groundwater table lies at a depth of 3.0 m. The piles are closed-toe pipe piles with a diameter (O. D.) of 12.75 inch. The strength parameters of the soil (the beta and toe bearing coefficients) are assumed to range from 0.35 through 0.50 and 20 through 80, respectively. A test pile is installed to an embedment depth of 15.0 m.

- A. Determine the range of bearing capacity to expect for the 15-m test pile (i.e., its minimum and maximum capacities).
- B. A static loading test is now performed on the test pile and the pile capacity is shown to be 1,400 kN. Assume that the beta coefficients are of the same range as first assumed (i.e., 0.35 through 0.50) and determine the capacity range for a new pile driven to an embedment depth of 18 m.

**Problem 15.5.6.** A soil profile at a site consist of a 2.0 m thick layer of silt ( $\rho = 1,700 \text{ kg/m}^3$ ) followed by a thick deposit of sand ( $\rho = 2,050 \text{ kg/m}^3$ ). The groundwater table is located at a depth of 0.5 m and the pore pressures are hydrostatically distributed.

At the site, an industrial building is considered which will include a series of columns (widely apart), each transferring a permanent (dead) vertical load of 1,000 kN to the soil. The groundwater table will be lowered to a new stable level at a depth of 1.5 m below the ground surface.

A foundation option is to support the columns on 0.25 m diameter square piles installed to 10.0 m depth. The  $\beta$ -coefficients of the silt and sand are 0.35 and 0.55, respectively, and the toe bearing  $N_t$ -coefficient of the sand is 50.

Calculate using effective stress analysis how many piles that will be needed at each column if the Factor-of-Safety is to be at least 2.5.



## CHAPTER 16

### REFERENCES

- AASHTO Specifications, 1992. Standard specifications for highway bridges, 15th Edition. American Association of State Highway Officials, Washington.
- AASHTO Specifications 2010. LRFD Bridge Design Specification, 5th Edition. American Association of State Highway Officials, Washington.
- Altaee, A., Evgin, E., and Fellenius, B.H., 1992. Axial load transfer for piles in sand. I: Tests on an instrumented precast pile. *Canadian Geotechnical Journal*, 29(1) 11-20.
- Altaee, A., Evgin, E., and Fellenius, B.H., 1993. Load transfer for piles in sand and the critical depth. *Canadian Geotechnical Journal*, 30(2) 465-463.
- Altaee, A. and Fellenius, B.H., 1994. Physical modeling in sand. *Canadian Geotechnical Journal*, 31(3) 420-431.
- Aoki, N., 2000. Improving the reliability of pile bearing capacity prediction by the dynamic increasing energy test, DIET. Keynote Lecture. Proc. of the Sixth International Conference on the Application of Stress-Wave Theory to Piles. Sao Paulo, September 11-13, Balkema, pp. 635-650.
- API 2000. Recommended Practice for Planning, Designing, and Constructing Fixed Offshore Platforms - Working Stress Design, 21st Edition. American Petroleum Institute, 242 p.
- ASTM, 2007. D1143-07 Standard Test Method for Piles Under Static Axial Compressive Load. American Society for Testing and Materials, Annual Book of Standards, ASTM, Philadelphia, PA, Construction Vol. 4:08, 15 p.
- ASTM, 2007. D3689-07. Standard Test Method for Individual Piles Under Static Axial Tensile Load. American Society for Testing and Materials, Annual Book of Standards. ASTM, Philadelphia, PA, Construction Vol. 4:08.
- ASTM, 2010. D4945-10. Standard test method for high-strain dynamic testing of piles. American Society for Testing and Materials, Annual Book of Standards. ASTM, Philadelphia, PA, Construction Vol. 4:08.
- Amir, J.M., 1983. Interpretation of load tests on piles in rock. Proc. of the 7th Asian Regional Conference on Soil Mechanics and Foundation Engineering, Haifa, August 14-19, IV/4, pp. 235-238.
- Amir, J.M., Amir, E.J., and Lam, C., 2014. Modulus of elasticity in deep bored piles. Proc. of the DFI-EFFC International Conference on Piling and Deep Foundations, Stockholm, May 21-23, pp. 397-402.
- Aoki, N., 2000. Improving the reliability of pile bearing capacity prediction by the dynamic increasing energy test, DIET. Keynote Lecture, Proc. of the Sixth Int. Conference on the Application of Stress-Wave Theory to Piles. Sao Paulo, September 11-13, Balkema, pp. 635-650.
- Asaoka, A., 1978. Observational procedure of settlement prediction. *Soil and Foundations*, Japan 18(4) 87-101.
- Axelsson, G., 2000. Long-term set-up of driven piles in sand. Department of Civil and Environmental Engineering, Royal Institute of Technology, Stockholm, 193 p.
- Authier, J. and Fellenius, B.H., 1980. Quake values determined from dynamic measurements. Proc. of the First International Seminar on Application of Stress-Wave Theory to Piles, Stockholm, September 10-13, H. Bredenberg Editor, A. A. Balkema, Rotterdam, pp., 197-216.
- Baldi, G., Bellotti, R., Ghionna, R., Jamiolkowski, M., and Pasqualini, E., 1986. Interpretation of CPTs and CPTUs. 2nd Part: Drained penetration of sands. Proc. of the Fourth International Geotechnical Seminar on Field Instrumentation and In-situ Measurements, Singapore November 25-27, 1986, 143-156.

- Baligh, M. , Vivatrat, V., Wissa, A., Martin R., and Morrison, M., 1981. The piezocone penetrometer. Proc. of Symposium on Cone Penetration Testing and Experience, ASCE National Convention, St. Louis, October 26 - 30, pp. 247 - 263.
- Barbie, D.L, Reece, B.D., and Eames, D.R., 2005. Water Resources Data--Texas, Water Year 2004, Volume 6, Groundwater Data. U.S. Geological Survey, Texas Water Science Center, Water-Data Report TX-04-6, 754 p.
- Barron, R.R., 1947. Consolidation of fine-grained soils by drain wells. Proc. of the ASCE 73(6) In Transactions of the ASCE 1948 (113) 718-742.
- Baquerizo, A. 2015. New cost effective, schedule drive solution for tall building foundations. DFI Superpile Conference, Kissimmee, FL, May 6 - 7, 33 p.
- Bean K., Jefferies M.G., and Hachey, J., 1991. The critical state of sand, *Geotechnique* 41(3) 365-381.
- Begemann, H.K.S., 1953. Improved method of determining resistance to adhesion by sounding through a loose sleeve placed behind the cone. Proc. of the 3rd ICSMFE, August 16 - 27, Zurich, Vol. 1, pp. 213 - 217.
- Begemann, H.K.S., 1963. The use of the static penetrometer in Holland. *New Zealand Engineering*, 18(2) 41.
- Begemann, H.K.S., 1965. The friction jacket cone as an aid in determining the soil profile. Proc. of the 6th ICSMFE, Montreal, September 8-15, Univ. of Toronto Press, Vol. 2, pp. 229-233.
- Birmingham, P., Ealy, C.D., and White J.K., 1993. A comparison of Statnamic and static field tests at seven FHWA sites. Birmingham Corporation Limited, Internal Report.
- Bishop, A.W., 1955. The use of the slip circle in stability analysis of slopes. *Geotechnique* 5(1) 7-17.
- Bjerrum L., Jönsson, W. and Ostenfeld, C 1957. The settlement of a bridge abutment on friction piles. Proc. 4th ICSMFE, London, August 12-24, Vol. 2, pp. 14-18.
- Bjerrum, L., Johannessen, I.J. and Eide O., 1969. Reduction of negative skin friction on steel piles to rock. Proc. 7th ICSMFE, Mexico City, August 25-29, Vol. 2 pp. 27-33.
- Bjerrum, L. and Flodin, N., 1960. The development of soil mechanics in Sweden 1900 - 1925. *Geotechnique* 10(1) 1-18.
- Boardman, T.B., 2007. Discussion on Assessment of the liquefaction susceptibility of fine-grained soils. *ASCE J. Geotechnical and Geoenvironmental Engineering*, (134)7 1030-1031.
- Boulanger, R.W. and Idriss, I.M., 2007. Closure to Discussion on Liquefaction susceptibility criteria for silt and clays. *ASCE J. Geotechnical and Geoenvironmental Engineering*, (134)7 1027-1028.
- Bray, J.D. and Sancio, R.B., 2006. Assessment of the liquefaction susceptibility of fine-grained soils. *ASCE J. Geotechnical and Geoenvironmental Engineering*, (132)11 1165-1187.
- Bray, J.D. and Sancio, R.B., 2007. Closure to Discussion on Assessment of the liquefaction susceptibility of fine-grained soils. *ASCE, J. Geotechnical and Geoenvironmental Engineering*, (134)7 1031-1034.
- Boussinesq, J., 1885. *Application des potentiels a l'etude de l'equilibre et due mouvement des solides elastiques*. Gauthiers-Villars, Paris, (as referenced by Holtz and Kovacs, 1981).
- Bowles, J.E., 1988. *Foundation analysis and design*, Fourth Edition. McGraw-Hill Book Company, New York, 1004 p.
- Bozozuk, M. and Labrecque, A., 1968. Proc. of Symposium of Deep Foundations, STP 444, Edited by R. Lundgren and E. D'Appolonia, ASTM 71st Annual Meeting, ,San Francisco June 23-28, pp. 15-40.
- Bozozuk, M., Fellenius, B.H. and Samson, L., 1978. Soil disturbance from pile driving in sensitive clay. *Canadian Geotechnical Journal* 15(3) 346-361.
- Briaud, J-L and Gibbens, R.M., 1994. Predicted and measured behavior of five spread footings on sand. Proc. of a Symposium sponsored by the Federal Highway Administration at the 1994 American Society of Civil Engineers, ASCE, Conference Settlement '94, College Station, Texas, June 16-18, pp., 192-128.
- Briaud, J.-L., and Gibbens, R.M., 1999. Behavior of five large spread footings in sand. *ASCE J. Geotechnical and Geoenvironmental Engineering* 125(9) 787-796.
- Briaud, J-L, Nicks J, Rhee, K., and Stieben, G., 2007. San Jacinto Monument case history. *ASCE J. Geotechnical and Geoenvironmental Engineering*, (133)11 1337-1351.
- Broms, B.B., 1976. Pile foundations—pile groups. 6th ECSMFE ,Vienna, Vol. 2.1 pp. 103-132.



- Brown, M.J., Hyde, A.F.L., and Anderson, W.F. (2006). Analysis of a rapid load test on an instrumented bored pile in clay, *Geotechnique*, 56(9), 627-638.
- Brown, D., 2012. Recent advances to the selection and use of drilled foundations. ASCE GeoInstitute Geo-Congress Oakland, March 25-29, 2012, Keynote Lectures, State of the Art and Practice in Geotechnical Engineering, ASCE, Reston, VA, Rollins, K. and Zekkos, D., eds., *Geotechnical Special Publication 226*, pp. 519-548.
- Boulanger, R.W. and Idriss, I.M., 2007. Closure to Discussion on Liquefaction susceptibility criteria for silt and clays. *ASCE J. Geotechnical and Geoenvironmental Engineering*, (134)7 1027-1028.
- Buisman, A.S.K., 1935. De weerstand van paalpunten in zand. *De Ingenieur*, No. 50, pp. 25 - 28 and 31 - 35. (As referenced by Vesic, 1973).
- Buisman, A.S.K., 1940. *Grondmechanica*. Walman, Delft, 281 p. (As referenced by Vesic, 1973, and Tschebotarioff, 1951).
- Bullock, P., Schmertmann, J., McVay, M.C., and Townsend, F.C., 2005. Side shear set-up. Test piles driven in Florida. *ASCE Journal of Geotechnical and Geoenvironmental Engineering*, 131(3) 292-310.
- Bullock, P., 2012. Advantages of dynamic pile testing. ASCE GeoInstitute Geo-Congress Oakland, March 25-29, 2012, Full-scale Testing in Foundation Design, State of the Art and Practice in Geotechnical Engineering, ASCE, Reston, VA, M.H. Hussein, K.R. Massarsch, G.E. Likins, and R.D. Holtz, eds., *Geotechnical Special Publication 227*, pp. 694-709.
- Bustamante, M. and Gianselli, L., 1982. Pile bearing capacity predictions by means of static penetrometer CPT. *Proc. of the Second European Symposium on Penetration Testing, ESOPT II*, Amsterdam, May 24-27, A.A. Balkema, Vol. 2, pp. 493-500.
- Campanella, R.G., Gillespie, D., and Robertson, P.K., 1982. Pore pressures during cone penetration testing, *Proc. of the 2nd European Symposium on Penetration Testing, ESOPT-2*, Amsterdam, May 24 - 27, Vol. 2, pp. 507 - 512.
- Campanella, R.G., and Robertson, P.K., 1988. Current status of the piezocone test. *Proc. of First International Symposium on Penetration Testing, ISOPT-1*, Orlando, March 22 - 24, Vol. 1, pp. 93 - 116.
- Canadian Standard Council, 2006. Canadian Highways Bridge Design Code, Section 6, Foundations. Canadian Standard Association, CSA-S6-06, Code and Commentary, 1,340 p.
- Canadian Foundation Engineering Manual, CFEM, 1985. Second Edition. Canadian Geotechnical Society, BiTech Publishers, Vancouver, 456 p.
- Canadian Foundation Engineering Manual, CFEM, 1992. Third Edition. Canadian Geotechnical Society, BiTech Publishers, Vancouver, 512 p.
- Canadian Foundation Engineering Manual, CFEM, 2006. Fourth Edition. Canadian Geotechnical Society, BiTech Publishers, Vancouver, 488 p.
- Caputo, V. and Viggiani, C. 1984. Pile foundation analysis: a simple approach to nonlinearity effects. *Rivista Italiana di Geotecnica*, 18(2): 32-51.
- Carrillo N. 1942. Simple two- and three-dimensional cases in the theory of consolidation of soils. *Journal of Mathematics and Physics*, 21(1) 1-5.
- Caquot, A. and Kerisel, J., 1953. Sur le terme de surface dans le calcul des fondations en milieu pulvérulent. *Proc. of the 3rd ICSMFE, Zurich, August 16-27, Vol. 1*, pp. 336-337.
- Casagrande, A., 1935. Characteristics of cohesionless soil affecting the stability of slopes and earth fills. *Journal of the Boston Society of Soil Mechanics*. Vol. 23, pp. 13-32.
- Casagrande, L. and Poulos, S., 1969. On the effectiveness of sand drains. *Canadian Geotechnical Journal*, 6(3) 287-326.
- Chai, J.C., Carter, J.P., and Hayashi, S., 2005. Ground deformation induced by vacuum consolidation. *ASCE Journal for Geotechnical and Geoenvironmental Engineering*, 131(12) 1552-1561.
- Chang, Y.C.E., 1981. Long-term consolidation beneath the test fills at Väsby, Sweden. Swedish Geotechnical Institute, Report 13, 192 p.
- Chai, J.C., Carter, J.P., and Hayashi, S., 2006. Vacuum consolidation and its combination with embankment loading. *Canadian Geotechnical Journal* 43(10) 985-996.

- Chellis, R.D., 1951. Pile Foundations. McGraw Hill Book Company, 704 p.
- Chin, F.K., 1970. Estimation of the ultimate load of piles not carried to failure. Proc. of the 2nd Southeast Asian Conference on Soil Engineering, pp. 81-90.
- Chin, F.K., 1971. Discussion on Pile test. Arkansas River project. ASCE Journal for Soil Mechanics and Foundation Engineering, 97(SM6) 930-932.
- Chin, F.K., 1978. Diagnosis of pile condition. Lecture at 6th Southeast Asian Conference on Soil Engineering, Bangkok, 1977, Geological Engineering, Vol. 9, pp. 85 - 104.
- Clausen, C.J.F., Aas, P.M., and Karlsrud, K., 2005. Bearing capacity of driven piles in sand, the NGI approach. Proc. International Symposium. on Frontiers in Offshore Geotechnics, Perth, September 2005, A.A. Balkema Publishers, pp. 574 - 580.
- Cortlever, N.G., Visser, G.T., and deZwart, T.P., 2006. Geotechnical History of the development of the Suvarnabhumi International Airport. Special Issue of the Journal of South-East Asian Geotechnical Society, December 2006, 37(3) 189-194.
- Crawford, C.B., 1968. Instrumentation and downdrag. Proc. of Symposium of Deep Foundations, STP 444, Edited by R. Lundgren and E. D'Appolonia, ASTM 71st Annual Meeting, San Francisco June 23-28, pp. 223-226.
- Dahlberg, R., 1975. Settlement Characteristics of Preconsolidated Natural Sands. Swedish Council for Building Research, Document D1:1975, 315 p.
- Davissom, M.T., 1972. High capacity piles. Proc. of Lecture Series on Innovations in Foundation Construction, ASCE Illinois Section, Chicago, March 22, pp. 81-112.
- DeBeer, E.E., 1968. Proefondervindlijke bijdrage tot de studie van het grensdrag vermogen van zand onder funderingen op staal. Tijdschrift der Openbar Verken van België, No. 6, 1967 and No. 4, 5, and 6, 1968.
- DeBeer, E.E. and Walays, M., 1972. Franki piles with overexpanded bases. La Technique des Travaux, Liege, Belgium, No. 333.
- Decourt, L., 1982. Prediction of bearing capacity of piles based exclusively on N-values of the SPT. Proc. ESOPT II, Amsterdam, May 24-27, pp. 19-34.
- Decourt, L., 1989. The Standard Penetration Test. State-of-the-Art report. A.A. Balkema, Proc. of 12th International Conference on Soil Mechanics and Foundation Engineering, Rio de Janeiro, Brazil, August 13-18, Vol. 4, pp. 2405-2416.
- Decourt, L., 1995. Prediction of load-settlement relationships for foundations on the basis of the SPT. Proc. of the Conf. in honor of Leonardo Zeevaert, Mexico City, Oct. 28-Nov. 6, pp. 87-103.
- Decourt, L., 1999. Behavior of foundations under working load conditions. Proc. of 11th Pan-American Conference on Soil Mechanics and Geotechnical Engineering, Foz DoIguassu, Brazil, August 1999, Vol. 4, pp. 453-488.
- Decourt, L., 2008. Loading tests: interpretation and prediction of their results. ASCE GeoInstitute Geo-Congress New Orleans, March 9-12, Honoring John Schmertmann—From Research to Practice in Geotechnical Engineering, Geotechnical Special Publication, GSP 180, Edited by J.E. Laier, D.K. Crapps, and M.H. Hussein, pp. 452-488.
- Deep Foundations Institute, DFI, 1979. A pile inspector's guide to hammers, Sparta, New Jersey, 41 p.
- DeRuiter, J. and Beringen F.L., 1979. Pile foundations for large North Sea structures. Marine Geotechnology, 3(3) 267-314.
- Dobry R., Peck, R.B., and Pecker, A., 2007 Rion-Antirion Bridge. An Olympian effort to overcome extreme geohazards. Deep Foundations Institute Magazine, Fall issue, pp. 5- 8.
- Duncan, J.M., Evans, L.T., and Ool, P.S.K., 1992. Lateral load analysis of single piles and drilled shafts. ASCE Journal of Geotechnical Engineering Division, 120(5) 1018-1033.
- Douglas, B.J., and Olsen, R.S., 1981. Soil classification using electric cone penetrometer. ASCE Proc. of Conference on Cone Penetration Testing and Experience, St. Louis, October 26 - 30, pp. 209 - 227.
- Dunnicliff, J., 1988. Geotechnical Instrumentation for monitoring field performance. John Wiley & Sons, New York, 577 p.

- Elisio, P.C.A.F., 1983. Celula Expansiva Hidrodinamica – Uma nova maneira de executar provas de carga (Hydrodynamic expansive cell. A new way to perform loading tests). Independent publisher, Belo Horizonte, Minas Gerais State, Brazil, 106 p.
- Elisio, P.C.A.F., 1986. Celula expansiva hidrodinamica; uma nova maneira de executar provas de carga (Hydrodynamic expansion cell; a new way of performing loading tests). Proc. of VIII Congresso Brasileiro de Mecânica dos Solos e Engenharia de Fundações, VIII COBRAMSEF, Porto Alegre, Brazil, October 12-16, 1986, Vol. 6, pp. 223-241.
- Endley, S.N., Yeung, A.T., and Vennalaganti, K.M., 1996. A study of consolidation characteristics of Gulf Coast clays. Proc. of Texas Section of ASCE, Fall Meeting, San Antonio, Texas, September 18-21, 152-160.
- Endo M., Minou, A., Kawasaki T, and Shibata, T, 1969. Negative skin friction acting on steel piles in clay. Proc. 7th ICSMFE, Mexico City, August 25 - 29, Vol. 2, pp. 85- 92.
- Erwig, H., 1988. The Fugro guide for estimating soil type from CPT data. Proc. of Seminar on Penetration Testing in the UK, Thomas Telford, London, pp. 261-263.
- Eslami, A., 1996. Bearing capacity of piles from cone penetrometer test data. Ph. D. Thesis, University of Ottawa, Department of Civil Engineering, 516 p.
- Eslami, A., and Fellenius, B.H., 1995. Toe bearing capacity of piles from cone penetration test (CPT) data. Proc. of the International Symposium on Cone Penetration Testing, CPT 95, Linköping, Sweden, October 4 - 5, Swedish Geotechnical Institute, SGI, Report 3:95, Vol. 2, pp. 453 - 460.
- Eslami, A., and Fellenius, B.H., 1996. Pile shaft capacity determined by piezocone (CPTU) data. Proc. of 49th Canadian Geotechnical Conference, September 21 - 25, St. John's, Newfoundland, Vol. 2, pp. 859 - 867.
- Eslami, A. and Fellenius, B.H., 1997. Pile capacity by direct CPT and CPTu methods applied to 102 case histories. Canadian Geotechnical Journal 34(6) 886–904.
- Eurocode, 1990. Eurocode, Chapter 7, Pile Foundations (preliminary draft), 25 p.
- Federal Highway Administration, FHWA, 2016. Geotechnical Engineering Circular No. 12, Design and Construction of Driven Pile Foundations, Report No. FHWA-NH-16-009, Volumes 1 and 2., 539 p.
- Fellenius, W. 1918. Kaj- och jordrasen i Göteborg (The quay and earth slides in Gothenburg). Teknisk Tidskrift 48 17-19.
- Fellenius W., 1926. Erdstatische Berechnungen mit Reibung und Kohäsion (Adhäsion) und unter Annahme kreiszylindrischer Gleitflächen. Verlag von Ernst und Sohn, Berlin. 47 p.
- Fellenius, W. 1926. Jordstatiska beräkningar med friktion och kohesion för cirkulär cylindriska glidytor (Earth stability calculations with friction and cohesion for circular-cylindrical slip surfaces). Kungl. Väg- och Vattenbyggarkårens 75-årsskrift, pp. 79-127.
- Fellenius, W. 1926. Erdstatische Berechnung mit Reibung und Kohäsion (Adhäsion) und unter Annahme Kreiszylindrischer Gleitflächen. Ernst, Berlin, 40 p.
- Fellenius, W. 1929. Jordstatiska beräkningar för vertikalbelastning på horisontal markyta under antagande av cirkulär cylindriska glidytor (Stability calculations for vertical loads on horizontal ground surface assuming cylindrical failure surfaces). Teknisk Tidskrift 29 57-63.
- Fellenius, W. 1936. Calculation of the stability of earth dams. Proc. of the Second Congress on Large Dams, Washington, DC, p. 445-462.
- Fellenius, B.H., 1972. Bending of piles determined by inclinometer measurements. Canadian Geotechnical Journal 9(1) 25-32.
- Fellenius B.H., 1975. Reduction of negative skin friction with bitumen slip layers. Discussion. ASCE Journal of Geotechnical Engineering Division, 101(GT4) 412-414.
- Fellenius B.H., 1975. Test loading of piles. Methods, interpretation, and new proof testing procedure. ASCE Journal of Geotechnical Engineering Division, 101(GT9) 855-869.
- Fellenius B.H., 1977. The equivalent sand drain diameter of the bandshaped drain. Discussion. Proc. 9th ICSMFE, Tokyo, July 10-15, Vol. 3, p. 395-396.
- Fellenius B.H., 1979. Downdrag on bitumen coated piles. Discussion. ASCE Journal of Geotechnical Engng., 105(GT10) 1262-1265.

- Fellenius, B.H., 1980. The analysis of results from routine pile loading tests. *Ground Engineering*, London, 13(6) 19-31.
- Fellenius, B.H., 1981. Consolidation of clay by band-shaped premanufactured drains. Discussion. *Ground Engineering*, London, 14(8) 39-40.
- Fellenius, B.H., 1984. Negative skin friction and settlement of piles. *Proc. of the Second International Seminar, Pile Foundations*, Nanyang Technological Institute, Singapore, 18 p.
- Fellenius, B.H., 1984. Ignorance is bliss—and that is why we sleep so well. *Geotechnical News*, 2(4) 14-15.
- Fellenius, B.H., 1984. Wave equation analysis and dynamic monitoring. *Deep Foundations Journal*, Deep Foundations Institute, Springfield, New Jersey 1(1) 49-55.
- Fellenius, B.H., 1988. Unified design of piles and pile groups. *Transportation Research Board*, Washington, TRB Record 1169, pp. 75-82.
- Fellenius, B.H., 1989. Tangent modulus of piles determined from strain data. *The ASCE Geotechnical Engineering Division, 1989 Foundation Congress*, Edited by F. H. Kulhawy, Vol. 1, pp. 500 - 510.
- Fellenius, B.H., 1994. Limit states design for deep foundations. *FHWA International Conference on Design and Construction of Deep Foundations*, Orlando, December 1994, Vol. II, pp. 415 - 426.
- Fellenius, B.H., 1995. Foundations. Chapter 22 in *Civil Engineering Handbook*, Edited by W. F. Chen. CRC Press, New York, pp. 817 - 853.
- Fellenius, B.H., 1996. Reflections on pile dynamics. *Proc. of the 5th International Conference on the Application of Stress-Wave Theory to Piles*, September 10 through 13, Orlando, Florida, Edited by M.C. McVay, F. Townsend, and M. Hussein, Keynote Paper, pp. 1 - 15.
- Fellenius, B.H., 1998. Recent advances in the design of piles for axial loads, dragloads, downdrag, and settlement. *Proc. of a Seminar by ASCE and Port of New York and New Jersey*, April 1998, 19 p.
- Fellenius, B.H., 1999. Bearing capacity of footings and piles—A delusion? *Proc. of the Deep Foundation Institute Annual Meeting*, October 14 though 16, Dearborn 17 p.
- Fellenius, B.H., 2000. The O-Cell — A brief introduction to an innovative engineering tool. *Väg- och Vattenbyggaren* 47(4) 11-14.
- Fellenius, B.H., 2002. Determining the resistance distribution in piles. Part 1: Notes on shift of no-load reading and residual load. Part 2: Method for Determining the Residual Load. *Geotechnical News Magazine*. *Geotechnical News Magazine*, 20(2 35-38), and 20(3 25-29).
- Fellenius, B.H., 2002. Pile Dynamics in Geotechnical Practice—Six Case Histories. *ASCE International Deep Foundation Congress, An International Perspective on Theory, Design, Construction, and Performance*, *Geotechnical Special Publication No. 116*, Edited by M.W. O'Neill, and F.C. Townsend, Orlando Florida February 14 - 16, 2002, Vol. 1, pp. 619 - 631.
- Fellenius, B.H., 2004. Unified design of piled foundations with emphasis on settlement analysis. *Current Practice and Future Trends in Deep Foundations GeoInstitute Geo-TRANS Conference*, Los Angeles, July 27-30, 2004, Edited by J.A. DiMaggio and M.H. Hussein. *ASCE Geotechnical Special Publication*, GSP 125, pp. 253-275.
- Fellenius, B.H., 2006. Results from long-term measurement in piles of drag load and downdrag. *Canadian Geotechnical Journal* 43(4) 409-430.
- Fellenius, B.H., 2008. Effective stress analysis and set-up for shaft capacity of piles in clay. *ASCE GeoInstitute Geo-Congress New Orleans*, March 9-12, Honoring John Schmertmann—From Research to practice in Geotechnical Engineering, *ASCE Geotechnical Special Publication*, Edited by J.E. Laier, D.K. Crapps, and M.H. Hussein, GSP180, pp. 384-406.
- Fellenius, B.H., 2011. Capacity versus deformation analysis for design of footings and piled foundations. *Southeast Asian Geotechnical Society, Bangkok*, *Geotechnical Engineering Journal* 41(2) 70-77.
- Fellenius, B.H., 2012. Critical assessment of pile modulus determination methods—Discussion. *Canadian Geotechnical Journal* 49(5) 614-621.
- Fellenius, B.H., 2013. Capacity and load-movement of a CFA pile: A prediction event. *GeoInstitute Geo Congress San Diego*, March 3-6, 2013, Honoring Fred H. Kulhawy—Foundation Engineering in the Face of Uncertainty, *ASCE*, Reston, VA, James L. Withiam, Kwok-Kwang Phoon, and Mohamad H. Hussein, eds., *Geotechnical Special Publication*, GSP 229, pp. 707-719.

- Fellenius, B.H., 2014. Analysis of results from routine static loading tests with emphasis on the bidirectional test. Proceedings of the 17th Congress of the Brasileiro de Mecanica dos Solos e Engenharia, Comramseg, Goiania, Brazil, September 10 - 13, 22 p.
- Fellenius, B.H., 2014. Piled foundation design as reflected in codes and standards. Proc. of the DFI-EFFC International Conference on Piling and Deep Foundations, Stockholm, May 21-23, pp. 1013-1030.
- Fellenius, B.H., 2015. The response of a "plug" in an open-toe pipe pile. Geotechnical Engineering Journal of the SEAGS & AGSSEA 46(2) 82-86.
- Fellenius, B.H., 2015. Static tests on instrumented piles affected by residual load. Journal of the Deep Foundation Institute, 9(1) 11-20.
- Fellenius, B.H., 2016. The unified design of piled foundations. The Sven Hansbo Lecture. Geotechnics for Sustainable Infrastructure Development – Geotec Hanoi 2016, edited by Phung Duc Long, Hanoi, November 23-25, pp. 3-28.
- Fellenius, B.H., 2016. Fallacies in piled foundation design. Geotechnics for Sustainable Infrastructure Development– Geotec Hanoi 2016, edited by Phung Duc Long, Hanoi, November 23-25, pp. 41-46.
- Fellenius, B.H., 2016. An Excel template cribsheet for use with UniPile and UniSettle. [www.Fellenius.net](http://www.Fellenius.net).
- Fellenius, B.H., 2017. Report on the results of the prediction survey of the 3rd CBFP event. 3rd Bolivian International Conference on Deep Foundations, Santa Cruz de la Sierra, Bolivia, April 27-29, Vol. 3, 19p.
- Fellenius B.H., Samson, L., Thompson, D. E., and Trow, W., 1978. Dynamic Behavior of foundation piles and driving equipment. Terratech Ltd. and the Trow Group Ltd., Final Report, Department of Supply and Services, Canada, Contract No. 1ST77.00045, Vol. I and II, 580 p.
- Fellenius, B.H., Riker, R. E., O'Brien, A. J. and Tracy, G. R., 1989. Dynamic and static testing in a soil exhibiting setup. ASCE Journal of Geotechnical Engineering, 115(7) 984-1001.
- Fellenius, B.H. and Altaee, A., 1994. The critical depth—How it came into being and why it does not exist. Proc. of the Institution of Civil Engineers, Geotechnical Engineering Journal, London, 113(2) 107-111.
- Fellenius, B.H. and Altaee, A., 1996. The critical depth – How it came into being and why it does not exist. Reply to Discussion. Proc. of the Institution of Civil Engineers, Geotechnical Engineering Journal, London, 119(4) 244-245.
- Fellenius, B.H., Altaee, A., Kulesza, R, and Hayes, J, 1999. O-cell Testing and FE analysis of a 28 m Deep Barrette in Manila, Philippines. ASCE Journal of Geotechnical and Environmental Engineering, 125(7) 566-575.
- Fellenius, B.H., Brusey, W. G., and Pepe, F., 2000. Soil set-up, variable concrete modulus, and residual load for tapered instrumented piles in sand. ASCE Specialty Conference on Performance Confirmation of Constructed Geotechnical Facilities, University of Massachusetts, Amherst, April 9 - 12, 2000, Special Geotechnical Publications, GSP94, pp. 98 - 114.
- Fellenius, B.H. and Eslami, A., 2000. Soil profile interpreted from CPTu data. Proc. of Year 2000 Geotechnics Conference, Southeast Asian Geotechnical Society, Asian Institute of Technology, Bangkok, Thailand, November 27-30, 2000, Editors Balasubramaniam, A.S., Bergado, D.T., Der Gye, L., Seah, T.H., Miura, K., Phien wej, N., and Nutalaya, P., Vol. 1, pp. 163-171.
- Fellenius, B.H., Harris, D., and Anderson, D.G., 2004. Static loading test on a 45 m long pipe pile in Sandpoint, Idaho. Canadian Geotechnical Journal 41(4) 613-628.
- Fellenius, B.H. and Massarsch, K.M., 2008. Comments on the current and future use of pile dynamic testing. Keynote Lecture, The 8th International Conference on the Application of Stress Wave Theory to Piles. Edited by L.A. Santos, Lisbon September 8 10, 2008, pp. 7-17.
- Fellenius, B.H. and Siegel, T.C, 2008. Pile design consideration in a liquefaction event. ASCE Journal of Geotechnical and Environmental Engineering, 132(9) 1312-1416.
- Fellenius, B.H., Kim, S.R., and Chung, S.G., 2009. Long-term monitoring of strain in instrumented piles. ASCE Journal of Geotechnical and Geoenvironmental Engineering, 135(11) 1583-1595.
- Fellenius, B.H. and Ochoa, M., 2009. San Jacinto Monument Case History. Discussion. ASCE Journal of Geotechnical Engineering, 133(1) 162-167.

- Fellenius, B.H., and Ochoa, M., 2009. Testing and design of a piled foundation project. A case history. Southeast Asian Geot. Society, Bangkok, Geotechnical Engineering. Journal 40(3) 129-137.
- Fellenius, B.H. and Tan, S.A., 2010. Combination of O-cell test and conventional head-down test. Honoring Clyde Baker—the Art of Foundation Engineering Practice, eds., ASCE Geotechnical Special Publication, GSP198, pp. 240-259.
- Fellenius, B.H. and Tan, S.A., 2012. Analysis of bidirectional-cell tests for Icon Condominiums, Singapore. Proc. of the 9th International Conference on Testing and Design Methods for Deep Foundations, Kanazawa, Japan, September 18-20, 2012. 10 p.
- Fellenius, B.H., and Nguyen, M.H., 2013. Large diameter long bored piles in the Mekong delta. International Journal of Case Histories 2(3) 196-207.
- Fellenius, B.H. and Nguyen M.H., 2013. Wick Drains and Piling for Cai Map Container Port, Vietnam. Honoring Robert D. Holtz—Sound Geotechnical Research to Practice. ASCE Geotechnical Special Publication, GSP 230, Edited by A.W. Stuedlein and B.R. Christopher. pp. 445-462.
- Fellenius, B.H., and Nguyen, M.H., 2014. Bidirectional-cell tests on two 70 m long bored piles in Vietnam. GeoInstitute Geo Congress, Atlanta, February 23-26, ASCE, Reston, VA, Honoring Roy Olson—From Soil Behavior Fundamentals to Innovations in Geotechnical Engineering, Magued Iskander, John E. Garlanger, and Mohamad H. Hussein, editors, Geotechnical Special Publication, GSP 233, pp. 482-496.
- Fellenius, B.H. and Ochoa, M., 2016. Wide storage tanks on piled foundations. Geotechnical Engineering Journal of the SEAGS & AGSSEA 47(1) 50-62.
- Finno, R. J., 1989. Subsurface conditions and pile installation data. American Society of Civil Engineers, Proc. of Symposium on Predicted and Observed Behavior of Piles, Evanston, June 30, ASCE Geotechnical Special Publication, GSP23, pp. 1-74.
- Flodin, N. and Broms, B.B., 1981 History of civil engineering in soft clay. In "Soft Clay Engineering" Edited by. E.W. Brand and R.P. Brenner., Elsevier Scientific Publishing Co., Chapter 1, pp.27 - 156.
- Frank, R., Baudin, C., Driscoll, M., Kavvada, M., Krebs Ovesen, N., Orr, T., and Schuppener, B., 2004. Designers' Guide to EN 1997-1. Eurocode 7: Geotechnical Design, General Rules. Thomas Telford, 216 p.
- Franke E., 1991. Measurements beneath piled rafts. International Conference on Deep Foundations, Ecole National des Ponts et Chaussees, Paris, March 19 21, pp. 599-626.
- Gibson, G.L. and Devenny, D.W., 1973. Concrete to bedrock testing by jacking from bottom of a borehole, Canadian Geotechnical Journal 10(2) 304-306.
- Gilboy, G., 1928. The compressibility of sand-mica mixtures. Proc. of ASCE Vol. 54, 555-568.
- Goossens, D. and Van Impe, W.F., 1991. Long-term settlement of a pile group foundation in sand, overlying a clayey layer. Proc. 10th European Conference on Soil Mechanics and Foundation Engineering, Firenze, May 26-30, Vol. I, pp. 425-428.
- Goble, G. G., Rausche, F., and Likins, G.E., 1980. The analysis of pile driving—a state-of-the-art. Proc. of the 1st International Seminar of the Application of Stress-wave Theory to Piles, Stockholm, Edited by H. Bredenberg, A. A. Balkema Publishers Rotterdam, pp. 131 - 161.
- Goudreault, P.A. and Fellenius, B.H., 2011. UniSettle Version 4 tutorial with background and analysis examples. UniSoft Geotechnical Solutions Ltd. [www.UniSoftLtd.com]. 85 p.
- Goudreault, P.A. and Fellenius, B.H., 2014. UniPile Version 5, User and Examples Manual. UniSoft Geotechnical Solutions Ltd. [www.UniSoftLtd.com]. 120 p.
- Gregersen, O.S., Aas, G., and DiBiagio, E., 1973. Load tests on friction piles in loose sand. Proc. of 8th ICSMFE, Moscow, August 12-19, Vol. 2.1, Paper 3/17, pp. 109–117.
- Greenfield, M. and Filtz, G. 2009. Downdrag and drag loads on piles. Virginia Tech Center for Geotechnical Practice and Research, Blacksburg, CGPR #56, 108 p.
- GRL, 2002. Background and Manual on GRLWEAP Wave equation analysis of pile driving. GRL Engineers Inc., Cleveland.
- Grozic, J.L.H., Lunne, T., and Pande, S, 2003. An oedometer test study of the preconsolidation stress of glaciomarine clays. Canadian Geotechnical Journal, 40(5) 857-872.

- Gwizdala, K., 1996. The analysis of pile settlement employing load-transfer functions (in Polish). *Zeszyty Naukowe* No. 532, *Budownictwo Wodne* No.41, Technical University of Gdansk, Poland, 192 p.
- Hanifah, A.A. and Lee S.K., 2006. Application of global strain extensometer (Glostrext) method for instrumented bored piles in Malaysia. *Proc. of the DFI-EFFC 10th Int. Conference on Piling and Deep Foundations*, May 31 - June 2, Amsterdam, 8 p.
- Hannigan, P.J., 1990. Dynamic monitoring and analysis of pile foundation installations. Deep Foundation Institute, Sparta, New Jersey, 69 p.
- Hannigan, P.J., Goble, G.G, Likins, G.E., and Rausche, F. 2006 Design and Construction of Driven Pile Foundations, Federal Highway Administration, FHWA, Reference Manual – Volume I and II, National Highway Institute, NHI-05-042, Courses Nos. 132021 and 132022, 1,454 p.
- Hansbo, S., 1960. Consolidation of clay with special reference to influence of vertical sand drains. Swedish Geotechnical Institute, Stockholm, *Proceedings* No. 18, 160 p.
- Hansbo, S., 1979. Consolidation of clay by band-shaped prefabricated drains. *Ground Engineering*, London, 12(5) 16-25.
- Hansbo, S., 1981. Consolidation of fine-grained soil by prefabricated drains. 10th ICSMFE, Stockholm June 15-19, A.A. Balkema, Rotterdam, pp. 677-682.
- Hansbo, S. 1984. Foundations on creep piles in soft clays. First International Conference on Case Histories in Geotechnical Engineering, St. Louis, May 6-11, 1984, pp. 259-264.
- Hansbo, S., 1993. Interaction problems related to the installation of pile groups. *Proceedings of the 2nd International Geotechnical Seminar on Deep Foundations on Bored and Auger Piles*, Ghent, 1–4 June, 1993, pp. 119–130.
- Hansbo, S., 1994. *Foundation Engineering*. Elsevier Science B. V., Amsterdam, *Developments in Geotechnical Engineering* No. 75, 519 p.
- Hansbo, S. and Jendebý, L., 1998. A follow-up of two different foundation principles. Foundations on friction creep piles in soft clays. *International Conference on Case Histories in Geotechnical Engineering*. St. Louis, March 9-12, 259-264.
- Hansen, J.B., 1961. A general formula for bearing capacity. *Ingeniøren International Edition*, Copenhagen, Vol. 5, pp. 38 - 46. Also in *Bulletin* No. 11, Danish Geotechnical Institute Copenhagen, 9 p.
- Hansen, J.B., 1963. Discussion on hyperbolic stress-strain response. Cohesive soils. *ASCE Journal for Soil Mechanics and Foundation Engineering*, 89(SM4) 241 - 242.
- Heckman, W.S. and Hagerty, D.J., 1978. Vibrations associated with pile driving. *American Society of Civil Engineering, Journal of the Construction Division*, 104 (CO4) 385 394.
- Harris, D., Anderson, D.G., Fellenius, B.H., Butler, J.J., and Fischer, G.S., 2003. Design of Pile Foundations for the Sand Creek Byway, Sandpoint, Idaho. *Proc. of Deep Foundation Institute Annual Meeting*, Miami, October 23 - 26, 2003.
- Holloway, D.M., Clough, G.W., and Vesic A.S., 1978. The effects of residual driving stresses on pile performance under axial load. *Proc. of the 10th Offshore Technology Conference*, Houston, TX., Vol. 4, pp. 2225-2236.
- Holtz, R.D. and Wager, O., 1975. Preloading by Vacuum—Current Prospects. *Transportation Research Record* 548, pp. 26-29.
- Holtz, R.D. and Kovacs, W.D., 1981. *An introduction to geotechnical engineering*. Prentice-Hall Inc., New York, 780 p.
- Holtz, R.D., 1990. Stress distribution and settlement of shallow foundations. Chapter 5, *Foundation Engineering Handbook*, 2nd Edition, H-Y Fang, Editor, Van Nostrand Reinhold Book Co., pp. 166-216.
- Holtz, R.D., Jamiolkowski, M. B., Lancelotta, R., and Peroni, R., 1991. Prefabricated vertical drains. Design and Performance. *Construction Industry Research and Information Association*, CIRIA, London, 131 p.
- Holtz, R.D., Kovacs, W.D., and Sheahan, T., 2011. *An introduction to geotechnical engineering*, 2nd Edition. Pearson, New York, 853 p.

- Hong Kong Geo, 2006. Foundation design and construction. Hong Kong Geotechnical Engineering Office, No. 1/2006, 376 p.
- Horvath, R.G., Kenney, T.C., and Kozicki, P., 1983. Methods of improving the performance of drilled piers in weak rock. *Canadian Geotechnical Journal*, 20(3) 758-772.
- Housel, W.S., 1956. Field and laboratory correlation of the bearing capacity of hardpan for the design of deep foundation. *Proc. of American Society for Materials and Testing, ASTM*, Vol. 56, pp. 1,320 - 1,346.
- Huang, A.B., Huai, H.H., and Chang, J.W. 1999. The behavior of a compressible silty fine sand, *Canadian Geotechnical Journal*, 36(1) 88-101.
- Hunter A.H. and Davisson M.T., 1969. Measurements of pile load transfer. *Proc. of Symposium on Performance of Deep Foundations*, San Francisco, June 1968, American Society for Testing and Materials, ASTM, Special Technical Publication, STP 444, pp. 106-117.
- Ismael, N.F., 1985. Allowable bearing pressure from loading tests on Kuwaiti soils. *Canadian Geotechnical Journal*, 22(2) 151-157.
- Iwanowski, T. and Bodare, A., 1988. On soil damping factor used in wave analysis of pile driving. *Third International Conference on Application of Stress-wave Theory to Piles*, Ottawa, May 25-27, 1988, Edited by B.H. Fellenius, pp. 343-352.
- Jaky, J., 1948. Earth pressure in silos. *Proc. 2nd ICSMFE*, Rotterdam, June 21-30, Vol. 1, pp. 103 - 107.
- Jamiolkowski, M., Ghionna, V. N., Lancelotta R. and Pasqualini, E., 1988. New correlations of penetration tests for design practice. *Proc. Penetration Testing, ISOPT-1*, DeRuiter (ed.), Balkema, Rotterdam, ISBN 90 6191 801 4, pp 263-296
- Janbu, N., 1963. Soil compressibility as determined by oedometer and triaxial tests. *European Conference on Soil Mechanics and Foundation Engineering*, Wiesbaden, October 15 -18, Vol. 1, pp., 19-25, and Discussion contribution, Vol. 2, pp. 17-21.
- Janbu, N., 1965. Consolidation of clay layers based on non-linear stress-strain. *Proc. 6th ICSMFE*, Montreal, Vol. 2, pp. 83-87.
- Janbu, N., 1967. Settlement calculations based on the tangent modulus concept. University of Trondheim, Norwegian Institute of Technology, Geotechnical Institution, Bulletin 2, 57 p.
- Janbu, N., 1998. Sediment deformations. University of Trondheim, Norwegian University of Science and Technology, Geotechnical Institution, Bulletin 35, 86 p.
- Janbu, N., Bjerrum, L., and Kjaernsli B, 1956. Veiledning ved losning av fundamenteringsoppgaver. Norwegian Geotechnical Institute, Publication No. 16, 93 p. (in Norwegian).
- Jardine, J., Chow, F., Overy, R., and Standing, J., 2005. ICP design method for driven piles in sands and clays. Thomas Telford Publishing Ltd., London, 105 p.
- Jefferies, M.G., and Davies, M.P., 1991. Soil classification using the cone penetration test. Discussion. *Canadian Geotechnical Journal*, 28(1) 173-176.
- Johannessen, I.J. and Bjerrum, L. 1965. Measurements of the compression of a steel pile to rock due to settlement of the surrounding clay. *Proc. 6th ICSMFE*, Montreal, September 8-15, Vol. 6, pp. 261-264.
- Jones G.A., and Rust, E., 1982. Piezometer penetration testing, CUPT. *Proc. of the 2nd European Symposium on Penetration Testing, ESOPT-2*, Amsterdam, May 24-27, Vol. 2, pp. 607-614.
- Justason, M. and Fellenius, B.H., 2001. Static capacity by dynamic methods for three bored piles. Discussion. *ASCE Journal of Geotechnical Engineering*, Vol. 127, No. 12, pp. 1081 - 1084.
- Kakurai, M., Yamashita, K., and Tomono, M., 1987. Settlement behavior of piled raft foundations on soft ground. *Proceedings of the 8th Asian Regional Conf. on SMFE ARCSMFE*, Kyoto, 20 -24 July 1987, Vol. 1. pp. 373 -376.
- Justason, M., Mullins, A.G., Robertson, D., and Knight, W., 1998. A comparison of static and Statnamic load tests in sand: a case study of the Bayou Chico bridge in Pensacola, Florida. *Proc. of the 7th Int. Conf. and Exhibition on Piling and Deep Foundations*, Deep Foundations Institute, Vienna, Austria, 5.22.2 - 5.22.7.
- Kany M., 1959. Beitrag zur berechnung von flachengrundungen. Wilhelm Ernst und Zohn, Berlin, 201 p. (as referenced by the Canadian Foundation Engineering Manual, 1985).



- Karlsrud, K., Clausen, C.J.F., and Aas, P.M., 2005. Bearing capacity of driven piles in clay, the NGI approach. *Proc. of Int. Symp. on Frontiers in Offshore Geotechnics*, Perth, September 2005, A.A. Balkema, Publishers, pp. 775 - 782.
- Kim, S.R., Chung, S.G., and Fellenius, B.H., 2011. Distribution of residual load and true shaft resistance for a driven instrumented test pile. *Canadian Geotechnical Journal*, 48(4) 384-398.
- Kjellman, W., 1947. Consolidation of fine-grained soils by drain wells. Discussion. *Proc. of the ASCE* 73(6) In *Transactions of the ASCE* 1948 (113) 748-751.
- Kjellman, W., 1948a. Accelerating consolidation of fine-grained soils by means of cardboard wicks. *Proc. 2nd ICSMFE*, Rotterdam, June 21–30, Vol. 2, pp. 302 - 305.
- Kjellman, W., 1948b. Consolidation of fine-grained soils by drain wells. Discussion. *ASCE Transactions*, Vol. 113, pp. 748 - 751.
- Ko, J. and Jeong, S., 2015. Plugging effect of open-end piles in sandy soil. *Canadian Geotechnical Journal* 52(1) 1-13.
- Kondner, R.L., 1963. Hyperbolic stress-strain response. Cohesive soils. *ASCE Journal for Soil Mechanics and Foundation Engineering* 89(SM1) 115-143.
- Kulhawy, F.H. and Mayne, P.W., 1990. *Manual on estimating soil properties for foundation design*. Electric Power Research Institute, EPRI, 250 p.
- Ladd, C.C., 1991. Stability evaluation during staged construction. The Twenty-Second Terzaghi Lecture, *ASCE Journal of Geotechnical Engineering* 117(4) 540-615.
- Larsson, R., and Mulabdic, M., 1991. Piezocone tests in clay. Swedish Geotechnical Institute, SGI, Report No. 42, 240 p.
- Lee, K.M. and Xiao, Z.R., 2001. A simplified nonlinear approach for pile group settlement analysis in multilayered soils. *CGJ* 38(10) 1063-1080.
- Liew, S.S., Gue, S.S. and Tan, Y.C., 2002. Design and instrumentation results of a reinforced concrete piled raft supporting 2500-tonne oil storage tank on very soft alluvium deposits. 9th Int. Conf. on Piling and Deep Foundations, Nice, June 3-5, pp. 263-269.
- Likins, G.E., Fellenius, B.H., and Holtz, R.D., 2012. Pile Driving Formulas—Past and Present. Full-scale Testing in Foundation Design, M.H. Hussein, R.D. Holtz, K.R. Massarsch, and G.E. Likins, eds. *ASCE GeoInstitute Geo-Congress Oakland March 25-29, 2012, State of the Art and Practice in Geotechnical Engineering*, ASCE, Reston, VA., *Geotechnical Special Publication* 227, 737-753.
- Lutenegger, A.J. and Miller, G.A., 1995. Uplift capacity of small diameter drilled shafts from in situ tests. *American Society of Civil Engineers, ASCE, Journal of Geotechnical Engineering*, Vol. 120. No. 8, pp. 1362-1380.
- Lunne, T., Eidsmoen, D., and Howland, J. D., 1986. Laboratory and field evaluation of cone penetrometer. *American Society of Civil Engineers, Proc. of In-Situ* 86, ASCE SPT 6, Blacksburg, June 23 - 25, pp. 714 - 729.
- Lunne, T. Robertson, P.K., and Powell, J.J.M., 1997. *Cone penetration testing in geotechnical practice*. Spon Press, London, 312p.
- Mandolini, A., Russo, G. and Viggiani, C. (2005). Pile foundations: experimental investigations, analysis, and design. *Proc. 16th ICSMGE*, September 12 -16, Osaka, Japan, pp. 177-213
- Massarsch, K.R. 1991. Deep Vibratory Compaction of Land Fill using Soil Resonance. *Proceedings, Infrastructure'91, Intern. Workshop on Technology for Hong Kong's Infrastructure Development*, December 1991, pp. 677-697.
- Massarsch, K.R. 1991. Deep soil compaction using vibratory probes. In *ASTM Symposium on Design, Construction, and Testing of Deep Foundation Improvement: Stone Columns and Related Techniques*. Ed. by R.C. Bachus. *ASTM STP* 1089, pp. 297–319.
- Massarsch, K.R., 1992. Static and dynamic soil displacements caused by pile driving. Keynote Lecture, *Fourth International Conference on the Application of Stress Wave Theory to Piles*, the Hague, the Netherlands, September 21-24, 1992, pp. 15-24.
- Massarsch, K.R., 1994. Settlement analysis of compacted fill. *Proc. of 13th ICSMFE*, New Delhi, January 5-10, Vol. 1, pp. 325-328.

- Massarsch, K.R. 2000. Settlement and damage caused by construction-induced vibrations. Proc., Int. Workshop, Wave 2000, Bochum, Germany, December 13-15, 2000, pp. 299–315.
- Massarsch, K.R. 2002. Effects of vibratory compaction. TransVib 2002 – International Conference on Vibratory Pile Driving and Deep Soil Compaction. Louvain-la-Neuve. Keynote Lecture, pp. 33–42.
- Massarsch, K.R., 2004. Deformation properties of fine-grained soils from seismic tests. Keynote Lecture, International Conf. on Site Characterization, ISC'2 Sept. 19-22, 2004, Porto, pp. 133-146.
- Massarsch, K.R. 2004. Vibrations caused by pile driving. Deep Foundations Institute, DFI Magazine, Part 1: Summer Edition, pp. 41–44, Part 2: Fall Edition, pp. 39–42.
- Massarsch, K.R., 2005. Ground vibrations caused by impact pile driving. Keynote Lecture, Second International Conference on Prediction Monitoring, Mitigation, and Evaluation, September 20-22, Okayama University, Okayama, Taylor and Francis Group, London, pp. 369-379.
- Massarsch, K.R. and Westerberg, E., 1995. The active design concept applied to soil compaction. Proc. of Bengt B. Broms Symposium in Geotechnical Engineering, Singapore, December 13 15, pp. 262-276.
- Massarsch, K.R., Westerberg, E., and Broms, B.B., 1997. Footings supported on settlement-reducing vibrated soil nails. 14th, Hamburg 97, Vol. 3, pp. 1533 - 1539.
- Massarsch, K.R. and Fellenius, B.H., 2002. Dynamic compaction of granular soils. Canadian Geotechnical Journal 39(3) 695-709.
- Massarsch, K.R. and Fellenius, B.H. 2005. Deep vibratory compaction of granular soils. In Ground Improvement Case Histories, Geo-Engineering Series Vol. 3, Chapter 19, Elsevier Publishers (UK), Edited by Buddhima Indraratna and Jian Chu, pp. 633-658.
- Massarsch, K.M., and Fellenius, B.H., 2008. Prediction of ground vibrations induced by impact pile driving, The Sixth International Conference on Case Histories in Geotechnical Engineering, Edited by S. Prakash, Missouri University of Science and Technology, August 12-16, 2008, Arlington, Virginia, 38 p.
- Massarsch, K.R. and Fellenius, B.H., 2012. Early Swedish Contributions to Geotechnical Engineering. ASCE GeoInstitute Geo-Congress Oakland, March 25-29, 2012, Full-scale Testing in Foundation Design, State of the Art and Practice in Geotechnical Engineering, ASCE, Reston, VA, M.H. Hussein, K.R. Massarsch, G.E. Likins, and R.D. Holtz, eds., Geotechnical Special Publication, GSP 227, pp. 239-256.
- Massarsch, K.R. and Fellenius, B.H., 2014. Ground vibrations from pile and sheet pile driving. Part 2. Review of Vibration Standards. Proc. of the DFI-EFFC International Conference on Piling and Deep Foundations, Stockholm, May 21-23, pp. 487-501.
- Massarsch, K.R. and Fellenius, B.H., 2014. Ground vibrations from pile and sheet pile driving. Part 1 Building Damage. Proc. of the DFI-EFFC International Conference on Piling and Deep Foundations, Stockholm, May 21 23, pp. 487-502.
- Mayne, P.W., 2007. Cone penetration testing, a synthesis of highway practice. NCHRP Synthesis 368, Transportation Research Board, Washington, DC, 120 p.
- Mayne, P.W., 2011. Engineering design using the cone penetration test. Geotechnical Applications Guide, ConeTec Inc., Third printing, 165 p.
- Mayne, P.W., Kulhawy, F, and Kay, J.N., 1990. Observations on the development of pore water pressure during piezocone penetration in clays. Canadian Geotechnical Journal 27(4) 418-428.
- Mayne, P.W., Christopher, B.R., and DeJong, J. 2001. Geotechnical Site Characterization. Manual on Subsurface Investigations, National Highway Institute Publication No. FHWA NHI-01-031, FHWA, Washington, DC. 305 p.
- Mayne, P.W, Christopher, B.R. and DeJong, J. 2002. Manual on Subsurface Investigations, Geotechnical Site Characterization. National Highway Institute Publication No. FHWA NHI-01-031, Federal Highway Administration, U.S. Department of Transportation, Washington, DC. 332 p.
- Mazurkiewics, B.K., 1972. Test loading of piles according to Polish Regulations. Preliminary Report No. 15, Commission on Pile Research, Royal Swedish Academy of Engineering Sciences, Stockholm, Sweden.

- McVay, M.C., Schmertmann, J., Townsend, F., and Bullock, P., 1999. Pile freeze, a field and laboratory study. Final Report, Florida Department of Transportation, Research Center, Contract No. B-7967, 1,314 p.
- Meyerhof, G.G., 1951. The bearing capacity of foundations. *Geotechnique* 2(4) 301-332.
- Meyerhof, G.G., 1963. Some recent research on bearing capacity of foundations. *Canadian Geotechnical Journal* 1(1) 16-26.
- Meyerhof, G.G., 1976. Bearing capacity and settlement of pile foundations. The Eleventh Terzaghi Lecture, November 5, 1975. *ASCE Journal of Geotechnical Engineering* 102(GT3) 195-228.
- Middendorp, P., Bermingham, P., and Kuiper, B., 1992. Statnamic loading test of foundation piles. *Proc. 4th Int. Conf. on the Application of Stress Wave Theory to Piles*, edited by B.J. Barends, Balkema, Rotterdam, The Netherlands, 581 - 588.
- Middendorp, P., Beck, C., and Lambo, A., 2008. Verification of Statnamic load testing with static testing in a cohesive soil type in Germany. *Proc. of the 8th International Conference on the Application of Stress-wave Theory to Piles*, pp. 531-536.
- Moh, Z.C. and Lin, P.C., 2006. Geotechnical History of the development of the Suvarnabhumi International Airport. Special Issue of the *Journal of South-East Asian Geotechnical Society*, *Geotechnical Engineering*, December 2006, 37(3) 143-155.
- Mokwa, R.L., and Duncan, J.M., 2001. Experimental evaluation of lateral load resistance of pile caps. *ASCE, Journal of Geotechnical and Geoenvironmental Engineering*, 127(2) 185-192.
- Moss, R.E.S., Seed, R.B., Kayen, R.E., Stewart, J.P., DerKiureghian, A., and Cetin, K.O. 2006, CPT-based probabilistic and deterministic assessment of in situ seismic soil liquefaction potential. *ASCE, Journal of Geotechnical and Geoenvironmental Engineering*, 132(8) 1032-1051.
- NAVFAC DM7, 1982. Design Manual for Soil Mechanics, Foundations, and Earth Structures. US Department of the Navy, Washington, DC.
- Newmark, N.M., 1935. Simplified computation of vertical stress below foundations. Univ. of Illinois Engineering Experiment Station, Circular 24, Urbana, Illinois, 19 p. (as referenced by Holtz and Kovacs 1985).
- Fellenius, B.H., 1984. Wave equation analysis and dynamic monitoring. *Deep Foundations Journal*, Deep Foundations Institute, Springfield, New Jersey 1(1) 49-55.
- Newmark, N.M., 1942. Influence chart for computation of stresses in elastic foundations. University of Illinois Engineering Experiment Station, Bulletin Series 338, Vol. 61, No. 92, Urbana, Illinois, 28 p. (as referenced by Holtz and Kovacs 1981, Holtz et al 1999).
- Nilsson, G., 1989. Markvibrationer vid påslagning (Ground vibrations during pile driving). Examensarbete Nr. 3:89. Dept. of Soil and Rock Mechanics, Royal Institute of Technology (KTH). Stockholm, Sweden, 43 p. and Appendix (In Swedish).
- Nishimura, S., Matsumoto, T., Kusakabe, O., Nishiumi, K., and Yoshizawa, Y., 2000. Case studies of Statnamic loading test in Japan. *Proc. 6th Int. Conf. on the Application of Stress Wave Theory to Piles*, Edited by S. Niyama and J. Beim, Balkema, Rotterdam, The Netherlands, 591-598.
- Nordlund, R.L., 1963. Bearing capacity of piles in cohesionless soils. *ASCE Journal of Soil Mechanics and Foundation Engineering* 89(SM3) 1-35.
- Nottingham, L.C., 1975. Use of quasi-static friction cone penetrometer data to predict capacity of displacement piles. Ph.D. thesis, Dept of Civil Engineering, Univ. of Florida, 553 p.
- OHBD, 1991. Ontario Highway Bridge Design Code, 3rd. Edition, Code and Commentary, Min. of Transp., Quality and Standards Division, Toronto.
- Okabe, T., 1977. Large negative friction and friction-free piles methods. 9th ICSMFE, Tokyo, July 11-15, Vol.1, pp. 679-682.
- Olson R.E., 1998. Settlement of Embankments on Soft Clays. *ASCE Journal of Geotechnical Engineering*, 124(4) 278-288.
- Oliveira, M.A., Falconi, F.F., and Perez, W., 2008. Estaca hélice contínua – ensaio dinâmico e prova de carga estática. 6th Seminário de Engenharia de Fundações Especiais e Geotecnia, SEFE VI, Sao Paulo, Brazil, November 3-5, Vol. 1 pp. 423-431.

- Olsen, R.S., and Farr, V., 1986. Site characterization using the cone penetration test. American Society of Civil Engineers, Proc. of In-Situ 86, ASCE SPT 6, Blacksburg, June 23-25, pp. 854-868.
- Olsen, R.S., and Malone, P.G., 1988. Soil classification and site characterization using the cone penetrometer test. Proc. of First International Symposium on Cone Penetration Testing, ISOPT-1, Orlando, March 22-24, Vol. 2, pp. 887-893.
- Olsen, R.S., and Mitchell, J.K., 1995. CPT stress normalization and prediction of soil classification. Proc. of International Symposium on Cone Penetration Testing, CPT95, Linköping, Sweden, SGI Report 3:95, Vol. 2, pp. 257-262.
- O'Neill, M.W., Hawkins, R.A., and Audibert, J.M.E., 1982. Installation of pile group in overconsolidated clay. ASCE Journal of Geotechnical Engineering Div., Vol. 108(11) 1369-1386.
- O'Neill, M.W., Hawkins, R.A., and Mahar, L.J., 1982. Load transfer mechanisms in piles and pile groups. ASCE Journal of Geotechnical Engineering Div., Vol. 108(12) 1605-1623.
- O'Neill, M.W. and Raines, R.D., 1991 Load transfer for pipe piles in highly pressured dense sand. ASCE Journal of Geotechnical Engineering, 117(8) 1208-1226.
- O'Neill, M.W. and Reese, L.C., 1999. Drilled shafts. Construction procedures and design methods, Federal Highway Administration, Transportation Research Board, Washington, FHWA-IF99-025.
- Osterberg, J., 1989. New device for load testing driven piles and bored piles separates friction and end-bearing. Deep Foundations Institute, Proc. of the International Conference on Piling and Deep Foundations, London, London June 2-4, Eds. J.B. Burland and J.M. Mitchell, A.A. Balkema, Vol. 1, pp. 421-427.
- Osterberg, J.O., 1998. The Osterberg load test method for drilled shaft and driven piles. The first ten years. Deep Foundation Institute, Seventh International Conference and Exhibition on Piling and Deep Foundations, Vienna, Austria, June 15 - 17, 1998, 17 p.
- Paik, K.H., Salgado, R., Lee, J.H., Kim B.J., 2003. Behavior of open- and closed-end piles driven into sands. ASCE Journal of Geotechnical and Geoenvironmental Engineering 129(4) 296-306.
- Paniagua, W., Ibarra, E., and Valle, J.A., 2007. Rigid inclusions for soil improvement in a 76 building complex. Deep Foundations Institute Magazine, Fall issue. 7p.
- Peck, R.B., Hanson, W.E., and Thornburn, T. H., 1974. Foundation Engineering, Second Edition. John Wiley and Sons Inc., New York, 514 p.
- Pecker, A., 2004. Design and Construction of the Rion Antirion Bridge. Proc. of the Conference on Geotechnical Engineering for Transportation Projects, , Geo-Trans, ASCE GeoInstitute, Los Angeles July 27 - 31, 2004, Eds. M.K. Yegian and E. Kavazanjian, Vol. 1 pp. 216 - 240.
- Perloff W.H. and Baron W., 1976. Soil mechanics principles and applications. John Wiley and Sons, New York, 745 p.
- Poulos, H.G., 2013. Pile design for ground movement. Proc. of the Int. Conf. on State-of-the-Art of Pile Foundations and Case Histories, Bandung, Indonesia, June 2-4, pp. A2-1 - A2-18.
- Rausche, F., Moses, F., and Goble, G.G., 1972. Soil resistance predictions from pile dynamics. ASCE Journal of Soil Mechanics and Foundation Engineering 8(SM9) 17-937.
- Rausche F. and Goble G. G., 1979. Determination of pile damage by top measurements. American Society for Testing and Materials, ASTM, Proceeding of Symposium on Behavior of Deep Foundations, R. Lundgren Editor, ASTM STP 670, pp. 500-506.
- Rausche, F., Goble, G.G., and Likins, G.E., 1985. Dynamic determination of pile capacity. ASCE Journal of the Geotechnical Engineering Division 111(GT3) 367-383.
- Robertson, P.K., 1986. In-Situ testing and its application to foundation engineering. 1985 Canadian Geotechnical Colloquium, Canadian Geotechnical Journal 23(4) 573-594.
- Robertson, P.K., 1990. Soil classification using the cone penetration test. Canadian Geotechnical Journal 27(1) 151-158.
- Robertson, P.K., 2007. Cone penetration testing. Geotechnical applications guide. Cone Tech Inc., Fifth Edition, 600 p.
- Robertson, P.K., 2007. Cone penetration test (CPT)-based soil behaviour type (SBT) classification system— an update. Canadian Geotechnical Journal 53(11) 1-18.

- Robertson, P.K., 2016. Cone penetration test (CPT)-based soil behaviour type (SBT) classification system--an update. *Canadian Geotechnical Journal*, 53(12) 1910-1927.
- Robertson, P.K., Campanella, R.G., and Wightman, A., 1983. SPT-CPT correlations. *ASCE Journal of the Geotechnical Engineering Division* 109(GT11) 1449-1459.
- Robertson, P.K. and Campanella, R.G., 1983. Interpretation of cone penetrometer tests, Part I sand and Part II clay. *Canadian Geotechnical Journal*, (20)4 718 - 733 and 734 - 745.
- Robertson, P.K., and Campanella, R.G., 1985. Liquefaction potential of sands using the cone penetration test. *Journal of Geotechnical Engineering, ASCE*, 22(GT3) 298-307
- Robertson, P.K., Campanella, R. G., Gillespie, D., and Grieg, J., 1986. Use of piezometer cone data. *Proc. of ASCE In-Situ 86 Specialty Conference*, Edited by S. Clemence, Blacksburg, June 23 - 25, *Geotechnical Special Publication GSP No. 6*, pp. 1263 - 1280.
- Robertson, P.K. and Campanella, R.G., 1986. Guidelines for use, interpretation, and application of the CPT and CPTU. *Manual, Hogentogler & Company, Inc.*, 196 p.
- Robertson, P.K. and Wride, C.E., 1998. Evaluating cyclic liquefaction potential using the cone penetration test. *Canadian Geotechnical Journal* 35(3) 442-459.
- Robertson, P.K., 1990. Soil classification using the cone penetration test. *Canadian Geotechnical Journal*. 27(1) 151-158.
- Rollins, K.M., Clayton, R.J., Mikesell, R.C., and Blaise, B.C., 2005. Drilled shaft side friction in gravelly soils. *ASCE Journal of Geotechnical and Geoenvironmental Engineering*, 131(8) 987-1003.
- Roscoe, K.H., Schofield, A.N., and Wroth, C.P., 1958). On the yielding of soils. *Geotechnique* 8(1) 22-53.
- Russo, G. and Viggiani C. (1995). Long-term monitoring of a piled foundation. *Fourth International Symposium on Field Measurements in Geomechanics*, Bergamo, pp. 283-290.
- Sampaco, K., Pham, H., and Anderson, D. 2008. The Golden Ears Bridge design-build project: foundation design for segment 4 approach structures. *Proc. of the FHWA, and SCDOT Sixth National Seismic Conference on Bridges and Highways*, Charleston, South Carolina, July 27-30, Paper 2B1-2, 12 p.
- Salem, H., Agharazi, F. and Fellenius, B.H., 1995. Detection of toe damage in steel piles driven to bedrock. *1995 PDA User's Days*, Cleveland, 14 p.
- Sanglerat, G., Nhim, T.V., Sejourne, M., and Andina, R., 1974. Direct soil classification by static penetrometer with special friction sleeve. *Proc. of the First European Symposium on Penetration Testing, ESOPT-1*, June 5 - 7, Stockholm, Vol. 2.2, pp. 337 - 344.
- Schmertmann, J.H., 1970. Static cone to compute settlement over sand. *ASCE Journal Soil Mechanics and Foundation Engineering* 96(SM3) 1011-1043.
- Schmertmann, J.H., 1975. Measurement of In-situ Shear Strength. *Proc. of ASCE Geotechnical Division, Specialty Conference on In-Situ Measurement of Soil Properties*, June 1 - 4, 1974, Raleigh, NC, Vol. 2. pp. 57 - 138.
- Schmertmann, J.H., 1978. Guidelines for cone penetration test, performance, and design. *U.S. Federal Highway Administration, Washington*, Report FHWA-TS-78-209, 145 p.
- Schmertmann, J.H., 1991. The mechanical aging of soil. *The 25th Terzaghi Lecture, ASCE J. of the Geot. Engng. Div.*, 115(7) 1003-1018.
- Schmertmann, J.H. and Schmertmann, C.P., 2009. "Test every non redundant foundation bored pile to reduce uncertainty and cost". *Lecture to Hong Kong Institution of Engineers, Polytech University, Hong Kong*, July 11, 2009, 41 p.
- Schmertmann, J.H. and Schmertmann, C.P., 2012. "Testing and Remediation Observational Method for the Design and Construction of Pile Foundations." *The Role of Full-Scale Testing in Foundation Design*, *ASCE Geotechnical Special Publication*, Ed. by M.H. Hussein, R.D. Holtz, K.R. Massarsch, and G.E. Likins, GSP 227, pp. 349 -361.
- Searle, I.E., 1979. The interpretation of Begemann friction jacket cone results to give soil types and design parameters. *Proc. of 7th European Conference on Soil Mechanics and Foundation Engineering, ECSMFE*, Brighton, Vol. 2, pp. 265-270.

- Seed, H.B., and Idriss, I.M. (1971). 'Simplified procedure for evaluating soil liquefaction potential. ASCE J. Geotech. Engng. Div.97(9) 1249–1273.
- Sheah, T.H., 2006. Design and Construction of ground improvement works at Suvarnabhumi Airport. Special Issue of the Journal of South-East Asian Geotechnical Society, Geotechnical Engineering, December 2006, 37(3) 171-188.
- Shen Bao-Han and Niu Dong-Sheng, 1991. A new method for determining the yield load of piles. Proc. of the Fourth International Conference on Piling and Deep Foundations, Deep Foundation Institute, Stresa April 7 - 12, Balkema Publishers, Vol. 1, pp. 531 - 534.
- Simpson, B. and Driscoll, R., 1998. Eurocode 7A Commentary. Construction Research Communications, Watford.
- Sinnreich, J., 2012. Strain gage analysis for nonlinear pile stiffness. Geotechnical Testing Journal. American Society for Testing Materials, ASTM 35(2) 1-8.
- Smith, E.A.L., 1960. Pile driving analysis by the wave equation. Journal of the Soil Mechanics and Foundation Engineering Division, Proc. ASCE 86(SM4) 35-61.
- Sridharan, A., Abraham, B.M., and Jose, B.T., 1991. Improved technique for estimation of preconsolidation pressure. Geotechnique 41(2) 263-268.
- Stark, T.D., and Olsen, S.M., 1995. Liquefaction resistance using CPT and field case histories. Journal of Geotechnical Engineering, ASCE, 121(GT12) 856–869.
- Steinbrenner, W., 1934. Tafeln sur Setzungberechnung. Die Strasse 1:221.
- Steinbrenner, W., 1936. A rational method for the determination of the vertical normal stresses under foundations. 1st ICSMFE, Vol. 2, pp. 142-143.
- Stoll, M.U.W., 1961. Discussion on New approach to pile testing by T. Whitaker and R. W. Cooke, Proc. 5th ICSMFE, Paris, July 17-21, Vol. 3, pp. 279 - 281.
- Swedish State Railways Geotechnical Commission, 1922. Statens Järnvägars Geotekniska Kommission – Slutbetänkande. Swedish State Railways, Bulletin 2 (in Swedish with English summary), 228 p.
- Tanaka, H., Ritoh, F., and Omukai, N, 2002. Quality of samples retrieved from great depth and its influence on consolidation properties. Canadian Geotechnical Journal (39)6 1288-1301.
- Tavenas, F. and LaRochelle, P., 1972. Accuracy of relative density measurements. Geotechnique 22(4) 549-562.
- Taylor, D.W., 1948. Fundamentals of soil mechanics. John Wiley & Sons, New York, 700 p.
- Teparaksa, W. 2015. Deep barrette pile capacity with aging effect. Geotechnical Engineering Journal of the SEAGS & AGSSEA 46(2) 68-76.
- Tschebotarioff, G.P., 1951. Soil mechanics, foundations, and earth structures. McGraw-Hill Book Company Inc., New York, 655 p.
- Tschebotarioff, G.P., and Palmer, L.A., 1948. Some experiences with tests on model piles. Proc. of 2nd ICSMFE, Rotterdam, June 21–30, Vol. 2, p. 196.
- Tschebotarioff, G.P., 1951. Soil Mechanics, Foundations, and Earth Structures. McGraw Hill Book Co. Inc., New York, p. 440 (p. 230 in 2nd Ed., 1979).
- Terzaghi, K., 1942. Discussion of the Progress Report of the Committee on the Bearing Capacity of Pile Foundations. ASCE Proc. 68(2) 311-323.
- Terzaghi, K., 1943. Theoretical Soil Mechanics. John Wiley and Sons, New York, 511 p.
- Terzaghi, K., 1954. Anchored bulkheads. ASCE Transactions, 119 1243-1324.
- Terzaghi, K. and Peck, R.B., 1948. Soil Mechanics in Engineering Practice. John Wiley and Sons, New York, 566 p.
- Terzaghi, K., 1955. Evaluation of coefficients of subgrade reaction. Geotechnique 5(4) 297-326.
- Terzaghi, K., Peck, R.B., and Mesri G., 1996. Soil Mechanics in Engineering Practice, Third Edition. John Wiley and Sons, New York, 549 p.
- Tomlinson, M.J., 1980. Foundation design and construction, Fourth Edition. Pitman Publishing Inc., London, 793 p.
- Tumay, M. T., and Fakhroo, M., 1981. Pile capacity in soft clays using electric QCPT data. ASCE Cone Penetration Testing and Experience, St. Louis, October 26-30, pp. 434-455.

- US Corps of Engineers (USCOE), 2012. Hurricane and storm damage risk reduction systems design guidelines (HSDRRSDG), Chapter 3, Geotechnical, 67 p.
- Van der Veen, C., 1953. The bearing capacity of a pile. Proc. of the 3rd ICSMFE, Zurich, Switzerland, August 16-27, Vol. 2, pp. 84-90.
- Vesic, A.S., 1973. Analysis of ultimate loads of shallow foundations. ASCE Journal of Soil Mechanics and Foundation Engineering 99(SM1) 45-73.
- Vesic, A.S., 1975. Bearing capacity of shallow foundations. In Foundation Engineering Handbook, edited by H.F. Winterkorn and H-Y Fang, VanNostrand Reinhold Co., New York, pp. 121 - 147.
- Vijayvergiya, V.N. and Focht, J.A. Jr., 1972. A new way to predict the capacity of piles in clay. Fourth Annual Offshore Technology Conference, Houston, Vol. 2, pp. 865 - 874.
- Vijayvergiya, V.N., 1977. Load-movement characteristics of piles. Proc. of Port '77 Conference, ASCE, Long beach, Ca, March 9 - 11, Vol. 2, pp. 269-284.
- Vos, J.D., 1982. The practical use of CPT in soil profiling, Proc. of the Second European Symposium on Penetration Testing, ESOPT-2, Amsterdam, May 24 - 27, Vol. 2, pp. 933 - 939.
- Wellington, A.M., 1988. Formulae for safe loads of bearing piles. Engineering News Records, pp 500-512.
- Westergaard, H.M., 1938. A problem of elasticity suggested by a problem in soil mechanics: A soft material reinforced by numerous strong horizontal sheets. In Contributions to the Mechanics of Solids, Stephen Timoshenko 60th Anniversary Volume, MacMillan, New York, pp. 260 - 277 (as referenced by Holtz and Kovacs 1981).
- Youd, T.L., Idriss, I.M., Andrus, R.D., Arango, I., Castro, G., Christian, J.T., Dobry, R., Finn, W.D.L., Harder, L.F., Hynes, M.E., Ishihara, K., Koester, J.P., Liao, S.S.C., Marcuson, W.F., Martin, G.R., Mitchell, J.K., Moriwaki, Y., Power, M.S., Robertson, P.K., Seed, R.B., Stokoe, K.H. 2001. Liquefaction resistance of soils: Summary report from the 1996 NCEER and 1998 NCEER/NSF Workshops on evaluation of liquefaction resistance of soils, ASCE Journal of Geotechnical and Geoenvironmental Engineering 127(4) 297-313.
- Zhang Q.Q. and Zhang, Z.M., 2012. Simplified non-linear approach for single pile settlement analysis. Canadian Geotechnical Journal, 49(11) 1256-1266.
- Yamashita, K. Hamada, J., Takeshi, Y., 2011. Field measurements on piled rafts with grid-form deep mixing walls on soft ground. Geotechnical Engineering Journal of the SEAG & AGSSEA, 42(2) 1-10.
- Yamashita, K. Hamada, J., Takeshi, Y., 2011. Investigation of settlement and load sharing on piled rafts by monitoring full-scale structures. Soil and Foundations 51(3) 513-532.
- Yamashita, K., Wakai, S., and Hamada, J. 2013. Large-scale piled raft with grid-form deep mixing walls on soft ground. Proc. 18th ICSMGE, September 2-6, Paris, France, Vol. 3, pp. 2637-2640.
- Yang, Y., Them, E.G., Lee, P.K.K., and Yu, F., 2006. Observed performance of long steel H-piles jacked into sandy soils. ASCE Journal of Geotechnical and Environmental Engineering 132(1) 24-35.





## CHAPTER 17

### INDEX

Aquifer	1.7	Degree of consolidation	3.14
Average degree of consolidation	4.3	Degree of saturation	1.2
		Density	1.2
Bearing capacity factors	6.1	Density, bulk	1.2
Bearing capacity formula	6.1	Density, dry	1.2
Beta coefficient	7.2	Density, saturated	1.2
Bidirectional test	8.20	Density, solid	1.2
Bitumen coating	7.51	Density, total	1.2
Block analysis	3.19	DIET	9.11
Blow rate	9.9	Discharge capacity	4.14
Boussinesq	1.12	Downdrag	7.5, 7.34
Buckling	7.51	Drag force	7.5, 7.34
		Drainage blanket	4.4
CAPWAP	9.33	Drains	4.1
Case method estimate of capacity	9.30		
Characteristic Point	1.15	Earth pressure	5.1
Chin.Kondner method	8.4	Earth stress	5.1
Coefficient of consolidation	3.14	Earth stress coefficient	5.2
Coefficient of horizontal consolidation	4.3	Eccentric load	5.2
Coefficient of restitution	9.16	Energy ratio	9.4
Coefficient of secondary compression	3.15	Equivalent cylinder diameter	4.3
Coefficient, earth pressure	5.2	Equivalent footing width	6.4
Coefficient, shaft correlation	7.25	Exponential function	8.16
Compression index	3.3	Factor of safety	6.2, 7.9, 8.9
Compression ratio	3.3, 3.4	Factor, inclination	6.3
Compaction	9.16	Factor, shape	6.4
Compression wave	9.12	Filter jacket	4.11
Cone penetrometer, electric	2.1	Follower	9.14
Cone penetrometer, mechanical	2.1	Force, pile head	9.15
Cone penetrometer, piezocone	2.1, 7.15	Force, pile toe	9.17
Cone resistance	2.2	Friction angle, internal	5.2
Cone resistance, "effective"	2.13	Friction angle, wall	5.2
Cone resistance, corrected	2.7	Friction ratio	3.2, 3.3, 3.5
Cone resistance, normalized	2.9	Friction ratio, normalized	2.10
Continuous sampling	2.20	Fundex test	9.37
CPTU.method for piles	7.11		
Creep	3.1, 3.15, 8.7	Gradient	1.7, 4.4, 4.7
Crimping	4.13	Grain size diagram	1.6
Critical depth	7.9	Groundwater table	1.7
Damping	9.18	Hammer efficiency	9.4
Damping factor	9.19, 9.20, 9.31	Hammer function	9.2
Davisson Offset limit	8.2	Hammer selection	9.22
DeBeer method	8.6	Hammer types	9.5
Decourt method	8.5	Hansen method	8.2
Deformation	1.1, 3.1	Hansen 80.% function	8.17

High strain testing	9.24	Permeability, filter jacket	4.12
Hooke's Law	3.3	Phase parameters	1.1
Horizontal loading	7.46	Phreatic height	1.7
Hydraulic conductivity	4.1, 4.10	Pile Driving Analyzer, PDA	9.24
Hydraulic pore pressure	1.7	Pile group effect	7.39
Hyperbolic function	8.16	Pile integrity	9.29
		Piled pad	7.12
Impact duration	9.3	Piled raft	7.11
Impedance, Z	9.25	Plugged toe	9.15
Inclination facto	6.4	Poisson's Ratio	3.2
Inclined load	6.3	Pore pressure	1.7
Instrumented test	8.17	Pore pressure at shoulder, U2	2.3, 2.10
		Pore pressure gradient	4.7
Jetting	7.50	Pore pressure ratio	2.10
		Pore pressure ratio, "effective"	2.10
Kjellman.Barron method	4.2	Porosity	1.2
		Preconsolidation	3.6
Lambda method	7.28	Preconsolidation margin	3.7
Lateral movement	4.8	Proctor test	3.5.7
Limit States Design	6.13	Quake	9.15
Load and Resistance Factor Design	6.13	q.z curve	8.12
Load, eccentric	6.3		
Load, inclined	6.4	Racking	9.9
Load, line	5.6	Ratio function	8.14
Load, residual	7.12	RAU	9.32
Load, strip	5.8	Recompression index	3.3
Load, surcharge	5.8	Recompression modulus number	3.7
Low strain testing	9.29	Residual force	8.15, 8.16, 8.22, 8.29
		Resistance, shaft	8.1
Maximum curvature method	8.8	Resistance, toe	8.2
Maximum stress	9.17	Resistance, ultimate	8.3
Microfolding	4.14	RSP	9.31
Mineral density	1.3	RSU	9.31
Modulus number, m	3.4, 3.7		
Modulus of elasticity	8.33	Scour	7.23
Modulus, constrained	3.2	Salt content	1.3
Modulus, elastic	3.2	Sand drains	4.10
Modulus, from CPTU	3.21	Sand drains	4.3, 4.8
Modulus, Janbu tangent	3.4	Scour	
Modulus, tangent for piles	8.31	Secondary compression	3.9, 3.14, 4.4
Modulus, Young's	3.2	Seismic design	7.49
Movement	3.1	Settlement	1.1, 3.1
		Settlement, acceptable	3.15
Negative skin friction	7.4	Settlement of piled foundations	7.37
Neutral plane	7.8	Settlement below pile toe level	7.38
		Shape factor	6.4
Newmark Influence Chart	1.13	Shoulder area ratio, a	2.7
Overconsolidation ratio, OCR	3.6	Sleeve friction	2.4
Overturning	6.6	Sliding	6.7
		Smear zone	4.15
PDA diagram	9.35	Spacing of drains	4.12

---

Spacing of piles	7.21	Transferred energy	9.21
Stage construction	4.8	Unified pile design method	7.17
Stage construction	4.6	Unit weight, buoyant	1.4
Standard penetration test, SPT	7.14	Unit weight, total	1.4
Statnamic test	9.37	Unloading Point Method, UPM	9.39
Stiffness	9.15		
Strain wave	9.10	Vacuum loading	4.9
Strain wave length	9.13	Vibrations	2.12.8
Stress distribution	1.6	Vibratory hammer	9.3
Stress exponent, j	3.4	Vibratory driving	9.14
Stress wave	9.10	Vibratin damage	9.15
Stress, effective	1.7	Void ratio	1.2
Stress, effective	1.7		
Stress, impact	9.17	Water content	1.2
Stress, overburden	1.7	Water ponding	4.4
Surcharge	4.6, 5.5	Wave equation analysis	9.21
Swelling soil	7.38	Wave traces	9.25
		Westergaard distribution	1.14
Tangent Modulus Method	8.16	Wick drains	4.6
Tapered pile	7.8	Winter conditions	4.5
Telltale	8.13		
Ternary diagram	1.7		
Time coefficient	3.14		
Time dependent settlement	3.14		
Toe coefficient	7.4		
Transition zone	7.15		
t.z curve	8.12		

---

